BUILDING RESPONSE DUE TO GROUND MOVEMENTS

Holger Netzel

Building Response due to Ground Movements

Proefschrift

ter verkrijging van de graad van doctor

aan de Technische Universiteit Delft,

op gezag van de Rector Magnificus Prof.dr.ir. J.T. Fokkema,

voorzitter van het College voor Promoties,

in het openbaar te verdedigen

op vrijdag 17 april 2009 om 12.30 uur

door

Holger Dirk NETZEL

Diplom-Ingenieur

(Technische Universiteit Stuttgart)

geboren te Stuttgart, Duitsland

CRUX

ACKNOWLEDGEMENTS

ABSTRACT

Building Response due to Ground Movements

Prediction of ground deformations due to excavations works and consequently the determination of potential building damage of the adjacent structures forms an important part of settlement risk management for underground works in urban surrounding. The requirements of the surroundings form a crucial boundary condition to the design of underground construction works in urban environment.

This thesis focuses on prediction methods, which can either be used in the design engineering stage to predict building damage due to imposed ground deformations by excavation works, but can also be applied for a postdiction to analyse relations between excavation works and claimed building damage.

Due to the great variety of excavation sources, foundation and type of surrounding buildings in the engineering practice, it is decided to focus in this thesis on the building response of masonry structures, founded on shallow foundations, due to TBM-tunnelling induced ground deformations. However the principles of the developed damage prediction methods also apply to other sources causing differential ground deformations on adjacent buildings.

This thesis first focuses on the empirical analytical prediction of *greenfield ground deformations* due to three relevant sources of ground deformations for projects in urban surrounding: TBM-tunnelling, the excavation of building pits and groundwater lowering. International developments on empirical analytical methods are summarized from a literature study. Recent monitoring data from three TBM-tunnelling projects in the Netherlands are used to develop prediction methods for ground movements due to TBM-tunnelling in the soft soil conditions of the Netherlands. These prediction methods can be used in a preliminary design stage in order to get a first indication of the range of expected ground movements.

Next is the *review and further development of the existing LTSM (Limiting Tensile Strain Method)*, which is currently used in the engineering practice to predict building damage due to excavation induced ground deformations. The prediction method is based on the calculation of induced tensile strains in a structure due to imposed differential vertical and horizontal ground deformations. The review was considered necessary, because the practical use of the method raised some important fundamental questions about basic assumptions in the method. The review investigates the assumptions and backgrounds of the prediction method. It is shown that several assumptions in the current method can lead to significant under- or overestimations of the damage. Finally, a modified LTSM is developed, which takes into account refined assumptions and procedures which are derived from analytical and numerical considerations.

Subsequently the thesis includes an intensive *numerical study on the effects of soil-structure interaction* on the building response due to excavation induced ground deformations. The soil-structure interaction is neglected in the empirical analytical LTSM, that assumes full transfer of the greenfield ground movements to the building. The advanced numerical finite element calculations include nonlinear smeared cracking response of the masonry wall and a nonlinear interface model between soil and building. The final results of the numerical calculations are presented in terms of cracking damage (crack widths en crack patterns) in the walls, which are classified in the LTSM damage classification system in order to be able to compare the numerical results with the results of the modified LTSM. The case of ground deformations induced by TBM-tunnelling and its influence on masonry walls founded on shallow foundations is investigated. For all considered numerical interaction analyses it is shown that for the same distribution of imposed greenfield ground deformations, the damage sensitivity of a masonry wall increases with increasing soil stiffness. A decreasing soil stiffness results in beneficial interaction effects, reducing the building damage. Furthermore the nonlinear material behaviour of the wall, including the modelling of smeared cracking, shows to have significant influence on the damage

Abstract

development once a crack is initiated. A numerical interaction analyses should take into account nonlinear material behaviour of the wall and the interface in order to obtain appropriate damage results. Detailed conclusions are drawn from the comparison of the damage results obtained with the advanced numerical interaction analyses and the results of the modified LTSM. It has to be distinguished carefully between the influence of interaction in a hogging zone situation and a sagging zone situation, because for the considered cases of tunnelling induced ground deformations, the combination of imposed horizontal and vertical differential ground movements causes very different effects on the building response in both zones.

Furthermore, some important aspects for the ***translation of the prediction results to monitoring criteria***, used for risk control during the construction stage, are addressed. Designers are often not aware of the need of these considerations. It is shown that the consequences can be significant if these issues are not correctly handled in engineering practice. Recommendations are given for the correct derivation of the monitoring criteria from a damage prediction in the design stage.

Finally the ***evaluation of a full scale test on the influence of TBM-tunnelling on the adjacent soil and building*** for the Sophia railway tunnel is presented. The monitoring results of ground deformations, building deformations and damage results of an adjacent building are analysed and compared to results of the previously developed prediction methods. The results show good agreement between predicted and observed damage level. Unfortunately, the differential ground deformations caused by the tunnelling process at the location of the building were that small, that the damage level on the building was negligible. The negligible damage is however observed from the defect surveys as well as predicted with the reviewed empirical analytical LTSM and the numerical damage prediction.

Holger Netzel

TABLE OF CONTENTS

Table of Contents

Table of Contents

Table of Contents

APPENDICES

Appendix 1 Settlements due to groundwater lowering

Appendix 2 Relation between angular distortion and deflection ratio for a simply supported beam with a central point load

Appendix 3 Settlements due to groundwater lowering

Appendix 4 Design charts for the determination of the angular distortions in a Gaussian settlement trough

Appendix 5 Eccentricity effect due to transfer of horizontal differential ground movements

1 INTRODUCTION

1.1 Problem description

Prediction of ground movements and consequently the building damage of adjacent structures forms an important part of settlement risk management for excavation works in urban surrounding. The assessment of the influence of the construction works on the immediate surroundings is a major political, technical and financial challenge for the design of projects in urban areas. The requirements imposed by the surroundings and various parties like building owners or service companies restrict the design of the construction works. Reliable prediction methods for ground movements associated with the excavation works and calculation methods for the prediction of the resulting building damage are required as a crucial engineering tool for the quantification of damage risks in an early design stage.

If the damage prediction in the design stage results in an unacceptable damage profile of the surroundings, additional design measures have to be taken in order to restrict the differential deformations up to an acceptable level. The design of underground works has to fulfil the requirements regarding stability, strength and serviceability of the new structure, but also has to limit the deformations and consequently the introduced stresses and strains in the existing neighbouring structures up to an acceptable level. In the engineering practice the designers are often not aware of the importance of the latter boundary condition.

Design considerations in combination with monitoring should be used during construction of the excavation works to control the influence on the surroundings and consequently minimize the impact on the adjacent buildings. A proactive risk control strategy has to be followed in the construction stage in order to be able to assign mitigating measures in time, preventing damage to develop. The decision to implement mitigating measures has to be taken on the basis of the predictions in the design stage combined with the expert interpretation of the monitoring results during the construction works. It is emphasized that monitoring in itself is not a mitigating measure, but a supporting tool during the construction work to be able to recognize the development of deformations in time, before irreversible damage has occurred.

This thesis focuses on the damage prediction methods used in the design engineering stage.

1.2 Scope of the research

The scope of this research is the investigation and development of calculation methods to predict the potential building damage due to ground movements. Simplified empirical analytical methods widely used in engineering practice are considered as well as advanced nonlinear numerical modelling of soil-structure interaction.

First the backgrounds of the existing empirical analytical damage prediction method are reviewed. This method, the Limiting Tensile Strain Method, further referred to as LTSM, is used to predict the building damage due to imposed ground deformations in the design stage of building projects in urban surrounding. The frequent use of the current LTSM in engineering practice has raised several fundamental questions to me. The aim of this part of the research is to critically review the backgrounds and assumptions of the methods and their consequences on the predicted building damage and to amend and further develop recommendations for the reliable use of the method in design practice.

The prediction of building damage due to excavation induced ground movements is influenced by many factors. One important aspect is the soil-structure interaction. The currently used LTSM neglects the interaction, assuming that the buildings fully follow the imposed ground movements. The influence of the soil-structure interaction on the damage response of building will be investigated with the support of advanced numerical soil-structure interaction analyses using nonlinear models for the interface properties and nonlinear fracture mechanics based crack models for the building. The nonlinear finite element studies provide insight into the stress redistribution processes in the building and the

consequent initiation and propagation of cracks. The comparison of the damage results according to the LTSM with the cracking results of the advanced interaction analyses forms an important part of the research. The major aspiration is to achieve a better understanding of the way buildings respond on imposed ground movements and to be able to qualitatively judge the influence of the soil-structure interaction including the nonlinear behaviour of the structure and the interface between soil and structure on the LTSM prediction results.

1.3   Outline of the thesis

In this thesis the following research topics are outlined:

Chapter 2 focuses on a literature study on empirical analytical prediction methods of ***greenfield ground movements*** for different sources of excavation works in urban surrounding. These sources include TBM-tunnelling, excavation of building pits and groundwater lowering. Moreover, field data of ground movements from three Dutch TBM-tunnelling projects are analysed.

Chapter 3 presents a review and further development of the existing empirical analytical prediction method (<u>L</u>imiting <u>T</u>ensile <u>S</u>train <u>M</u>ethod; LTSM), which is widely used in engineering practice to predict building damage due to imposed greenfield ground deformations.

Chapters 4 to 7 show the results of an intensive numerical study on the effects of soil-structure interaction on the damage response of masonry buildings founded on shallow foundations for the example of tunnelling induced ground movements. The interpretation of the numerical calculations and the comparison of the damage results with the modified LTSM is presented.

Chapter 8 addresses the translation of the settlement predictions in the design stage into monitoring criteria of buildings, used for the risk control during the construction stage.

Chapter 9 presents the analyses of the monitoring data of a full scale test, showing the response of a masonry building founded on a shallow foundation due to TBM-tunnelling. The monitored results are compared with the different prediction methods for the building damage.

Chapter 10 summarizes the previous chapters and gives the main conclusions.

Chapter 11 gives recommendations for future research.

2 PREDICTION OF GREENFIELD GROUND MOVEMENTS DUE TO EXCAVATION WORKS

2.1 General

The first step in risk analyses of building projects regarding possible damage on the surroundings is the prediction of so called "greenfield" ground movements in the nearby surrounding of the construction work. The influence of the presence of the surrounding buildings with their loads and stiffness is neglected in the calculation of greenfield ground movements. It presents purely the effects in the ground. "Greenfield" describes the absence of any surrounding structures. This consideration would also be used for a project on the country side (greenfield area) without any surrounding structures. It should be noted that these greenfield ground movements can be modified significantly due to the interaction with the surrounding structures. This aspect is excluded in this section, but considered in section 4 to 7.

Sections 2.2, 2.3 and 2.4 describe empirical analytical prediction methods for three important sources of ground movements due to construction works in urban surrounding:

- TBM (Tunnel Boring Machine)-tunnelling in soft soil
- Excavation of building pits
- Groundwater lowering

It should be emphasized, that the presented calculation methods can be used in the preliminary design stage to determine expected ground movements within empirical bandwidths. Advanced numerical prediction methods are considered to be necessary for the detailed design stage to take into account the specific conditions for each project including soil properties, details of the construction sequences etc..

Section 2.5 reflects some important aspects of the development of ground movements in time. The influence of long term and short term settlements on the prediction of possible settlement damage on adjacent buildings are discussed.

2.2 Ground movements due to TBM-tunnelling in soft soils

2.2.1 General

The empirical analytical methods for the prediction of greenfield ground movements due to TBM-tunnelling derived by different authors from monitoring data of international tunnelling projects are described in Section 2.2.2. Section 2.2.3 presents design charts which can be used to determine characteristic values like the settlement influence area, the maximum settlement and the maximum slope for a given situation. Section 2.2.4 extends and validates the empirical analytical methods for Dutch conditions.

Several recently completed Dutch TBM tunnelling projects have been assigned to be part of a national research program managed by the Netherlands Centre for Underground Construction (COB). One of the objectives of this research program is to improve the settlement control of a TBM-boring process in Dutch soft soil with high groundwater level. The settlement field data of three COB-projects (two TBM-tunnels built with a slurry shield and one built with an EPB shield) is analysed in section 2.2.4 and compared with the international experience. Recommendations for the use of the methods for Dutch conditions are given.

The magnitude and the distribution of ground movements due to TBM-tunnelling is influenced by boring process parameters like the tail void injection volumes and the tail void pressures, the face pressure and by the conical shape of the TBM, the layering of the soil and the variation of soil

properties. Advanced numerical calculations are currently developed for the settlement prediction and control in the final design and construction stage. These models are often 3D or even 4D, indicating that the time factor is included by modelling the construction sequences of the TBM process.

It should be emphasized that these complex models involve a lot of input parameters and the results are shown to be very sensitive to the variation of certain TBM process parameters and the modelling of the sequential excavation process see Visschedijk et al. (2005), Maidl et al. (2005) and Vermeer et al. (2002). Besides the important qualitative insight in the sensitivity of different parameters, the quantitative use of these models for the prediction of absolute values of ground movements requires highly qualified engineering judgement of the numerical results. One should be always aware that in reality there are still a lot of variations on site which cannot be easily implemented in the numerical models. The reliability of these models for the realistic prediction of ground movements has therefore first to be further proved by validation with real monitoring data of the TBM-processes and corresponding ground movements, before they can be used as a powerful design tool.

The use of the empirical analytical methods described in the following sections in combination with advanced numerical approaches for the determination of bandwidths of TBM–tunnelling induced ground movements and their distributions is strongly recommended.

2.2.2   Empirical analytical prediction of tunnelling induced ground movements

2.2.2.1   *General*

TBM-tunnelling in soft soil causes a 3D ground deformation field, developing in longitudinal direction, parallel to the axis of the tunnel and transverse direction, perpendicular to the axis of the tunnel. Empirical analytical based methods are used for the prediction of the distribution of ground movements in both directions. In the following section a distinction is made between vertical ground movements (settlements) and horizontal ground movements.
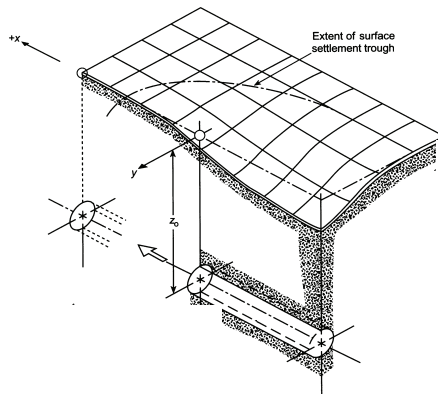
(a) 3D visualisation surface settlement trough due to tunnelling, Burland et al. (2001)

Iso settlement lines 3D-trough in map view

Symmetric half of the transverse trough (B-B):

$W_{transverse(y)}$

$W_{max, transverse}$

y

Axis bored tunnel

A

B

B

y

Longitudinal trough (A-A):

$W_{max, transverse}$
$= W_{max, longitudinal}$

x

$W_{y=0, longitudinal}(x)$

x

A
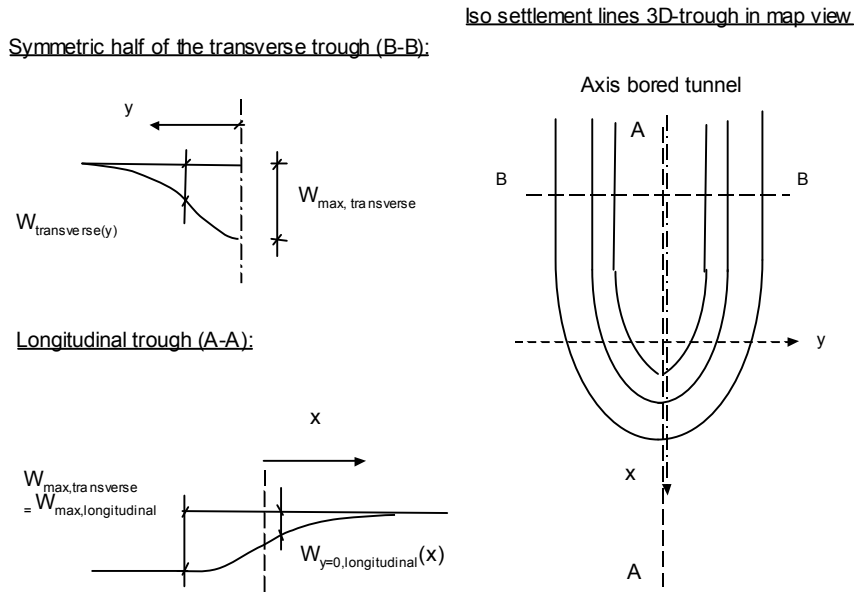
(b) Settlement trough in transverse and longitudinal direction

Figure 2.1: 3D settlements due to tunnelling

It is emphasized, that the longitudinal trough is a temporary phenomenon, which occurs during the passage of the tunnel. The transverse settlement trough is the permanent trough perpendicular to the tunnel axis, remaining after the TBM passage. It should be mentioned that due to varying ground conditions, varying tunnel depth and workmanship a certain permanent longitudinal trough can also occur. This longitudinal trough cannot be predicted with the approaches given in the following sections and is neglected in the present study.

2.2.2.2 *Vertical settlements in transverse direction*

Peck (1969) suggested to use a Gaussian normal distribution curve to describe the form of the transverse settlement trough. Two parameters are determining the shape and magnitude of the trough: The point of inflection i and the volume loss V. These parameters depend on the tunnel depth, the tunnel diameter and the soil properties. Figure 2.2 shows the transverse settlement troughs on surface level and on subsurface level at depth z.

Volume loss $V = A_{trough} / A_{tunnel}$
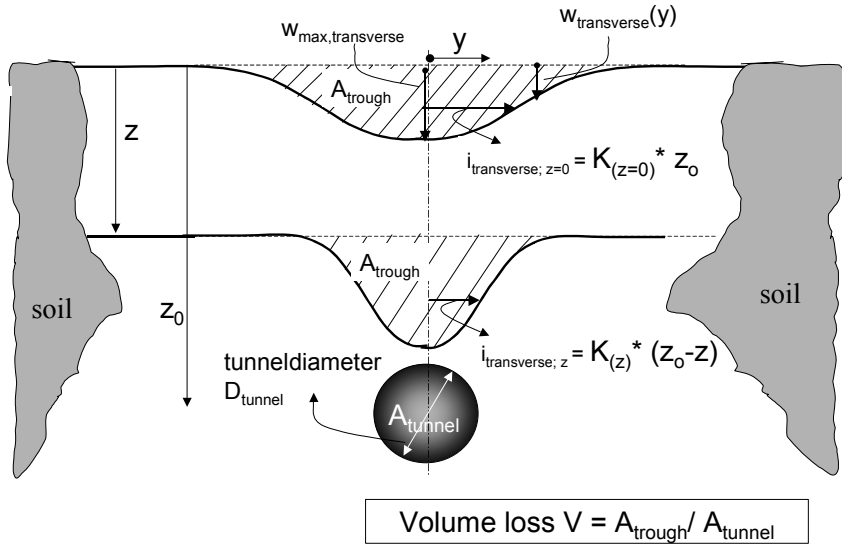
Figure 2.2: Transverse settlement trough

The equations describing the transverse trough are given by Mair et al. (1996):

$$w_{transverse, z}(y) = w_{max, transverse, z} \cdot e^{-\left(\frac{y^2}{2 \cdot \left(i_{transverse, z}\right)^2}\right)} \tag{2.1}$$

with

$w_{max, transverse, z}$	maximum settlement of the transverse trough at the tunnel centre line
$i_{transverse, z}$	horizontal distance between the location of the point of inflection and the vertical tunnel axis
y	horizontal distance from the vertical tunnel axis

The area of the settlement trough A_{trough} in the transverse direction can be derived by integration of equation (2.1) as:

$$A_{trough} = \sqrt{2\pi} \cdot i_{transverse, z} \cdot w_{max, transverse, z} \tag{2.2}$$

The volume loss V (see Figure 2.2) describes the quotient of A_{trough} and the circular tunnel area A_{tunnel} and is expressed as a percentage:

$$V = \frac{A_{trough}}{A_{tunnel}} = \frac{\sqrt{2\pi} \cdot i_{transverse, z} \cdot w_{max, transverse, z}}{\left(\frac{\pi \cdot D^2}{4}\right)} \tag{2.3}$$

with
	V	volume loss [%]
	D	diameter of the tunnel

Prediction of Greenfield Ground Movements

The point of inflection $i_{transverse,z}$ can be described by:

$$i_{transverse,\,z} = K_z \cdot (z_0 - z) \qquad (2.4)$$

K_z dimensionless factor varying with depth z
z_0 tunnel depth (see Figure 2.2)
z   considered depth of the settlement trough (orientation of z see Figure 2.2)

Combining equations (2.2) to (2.4) and substitution in equation (2.1) gives the settlement by:

$$w_{transverse,\,z}\,(y) = 0.313 \cdot \frac{V \cdot D^2}{K_z \cdot (z_0 - z)} \cdot e^{-\left(\frac{y^2}{2 \cdot (K_z \cdot (z_0 - z))^2}\right)} \qquad (2.5)$$

The **volume loss V** develops due to different processes during tunnelling, e.g. the unbalance of the applied front and tail void pressures in the TBM with the initial soil pressures, due to overcutting and due to the conicity of the TBM. The **point of inflection $i_{transverse,z}$** determines the distribution of differential settlements and thus the steepness of the settlement trough and has therefore an important influence on the prediction of damage risks for adjacent buildings. The K_z**-value** presents a dimensionless, empirical factor for determining $i_{transverse,z}$ and is different for surface and subsurface levels.

Point of inflection i

The value $i_{transverse,z}$ represents statistically the standard deviation of the Gaussian normal distribution and describes the location of the point of inflection of the settlement curve. The value $i_{transverse,z}$ determines the form and steepness of the trough and is therefore of particular interest for the prediction of building damage. $I_{transverse,z}$ gets smaller with increasing depth z, see Figure 2.2. The value K_z and (z_0-z) determine the magnitude of $i_{transverse,z}$ according to equation 2.5. Empirical bandwidths for the value K_z depending on (z_0-z) are derived from different field data all over the world throughout the last years (Mair et al. (1993),(1996), O'Reilly et al. (1982), Clough et al. (1977), Moh et al. (1996), Peck (1969) and Leach). K_z is dependant on the ground conditions, the tunnel diameter, the tunnel depth and the depth z. The approaches of several authors for the determination of the depth-dependant K_z-value are summarized in Figure 2.3 for the example of a TBM-diameter of 9m and a tunnel depth of z_0=20m. The dimensionless factor K_z increases with depth as shown in Figure 2.3. Differences between clay and sand are noted.

Prediction of Greenfield Ground Movements

K_z - values of international field observations
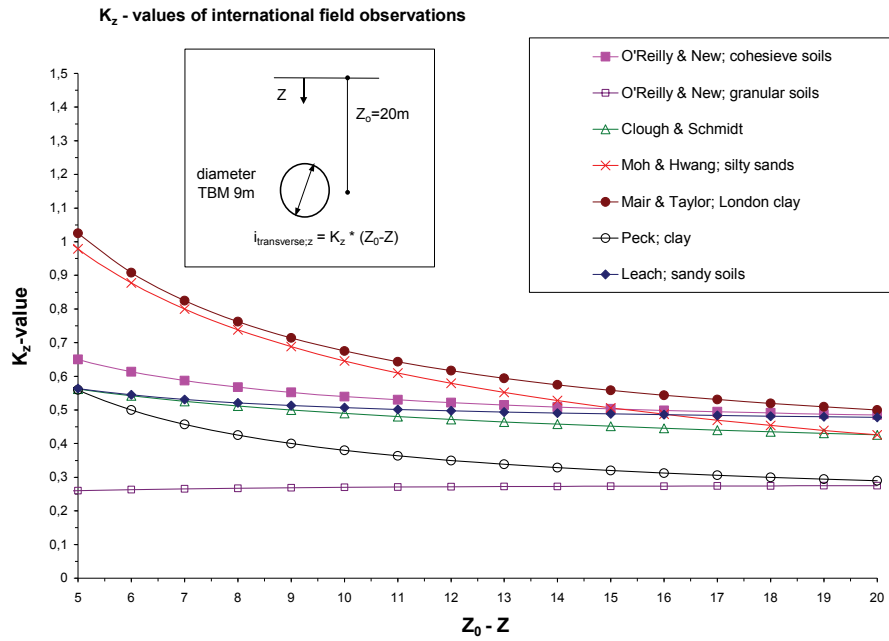
Figure 2.3: Empirical K_z-values for different projects

These empirical approaches do not explicitly derive a relation between $i_{transverse,z}$ and the TBM-process parameters (front pressure, tail void pressures and injection volumes) due to the lack of complete datasets of tunnelling operation and monitoring of ground movements. Rather the combination of all relevant process parameters is accounted for implicitly via empirics.

Volume loss V

The volume loss V is a measure for the quality of the boring process with regard to the ground movements in the surrounding. The volume loss is a simplified approach of the three-dimensional boring process and is defined as the relation between the area of the settlement trough versus the area of the tunnel in a two dimensional section, see Figure 2.2 and equation (2.4). The volume loss is used as input parameter for the settlement prediction in the preliminary design stage and it generally varies between practical bandwidths of 0.5% to 2%.

In general the volume loss is taken constant over the depth, which means that the volume loss on surface level is equal to the volume loss on subsurface levels. From field data of subsurface settlements compared to surface settlements it has been deduced, that the volume loss can vary with increasing depth due to for example dilatation and arching action in the soil on different levels, Cording et al. (1975). This variation depends on the soil properties and soil layering and on the depth of the tunnel and can be analysed only with advanced computational methods.

It should be noted that the volume loss is an important input parameter in the empirical analytical prediction method. It is in fact a rude simplification for all the different processes within TBM-tunnelling contributing to the overall settlement performance. It should be realized that no "volume loss" button is available in the TBM. To specify the volume loss in more detail a future challenge is to collect and evaluate more TBM-data and corresponding settlement monitoring data in order to be able to develop relations between TBM process parameters and their contributions to the volume loss.

2.2.2.3   *Vertical ground movements in longitudinal direction*

The longitudinal trough and the transverse trough together form the 3D deformation field, see Figure 2.1. Generally the method suggested by Attewell et al. (1986) is applied to determine the temporary

settlement profile in longitudinal direction at surface level, the "settlement wave". This method adopts the shape of a cumulative probability curve based on the statistical mean value corresponding with $w_{transverse}(y)$ and the standard deviation corresponding with $i_{transverse}$ as previously used to define the transverse Gaussian shaped trough. Equation (2.6) describes the longitudinal wave on a transverse distance y from the tunnel axis:

$$w_{y,longitudinal}(x) = w_{transverse}(y) \cdot \left\{ G\left(\frac{(x-x_i)}{i_{transverse}} \right) - G\left(\frac{(x-x_f)}{i_{transverse}} \right) \right\} \tag{2.6}$$

The terms for $G(x-x_i)$ and $G(x-x_f)$ for the cumulative probability curve may be determined from tabulated statistical texts, also given by Attewell et al. (1986). The longitudinal settlement curve described by equation (2.6) is shown in normalized form in Figure 2.4. The distance on the horizontal axis of Figure 2.4 is expressed in terms of $i_{transverse}$ and the settlement on the vertical axis is expressed in percentages of the maximum settlement. This maximum settlement is corresponding with the maximum transverse settlement $w_{transverse}(y)$. This curve is used for the prediction of longitudinal TBM-settlements on a distance y parallel to the tunnel axis with x being the coordinate in longitudinal direction starting at 50% of the maximum settlement of the longitudinal trough (see sketch in Figure 2.4). This assumption for the origin coordinate system is derived by Attewell due to validation with field data. Attewell remarks that compared with field data the use of equation (2.6) can lead to a slightly steeper trough as compared to field data especially for clay soil. Therefore it is assumed to be conservative for the damage assessment of adjacent buildings. It should be noted, that this statement has to be seen in relation with the length of the building undergoing the longitudinal settlement trough.

Longitudinal trough
(cumulative probability curve)
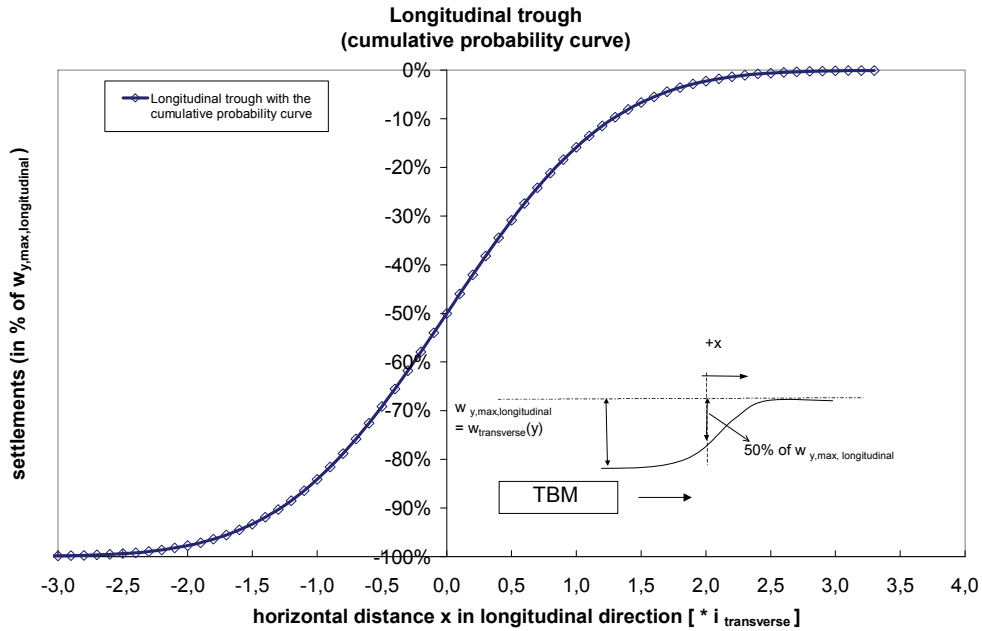
Figure 2.4: Longitudinal settlement trough according to Attewell et al. (1986)

2.2.2.4   *Horizontal ground movements in transverse direction*

The horizontal movements in transverse direction can be determined based on the approach of O'Reilly et al. (1982) stating that the resultant vectors of ground movement are directed towards the tunnel axis

Prediction of Greenfield Ground Movements

(see Figure 2.5). This approach is derived from validation with field data and is considered generally conservative with respect to the magnitude of horizontal ground movements, but reasonable.

$$h = \frac{w}{(z_0 - z)} \cdot y$$
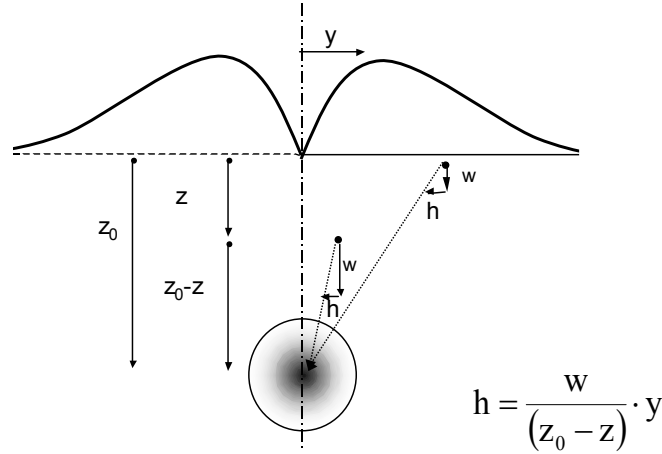
Figure 2.5: Distribution of horizontal ground movements in transverse direction

Assuming this tunnel-centric directed ground movement, the horizontal ground movement $h_{transverse}(y)$ can be related to the vertical settlement $w_{transverse}(y)$ by the expression:

$$h_{transverse}(y) = \frac{w_{transverse}(y)}{z_0 - z} \cdot y \tag{2.7}$$

Replacing $w_{transverse}(y)$ from equation (2.1) it can be shown that the maximum horizontal displacement occurs at the horizontal distance $y = i_{transverse}$ as derived by Attewell et al. (1986). The maximum horizontal movement is:

$$h_{max,transverse} = \frac{0.606 \cdot i_{transverse} \cdot w_{max,transverse}}{z_0 - z} \tag{2.8}$$

The distribution of the (differential) horizontal ground movements (see Figure 2.5) causes horizontal strains in the soil. The maximum horizontal tensile strain occurs at $y = 1.73 * i_{transverse}$ and is derived by Attewell et al. (1986) with:

$$\varepsilon_{max,transverse,tensile} = 0.446 \cdot \frac{w_{max,transverse}}{z_0 - z} \tag{2.9}$$

The maximum horizontal compressive strain occurs at the tunnel centre line and is given by Attewell et al. (1986) with:

$$\varepsilon_{max,transverse,compressive} = \frac{w_{max,transverse}}{z_0 - z} \tag{2.10}$$

2.2.2.5   Horizontal ground movements in longitudinal direction

Horizontal movements of the longitudinal trough are derived by Attewell et al. (1986) with the expression:

$$h_{y,longitudinal}(x) = \frac{V}{2 \cdot \pi \cdot (z_0 - z)} \cdot e^{\left(\frac{-y^2}{2 \cdot i_{transverse}^2}\right)} \cdot \left(e^{\left(\frac{-(x-x_i)^2}{2 \cdot i_{transverse}^2}\right)} - e^{\left(\frac{-(x-x_f)^2}{2 \cdot i_{transverse}^2}\right)} \right) \quad (2.11)$$

The terms *(x-x_i)* and *(x-x_f)* can be determined from tabulated statistical texts, given by Attewell et al. (1986). The normalized relation between the horizontal movement in longitudinal direction $h_{y,longitudinal}(x)$ and the maximum settlement of the transverse trough $w_{y,max,\,longitudinal}$ at the transverse distance y is shown in Figure 2.6.
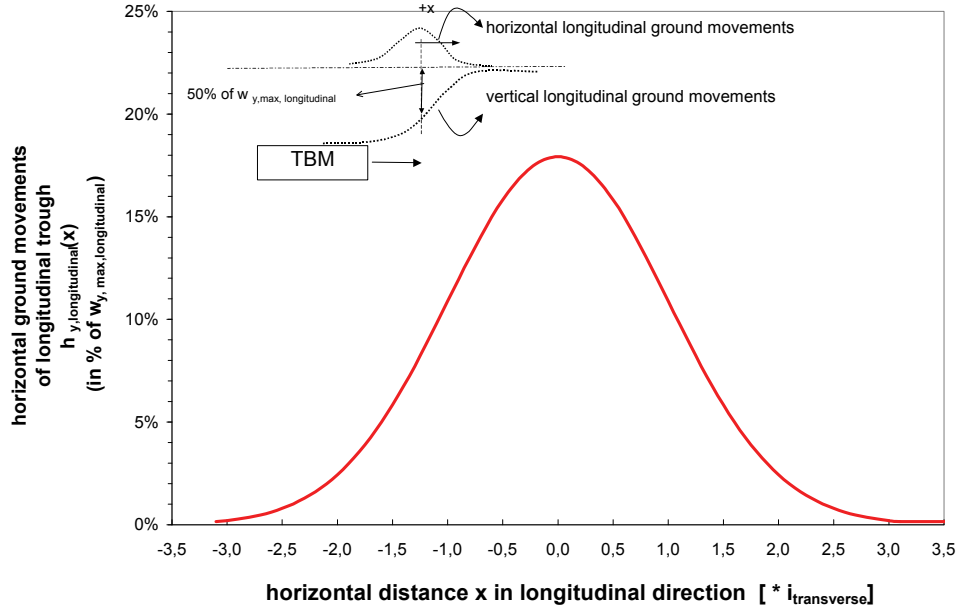
Figure 2.6: Horizontal movements longitudinal trough

Finally the maximum horizontal ground movement of the longitudinal trough on a transverse distance *y* has been derived by Attewell et al. (1986):

$$h_{y,max,longitudinal} = 0.399 \cdot \frac{w_{y;max,longitudinal}}{z_0 - z} \cdot i_{transverse} \quad (2.12)$$

2.2.3   Design charts

2.2.3.1   General

The equations for the Gaussian transverse settlement trough presented in 2.2.2.2 have been analysed by the author and translated into design charts. The charts can be used to get a first magnitude of

characteristic TBM-tunnelling influences in terms of the maximum settlement, the influence area (width of the transverse settlement trough) and the maximum slope of the transverse settlement trough.

2.2.3.2   Dimensionless input parameter

It appears to be convenient to use the dimensionless parameter $V*D^2/i_{transverse}^2$ as input for the design charts. It is emphasized that this parameter has no physical meaning, but is purely a fictitious parameter which incorporates the three dominant input parameters. The units of the tunnel diameter D and the point of inflection $i_{transverse}$ are mm and the volume loss is taken as a decimal value (as example 0.01 for V=1%). Figure 2.7 shows the parameter $V*D^2/i_{transverse}^2$ for practical ranges of the tunnel diameter (between 7m and 14m), the volume loss (between 0.5% en 2%) and the point of inflection (between 4m en 16m).
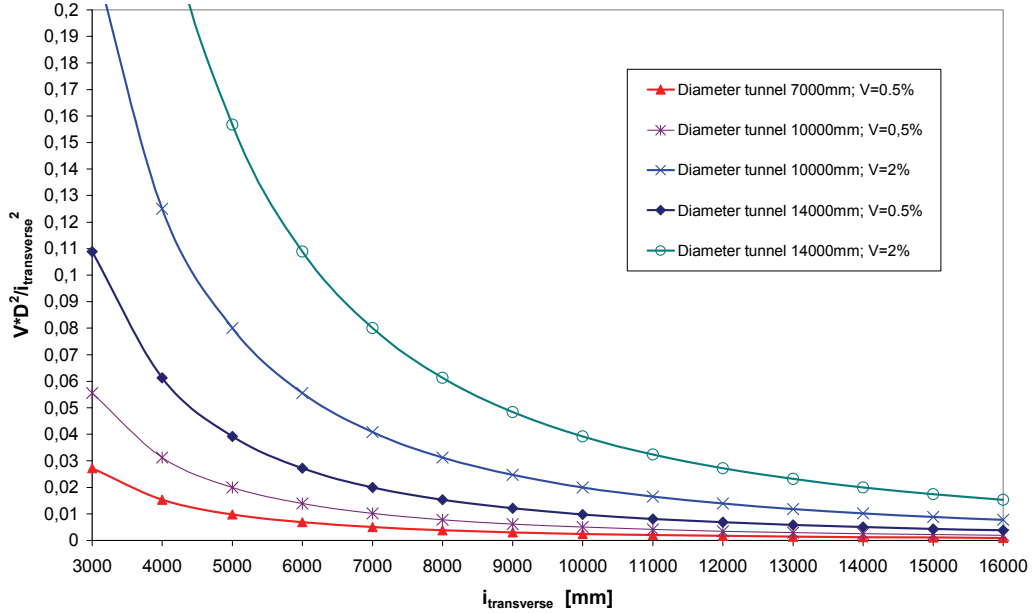
Figure 2.7: Practical range of dimensionless parameter $V*D^2/i_{transverse}^2$

2.2.3.3   Determination of the influence area in transverse direction

Strictly speaking the Gauss settlement distribution extends infinitely. However at distances far from the tunnel axis the settlements will be very small. The 1mm settlement line is generally adapted to determine the boundary of the influence area of the transverse settlement trough. The equations to calculate the symmetrical half width of the settlement trough ($b_{half\ trough,\ 1mmm}$) up to the 1mm for each arbitrary combination of volume loss (V), tunnel diameter (D) and point of inflection ($i_{transverse}$) are derived from the equations given in 2.2.2 and are as follows:

$$b_{half\ trough,1mm} = i_{transverse} \cdot \sqrt{2} \cdot \sqrt{\ln\left(0.313 \cdot \frac{V \cdot D^2}{i_{transverse}}\right)}$$

$$= i_{transverse} \cdot \sqrt{2} \cdot \sqrt{\ln(w_{max,transverse})} \qquad (2.13)$$

Figure 2.8 visualizes this equation for a wide practical range of the input parameters. The diagram shows that the range for the symmetrical half width of the settlement trough varies between:
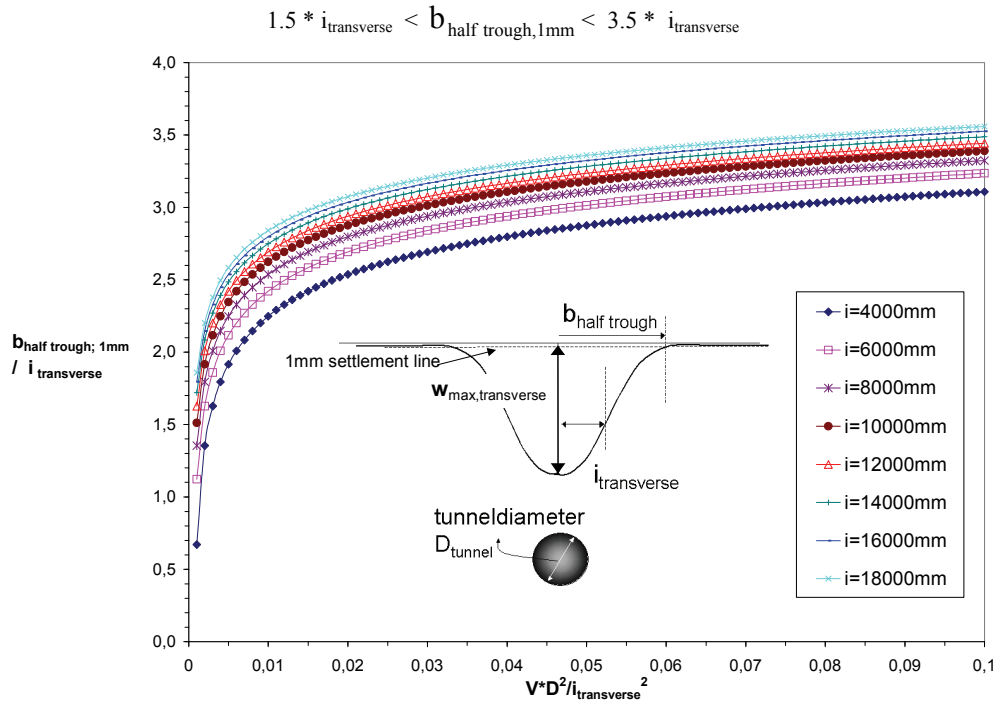
Figure 2.8: Settlement influence area

2.2.3.4 Maximum settlement

The maximum settlement of the transverse trough gives a first indication of the magnitude of the settlement trough and is often used as a performance criterion for tunnelling works regarding the contractual design limits of surrounding influences (see section 8.3).

The maximum settlement $w_{max,transverse,z}$ at the depth z occurs at the tunnel axis and can be derived with equation (2.5) by using $y=0$:

$$w_{max,transverse,z} = 0.313 \cdot \frac{V \cdot D^2}{i_{transverse,z}} \qquad (2.14)$$
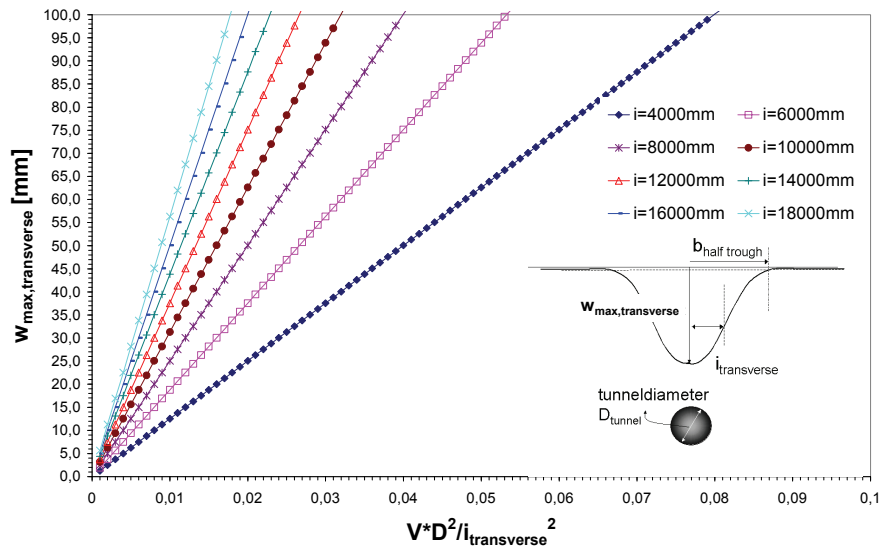
Figure 2.9: Maximum settlement of the transverse trough

2.2.3.5   *Maximum slope in transverse direction*

The maximum slope of the settlement trough gives an important indication of the steepness of the trough. The maximum slope in the Gaussian settlement trough occurs at the point of inflection (see sketch in Figure 2.10) and can be determined by derivation of equation 2.5 for the settlement $w_{transverse,z}(y)$:

$$\rho_{transverse,max,z} = \frac{d'' \, w_{transverse,z}(y)}{dy} = 0$$

$$\rho_{transverse,max,z} = 0.606 \cdot \frac{w_{max,transverse,z}}{i_{transverse,z}} \tag{2.15}$$
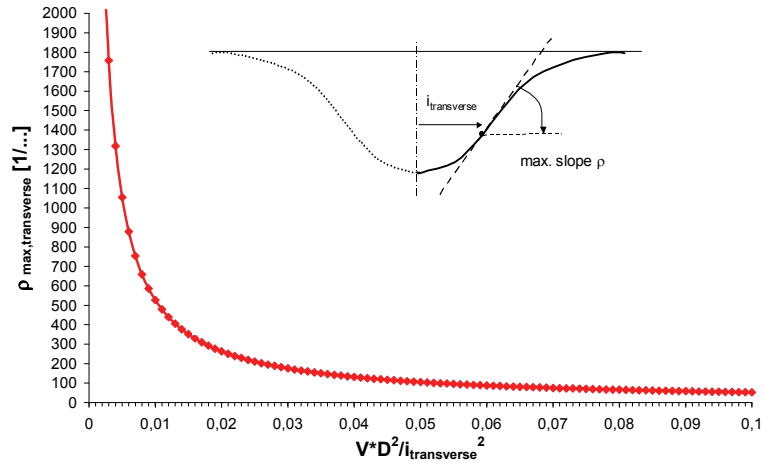
Figure 2.10: Maximum slope of the transverse trough

It is remarkable, that the maximum slope from Figure 2.10 results in one curve for different combinations of i, D en V. This has no physical meaning but is purely a fictitious relation with the chosen input parameter $V*D^2/i_{transverse}^2$ and the maximum slope of a Gaussian settlement curve.

2.2.4 Analyses of Dutch field data

2.2.4.1 General

To fit the measured settlement data of Dutch tunnelling projects with the empirical analytical methods the following procedure has been used. The volume loss of the monitored transverse settlement trough is calculated and used as input for the empirical analytical approach described in 2.2.2. Subsequently two *K*-values are derived from a fit of the maximum settlement monitored and the maximum slope monitored for the transverse trough according to the equations presented in the previous sections. Finally the measured longitudinal troughs are fit with the empirical analytical approach described in section 2.2.2.3 using the input parameters derived of the fit for the corresponding transverse trough.

In the following sections an example for the fit of the field data for each of the three Dutch TBM-tunnelling projects is presented. The fit of the transverse trough is made for a monitoring section of the Second Heinenoord tunnel and the Sophia Railway tunnel and the fit of the longitudinal trough is shown for the Botlek Railway tunnel. In section 2.2.4.5 the fitted *K*-values for all considered monitoring sections of the three projects are summarized and compared to the approaches suggested by the authors specified in Figure 2.3, also the monitored volume losses are summarized.

2.2.4.2 Second Heinenoord Tunnel

The characteristic soil profile and the variation of the tunnel depth in the monitoring cross sections of the tunnel track are shown in Figure 2.11. The twin tunnels of the Second Heinenoord Tunnel are built close to Rotterdam in the Netherlands. The soil in the monitored cross sections consists mainly of Holocene and Pleistocene sand layers. The groundwater level is about 3m below surface level. The TBM-diameter is 8.3m. The twin tunnels have been bored with a slurry shield.
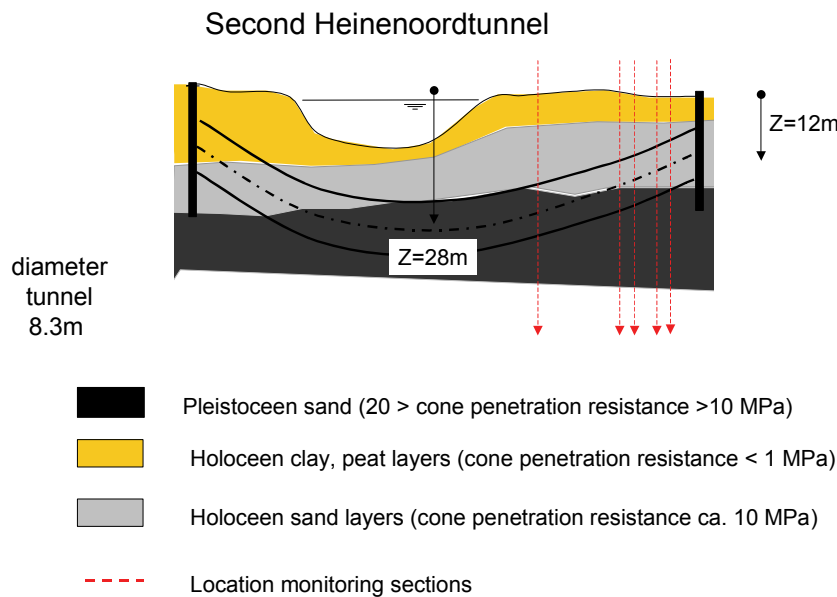
Figure 2.11: Second Heinenoord Tunnel

Prediction of Greenfield Ground Movements

Figure 2.12 provides the fit of the monitoring data with the empirical analytical approaches for the symmetric transverse trough on surface level. The tunnel depth of the considered monitoring section is 20m. The settlement distribution appears to match well with the Gaussian form for the bandwidth of *K* between 0.39 en 0.42.
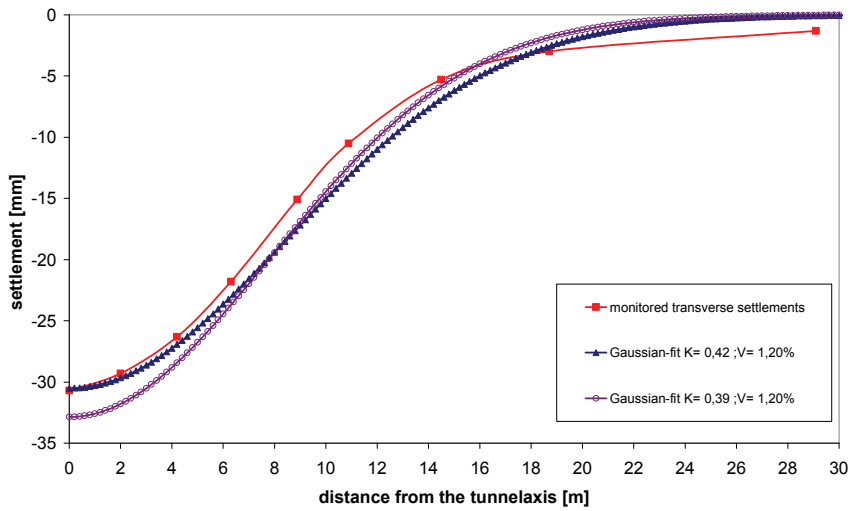
Figure 2.12: Fit of the symmetric transverse settlement trough for the Second Heinennoord tunnel

The *K*-value of 0.42 provides the best match with the maximum settlement, see Figure 2.12 and the *K*-value of 0.39 provides the best match with the maximum slope, see Figure 2.13.
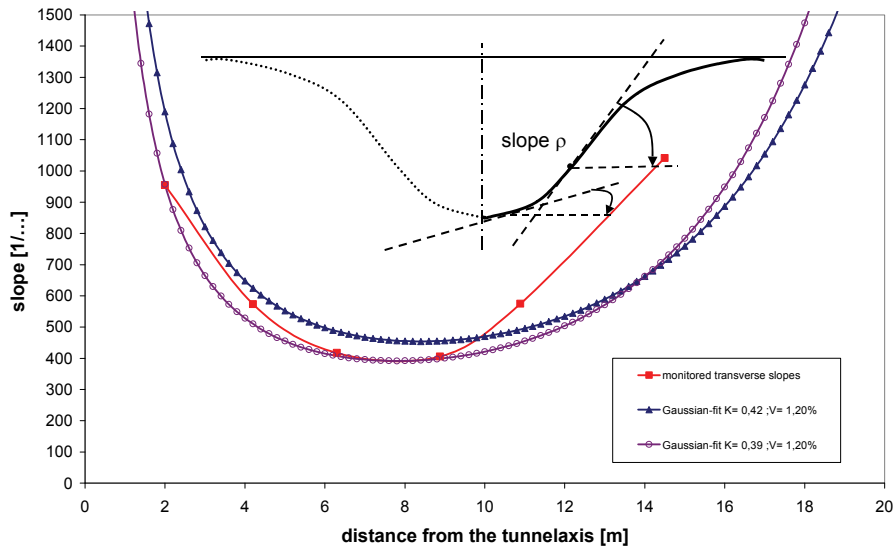
Figure 2.13: Fit of the slopes of the symmetric transverse tough

The differences of the match of the slopes according to Figure 2.13 between the horizontal distances of 11m to 14m can be explained by the greater distance of the monitoring points in this part compared to the theoretical continuous Gaussian line. As the monitored slopes are derived geometrically from the

monitored settlements, a greater distance between the monitored settlements influences the calculated slopes. It can be concluded that the monitored transverse trough (V=1.2%) shows a good match with the empirical analytical Gaussian approach for a bandwidth of the K-value between 0.39 en 0.42.

2.2.4.3   Botlek Railway Tunnel

The characteristic soil profile and the variation of the tunnel depth in the monitored cross sections of the tunnel track are shown in Figure 2.14. The twin tunnels have been built close to Rotterdam and are part of the Betuwe cargo line.

Botlek Railway Tunnel
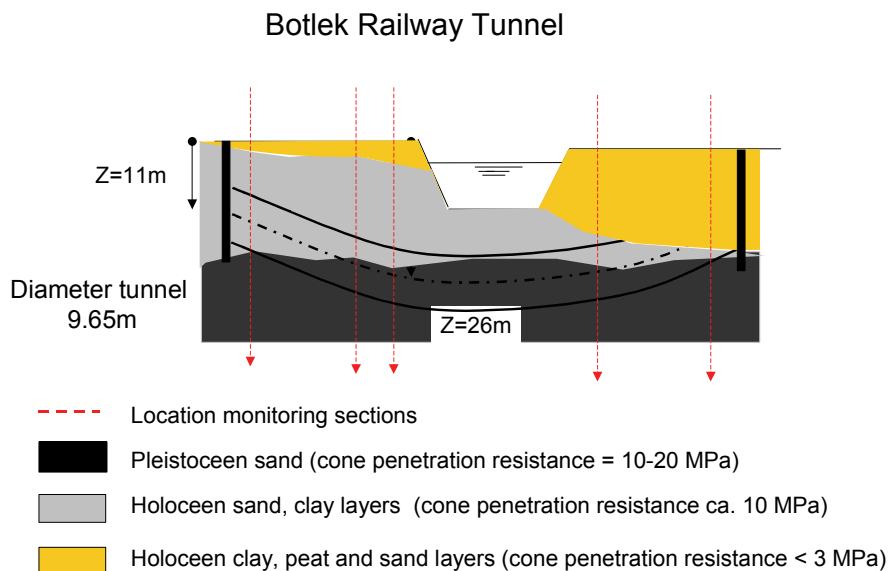
Figure 2.14: Botlek RailwayTunnel

The soil in the monitoring sections consists mainly of soft Holocene sand/clay layers and Pleistocene sand layers. The groundwater level is ca. 3m below surface level. The TBM-diameter is 9.65m. The twin tunnels are bored in the EPB (Earth Pressure Balance)-mode. **Fout! Verwijzingsbron niet gevonden.** and Figure 2.16 show examples of the fit of the monitoring data with the analytical, empirical approaches for the longitudinal trough along the tunnel axis on surface level. The corresponding transverse trough on this location (V=1.3%) shows a good fit for a bandwidth of the K-value between 0.39 and 0.4.
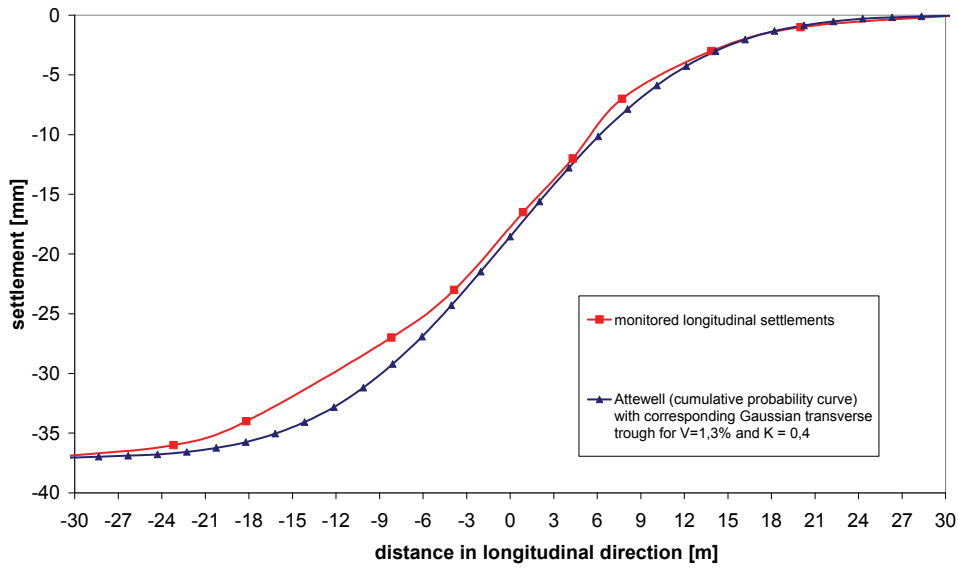
Figure 2.15: Fit of the longitudinal settlement trough
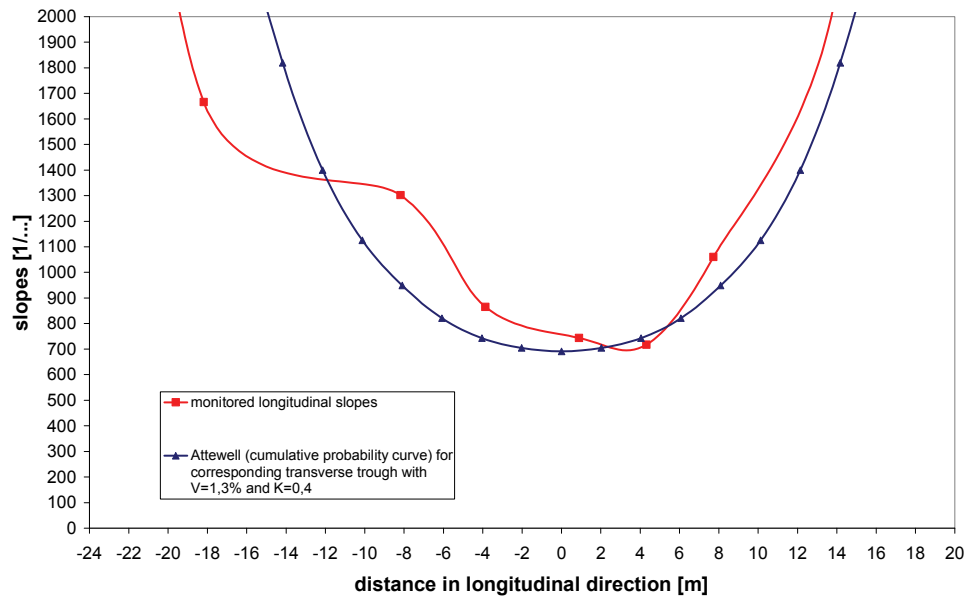
Figure 2.16: Fit slopes longitudinal trough

The Attewell approach gives a good fit for the longitudinal trough. The differences in slopes between the horizontal distances of -8m to -18m can be explained by the greater distance of the monitoring points in this part compared to the theoretical continuous fit line.

2.2.4.4 *Sophia Railway Tunnel*

The characteristic soil profile and the variation of the tunnel depth in the monitoring cross sections of the tunnel track are shown in Figure 2.17. The twin tunnels of the Sophia Railway Tunnel are built close to Rotterdam and are part of the Betuwe cargo line. The soil in the monitoring cross sections consists mainly of soft Holocene sand/clay layers and Pleistocene sand layers. The groundwater level is ca. 3m below surface level. The TBM-diameter is 9.65m. The twin tunnels have been bored in the slurry-mode.

Sophia Railway Tunnel

Z=11m

Z=19.5m

Diameter tunnel 9.5m

Clay layer of Kedichem (cone penetration resistance ca. 5 MPa)

Pleistoceen sand (cone penetration resistance > 10 MPa)

Holoceen clay, peat layers (cone penetration resistance < 1 MPa)

Sandy toplayer (cone penetration resistance ca. 2-3 MPa)

Location monitoring sections
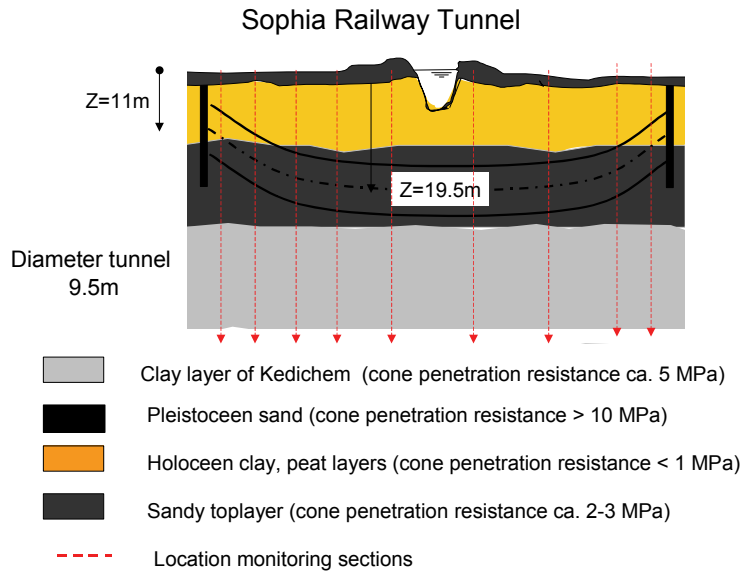
Figure 2.17: Sophia Railway tunnel

Figure 2.18 and Figure 2.19 show examples of the fit of monitoring data with the analytical, empirical approaches. It should be noted, that the field data in this specific example represents heave of the ground surface instead of a trough, as shown in the previous examples. However the empirical methods given in previous sections are also applied for fitting the heave monitoring results by using a negative "volume loss", which for this case was 0.9%. The distribution of the transverse heave is represented accurately for a bandwidth of the K-value between 0.3 en 0.32.

The heave in this monitoring section occurred due to locally high applied front pressures and tail void pressures in the TBM. Detailed analyses of the relationship between TBM-pressures and surface ground movements are carried out by Visschedijk et al. (2005).
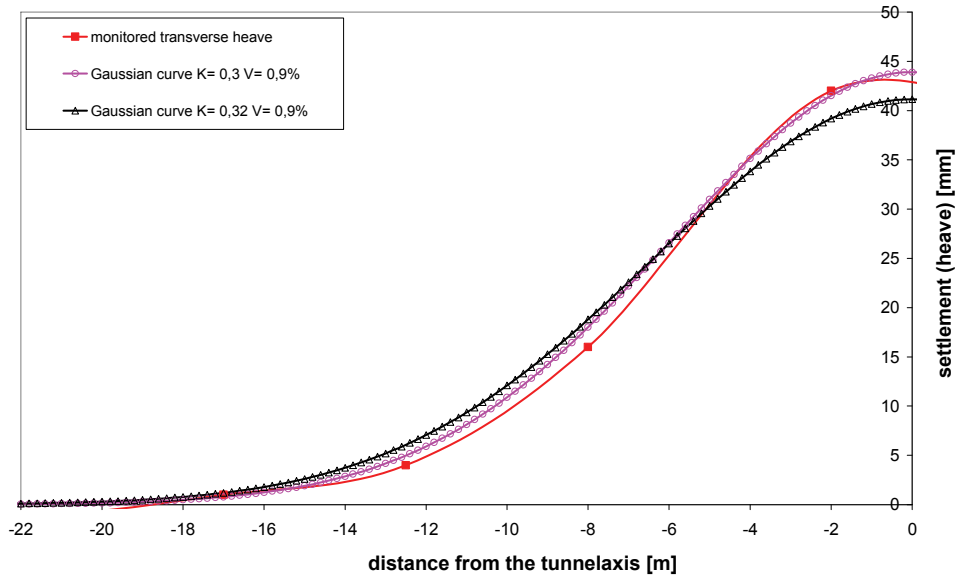
Figure 2.18: Fit of the transverse trough (heave)
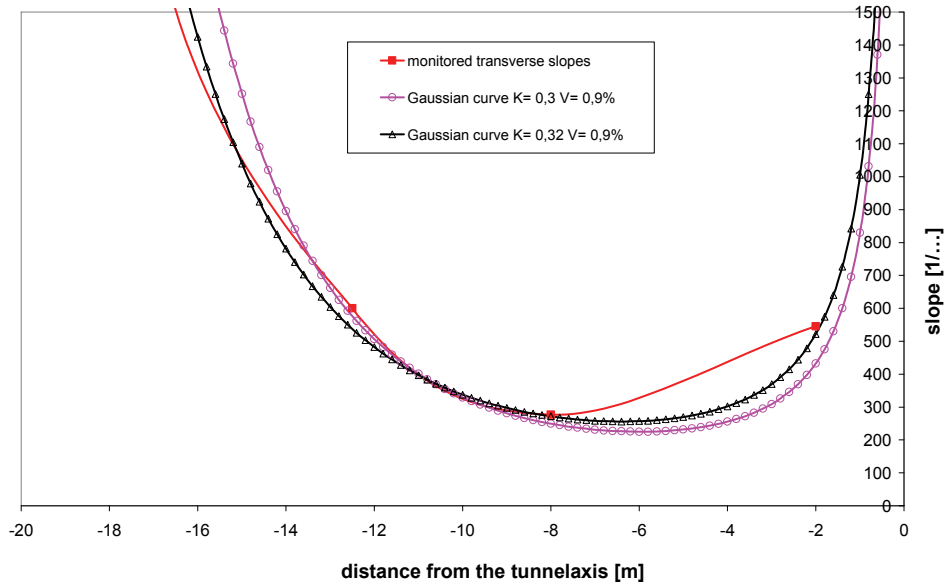
Figure 2.19: Fit slopes transverse heave

2.2.4.5   Comparison Dutch field data with literature

<u>**K-values**</u>

The fitted *K*-values of all considered surface monitoring sections of the three Dutch tunnelling projects are summarized in Figure 2.20 as a function of the depth of the tunnel. Different approaches for *K*-

values for surface settlement troughs obtained by other authors (see Figure 2.3) from international tunnelling projects in sandy soils are also included in the graph.
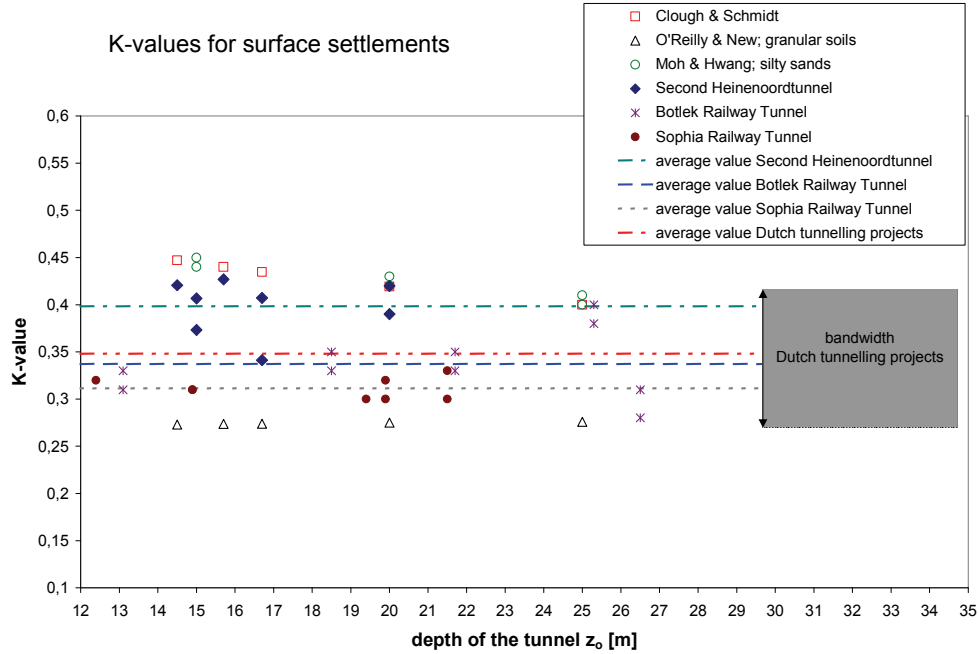
Figure 2.20: *K*-values for surface ground movements due to TBM-tunnelling

For the three Dutch tunnelling projects a bandwidth for the *K*-value of 0.28 to 0.43 covers the entire range of the monitored surface settlements indicated by the shaded area in Figure 2.20. This bandwidth fits well within the approaches suggested by the other authors for sandy soils. The average *K*-value for all Dutch projects is 0.35 with a standard deviation of 0.045.

TBM performance (volume loss cq. heave)
Figure 2.21 shows the monitored TBM-performances at surface level in terms of volume loss or heave. It should be noted that heave effects (as occurring in section 2.2.4.4) are also included in the figure as positive values, because the figure is meant to show the overall performance of TBM-tunnelling compared to the initial undisturbed situation regardless the fact whether the volume change is negative or positive. Both effects can cause damage to the adjacent buildings although the hogging and sagging parts will be opposite for a settlement trough and a heave effect respectively. The heave of 0.9% shown in section 2.2.4.4 was an exception. Small heave values around 0.2% were observed in only a few other monitoring sections. The volume changes vary between 0.15 and 1.5% with an average value of all three projects of 0.6% and a standard deviation of 0.4.

Prediction of Greenfield Ground Movements
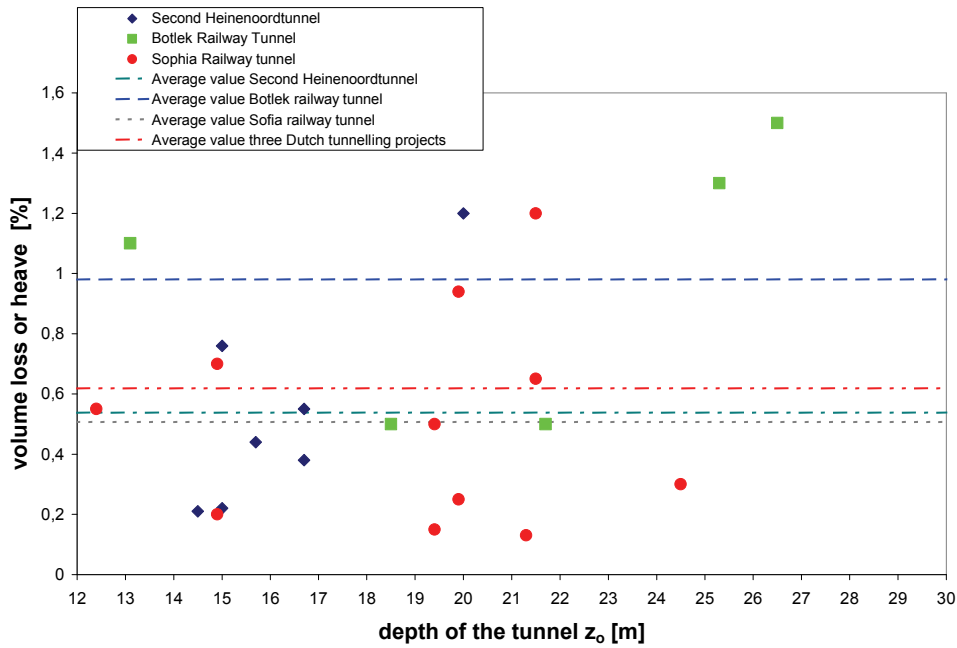
Figure 2.21: Monitored TBM performances at surface level for Dutch tunnelling projects

Conclusions

The settlement field data of three TBM-projects have been be properly fitted with empirical analytical methods. An average K-value of 0.35 with a standard deviation of 0.05 is suggested for the prediction of the surface transverse trough for comparable Dutch soil conditions. The K-value determines the point of inflection and thus the steepness of the trough.

The fit of the longitudinal wave using the cumulative probability curve according to Attewell et al. (1986) showed slight underestimations of the steepness of the longitudinal troughs, but is proven to be a good approach, also for Dutch tunnelling projects. The longitudinal trough is a temporary trough that occurs during the passage of the TBM, whereas the transverse trough is permanent.

The measured volume changes at the surface due to TBM-tunnelling in Dutch soil conditions vary between 0.15 and 1.5% and showed settlements ("volume loss") as well as heave effects.

2.3 Ground movements due to excavation of building pits

2.3.1 General

The construction of building pits in urban surrounding implies several sources of ground movements:

- Installation and removal of retaining walls
- Groundwater lowering due to leakage of a retaining wall or due to construction dewatering
- Excavation and as a consequence the deformation of the retaining wall of the building pit

The present section is focused mainly on the prediction of the latter source, reflecting the ground movements behind the retaining wall due to deformation of the wall during the excavation process. For information on the prediction of ground movements due to the installation and removal of the retaining walls the reader is referred to Clough et al. (1990), Finno et al. (1991a), Wit, de et al. (1999) and Hergarden (2000). Settlements due to dewatering are described in section 2.4.

The presented empirically derived approaches in the following sections can be used in a preliminary design stage to predict ground movements within a broad bandwidth. It is strongly recommended to carry out advanced finite element studies to predict ground movements due to excavations within a smaller and more accurate bandwidth for the detailed design stage. Numerical models take into account the inhomogeneity of the soil, the nonlinear soil properties (stress dependant soil stiffness) and the detailed sequences of the excavation works. These issues play an important role in the prediction of ground movements due to excavation of building pits.

Many authors derived empirical analytical methods to determine the lateral movement of the retaining wall dependant of the excavation depth and the soil conditions. However it is not so much this parameter but rather the distribution of the (differential) ground movements of the soil mass behind the retaining walls that is of particular interest to the damage prediction of surrounding buildings. The selection of the presented approaches in 2.3.2 is made from this point of view.

2.3.2 Literature study

2.3.2.1 Vertical ground settlements behind the retaining wall

Peck

The basis for estimating ground movements adjacent to excavations was presented by Peck (1969). He compiled ground surface settlement data measured adjacent to temporary braced sheet pile walls and soldier pile walls, and summarized the data in a chart, see Figure 2.22a. The chart presents the maximum ground settlement plotted against the distance from the excavation. Both of these input parameters are expressed relative to the final depth of the excavation. Peck (1969) grouped the data on the chart into three categories. The three categories were developed on the basis of the soil conditions and the margin of safety against basal stability (excavation base heave). The relation of maximum ground movement versus excavation depth varies between a maximum of 1% for category I up to >2% for category III.
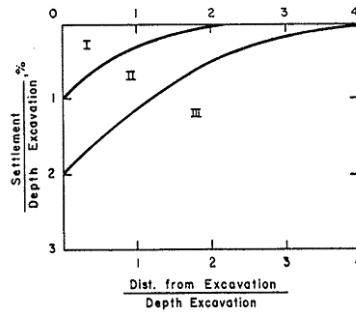
Category I: SAND and SOFT to HARD CLAY
Average workmanship

Category II: VERY SOFT to SOFT CLAY
With either a limited depth of soft clay beneath excavation
or a significant depth of soft clay with a high
margin of safety against base heave

Category III: VERY SOFT to SOFT CLAY
With a low margin of safey against excavation base heave

Figure 2.22: Ground settlement trough according to Peck (1969)

Clough & O'Rourke

The work of Peck (1969) has been comprehensively reviewed and extended with additional empirical field data supported by several nonlinear finite element analyses by Clough et al. (1990).

For sands and stiff to very hard clays (see Figure 2.23 (a) and (b)) the maximum surface ground movement was found to be about 0.3% of the excavation depth H, which is significant lower than suggested by Peck for category I. Clough et al. explained these differences by the improved control of the excavation process covering new methods of construction and strutting processes developed during the years and reflected in the recent field observations.

For soft to medium clays the consideration of the safety factor against base heave and the system stiffness, as defined by Clough et al. (1990), has to be taken into account to determine the maximum lateral wall movement and the maximum ground settlement respectively. The obtained yield values for the maximum lateral wall movement vary between 0.5% H and 2% H depending on the safety factor and the system stiffness see Figure 2.23 (c).

Clough et al. also presented dimensionless settlement profiles as a basis for estimating vertical movement patterns adjacent to excavations, see Figure 2.24. With knowledge of the maximum ground settlement, the dimensionless diagrams in Figure 2.24 can be used to estimate the surface settlement on different distances of the excavations.
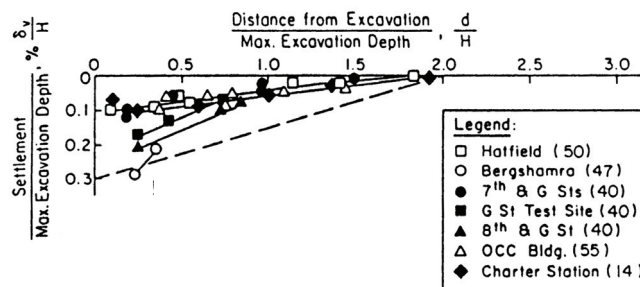
(a) Sand
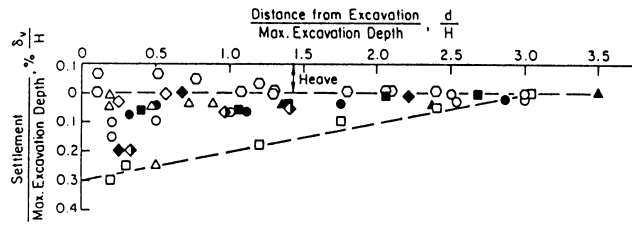
(b) Stiff to very hard clay
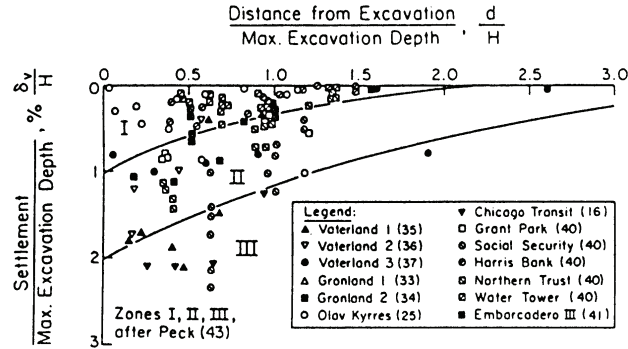
(c) Medium to soft clay

Figure 2.23: Ground settlement trough according to Clough et al. (1990)
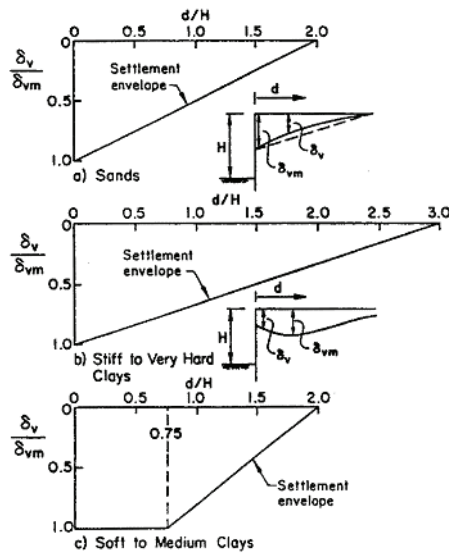
Figure 2.24: Dimensionless settlement profiles suggested by Clough et al. (1990) for three different types of soil

Boone

Boone (1998) presents the approach shown in Figure 2.25 to estimate the surface settlement distribution due to the excavation of a building pit of an excavation depth of 20m in stiff glacial till and highly overconsolidated sand, silt and clay deposits.
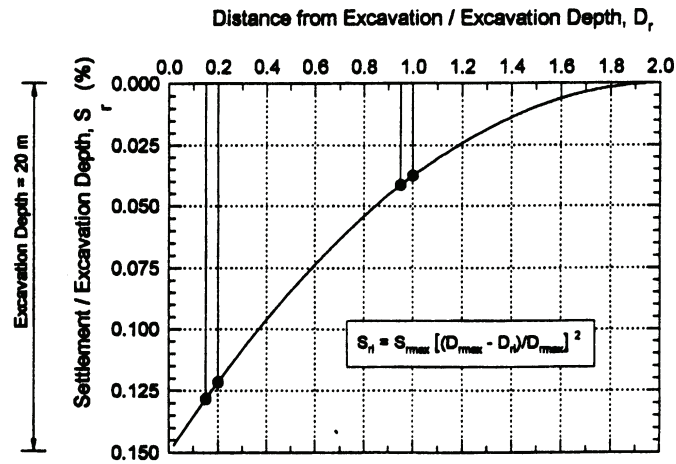
Figure 2.25: Surface settlement distribution according to Boone (1998)

The distribution of the surface settlement S_r on a distance D_r from the retaining wall can be determined with:

$$S_r = S_{max} \cdot \left[(D_{max} - D_r)/D_{max} \right]^2 \tag{2.16}$$

with D_{max} width of the influence area (chosen as 2H for the case presented in Boone (1998))
             S_{max} maximum settlement (chosen as 0.15% H for the case presented in Boone (1998))
             H   excavation depth

Dhanjal, Thurlow and Bailey

The approach used to predict the surface settlements for the design of the deep building pits for the construction of the Copenhagen metro is described by Dhanjal et al. (2001). The ground conditions in Copenhagen consist of made ground and glacial till overlying Copenhagen limestone. The glacial till consists of overconsolidated sandy clay or clayey sand with bands of water bearing meltwater sands and gravels. The authors mention that the shape of the ground surface settlement trough is often assumed as a projection of the shape of the deflected retaining wall. However in practice the ratio of surface settlements to lateral wall deflection tends to be between 0.6 and 0.8 as conformed by case studies. They used the charts (including the approach of Clough et al. (1990) for sands) as shown in Figure 2.26.

Prediction of Greenfield Ground Movements
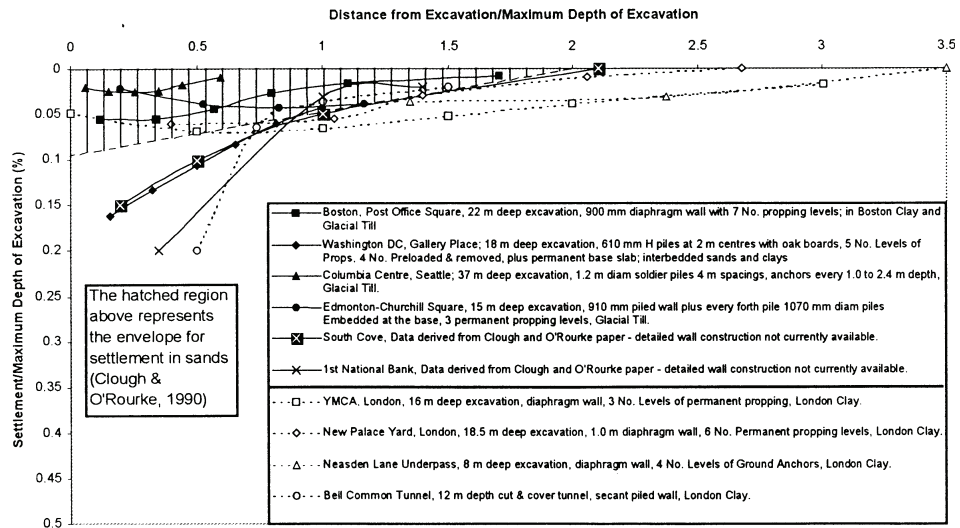
(a) Empirical field data from other international projects summarized by Dhanjal et al. (2001)
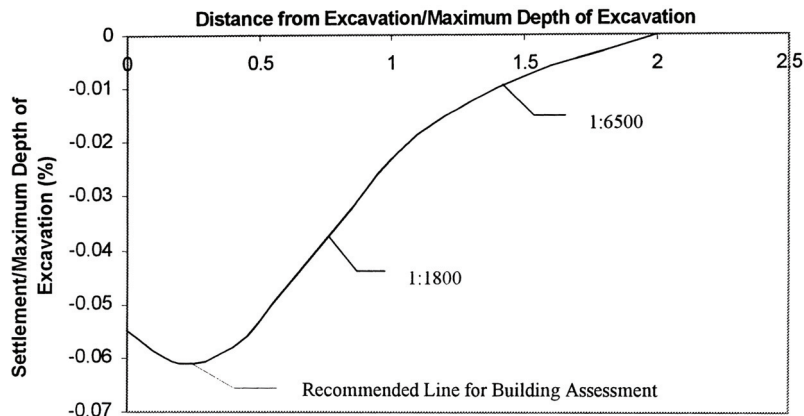
(b) Chosen design curve for the Copenhagen building pits

Figure 2.26: Predicted ground surface movements for the building pits of the Copenhagen metro, Dhanjal et al. (2001)

Hashah, Whittle

Hashah et al. (1996) carried out extensive numerical parametric studies to develop charts for estimating maximum lateral wall movements and maximum ground movements for deep excavations in soft soils as functions of the excavation depth, support conditions, the wall length and the stress history of the soil. They focused on a braced diaphragm wall in a deep soft clay deposit. The results of the study are used for the design of the construction of underground highways in Boston. The authors emphasize the use of advanced nonlinear constitutive soil models including the nonlinear stiffness properties at small shear strains and the anisotropic stress-strength behaviour for reliable settlement predictions. The magnitude and location of the maximum ground movements are in broad agreement with the field data reported for excavations in soft clay by Clough et al. (1990). Figure 2.27 shows the effect of the wall length on the wall deflection and the vertical surface settlements.

Prediction of Greenfield Ground Movements

(a) Surface Settlements

(b) Lateral Wall Deflections

Over consolidation ratio (OCR) =1

h = equal support spacing
h_e = excavation depth below support

H = excavation depth
h_u = unsupported excavation
L = wall length
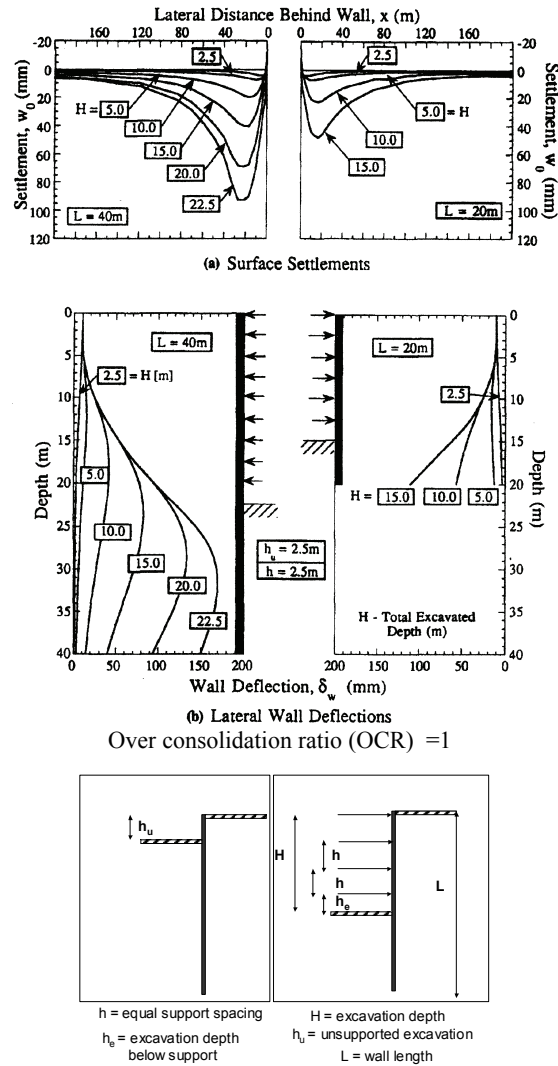
Figure 2.27: Effect of wall length on lateral wall deflection and surface settlements, Hashah et al. (1996)

Whittle et al. (1993) demonstrated the predictive capabilities and limitations of advanced nonlinear numerical analyses through detailed comparisons with extensive field monitoring data like wall deflections, surface settlements and piezometric levels. The considerations were carried out for the case study of a braced excavation in Boston used for the construction of a deep underground garage adjacent to existing buildings. They conclude that an improved laboratory characterization of the deformation properties of the soil layers and the realistic modelling of piezometric elevations is necessary to make reliable predictions of ground movements. They also emphasize that the interpretation of the monitoring data requires careful engineering judgement. Effects as for example the contributions of post construction deformations of concrete floor and roof slabs have played an important role in the development of wall deflections for the Boston case.

Prediction of Greenfield Ground Movements

Long

Long (2001) has summarized the results of a worldwide database for maximum lateral wall movements and maximum ground settlements due to the excavation of retaining walls. He subdivided the data in four sets depending on the types and strength of the soil, the safety factor against base heave (FOS). The cantilever walls are considered as a separate set. The sets are shown in Figure 2.28.
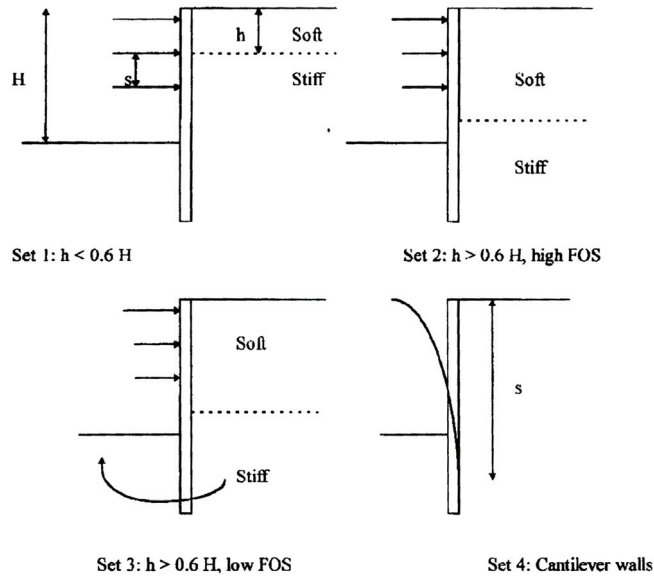
Figure 2.28: Categorisation by Long in four different sets

For stiff soils (set 1) and situations for soft soils with a high safety factor against base heave (set 2) the values derived by Long show good agreement with those of Clough et al. (1990). An exception in this category form the cases which have soft soil at the dredge level. The wall deflections are significantly increased and the charts presented by Clough et al. (1990) can considerably underestimate the movements.

For soft soils with a low safety factor against base heave (set 3) large wall deflections have been recorded (up to 3.2% *H*). The relationship between movement, system stiffness and FOS according to Clough et. al can be taken as a good starting point.

Cantilever walls (set 4) show an average of the maximum wall deflection of 0.36% *H*. Long states that surprisingly the lateral wall movements appear to be independent of the system stiffness and therefore concludes that the worldwide design practice for cantilever walls may be conservative.

2.3.2.2   *Horizontal ground movements behind the retaining wall*

Burland et al. (2001) stated that the horizontal movements of the ground behind the retaining wall can be significantly larger than the vertical deformations in case of a cantilever excavation in stiff clays. For other reported cases the horizontal movements are in general similar to the vertical movements.

Boone (1998) assumed that lateral surface movements due to the excavation of a building pit are considered to be about half of the vertical movements. In 1999 Boone however presents the design approach of a large braced excavation in glacial till and highly overconsolidated sand, silt and clay deposits. Due to local experience and the work of O'Rourke (1976) and Milligan (1974) the maximum horizontal movements can be assumed to be equal to maximum vertical movements.

Dhanjal et al. (2001) stated that from the limited information of case records the expected horizontal movements for the design of the excavation pits for the construction of the Copenhagen metro (glacial till of overconsolidated sandy clay or clayey sand) should be considerably less than 0.1% H and may be assumed to tend to zero at a distance of 1.5H.

Clough et al. (1990) presented the graph shown in Figure 2.29 based on field observations of different excavations in stiff to very hard clay. The maximum horizontal ground movement falls within a bandwidth up to 0.8% H and tends to even exceed the corresponding vertical ground movements that were presented in Figure 2.23(b).
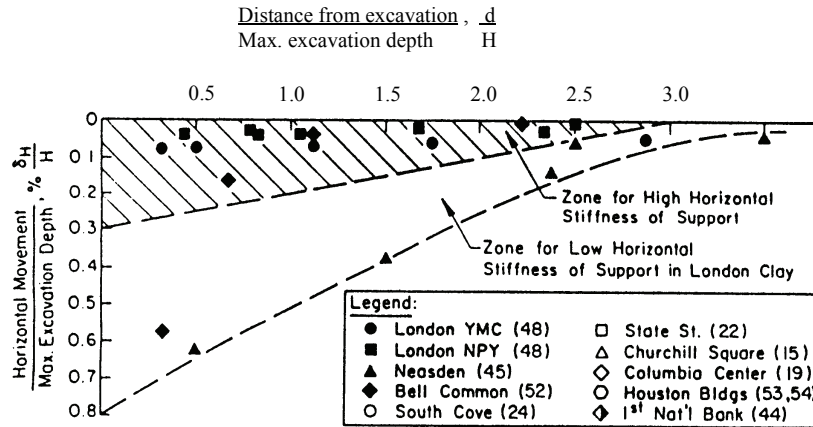
Figure 2.29: Horizontal ground movements due to excavation in stiff to very hard clay (Clough et al. 1990)

2.3.3   Conclusions

The wide bandwidths of the empirical approaches to predict ground movements due to excavation of retaining structures show the restrictions of these methods and requires careful engineering judgement, when applying them in a preliminary design stage for a project. The methods should only be used as initial guidance and special attention is required when extrapolating the empirical observations of other projects to the project-specific conditions of a new situation. For detailed design purposes it is however necessary to use powerful numerical modelling to achieve more reliable predictions of ground movements, taking into account the detailed site-specific circumstances like construction sequence, nonlinear soil properties and strutting support per project.

2.4   Ground movements due to groundwater lowering

2.4.1   General

If the groundwater level is lowered the pore water stresses in the soil are reduced and the effective soil stresses are increased. This increase causes compression of the soil and results in ground settlements. The magnitude and distribution of the settlements depend on the groundwater flow pattern and the soil properties in particular the permeability and compressibility and represents a complex three-dimensional and time-dependent problem. Detailed analyses would require a site-specific numerical model. However empirical analytical approaches have been developed to get a global indication of surface settlements due to dewatering. Such methods are described in section 2.4.2.

Prediction of Greenfield Ground Movements

An important difference between settlements from dewatering and settlements from tunnelling or excavation of building pits is the extent of the influence zone. While ground movements due to excavations and tunnelling are a relatively local phenomenon, settlements due to dewatering can extend up to a much larger distance from the source.

2.4.2   Literature study

SBR (Dutch organisation "Stichting Bouwresearch")
The SBR (2003) presents the combined equation of Terzaghi and Keverling-Buisman for the determination of the maximum settlement due to groundwater lowering:

$$\frac{\Delta d}{d} = \left(\frac{1}{C_p} + \frac{1}{C_s} \cdot \log \frac{t}{t_0} \right) \cdot \ln \frac{P + \Delta P}{P} \qquad (2.17)$$

with
$\Delta d/d$	= relative compression of the soil layer	[-]
d	= thickness compressible soil layer	[m]
C_p	= primary compressibility index	[-]
C_s	= secondary compressibility index (including creep of the soil)	[-]
t_0	= 1 day	
t	= time period when maximum settlements are developed	[day]
P	= initial effective soil stresses	[N/m^2]
ΔP	= increase of effective soil stresses (dependant of the drawdown)	[N/m^2]

The input for the influence of the groundwater lowering is the increase of effective soil stresses *ΔP* due to the drawdown of the groundwater level.

To determine the period *t* when the maximum settlement has developed, the following equation can be used:

$$t = 2 \cdot \frac{(d/2)^2}{C_v} \qquad (2.18)$$

with C_v = consolidation coefficient   [m^2/s]

For the use of equation (2.18) one should be aware that it is assumed that pore water pressures can flow away at two sides. Equation (2.17) and (2.18) give a first conservative estimation of the maximum settlement due to dewatering and the corresponding increase of the effective soil stresses after a long time. The settlements can occur directly in case of highly permeable sand or after a longer time in case of less permeable clay and peat, depending on the consolidation and creep properties of the soil and the thickness of the soil layer.

CUR 162
CUR 162 (1993) presents a more complex equation to determine the settlements caused by an increase of effective soil stresses due to dewatering, which takes into account the stress history of the soil in terms of the overconsolidation ratio *OCR* and its influence on the predicted settlements. The equations are given and explained in Appendix 1. By introducing different soil stiffness in terms of the compressibility index *C* and *C'* for stresses above or below the limit stress state, different settlement contributions are encountered.

Different parameters are used in the literature to describe the compressibility of soil. It is distinguished between parameters *Cp*, *Cs*, *C*, *C'p*, *C's* and *C'*. The *C* values with the index (') indicate the compression for stress levels lower than the limit stress state. The values without index represent the stiffness before the limit stress state.

Prediction of Greenfield Ground Movements

A comprehensive overview of the effects of groundwater lowering on the surrounding for Dutch circumstances is presented in SBR (1986). The influence has been considered for a great variety of soil profiles in the Netherlands, see Figure 2.30. To get a rough indication of the relation between the surface settlement and the lowering of the groundwater for the different locations in the Netherlands the results given in Table 2.1 can be useful. The percentages are derived for lowering of the freatic groundwater level of 0.25m over a period of 30 years.

Legenda

Grondgesteldheid

- draagkrachtig zand
- zand met leem/silt/kleilagen
- rivierklei
- slappe klei/veenlagen: dikte <10 m
- slappe klei/veenlagen: dikte >10 m
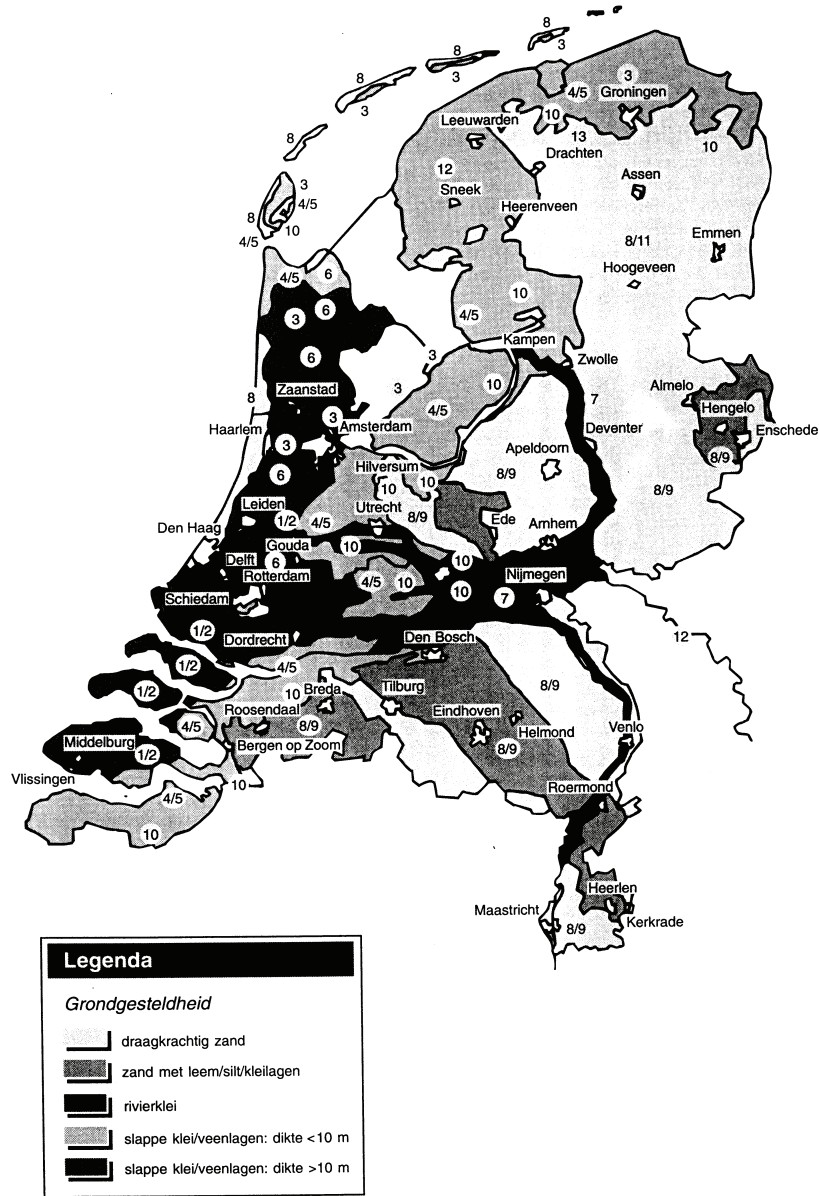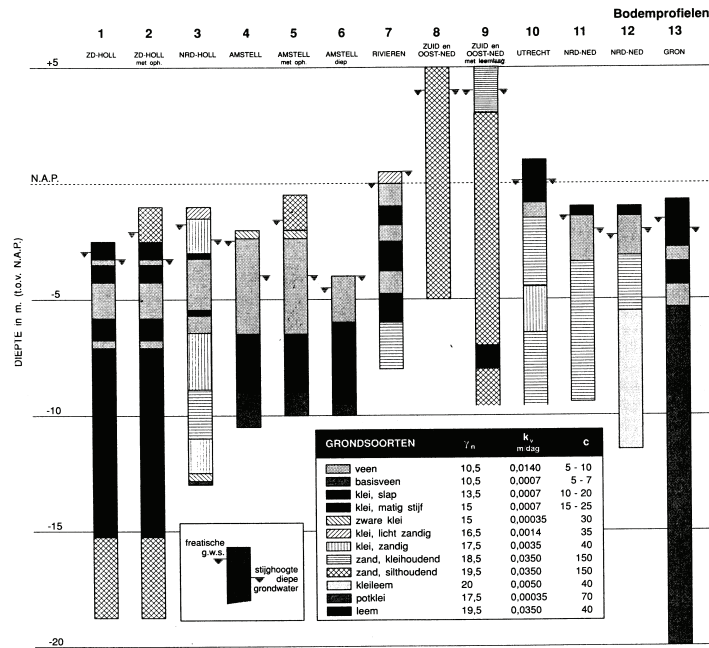
Figure 2.30: Characteristic soil profiles in the Netherlands given in SBR (1986)

Soil profile	Calculated surface settlement due to drawdown of the freatic level of 0.25m after 30 years [mm]	Relation of the surface settlement versus drawdown [%]
1	59	24
2	41	16
3	33	13
4	82	33
5	47	19
6	49	20
7	47	19
8	0	0
9	4	2
10	13	5
11	40	16
12	16	6
13	40	16

Table 2.1: Relation of surface settlement versus drawdown of the freatic groundwater level; SBR (1986)

The surface settlements strongly depend of the local ground properties and layering en varies up to a maximum of 33% of the drawdown. It should be emphasized that these results are derived for Dutch conditions and only give a rough estimate of the maximum surface settlement due to lowering of the freatic water level in Dutch conditions.

Prediction of Greenfield Ground Movements

To determine the settlement curve the drawdown curve on distance of the maximum drawdown has to be determined by hydrological calculation methods, see Preene (2000) or SBR (2003), taking into account the time-dependence of the groundwater flow. For detailed design purposes numerical calculations have to be carried out.

A special aspect related to groundwater lowering is the risk of damage to rot of wooden piles. It can occur if water levels are drawn drown that much that the top of the piles are exposed to air. The influence factors to be considered are:

- The period and magnitude of the drawdown, assuming the drawdown leads to a temporary groundwater lowering below the pile head.
- Natural fluctuations of the groundwater table.
- Type of wood (pine or spruce).

A general recommendation to avoid rot and consequently damage of wooden piles for Dutch conditions is given in SBR (1986) and says that the pile head has to be situated at least 0,5m below the lowest groundwater table. Decay fungi, such as brown, white and soft rot are known to remain present even if the ground water level is restored and the foundation wood is again immersed in water. When the ground water level is lowered again in the future, the rotting will continue and, depending on the amount of oxygen supply it will eventually result in a total loss of the foundation wood, Peek et al. (1981) and Hoekstra (1974). In the Netherlands many problems due to decay fungi have been experienced in Rotterdam, Haarlem, Dordrecht and Breda.

As rough indication the SBR (1986) states that for a groundwater level of ca. 20cm below the pile head during a period of ca. 3 months the risk of damage is low and for 50cm over a period of 4 to 6 months, the damage risk is high. Pine is more susceptible than spruce.

Preene

Preene (2000) presents a systematic method for the prediction of the distribution of ground settlements due to groundwater lowering. Important factors in the determination of the settlement distribution are the maximum target drawdown, the permeability and compressibility of the soils and the period of dewatering. Different situations of soil layering of aquifers (a significantly permeable stratum), aquitards (a stratum of lower permeability) and aquicludes (a stratum of very low permeability) can be encountered in the method. Preene provided design charts to determine:

- The distribution of drawdown with distance of the location of the maximum target drawdown. As this distribution is time-dependent, the period of dewatering and the permeability is included as input parameter.
- The distribution of the ground settlements with distance are determined from the previous calculated distribution of the drawdown and the corresponding increase of the vertical effective stresses. Elastic analyses taking into account the stiffness of the soil in one dimensional compression are used to determine the compression of the soil layers and the settlements respectively.

A significant difference in the calculation of the settlements between the approaches of the SBR (2003) and Preene (2000) is, that Preene uses the simplified one dimensional E'_0 instead of the compressibility indexes C_p and C_s to determine the compression and the settlement respectively.

2.5 Development of ground movements in time

The timely development of ground movements and its influence on the surrounding structures has to be incorporated in damage risk analyses. It is a popular premise that buildings undergoing slow settlement are damaged less than buildings sustaining rapid settlements. Long term settlements imposed to adjacent structures have to be judged in combination with the accompanying effects of creep or relaxation of the structural material. If the settlements occur slowly, creep and relaxation of the structure reduces the stress changes occurring due to redistribution of the building loads and

Prediction of Greenfield Ground Movements

consequently also the damage risks can be reduced. This is particularly true for structures from quasi-brittle material like masonry. A rapid process of imposing ground movements (short term settlements) implies that creep is less or even not able to accommodate imposed deformations in the structure. An empirical approach to take into account the beneficial effects of long term settlements in the building damage prediction is given in section 3.4.2. In the present section the considerations are focused on long term effects in the soil.

The definition of the SBR (1986) for the settlement rates can be used to distinguish between short term, medium term and long term settlements:

- Short term movements: 70 - 100% of the maximum settlements occur within 1 year
- Medium term movements: 35 - 50% of the maximum settlements occur within 1 year
- Long term movements: 10 - 15% of the maximum settlements occur within 1 year

The fact that the ground movement will develop gradually over a longer time is caused by the cohesive creep properties of soil layers and is only to be expected in clayey layers. Sandy layers will show a non-cohesive behaviour resulting in the almost immediate occurrence of the ground movement reaction when the excavation source is activated.

The main factors contributing to the development of post-construction long term settlements for TBM–tunnelling are given by Mair et al. (1997):

- The *compressibility and permeability of the soil.* If the horizontal permeability is for example significantly larger than the vertical permeability it gives raise to the widening of the short term settlement trough.

- The *initial pore pressure distribution in the ground* before tunnel construction and the *magnitude and distribution of excess pore pressures generated by the construction of the tunnel* play an important role in the development of long term settlements. Lower initial pore pressures show clearly smaller long term settlements.

- The *permeability of the tunnel lining* relative to the permeability of the soil. The time-dependent settlements result from increase in effective soil stresses due to the fact that the tunnel acts as a permeable drain.

There is a lack of longer-term measurements of excavation induced ground movements. The intensive research project of the JLE (Jubilee Line Extension) however presents some interesting case records of the development of long term ground movements in London soil conditions over a period of two to three years after construction see Burland et al. (2001) and Figure 2.31. The tunnels of the JLE were constructed in the stiff London clay and the Lambeth group (silty sand). For details about the geology and the soil properties it is referred to Burland et al. (2001).
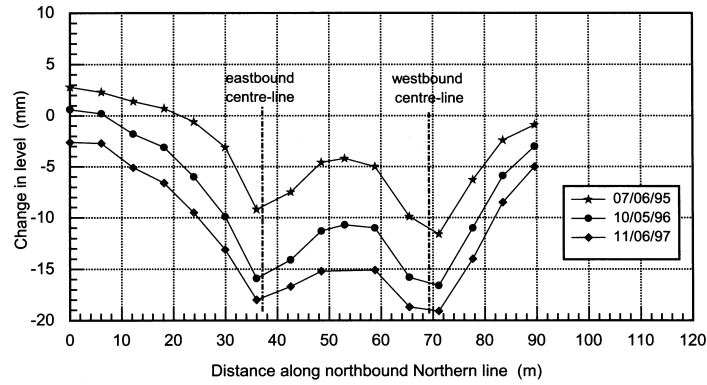
Figure 2.31: Development of long term transverse settlement trough due to twin tunnelling at the JLE, Burland et al. (2001)

Some essential conclusions from the analyses of these monitoring field data are:

- The influence area of the long term settlements is clearly widened compared to the short term settlements. This means that areas which do not fall in the short term influence area will well be subjected to ground movements due to the long term ground movements. This should be taken into account when assessing the influence area for the damage risks of short term and long term influences.
- However the slopes and differential settlements (potential for settlement damage to adjacent buildings) in the short term settlement zone are not increased in the long term situation. This gives raise to the assumption that for the considered cases in London the damage assessment of structures due to the short term ground movements will not be modified due to the long term ground movements.

3 REVIEW OF THE EMPIRICAL ANALYTICAL BUILDING DAMAGE PREDICTION METHOD

3.1 General

Predicting settlement building damage due to excavation induced ground movements is of increasing importance to the viability of urban building projects, Netzel et al. (1999a, 1999b, 2001a). The predicted greenfield ground movements derived by the numerical or empirical analytical methods from section 2 serve as input and have to be projected on the adjacent buildings to predict damage in these. An empirical analytical prediction method, the limiting tensile strain method (LTSM), has been developed throughout the last years for the prediction of building damage.

The design of urban excavation projects requires a two staged approach of settlement risk assessment studies. Stage I explores the potential damage risk areas and structures in the nearby surrounding on the basis of the LTSM. Stage II assessments are carried out on the hot spot locations in order to determine the need and efficiency of mitigating (protective) measures. This stage II takes into account the effects of soil-structure interaction and implies a consideration of structural details and 3D-effects. The calculations in stage II have to be carried out with advanced numerical techniques, as for example presented in sections 4 to 7.

Section 3.2 describes the currently used LTSM as it is applied in the design practice for the stage I assessment of potential building damage. Section 3.3 gives a detailed review of the empirical analytical backgrounds of this method and addresses some important aspects for the reliable use of this method. Section 3.4 develops recommendations for implementation of additional aspects like the building condition, long term settlements, creep of structures etc. which can affect the predicted damage and which are not yet encountered in the current LTSM.

The LTSM method implies simplifying assumptions to model the structures and the transfer of soil movements to the structures. The use of the current LTSM in engineering practice has raised several fundamental/basic questions especially from the structural point of view. The goal of this section is to critically review the assumptions and their consequences on the predicted building damage and develop recommendations for the reliable use of the method in the design practice.

The considerations in this section focus on the example of TBM-tunnelling induced ground movements and its effects on surrounding buildings. The principle of the projection of differential ground movements to predict potential building damage can however be used for all other sources of ground deformations (see section 2).

3.2 The current Limiting Tensile Strain Method (LTSM)

3.2.1 The principles of the current LTSM

The empirical analytical LTSM is commonly used in the design stage to determine the risk profile for settlement damage on the surroundings. The method was initiated by the work of Burland et al. (1974) and Boscardin et al. (1989). The basic principle of the limiting tensile strain method is that settlement induced damage in buildings results from the development of tensile strains induced by imposed ground movements. The level of expected tensile strains is determining the degree and amount of damage. The method is quite popular in practical engineering for settlement risk assessment in the design stage of excavation works in urban surrounding. It is emphasized that this section describes the current state of the art of the method with the assumptions and recommendations of the initiators of the method. The review of the backgrounds, certain assumptions and simplifications of the current method is presented in section 3.3.

The stage I damage prediction for structures according to the limiting tensile strain method is carried out in a 4-step approach as shown schematically in Figure 3.1.
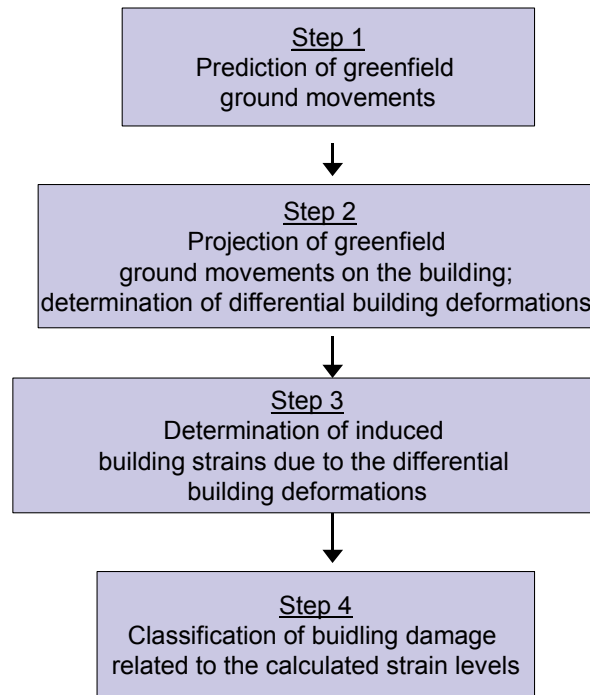
Figure 3.1: 4-step approach of the LTSM

The details of the four steps are illustrated for an example of tunnelling induced ground deformations on a masonry wall (Figure 3.2 to Figure 3.5).

Step 1: Prediction of greenfield ground movements

The greenfield ground movements are calculated with numerical or empirical analytical methods, see section 2. These methods neglect the presence (stiffness and loads) of the adjacent buildings implying an uncoupled approach. Figure 3.2 shows an example of the horizontal and vertical greenfield ground movements due to TBM-tunnelling. The predicted 1mm settlement line is assumed to be the limit of the influence area for the horizontal and vertical ground movements. The differential settlements beyond the 1mm line are considered to cause no damage to the structures. Regarding the accuracy of deformation monitoring the 1mm line is generally accepted as a reasonable limit of the measurable settlement influence.
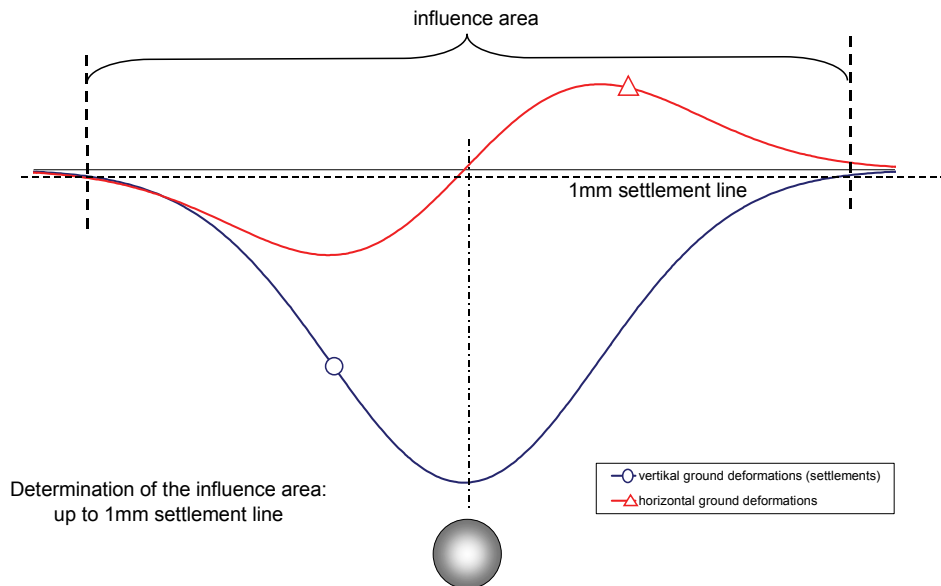
Figure 3.2: Step 1 in the LTSM

Step 2: Projection of the greenfield ground movements on the building

In step 2 the ground movement curves from step 1 have to be projected on the building as predescribed displacements. Figure 3.3 shows step 2 at the example of TBM-tunnelling induced ground deformations on an adjacent building.

- Determination of the building part inside the influence area

- splitting building into hogging and sagging part

- determination of damage parameters (angular distortion, deflection ratio, horizontal strain)

average horizontal strain
$$\varepsilon_h = (h_1 - h_2)/L_h$$

deflection ratio
$$\Delta/L_h$$

angular distortion β:
$$\varphi - \omega$$
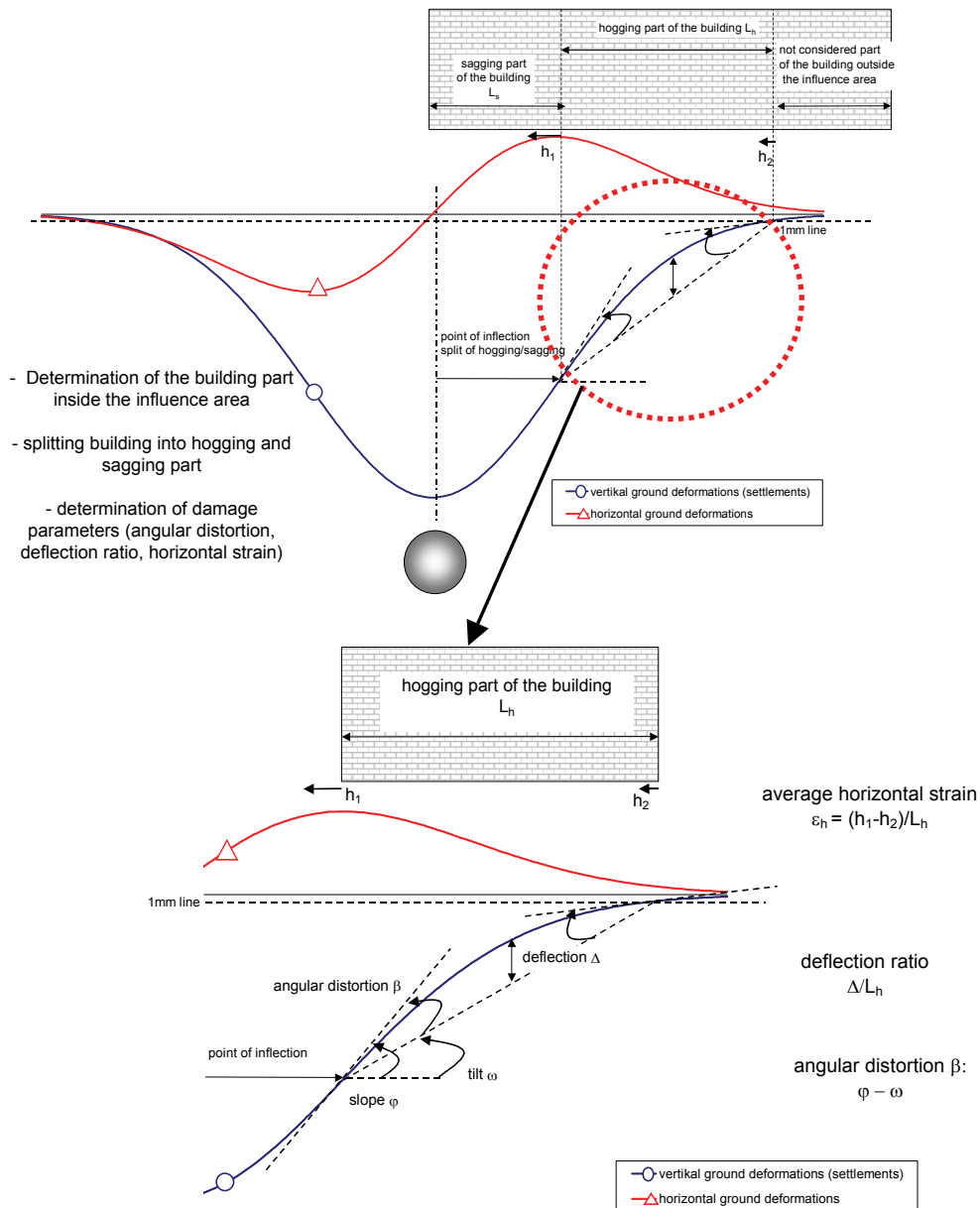
Figure 3.3: Step 2 in the LTSM

Mair et al. (1996) suggested to consider only the part of the building which is situated inside the 1mm settlement influence area. Consequently it is distinguished between the effects of imposed vertical and horizontal differential deformations.

The *vertical settlement curve* is used to split the building at the point of inflection into a hogging part (convex curvature of the settlement profile) and a sagging part (concave curvature of the settlement profile). It is assumed that the hogging and the sagging part of a building can be considered separately for the determination of the damage criteria and the tensile strains, Mair et al. (1996). The influence of

differential greenfield settlements on the location of the adjacent building, can be expressed in terms of the damage criteria angular distortion (β) or the deflection ratio (Δ/L). The definition of both parameters is shown in Figure 3.3. Different authors use one of these parameters as the dominating parameter for the determination of the induced building strains due to the vertical differential settlements (see step 3). It is noted that the rigid body rotation (tilt ω) is eliminated in the geometrical calculation of the angular distortion and the deflection ratio (see Figure 3.3) as it is assumed not to cause any strains in the structure.

The influence of differential ***horizontal greenfield ground movements*** on the building is expressed with the (average) horizontal strain (ε_h) (see Figure 3.3).

The geometric determination of the damage criteria from the greenfield ground deformations (angular distortion β, deflection ratio Δ/L and average horizontal strain ε_h) is shown in Figure 3.3(b) for the example of a building situated in the hogging area.

Step 3: Determination of induced building strains

Figure 3.4 shows the fictitious beam model used to calculate the tensile strains in the structure due to the differential ground deformations calculated in step 2.
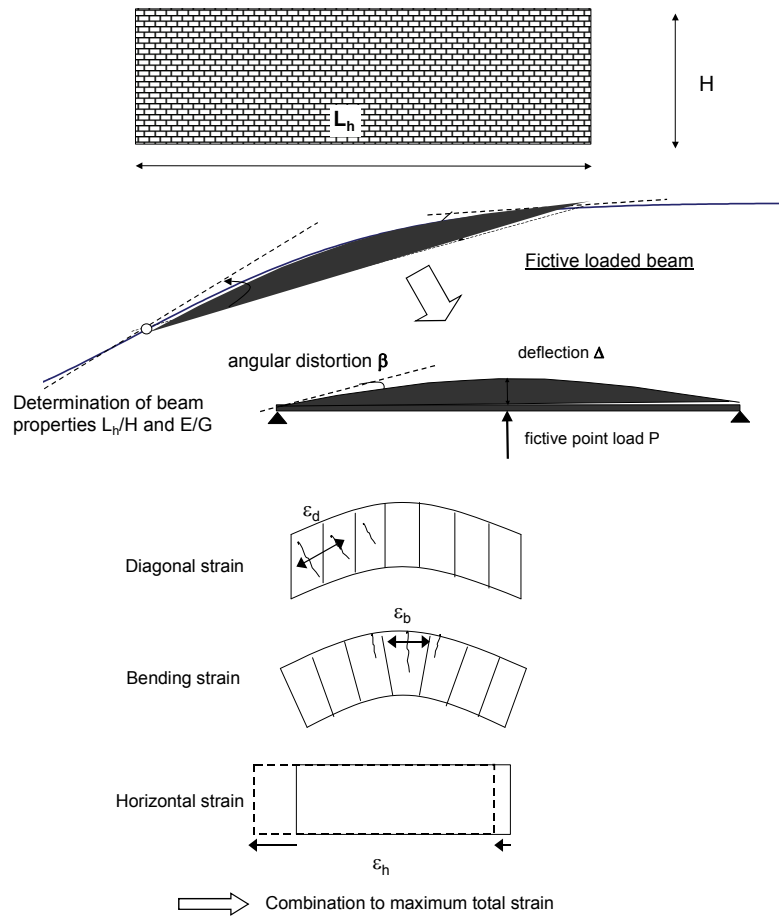
Figure 3.4: Step 3 in the LTSM

Review

The structural section of a building is modelled as a weightless, rectangular, isotropic elastic beam of length *L*, height *H* and material parameter *E/G*. The *H* value represents purely the geometrical height of the building, taken from foundation level to the eaves, usually ignoring the roof construction. Different *L/H*-ratios are determined for the sagging (L_{sag}/H) and the hogging zone (L_{hog}/H) as the length of the building parts in the sagging and the hogging zone can be different. For a massive wall, the material value of *E/G* of 2.6 is suggested by Burland et al. (1974, 2001). This value corresponds with the well known relation for *E/G* of an isotropic elastic material with a Poisson's ratio ν of 0.3 (see equation 3.1).

$$E = \frac{G}{2 \cdot (1+\nu)} \text{ and thus } \frac{E}{G} = 2 \cdot (1+\nu) = 2.6 \text{ for } \nu = 0.3 \qquad (3.1)$$

For a concrete framed structure Burland et al. (1974) suggest to use the *E/G*-value of 12.5, which is explained by the more flexible frame structure in shear leading to a reduction of the shear modulus *G* and thus an increase of the *E/G* value. It should be emphasized that the value of 12.5 is not a material parameter (as chosen for a massive wall construction), but a fictitious value, which has to take into account the expected structural behaviour of a framed structure.

The tensile strains (bending strains and diagonal strains) in the structure due to the settlements are calculated with analytical beam equations for a simply supported beam, which is loaded with a fictitious point load causing a similar deflection or angular distortion, as imposed by the pre-described vertical ground deformations. In the beam equations both shear and bending deformations are taken into account. For low ratios of *L/H* the shear deformations can cause an important part of the overall deflections whereas for high *L/H*-ratios the bending mode prevails. Burland et al. (1974) and Boscardin et al. (1989) refer to the equations given by Timoshenko (1957) to calculate the building strains. An essential difference between the approaches from Burland et al. (1974) and Boscardin et al. (1989) is the choice of the driving parameter, the deflection ratio or the angular distortion. Both approaches are described hereafter.

Burland et al. (1974) uses the deflection ratio as the driving parameter describing the imposed differential settlements. Based on Timoshenko (1957) they present the following equations to calculate the maximum bending strain $\varepsilon_{b,max}$ and the maximum diagonal strain $\varepsilon_{d,max}$:

$$\varepsilon_{b,\,max} = \frac{\Delta/L}{\left(\dfrac{L}{12 \cdot t} + \dfrac{3 \cdot I}{2 \cdot t \cdot L \cdot H} \cdot \dfrac{E}{G} \right)} \qquad (3.2)$$

$$\varepsilon_{d,\,max} = \frac{\Delta/L}{\left(1 + \dfrac{H \cdot L^2}{18 \cdot I} \cdot \dfrac{G}{E} \right)} \qquad (3.3)$$

with

	L	length of the beam i.e. the considered part of the building
	I	moment of inertia of the beam
	E	Young's modulus of the beam
	G	shear modulus of the beam
	t	furthest distance from the neutral axis to the edge of the beam in tension (if the neutral axis is in the middle of the beam t = H/2; if the neutral axis is at the bottom edge of the beam t = H)

Similar relationships can be derived for the case of a uniformly distributed load used as the fictitious loading on the beam and Burland et al. (1974) showed that the relationships for the maximum tensile strains are not sensitive to the type of loading.

An essential difference is suggested by Burland et al. (1974) for the calculation of strains in the sagging and the hogging zone. Burland et al. (1974) state, that a hogging mode deformation is generally more susceptible to damage than the sagging mode – a result that is borne out of practice by empirical observations of building damage. To implement this empirical aspect in the LTSM, it is recommended by Burland et al. (1974) to use the equations (3.2) and (3.3) for the hogging zone with the assumption of the neutral axis at the lower edge of the beam. They argue that in real structures the foundation and the soil would offer considerable restraint to the beam at the lower edge justifying the assumption that the neutral axis can be situated at the lower edge for the hogging zone. For the sagging zone they suggest to use the equations (3.2) and (3.3) for the neutral axis at the middle of the beam.

Boscardin et al. (1989) suggest to use the angular distortion β to quantify the influence of the vertical differential settlements. They present the following relationship between the angular distortion and the deflection ratio for a simply supported beam, centrally loaded with a point load and the neutral axis at the lower edge of the beam (assumed for the hogging zone):

$$\beta = 3 \cdot \frac{\Delta}{L} \cdot \left[\frac{1 + 4 \cdot \left(\frac{E}{G}\right) \cdot \left(\frac{H}{L}\right)^2}{1 + 6 \cdot \left(\frac{E}{G}\right) \cdot \left(\frac{H}{L}\right)^2} \right] \qquad (3.4)$$

The relation given in equation (3.4) is presented in Boscardin et al. (1989) and derived from the work of Timoshenko (1957).

Next step to derive the maximum total strain is, that the strains due to the vertical settlements (bending strains and diagonal strains respectively) and the horizontal ground movements (horizontal strain) are combined to a total tensile strain. It is distinguished between a total strain derived by the combination of the maximum bending strain and the average horizontal strain (ε_{bt}) and the combination of the maximum diagonal strain and the average horizontal strain to (ε_{dt}). The highest value of these two is considered as the dominant tensile strain in the structure imposed by vertical and horizontal ground movements.

Boscardin et al. (1989) suggested to determine ε_{bt} by simple superposition with:

$$\varepsilon_{bt} = \varepsilon_h + \varepsilon_b \qquad (3.5)$$

This assumption is valid for the case of the hogging zone were the neutral axis is assumed at the bottom edge of the beam. If the horizontal strain is transferred at the neutral axis, a central horizontal tensile strain would be imposed on the building over the entire height. The maximum value of ε_{bt} will than occur for the hogging zone at the top fibre due to bending and horizontal strain.

As the diagonal strain is inclined it cannot directly be superimposed to the horizontal strain. The strain relationships given by Timoshenko et al. (1971) for the calculation of the principal strains ε_1 and ε_2 have to be used to determine ε_{dt}.

$$\varepsilon_{1,2} = \frac{\varepsilon_x + \varepsilon_y}{2} \pm \sqrt{\left(\frac{\varepsilon_x - \varepsilon_y}{2}\right)^2 + \left(\frac{\gamma_{xy}}{2}\right)^2} \qquad (3.6)$$

The value ε_{dt} represents the maximum principal tensile strain and can be derived by equation (3.6) with:

$$\varepsilon_y = 0$$

$$\varepsilon_x = \varepsilon_h$$

$$\gamma_{xy} = 2 \cdot \varepsilon_d$$

$$\varepsilon_{dt} = 0.5 \cdot \varepsilon_h + \sqrt{0.25 \cdot \varepsilon_h{}^2 + \varepsilon_d{}^2} \qquad (3.7)$$

Step 4: Classification of damage related to strain levels

The maximum of the calculated maximum total strains (ε_{bt} or ε_{dt}) from step 3 has to be related to possible damage in step 4 (see Figure 3.5).

Burland et al. (1974) analysed numerous large scale tests on masonry structures and found the tensile strain as the fundamental parameter in the determination of the onset of cracking. They showed that the onset of visible cracking is associated with an average value of tensile strain. The limiting tensile strain is found not to be sensible for the deformation mode. For masonry structures they reported values between 0.05% and 1% and for reinforced concrete structures lower values of 0.035% to 0.05% were observed. It is emphasized that these strain limits for the initiation of visible cracking are not related to the strain corresponding with tensile failure (i.e. loss of tensile strength). They are obviously larger. The bandwidth for reinforced structures is derived from a wide variety of tests for concrete strengths and type of reinforcement by Base et al. (1966) and Burhouse (1969).

A system for the classification of damage to masonry structures has first been put forward by Burland et al. (1977) and only changed slightly by BRE (1981),(1990). It is shown in Figure 3.5. The system has proved to be an objective framework for assessment of damage risk to buildings. The expected damage is defined in terms of ease of repair. The BRE classification is developed for masonry and the degree of severity given in the table only applies to standard domestic or office buildings and may not be appropriate for sensitive finishes. More stringent criteria may also be necessary when the cracking can lead to corrosion or penetration of liquids and for watertight structures.

A very important threshold for practical engineering forms the boundary from aesthetical damage (up to damage class "slight") to functional damage. Damage predictions up to damage class slight are generally considered acceptable for urban building projects if no special consideration is required due to poor building or foundation condition, the historical or architectural significance of buildings or restrictions on the particular sensitivity of parts of the structure. Burland et. al. (2001) state that buildings can be considered at "low" risk, if predicted damage falls into the categories negligible to slight and that a major objective of design is to maintain the level of risk below this threshold. Damage up to class slight can also result from shrinkage or thermal effects of the structure itself.

Boscardin et al. (1989) appointed bandwidths of strain levels to the different damage categories defined in the BRE classification. They derived these relationships from the limiting tensile strains for the onset of cracking, analysed from the large scale tests of Burland et al. (1974) and additional empirical data of several case records.

Category of damage	Damage class	Description of typical damage and ease of repair	Approximate crack width (mm)	Limiting tensile strain levels (Bosardin et al. (1989)) (%)
Aesthetic damage	Negligible	Hairline cracks of less than about 0,1mm width	up to 0,1mm	0 - 0.05
	Very slight	Fine cracks which can easily be treated during normal decoration. Perhaps isolated slight fracturing in building. Cracks in external brickwork visible on close inspection.	Up to 1mm	0.05 – 0.075
	Slight	Cracks easily filled. Redecoration probably required. Several slight fractures showing inside of building. Cracks are visible externally and some repainting may be required externally to ensure water tightness. Doors and windows may stick slightly	Up to 5mm	0.075 – 0.15
Functional damage, affecting Serviceability	Moderate	The cracks require some opening up and can be patched by a mason. Recurrent cracks can be Masked by suitable linings. Repainting of external brickwork and possibly a small amount of brickwork to be replaced. Doors and windows sticking. Service pipes may fracture. Weather-tightness often impaired.	5 to 15mm or a number of cracks > 3 mm	0.15 – 0.3
	Severe	Extensive repair work involving breaking out and replacing sections of walls, especially over doors and windows. Windows and door frames distorted, floors sloping noticeably. Walls leaning or bulging noticeably, some loss of bearing in beams. Service pipes disrupted.	15 to 25mm , but also depends on number of cracks	> 0.3
Structural damage affecting stability	Very severe	This requires a major repair involving partial or complete rebuilding. Beams loose bearing, walls lean badly and require shorting. Windows broken with distortion. Danger of instability.	Usually > 25mm, but depends on number of cracks	

Notes for table:
1. There is no simple relationship between serviceability and degree of visible damage
2. It must be emphasized that in assessing the degree of damage, account must be taken of both the location and market value of the building.
3. Crack width is one factor in assessment and should not be used on its own as a direct measure of damage.
4. Boscardin et al. (1989) describe the damage corresponding to the tensile strain in the range $0,15 – 0,3\%$ as 'moderate to severe'. However none of the cases quoted by them exhibit severe damage for this range of strains.

Figure 3.5: Step 4 in the LTSM (according to BRE (1981) , (1990) and Boscardin et al (1989))

3.2.2   Basic assumptions of the LTSM

The LTSM forms an important framework for predicting damage of buildings due to excavation induced ground movements. The method is developed for practical engineering and is used in the design stage. As shown in the 4-step approach of section 3.2.1 it implies some important simplifications of the real behavior of soil and structure in order to achieve a simple and transparent method. Burland et al. (2001) state that the simplified approach is usually considered to be conservative for the prediction of building damage as in the majority of cases the damage likely to occur will be less than the assessed category. The reason for this is that the imposed (horizontal and vertical) greenfield ground deformations on foundation level, caused by an external source (tunnelling, excavation etc. see section 2), are assumed to be fully transferred to the building regardless soil-structure interaction effects. The full transfer of the (differential) green field ground movements implies the building to be forced to follow the pre-described differential settlements, causing the largest distortion of the building. In reality the interaction of the soil and the structure tends to reduce the distortions at the building. The method is therefore considered to provide a ***conservative estimate*** for the expected damage.

Despite this explanation given by Burland et al. (2001) one should be aware of other basic assumptions of the LTSM which will not necessarily always provide a conservative result for the predicted damage for all kind of structures:

- The structure is simplified schematised to behave as a linear elastic beam. The strains are calculated using the assumptions of linear–elastic beam theory, including bending and shear components. Geometrical discontinuities like doors and window openings are not taken into account. Consequently unfavourable local strain concentrations around openings which could result in increased damage are ignored. Additionally a modification of the strains due to the shell behaviour of walls for low *L/H*-ratio's is not taken into account.

- Initial loading and initial damage of the building is ignored. The strains in the building due to the ground deformations are determined by a fictitious loading approach, neglecting the possible superposition with existing initial strains. Thus no superposition of the initial and the additional strains is taken into account. As a consequence redistribution of existing forces on the building, which is in fact causing strain redistribution and concentrations is not taken into account.

- Linear elastic strain levels are used for the determination of damage in an average manner. The effect of local reduction of the stiffness, if a crack develops, is not taken into account. The relation between linear elastic strain levels and the severity of damage (see last column in Figure 3.5) is derived from empirical observations and material tests, but the influence of nonlinear material behaviour and the development of local cracking in a entire wall structure (for example near openings of doors and windows) is not taken into account.

The influence of these aspects will be investigated with the support of advanced numerical modelling in section 4 to 7.

3.2.3   Design charts from the literature

Boscardin et al. (1989) worked out the equations presented in the previous section in a design chart including also the strain limits for the different damage classes (see Figure 3.5) and included data of case records in the diagram. It is emphasized that the curved boundary lines of the damage classes represent the LTSM results for a wall of *L/H*=1 and *E/G*=2.6 in the hogging zone, derived with greenfield values for the horizontal strain as a measure for the impact of differential horizontal ground movements and the greenfield angular distortion as a measure for the vertical differential settlements. Boscardin et al. describe that the monitoring data of the cases considered in their validation is the data on the structures and not in the soil, but as all cases have no grade beams and are considered flexible they are assumed to almost not alter the differential greenfield movements. Thus the input parameters

for the angular distortion and the horizontal strain in their diagram, used for the validation of the LTSM with the data of the case records, are considered greenfield values.

The design chart is shown in Figure 3.6. It should be emphasized that the data of the case records were not always complete as horizontal strains were not measured at all cases and the authors therefore assumed a range for the horizontal strains for the interpretation of the data. Furthermore the diagram includes data from a few records were the differential movements were caused by self weight settlements of the building as well as excavation induced movements on existing buildings. More complete recorded cases should be analysed to reduce the shortcomings and scatter in the data used by Boscardin et al. (1989).
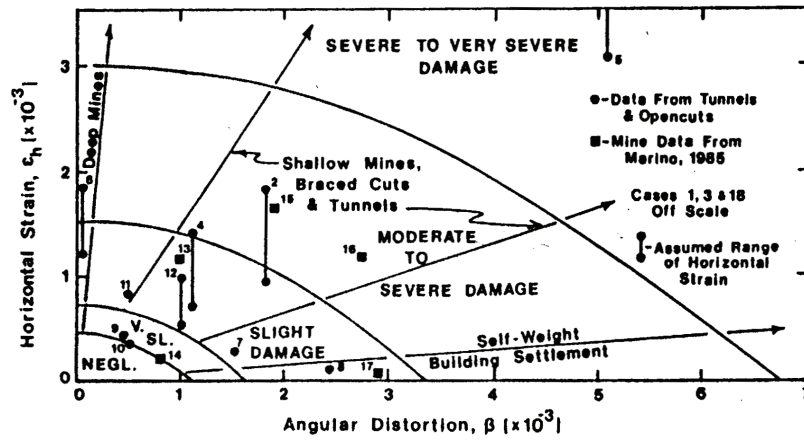
Figure 3.6: Design chart developed by Boscardin et al. (1989)

Burland (1995) presented a comparable diagram based on the results of LTSM calculations for *L/H*=1, *E/G*=2.6 and the hogging zone with the difference, that the deflection ratio is used as a measure for the vertical differential settlements instead of the angular distortion used by Boscardin et al..
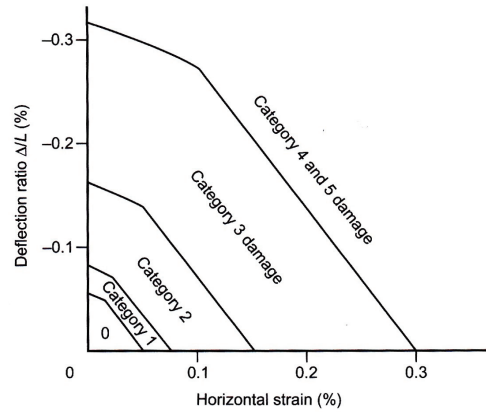
Category 0	Negligible damage
Category 1	Very slight damage
Category 2	Slight damage
Category 3	Moderate damage
Category 4 and 5	Severe to very severe damage

Figure 3.7: Design chart developed by Burland (1995)

It is strongly emphasized to be aware of the fact, that both diagrams only apply to a structure of a *L/H*-ratio equal to 1, an *E/G*-value of 2.6, situated in the hogging zone (with the assumption of the neutral axis at the bottom edge of the structure). Other situations of varying *L/H*, *E/G* and the sagging zone can therefore **not** be considered with these diagrams. In engineering practice the designers using these charts are often not aware of these important restrictions of the diagrams of Boscardin et al. (1989) and Burland (1995), with the consequence of incorrect damage predictions.

3.3 Review of the backgrounds

3.3.1 Shear form factor

To calculate the deflection *Δ* of a fictitious loaded beam, Burland et al (1974) and Boscardin et al. (1989) refer to the equations presented by Timoshenko (1957) and suggest to use equation (3.8) to calculate the overall beam deflection of a beam with the neutral axis at the mid of the beam, loaded with a fictitious point load *P* taking into account shear and bending deformations.
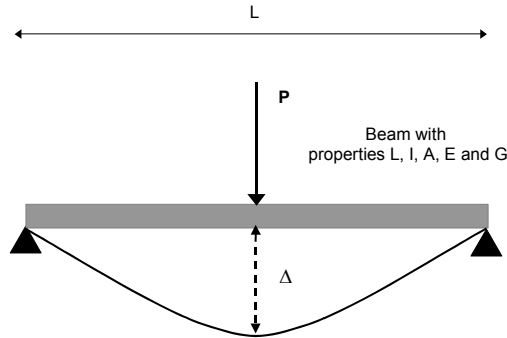
$$\Delta = \frac{P \cdot L^3}{48 \cdot EI} + \frac{P \cdot L \cdot 1,5}{4 \cdot G \cdot A} \tag{3.8}$$

with
	P	point load
	L	span width of the beam
	G	shear modulus
	E	Young's modulus
	I	moment of inertia $(B*H^3)/12$ for a rectangular cross section
	A	cross section area $(B*H)$ for a rectangular cross section

Figure 3.8: Equation used by Burland et al. (1974) and Boscardin et al. (1989)

The first term in equation (3.8) presents the deflection due to bending and the second term the deflection due to shear. The contribution of the shear deformations to the overall deflection includes the shear form factor α_s. The current LTSM uses the equations with a shear form factor of 1.5, based on the maximum shear stress and shear strain at the neutral axis of the beam. The variation in shear stresses and corresponding strains over the height of the beam is not taken into account in the contribution to the overall deflection (see Figure 3.9).
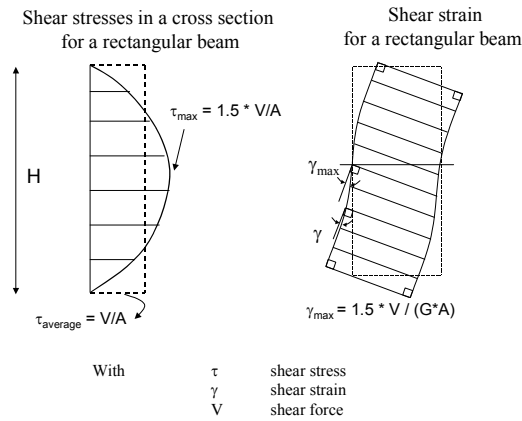
Figure 3.9: Distribution of shear stresses and shear strains in the cross section of the beam

This leads to an overestimation of the shear deflection contribution and consequently to an underestimation of the tensile strains, because the fictitious point load which is necessary to force the beam to deflect equal to a given greenfield deflection (see step 3 of the LTSM; section 3.2.1.) is underestimated.

Timoshenko et al. (1971) however also presents solutions derived from the more exact theory of elasticity and the method of virtual work respectively. These equations differ from the equations used in the current LTSM-approach, because the influence of the shear strain distribution over the height of the beam is properly taken into account when calculating the contributions of the shear deflections to the overall deflection of the beam. For a rectangular beam a shear form factor of 1.2 is derived (Timoshenko et al. (1971)), instead of the simplified shear factor of 1.5 used currently in the LTSM. Using this modified shear form factor, the equations for the deflection ratio due to a fictitious point load *P* and the neutral axis in the mid of the beam are:

$$\Delta = \frac{P \cdot L^3}{48 \cdot EI} + \frac{P \cdot L \cdot 1{,}2}{4 \cdot G \cdot A} \tag{3.9}$$

To quantify the contribution of the shear deformations to the total deflection *Δ*, equation 3.9 is analysed. The results show the results depending of the *L/H*-ratio.
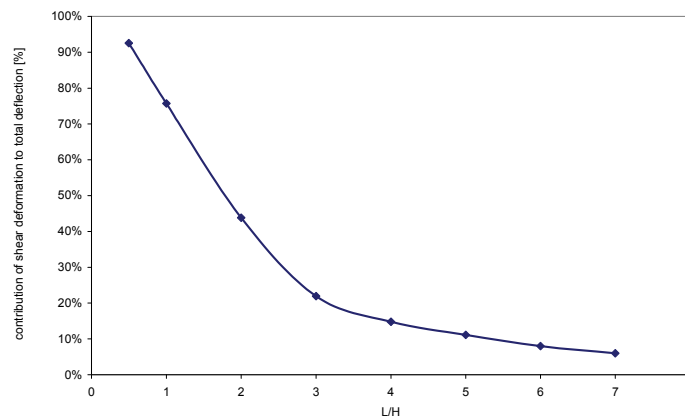
Figure 3.10: Contribution of shear deformations to total deflection according to equation 3.9

Review

The influence of the modification of the shear form factor on the calculation of the tensile strains $\varepsilon_{b,max}$ and $\varepsilon_{d,max}$ for the LTSM is analysed. The equations for the neutral axis at the centre of the beam are derived as follows:

Neutral axis at the centre of the beam
(sagging zone)
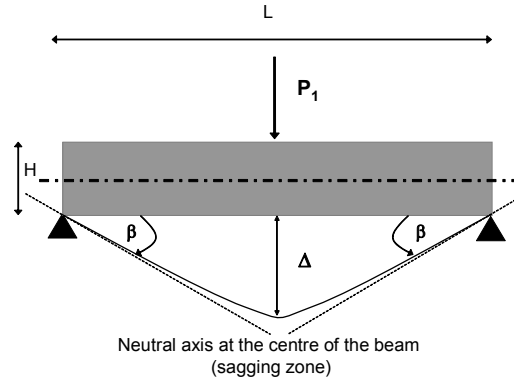
Bending strains

$$\varepsilon_{b,max} = \frac{\sigma_b}{E} = \frac{M_{max}}{E \cdot W_1} = \frac{P_1 \cdot L \cdot H}{4 \cdot E \cdot I_1 \cdot 2} \tag{3.10}$$

Substitution of equation (3.9) gives

$$\varepsilon_{b,max} = \frac{\left(\frac{\Delta}{L}\right)}{\frac{L^2}{48 \cdot E \cdot I_1} + \frac{1.2}{4 \cdot G \cdot A_1}} \cdot \frac{L \cdot H}{8 \cdot E \cdot I_1}$$

$$\varepsilon_{b,max} = \left(\frac{\Delta}{L}\right) \cdot \left[\frac{6 \cdot \left(\frac{L}{H}\right)}{\left(\frac{L}{H}\right)^2 + 1.2 \cdot \left(\frac{E}{G}\right)} \right] \tag{3.11}$$

with

$\sigma_{b,\,max}$	maximum bending stresses	
M_{max}	maximum bending moment ($1/4 * P_1 L$)	
W_1	section modulus for the neutral axis in the mid ($B*H^2/6$ for a rectangular cross section)	
I_1	moment of inertia for the neutral axis in the mid ($B*H^3/12$ for a rectangular cross section)	
A_1	cross section area ($B*H$)	

Diagonal strains

The relation between the diagonal strain $\varepsilon_{d,max}$ and the shear strain γ according to Timoshenko et al. (1971) is shown in Figure 3.11.

Deformation of a square
element due to shear strain γ
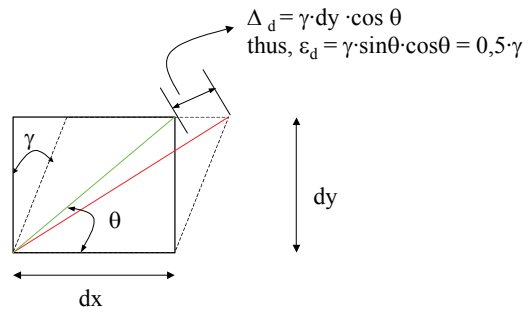
Figure 3.11: Shear deformation and diagonal strain

$$\varepsilon_{d,max} = \frac{1}{2} \cdot \gamma_{max} = \frac{1}{2} \cdot \frac{\tau_{max}}{G} = \frac{1}{2} \cdot \frac{3}{2} \cdot \frac{V_{max}}{G \cdot A_1} = \frac{3 \cdot P_1}{8 \cdot G \cdot A_1} \tag{3.12}$$

Substituting equation (3.9) gives

$$\varepsilon_{d,max} = \frac{\left(\Delta/L\right)}{\dfrac{L^2}{48 \cdot E \cdot I_1} + \dfrac{1.2}{4 \cdot G \cdot A_1}} \cdot \frac{3}{8 \cdot G \cdot A_1}$$

$$\varepsilon_{d,max} = \left(\Delta/L\right) \cdot \left[\frac{3 \cdot \left(\dfrac{E}{G}\right)}{2 \cdot \left(\dfrac{L}{H}\right)^2 + 2 \cdot 1.2 \cdot \left(\dfrac{E}{G}\right)} \right] \tag{3.13}$$

With

	γ_{max}	maximum shear strain
	τ_{max}	maximum shear stress
	V_{max}	maximum shear force ($P_1/2$)

For the case of the assumption with the neutral axis at the bottom of the beam, a fictitious beam with the height of *2H* (compared to the beam with the neutral axis in the mid and the beam height *H*) is used to derive the strains. It should be emphasized that this fictitious approach is based on the kinematic consideration of the deformation of the beam where the neutral axis at the physical bottom edge of the beam is assumed to undergo no extension or shortening.

The equations for the neutral axis at the bottom edge of the beam are derived as follows:

Neutral axis at the bottom of the beam
(hogging zone)
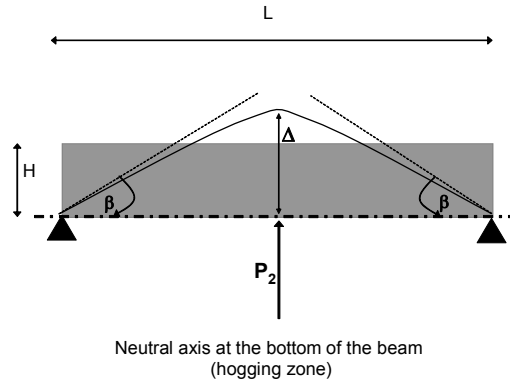
Figure 3.12: Neutral axis at bottom edge for hogging zone

It is noted, that the above figure is not consistent from static point of view for a rectangular cross section of the beam. The chosen approach for the translation of imposed deformation of a beam into strains is therefore dominated from the kinematic point of view considering an imposed deformation of the beam, with a neutral bottom fibre of the beam.

<u>Bending strains:</u>

$$\varepsilon_{b,max} = \frac{\sigma_b}{E} = \frac{M_{max}}{E \cdot W_2} = \frac{P_2 \cdot L \cdot (2H)}{4 \cdot E \cdot I_2 \cdot 2} \tag{3.14}$$

$$\varepsilon_{b,max} = \frac{\left(\Delta/L\right)}{\dfrac{L^2}{48 \cdot E \cdot I_2} + \dfrac{1.2}{4 \cdot G \cdot A_2}} \cdot \frac{L \cdot H}{4 \cdot E \cdot I_2}$$

$$\varepsilon_{b,max} = \left(\Delta/L\right) \cdot \left[\frac{3 \cdot \left(\dfrac{L}{H}\right)}{\dfrac{1}{4} \cdot \left(\dfrac{L}{H}\right)^2 + 1.2 \cdot \left(\dfrac{E}{G}\right)} \right] \tag{3.15}$$

with W_2 section modulus for the neutral axis at the bottom
(consideration of fictitious beam with height 2H, thus $W_2=B*(2H)^2/6$ for a rectangular cross section)

I_2 moment of inertia for the neutral axis at the bottom
(consideration of fictitious beam with height 2H, thus $I_2=B*(2H)^3/12$ for a rectangular cross section)

A_2 cross section area for fictitious beam of the height 2H , thus $A_2=B*2H$

Review

Diagonal strains:

$$\varepsilon_{d,max} = \frac{1}{2} \cdot \gamma_{max} = \frac{1}{2} \cdot \frac{\tau_{max}}{G} = \frac{3 \cdot P_2}{8 \cdot G \cdot A_2} \qquad (3.16)$$

$$\varepsilon_{d,max} = \frac{\left(\Delta / L\right)}{\dfrac{L^2}{48 \cdot E \cdot I_2} + \dfrac{1.2}{4 \cdot G \cdot A_2}} \cdot \frac{3}{8 \cdot G \cdot A_2}$$

$$\varepsilon_{d,max} = \left(\Delta / L\right) \cdot \left[\frac{3 \cdot \left(\dfrac{E}{G}\right)}{\dfrac{1}{2} \cdot \left(\dfrac{L}{H}\right)^2 + 2 \cdot 1.2 \cdot \left(\dfrac{E}{G}\right)} \right] \qquad (3.17)$$

Figure 3.13 presents the different tensile strains for different shear factors (1.2 versus 1.5) for the assumption of the neutral axis at the mid of the beam (a) and the neutral axis at the bottom edge of the beam (b) dependant of the *L/H*-ratio of the beam (the *E/G*-value is taken as 2.6 for a massive wall, see section 3.2.1).
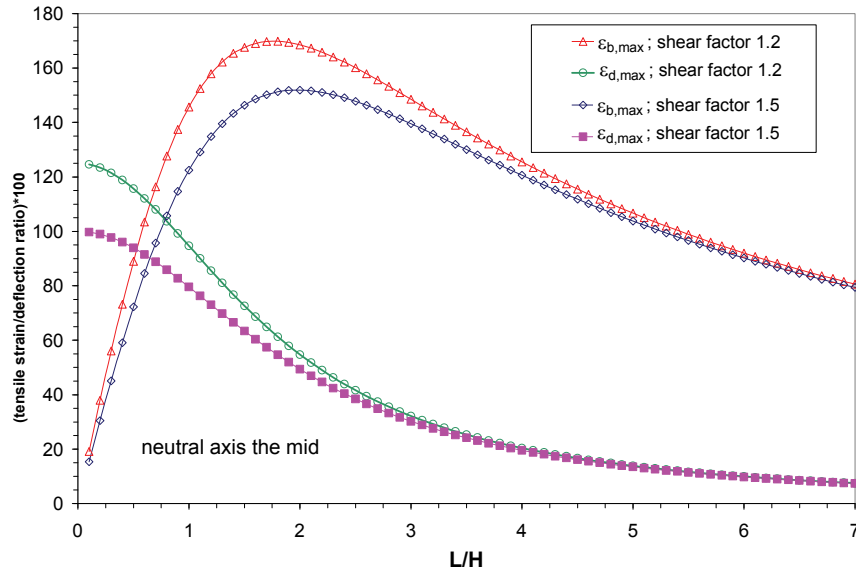
(a) strains for different shear factors and the neutral axis in the centre of the beam
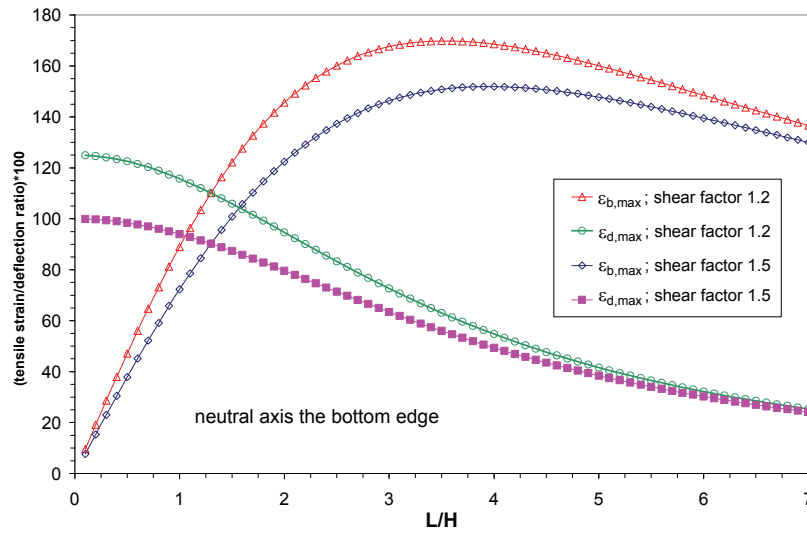
(b) strains for different shear factors and the neutral axis at the bottom edge of the beam

Figure 3.13: Influence of shear factors on maximum tensile strains

Figure 3.14 shows modification factors for the tensile strains for the assumption of the neutral axis in the mid and the bottom edge of the beam. The modification factor is independent of the type of strain, thus the relation of $\varepsilon_{b,max,1,2} / \varepsilon_{b,max,1,5}$ and $\varepsilon_{d,max;1,2} / \varepsilon_{d,max;1,5}$ are equal for each assumption of the neutral axis. Therefore only two modification lines are presented in Figure 3.14. The correct shear form factor of 1.2 leads to an increase of the strains of up to 25%. It is therefore recommended to use the above equations with a shear form factor of 1.2 when predicting the building damage using the LTSM.
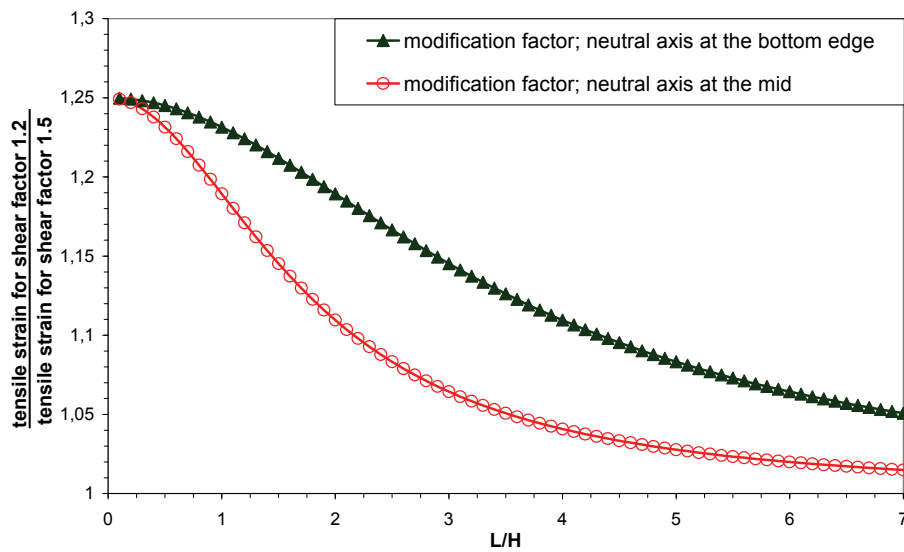
Figure 3.14: Modification factors tensile strains for different shear factors

3.3.2   Long buildings extending the 1mm line

If a building is longer than the influence area of a settlement trough, the current LTSM only considers the part of the building inside the influence area for the determination of the relevant maximum strains. The building span length L of the fictitious beam is then limited by the extent of the settlement trough. The 1mm settlement line is generally used to determine the limit of the influence area of a Gaussian formed settlement trough. The example in Figure 3.15 shows the case of a 30m long building, where only the part up to the 1mm line is considered.
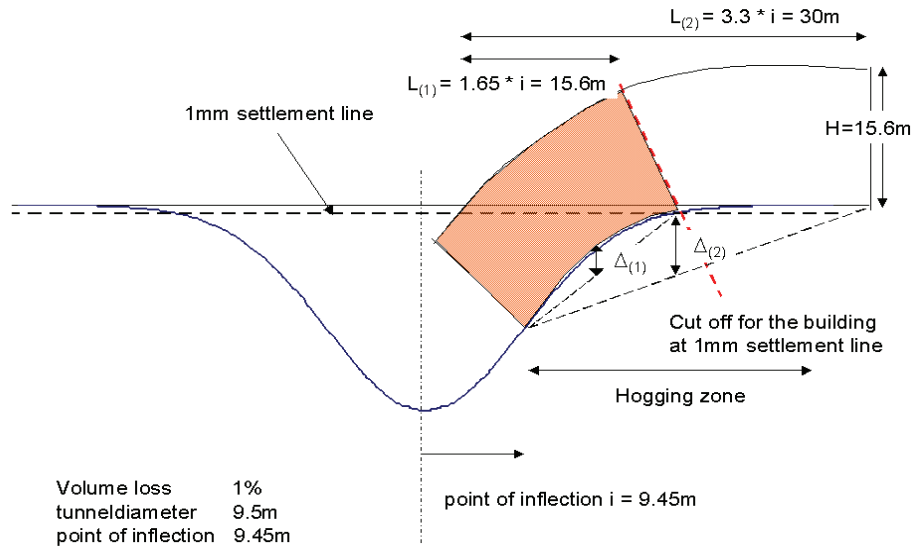
Figure 3.15: Example for "cutting off" a long structure at the 1mm line

The "cantilever" effect of long structures is obviously neglected in the current LTSM. The influence of this assumption is analysed by comparing the calculated strains for the "short" (the "cut off" part of the building inside the 1mm line) and the "long" structure (the entire building), as shown in the example of Figure 3.15). The cantilever effect for structures, which are extending beyond the 1mm line can be estimated in terms of the development of the deflection ratio in combination with the change in L/H.

For the considered case of Figure 3.15 the length $L_{(1)}$ of the "short structure" of 15.6m leads to the $L_{(1)}/H$-value of 1. The total length of the "long" structure $L_{(2)}$ is 30m thus the $L_{(2)}/H$-value is ca. 2. The different L/H-ratio's lead to an increase of the bending strains of circa 60% for the longer structure (see difference of bending strains depending of L/H in Figure 3.13 (b)).

A comparison of the deflection ratio's for both cases (the $\Delta_{(1)}/L_{(1)}$ and $\Delta_{(2)}/L_{(2)}$ values) show an increase of the deflection ratio for the long structure of circa 10%. Combination of these two effects leads to ca. 75% higher bending strains for the long structure in the considered case.

The above example shows clearly, that the "cantilever" effect can cause a significant increase of the strains and has therefore to be considered. Neglecting the length of a longer building extending the 1mm line can significantly underestimate the strains.

3.3.3   Partitioning of the structure at the point of inflection

As described in section 3.2.1 the current LTSM assumes that a building situated in the hogging and the sagging part can be considered separately for the determination of the strains. This assumption is reviewed with the support of numerical beam calculations for two cases of structures undergoing an tunnel induced Gaussian settlement profile see Figure 3.16.

$i_{transverse}$ [m]	9,5
V [%]	2
Diameter tunnel [m]	9,5
depth tunnel [m]	21

(a) case 1

i transverse [m]	9,5
V [%]	2
Diameter tunnel [m]	9,5
depth tunnel [m]	21
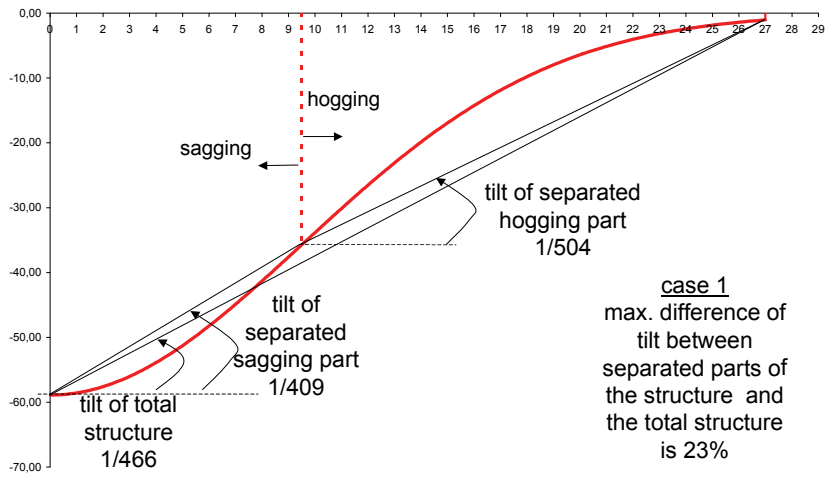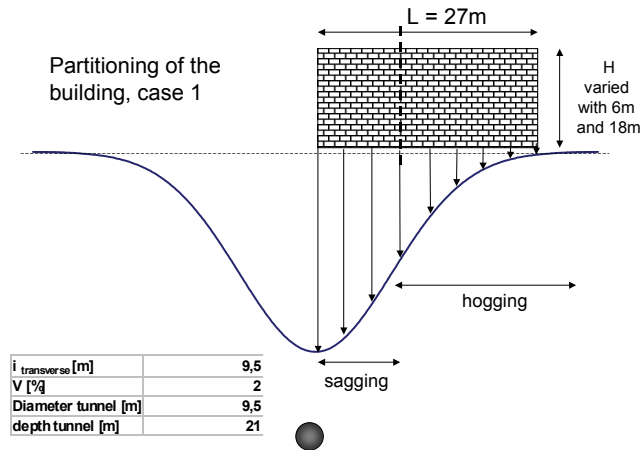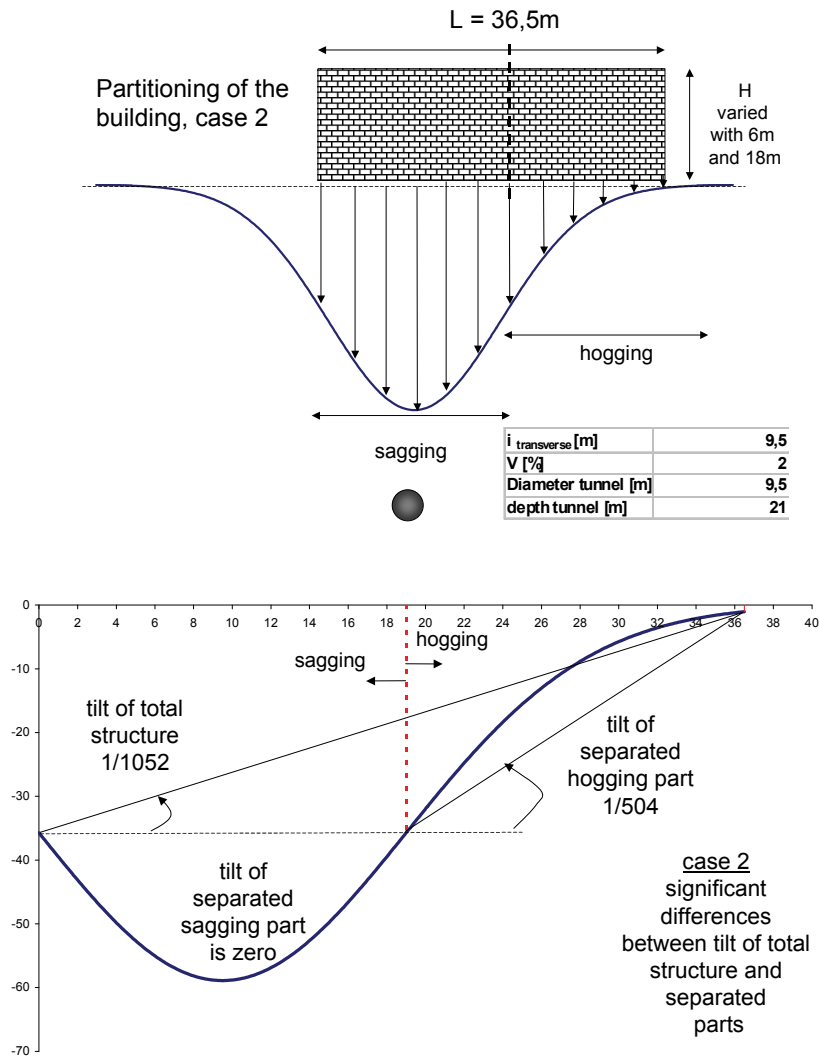
(b) case 2

Figure 3.16: Considered cases for structures situated in the sagging and hogging zone

The building is modelled in the numerical beam calculations as a fully supported Timoshenko beam with the numerical finite element code DIANA. The settlement profiles are imposed as support settlements on the Timoshenko beams. To be able to analyse the effects of partitioning of the building on the induced moments and shear forces in the beam it is distinguished between three models:

- Model A (entire building, without partitioning of the building)
- Model B (separated sagging part)
- Model C (separated hogging part)

The three models are shown in Figure 3.17 at the example of case 1. The element width of the beam elements is the same for all three models (0.1m) in order to avoid numerical influences due to the mesh

density. Model A serves as reference for the real situation of the entire building without partitioning the building. The moments and shear forces induced in the building models A to C are calculated and compared with each other. In order to investigate the influence of the *L/H*-relation of the building on the partitioning of the building, two different heights of the building are considered (*H*=18m and *H*=6m). The different building heights cover a wide range of possible *L/H*-ratios.
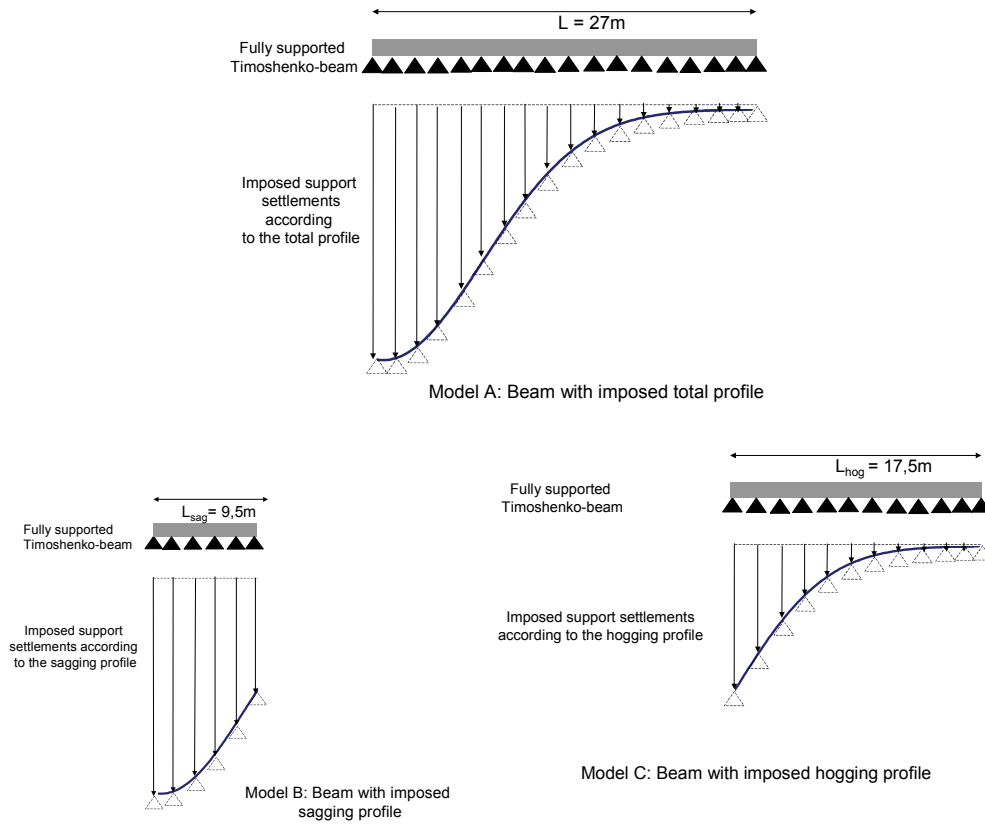
Figure 3.17: Considered numerical Timoshenko beam models

Figure 3.18 shows the results of the numerical calculations in terms of the distribution of moments and shear forces for the building height of 6m and 18m for case 1.

Review

case 1; H=18m

case 1, H=18m
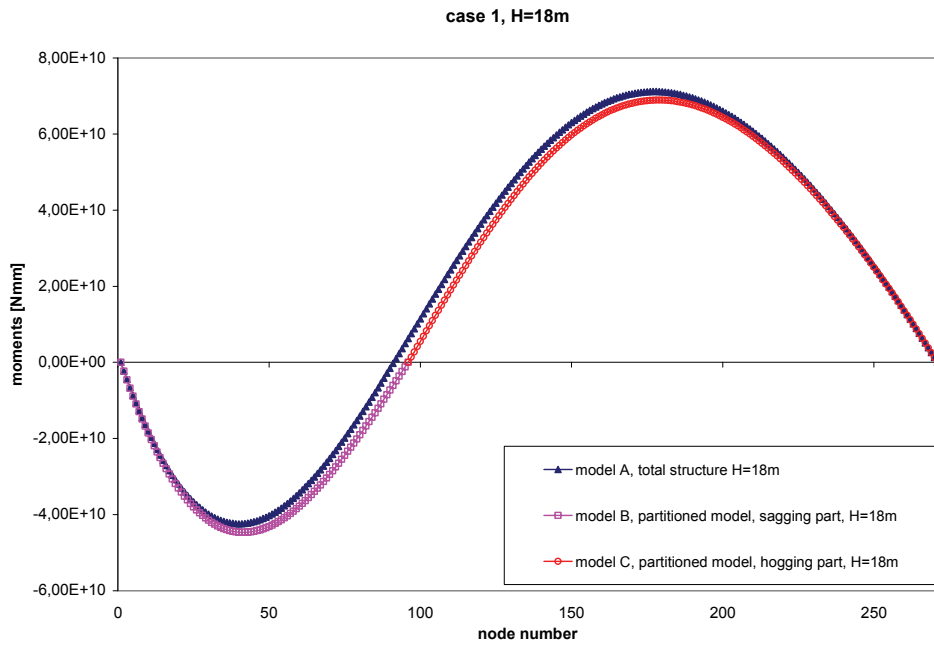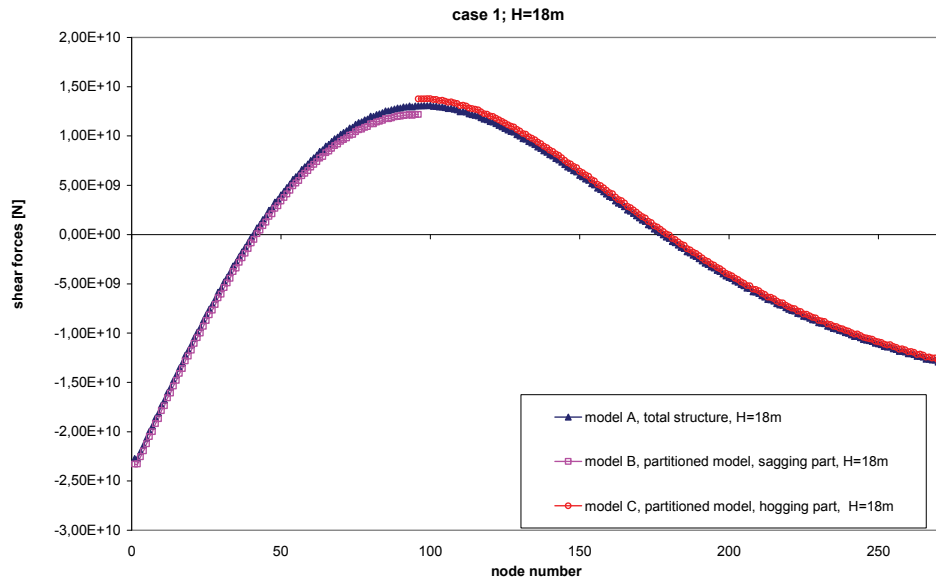
(a) $H_{building}$ = 18m
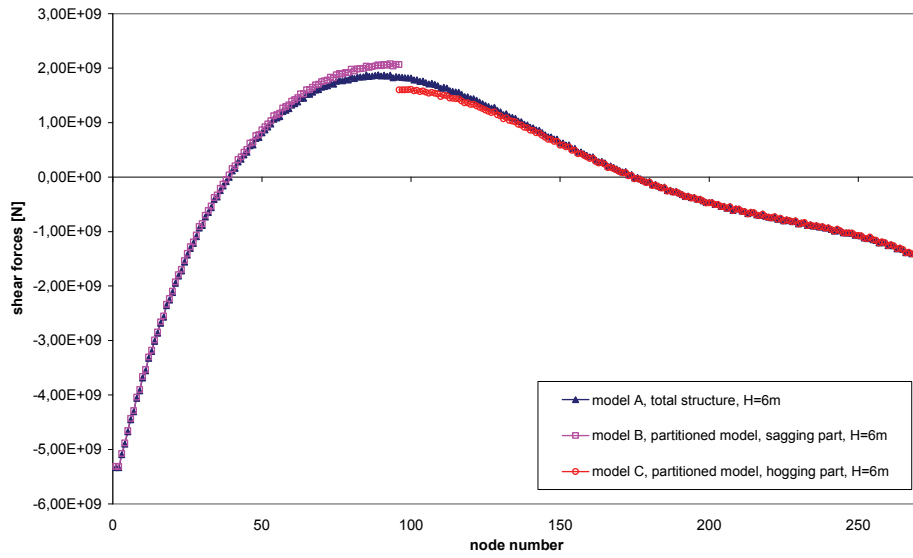
case 1, H=6m

case 1; H=6m
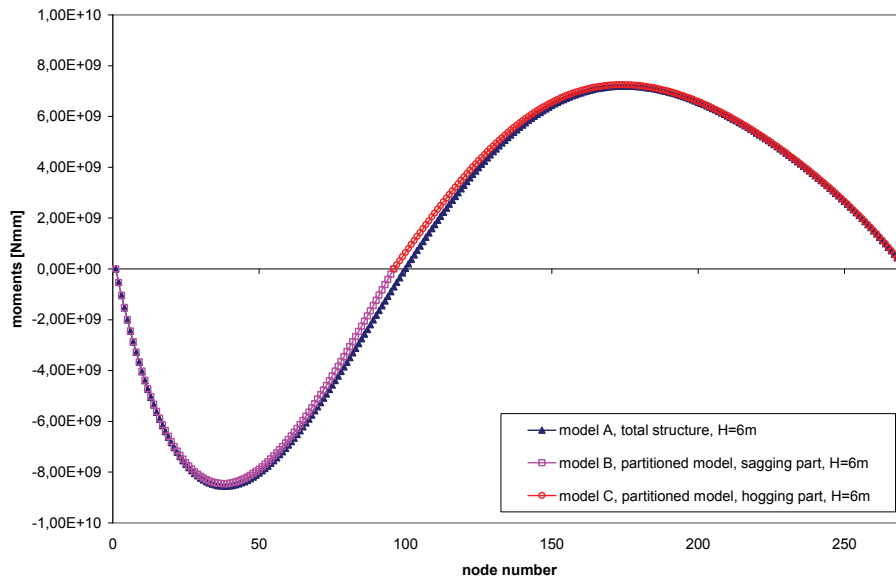
(b) $H_{building}$ = 6m

Figure 3.18: Results of the numerical beam calculations for case 1 (a) $H_{building}$ = 18m and (b) $H_{building}$ = 6m

Small differences are recognized for case 1 and the building height of 18m. The maximum shear forces in the separated models B and C vary between 5% and 7% with the maximum shear forces of model A.

Review

The maximum bending moments in the separated models B and C vary between 3% and 5% with the maximum bending moments of model A.

For the building height of 6m the maximum shear forces in the separated models B and C vary between 10% and 15% with the maximum shear forces of model A. The maximum bending moments in the separated models B and C vary between 0.7% and 1% with the maximum bending moments of model A.

case 2, H=18m

case 2, H=18m
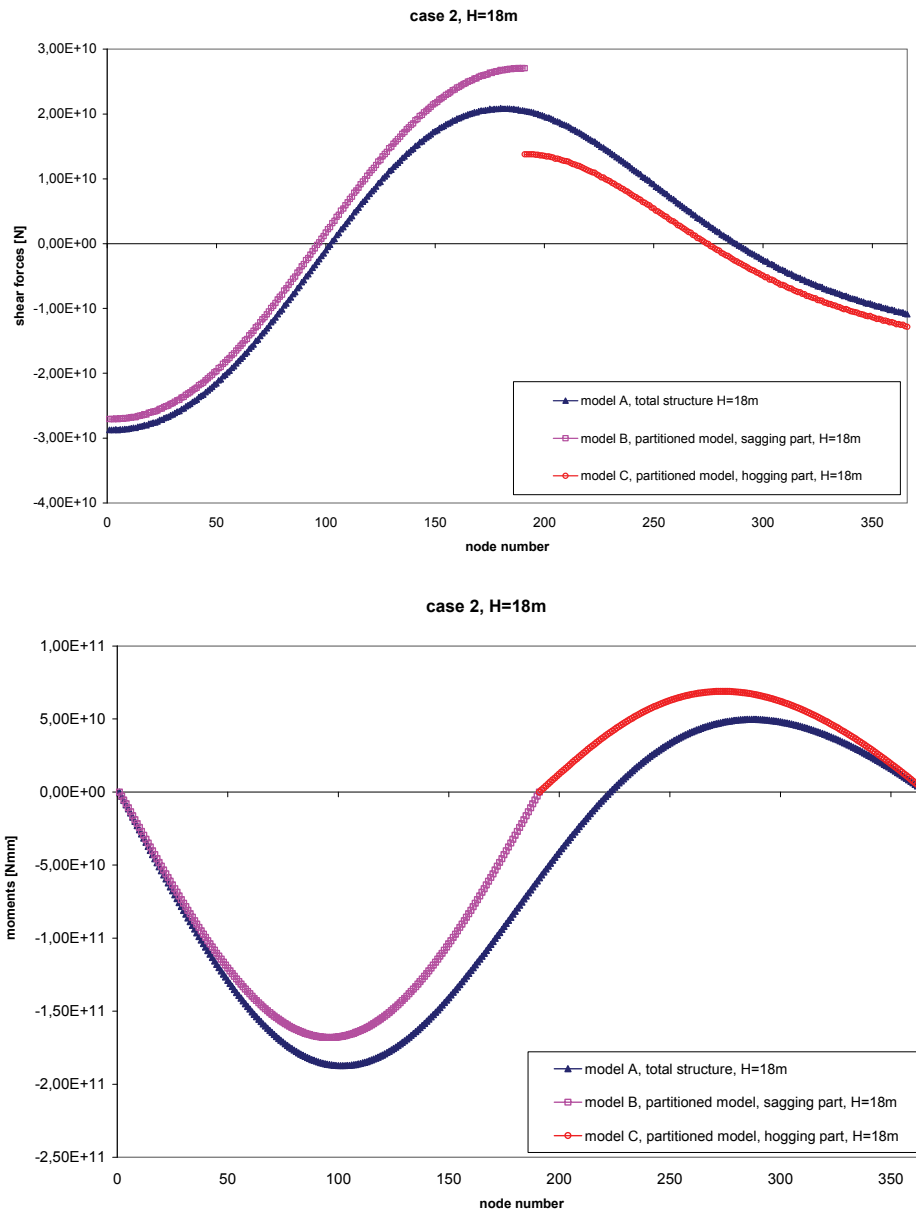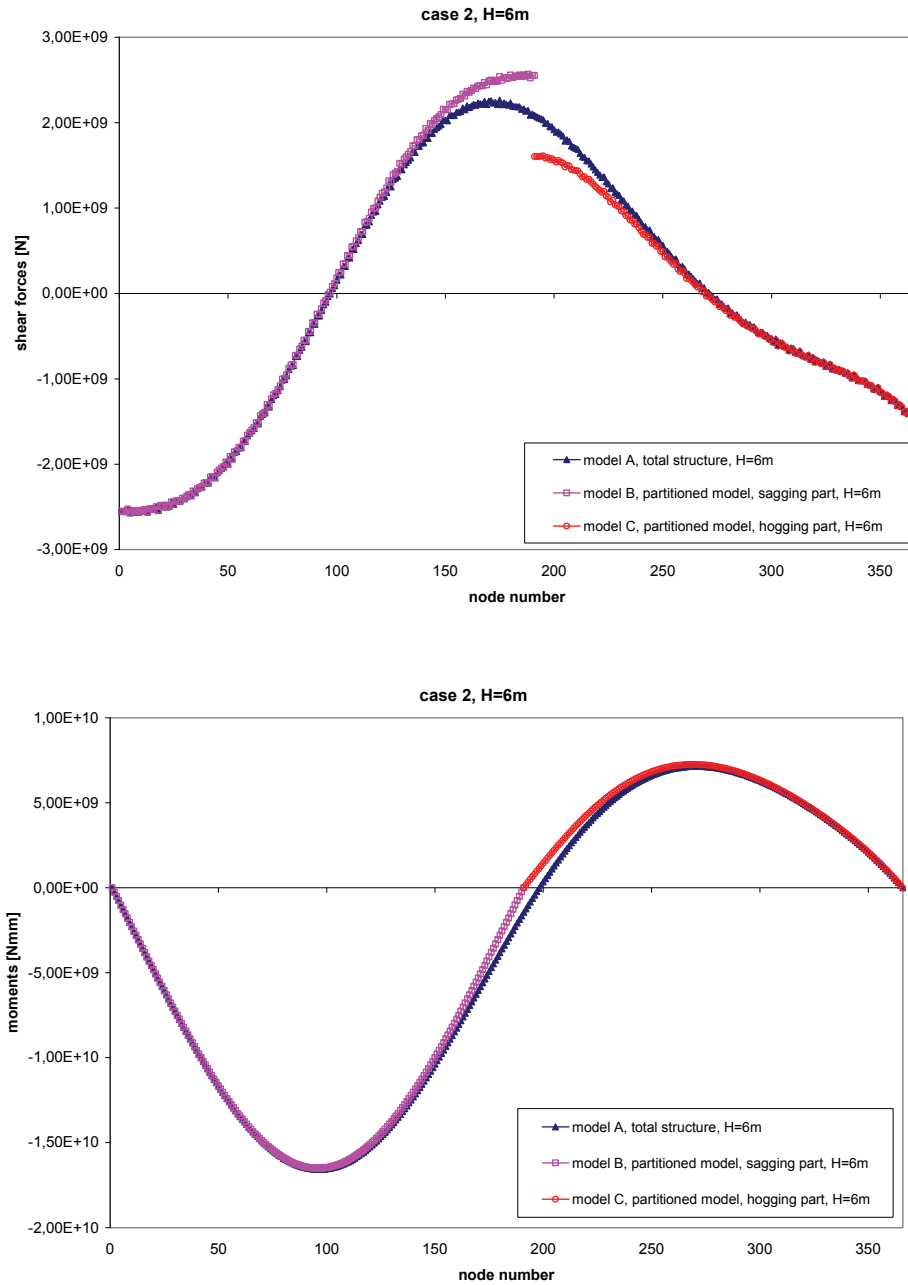
(a) H_{building} = 18m

(b) $H_{building}$ = 6m

Figure 3.19: Results of the numerical beam calculations for case 2 and (a) $H_{building}$ =18m and (b) $H_{building}$ = 6m

Review

The differences in case 2 are significant greater than for case 1. For the building height of 18m the maximum shear forces in the separated models B and C vary between 29% and 49% with the maximum shear forces of model A. The maximum bending moments in the separated models B and C vary between 11% and 38% with the maximum bending moments of model A.
For the building height of 6m the maximum shear forces in the separated models B and C vary between 14% and 31% with the maximum shear forces of model A. The maximum bending moments in the separated models B and C vary between 1% and 1.5% with the maximum bending moments of model A.

The results show, that the partitioning is **not appropriate for case 2**, because the results of the moments and shear forces in the separated hogging and sagging parts differ significantly from the values of the total model.

The differences for **case 1** are small except the deviation of the shear forces for the building height of 6m. The situation for a building height of 6m leads to an underestimation of the shear forces in the separated hogging part with 15%, which is not considered negligible. The difference in tilt values between the separated parts and the total structure for the considered case 1 is 25%. If the difference would be smaller than 25% also the above mentioned underestimation of the shear forces would be reduced further. Without further detailed parametric studies it is suggested to set the limit of the difference in greenfield tilt values between the separated parts and the total structure on 15%. For these initial tilt differences, the deviations of moments and shear forces in the separated parts and the total structure are considered acceptable.
It is therefore recommended to consider the assumption of splitting up a structure in a hogging and a sagging part correct for the concept of the LTSM, **if the tilt values between the total structure and the separated parts vary less than 15%.**

It is shown, that for situations where the tilt values in the hogging, the sagging and the overall structure are significant different, the separation into two apart simply supported beam situations is not appropriate. Additional interaction forces are required between the separated parts to guarantee the compatibility of the entire structure. These additional effects can cause underestimations in the moments and shear forces between the separated parts and the entire structure. To quantify these differences it is recommended to carry out numerical beam calculations if the variation of tilt values for the separated parts and the total structure is greater than 15%.

3.3.4 Angular distortion versus deflection ratio

3.3.4.1 *General*

The significant input parameter in the LTSM method, describing the influence of differential greenfield settlements on the adjacent building, is either expressed in terms of the angular distortion or the deflection ratio (see section 3.2.1 and 3.2.3). This section investigates the influence of the use of these two parameters on the predicted strains and damage in structures with the fictitious beam approach of the LTSM.

The theoretical relation of the two different parameters for a deflection line of a simply supported Timoshenko beam with a central point load is shown in Figure 3.20, dependant of the *L/H*-ratio of the beam. The theoretical derivation of the line shown in this figure is given in Appendix 2.
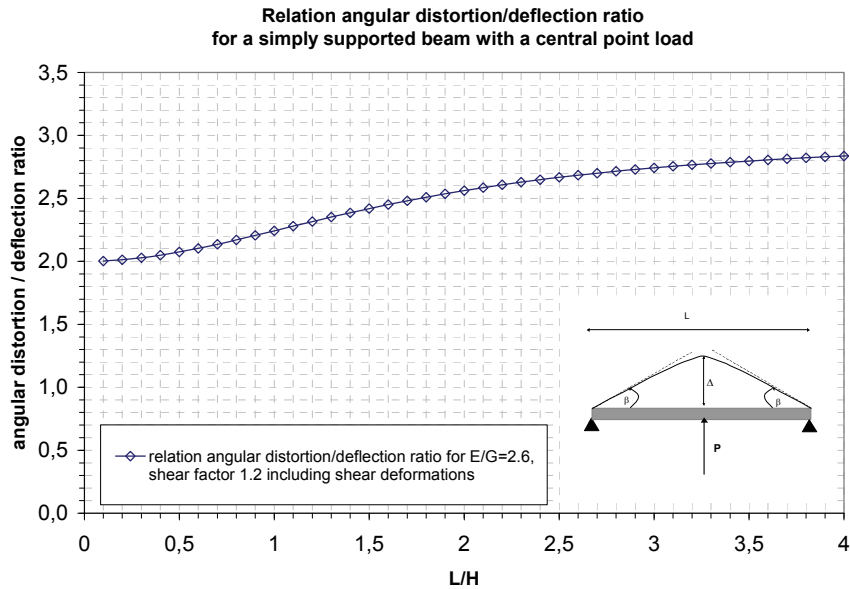
Figure 3.20: Relation of angular distortion to deflection ratio for a beam with a fictitious point load

3.3.4.2 *Angular distortion*

The geometrical determination of the angular distortion for a building in a symmetric greenfield settlement trough is shown in Figure 3.3. By using the LTSM in practical engineering it is recognized, that, dependant on the location of the building in the settlement trough different values for the angular distortions at the outer ends of the building can be derived. That means that the distortion of the building is asymmetric. This is shown in the following examples for buildings in the hogging and the sagging zone of a Gaussian settlement trough due to tunnelling.
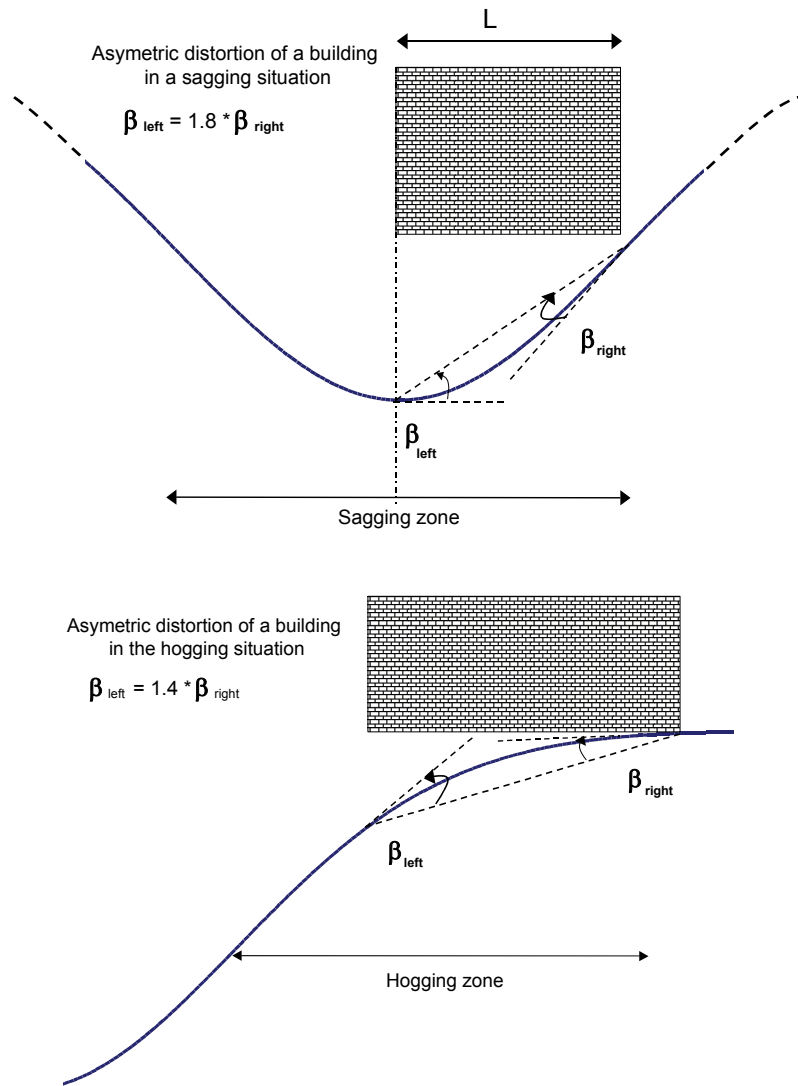
Figure 3.21: Example of asymmetric angular distortions at the outer ends of a building in a Gaussian settlement trough

The first example in Figure 3.21 for the sagging zone shows a relation of $\beta_{left} / \beta_{right}$ of 1.8, or in other words the angular distortion at the left end of the building is 1.8 times larger than the distortion at the right end. The question raises which of the two values should be used as input for the fictitious beam approach in the LTSM or the determination of the strains (see 3.2.1).

This relation between the angular distortions at the outer ends is analysed for various building locations in a Gaussian formed sagging and hogging zone. A design chart is developed using the input factors L, point of inflection i (see section 2.2) and s_{sag}. Their influence on the relation $\beta_{left} / \beta_{right}$ is graphically presented in a normalized design chart. Figure 3.22 is valid for each location of a building in the sagging zone and can be used to directly determine the relation $\beta_{left} / \beta_{right}$. Important input parameter to define the location of the building in the trough is the value s_{sag} (see Figure 3.22(a)). The value for s_{sag}

and the length L of the building have to be expressed in terms of i for use in the design charts (Figure 3.22(b)).
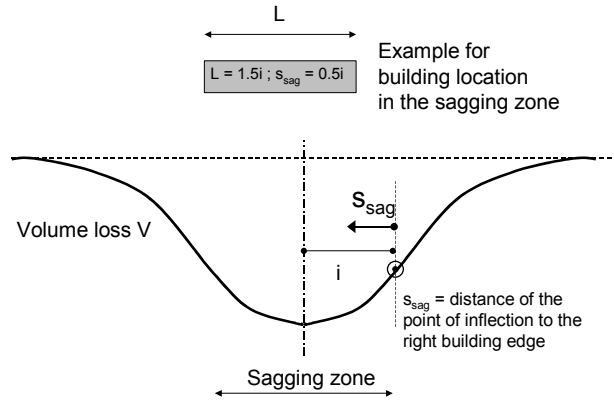
(a) determination of s_{sag}
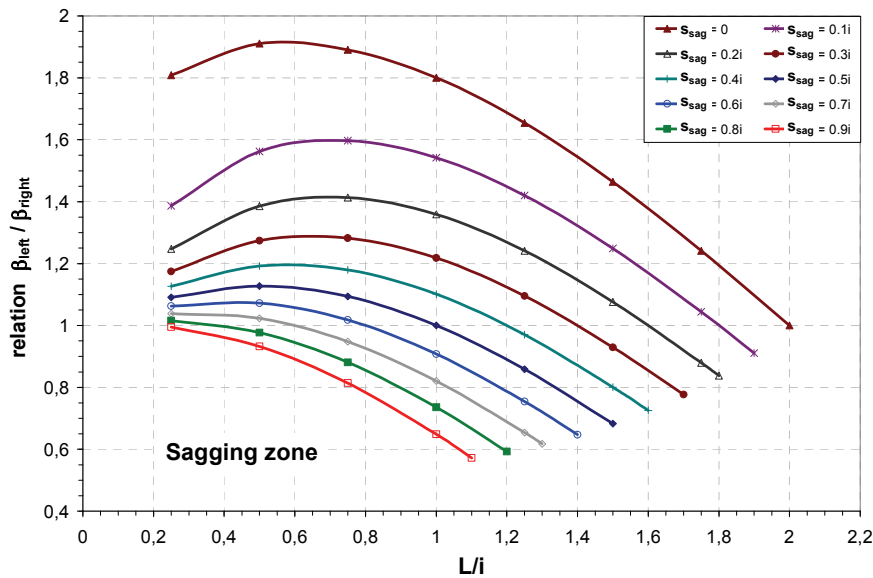
(b) design chart for determination of $\beta_{left}/\beta_{right}$ for an arbitrary location of the building in the sagging zone

Figure 3.22: Determination of the relation $\beta_{left}/\beta_{right}$ in the sagging zone of a Gaussian formed trough due to tunnelling

Figure 3.22(b) shows for example that for a building of $L/i = 2$, that means a building which covers the entire sagging trough, the relation of $\beta_{left}/\beta_{right}$ is 1 representing a symmetric sagging situation of the building.

The design chart in Figure 3.23 is developed for a variable location and length of a building in the hogging zone. The chart can be used to directly determine the relation $\beta_{left}/\beta_{right}$. Important input parameter to define the location of the building in the hogging zone of the trough is the value s_{hog} (see Figure 3.23 (a)). The value for s_{hog} and the length L of the building have to be expressed in terms of i for use in the design charts (Figure 3.23 (b)).
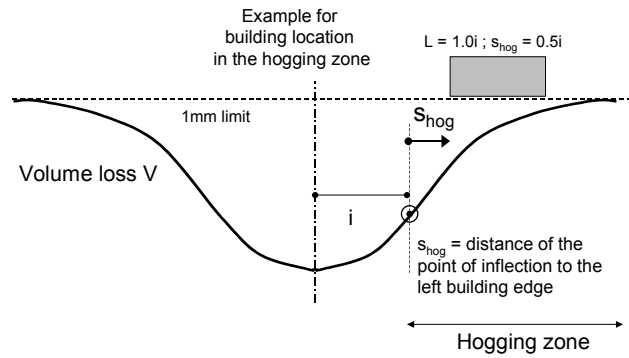
(a) determination of s_{hog}
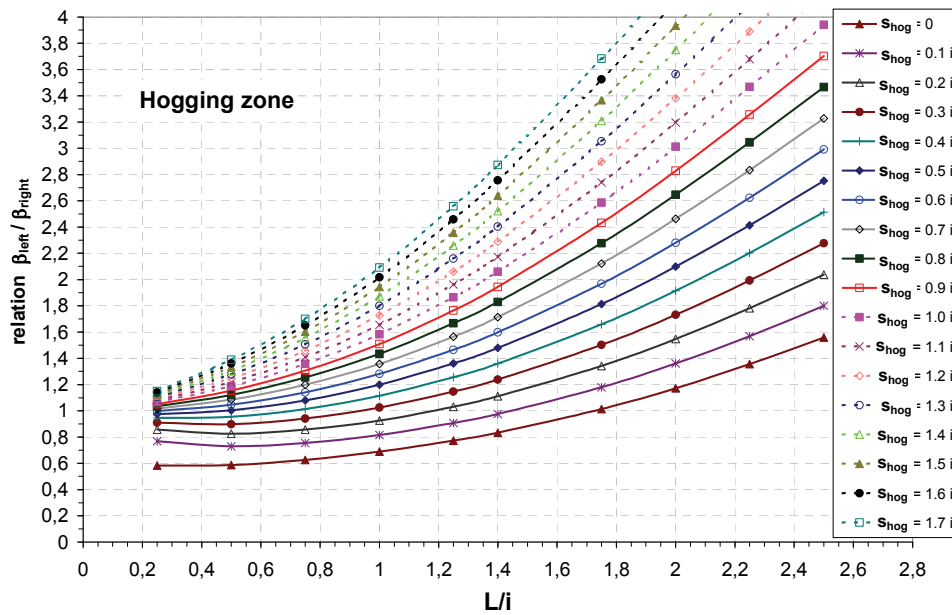
(b) design chart for determination of $\beta_{left}/\beta_{right}$ for an arbitrary location of the building in the hogging zone

Figure 3.23: Determination of the relation $\beta_{left}/\beta_{right}$ in the hogging zone of a Gaussian formed trough due to tunnelling

Design charts to determine the absolute values β_{left} or β_{right} and the average value $\beta_{average}$ (equal to ($\beta_{left +}$ β_{right}) / 2), depending on the location of a building in a Gaussian trough are given in Appendix 3.

3.3.4.3   Deflection ratio

The deflection ratio is defined as the maximum vertical deflection between the tilt line of the building and the imposed settlement curve, divided by the length of the building L. It is noted, that the difference between the vertical deflection component (Δ) and the deflection component perpendicular to the tilt line (Δ_l) is negligible for practical values of the tilt (see Figure 3.24). It is therefore appropriate to use Δ for the correct determination of the deflection ratio.
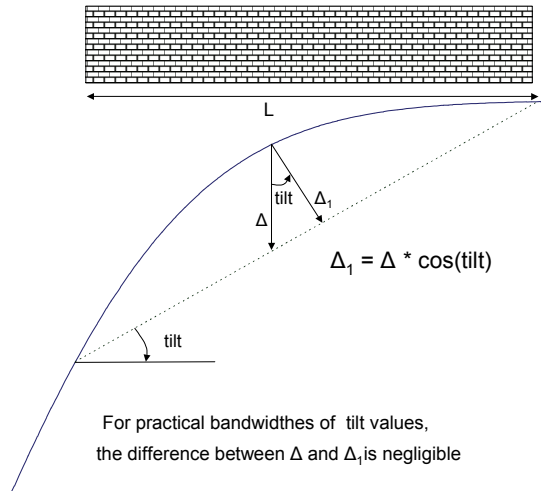
Figure 3.24: Deflection ratio

Figure 3.25 shows the design chart, which is developed to determine the deflection ratio in the sagging zone for a Gaussian formed settlement trough. Input parameters are the volume loss V, the point of inflection i, the tunnel diameter D, the building length L and the positional factor s_{sag} (see Figure 3.22(a)).
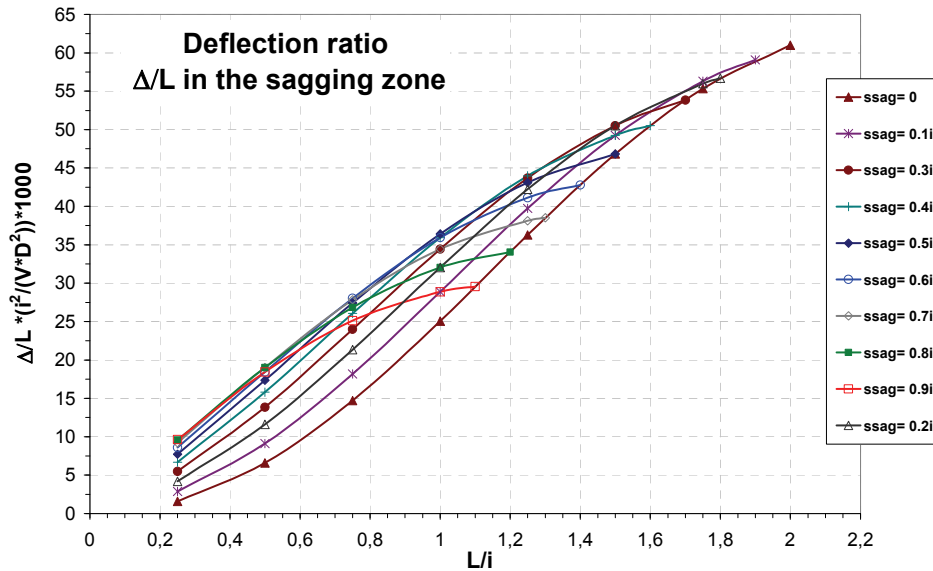
Figure 3.25: Design chart for the deflection ratio of a Gaussian formed trough in the sagging zone

Figure 3.26 shows the design chart which is developed to determine the deflection ratio in the hogging zone for a Gaussian formed settlement rough. Input parameters are the volume loss V, the point of inflection i, the tunnel diameter D, the building length L and s_{hog} (see Figure 3.23(a)).
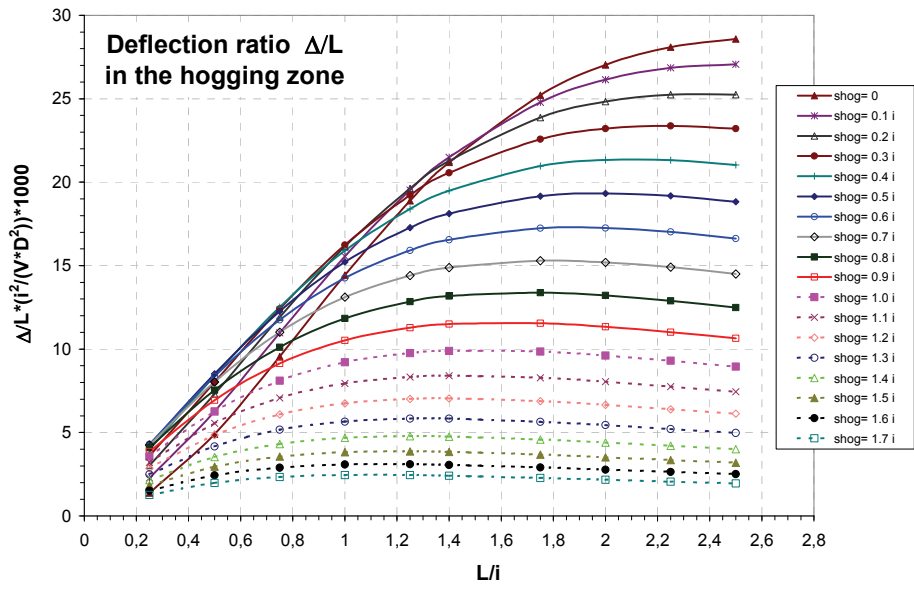
Figure 3.26: Design chart for the determination of the deflection ratio for a Gaussian formed trough in the hogging zone

3.3.4.4 Influence of the use of the deflection ratio or the angular distortion on the tensile strains

3.3.4.5 Principles of the analyses

To investigate the influence of the use of the deflection ratio and the angular distortion respectively different situations of buildings in the sagging and the hogging zone are considered. The principle of the analyses is schematised in Figure 3.27 for the example of a building undergoing an asymmetric distortion in the sagging zone.
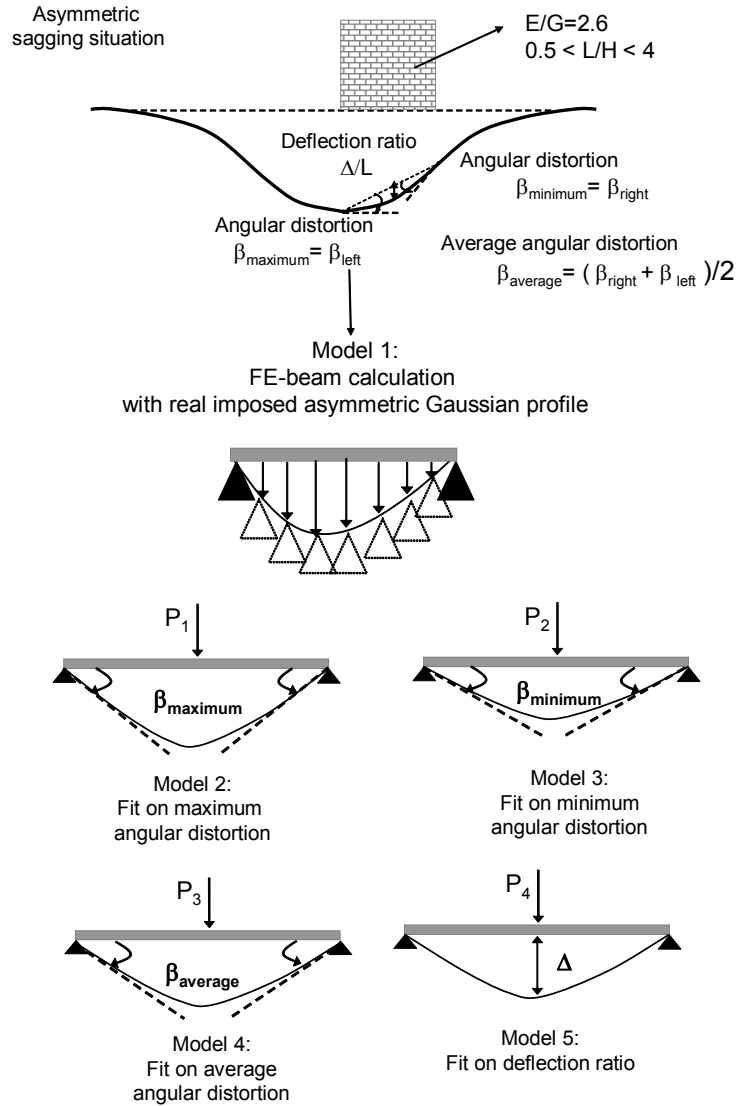
Figure 3.27: Principle of the analyses at the example of the asymmetric sagging zone situation

Review

Different numerical beam calculations are carried out to quantify the influence of the damage criteria on the calculation of the tensile strains. The numerical beam calculations with the fully imposed Gaussian deflection profile (model 1 in Figure 3.27) is used as reference as it represents the correct strains in the beam for the real imposed Gaussian deflections. The tensile strains calculated from model 1 are consequently compared to the tensile strains calculated with the LTSM and the fictitious point load approach with the fit on the maximum angular distortion (model 2), the minimum angular distortion (model 3), the average angular distortion (model 4) and the deflection ratio (model 5). Modification factors are derived representing the relations of the tensile strains of the models 2 to 5 versus those of the reference model 1. Thus for example:

$$\text{modification factor (model 2)} = \frac{\text{tensile strain model 2}}{\text{tensile strain reference model 1}}$$

A modification factor >1 for example means that the fictitious point load approach overestimates the correct strains from model 1.

It is distinguished between sagging and hogging cases, symmetric and asymmetric situations and different L/H-ratio's to cover a wide range of possible situations. The example of a symmetric situation in the sagging zone is shown in Figure 3.28. It is emphasized, that for the symmetric situation only three models have to be considered, because the angular distortion is symmetric.
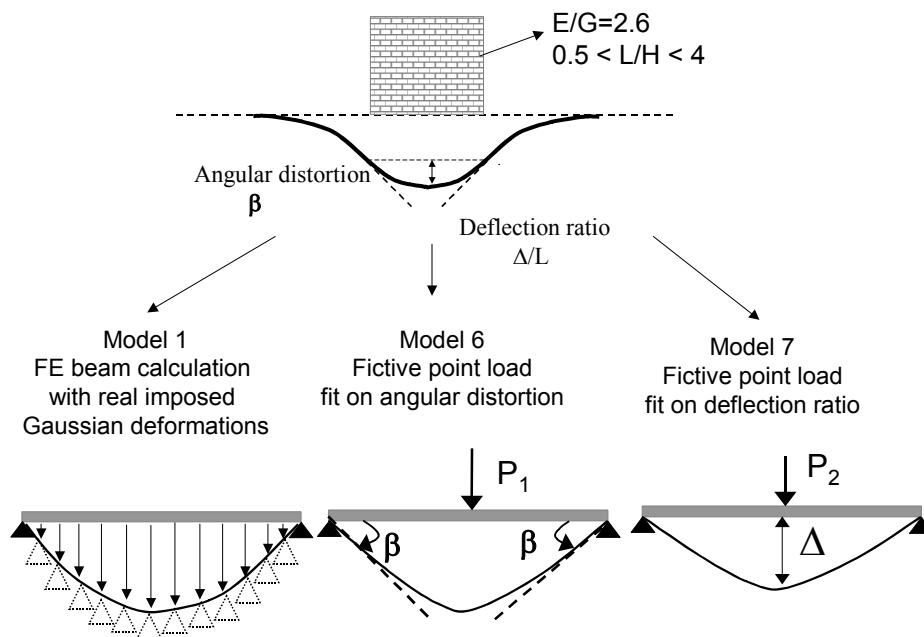
Figure 3.28: Principle of the analyses for the example of the symmetric sagging zone situation

3.3.4.6   Results for the symmetric sagging situation

For the symmetric sagging situation the building is located symmetrically in the sagging zone according to Figure 3.28. The tensile strains of model 6 and 7 are calculated with the LTSM for different L/H-ratio's. The results for the modification factors for the symmetric sagging situation are shown in Figure 3.29 and Figure 3.30. It is distinguished between the influence on the bending strains and the diagonal strains.

Diagonal strain
for the symmetric sagging situation (β_{max}/β_{min} =1)
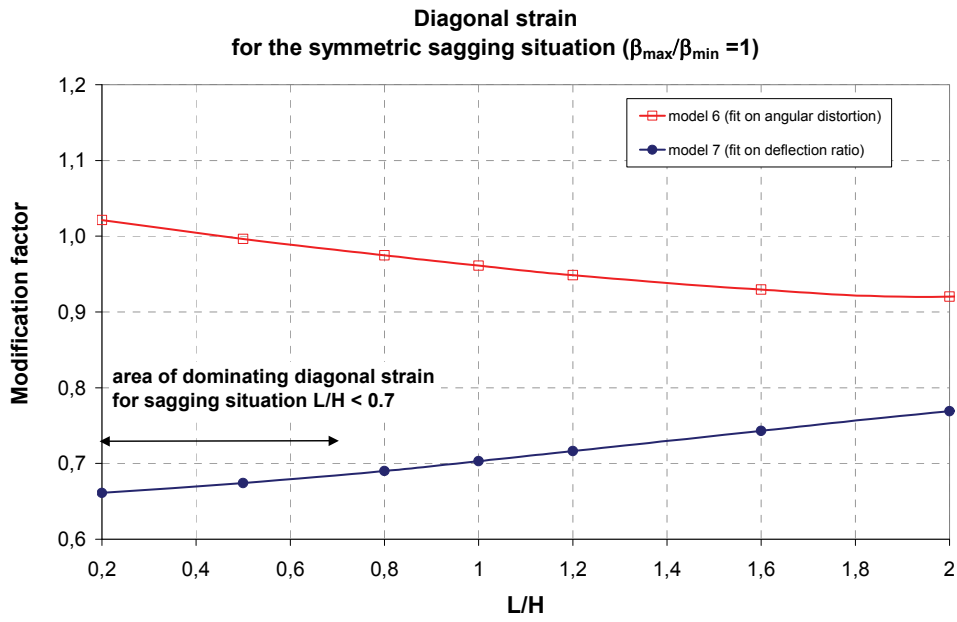
Figure 3.29: Modification factors for the diagonal strains in a symmetric sagging zone situation

Bending strain
for a symmetric sagging situation (β_{max}/β_{min}=1)

Figure 3.30: Modification factors for the bending strains in a symmetric sagging zone situation

Figure 3.29 shows that the use of the deflection ratio as fitting parameter for the fictitious point load (model 7) leads to a significant underestimation of the *diagonal strains* compared to model 1. The

difference is up to 35%. The angular distortion fit shows however a very good agreement with a negligible differences of circa ± 3% for the diagonal strains in the dominant *L/H*-area up to 0.7 (see Figure 3.29).

The ***bending strains*** in Figure 3.30 show other effects. The deflection ratio leads to an overestimation of the tensile bending strains from 2 to 18% for the relevant *L/H*-ratio's > 0.7. The angular distortion fit however overestimates the bending strains between 30 and 50%, see Figure 3.30.

In can be concluded that for the situation in the symmetric sagging zone the angular distortion should be used to determine the diagonal strains and the deflection ratio should be used to determine the bending strains. The use of ***one*** damage parameter for both strains leads to significant under-and/or overestimations of the strains.

3.3.4.7   *Asymmetric sagging situation*

As mentioned in section 3.3.4.2, the value for the angular distortion derived from a Gaussian profile is not straightforward, because different values can occur at the outer ends for an asymmetric situation. Figure 3.31 and Figure 3.32 show four modification lines (for the models 2 to 5 according to Figure 3.27), taking into account the deflection ratio fit and the fit on the maximum, minimum and the average value for the angular distortion for the example of an asymmetric sagging situation (with the relation of $\beta_{maximum} / \beta_{minimum} = 1.8$).
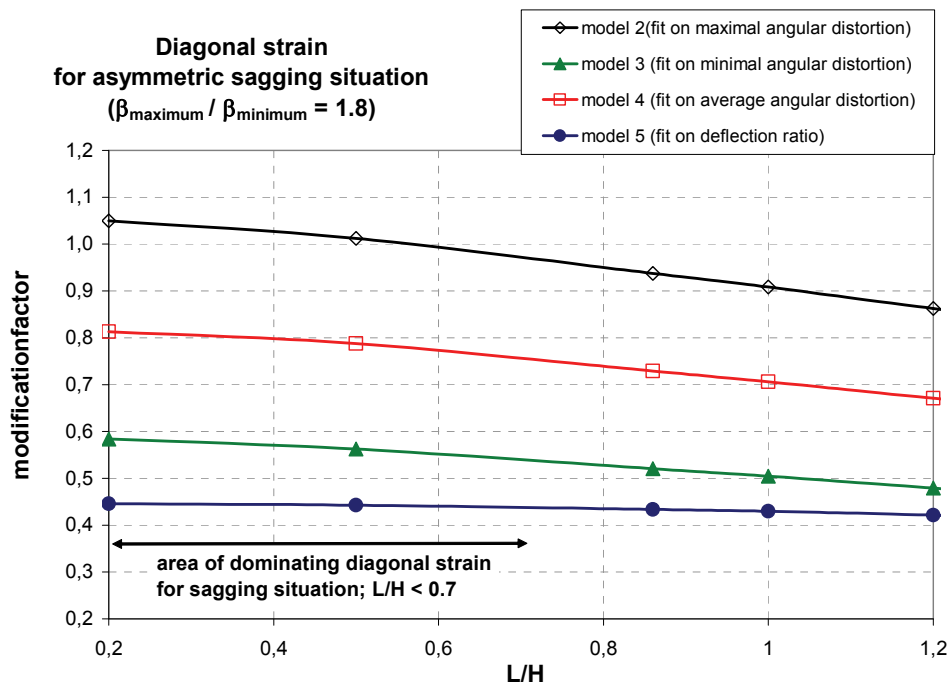
Figure 3.31: Modificationfactor for the diagonal strains in an asymmetric sagging situation
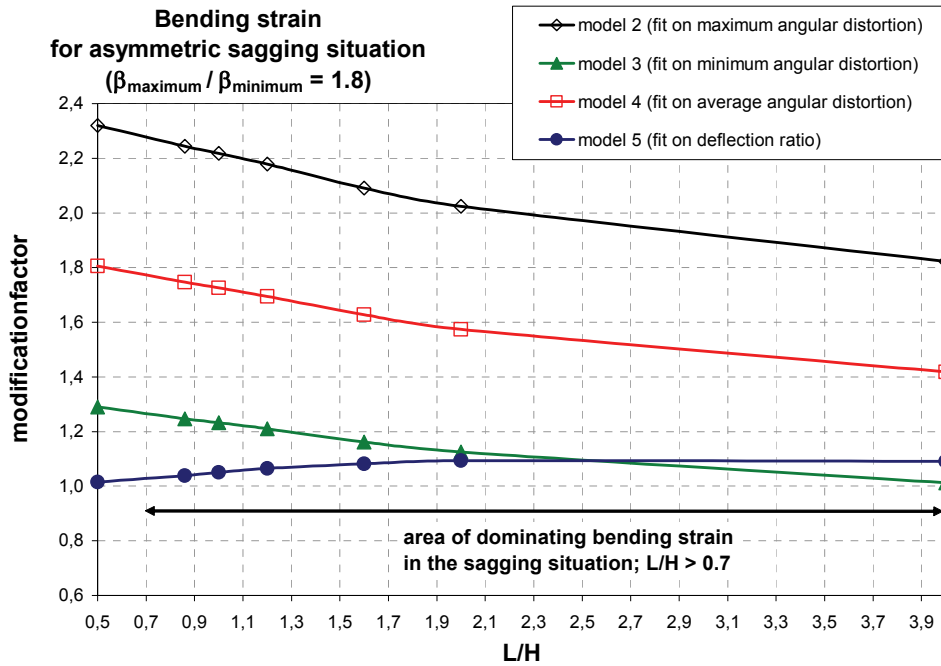
Figure 3.32: Modification factor for the bending strains in an asymmetric sagging situation

Figure 3.31 shows that the use of the deflection ratio as fitting parameter for the fictitious point load (model 5) leads to a significant underestimation of the *diagonal strains* of model 1 up to 55%. The fit on the maximum angular distortion (model 2) shows however a very good agreement with negligible differences of circa ± 3% with model 1 for the diagonal strains in the dominant *L/H*-area up to 0.7.

The ***bending strains*** in Figure 3.32 show other effects. The deflection ratio fit (model 5) leads to a good agreement with model 1 resulting in a slight overestimation of the tensile bending strains up to ca. 10% (dependant of the *L/H*-ratio). The fit on the maximum angular distortion (model 2) however overestimates the bending strains up to ca. 120%.

It can be concluded that for the situation in the asymmetric sagging zone the maximum angular distortion should be used to determine the diagonal strains and the deflection ratio should be used to determine the bending strains. The use of ***one*** damage parameter for both strains leads to significant under-and/or overestimations of the strains.

3.3.4.8   Symmetric hogging situation

The analyses for the hogging zone are carried out according to the same principle as for the sagging zone (see Figure 3.27 and Figure 3.28), but with hogging formed Gaussian deflection profiles. The LTSM assumption of the neutral axis at the bottom of structure is used for the calculation of the strains with the fictitious point load approach and the FE-beam calculations (model 1).
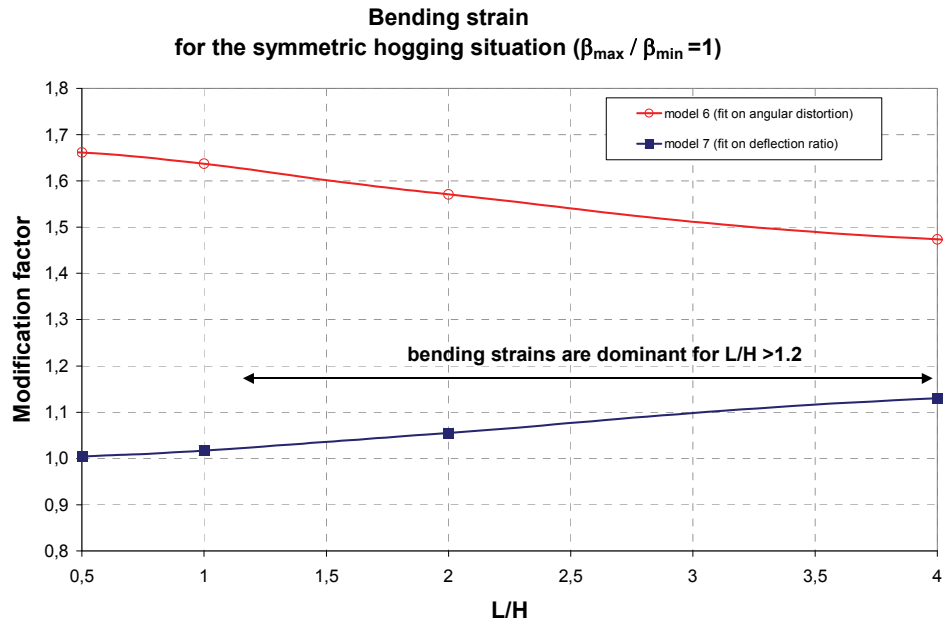
Figure 3.33: Modification factors for the bending strains in a symmetric hogging situation
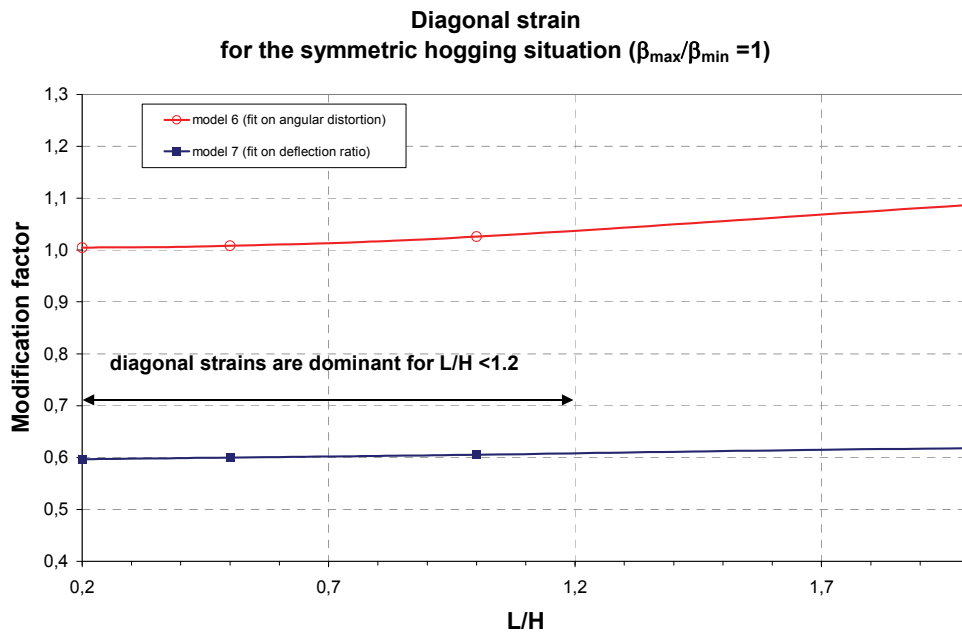
Figure 3.34: Modification factors for the diagonal strains in a symmetric hogging situation

Figure 3.34 shows that the use of the deflection ratio as fitting parameter for the fictitious point load (model 3) leads to a significant underestimation of the *diagonal strains* of model 1 up to 40%. The angular distortion fit shows however a very good agreement with a negligible difference of circa $\pm$ 4% for the diagonal strains (in the dominant *L/H*-area up to 1.2).
The **bending strains** in Figure 3.33 show other effects. The deflection ratio leads to an overestimation of the tensile bending strains from up to 12% (dependant of the *L/H*-ratio). The angular distortion fit however overestimates the bending strains between 50 and 65%.

In can be concluded that for the situation in the symmetric hogging zone the angular distortion should be used to determine the diagonal strains and the deflection ratio should be used to determine the bending strains. The use of *one* damage parameter for both strains leads to significant under-and/or overestimations of the strains.

3.3.4.9 *Asymmetric hogging situation*

In contrast to section 3.3.4.7 for the asymmetric sagging situation it is noted, that only the results for the modification factors for model 2 (fit on maximum angular distortion) and model 5 (fit on deflection ratio) are presented in Figure 3.35 and Figure 3.36. These two fits are dominant, see conclusions for the asymmetric sagging zone in section 3.3.4.7.
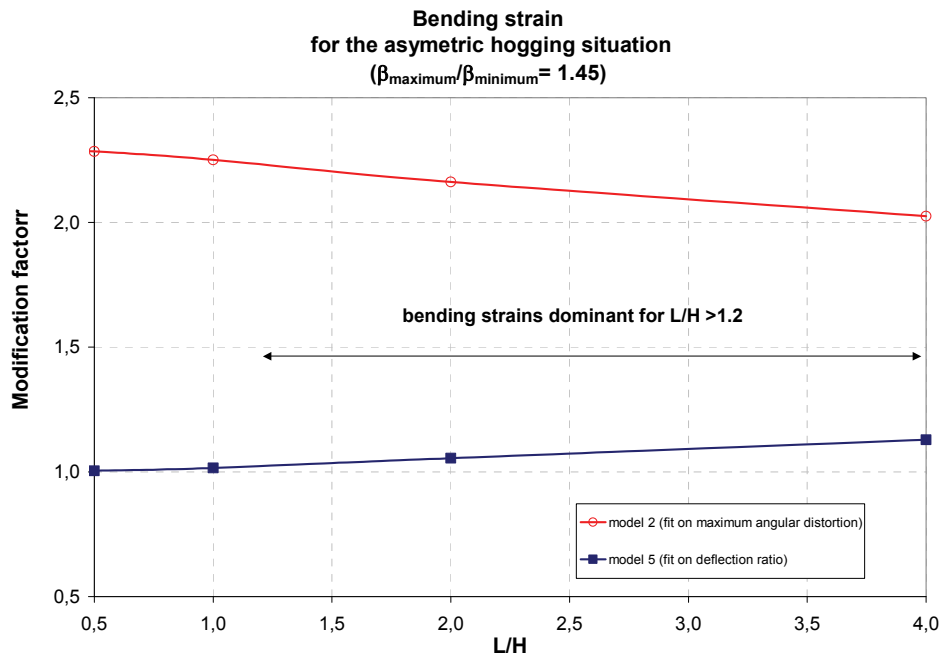
Figure 3.35: Modification factors for the bending strains in a asymmetric hogging situation

**Diagonal strains
for the asymmetric hogging situation
($\beta_{maximum}$ / $\beta_{minimum}$ = 1.45)**

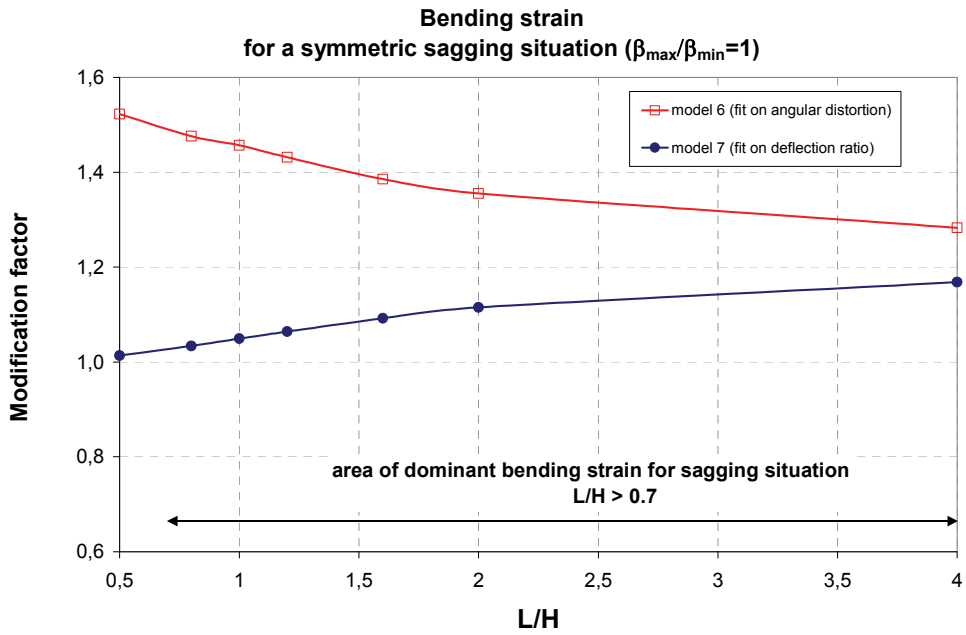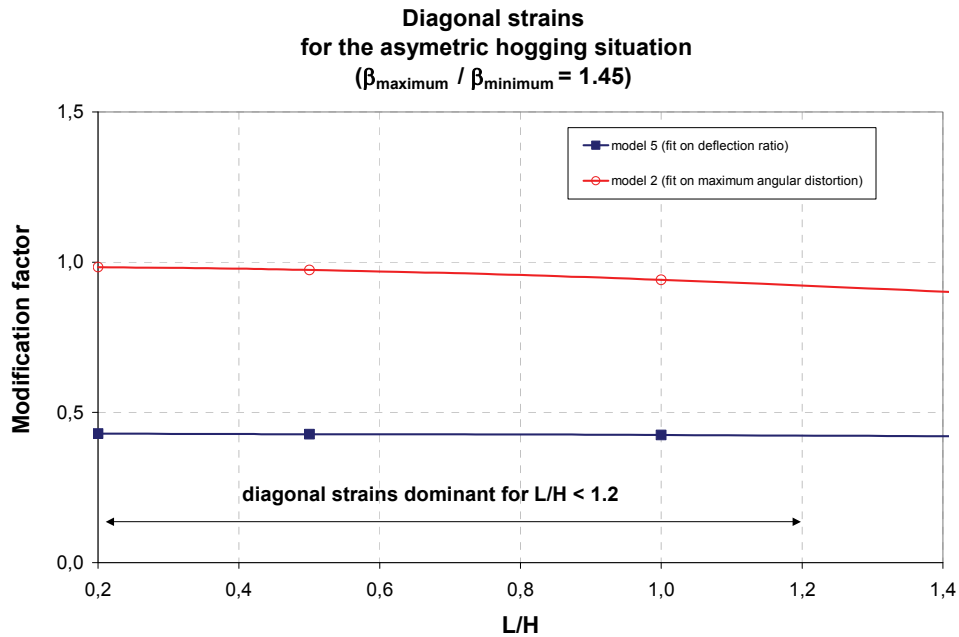**Figure 3.36: Modification factors for the diagonal strains in an asymmetric hogging situation**

Figure 3.36 shows that the use of the deflection ratio as fitting parameter for the fictitious point load (model 5) leads to a significant underestimation of the *diagonal strains* of model 1 up to 60%. The fit on the maximum angular distortion (model 2) shows however a very good agreement with negligible differences of circa ± 5% with model 1 for the diagonal strains (in the dominant *L/H*-area up to 1.2).

The **bending strains** in Figure 3.35 show other effects. The deflection ratio fit (model 5) leads to a good agreement with model 1 resulting in a slight overestimation of the tensile bending strains up to ca. 15% (dependant of the *L/H*-ratio). The fit on the maximum angular distortion (model 2) however overestimates the bending strains up to 130%.

In can be concluded that for the situation in the asymmetric hogging zone the maximum angular distortion should be used to determine the diagonal strains and the deflection ratio should be used to determine the bending strains. The use of **one** damage parameter for both strains can lead to significant under-and/or overestimations of the strains.

3.3.4.10   Conclusions

The influence of using either the angular distortion or the deflection ratio as input parameter for the calculation of the tensile strains according to the LTSM has been investigated and the following conclusions can be drawn:

- Depending on the location of a building in a Gaussian formed settlement trough, significant differences in the values of the angular distortions at the outer ends of the building can occur. The angular distortion is therefore not a clear defined parameter and considered not straightforward.
- The use of the deflection ratio as damage parameter in the LTSM can lead to a significant underestimation of the **diagonal strains** of Gaussian formed settlement profiles, up to 60%.

- The use of the maximum angular distortion at the location of the building in the LTSM can lead to a significant overestimation of the **bending strains** of Gaussian formed settlement profiles, up to 130%.
- The author strongly recommends to use the maximum angular distortion for the determination of the diagonal tensile strains and the deflection ratio to determine the bending tensile strains with the LTSM for **Gaussian formed settlement profiles**. This approach leads to correct determination of the tensile strains with the fictitious point load approach of the LTSM within practical acceptable bandwidths.

The above given results of the investigations and the recommendations can be qualitatively explained by the fact that the deflection ratio for the point load approach gives the best match of the bending distortion of the beam at the mid cross section, thus at the same location where also the maximum bending strains occur. The angular distortion for the point load is shown to be the appropriate parameter for determination of the diagonal strains with the LTSM beam approach.

3.3.5   Hogging versus sagging zone

3.3.5.1   General

It is generally considered that hogging mode deformations are more severe for building damage than sagging deformations. This phenomena is born out in practice based on empirical observations by Burland et al. (1974, 2001) and Boscardin et al. (1989). For the prediction of building damage with the LTSM the authors therefore suggested to assume different locations of the neutral axis in the beam for the hogging and the sagging zone respectively. It is emphasized, as already mentioned in section 3.2.1., that this approach is only a fictitious assumption and has no relevance or background in static's or beam theory.

It should be emphasized that it is important to consider the combination of vertical and horizontal ground movement effects carefully in the explanation of the higher hogging sensitivity for damage. Gaussian formed ground movements due to tunnelling will for example in general cause horizontal tensile strains in the hogging zone whereas in the sagging zone horizontal compressive strains develop (see explanations in section 3.2.1). This section therefore distinguishes between a consideration of vertical ground deformations only and the combination of horizontal and vertical ground deformations on the results for the strains and damage for different assumptions for the locations of the neutral axis.

The objective of this section is to analyse the influence of the assumption of the location of the neutral axis on the calculated strains with the LTSM.

3.3.5.2   The influence of the location of the neutral axis for only differential vertical settlements

The differences in the strain distributions for the neutral axis at the centre of the beam or the empirical based assumption of the neutral axis at the bottom of the beam in the sagging and the hogging zone respectively are schematically shown in Figure 3.37. It is emphasized that Figure 3.37 shows the effect of the neutral axis location for only vertical differential settlements.
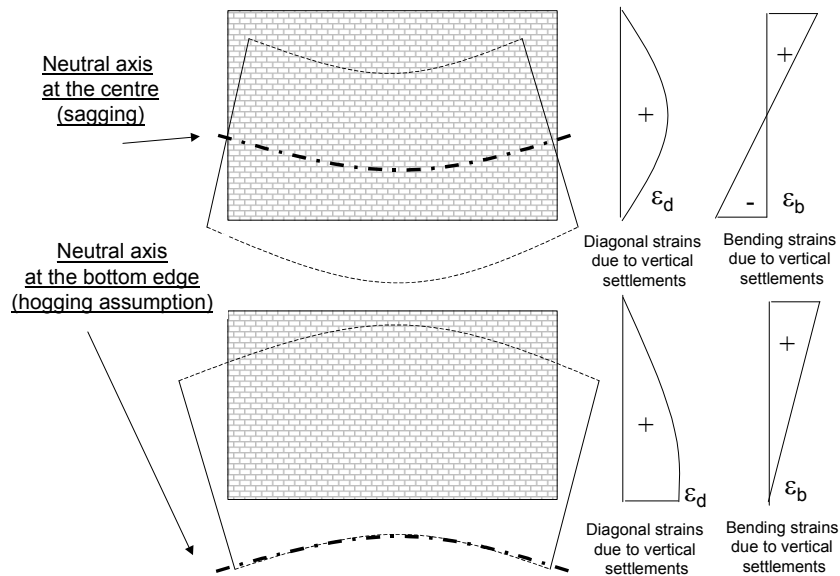
Figure 3.37: Strain distributions for different locations of the neutral axis and vertical differential settlements only

The differences of the magnitudes of the bending strains ε_b and the diagonal strains ε_d normalized with the imposed deflection ratio for the sagging and the hogging model are shown in Figure 3.38 and Figure 3.39. The results are calculated for the shear form factor of 1.2 (see section 3.3.1) and an *E/G*-value of 2.6. A wide range of *L/H*-values is considered.

Figure 3.38 shows the difference in bending strains calculated with the LTSM for the hogging and the sagging approach for *L/H* factors from 0.1 to 10. The vertical axis gives the bending strains normalized with the imposed deflection ratio.
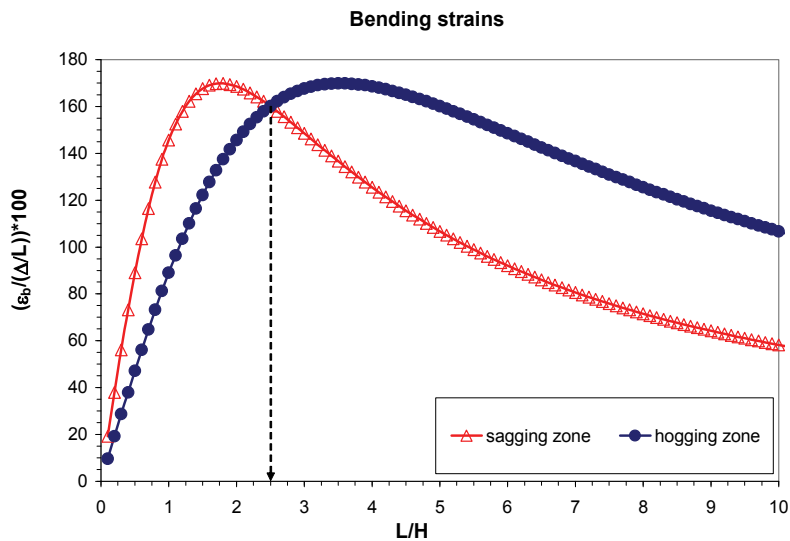
Figure 3.38: Difference of bending strains for the hogging and sagging approach

Review

It can be concluded, that for *L/H*-values up to 2.5 the bending strains for the hogging zone are smaller than for the sagging zone, which means, that with the assumption of the neutral axis at the lower edge of the beam for the hogging model, the LTSM approach predicts lower bending strains and thus less damage than for the sagging model, which is in contrast to the general assumption that the hogging deformation mode is always considered more susceptible to damage. For *L/H*-values larger than 2.5 the hogging bending strains are larger than for the sagging zone, which corresponds with the empirical statement that hogging deformation is more harmful than sagging deformation.

Figure 3.39 shows the results of the calculation of the diagonal strains for the hogging and the sagging approach.
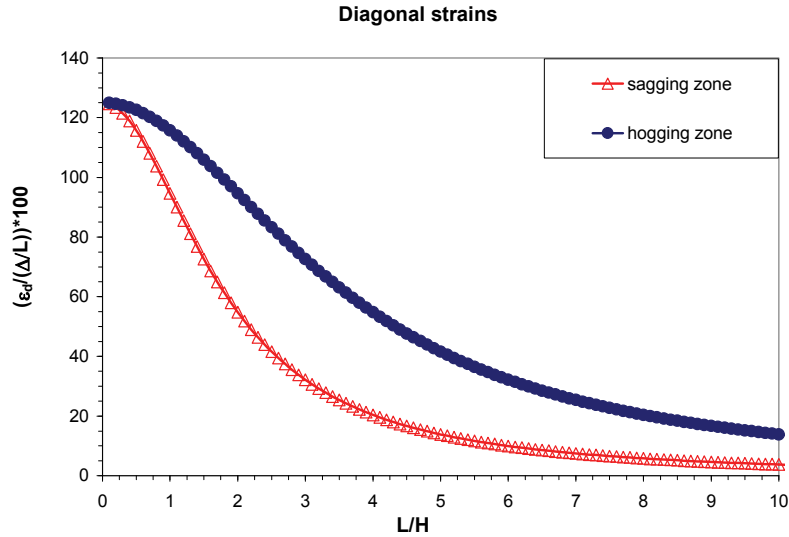
Figure 3.39: Difference of diagonal strains for the hogging and sagging approach

It can be concluded, that for all *L/H* values the hogging approach gives higher diagonal strains which corresponds with the empirical statement that hogging deformation is more harmful than sagging deformation.

Combination of Figure 3.38 and Figure 3.39 derives the dominant strain shown in Figure 3.40. The dominant strain is the maximum value of the bending or the diagonal strain for each *L/H* value and is used for the final damage classification.

Dominant tensile strains
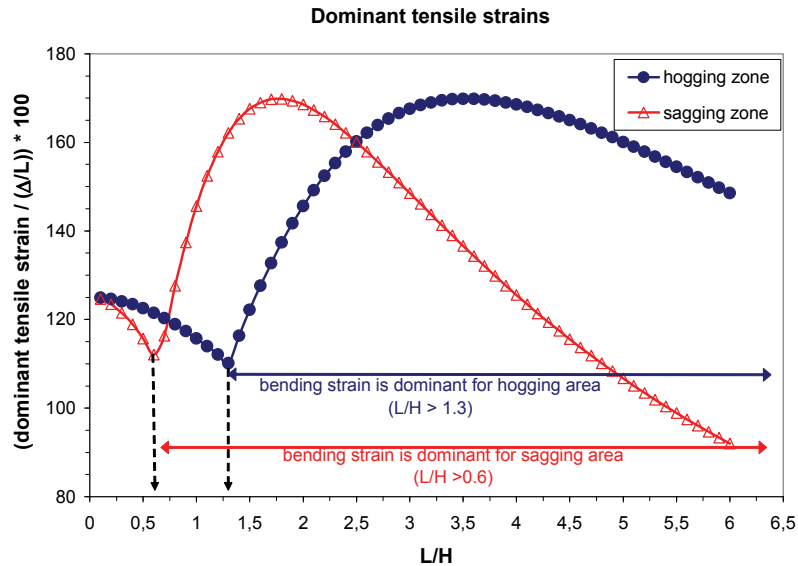
Figure 3.40: Differences of dominant total strains for the hogging and the sagging zone

Figure 3.40 shows that for the hogging zone the bending strain is dominant for *L/H*-values greater than 1.3. For the sagging zone the bending strains become dominant for *L/H*-values greater than 0.6. This means, that the hogging approach leads to a horizontal shift of the threshold where bending and diagonal strain become dominant.

Considering the absolute dominant strains it is recognized, that in the *L/H*-range between 0.75 and 2.5, the absolute dominant strains for the sagging approach are larger than for the hogging approach. This means, that the analytical approach of the LTSM for a building in a hogging zone does not lead to more severe damage susceptibility than a building in the sagging zone for the practical range of *L/H* between 0.75 en 2.5, *if only the effect of vertical settlements is considered*. For all other *L/H*-ratio's the assumption for the neutral axis at the bottom edge and the resulting strain calculated with the LTSM however reflects the higher damage sensitivity of the hogging mode.

3.3.5.3 *The influence of the location of the neutral axis for differential vertical and horizontal ground movements*

Considering the combination of vertical differential movements and horizontal tensile ground strains in the hogging zone (see Figure 3.41), the assumption of the neutral axis at the bottom edge of the wall causes central tension over the entire height of the beam due to the horizontal tensile forces induced by the tensile ground strains at the bottom of the wall. If the neutral axis would be situated at the centre of the wall, the horizontal forces induced by the transfer of horizontal ground strains at the bottom edge of the wall would cause an eccentric moment, leading to a compression of the top edge of the wall. This compression consequently reduces the tensile strains at the top edge of the wall, which are induced by the vertical hogging mode deformations. If the neutral axis is chosen fictitiously at the bottom edge of the wall, this reduction effect is not taken into account in the calculation of the strains and leads therefore to higher strains at the top edge.

When the neutral axis is assumed at the centre of the wall the eccentric moment however also causes tensile strains at the bottom edge which are superposed to the centric horizontal tensile strains. These strains are however reduced by the compressive strains, which are induced at the bottom edge due to the vertical bending hogging mode. The magnitude of the eccentric moment finally determines whether the resulting dominant tensile strain occurs at the bottom or the top edge.

Combination of strains
with principal strain equations

Neutral axis at the
bottom of the wall

Central tension
due to the transfer
of horizontal forces
at the bottom of the wall

ε_d

Diagonal strains
due to vertical
settlements

ε_h

Horizontal
strain

ε_b

Bending strains
due to vertical
settlements

ε_h

Horizontal
Strain

(a) neutral axis at the bottom of the wall

Combination of strains
with principal strain equations

Neutral axis the centre
of the wall

Eccentric moment loading
due to the transfer of
horizontal forces at the bottom
of the wall

ε_d

Diagonal strains
due to vertical
settlements

ε_h

Horizontal
strain

$\varepsilon_{hb,ex}$

eccentricity effect
due to horizontal
strain

ε_b

Bending strains
due to vertical
settlements

ε_h

Horizontal
Strain

$\varepsilon_{hb,ex}$

eccentricity effect
due to horizontal
strain

(b) neutral axis at the centre of the wall

Figure 3.41: Strain distributions for combination of vertical and horizontal ground movements in the hogging zone

Review

The example of a hogging situation shown in Figure 3.42 is used to analyze the influence of the eccentric moment on the dominant strains for a special case.

$\beta_{left} = \beta_{right} = 1/1180$

$\Delta/L = 0.00026$

point of inflection

depth of the tunnel axis:	21m
diameter of the tunnel:	9.5m
point of inflection:	9.5m
K surface level:	0.45
volume loss:	1%
Gaussian profile	
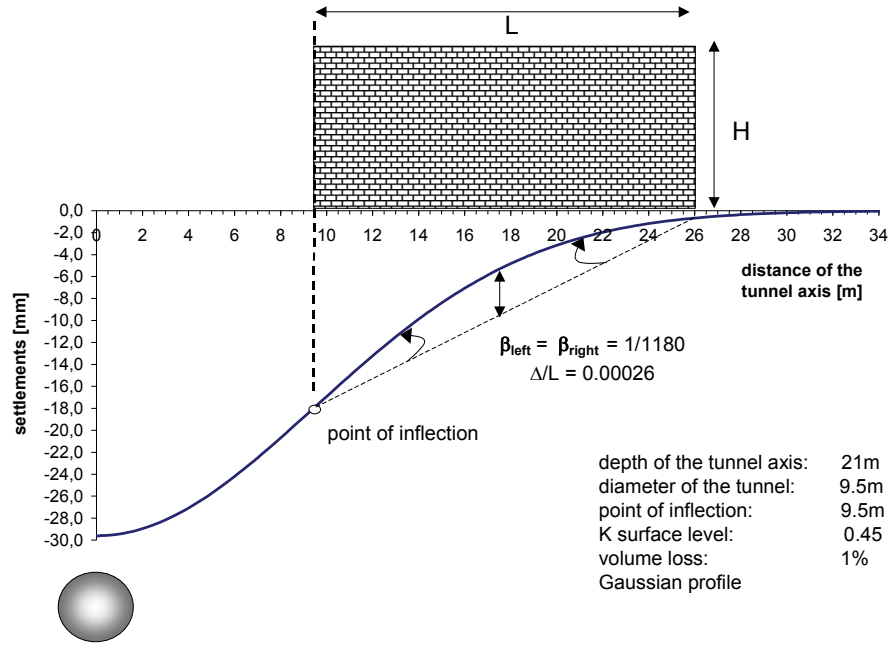
(a) influence of vertical settlements in a hogging case

Average horizontal strain

$\varepsilon_h = (h1 - h2) / L$

$= 0{,}00044$
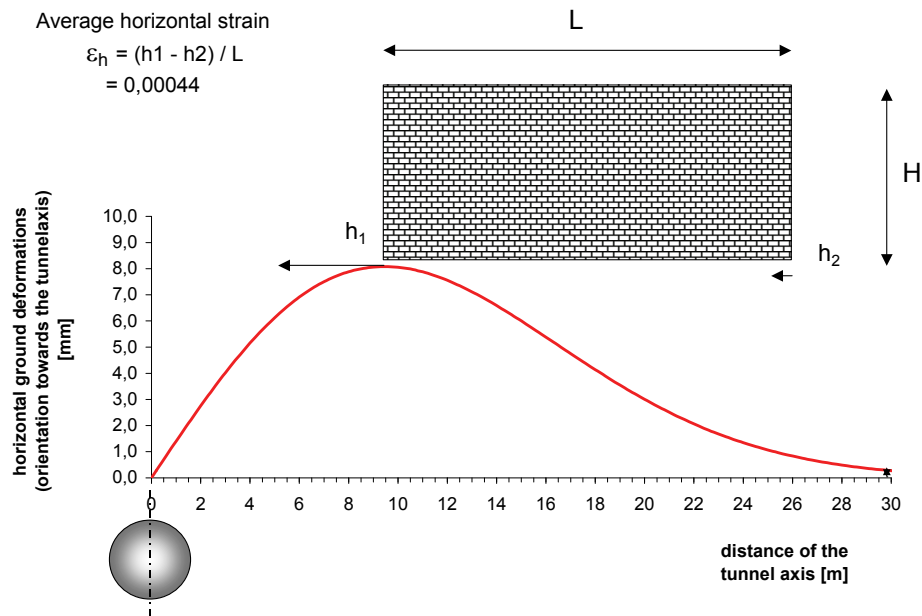
(b) influence of horizontal ground movements in a hogging case

Figure 3.42: Example for a hogging case

The differential vertical and horizontal ground deformations of the above case are used to calculate the

total strains for two different assumptions:

- Neutral axis at the centre and full eccentricity of the horizontal forces induced due to the transfer of the horizontal differential movements at the bottom edge is taken into account.
- Neutral axis at the bottom edge with the consequence that no eccentricity due to the transfer of horizontal differential movements has to be taken into account.

The height H of the building is varied and the length of the building L is fixed in order to cover a wide range of L/H-ratio's. The backgrounds for the strain calculations and the different contributions of bending strains at top and bottom edges and the diagonal strains are given in Appendix 5.
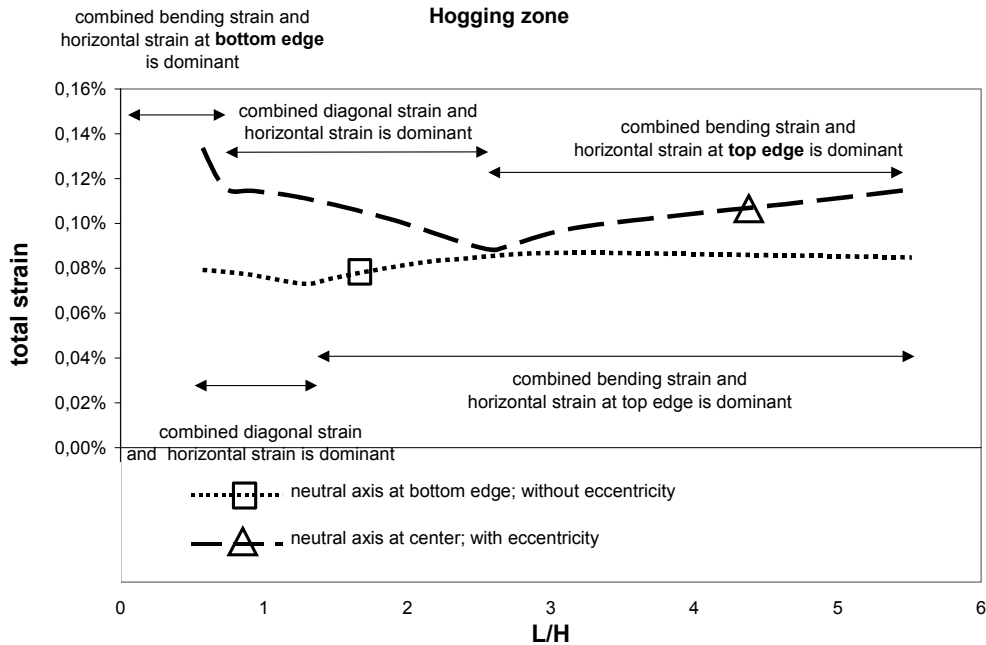
Figure 3.43: Influence of the eccentricity and the location of the neutral axis on the total strains for the considered hogging case

Figure 3.43 shows the results for the dominant total strains, which are determined from the combination of induced strains due to the horizontal and vertical differential displacements. The case with the neutral axis at the centre and the inclusion of the eccentricity provides higher total strains than the case with the neutral axis at the bottom edge of the wall. It is also noted that, if eccentricity is taken into account, the dominant bending strain can either occur at the bottom or the top edge of the wall. For L/H-ratio's greater than 2.7 the bending strain at the top edge is dominant and for L/H-ratio's smaller than 0.7 the bending strain at the bottom edge is dominant. This phenomena can be explained by the fact that with increasing L/H the building height H and thus the eccentric moment is reduced and does not overrule the tensile strains at the top edge due to the vertical hogging bending mode. For smaller L/H-ratio's and thus greater building height H the tensile strains at the bottom edge due to the eccentric moment cause the maximum total strains in the building.

It is emphasized, that the chosen example does not allow a general conclusion, because the degree of dominance of the eccentricity effect depends on the relation between the magnitudes of the differential vertical and horizontal displacements and also on the absolute dimensions of L and H of the wall. Each situation can therefore provide another result.

It should however be realized that the theoretical eccentric moment of the horizontal forces is clearly overestimated for practical situations, because the LTSM assumes full transfer of horizontal differential ground movements to the building. This causes large horizontal forces at the bottom of the wall, because the horizontal forces have to elongate the stiff structure (high *EA*) with the full magnitude of the differential horizontal ground movements. These high horizontal forces cause high eccentric moments. In practice these forces are restricted to much smaller values due to the interaction and the limitation of the friction transfer between building and soil.

3.3.5.3.1 CONCLUSIONS

Buildings undergoing hogging mode ground deformations are considered more susceptible to damage than buildings in the sagging zone. This observation is born out empirical experience in practice. This aspect is reflected in the LTSM by a fictitious assumption for the location of the neutral axis in the structure. In the hogging zone the neutral axis is chosen at the bottom edge of the wall. With this assumption the tensile strains due to horizontal differential ground movements at the bottom edge of the wall in a hogging zone cause a central tension of the wall.

It is shown in the above section, that if **no horizontal ground strains** would be considered in the damage calculation, the LTSM assumption of the neutral axis at the bottom edge leads consequently to lower strains (compared to the neutral axis at the centre) for a *L/H*-range between 0.75 and 2.5. This means, that the analytical approach of the LTSM for a building in a hogging zone does not necessarily always lead to more damage susceptibility than a building in the sagging zone, if **only the effect of vertical settlements is considered**.

3.3.6   Frame structures in the LTSM

3.3.6.1   General

Burland et al. (2001) suggest to use a modified, fictitious *E/G*-factor of 12.5 for frame structures instead of 2.6 for massive walls. The empirical background of this suggestion is, that the frame structures are generally considered to be less susceptible to settlement damage than massive walls due to their flexibility and material ductility. This perception should, according to Burland et al. (2001), be reflected in the LTSM by the use of an increased fictitious *E/G*-value for the idealized beam representing the structure. The influence of the modification of the *E/G*-factor on the calculation of strains is analysed in section 3.3.6.2. The main objective of these considerations is to investigate whether the suggested fictitious *E/G* modification leads to the wished objective for all different geometries (*L/H* variations) in hogging and the sagging mode situations.

A second issue which is addressed in this section is the fact that the procedure of the calculation of tensile strains with the fictitious beam approach of the LTSM is used for frame structures as well as for the massive walls. However this is questionable from structural point of view, because the tensile strains calculated for a fictitious beam representing a frame structure are not consequently representative for the corresponding strains in beams or columns of the open frame structure. The influence of imposed ground deformations on the beams and columns of a frame structure should be expressed in terms of a modification of bending moments, shear forces and normal forces. A new approach for frame structures is therefore presented in this section.

It is emphasized that this section only focuses on the settlement influence on the structural members of the frame structure. The existence of in-fill masonry walls or façade elements fixed to the frame structure requires special consideration.

3.3.6.2   Influence of the E/G-factor on the tensile strains

A frame structure is more flexible than a massive wall, because of the open structure of beams and columns. Due to this reduced stiffness, the structure tends to follow the imposed differential soil deformations more easily than a stiff massive wall. Although it will deform more due to its greater

flexibility, the need to redistribute loads will decrease causing less changes of strains and stresses and thus less damage in the structural parts of the frame. Another important beneficial aspect regarding the damage susceptibility is the more ductile material of the structural members of a frame structure as they are usually made of reinforced concrete or steel.

For a frame structure the fictitious *E/G*-value of 12.5 is suggested by Burland et al. (2001) for the damage prediction with the concept of the LTSM. It should be emphasized that the *E/G*-value of 12.5 is not a realistic material parameter, compared to the *E/G*-value of 2.6 for massive walls, but a fictitious value, which has to take into account the expected structural behaviour (more flexibility) of a frame structure compared to a massive wall.

E/G = 12,5   **E/G = 2,6**
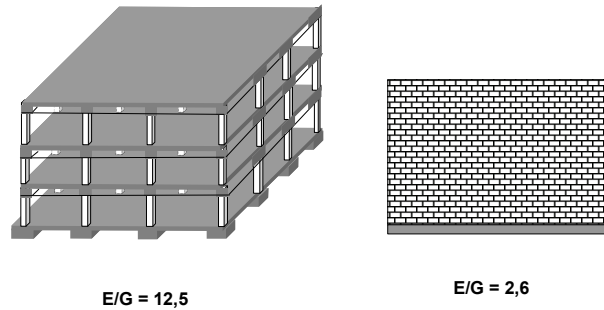
Figure 3.44: *E/G*-**value for frame structure and massive wall structure**

The intention of the authors (Burland et al. (2001)) is thus to calculate reduced strains with the LTSM for frame structures by using an empirical derived fictitious value of *E/G*=12.5 instead of *E/G*=2.6. The choice of the *E/G*-factor and its consequences on the determination of the tensile strains with the LTSM is investigated.

Equations (3.10) to (3.17) are used for the analyses of the influence of the *E/G*-factor on the normalized bending and diagonal strains in the sagging zone (neutral axis in the centre) and the hogging zone (neutral axis at the bottom edge of the beam) calculated with the fictitious beam approach of the LTSM. The results are given in Figure 3.45 (for the neutral axis at the centre of the beam) and Figure 3.46 (neutral axis at the bottom edge of the beam) and a wide range of *L/H*-ratio's.
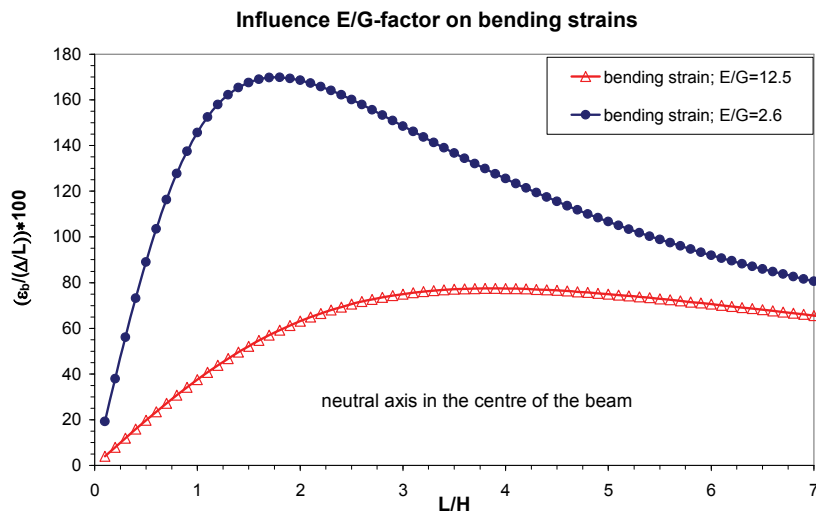
(a) bending strains for the neutral axis at the centre

Influence E/G-factor on diagonal strains
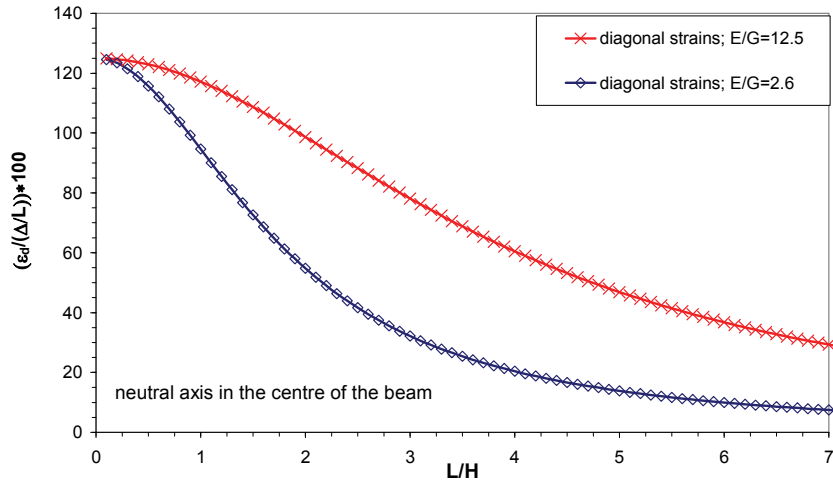
(a) diagonal strains for the neutral axis at the centre

Figure 3.45: Influence of *E/G*-factor on diagonal and bending strains for the neutral axis at the centre of the beam (assumed for the sagging mode)

Influence of E/G-factor on bending strains
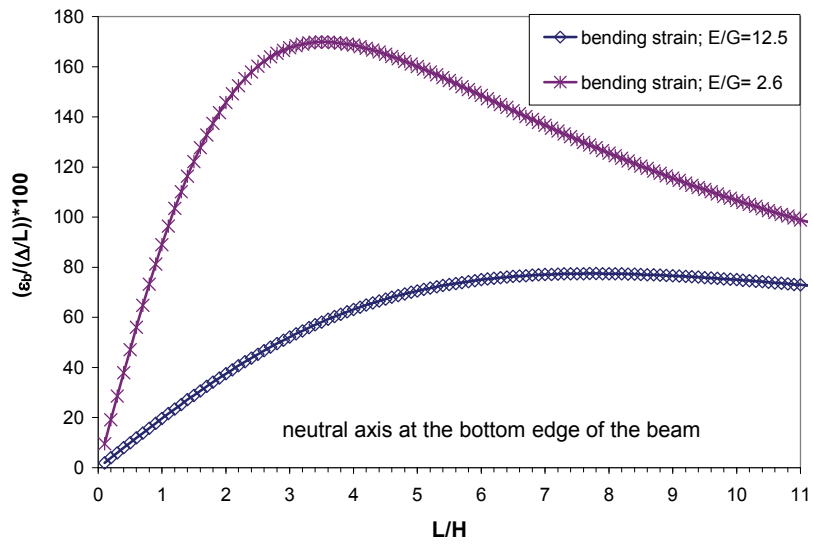
(a) bending strains for the neutral axis at the bottom edge of the beam

Influence of E/G-factor on the diagonal strains
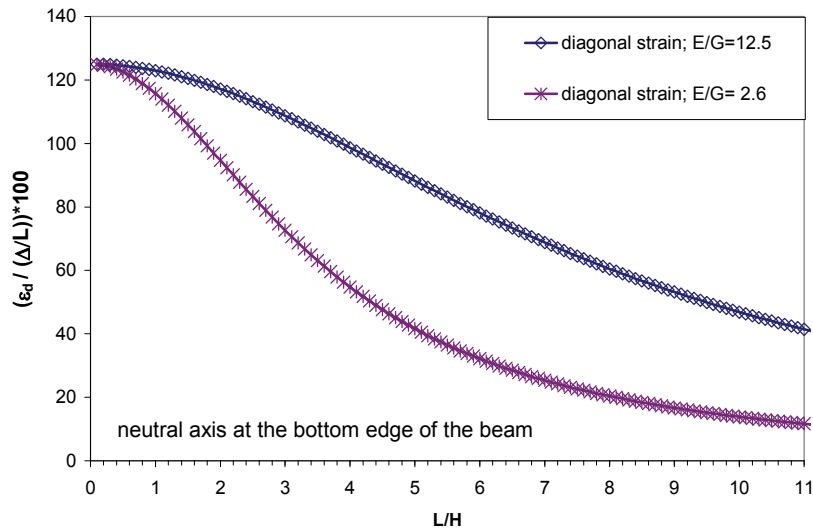
(b) diagonal strains for the neutral axis at the bottom edge of the beam

Figure 3.46: Influence of *E/G*-factor on diagonal and bending strains for the neutral axis at the bottom edge of the beam

For the *bending strains* Figure 3.45 and Figure 3.46 show a significant reduction if the *E/G*-factor of 12.5 is used instead of 2.6. The magnitude of the reduction depends on the *L/H*-ratio. The maximum reduction is ca. 75% and occurs at low *L/H*-ratio's and the reduction decreases with increasing *L/H*-ratio.

The *diagonal strains* however appear to increase up to a maximum of ca. 70%, if the *E/G*-factor of 12.5 is used instead of 2.6. The maximum increase occurs for high *L/H*-ratio's and the increase reduces with decreasing *L/H*-ratio.

Subsequently the bending strains and the diagonal strains from Figure 3.45 and Figure 3.46 are combined to the dominant strains. The dominant strains present the higher value of the two strains for each *L/H*-ratio and thus represent the strain to be used for the final damage classification in the LTSM. The dominant strains for the *E/G*-values of 12.5 and 2.6 and the neutral axis in the centre of the beam and at the bottom of the beam are shown in Figure 3.47 and Figure 3.48 respectively.

Influence E/G-factor on dominant strains
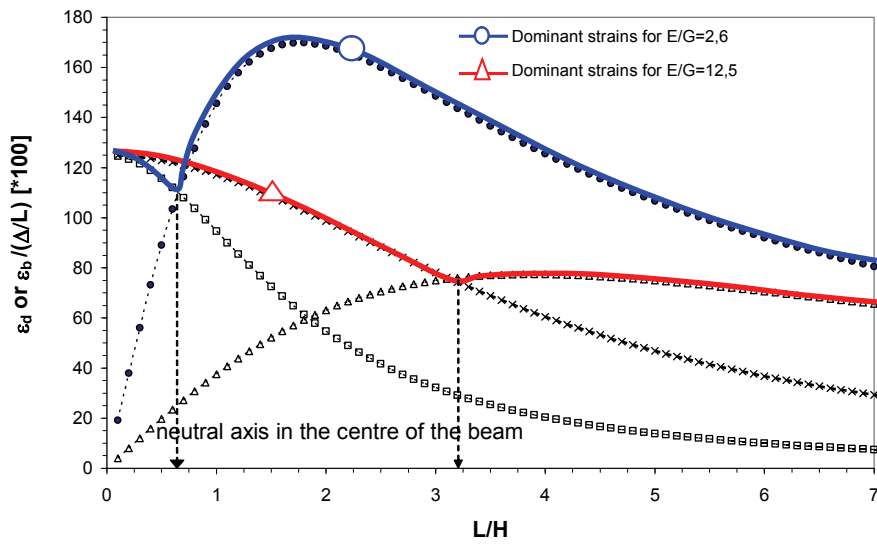
Figure 3.47: *E/G* **influence on the dominant strains for the neutral axis at the centre of the beam**

Influence of E/G-factor on the dominant strains
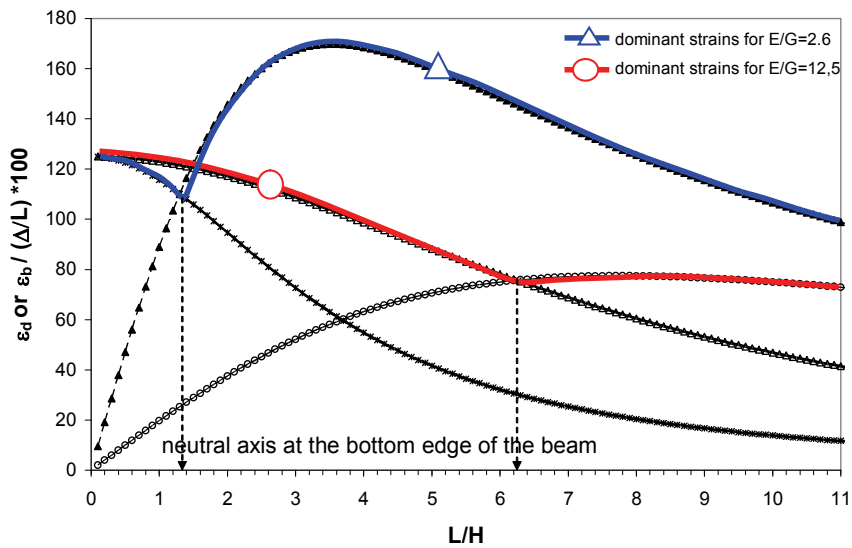
Figure 3.48: *E/G* **influence on the dominant strains for the neutral axis at the bottom edge of the beam (assumed for the hogging mode)**

Figure 3.47 and Figure 3.48 show, that the aimed reduction effect of the dominant tensile strains for a factor 12.5 instead of 2.6 strongly depends on the *L/H*-ratio of the structure.

For the **neutral axis in the centre of the beam** and *L/H* smaller than 0,8, the dominant tensile strains for the *E/G*-value of 12.5 are increased up to max. 10%. For values of *L/H* greater than 0.8 the dominant strains are reduced up to max. 50% (for *L/H* =3.2) compared to the strains for an *E/G* value of 2.6.

For the **neutral axis at the bottom edge of the beam** and *L/H* smaller than 1.4, the dominant tensile strains (being the diagonal tensile strain) for the *E/G*-value of 12.5 are up to max. 10%. For values of *L/H* greater than 1.4 the dominant strains are reduced up to max. 50% (for *L/H* =6.2) compared to the strains for an *E/G* value of 2.6.

It is also noted that the increase of the *E/G*-factor from 2.6 tot 12.5 leads to a horizontal translation of the *L/H* threshold where diagonal strains or bending strains are getting dominant. The threshold is moved from *L/H* of 0.7 to *L/H* of 3.2 for the neutral axis at the centre of the beam and from *L/H* of 1.3 to *L/H* of 6.2 for the neutral axis at the bottom edge of the beam.

It can be concluded that the aimed damage reduction for a frame structure compared to a massive wall with the implementation of the suggested fictitious *E/G*-factor of 12.5 in the current LTSM *is not achieved for all L/H-ratios*. This approach can therefore not considered to be a straightforward/appropriate approach to take into account the damage susceptibility of frame structures for all kind of situations. Additionally it is emphasized that the choice for a single fictitious *E/G* adaptation of 12.5 suggested by Burland et al. (2001) for a "general" frame structure cannot be considered representative for all kind of frame structures. The structural details for each frame structure as for example the connections of columns and beams, the foundation (strip footings or foundation plate) play an important role in the determination of the overall stiffness of a frame structure.

These conclusions therefore require a modified approach to deal with the damage prediction of frame structures. Recommendations are made in the following section.

3.3.6.3   Modified approach for damage prediction in frame structures

The procedure of the calculation of tensile strains with the fictitious beam approach of the LTSM for massive walls is considered inappropriate for frame structures. The tensile strains calculated at a fictitious beam for a massive wall with the LTSM are not comparable to discrete strains in beams or columns of a frame structure. The influence of imposed ground deformations on the beams and columns of a frame structure should be expressed in terms of a modification (increase or decrease) of bending moments and shear forces. A modified approach for frame structures is presented hereafter. It is distinguished between three kind of frame structures depending of the structural connections between floors and columns.

To determine the fictitious point load P according to the LTSM which forces the frame structure to follow the imposed ground deflection Δ, a simplified approach is assumed taking account only the contribution of bending deformations. This assumption forms a conservative upper bound value for the fictitious load and therefore provides an upper bound of the possible damage. Additionally it makes the presented approach more transparent and applicable for the design practice. Equation (3.9) is therefore reduced to:

$$\Delta = \frac{P \cdot L^3}{48 \cdot EI_{eq}}$$

(3.18)

With   P   Point load necessary to deflect the fictitious beam with the pre-described deflection Δ

I_{eq} the equivalent moment of inertia of the overall frame structure

E   the Young's modulus of the structural material of the beams and columns of the frame

Netzel D. (2000) presents guidelines to determine the equivalent moment of inertia (I_{eq}) for three different categories for frame structures:

- *Hinged connections between beams and columns of the frame structure*

An example of a part of a prefab structure with one-field beams is shown in Figure 3.49. It is noted that the considered structure requires in reality a stability tower to guarantee the overall stability. For the following considerations it is assumed that this tower is situated outside the influence area. The equivalent moment of inertia I_{eq} of the frame structure shown in Figure 3.49 can be determined with I_{fo} representing the moment of inertia of the foundation plate, because the floors do not contribute to the overall bending stiffness for hinged connections. The value I_{fo} represents the moment of inertia of the continuous foundation plate.

$$I_{eq} = I_{fo}$$
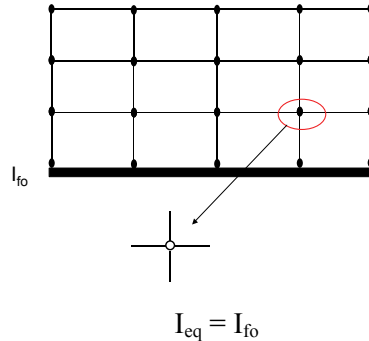
Figure 3.49: Hinged prefab frame structure

- *Continuous beams but hinged connections of the columns or walls*

An example of a part of a structure where the floor beams are continuous elements and the columns are hinged connected to the floors is shown in Figure 3.50. With the assumption that all floor beams have the same I_{fl} the equivalent moment of inertia of the overall frame structure can be determined with:

$$I_{eq} = I_{fo} + n_h \cdot I_{fl} \tag{3.19}$$

with

	n_h	the amount of storey's
	I_{fl}	the moment of inertia of one floor slab
	I_{fo}	the moment of inertia of the foundation plate
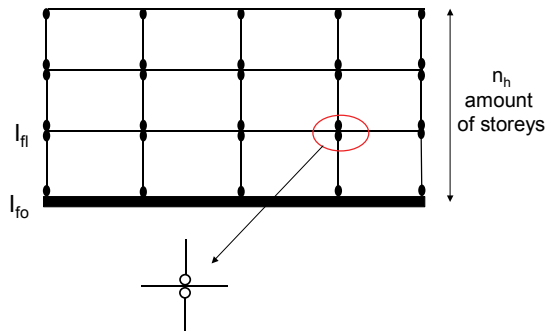
Figure 3.50: Partly hinged frame structure

The overall bending stiffness of the entire structure can thus be considered as a staple of all floors without shear connections.

It is emphasized that this equation is only valid for the assumption that the axial deformation of the vertical elements (walls and or columns) can be neglected for the interaction between foundation plate

and frame structure, see Netzel D. (2000). If the axial deformations of the vertical elements are taken into account the equivalent moment of inertia according to equation (3.19) must be reduced as only the floor slabs up to a certain level will contribute to the overall bending stiffness. The contribution of the floor levels to the overall stiffness of the structure with increasing height has then to be modified with a reduction factor. This reduction factor has to be determined specifically for each frame structure with numerical calculations. The example in Figure 3.51 shows the principal effect of the influence of the axial deformation of the vertical elements on the overall stiffness due to interaction between foundation plate and frame structure for a dead weight load case. The interaction between the foundation plate and the frame structure can change the normal forces in the columns and beams. For the case of Figure 3.51 the outer columns are compressed and the inner columns are elongated relatively to each other. These differential axial deformations of the columns lead to a reduction of the equivalent bending stiffness. The floors only contribute to the overall stiffness of the frame up to the level, where the settlement from the bottom is compensated.
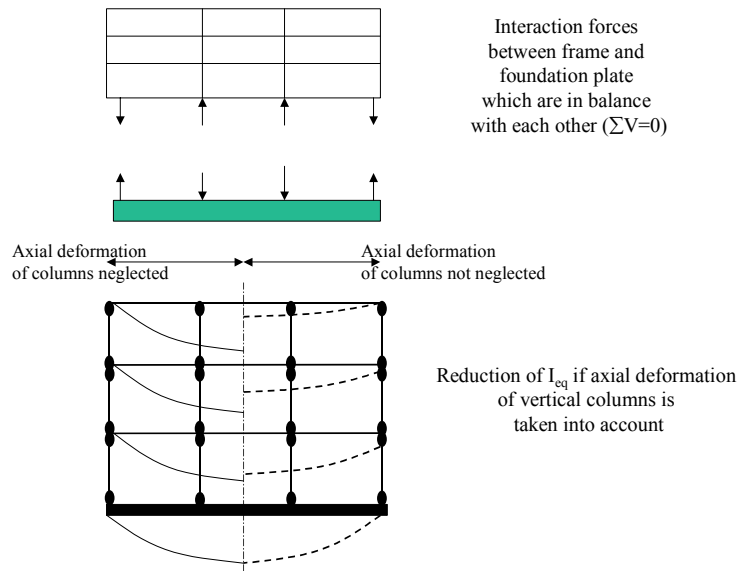
Figure 3.51 Reduction effect of I_{eq} if axial deformation of vertical elements is considered

Equation (3.19) however provides an upper bound of the I_{eq} value, which leads, for the input in equation (3.18) a conservative value for the fictitious point load P and thus forms a safe case for the damage prediction.

- *Full monolith connection of beams and columns*

The overall bending stiffness increases for a monolithically connected frame structure, compared to the partly hinged structure due to the dowel effect of the vertical elements (Netzel D. (2000)). Meyerhof (1953) presents the following approach to determine the equivalent moment of inertia for a monolith connected frame structure:

$$I_{eq} = I_{fo} + \sum_{1}^{n_h} I_{fl} \cdot \left[1 + \frac{1}{\dfrac{(I_{fl}/L)}{\dfrac{I_o}{h_o} + \dfrac{I_u}{h_u}} + 1} \cdot n_L{}^2 \right] \tag{3.20}$$

The input parameters of equation (3.20) are shown in Figure 3.52. The equation between the brackets represents a factor which takes into account the dowel effect of each story. As the dimensions of the columns or walls and thus the I_o and I_u values can vary in each story it has to be considered separately for each story.
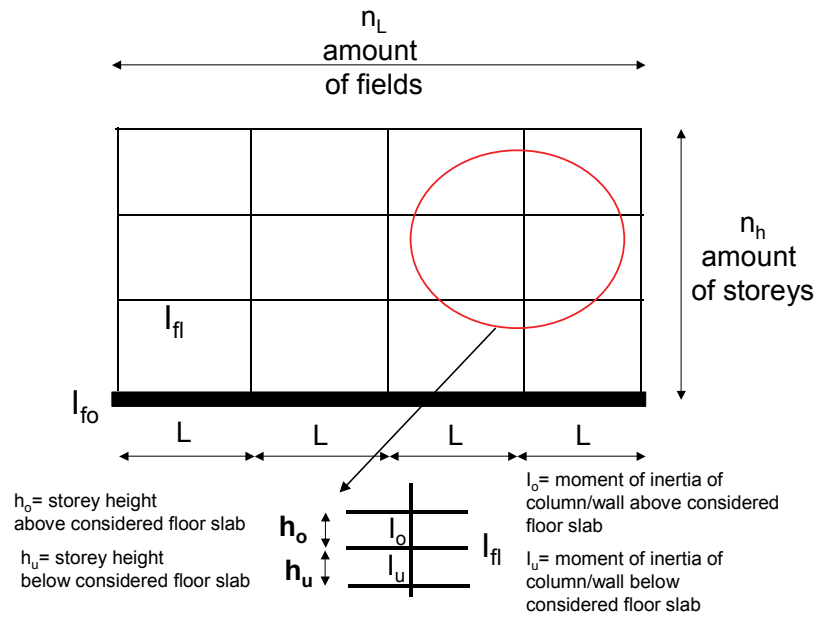
Figure 3.52: Monolith frame structure

For an extreme case of columns or walls with a negligible small bending stiffness compared to the floors, the dowel effect becomes negligible. This is reflected in equation (3.20) because the dowel factor between the brackets becomes 1 if the term $(I_o/h_o + I_u/h_u)$ is chosen negligible small. This means that for this extreme case of negligible small bending stiffness of the columns, the I_{eq} would be corresponding with the value according to equation (3.19). For theoretically infinite high bending stiffness of the vertical elements the maximum dowel factor converges to $[1+n_L{}^2]$. The principle of the dowel effect is shown in Figure 3.53.

(EA = ∞ assumed for the floors)
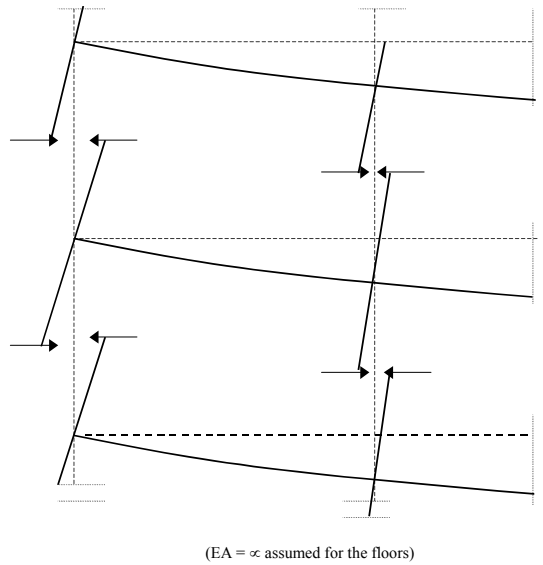
Figure 3.53: Principle of dowel effect of the vertical frame elements (columns or walls)

It should also be mentioned, that this upper limit of the equivalent moment of inertia is still significant lower than the moment of inertia which would be calculated for the assumption of a common cross section consisting of the floors, where the "Steiner" contributions of each floor level is taken into account (see Figure 3.54).

$$I_{eq} = [I_{fo} + y_{fo}^2 \cdot A_{fo}] + \sum_{i=1}^{n_h} [I_{fl} + y_{si}^2 \cdot A_{fl}]$$
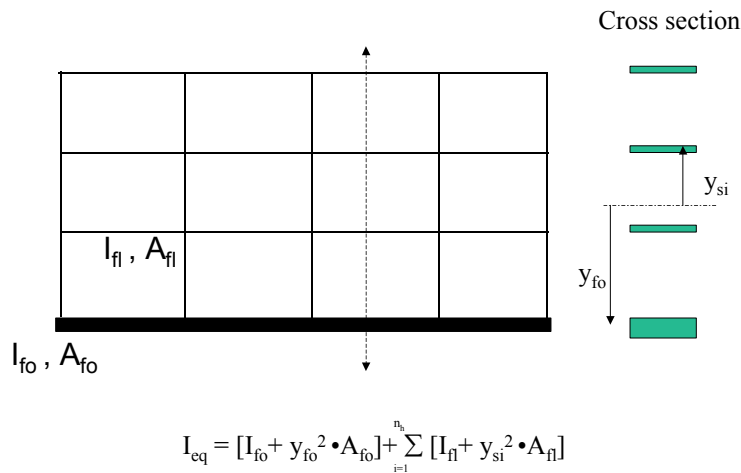
Figure 3.54: Consideration of cross section with Steiner contributions

The approach of Figure 3.54 should therefore be ***considered*** as an unrealistic stiff estimation of the equivalent moment of inertia for a monolith frame structure and the above described approach of Meyerhof should be used instead.

The good agreement of the Meyerhof approach and the bending stiffness of a frame, calculated with finite element calculations, is shown in Figure 3.55. For details regarding the numerical calculations it is referred to Netzel D. (1972).
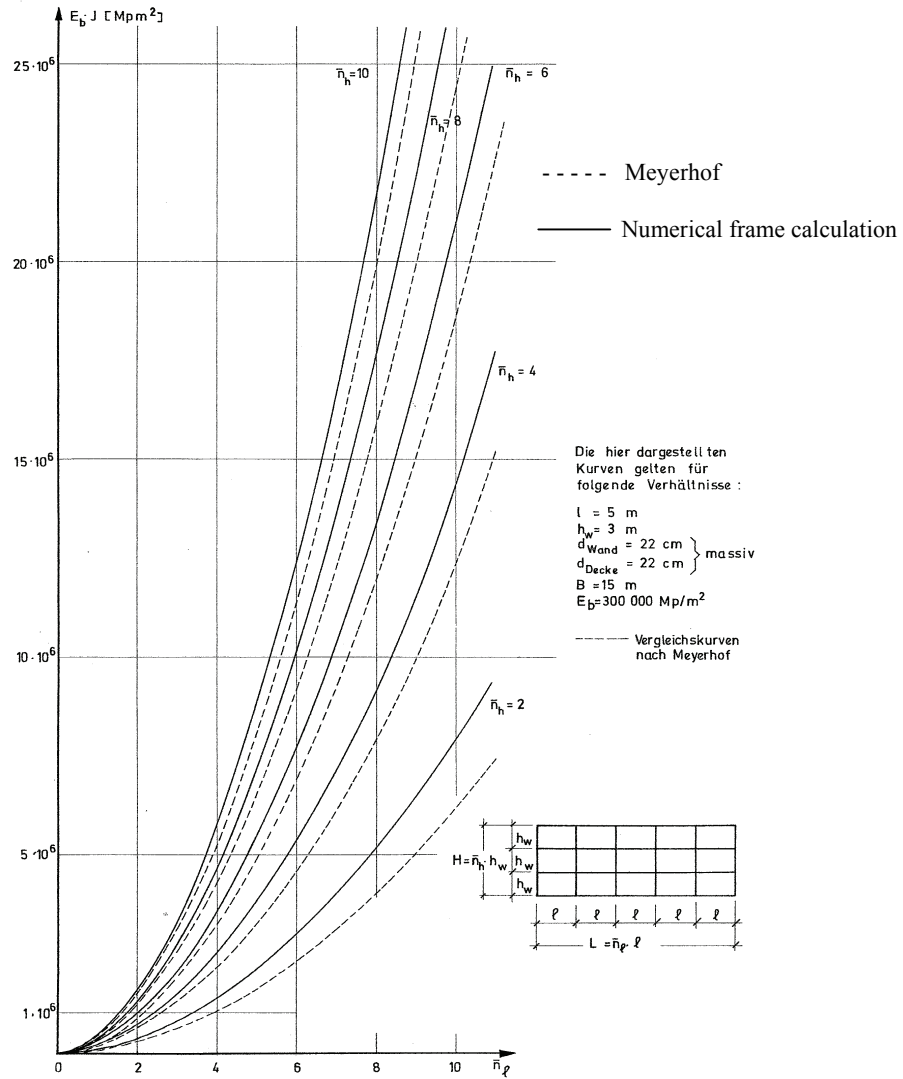
Figure 3.55: Comparison of Meyerhof approach with numerical calculations Netzel D. (1972)

The influence of the axial stiffness of the vertical structural elements (columns) is not taken into account in equation (3.20) and can lead to a reduction of the overall stiffness in the same way as previously described for the partly hinged structure. This special reduction factor has to be determined specific for each frame structure with numerical calculations. Equation (3.20) however provides an upper bound of the I_{eq} value, which leads, for the input in equation (3.18) a conservative value for the fictitious point load P and thus forms a safe case for the damage prediction.

After determination of the value I_{eq} and the use of equations for the fictitious beam with a central point load, the maximum bending moment M_{max} and the maximum shear force V_{max} can be expressed with:

$$M_{max} = \frac{P \cdot L}{4} = \left(\frac{\Delta}{L}\right) \cdot \frac{12 \cdot E \cdot I_{eq}}{L} \tag{3.21}$$

$$V_{max} = \frac{P}{2} = \left(\frac{\Delta}{L}\right) \cdot \frac{24 \cdot E \cdot I_{eq}}{L^2} \tag{3.22}$$

Subsequently these maximum bending moments and shear forces at the fictitious beam have to be redistributed to the foundation and the floor beams, proportional to their stiffness contribution in relation to the overall stiffness of the structure. The corresponding moments and shear forces have to be superimposed to the initial internal loadings in the beams and columns of the frame. The judgement whether a certain increase of bending moments or shear forces can considered to be acceptable can only be made with detailed consideration of the current margin of safety and capacity of the beams and columns/walls. Apart from these safety requirements also crack width requirements for reinforced concrete can set limits for the allowable increase of moments.

For the *frame structure with hinged connections* between floors and columns the moments and shear forces introduced by the imposed settlements, are concentrated in the foundation plate. No moments and shear forces are introduced in the floor beams and columns (see Figure 3.56).

$$I_{fo}, A_{fo}$$

$$M_{fo} = \underbrace{(I_{fo} / I_{eq})}_{=1} \cdot M_{max}$$

$$V_{fo} = \underbrace{(A_{fo} / A_{eq})}_{=1} \cdot V_{max} \text{ with } A_{eq} = A_{fo}$$

No bending moments and shear forces
are introduced in the superstructure
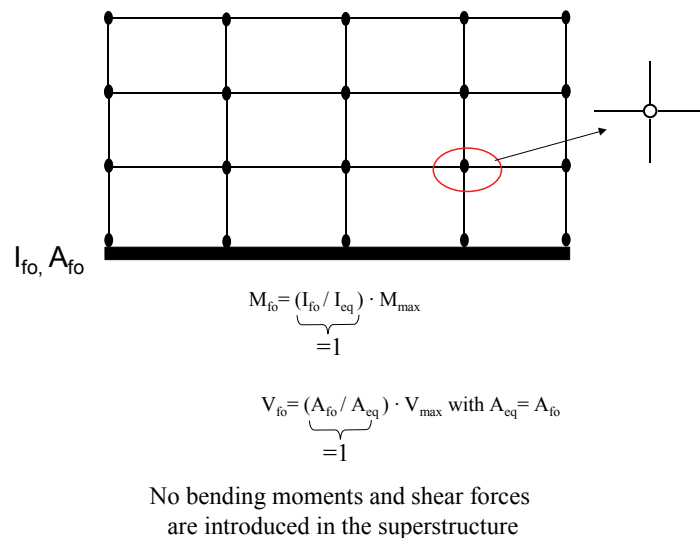
Figure 3.56: Moments and shear forces in a prefab structure with hinged connections

For the *frame structure with continuous beams but hinged connections of columns/or walls* the moments and shear forces introduced by the imposed settlements, are divided on the foundation plate and the different floor beams according to their stiffness contribution to the overall stiffness of the frame structure, see Figure 3.57.

$$M_{fo} = (I_{fo} / I_{eq}) \cdot M_{max}$$
$$M_{fl} = (I_{fl} / I_{eq}) \cdot M_{max} \text{ for each floor level}$$

$$V_{fo} = (A_{fo} / A_{eq}) \cdot V_{max}$$
$$V_{fl} = (A_{fl} / A_{eq}) \cdot V_{max} \text{ for each floor level}$$

$$\text{with } A_{eq} = A_{fo} + n_h \cdot A_{fl}$$
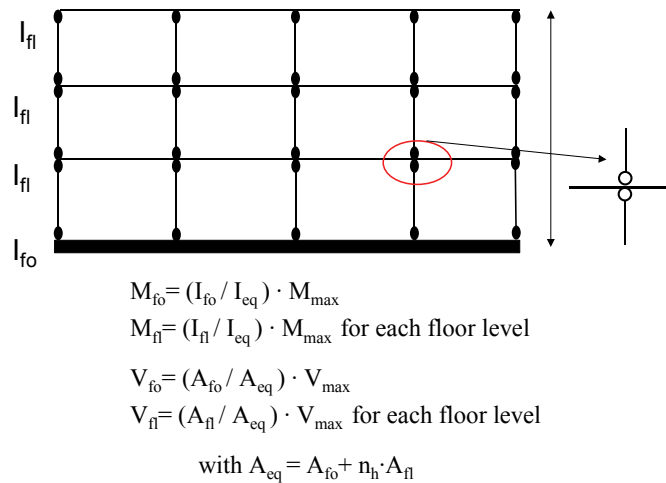
Figure 3.57: Moments and shear forces in a frame structure with continuous beams and hinged connections between columns/walls and the floor beams.

For a ***frame with monolith connections between floors and columns/walls*** the redistribution of the moments and the shear forces to the individual floors and columns is far more complex and cannot be covered with simplified approaches as described for the frames with hinged connections. The complexity is due to the dowel effect of the columns/walls, which introduces additional moments with varying magnitude at each column. This effect modifies the moments in the floors and is schematically shown in Figure 3.58 for a part of the frame for the example of a sagging situation. A detailed numerical analyses of the frame structure is required to analyse the moment and shear force of each part of the frame for a monolith connected structure.
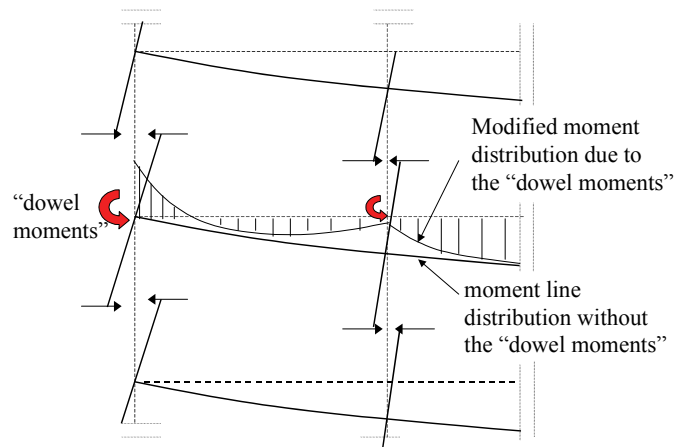
Figure 3.58: Dowel effect for the moment distribution in a floor of a monolith frame structure

3.3.6.4   Conclusions

Framed structures are generally considered to be less susceptible to settlement damage than massive walls due to the flexibility and the material ductility of the structural members being steel or reinforced concrete beams and columns. According to Burland et al. (2001) this perception should be reflected in

the LTSM by the use of an increased fictitious *E/G*-value for the idealized beam representing the structure. They propose a value of 12.5 compared to a realistic material parameter of 2.6 for massive wall structures. This increased value should reduce the calculated tensile strains and thus the damage according to the LTSM for all kind of frame structures.

In the present section it has been shown that this approach is not straightforward. The effect of the *E/G* factor of 12.5 on the tensile strains turns out to strongly depend on the *L/H*-ratio. For low *L/H*-ratio (up to 1.4) the increase of the *E/G*-factor even leads to an increase of the strains (max. ca. 10%) instead of the aimed decrease. For *L/H*-ratio's beyond 1.4 the tensile strains are reduced up to max. 50%, providing the desired effect. Additional to these shortcomings it is emphasized that the choice for a single fictitious *E/G* adaptation of 12.5 suggested by Burland et al. (2001) for a "general" frame structure cannot be considered representative for all kind of frame structures. The structural details for each frame structure play an important role in the determination of the overall stiffness of a frame structure.

Another important aspect which is addressed in the previous section is that the principle of the LTSM, calculating strains at a fictitious beam cannot be applied for the calculation of internal loadings in the beams and columns in an open frame structure due to imposed deformations.

The newly developed approach described in section 3.3.6.3 is therefore recommended for the determination of the modification of bending moments and shear forces in beams and columns of different types of frame structures due to imposed settlements.

It is also emphasized that the particular damage sensitivity of in-fill masonry walls or façade elements fixed to the frame structure is not part of this research. Anyhow special considerations can be required, as they can be the dominating damage factor, before structural parts of the frame itself undergo unacceptable loadings. These considerations have to be taken into account in a site-specific damage prediction of frame structures using numerical methods.

3.4 Implementation of additional influence factors in the current LTSM approach

3.4.1 General

The current LTSM does not give guidance on special aspects which can influence the damage susceptibility of buildings, as for example the timely development of ground movements and the initial condition of the building. Beside differential ground movements and the induced strains calculated with the LTSM, also absolute values for settlements and the tilt can set tolerance limits for specific structures or parts of structures. These issues will be addressed in the present section.

3.4.2 Implementation of settlement rates in combination with creep or relaxation of structural material

Long term settlement can play an important role in the damage prediction of the adjacent buildings, because the accompanying beneficial effects of creep or relaxation of the structural material could possibly be considered. Creep is the timely increase of the deformation and the strains of a structure due to an imposed, constant loading. Relaxation is the timely reduction of the stresses due to an imposed, constant strain. The principle relationships of the development of strains and stresses for both phenomena are shown in
Figure 3.59.
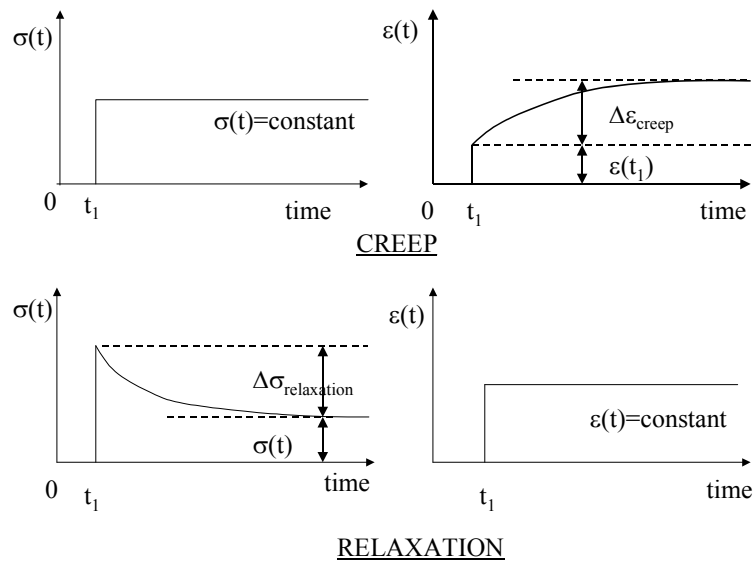
CREEP

RELAXATION

Figure 3.59: Schematic strain and stress developments for creep and relaxation

If the imposed settlements develop slowly and comparable with the timely development of the stiffness reduction due to creep or relaxation of the material, the damage susceptibility will decrease. A rapid development of ground movements (short term settlements) implies that creep or relaxation is not able to reduce the damage effects in the structure.

The capacity of the structural material for creep and relaxation is dependant of:

- Age of the structure when the loading is imposed. The creep and relaxation capacity is reduced with increasing age of the structure.
- Temperature. The creep and relaxation capacity is reduced with increasing temperature.

The SBR (1998) gives an empirically derived indication for the beneficial effects of creep due to the imposure of long term settlements. These recommendations can be used in the LTSM to increase the tolerable strain limits (last column in Figure 3.5) with the percentages given in Table 3.1. It is emphasized that these percentages are only applicable for structural materials like concrete, masonry and other quasi brittle materials which have enough creep or relaxation capacity to beneficially reduce the imposed stress and strain concentrations in the building.

Settlement rate	Increase of the tolerable strain limits
Medium term settlements compared to short term settlements	20%
Long term settlements compared to short term settlements	55%

Table 3.1: Increase of tolerable strain limits for buildings due to creep of the structural material in combination with long term settlement effects

The definition of short term, long term and medium settlements has been given in section 2.5.

3.4.3 Implementation of building/foundation condition

A structure may have undergone previous damage and displacements during its lifetime. Additionally imposed differential ground movements often tend to concentrate in the pre-weaked locations of a building, e.g. in existing cracks. This can result in a rapid increase of the existing cracks and the degree of damage if the building is in a poor condition. It is therefore important that the initial building condition is taken into account in the damage prediction.

The initial building condition can be classified by a defect survey carried out in the design stage. The following aspects should be accounted for in the classification of the initial building/foundation condition:

- Archive investigation to collect detailed information about the foundation and the structure
- Visual inspection of damage (degree, amount, orientation and location of cracking etc.)
- floor levelling (determination of differential settlements and rotations of the building)
- precise levelling of the structure to determine the settlement rate over the last period (determination of recent settlement behaviour and development respectively)

If these information are not completely available or do not give a clear picture of the current condition, a foundation inspection is recommended. The procedure for an inspection of wooden pile foundations is described by Stoel, van der (2001). Oversteegen (1998) describes an example of a framework for a classification system to judge the condition of buildings in Amsterdam, developed by the municipality of Amsterdam. It is distinguished between good, moderate and poor condition of the buildings and the pile foundations.

The SBR (1998) has derived some empirical bandwidths to take into account the initial condition of the building in a damage prediction. The increased damage susceptibility of a building in a moderate or poor condition should be reflected in the LTSM by reducing the tolerable strain limits (last column in Figure 3.5) with the percentages given in Table 3.2.

Building condition	Reduction of the tolerable strain limits
poor building condition versus good building condition	55 - 75%
moderate building condition versus good building condition	20 - 30%

Table 3.2: Reduction of the tolerable strain limits due to the initial condition of the building

Due to the wide variety of different damage patterns and structures the empirical approach can only give an indication of the increased damage susceptibility. Engineering judgement plays an important role in this respect. For listed buildings it is recommended to carry out a detailed defect survey.

3.4.4   Settlement criteria for connections between services and structures

To avoid damage at the connection of services to buildings the differential settlements at the location of the connection have to be limited. This has to be checked particularly if the building is founded on piled foundations and the service on a raft foundation. Figure 3.60 presents an example for a building founded on end bearing piles and the services on a shallow foundation.

These limits are dependent of each case and should be derived in close correspondence with the involved parties (building owners, service companies etc.). Some indications of bandwidths from empirical experience are given in this section. Further well documented case records are required and form an important aspect for future research.
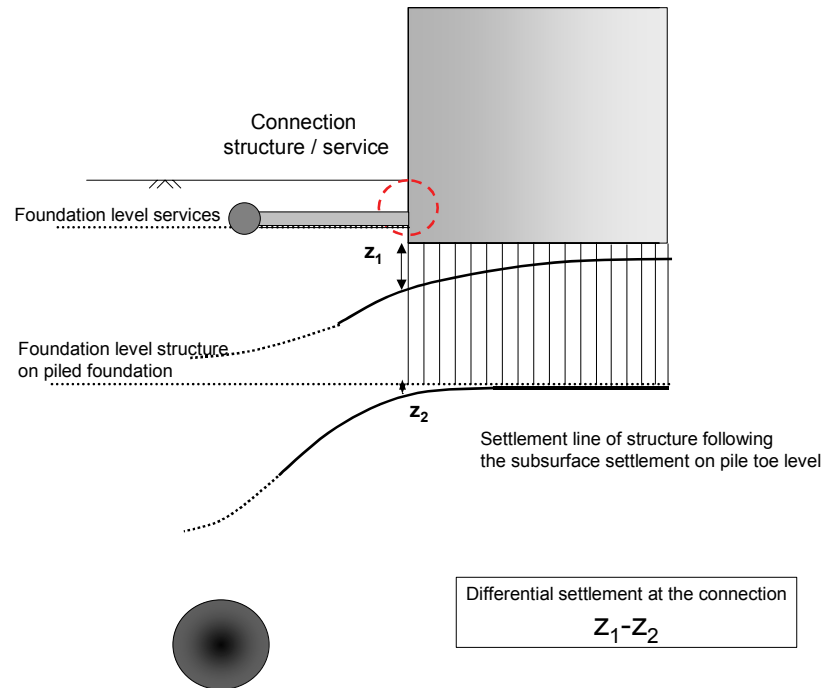
Figure 3.60: Differential settlements at the connection of services and buildings

A worst case for the situation of Figure 3.60 is that the building follows the settlement on the pile toe level (foundation on end bearing piles) whereas the services will follow the surface movements. The resulting differential movements of the connection between the services and the building is than equal to the difference between the absolute settlements at the different foundation levels z_1-z_2, see Figure 3.60. For the situation, that the settlement z_2 is very small compared to z_1, the difference z_1-z_2 equals the absolute settlement z_1 on surface level.

It is emphasized, that although if the building and the services would be founded on the same foundation level differential settlements at the connection of services to buildings can also occur due to different interaction between the stiff building with the soil compared to the interaction of the flexible service with the soil.

It should be noted that the tolerable settlement limits depend on the degree of flexibility and thus the type of connection of the services to the building. Information from services company should always be incorporated. As a first rough indication the following empirical value given by the SBR (1998) for Dutch conditions can be used:

Connection of services and buildings (without special flexible connections)	Tolerable differential settlements at the connection 50 mm	Negligible damage

Table 3.3: Indicative settlement limits for damage of connection between services and structures

3.4.5   Tilt limits for tall structures

Tall structures like for example towers require a restriction of the tilt to avoid stability problems. Indicative limits of the tilt ω (rigid body rotation) for tall structures are given by the empirical approach of Schultze (1990) with:

$$\max \omega = \frac{1}{0.005 \cdot \left(\dfrac{B_{building}}{H_{building}} \right)} \tag{3.23}$$

For the example of a building height H of 20m and a base width B of 5m the allowable limit for the tilt according to the above given equation is 1/800. It is recommended to carry out detailed stability analyses taking into account the soil-structure interaction if the structure is already considerably tilted in the initial stage.

3.5   Conclusions

The review leads to the following recommendations for a modified LTSM:

- The equations used for the calculations of the strains according to the current LTSM imply a simplified shear form factor to take into account the contribution of shear deformations. It is however shown that the use of this factor can lead to an underestimation of the damage. New Equations with a modified shear form factor, derived from the more exact theory of elasticity and the method of virtual work respectively, as presented by Timoshenko et al. (1971), are presented in this study. It is recommended to use these equations with the modified shear form factor for the LTSM.
- The currently used assumption of cutting off the beam model of a structure at the 1mm influence line and only considering the part of the structure inside the influence area is not straightforward. Structures extending the influence area of the ground deformations should be considered with their entire length. It is shown that when only a part of the structure inside the influence area is considered, this may result in a significant underestimation of the damage.
- The current approach of the LTSM assumes that a structure extending over the hogging and sagging part can be partitioned for the damage prediction into a separate hogging part and a sagging part. These parts can then be considered separately and independent from each other for the damage prediction. It is shown that this is only valid for structures where the difference between the tilt of the separated parts and tilt of the total structure does not differ more than 15%. If the difference is greater, additional numerical beam calculations for the entire structure are required to quantify the influence. Neglecting this guideline can lead to an underestimation of the damage.
- The two approaches of the current LTSM presented in literature are not consequent in the use of the greenfield damage parameter as input for the damage prediction. Boscardin e al. (1989) use the angular distortion and Burland et al. (1974, 2001) use the deflection ratio as input parameter for the influence of the differential vertical ground movements. It is shown that for Gaussian formed ground deformations the angular distortion has to be used for the calculation of the diagonal strains

in the structure and the deflection ratio has to be used for the calculation of the bending strains. Other procedures can cause a significant under- or overestimation of the strains and consequently the damage.

- The increasing damage susceptibility of the hogging deformation mode is an empirical observation born in practice. The current LTSM reflects this observation with the fictitious assumption of the location of the neutral axis of the structure at the bottom edge. It is shown, that if only the influence of vertical ground movements is considered, this assumption does not necessarily provide the aimed effect for all *L/H*-ratio's for structures, For the combination of vertical hogging mode deformations with differential horizontal ground movements introducing tensile strains at the bottom edge of the building, this assumption is however shown to be a reasonable approach.

- The current LTSM suggests a fictitious assumption of an *E/G* value of 12.5 for a frame structure. This is shown not to be straightforward. Additionally the concept of the LTSM for obtaining strains should be limited to wall structures. For frame structures the modification of moments and shear forces in the beams and columns of the structure due to the imposed ground deformations is of prime interest to judge the damage sensitivity. A first step for a modified approach for frame structures is therefore presented.

- Additional factors influencing the damage response of a structure are described in section 3.4. Empirical bandwidths for implementation in the LTSM are given for the influence of the initial building condition and the time dependant development of the ground deformations in combination with beneficial creep or relaxation effects in the structure. Additionally, empirically based limiting values for tilt of tall structures with respect to the stability and limiting differential settlement values for the functionality of the connections of services with buildings, as derived from the literature, are given.

4 SOIL-STRUCTURE INTERACTION

4.1 General

This section presents the results of extensive numerical parametric studies on the effects of soil-structure interaction on building damage for the case of tunnelling induced ground movements.

Main objective of the analyses is to gain insight in the influence of different configurations and combinations of soil stiffness, interface properties and type, geometry and location of the structure on the expected building damage. The comparison with the damage prediction using the modified LTSM (see section 3) forms an important aspect in the analyses, as this method neglects the soil-structure interaction.

The principles of the judgement of soil-structure interaction effects are applicable to other deformation sources than tunnelling (see section 2) as the results are presented in terms of imposed greenfield parameters (differential ground deformations as deflection ratio, angular distortion and horizontal ground strain).

4.2 Literature

Addenbrooke (1996) developed a procedure to incorporate the effects of soil-structure interaction in the LTSM. He carried out extensive numerical parametric studies to investigate the influence of the building stiffness and soil stiffness on the overall response of a building imposed to ground movements. The numerical model used by Addenbrooke (1996) is shown in Figure 4.1.
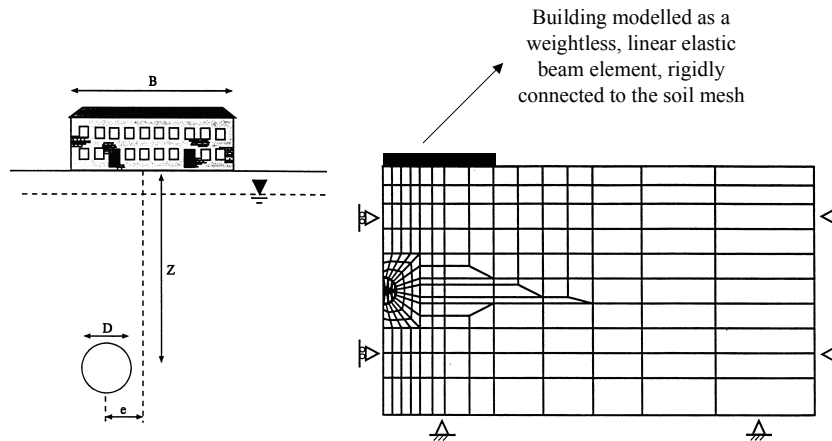
Figure 4.1: Interaction model of Addenbrooke (1996)

The parametric calculations were used to derive modification factors for the greenfield values of the deflection ratio, the angular distortion and the horizontal strain in the sagging and the hogging zone. These modification factors take into account the soil-structure interaction. They are presented in design charts (see Figure 4.2) and depend on the relation between relative axial and bending stiffness of the interaction system and the location of the building in the trough. The relative axial and bending stiffness describe the relation between building and soil stiffness.

The relative bending stiffness is defined by Addenbrooke (1996) as:

Soil-Structure Interaction

$$\rho^* = \frac{EI}{E_s \cdot H^4} \qquad (4.1)$$

with EI the bending stiffness of the building and E_s is the representative soil stiffness. They suggest to use the secant stiffness that would be obtained at 0.01% axial strain in a triaxial compression test performed on a sample from a depth of half the tunnel depth ($Z/2$; see Figure 4.1). H represents half the width of the beam ($=B/2$, see Figure 4.1).

The relative axial stiffness is defined by Addenbrooke (1996) as:

$$\alpha^* = \frac{EA}{E_s \cdot H} \qquad (4.2)$$

The modification factor for the greenfield deflection ratio (DR) value due to the soil-structure interaction is defined as:

$$M^{DR} = \frac{DR_{\text{interaction}}}{DR_{\text{greenfield}}} \qquad (4.3)$$

The modification factor for the greenfield horizontal strain value ε_h due to the soil-structure interaction is defined as :

$$M^{\varepsilon_h} = \frac{\varepsilon_{h,\text{interaction}}}{\varepsilon_{h,\text{greenfield}}} \qquad (4.4)$$

The modification factors derived by Addenbrooke (1996) from the numerical calculations are shown in Figure 4.2.

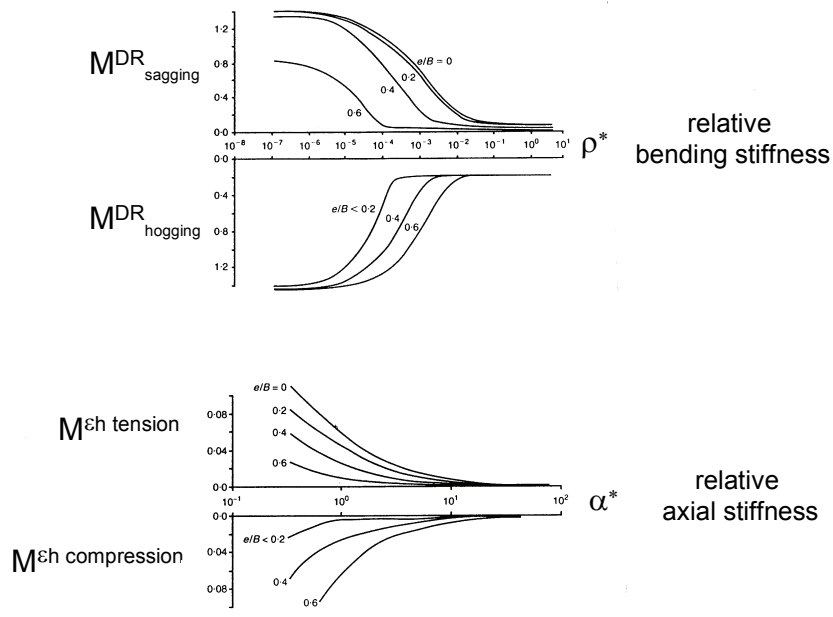**Figure 4.2: Modification factors for greenfield parameters due to soil-structure interaction**

The resulting modification factors show that the greenfield parameters for the deflection ratio and the horizontal strain are reduced with increasing values for the relative bending and axial stiffness. The modified values for the greenfield parameters are used in the LTSM approach of Burland et al. (2001)

for the prediction of the damage. A smaller modification factor leads to a higher reduction of the greenfield parameter and thus less damage of the building. The interaction reduces the horizontal greenfield strains up to a value between 0% and 10%.

Some limitations of this approach are:

- Focused on London clay.
- Interface between building and soil is assumed to be rough, thus the building is rigidly connected with the soil.
- No initial building loads (self weight or mobile loads) are considered.
- The building is modelled with a simplified beam with linear elastic material properties behaviour (axial and bending stiffness). Cracking and other nonlinear effects in the building or the interface have not been included. The influence of wall openings and the shell behaviour of walls is also not included in the model.

Although the approach represents a valuable addition to the existing LTSM it has to be considered as a first step towards including soil-structure interaction effects. The crucial restrictions on the model at the building side (rigid connection with soil, linear elastic material properties, neglecting the building loads and geometrical discontinuities like door and window openings in the structure) can have major impact on the building response. The method is developed within the research program of the JLE (Jubilee Line Extension) and is primarily meant for the special circumstances in London clay. The application of the method to other projects requires detailed engineering judgement.

The following section presents the results of numerical interaction studies which incorporate nonlinear behaviour of the building and the interface between soil and building. Furthermore advanced modelling of the building with plane stress finite elements and the real geometry, including doors and window openings for a facade wall, replace the simplified beam model used by Addenbrooke.

4.3 System stiffness parameter

It is emphasized that for the presentation of the interaction results of this thesis it is not chosen to use a system stiffness parameter to characterize and normalize the relation between the stiffness of the building and the soil. A great variety of different expressions for these system stiffness parameters are presented in the literature and used for the quantitative comparison of the interaction response of different interaction systems. One example is the definition of the system stiffness used by Addenbrooke (1996) as given in equation (4.1) of the previous section.

Schultze (1964) published a critical review of different widely used system stiffness parameter, compared the values with each other and addressed the shortcomings of the mostly used expressions. Using a system stiffness parameter for the comparison of different situations without being aware of the limitations can lead to wrong results and conclusions. The impact of the uncritical use of a system stiffness parameter is often underestimated in engineering practice. For dead weight cases it is shown in Netzel D. (1972), that different combinations of the often used simplified input parameters $EI_{building}$, E_{soil}, $L_{building}$ and $B_{building}$ for the system stiffness parameter do not necessarily lead to the same interaction response of internal loadings of buildings in terms of induced bending moments. This makes the approach of the system stiffness parameter as an absolute value not feasible to quantify interaction effects. The most important shortcomings which are not encountered in the standard definitions of the system stiffness parameters:

- thickness of the compressible, settlement causing, soil layer;
- difference in loading scheme of the building loads on the foundation element (single loads, line loads or uniform loads).

Only if these aspects are individually considered with difference influence factors in a system stiffness approach, such an approach could be able to give a feasible basis for comparing the influence effects of

different situations. This will however make the simplified system stiffness parameter far more complex and it therefore loses its power for practical application.

It is therefore not recommended to relate the interaction effects of different configurations and combinations of building and soil to a simplified value which is considered to be able to quantify the effects of different interaction systems dependant of the absolute value for the system stiffness parameter.

4.4 Numerical model

4.4.1 General

The numerical model and the parametric variation of its components (building, interface, soil and tunnelling), considered in this research, are schematically shown in the figure below.

Interface

Horizontal interaction — "rough"

Horizontal interaction — "smooth"

Vertical interaction — tension cut off

Building

Massive masonry bearing wall

Masonry facade wall

Smeared crack model for masonry

Variation of building location

Sagging   **Hogging**

Tunnel depth
22m

Tunnel
diameter 9m

44m

100m

**Volume loss variation modelled by an incremental
contraction of the tunnel area**
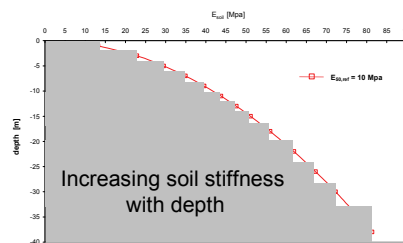
Soil

Increasing soil stiffness
with depth
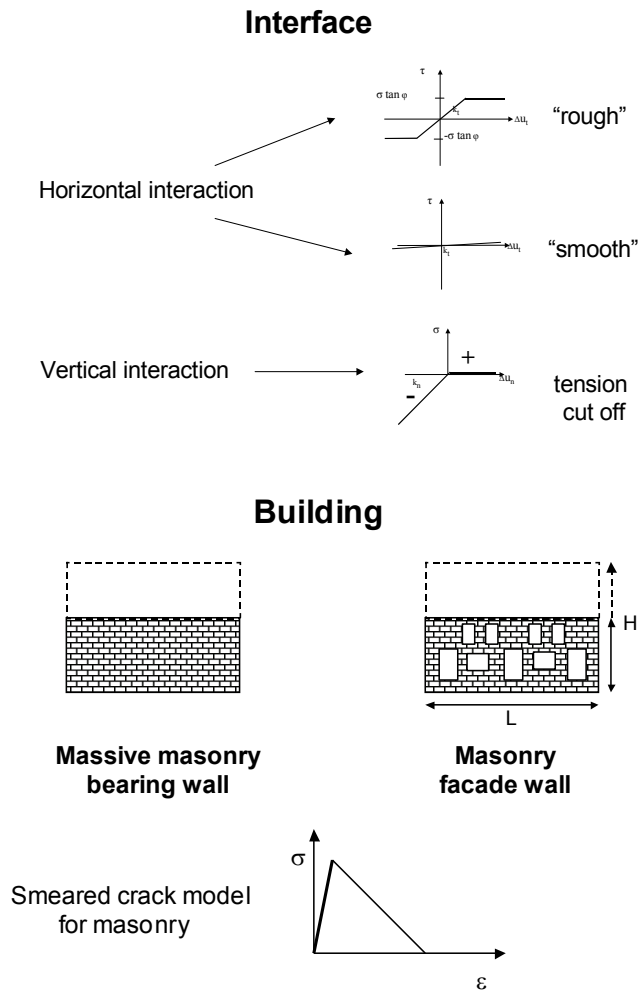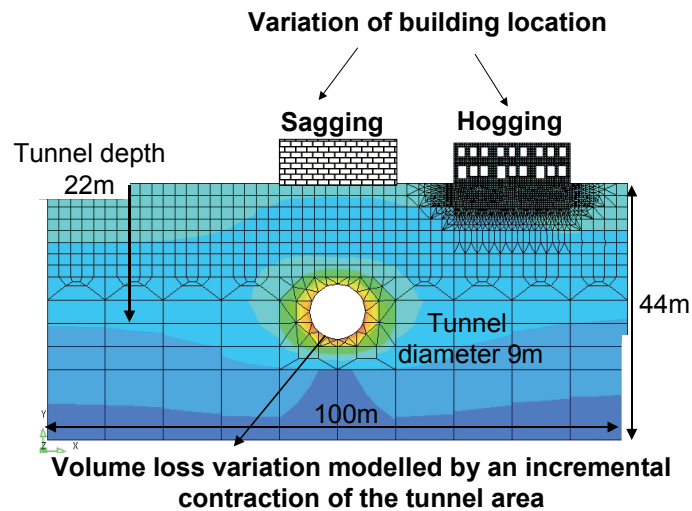
Variation of
soil stiffness

Soil type	$E_{50,ref}$ [Mpa]
A	10
B	50
C	100

Figure 4.3: Numerical model with parametric variations of its components

A systematic parameter study was designed, including:

- 3 different soil stiffness;
- 3 volume losses due to tunnelling causing differential imposed ground movements and distortions of the structures;
- 2 interface properties smooth and rough for variation of transfer of horizontal forces between soil and building;
- 2 different wall types; a massive masonry bearing wall and a masonry facade wall with openings of doors and windows;
- 2 different locations of the walls in the settlement area; hogging and sagging situation;
- 2 different heights of the building resulting in two different L/H ratio's.

Soil-Structure Interaction

Phased nonlinear calculations are carried out starting with the initial loading situation of the building and the soil (activation of self weight and mobile building loads). Subsequently the tunnelling process was simulated with an incremental increase of the volume loss in loading steps, causing differential ground movements. An incremental iterative procedure was applied taking into account cracking in the building and nonlinear behavior of the interface.

4.4.2   Soil

The parametric studies of the interaction calculations are carried out for a linear elastic soil model. Due to the numerical restrictions regarding the calculation time and the numerical stability of the complex interaction analyses the implementation of nonlinear material properties of *all* components of the model (soil, building and interface) are judged not to be feasible in the current stage of the research. It was therefore decided to carry out the parametric variations only for a linear soil model, while the building model and interface model were nonlinear. The combination of nonlinear soil, building and interface is a challenge for future research.

The soil was considered as an isotropic material with linear elastic material properties. The input parameters are the linear elastic soil stiffness $E_{soil,linear\ elastic}$ and Poisson's ratio ν. To take into account the increasing soil stiffness with depth the mesh was divided in different horizontal soil layers. Each layer in the mesh was assigned a constant E-value, increasing with the depth. Figure 4.4 shows an example for the case with the characteristic soil stiffness $E_{50,ref}$=10MPa. The Poisson's ratio was assumed to be 0.2.
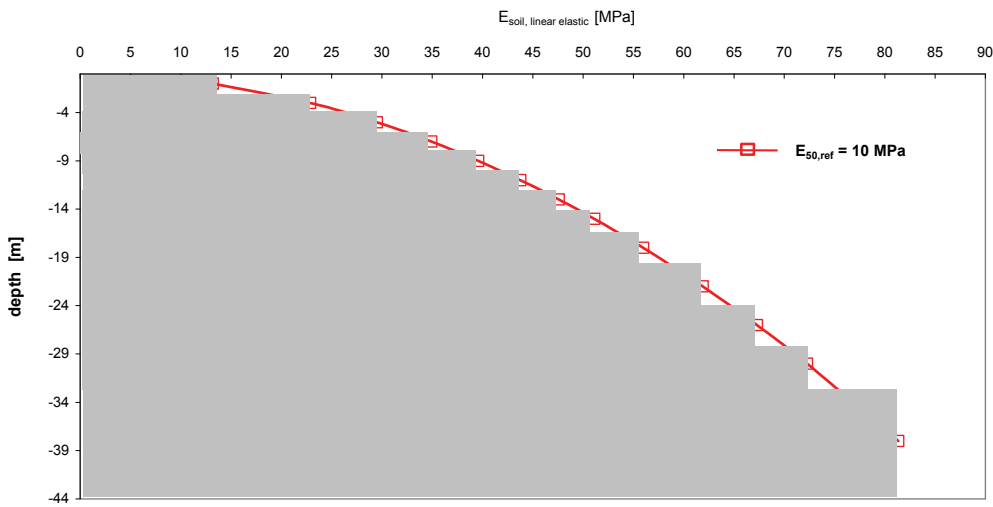
Figure 4.4: Example of the implementation of the increasing soil stiffness $E_{soil,linear\ elastic}$ with depth

The different soils used in the interaction calculations are meant to cover a broad range of soil stiffness in order to be able to judge the soil-structure interaction effects for different ratio's of soil and building stiffness. The different soils used in the numerical calculations are characterized in terms of the triaxial stiffness parameter $E_{50,ref}$, see Table 4.1. The determination of $E_{50,ref}$ from a triaxial test is described in Appendix 4.

Soil type	$E_{50,ref\ [MPa]}$
A	10
B	50
C	100

Table 4.1: Considered soils A to C

Soil-Structure Interaction

The relation between the linear elastic soil stiffness $E_{soil,\ linear\ elastic}$ used as input in the finite element code DIANA and the relation with the characteristic value for $E_{50,ref}$ is described in Appendix 4. The resulting variations of $E_{soil,\ linear\ elastic}$ with depth for the different soils A to C applied in the numerical calculations are shown in Figure 4.5.
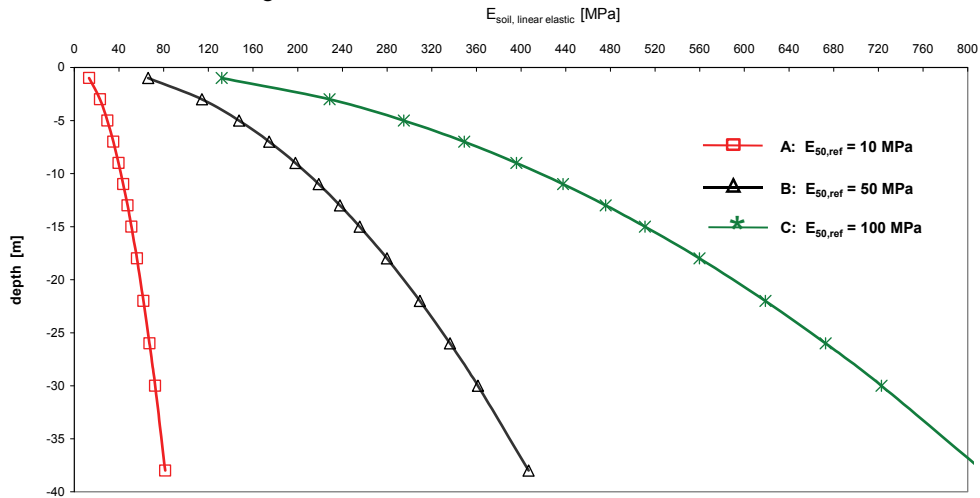

Figure 4.5: Increase of the linear elastic soil stiffness $E_{soil,linear\ elastic}$ with depth used in the numerical model

4.4.3   Tunnelling proces

The volume loss generated by the tunnelling process is simplified in the numerical model with a centric contraction of the tunnel area with a tunnel diameter of 9,5m. It is emphasized that this assumption does not lead to an optimal prediction of the ground movements due to TBM-tunnelling. The tunnelling operation is in fact a complex process, where face pressure, tail void grouting process, conicity and overcutting contributes to the overall performance regarding ground movements, see section 2.2.2.

In the present study it was decided to use the simplified contraction model, because this study is focused on the soil-structure interaction effects and consequently the building response due to *differential* ground movements rather than on the correct prediction of absolute ground movements due to TBM-tunnelling. Furthermore, the numerical interaction model would become far more complex with the risk of numerical instability, if the TBM-settlement performance would be modelled with an advanced grout pressure model. As mentioned already in section   2.2 these models are still under development.

Consequently the studies can not be used to define relations between the absolute values of the volume loss due to tunnelling and the building response. The induced greenfield movements at the buildings are described in terms of differential ground movements via characteristic deformation parameters (deflection ratio, angular distortion and horizontal ground strain).

Three different tunnelling performances were identified with the contraction model, referred to as volume loss 1 to 3. In the numerical calculations the tunnelling process is modelled as one loading case where the degree of contraction and consequently the volume loss is incrementally increased in small loading steps. Three loading levels representing the three volume losses were chosen for processing and interpretation of the results. The volume losses were first applied in a greenfield calculation (without the buildings) causing differential greenfield ground movements at the fictitious locations of the buildings.

The degree of contraction was adjusted for the different soil stiffness in order to achieve the same distribution of greenfield ground movements for all different soil stiffness. The greenfield results for horizontal and vertical ground movements for volume loss 1 to 3 are shown in Figure 4.6.
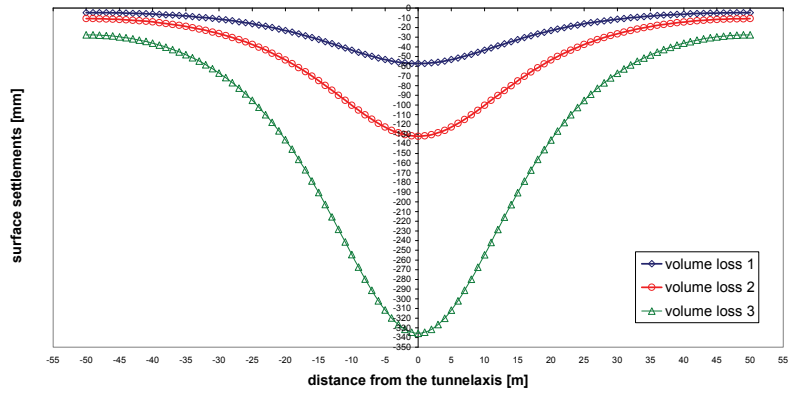
(a) vertical greenfield ground movements
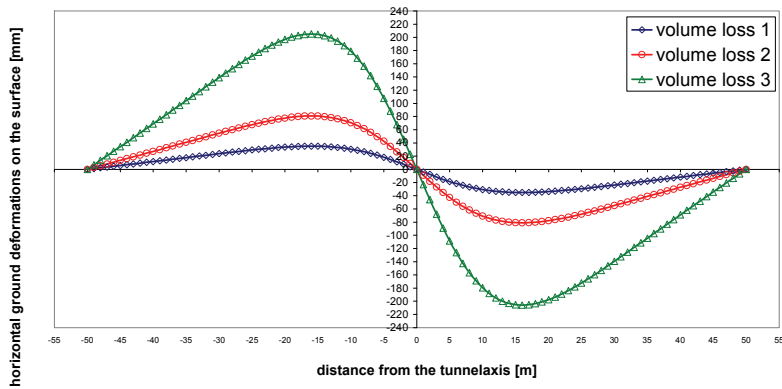
(b) horizontal greenfield ground movements

Figure 4.6: Greenfield ground deformations for volume loss 1 to 3

The numerical soil-structure interaction calculations include the following loading steps:

- Phase 0 Generation of initial soil stresses and strains under dead weight of the soil (without the tunnel, the building and the interface).

- Phase 1 Generation of initial soil and building stresses and strains due to the loading and the stiffness of the building (interaction with interface, building and soil).

- Phase 2 Tunnelling contraction gradually increased up to the volume loss 1.

- Phase 3 Tunnelling contraction gradually increased from volume loss 1 to volume loss 2.

- Phase 4 Tunnelling contraction gradually increased from volume loss 2 to volume loss 3.

Phased calculations integrate the strain and stress histories of previous loading steps in all components of the model. In order to be able to judge purely the deformation influence of the tunnelling process on the buildings, the influence of the initial displacements from phase 0 and phase 1 are set to zero, before the tunnelling process in phase 2 is activated. The initial stresses and strains from phase 0 and phase 1 however remain in the soil and the structure when tunnelling contraction starts in phase 2. An incremental iterative procedure is used for the nonlinear calculations to increase the contraction of the tunnel gradually.

4.4.4   Wall structure

4.4.4.1   General

The 2D calculations consider a massive masonry bearing wall and a masonry facade wall which are influenced by the transverse trough of the tunnelling process. These cases represent characteristic 2D cross sections of a building, as shown in Figure 4.7.
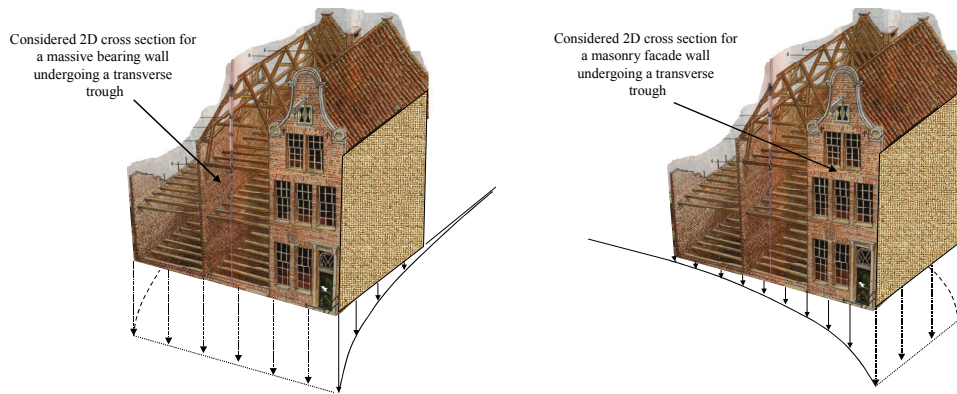

Figure 4.7: Considered 2D sections of a 3D building

The material behavior for the masonry structures was modeled with a nonlinear smeared crack model. For comparison also some analyses without cracking were performed with linear elastic masonry properties. The majority of the calculations was however carried out with the nonlinear crack model in order to be able to obtain realistic results regarding expectable cracking patterns and crack widths in the wall structures. The finite elements of the 2D model are quadratic eight-node plane stress type elements for the wall and plane strain elements for the soil, see Figure 4.8.
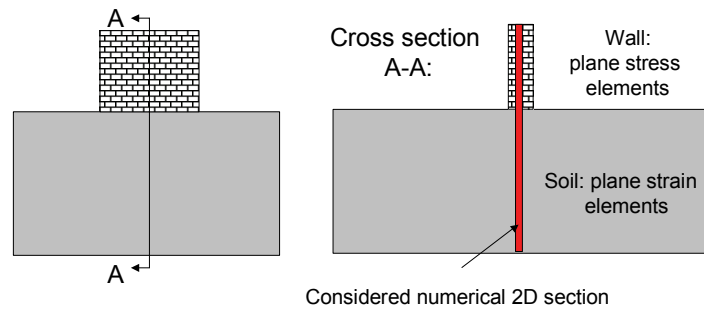

Figure 4.8: Plane stress elements for the wall and plain strain elements for the soil

4.4.4.2   Wall geometries and location

The height of the wall was varied in order to investigate the influence of different *L/H*-ratio's. The variation is shown for the example of the massive masonry walls in Figure 4.9. The same *L/H* variation was adopted for the masonry façade walls with door and window openings. The location of the structure was varied in order to study the building response in the hogging and the sagging mode.
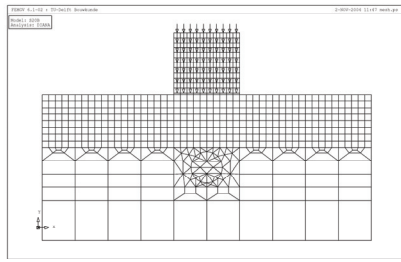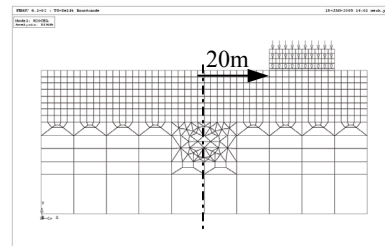

Sagging,
wall length 20m;
wall height 20m
L/H = 1
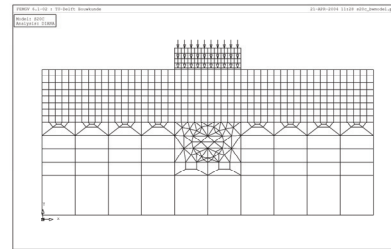
Sagging,
wall length 20m;
wall height 6.5m
L/H = 3
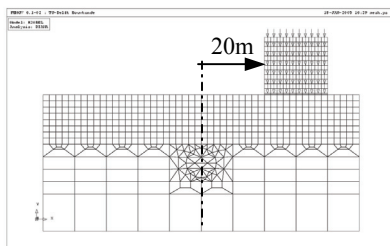
Hogging,
wall length 20m;
wall height 20m
L/H=1

Hogging
wall length 20m;
wall height 6.5m
L/H=3

Figure 4.9: Variation of geometry and location of the building for the example of the massive masonry wall

4.4.4.3   Building loads

The initial loading stage in the phased calculations represents the initial loading situation of the building. The walls are initially loaded under the influence of its self-weight and the floor loads. The finite element program automatically generates the self-weight of the masonry walls from the modelled geometry and prescribed density (γ =20 kN/m^3 for masonry). The applied floor loads on the masonry wall are calculated from the dead weight of timber floors in old masonry structures (0.5 kN/m^2 for the roof level and 0.75 kN/m^2 for all other floor levels) and the mobile floor loads (1 kN/m^2 for the roof level and 1.5 kN/m^2 for all other floor levels). For the mobile loads 50% of the maximum allowable values on all levels is taken into account for a representative loading situation.

A general span width of the timber floors of 7m perpendicular to the 2D-plane of the model is used to determine the line loads at each floor level for the *massive masonry bearing wall*, see Figure 4.10. The line loads from the floors are translated into wall stresses for the 2D calculations with a wall thickness of 0.3m.

Figure 4.10: Loading scheme massive masonry bearing wall for the example of L/H=3

A stroke of 1m perpendicular to the 2D-plane of the model is used to determine the line loads at each floor level for the *masonry facade wall,* see Figure 4.11. The line loads from the floors are translated into wall stresses for the 2D calculations with a wall thickness of 0.3m.

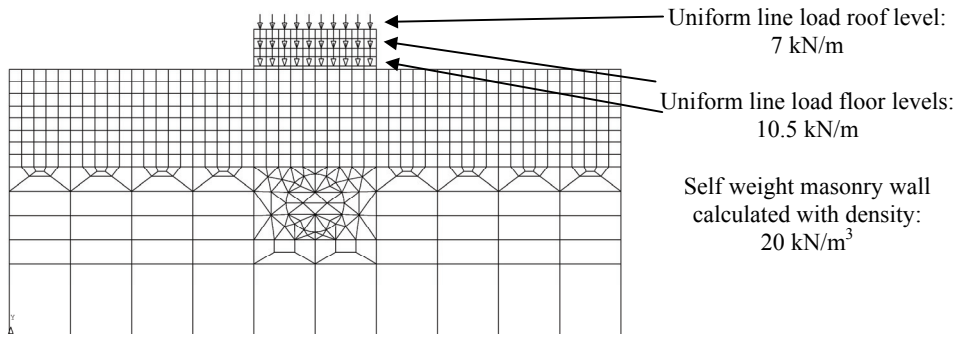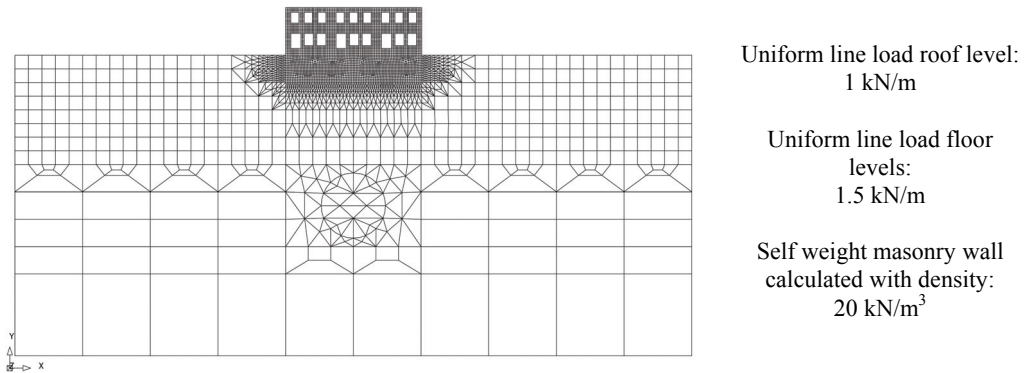**Figure 4.11: Loading scheme masonry facade wall for the example of *L/H=3***

The detailed dimensions of the door and window openings for the masonry facade wall are given in Figure 4.12.
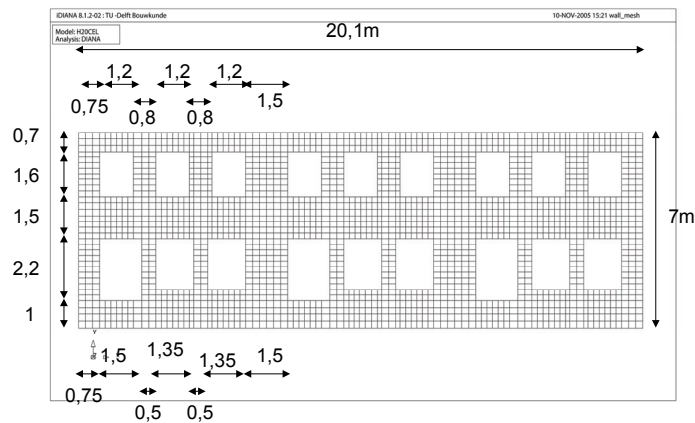

Figure 4.12: Geometry of masonry facade walls

4.4.4.4   Material model masonry

The masonry has been modelled as an elastic-softening material. In the initial uncracked stage the stress-strain behaviour is assumed to be isotropic and linearly elastic, while a softening law is inserted once cracking occurs.

The isotropic linear-elastic behaviour of the masonry wall in plane stress is described by two parameters, Young's modulus E and Poisson's ratio v, or alternatively via E and the shear modulus $G = E / (2 (1 + v))$. In the present study, E was taken as 6000 N/mm^2 and v was assumed to be 0.3, implying a shear modulus G of 2307 N/mm^2. The density of the masonry was assumed to be 2000 kg/m^3. The values are listed in Table 4.2 and are considered to be representative for a wide class of masonry, see e.g. Rots (1997).

The isotropic assumption certainly is a simplification of reality, as masonry is an orthotropic material with different behaviour in the direction of head joints and bed joints. Orthotropic models exist (e.g. Lourenco et al. (1998)), but are considered to be too detailed for this stage of the first nonlinear soil-wall interaction research. Refinements can be made in following studies. In addition, it should be mentioned that for settlement cases most of the tensile strain activity is in horizontal direction, leading to vertical cracks, implying that the horizontal elastic constants and cracking parameters prevail and can be the basis for the isotropic model.

Table 4.2: Linear-elastic masonry parameters

Masonry			
Parameter		Value	Unit
Young's modulus	E	6000	N/mm^2
Shear modulus	G	2307	N/mm^2
Density	ρ	2000	kg/m^3

A nonlinear smeared crack model has been used to model the cracking behaviour of the masonry beyond the linear-elastic stage, see e.g. Rots (1988). The effect of cracking is spread over the area that belongs to an integration point of the finite element, as sketched in Fig. 4.13. The stress-strain behaviour then switches from the linear-elastic relation to a softening stress-strain relation. As the model still departs from strains, not from discrete crack widths, the terminology smeared cracking is adopted. A smeared crack model is a continuum model which fits the nature of the finite element displacement method. It does not require re-meshing for discrete crack paths, but it uses existing nodes and existing degrees of freedom from the initial mesh. Another advantage is that smeared cracks can occur anywhere in the mesh in any direction.
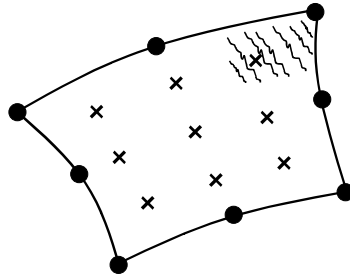
Figure 4.13: Impression of a smeared crack in an integration point of a finite element

A smeared crack model involves parameters that describe the initiation, the propagation and the possible unloading or closure of the crack.

For the initiation, a tension cut-off criterion is used, bounding the linear-elastic domain. In this study a single-parameter constant stress cut-off criterion in the principal stress space has been assumed, Fig. 4.14. Once the major principal tensile stress exceeds the value of the tensile strength f_t, a smeared crack is initiated perpendicular to the direction of this major principal tensile stress. This crack initiation

criterion orthogonal to principal stress is widely accepted for concrete and masonry. For cases with significant lateral compression, more sophisticated stress cut-off criteria might be considered.

Figure 4.14: Constant tension cut-off criterion in two-dimensional principal stress space, for crack initiation

For the propagation, a fracture mechanics based tension-softening relation is used. With n indicating the direction normal to the smeared crack, the stress σ_{nn} decreases as a function of the strain ε_{nn}, as shown in Fig. 4.15. The softening reflects the gradual process of micro-cracking and debonding, finally resulting in a fully open macro-crack wit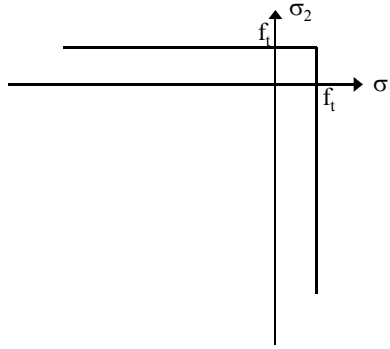h zero stress transfer. The parameters are the fracture energy G_f, the crack band width h and the shape of the softening diagram. The fracture energy G_f is defined as the energy required to create one unit of area of a macro crack. This energy is equal to the area underneath the stress-crack width diagram for a discrete crack, reflecting the work to create such crack. For a smeared crack, the crack width is smeared out into a strain over a certain width, the so-called crack band width h which is related to the size, type and integration scheme of the finite element. Consequently, the area underneath the crack normal stress-strain diagram equals G_f/h. In this study, a linear softening diagram is employed. Then, it can be shown that the ultimate strain ε_u of the linear softening branch equals $(2\,G_f)/(f_t\,h)$. Backgrounds of this tension-softening formulation can be found in e.g. Bazant et al. (1983), Rots (1988). The crack band width h also plays a role in interpreting the results of the analyses in this thesis, where smeared crack strain are converted back into a crack width, in order to make contact with damage classification systems based on notions of crack widths. The crack width w equals the crack strain ε_{nn} times the crack band width h.
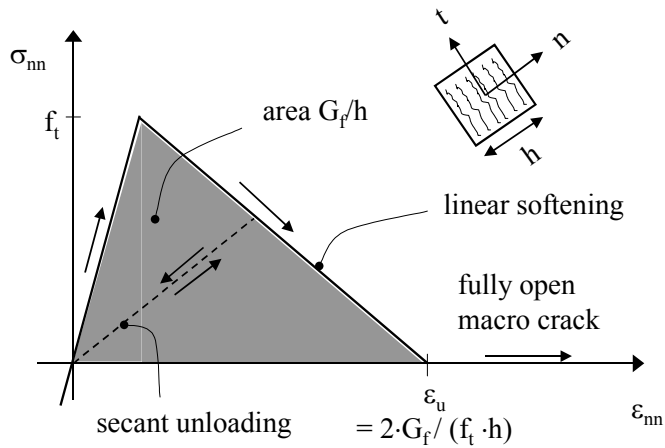

Figure 4.15: Linear tension-softening diagram and parameters, for crack propagation

Soil-Structure Interaction

For the unloading of cracks, a secant unloading/reloading branch is assumed back to the origin, as indicated in Fig. 4.15. In wall analyses, unloading cracks frequently occur. Due to the finite load steps in the incremental-iterative procedure, multiple integration points of multiple elements may crack simultaneously, with only a few of them surviving in the propagation process while others are arrested. In interpreting the crack outputs, mainly the active opening cracks will be considered, while unloading cracks will be omitted.

In the present study, the tensile strength f_t was assumed to be 0.3 N/mm^2, the fracture energy G_f was taken as 0.05 N/mm, a linear tension softening diagram was assumed and the crack band width h was calculated depending on the dimensions of the elements. This set of parameters is assumed to be representative for a wide class of masonry, see e.g. Rots (1997). Parameter variations for settlement damage studies have been reported by Boonpichetvong et al. (2003, 2005). The values and outcome in terms of the ultimate strain ε_u of the linear softening diagram are listed in Table 4.3.

Table 4.3: Material parameters for the nonlinear masonry behaviour

tensile strength f_t	0.3 N/mm^2
fracture energy G_f	0.05 N/mm
crack bandwidth h* (depending on element dimensions)	125mm (for elements of the façade wall) 875mm (for elements of the massive wall)
ultimate strain $\varepsilon_u^{cr} = \dfrac{2 \cdot G_f}{f_t \cdot h}$ * (depending on element dimensions)	2.6 E-3 (for elements of the façade wall) 3.8 E-4 (for elements of the massive wall)

*the values for the crack bandwidth and the ultimate strain depend on the element dimensions, which are different for the façade wall and the massive wall.

The above assumptions are simplifications of reality, as masonry is an orthotropic material and both the tensile strength as well as the fracture energy will depend on the angle between the crack and the head joints and bed joints respectively. Orthotropic models are considered to be too detailed in this stage of the first nonlinear soil-wall interaction research. Also, refinements towards exponential softening diagrams instead of linear softening diagrams, or towards more sophisticated assumptions for the crack band width can be made in following studies.

As a final remark, it is mentioned that the constitutive model adopted was based on a decomposition of the total strain into elastic strain and crack strain. This formulation has advantages for describing elastic-softening principles which inherently imply a split between the crack and the elastic material at either side of the crack. It includes the possibility of multiple orthogonal or non-orthogonal cracks having their own softening and unloading status. Also, this model belongs to the class of fixed crack models, where the direction of the crack is fixed upon crack initiation. The behaviour is described in this fixed crack system, as opposed to rotating crack models where the softening is described in the continuously rotating principal directions. Fixed crack models use a shear retention factor β for the description of shear transfer across the crack. A β of 1 implies that the full elastic shear modulus G is retained after cracking, corresponding to a rough interlocked crack. A β of 0 implies that the shear stiffness is set to zero after cracking, corresponding to a perfectly smooth crack. In the present study a small value of $\beta = 0.01$ was adopted in order to avoid stress locking and over stiff response. For detailed information about these backgrounds and the parameters of non-linear crack models for masonry and concrete the reader is referred to Rots et al. (1985), Rots (1988), Rots (1997) and DIANA (2002).

4.4.5   Interface

4.4.5.1   General

The connection between the soil and the structure is modelled with interface elements. These elements are situated along the boundary of the soil and the lower edge of the structure. The interface elements describe the interaction and thus the transfer of vertical and horizontal stresses between soil and building. Nonlinear material models should be used for the modelling of the interface behaviour in order to limit the normal and shear stresses transferred between building and soil to realistic values. The parameters of the interface models used in this study are described in the following sections.

4.4.5.2   Material model

The interface element relates the stresses acting on the interface (in horizontal and vertical direction) to the relative displacement of the two sides of the interface. The frictional behaviour of the interface can be described using the concept of the Coulomb friction criterion.

Two scenarios are considered for the possible transfer of *horizontal stresses* between building and soil:

- Smooth interface
  For the smooth interface, a very low value for the horizontal interface stiffness k_t is adopted (10^{-15} N/mm^3) to neglect any shear transfer between soil and structure (see Figure 4.16). A smooth type of interface can for example occur in case of very loose sands (the slipping is than occurring directly in the sand) or a very effective coating/foil, which reduces and even eliminates the mobilisation of friction between soil and building. The chosen value for this study is a lower bound used for the parametric study. This value neglects the transfer of shear stresses between soil and building, leading to immediate slipping if differential horizontal movements between soil and building occur. Different realistic values for different coating connections of the soil and the building are given by Schuette (1997).
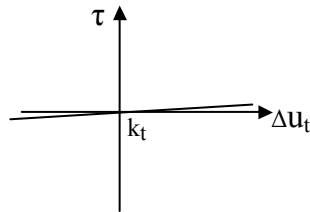

Figure 4.16: Interface properties in horizontal direction for smooth interface

- Rough interface
  For the rough interface the horizontal interface stiffness k_t is taken as 1 N/mm^3. Kolb (1988) defined a mobilisation function for the friction in sand and suggested to use a simplified bilinear relation with the stiffness $k_t = \sqrt{D}$ (see Figure 4.17). The value for k_t of 1 N/mm^3 is used in the numerical calculations and can be considered to be representative for a dense sand ($D > 0.5$). A lose sand (D=0.15-0.3) for example gives a k_t value of ca. 0.5. D describes the "Lagerungsdichte" (according to the German code DIN 18 126).

The equation shown on the right of the figure:

$$\frac{\tau}{\sigma_n \cdot \tan \delta_{sf}} = \frac{\dfrac{v}{d_v} + \left(1 - \dfrac{\sqrt{D}}{4}\right)\cdot\left(\dfrac{v}{d_v}\right)^2}{\left(\dfrac{v}{d_v}\right)^2 + \dfrac{1}{\sqrt{D}}}$$

σ_n = Sohlnormalspannung (lokal)
δ_{sf} = Bruchsohlreibungswinkel
D = Lagerungsdichte des Untergrunds
v = lokale Verschiebung an der Struktur der Sohlfläche
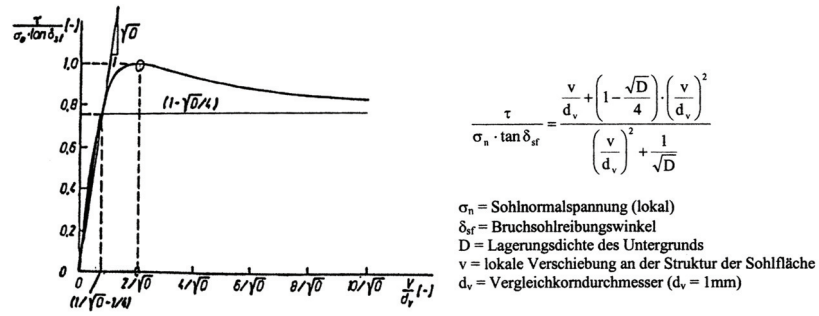d_v = Vergleichkorndurchmesser (d_v = 1mm)

Figure 4.17: Mobilisation function of friction for sandy soils according to Kolb (1988)

The yield function of horizontal stresses τ across the rough interface is modelled as elastoplastic behaviour controlled by the magnitude of normal stress σ and the angle of friction φ. A friction angle of 20° is generally used in the calculations resulting in a friction coefficient of 0.36 (tan 20^0). For one calculation a value of 35° is used as variation, resulting in a friction coefficient of 0.7. For interface shear stresses τ below the yield limit, the relative shear displacement Δu_t is related to shear stresses via $\tau = k_t \cdot \Delta u_t$ (see Figure 4.18). The Coulomb friction model is a plasticity based model which also includes a plastic potential function to describe the direction of plastic deformation. Here, the dilatancy angle ψ is used, reflecting the amount of uplift upon shearing. In the present study, ψ was assumed to be zero, i.e. no uplift upon shearing.
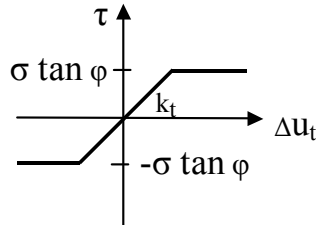

Figure 4.18: Interface properties in horizontal direction for rough interface

The *transfer of normal tensile stresses* between building and soil is eliminated for the smooth and the rough interface type by the introduction of a tension-cut off criterion for the normal interface stresses. The implemented stress-relative displacement relation in the normal direction of the interface for tensile stresses is shown in Figure 4.19. A gap is assumed to open between soil and building once the tension cut-off criterion is violated.
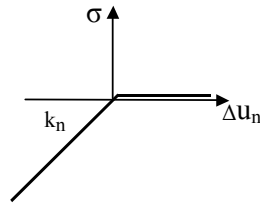

Figure 4.19: Interface properties in normal direction

The normal stiffness of the soil-structure interface k_n, is taken as 1 N/mm^3. In fact, this interface stiffness only serves to suppress the initial elastic normal deformation in the interface elements.

From numerical experience, a higher value of the normal interface stiffness must be avoided to relieve the problem of stress oscillation and numerical instability, see Rots (1988).

4.5   Empirical analytical damage prediction with the LTSM

4.5.1   General

The comparison of the numerical results with the LTSM approach forms an important aspect to judge the influence of soil-structure interaction as it is neglected in the empirical analytical LTSM approach. The greenfield ground movements of volume loss 1 to 3 (see Figure 4.6) are projected on the location of the building in the sagging and the hogging zone and the damage is predicted with the modified LTSM (see section 3.5). In this damage prediction it is distinguished between the consideration with or without horizontal ground movements, as the numerical analyses also distinguishes between smooth (neglecting the horizontal interaction) and rough interface behavior.

4.5.2   Hogging zone

The differential greenfield ground movements of volume loss 1 to 3 and the corresponding deformation parameters at the location of the building in the hogging zone (see Figure 4.9) are presented in this section.

4.5.2.1   Volume loss 1

Figure 4.20 shows the results of the damage parameters for the differential vertical ground movements and volume loss 1.
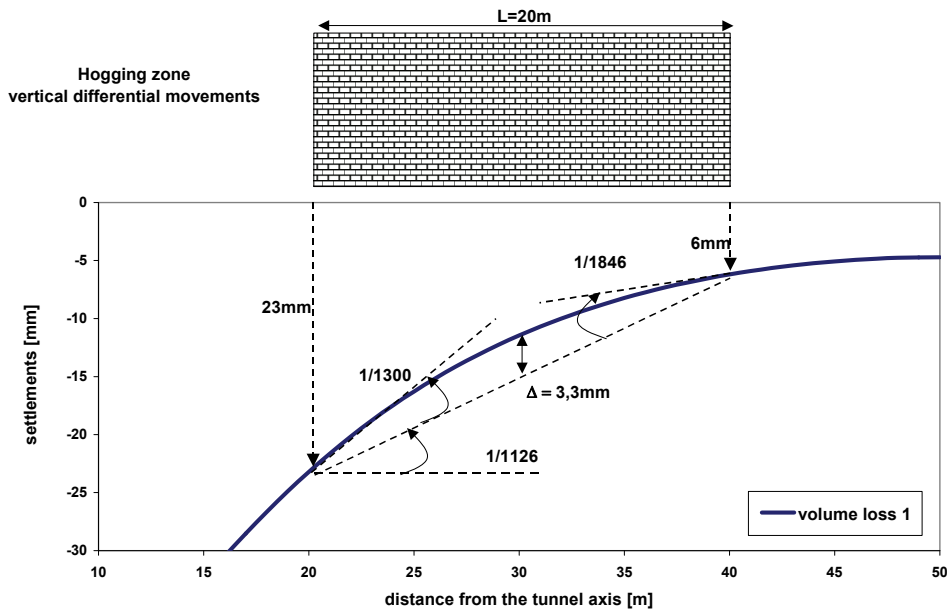

Figure 4.20 Damage parameters for differential vertical ground movements in the hogging zone; volume loss 1

Figure 4.21 shows the results of the damage parameters for the differential horizontal ground movements and volume loss 1.

Figure 4.21: Differential horizontal ground movements in the hogging zone; volume loss 1

4.5.2.2   *Volume loss 2*

Figure 4.22 shows the results of the damage parameters for the differential vertical ground movements and volume loss 2.

Figure 4.22: Damage parameters for differential vertical ground movements in the hogging zone; volume loss 2

Soil-Structure Interaction

Figure 4.23 shows the results of the damage parameters for the differential horizontal ground movements and volume loss 2.
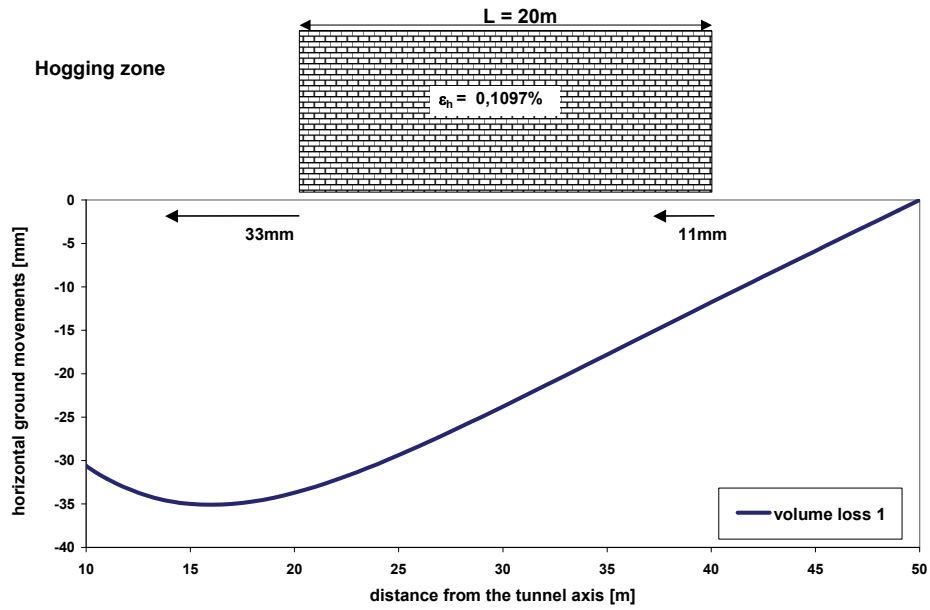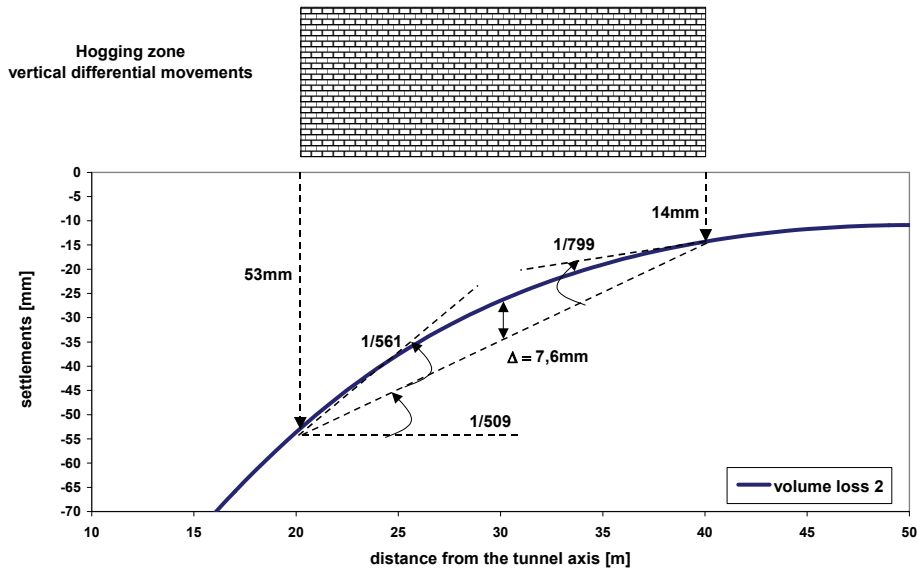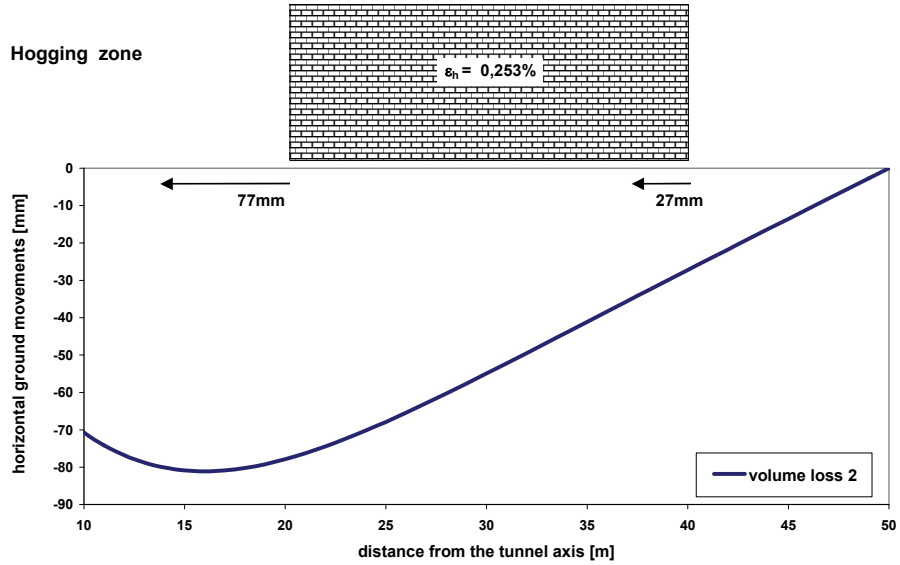

Figure 4.23: Differential horizontal ground movements in the hogging zone; volume loss 2

4.5.2.3   Volume loss 3

Figure 4.24 shows the results of the damage parameters for the differential vertical ground movements and volume loss 3.
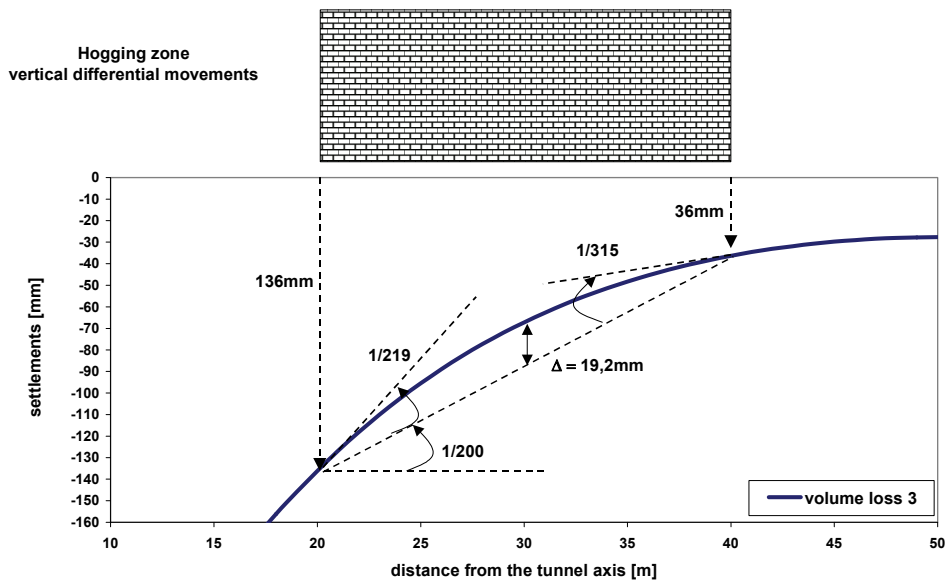

Figure 4.24: Damage parameters for differential vertical ground movements in the hogging zone; volume loss 3

Figure 4.25 shows the results of the damage parameters for the differential horizontal ground movements and volume loss 3.
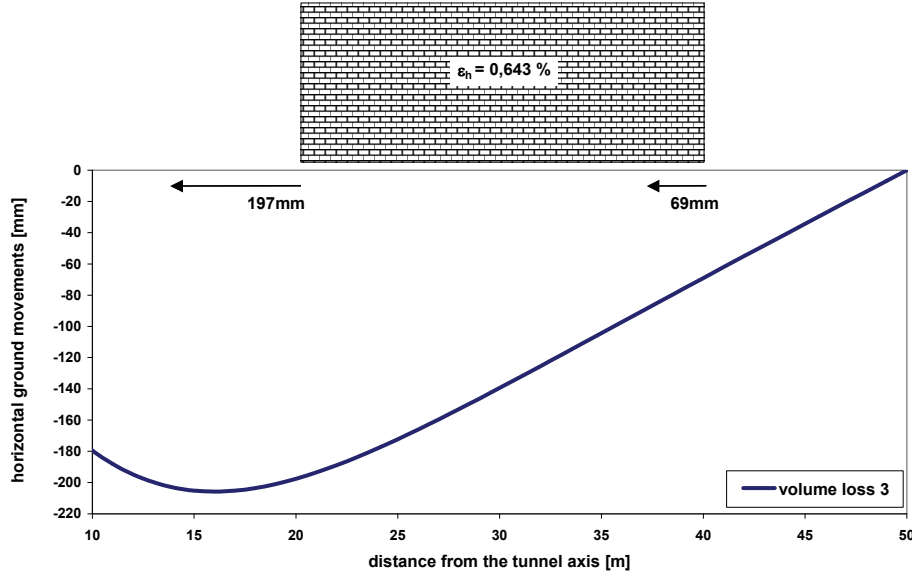

Figure 4.25: Differential horizontal ground movements in the hogging zone; volume loss 3

4.5.2.4   *Summary of LTSM results for the hogging zone*

The results for the relevant strains according to the modified LTSM and the corresponding damage classes are summarized in Table 4.4. It is emphasized that the approach of choosing the neutral axis at the bottom edge of the wall is used for the hogging zone, see section 3.5.

HOGGING	volume loss 1	volume loss 2	volume loss 3
L/H=3			
horizontal strain	0,110%	0,253%	0,643%
bending strain due to deflection ratio	*__0,027%__*	*__0,063%__*	*__0,161%__*
diagonal strain due to average angular distortion	0,020%	0,046%	0,116%
diagonal strain due to maximum angular distortion	0,023%	0,058%	0,137%
total strain; combined bending and horizontal strain	*0,137%*	*0,317%*	*0,804%*
total strain; combined average diagonal and horizontal strain	0,113%	0,261%	0,663%
total strain; combined maximum diagonal and horizontal strain	0,114%	0,266%	0,671%
rough (full transfer of horizontal strain)	*slight*	*moderate/severe*	*severe*
smooth (no transfer of horizontal strain)	*__negligible__*	*__very slight__*	*__slight/moderate__*
L/H=1			
horizontal strain	0,110%	0,253%	0,643%
bending strain due to deflection ratio	0,016%	0,036%	0,093%
diagonal strain due to average angular distortion	0,035%	0,083%	0,211%
diagonal strain due to maximum angular distortion	*__0,042%__*	*__0,106%__*	*__0,249%__*
total strain; combined bending and horizontal strain	*0,125%*	0,290%	*0,735%*
total strain; combined average diagonal and horizontal strain	0,120%	0,278%	0,706%
total strain; combined maximum diagonal and horizontal strain	0,124%	*0,292%*	0,728%
rough (full transfer of horizontal strain)	*slight*	*moderate*	*severe*
smooth (no transfer of horizontal strain)	*__negligible__*	*__slight__*	*__moderate__*

Table 4.4: Damage prediction with the LTSM for the hogging zone

The results show significant more damage for the rough cases than for the smooth cases. The reason for these differences is the fact, that the smooth cases neglect the transfer of horizontal differential ground movements on the building. As the horizontal differential ground movements cause additional tensile strains in the tunnelling hogging zone, the damage is increased if the transfer of horizontal differential ground movements is taken into account.

4.5.3   Sagging zone

The differential greenfield ground movements of volume loss 1 to 3 (Figure 4.6) and the corresponding damage parameters at the location of the building in the sagging zone (see Figure 4.9) are presented in this section.

4.5.3.1   *Volume loss 1*

Figure 4.26 shows the results of the damage parameters for the differential vertical ground movements and volume loss 1.

Figure 4.26: Damage parameters for differential vertical ground movements in the sagging zone; volume loss 1

Figure 4.27 shows the results of the damage parameters for the differential horizontal ground movements and volume loss 1.

Figure 4.27: Damage parameters for differential horizontal ground movements in the sagging zone; volume loss 1

4.5.3.2   Volume loss 2

Figure 4.28 shows the results of the damage parameters for only the differential vertical ground movements and volume loss 2.
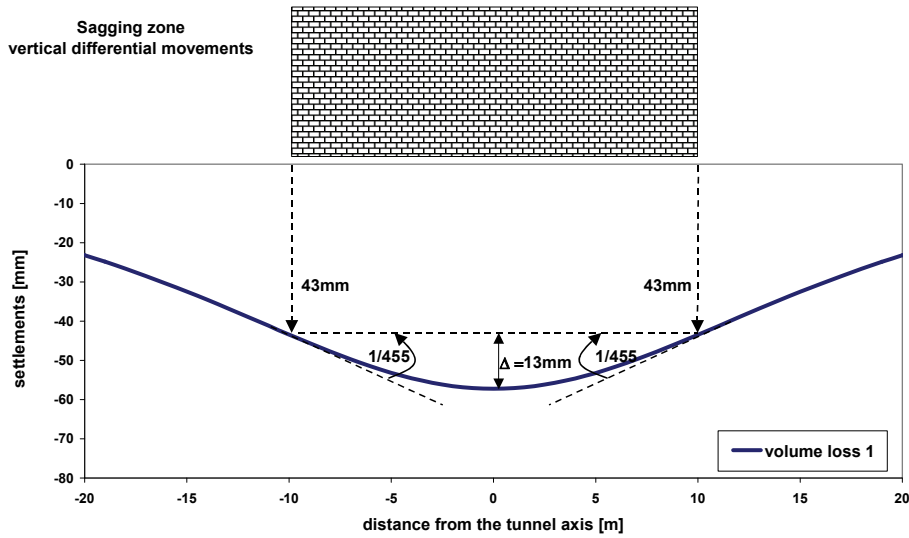

Figure 4.28: Damage parameters for differential vertical ground movements in the sagging zone; volume loss 2

Figure 4.29 shows the results of the damage parameters for the differential horizontal ground movements and volume loss 2.
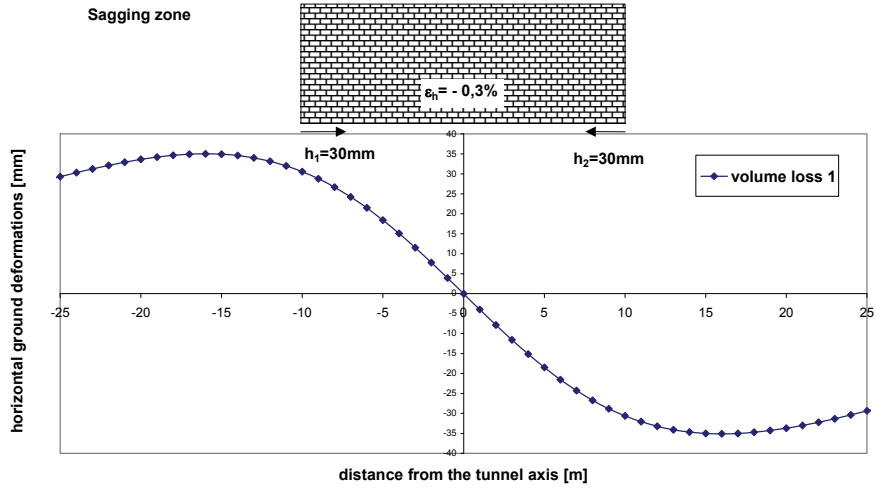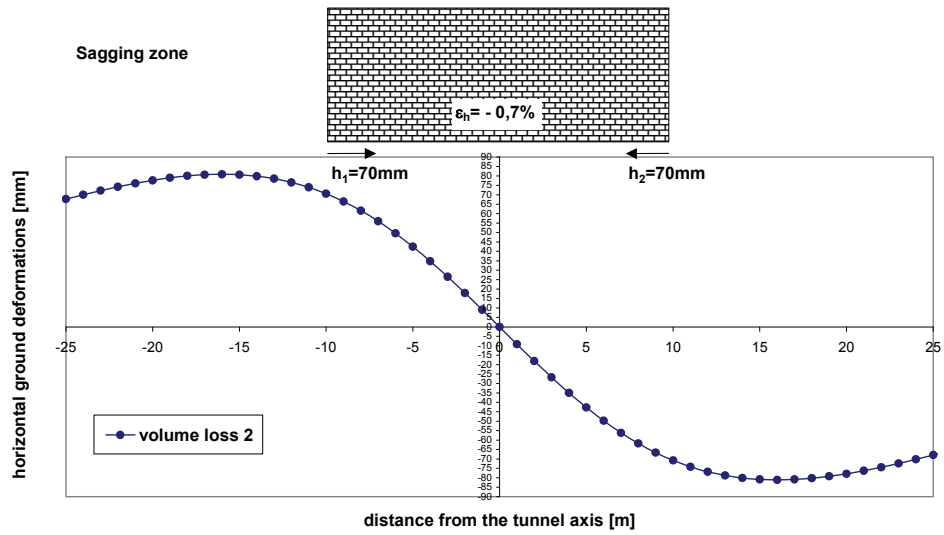
Figure 4.29: Damage parameters for differential horizontal ground movements in the sagging zone; volume loss 2

4.5.3.3   *Volume loss 3*

Figure 4.30 shows the results of the damage parameters for the differential vertical ground movements and volume loss 3.
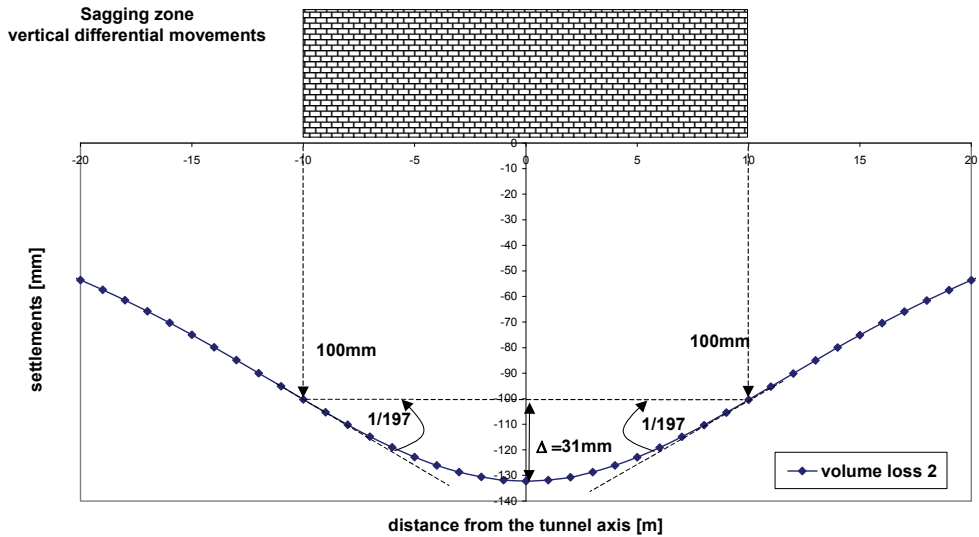

Figure 4.30: Damage parameters for differential vertical ground movements in the sagging zone; volume loss 3

Figure 4.31 shows the results of the damage parameters for the differential horizontal ground movements and volume loss 3.

Sagging zone

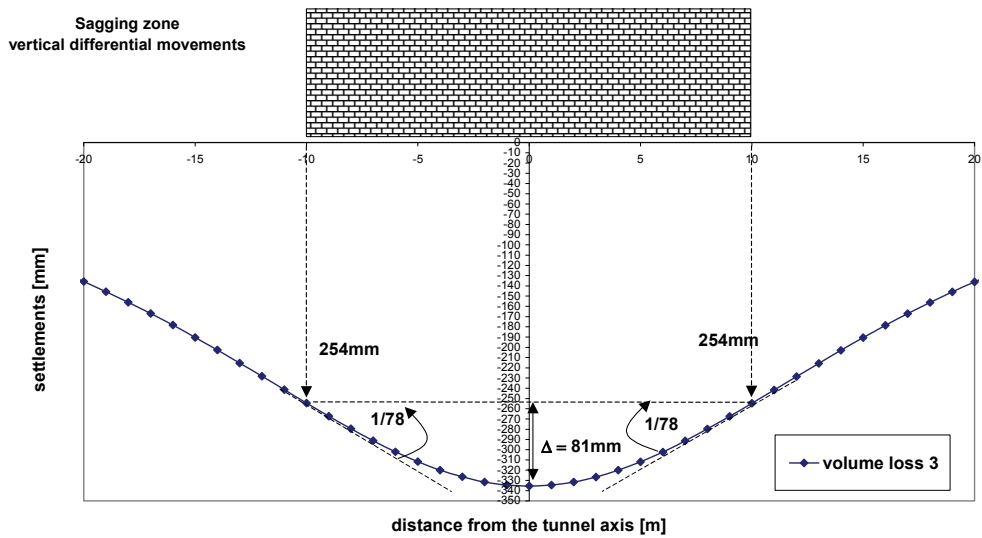$\varepsilon_h = -1.8\%$

$h_1 = 179mm$ $h_1 = 179mm$

horizontal ground deformations [mm]
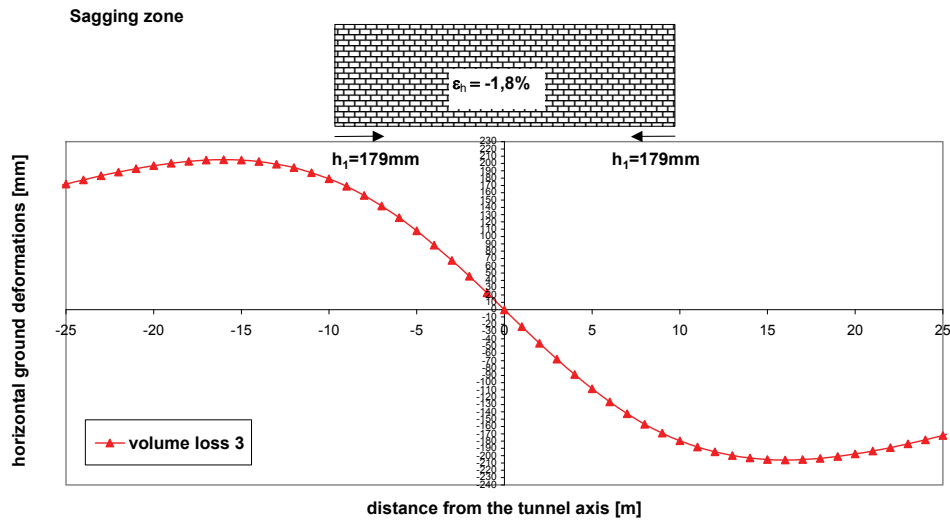
volume loss 3

distance from the tunnel axis [m]

Figure 4.31: Damage parameters for differential horizontal ground movements in the sagging zone; volume loss 3

4.5.3.4   Summary of the results for the sagging zone

The results for the relevant strains according to the LTSM and the corresponding damage classes are summarized in Table 4.5.

SAGGING	volume loss 1	volume loss 2	volume loss 3
L/H=3			
horizontal strain	-0,306%	-0,708%	-1,796%
bending strain due to deflection ratio	***0,103%***	***0,237%***	***0,602%***
diagonal strain due to angular distortion	0,026%	0,059%	0,150%
total strain; combined bending and horizontal strain	-0,204%	-0,471%	-1,205%
total strain; combined diagonal and horizontal strain	***0,002%***	***0,005%***	***0,012%***
rough (full transfer of horizontal strain)	*negligible*	*negligible*	*negligible*
smooth (no transfer of horizontal strain)	*slight*	*moderate*	*severe*
L/H=1			
horizontal strain	-0,306%	-0,708%	-1,796%
bending strain due to deflection ratio	***0,101%***	***0,232%***	***0,591%***
diagonal strain due to angular distortion	0,092%	0,214%	0,540%
total strain; combined bending and horizontal strain	-0,206%	-0,476%	-1,194%
total strain; combined diagonal and horizontal strain	***0,026%***	***0,060%***	***0,150%***
rough (full transfer of horizontal strain)	*negligible*	*very slight*	*slight*
smooth (no transfer of horizontal strain)	*slight*	*moderate*	*severe*

Table 4.5: Damage prediction with the LTSM for the sagging zone

The results show significant more damage for the smooth cases than for the rough cases. The reason for these differences is the fact, that the smooth cases neglect the transfer of horizontal differential ground movements on the building. As the horizontal differential ground movements cause compressive strains in the tunnelling sagging zone, they have a beneficial effect on the damage, because they reduce the tensile strains due to the differential vertical displacements.

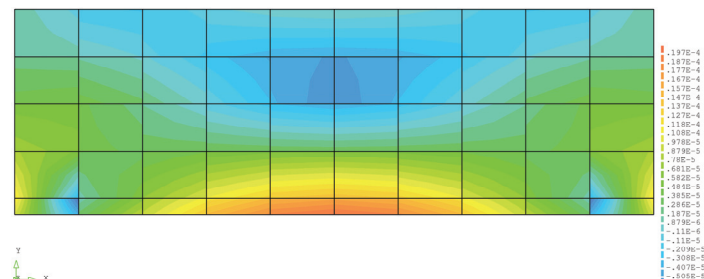# 5   SOIL-STRUCTURE INTERACTION - MASSIVE MASONRY WALL

5.1   Response of the massive masonry wall due to initial building loads

The first calculation stage in the numerical analyses is the activation of the initial building loads, consisting of the line loads and the dead weight of the wall. The results from this first calculation stage without any influence of the tunnelling are presented in this section. The initial stress and strain situation in the wall and the soil form the starting point for the phased analyses, where the incremental ground deformations are generated by the contraction of the tunnelling area in the following calculation stages.

The initial strains in the building and stresses in the interface due to the building loads given in 4.4.4.3 are shown in Figure 5.1 and Figure 5.5 for the example with the building geometry for L/H=3 and the E_{soil}=50MPa with the rough and the smooth interface respectively. The rough and the smooth cases are also considered here for the initial loading situation, because the degree of horizontal restraint is expected to have also influence on the corresponding initial strains in the building due to the initial building loads.

Figure 5.1 to Figure 5.4 show the results for the rough interface in terms of principal strains and horizontal and vertical interface stresses.

L/H=3; E_{soil}= 50MPa and ***rough*** interface

contours principal tensile strains ε_I
0.0019% (at the centre of the bottom edge)
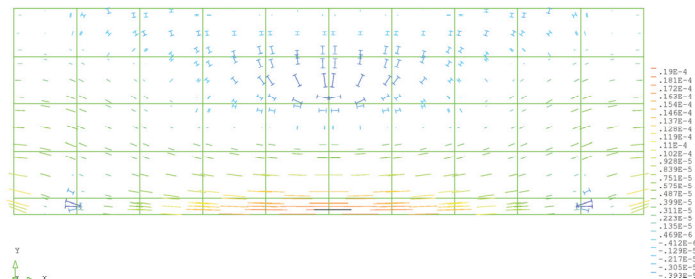
vectors principal strain ε_I

(a) principal tensile strains

Soil-Structure Interaction

L/H=3; E_{soil} = 50MPa and ***rough*** interface

contour principal compressive strains ε_2

vectors principal strain ε_2

(b) principal compressive strains
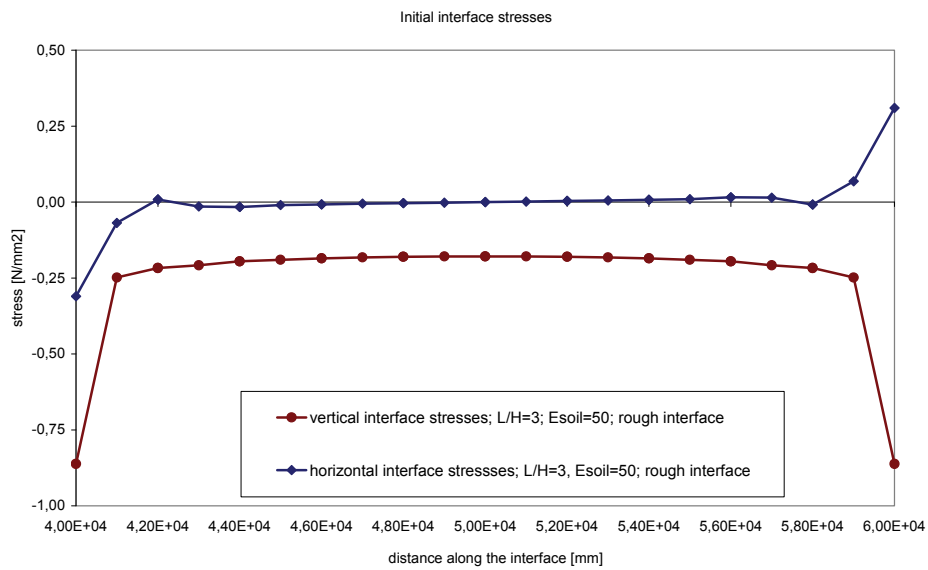
(c) interface stresses
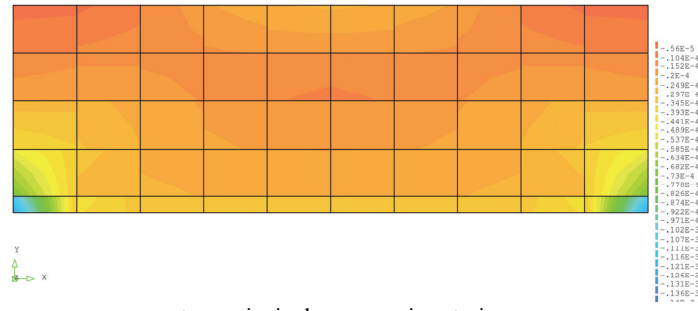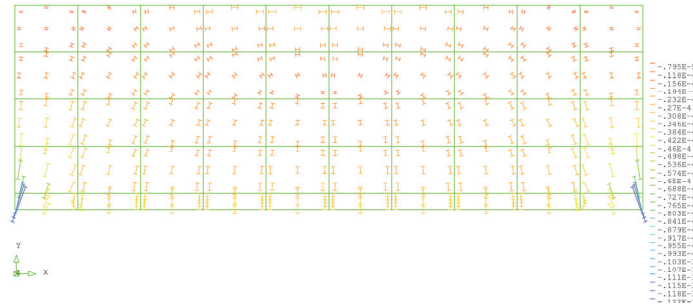
Figure 5.1: Initial stresses and strains in the building for the rough interface

Soil-Structure Interaction

The maximum initial tensile strain in the building occurs in horizontal direction at the centre of the bottom edge of the building and can be considered to be negligible (0.0019%). These small tensile strains are caused by the interaction of the stiff building and the soft soil, causing a concentration of vertical support pressures towards the bottom corners of the building. The vertical (compressive) interface stresses show the resulting peaks at the bottom corners of the building. Due to this interaction effect a small degree of arching occurs in the building, shown in the contour and vector plots. This causes the mentioned small horizontal tension at the bottom edge of the building.

For the calculation with a rough interface these tensile strains are reduced by the horizontal restraint with the soil via the rough interface. The activation of the horizontal interface stresses at the outer ends of the buildings are shown in the interface diagram. At the outer edges the relative horizontal displacements are the greatest and the vertical loads are the highest, leading to the transfer of increasing horizontal stresses between building and soil.

The initial tensile strains in the building increase with decreasing soil stiffness, which is explainable by the greater difference of stiffness between soil and building. The maximum principal tensile strain in the centre of the bottom edge for the case of E_{soil}=10MPa is 0.0024% (thus ca. 25% higher than for E_{soil}=50MPa). For all considered cases the initial values are however still of negligible magnitude. The qualitative explanation of the influence of different soil stiffness due to interaction is shown in Figure 5.2.
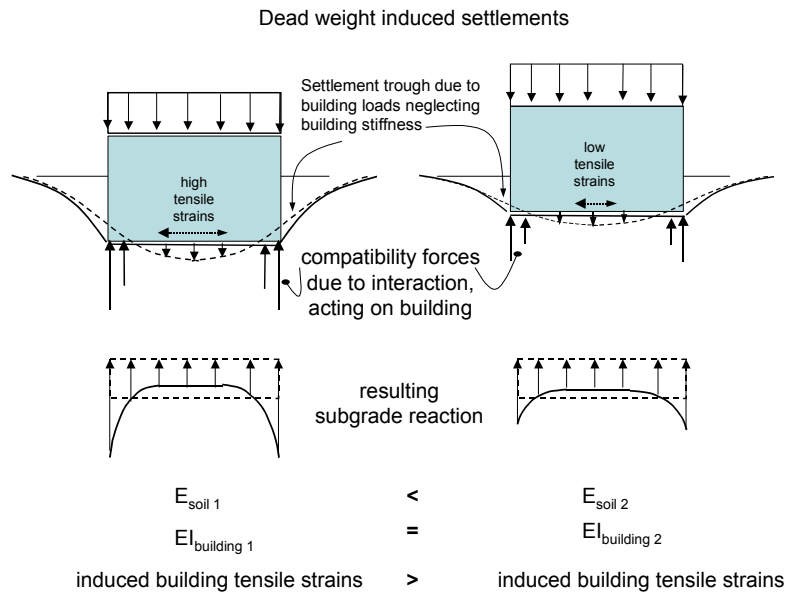
Figure 5.2 Interaction principles for initial load case and varying soil stiffness

For the lower soil stiffness, the building loads cause greater (differential) settlements. Compatibility forces develop due to the soil-structure interaction. The magnitude of these required compatibility forces increase for the softer soil compared to the stiffer soil. If the compatibility forces between soil and building are increased, the distribution of the subgrade reaction between soil and building is also further modified, which leads to increasing of loading redistribution in the building and consequently higher tensile strains at the bottom edge for the considered case.

The differences in vertical and horizontal interface stresses for two varying soil stiffness are shown for the case of *L/H*=3 and the rough interface in Figure 5.3 and Figure 5.4. The peaks of the horizontal and vertical interface stresses at the building corners are 10% higher for the soil stiffness of E_{soil}=50MPa than for E_{soil}=100MPa. The fact that the interface stress concentrations at the outer ends increase with

decreasing soil stiffness agrees with the observation that the maximum initial tensile strains at the bottom of the wall increase with decreasing soil stiffness. If the load distribution is more concentrated to the bottom corners arching is increasing and thus increases the initial tensile strain at the centre of the bottom edge.
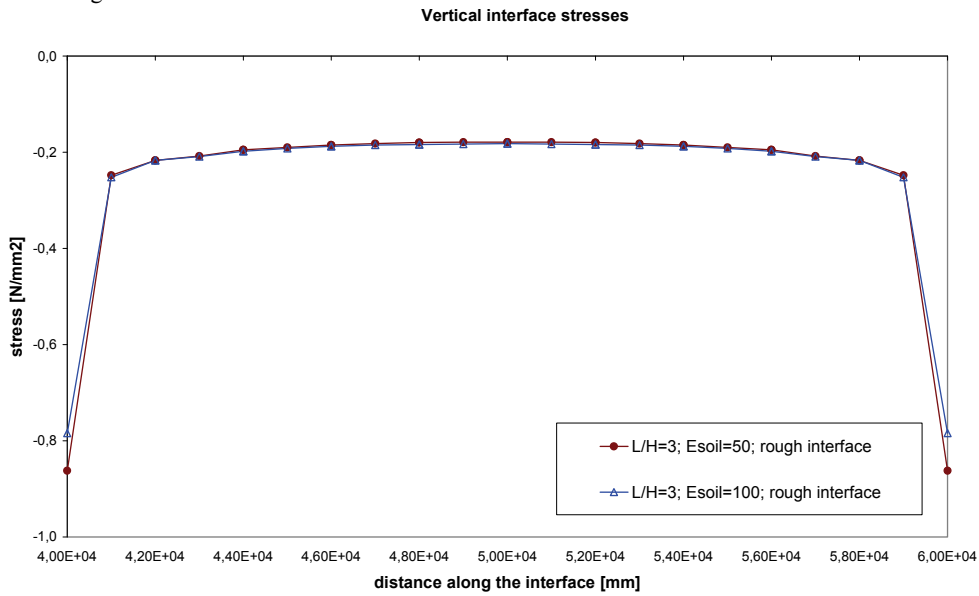

Figure 5.3: Vertical interface stresses for varying soil stiffness and the rough interface
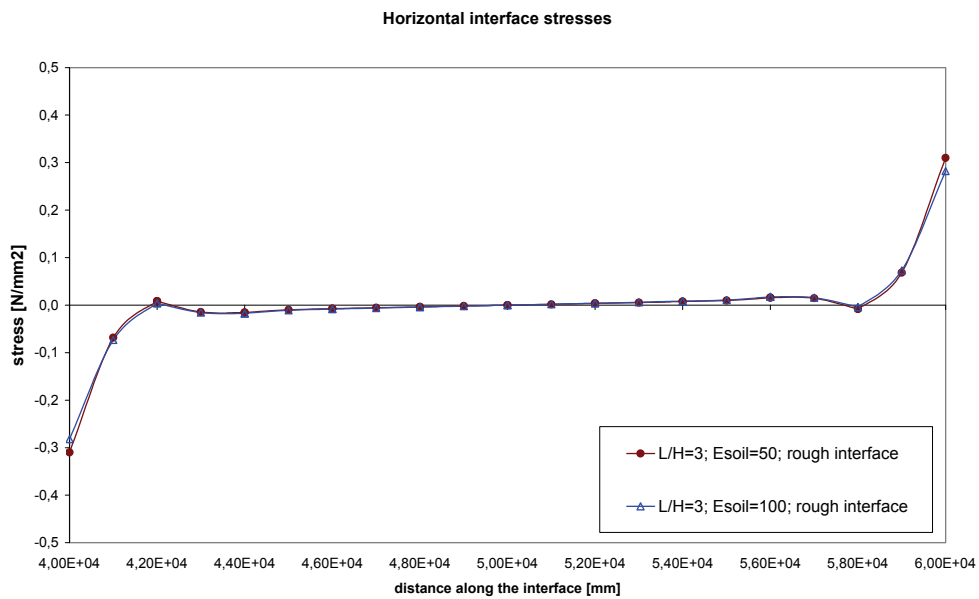
Figure 5.4: Horizontal interface stresses for varying soil stiffness and the rough interface

Soil-Structure Interaction

It is noted, that the sum of all vertical building loads (according to 4.4.4.3) corresponds with the integration of the vertical interface stresses. For the building with L/H=3 and building height of 6.5m, the initial vertical interface stress at the centre of the wall is 0.2 N/mm^2.

Figure 5.5 summarizes the results for L/H=3, E_{soil}=50MPa and the **smooth** interface. The smooth interface does not transfer horizontal forces between soil and building and is therefore also expected to offer no restraint at the bottom of the wall. Regarding the previously presented interpretations of the calculations with the rough interface one should expect increasing tensile strains in the initial loading situation due to the lack of the restraint effect.

L/H=3; E_{soil} = 50MPa and **smooth** interface

contour principal strain ε_1
max. 0.005% at the bottom corners
0.0045% (at the centre of the bottom edge)

contour principal strain ε_2

vectors principal strain ε_1

vectors principal strain ε_2

Figure 5.5: Initial stresses and strains in the building and the smooth interface

As expected, the calculations with the smooth interface show higher initial tensile strains in the wall compared to the rough case, because the beneficial horizontal restraint effect is neglected. No horizontal interfa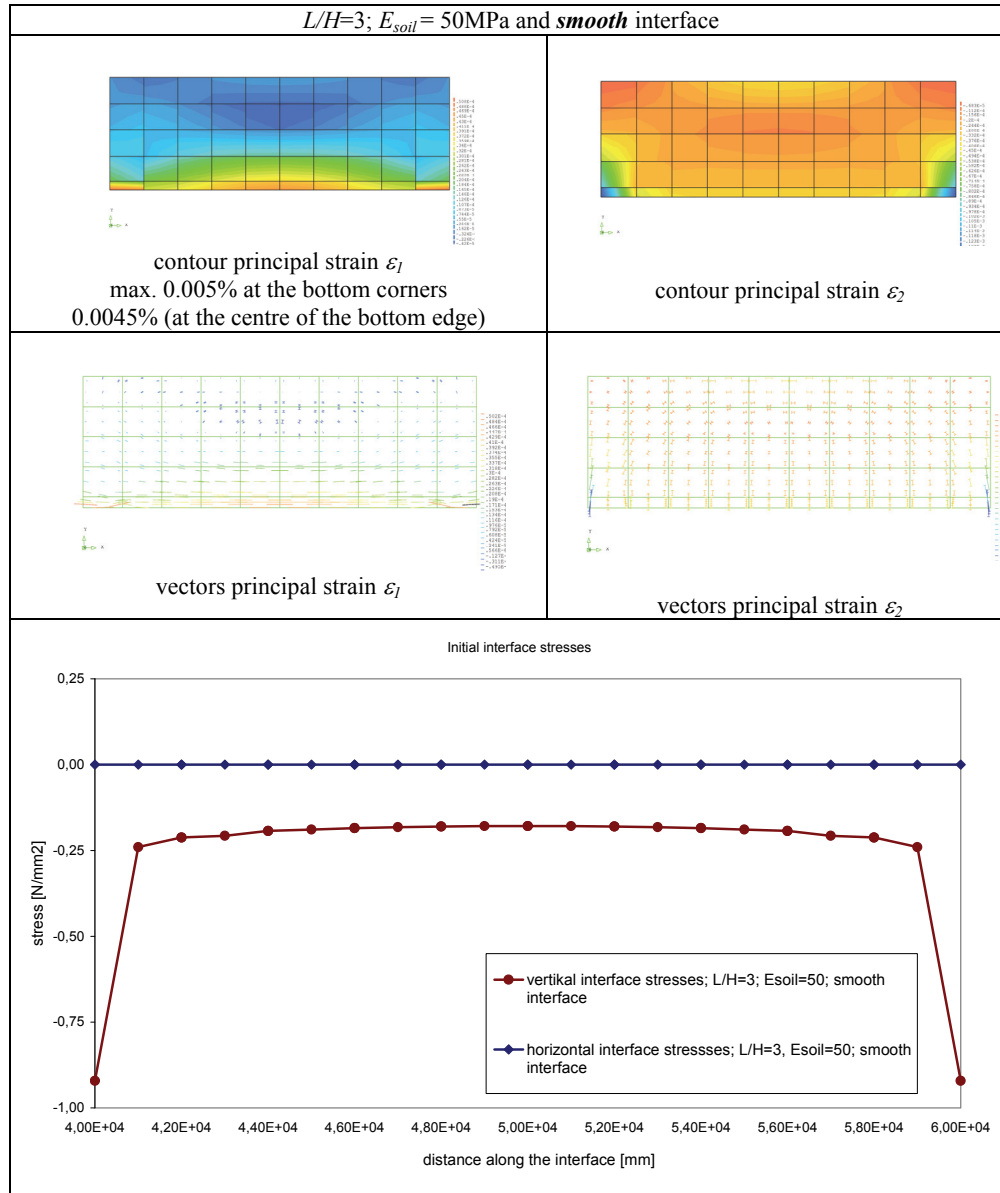ce stresses can be activated and transferred between soil and building. The calculation for E_{soil}=50MPa and the smooth interface show an increase of the maximum initial tensile strain of ca. 100% (0.0045% versus 0.0019% for the calculation with the rough interface). The magnitude of initial tensile strains is however still negligible as it does not cause any cracking. These differences show clearly the importance of the effects of the horizontal interaction also for the initial loading situation of buildings.

5.2 Response of the masonry walls due to the tunnelling induced ground movements

5.2.1 Principle of the interpretation of the numerical analyses

Each numerical calculation provides a huge amount of data. In order to extract the crucial information a standard principle is developed for the interpretation of the numerical calculations. In this section this procedure is explained in detail for one example of the parametric study, giving all considered output options for a calculation. Depending on the results of each calculation, the relevant output options for the interpretation and presentation are chosen and presented in the following sections.

In this section the chosen case is a sagging situation with the massive masonry bearing wall, the *L/H*-ratio of 3, the soil stiffness of E_{soil}=100MPa, a smooth interface and the contraction of the tunnel up to volume loss 1. It is emphasized that this section only serves to explain the different output options chosen for the interpretation of the calculations. For a detailed interpretation of the chosen case it is referred to a subsequent section.

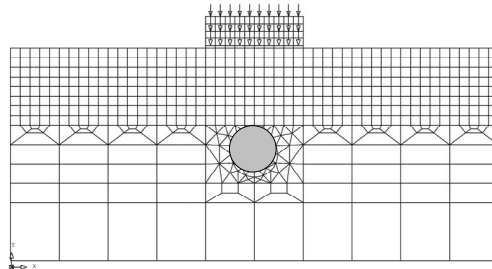**Figure 5.6: Reference case for explanation of the interpretation of the numerical analyses**

The following results are presented to evaluate the damage in the structure:

- **Contour plots and vector plots of the principle tensile strains** of the masonry wall.

These plots reveal the internal development of strains in the wall and consequently the redistribution of loads due to the soil-structure interaction.
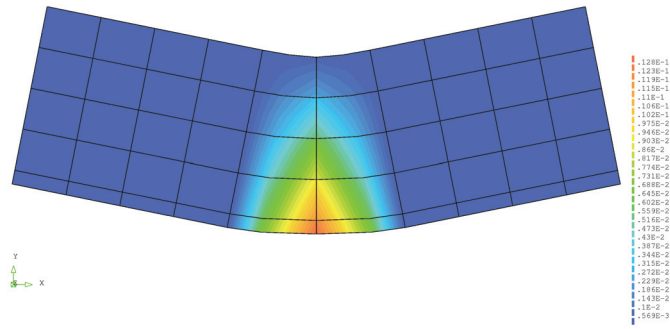
Figure 5.7: Contour plot of principal tensile strains in the deformed mesh

Figure 5.7 shows the contour plot of principal tensile strains in the deformed mesh. The current example shows the sagging mode deflection with maximum tensile strains at the centre of the bottom edge of the wall, decreasing towards the upper edge of the wall.
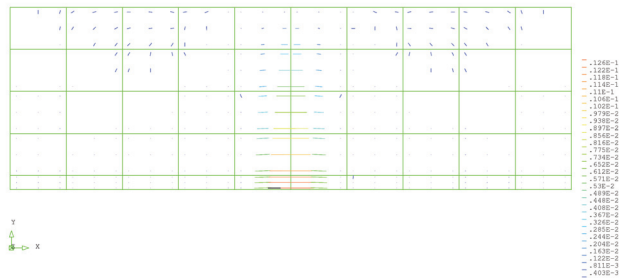
Figure 5.8: Vector plot of principal tensile strains

Figure 5.8 shows the vector plot of the principal tensile strains providing the orientation of the tensile strains. The current example shows the horizontal orientation of the tensile strains in the mid section due to bending of the sagging mode. The horizontal tensile strains correspond to vertical cracking.

- **Contour plots and vector plots of crack strains** in the deformed mesh of the masonry walls.
These plots reveal the crack patterns with the degree, the locations and the orientations of the cracking strains. The plotted crack strain ε_{nn}^{crack} is the strain perpendicular to the fixed smeared crack.
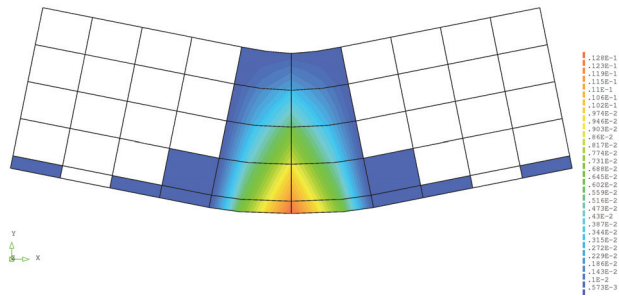
Figure 5.9: Contour plot of crack strains in the deformed mesh

Figure 5.9 shows the contour plot of the crack strains. The blank elements are uncracked. Only the coloured elements contain smeared cracks. The colour represents the level of crack strain. It is noted

that for this example the plot appears to be almost the same as the plot of the total principal tensile strain, indicating that the elastic part of the strains is very small and virtually all strain is crack strain.
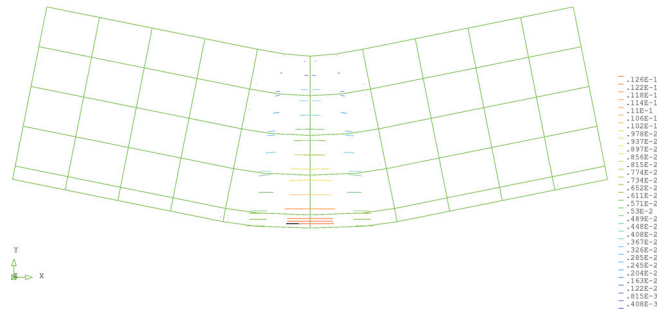
Figure 5.10:Vector plot of crack strains in the deformed mesh

Figure 5.10 shows the vector plot of crack strains in the deformed mesh. The direction of the vector is the direction normal to the smeared crack in the integration point. The length of the vector represents the magnitude of the crack normal strain.

- **Differential horizontal displacements** at the bottom corners and/or the top corners of the wall.

The numerical output of the horizontal displacements at the bottom corners is used to derive the differential wall displacements of the bottom edge.

horizontal displacements (x)

-13mm   13mm
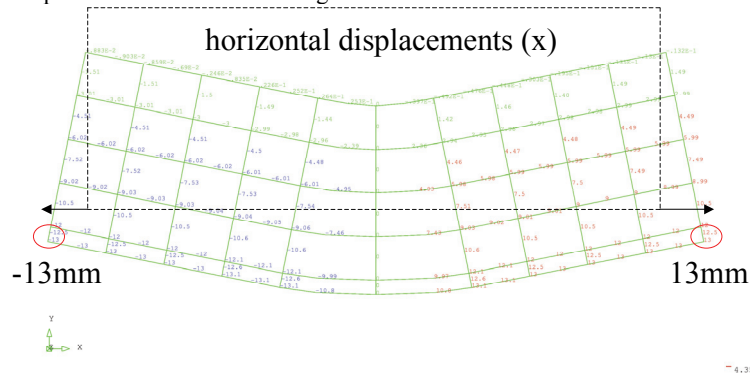
Figure 5.11: Horizontal displacements at the bottom corners

If relevant also the horizontal displacements at the top corners of the wall are presented, for example in case of a hogging bending mode causing extension of the top edge of the wall. In the example of Figure 5.11 the differential horizontal displacements at the bottom edge are 26mm.

- **Differential vertical displacements** at the bottom corners and the bottom mid of the wall

Figure 5.12: Vertical displacements at the bottom corners

- **Determination of the tilt and the deflection** of the wall structure

The differential vertical displacements at the bottom corners from Figure 5.12 are used to calculate the tilt of the structure. For the current example no tilt occurs as the wall is undergoing the symmetric sagging trough. The deflection at the bottom centre of the wall is determined from the differential vertical displacements at the bottom corners and the bottom mid. The current example gives a deflection of 60.9mm – 42.6mm = 18.3mm.
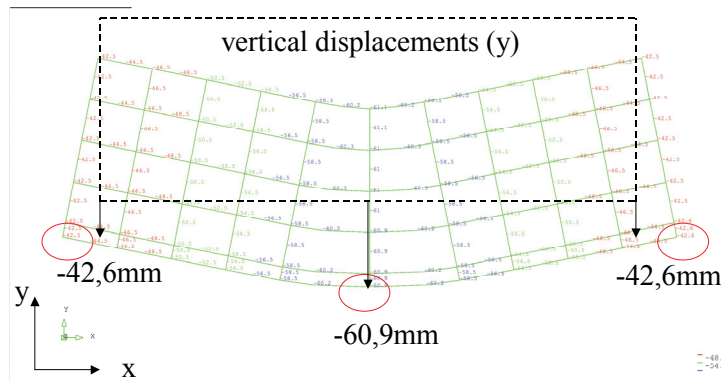
- **Determination of the average tensile strain** along the bottom and/or the top edge of the wall.

The differential horizontal displacements at the bottom corners shown in Figure 5.11 are used to determine the average tensile strain at the bottom fiber. The current example gives an average horizontal tensile strain of the wall of $2 \cdot 13.6$mm divided by the length 20000mm of the wall, leading to 0.136%. If relevant also the average horizontal strain at the top edge of the wall is determined, for example in case of a hogging mode bending deformation.

- **Determination of the cumulative crack width**

The maximum cumulative crack width is determined from the sum of the horizontal differential displacements at the bottom corners of the wall, which is valid if the cracking is orientated vertically as shown in the current case. It is noted that for some cases also the sum of the horizontal differential displacements at the top corners of the wall are presented as they can be the dominating factor for hogging mode deformations.

Depending of the crack pattern, this cumulative crack width can be assumed to be equal to the maximum crack width if crack strains concentrate at one location in the wall. This is valid for the current case. The cumulative crack width for the current case is 27mm. In this procedure the masonry is assumed to behave as an elastic-softening material. When the softening and cracking proceeds in the mid of the wall, the two wall parts at either side of the crack unload elastically. When the vertical crack is fully developed, i.e. the stress has reduced to zero beyond the softening branch, the material at either side of the crack has fully unloaded. Then, all horizontal strain in the wall concentrates as crack strain in the mid section.

In cases where cracking is not concentrating at one location in the wall also the distribution of cracking is presented.

- **Determination of the damage classification**

The determined cumulative crack width and/or the combination of number of cracks with corresponding crack widths are used to categorize the damage class. The classification given in Table 5.1, which is in accordance with the indications for crack widths of the Building Research Establishment (see Figure 3.5) is used to categorize the damage class of the numerical results.

Soil-Structure Interaction

Damage class	Approximate crack width (mm)
Negligible	< 0,1mm
Very slight	0,1 to 1mm
Slight	1 to 5mm
Moderate	5 to 15mm or a number of cracks > 3 mm
Severe	15 to 25mm, but depends also on the number of cracks
Very severe	> 25mm, but depends also on the number of cracks

Table 5.1: Damage classification for crack widths

The current example reveals a cumulative crack width of 27mm leading to severe/very severe damage. Cracking for the current example is concentrated in a single vertical crack at the centre of the wall.

- **Distribution of the horizontal and vertical interface stresses**

The distribution of the vertical and horizontal interface stresses are presented for each case, as they give good understanding of the soil-structure interaction and the redistribution of the initial bedding stresses. The current example in Figure 5.13 shows clearly the redistribution of the initial vertical bedding stresses due to the soil-structure interaction for volume loss 1. We observe an increase of the bedding stresses, compared to the initial situation, near the crack at the mid-section As the current example has a smooth interface neglecting the transfer of horizontal movements between building and soil, no horizontal interface stresses are given.
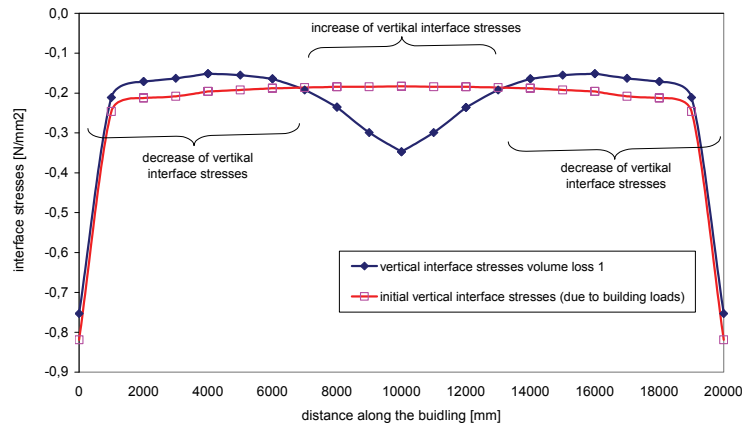

Figure 5.13: Vertical interface stresses

- **Summary of the results in a damage chart**

The results for each phased calculation are summarized in a chart as shown below in Figure 5.14. The horizontal axis of the chart describes the imposed greenfield deflection ratio. Additionally the

corresponding greenfield angular distortion and greenfield horizontal strain values are given for the three different volume losses.

The vertical axis presents the damage class determined with the cumulative crack width of the numerical interaction calculation. The three points in the charts present the results of the three considered volume losses. The points are connected with straight lines to characterize the development of damage.

It is once more emphasized, that the horizontal axis presents the greenfield values for the characteristic damage parameters (deflection ratio, angular distortion and horizontal strain) and not the values due to the interaction. The current example for volume loss 1 is marked in Figure 5.14.
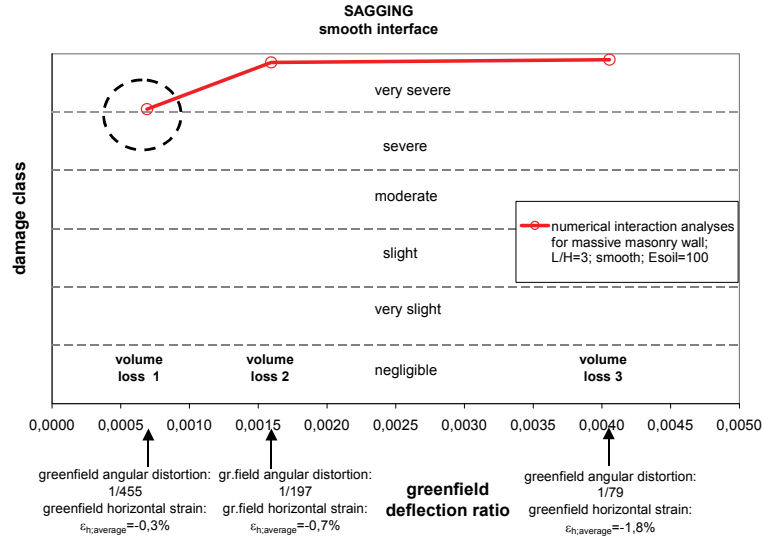

Figure 5.14: Summary numerical results with damage chart

It is noted that the linear connection lines between the three investigated greenfield distortions are only for visual purpose to identify the three results belonging to one case. No linear interpolation can be applied for intermediary greenfield distortions once cracking is initiated.

5.2.2 Hogging

5.2.2.1 *Influence of smooth and rough interface*

The interface properties determine the transfer of horizontal greenfield ground movements, induced by the tunnelling process, to the walls. As explained in section 4.4.5 the smooth interface neglects the horizontal transfer between soil and wall and the rough interface transfers differential horizontal movements and shear forces between soil and wall at the bottom edge of the wall. The magnitude of the mobilized horizontal forces depends on the vertical loading. These horizontal shear forces are mobilized up to a realistic value before horizontal slipping between soil and wall occurs. For the hogging situation the horizontal differential greenfield movements cause horizontal strain (see also section 4.5.2) and it is therefore expected that for the rough cases horizontal tensile strains are induced at the bottom edge of the walls.

The influence of the smooth and the rough interface for the hogging mode is analysed for the example of L/H=3 and E_{soil}=50MPa. The numerical model is shown in Figure 5.15.

Soil-Structure Interaction
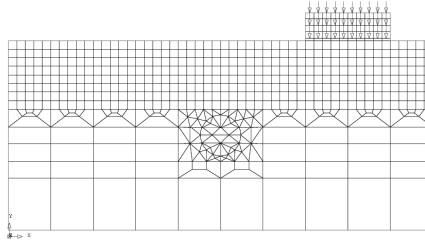
Figure 5.15: Numerical model for the wall in the hogging zone and *L/H*=3

Figure 5.16 shows the relevant results for the wall and volume loss 1.

Volume loss 1	E_{soil}= 50MPa smooth	E_{soil}= 50MPa rough
crack pattern	no cracking	
differential horizontal displacements at bottom/top edges [mm]	-0,2mm (bottom egde slightly in compression) +0,2mm (top egde slightly in tension)	+1,2mm (bottom egde in tension) -0,3mm (top edge in compression)
differential vertical displacements at bottom corners [mm]	16,8mm	17mm
tilt	1/1190	1 / 1190
deflection	0,2mm (hog)	0,6mm (sag)
tensile strains	average strain at top and bottom edge 0.001%	average strain bottom edge 0.006%
cumulative crack width	-	1,2mm
distribution of cracks	-	
damage class	negligible	very slight/slight

Figure 5.16: Comparison of rough and smooth cases for volume loss 1

The **rough case** clearly shows the transfer of horizontal tensile friction forces at the bottom edge of the wall. The bottom edge undergoes a tensile strain due to the transfer of the imposed differential horizontal greenfield ground movements. The eccentric moment induced by these tensile forces

imposed at the bottom edge of the wall even leads to a very small sagging deflection of the wall of 0.6mm. The vertical greenfield hogging mode ground movements are obviously overruled by the induced horizontal tensile forces at the bottom edge for volume loss 1. The wall undergoes almost a rigid body tilt due to its great stiffness relative to the soil stiffness and does not follow the hogging curvature of the differential vertical greenfield ground movements. The introduction of the horizontal strains at the bottom edge of the wall leads to very slight vertical cracking starting at the bottom edge of the wall with a cumulative crack width of 1.2mm and a maximum crack width at the centre of the wall of 0.8mm. The principle of the above described effects is shown in Figure 5.17.
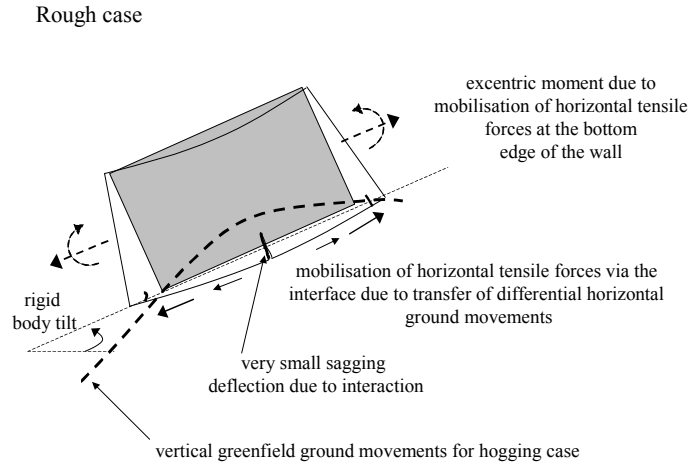
Rough case

Figure 5.17: Principle effects of interaction results of rough case

In contrast to the rough case, the **smooth case** clearly shows no effects of horizontal forces induced at the bottom edge of the wall, because the smooth interface neglects the transfer of horizontal differential ground movements. The bottom edge of the wall is under slight compression and the top edge shows slight horizontal tensile strains, which is corresponding with a hogging mode deflection due to the vertical greenfield deformations. However a strong reduction of the imposed hogging curvature due the vertical greenfield ground movements is caused by the soil-structure interaction of the stiff building and the soft soil. The wall almost tilts rigidly with a very small hogging deflection of 0.2mm. No cracking is induced for volume loss 1 for the smooth case. The principle of the above described effects is shown in Figure 5.18.

Figure 5.18: Principle effects of interaction results for smooth case
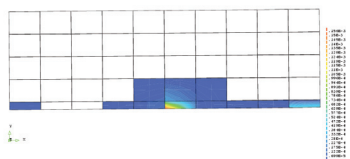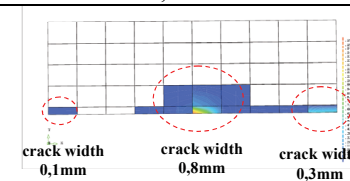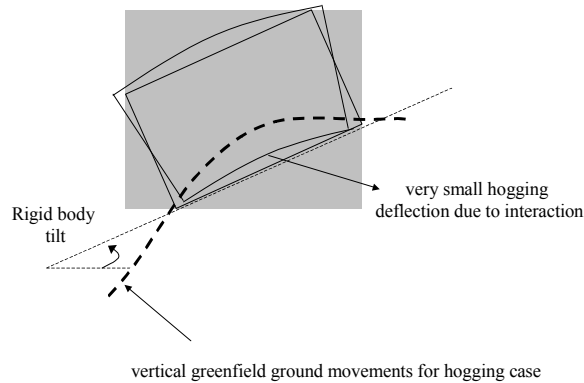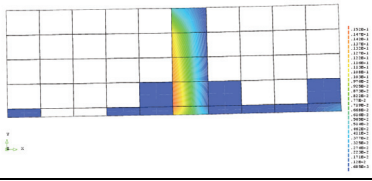
Figure 5.19 shows the relevant results for volume loss 2.

Volume loss 2	E_{soil}=50MPa Smooth	E_{soil}=50MPa Rough
crack pattern	no cracking	
differential horizontal displacements at bottom/top edges [mm]	-0.4mm (bottom edge in compression) +0.4mm (tension top edge)	+20mm (tension bottom edge) +10mm (tension top edge)
differential vertical displacements at bottom corners [mm]	38.6mm	39mm
tilt	1 / 518	1 / 514
deflection	0.5mm (hog)	4.1mm (sag)
tensile strains	average strain at top edge 0,002%	average strain bottom edge 0,1% average strain top edge 0,05%
cumulative crack width	-	20mm
distribution of cracks	-	
damage class	negligible	severe

Figure 5.19: Comparison of rough and smooth cases for volume loss 2

Volume loss 2 shows the same principal interaction effects as described previously for volume loss 1. The cumulative crack width for the **rough case** at the bottom edge is however increasing significantly for volume loss 2, leading to severe damage. Vertical cracking which is initiated at volume loss 1 is rapidly progressing for volume loss 2 and has developed over the entire height of the wall. The wall is separated into two parts, which is reflected in the crack width of 10mm at the centre of the top edge of the wall and 17mm at the centre of the bottom edge of the wall.

The hogging deflection for the wall of the **smooth case** increases compared to volume loss 1, although it is still very small (0.5mm). The smooth case is still remaining uncracked, because the strong interaction effect of the wall for the vertical differential ground movements is still minimizing the tensile strains in the wall. The wall shows an almost rigid body tilt.
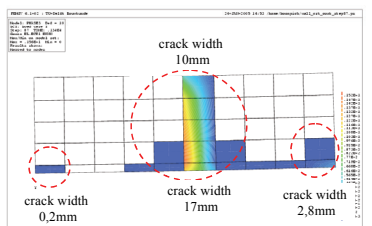
Figure 5.20 shows the relevant results for volume loss 3.
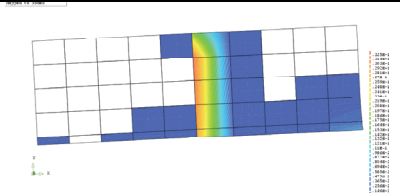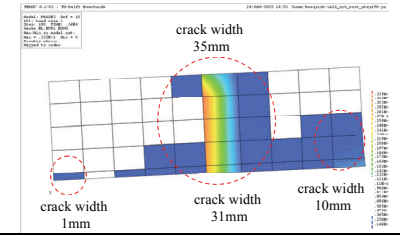
Volume loss 3	E_{soil} = 50MPa smooth	E_{soil} = 50MPa rough
crack pattern	no cracking	
differential horizontal displacements at bottom/top edges [mm]	-1mm (bottom edge in compression) +1mm (top edge in tension)	+42mm (bottom edge in tension) +35mm (top edge in tension)
differential vertical displacements at bottom corners [mm]	97.8mm	99.5mm
tilt	1 / 204	1/201
deflection	1.2mm (hog)	1.8mm (hog)
tensile strains	average strain top edge 0.005%	average strain bottom edge 0.21% average strain top edge 0.18%
cumulative crack width	-	42mm
distribution of cracks		
damage class	negligible	very severe

Figure 5.20: Comparison of rough and smooth cases for volume loss 3

The **rough case** is already vertically cracked over the entire height of the wall for volume loss 2 resulting in a separation of the wall in two parts. For volume loss 3 the damage is further increased to very severe damage. The crack opening at the location of the separation (in the centre of the wall) is increased to 31mm at the bottom of the wall and 35mm at the top of the wall. The two parts are also separately tilting slightly in a hogging mode, thus the sagging deflection of the total wall recognized in volume loss 1 and 2 is changed in a very small hogging deflection of the total wall for volume loss 3 (1.8mm). The **smooth case** shows a further increased hogging deflection which is however still very small with 1.2mm. The strong interaction of the stiff building with the relatively soft soil still causes an almost rigid body rotation and only imposes a very small bending deflection in the wall, still resulting in negligible damage.

Soil-Structure Interaction

Figure 5.21 shows the distribution of the interface stresses for the rough and the smooth case. For the rough case the horizontal and vertical interface stresses are presented. For the smooth case only the vertical interface stresses are presented because no horizontal interface stresses are transferred between wall and soil.

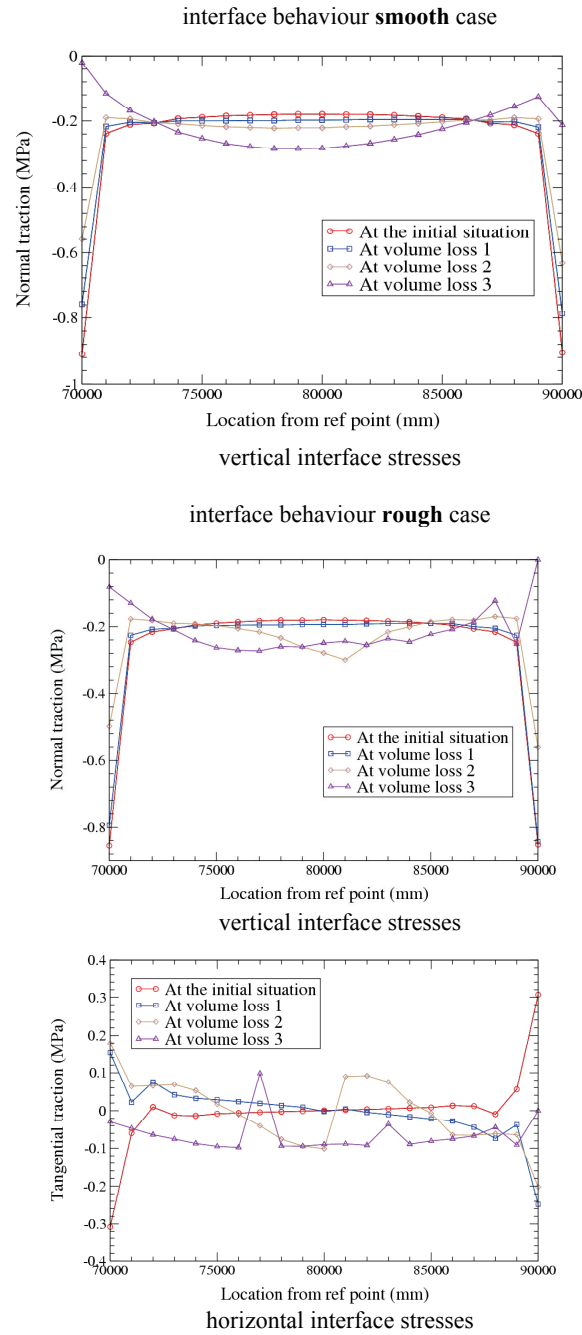interface behaviour **smooth** case

vertical interface stresses

interface behaviour **rough** case

vertical interface stresses

horizontal interface stresses

Figure 5.21: Interface stresses for the rough and the smooth case for all volume losses

It is noted that Figure 5.21 also includes the distribution of the interface stresses in the initial loading situation in order to show the redistribution of stresses due to the volume losses compared to the initial situation.

The **smooth case** shows very minor changes in the vertical interface stresses for volume loss 1 and 2. As a consequence, the redistribution of loads in the wall is also very small, which does not lead to damage. This corresponds with the resulting damage class negligible. The explanation for the minor redistributions of the interface stresses for the smooth case is the strong interaction of the stiff building with the relatively soft soil, which leads almost to a rigid body rotation and only imposes a very small bending deflection in the wall. This is however not sufficient to cause cracking damage. Volume loss 3 of the smooth case shows a clear redistribution corresponding with the hogging mode deflection, because the supporting pressures at the mid part of the wall increase and the pressures at the edges of the wall decrease. The pressure at the left bottom corner of the wall is almost reduced to zero. This redistribution however still does not cause cracking tensile strains in the wall. The corresponding hogging deflection of the wall for volume loss 3 and the smooth case is still small with 1.8mm and the damage class is still negligible.

For the **rough case** the change of the horizontal interface stresses is particularly interesting, because the transfer of horizontal strains and friction forces at the bottom edge of the wall is an important factor for the overall damage of the wall. This has been described in detail in the previous section. Anyhow, because the distribution of the vertical interface pressures also determines the magnitude of the horizontal stresses according to the Coulomb friction law, the combination of both is further analyzed below.

Volume loss 1 shows a minor change of the vertical interface stresses compared to the initial situation. The distribution of the vertical interface stresses is almost equal to the initial situation, characterized by the load concentrations at the bottom corners. The horizontal interface stresses however show a major change in the direction of the stresses. The initial horizontal interface stresses lead to compression in the wall due to the restraint in the initial situation. These compressive strains which are increasing towards the bottom corners are first demobilized and then turned into horizontal tensile stresses acting on the bottom edge of the wall. This effect develops due to the partial transfer of the greenfield horizontal differential ground movements induced by tunneling of volume loss 1 in the hogging zone. These effects for the rough case and volume loss 1 are schematically shown in Figure 5.22.
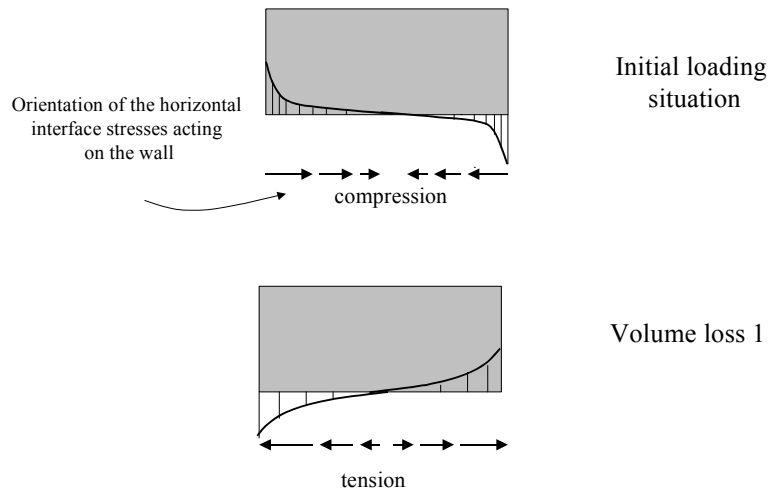

Figure 5.22: Schematic interpretation of the horizontal interface stresses in the initial situation and for volume loss 1

Volume loss 2 shows a significant change of the vertical and horizontal interface stresses for the rough case. Due to the vertical cracking at the centre of the wall and the resulting separation of the wall in two

parts the distribution of the horizontal and the vertical interface stresses for each part is of a comparable pattern as the distribution for the entire wall in volume loss 1. Horizontal tension is introduced at the bottom of the wall separately for both wall parts and tends to tear the wall parts further away from each other. The vertical interface stresses for volume loss 2 show qualitatively the same distribution of bedding stresses for each separated wall part as for the entire wall in volume loss 1. The vertical load concentrations at the inner corners of the two separated wall parts next to the vertical crack in the centre are however less pronounced than at the outer corners. The effects are schematically shown in Figure 5.23.
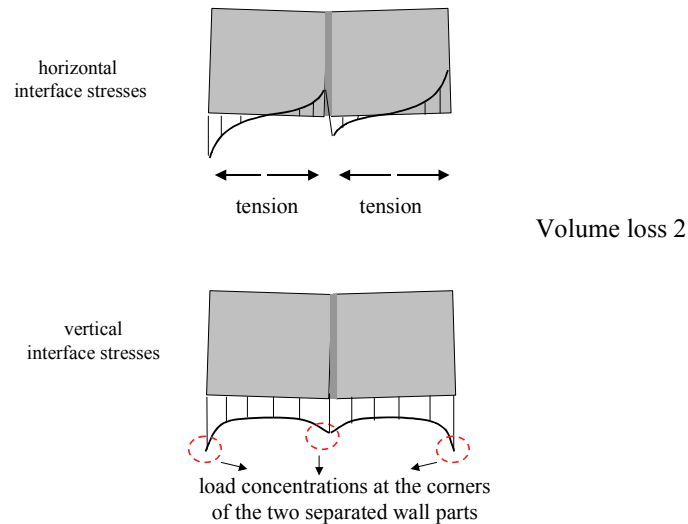
Figure 5.23: Schematic interpretation of the horizontal interface stresses for volume loss 2

Volume loss 3 shows a different pattern of the horizontal and the vertical interface stresses. Figure 5.24 shows the schematic interpretation of horizontal and vertical interface stresses. The hogging mode deflection of the separated parts leads to unloading of the four bottom corners of the two separated wall parts. This is clearly reflected in the distribution of the vertical interface stresses, showing even full vertical unloading at the right bottom corner of the wall. The reduction of the vertical stresses towards the corners leads consequently to a reduction of the horizontal interface stresses towards the bottom corners of the wall. The orientation of the shear stresses is also changed in certain parts of the wall due to the hogging mode deformation of the two separated wall parts.
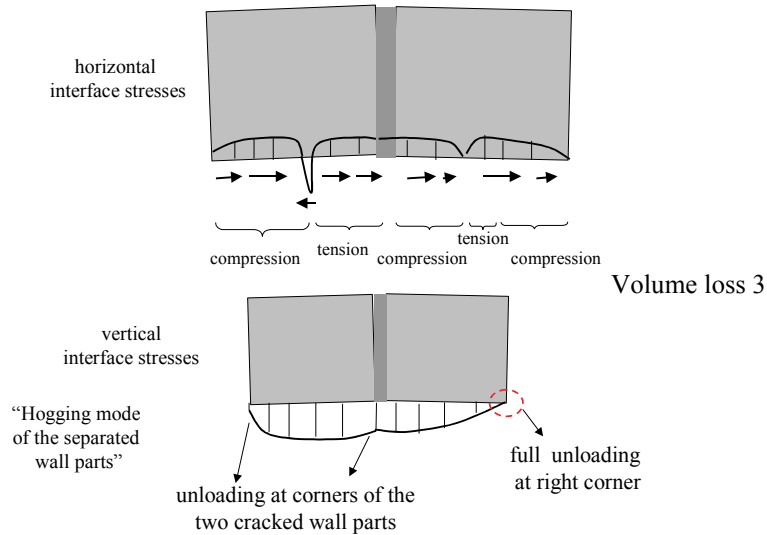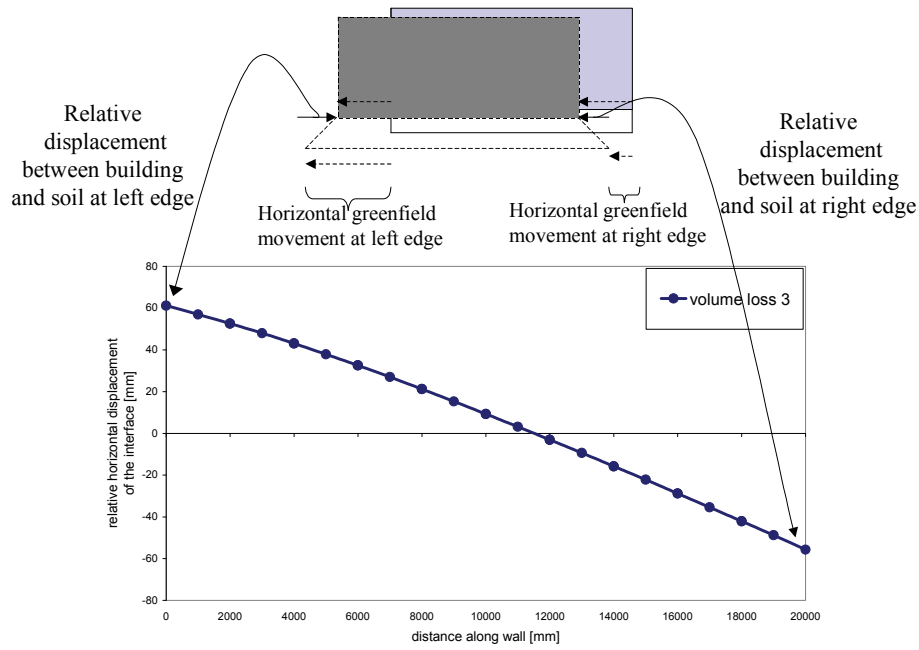
Figure 5.24: Schematic interpretation of the horizontal interface stresses for volume loss 3

For a better understanding of the differential horizontal interface deformations between building and soil, the relative horizontal displacements between the building side and the soil side of the interface are shown for the **smooth case** for volume loss 3 in Figure 5.25a. As expected the ground is horizontally slipping under the building, because of the lack of transfer of horizontal movements due to the smooth properties of the interface leading to high relative horizontal displacements in the interface. The sum of the absolute values of the relative displacements in the interface at the outer ends of the wall is in accordance with the differential horizontal greenfield ground movements along the building. It is emphasized, that the slipping in the interface is recognized for all three volume losses with the corresponding magnitude of the differential horizontal greenfield ground deformations. This confirms the correct behaviour of the smooth interface properties.

Figure 5.25b shows the case for the **rough interface** and volume loss 3, where the separation of the wall due to vertical cracking dominates the very severe damage in the wall. Horizontal opening of the crack in the centre is strongly increased. The diagram of the relative horizontal displacements of the interface shows also increasing slipping towards the bottom corners between soil and building interface for both separated wall parts at volume loss 3. The outer ends of the wall show significant relative horizontal movements in the interface (between 30mm and 40 mm). It is emphasized that this effect does not occur for the rough case and volume loss 1 (only very slight cracking in the wall) and only very little for volume loss 2 (where the wall is already cracked severely) as less slipping occurs in the first two volume loss for the rough case.

Relative displacement between building and soil at left edge

Horizontal greenfield movement at left edge

Horizontal greenfield movement at right edge

Relative displacement between building and soil at right edge
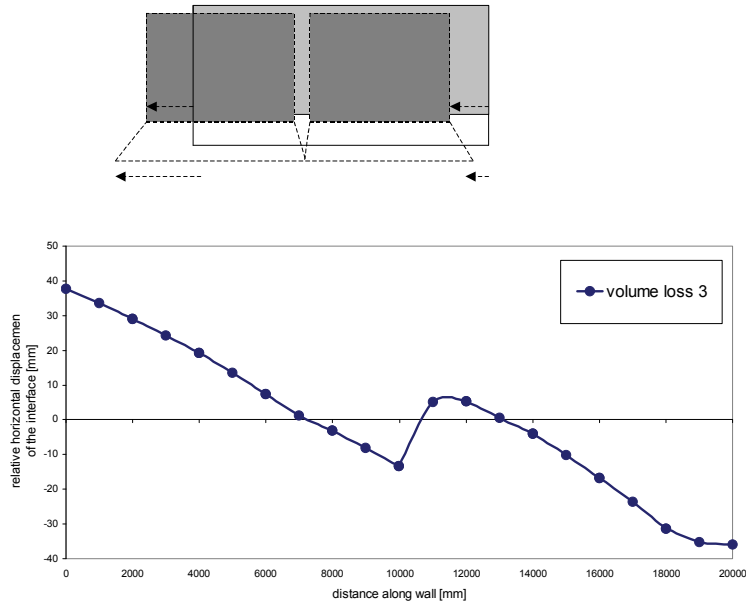
(a) smooth case

(b) rough case

Figure 5.25: Relative horizontal displacements of the interface for volume loss 3

Figure 5.26 summarizes the results of the rough and the smooth calculations for all three volume losses in terms of the damage class.

Hogging; L/H=3
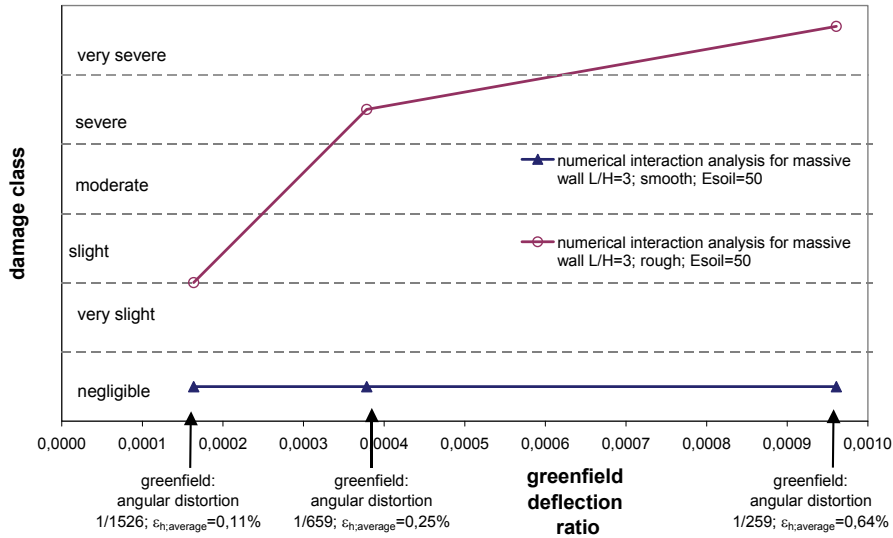
Figure 5.26: Damage class for rough and smooth case

It is emphasized that the values which are presented on the horizontal axis of Figure 5.26 for the greenfield values for the angular distortions in the hogging zone, are the average values between the front and the back side of the building.

The rough case shows significantly more damage than the smooth case. A significant increase in the damage of the rough case is noted between volume loss 1 and volume loss 2. The vertical crack is just initiated at the bottom centre of the wall at volume loss 1. For volume loss 2 the damage class is increased from very slight to severe, due to the complete opening of the vertical crack at the centre of the wall up to the top edge of the wall. The non-linear material behaviour of the wall including the modelling of smeared cracking shows to have significant influence on the damage development once a minor crack is initiated. As explained previously the increased damage susceptibility for the rough case compared to the smooth case is caused by the transfer of horizontal ground strains via the soil to the bottom of the building. This transfer is neglected for the smooth case. The smooth case is therefore only affected by the differential vertical hogging mode deformations. The strong vertical interaction between the relatively stiff wall compared to the soft soil reduces the vertical distortion of the wall, leading to negligible damage for all three volume losses.

Figure 5.26 shows the comparison of the damage prediction with the LTSM method and the numerical interaction damage prediction.

Figure 5.27: Damage classes compared to the LTSM

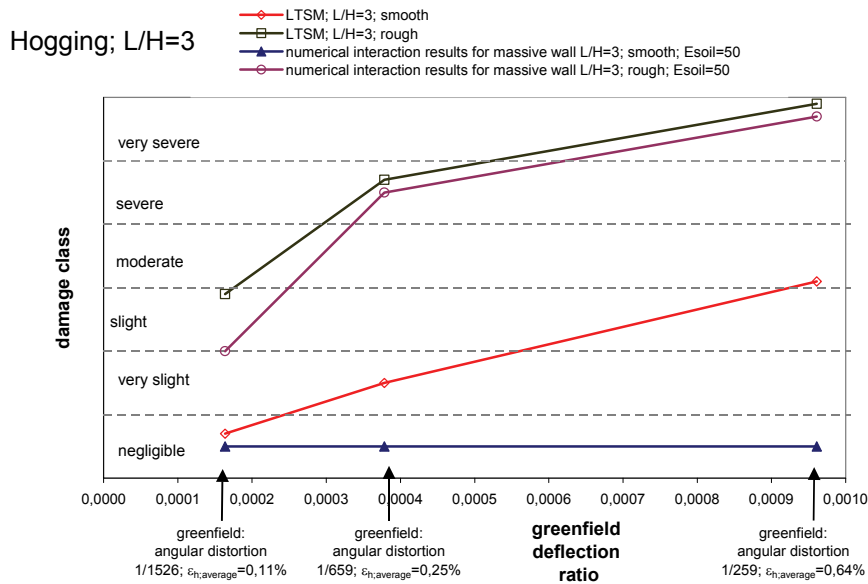The empirical analytical results calculated in section 4.5.2 with the modified LTSM for the smooth case, thus neglecting the influence of horizontal ground deformations, show a conservative prediction of the damage compared to the numerical interaction results. For volume loss 1 and 2 the difference is small as both approaches reveal negligible to very slight damage. For volume loss 3 the difference is significant as the LTSM predicts clearly more damage (slight/moderate for the LTSM versus negligible for the numerical interaction model). The numerical interaction model for the smooth case remains uncracked for all three volume losses, due to the strong interaction effect, which is neglected in the LTSM.

The LTSM results for the **rough case** are calculated with transfer of horizontal and vertical greenfield ground movements to the wall. The results show a very good agreement with the numerical results for the rough case for all three volume losses, even though the LTSM assumes a full transfer of the differential horizontal and vertical greenfield ground movements. The numerical interaction model however reduces the greenfield distortions due to interaction of the different stiffness of the wall and the soil. Nevertheless, as soon as cracking of the wall is initiated, the advanced numerical models show an overall damage pattern which is in good agreement with the LTSM prediction. Only volume loss 1 provides a conservative result with the LTSM, because minor cracking is just initiated for volume loss 1 in the numerical calculations. The damage class for the numerical analyses gives very slight/slight damage and the LTSM results in slight/moderate damage for volume loss 1.

It can be concluded, that the LTSM provides a good agreement with the numerical damage prediction for the considered cases for a massive wall and a rough interface between wall and soil. For the smooth case, when the transfer of horizontal differential ground movements is neglected, the LTSM provides a conservative estimation of the damage.

5.2.2.2   Influence of the soil stiffness

The analyses on the influence of the numerical models with different soil stiffness are considered separately for the rough cases and the smooth cases. The comparison of the results is presented for the lower and the upper bound value of the soil stiffness, E_{soil}=10MPa and E_{soil}=100MPa. It is emphasized that the case for E_{soil}=50MPa has been presented already in the previous section. The influence of the soil stiffness for the **smooth cases** is presented first in the following figures.
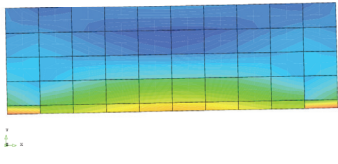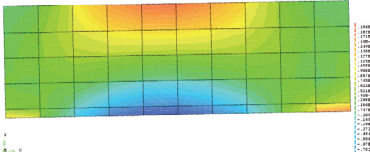
Soil-Structure Interaction

Figure 5.28 shows the results for volume loss 1.

Volume loss 1	E_{soil} =10MPa smooth	E$_{soil}$ =100MPa smooth
crack pattern	no cracking	no cracking
differential horizontal displacements at bottom/top edges [mm]	-0.04mm (bottom edge very slightly under compression) +0.03mm top edge very slightly under tension	-0.4mm (bottom edge slight under compression) +0.3mm (top edge slightly in tension)
differential vertical displacements at bottom corners [mm]	16.7mm	16.7mm
tilt	1 / 1176	1 / 1197
deflection	0.05mm (hog)	0,35mm (hog)
tensile strains	average strain at top edge is negligible	average strain at top edge 0.0015%
cumulative crack width	-	-
damage class	negligible	negligible

Figure 5.28: Comparison for different soil stiffness with smooth interface and volume loss 1

Figure 5.29 shows the results for volume loss 2.

Volume loss 2	E_{soil} =10MPa smooth	E_{soil} =100MPa smooth
crack pattern	no cracking	no cracking
principal tensile strains		

	-0.1mm (bottom edge very slightly under compression) +0.1mm (top edge very slightly under tension)	-0.7mm (bottom edge in compression) +0.6mm (top edge in tension)
differential horizontal displacements at bottom/top edges [mm]		
differential vertical displacements at bottom corners [mm]	38.6mm	38.7mm
tilt	1 / 518	1 / 516
deflection	0.1mm (hog)	0.9mm (hog)
tensile strains	average strain at top edge 0.05%	average strain at top edge 0.003%
cumulative crack width	-	-
damage class	negligible	negligible

Figure 5.29: Comparison for different soil stiffness with smooth interface and volume loss 2

Figure 5.30 shows the results for volume loss 3.

Volume loss 3	E_{soil} =10MPa smooth	E_{soil} =100MPa smooth
crack pattern	no cracking	
differential horizontal displacements at bottom/top edges [mm]	-0.3mm (bottom edge very slightly under compression) +0.3mm (top edge vey slightly under tension)	-1mm (bottom edge very slightly under compression) +20mm (top edge under tension)
differential vertical displacements at bottom corners [mm]	98.3mm	98.1mm
tilt	1 / 203	1/ 203
deflection	0.6mm (hog)	14mm (hog)
tensile strains	average top edge 0.0015%	average top edge 0.1%
cumulative crack width	-	20mm
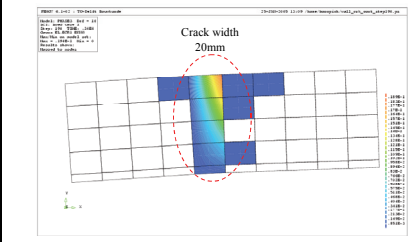
distribution of cracks		
damage class	negligible	severe

Figure 5.30: Comparison for different soil stiffness with smooth interface and volume loss 3

Figure 5.31 shows the results of the vertical interface stresses for all cases.
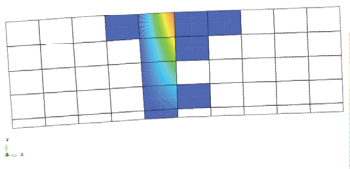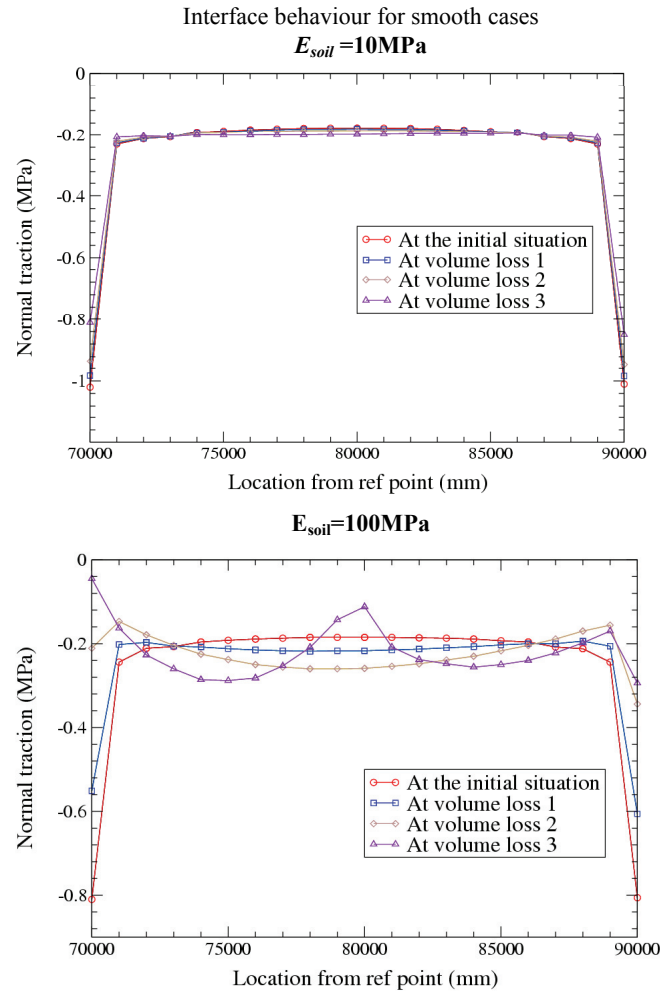

Figure 5.31: Vertical interfaces stresses for different soil stiffness and smooth interface

Soil-Structure Interaction

The considered hogging cases with smooth interface, thus without the transfer of differential horizontal ground movements, cause negligible damage except for the situation of volume loss 3 and E_{soil}=100MPa. For all volume losses the calculations with the low soil stiffness of 10MPa show clearly less introduction of tensile strains in the wall than for the case of 100MPa. This can be explained due to the increasing interaction effect of the soil and stiff building with decreasing soil stiffness.

However as soon as cracking is initiated, a significant increase of the damage is occurring, as shown in volume loss 3 for the upper bound value E_{soil}=100MPa for the soil stiffness. For this case the wall shows vertical cracking introduced at the top edge indicating a clear hogging mode deformation of the wall. The damage is categorized as severe damage, separating the wall into two parts. Both parts show a clear separate hogging mode deformation with unloading at the edges and an increase of the loads towards the centre of the wall. The distributions of vertical interface stresses shown in Figure 5.30 reflect this redistribution of support stresses. This hogging behaviour leads only to cracking for the case with the high soil stiffness and volume loss 3 for E_{soil}=100MPa. The introduced strains in the wall for volume loss 3 and the lower bound soil stiffness of E_{soil}=10MPa are not sufficient to cause cracking, leading to negligible damage.

It can be concluded that for the considered smooth cases, the beneficial interaction effect on the predicted damage increases clearly with decreasing soil stiffness, leading to less damage for the lower bound value of the soil stiffness. This conclusion is particularly valid if the imposed vertical ground distortions are greater than the distortions, which initiate first cracking in the wall.

Figure 5.32 presents the damage chart of the calculations with different soil stiffness for L/H=3 and the smooth interface. It is noted that the results for E_{soil}=50MPa, which are already presented in the previous section are also included in order to have the direct comparison of all three considered soil stiffness.
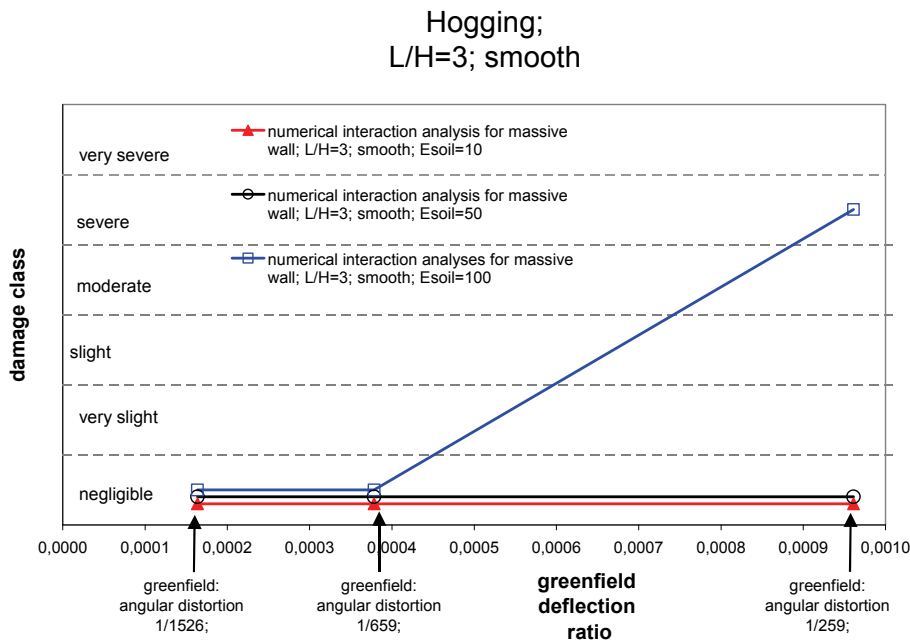
Figure 5.32: Damage results for numerical calculations with different soil stiffness and smooth interface

In Figure 5.33 the damage prediction result according to the LTSM is added to the chart of Figure 5.32.

Hogging;
L/H=3; smooth
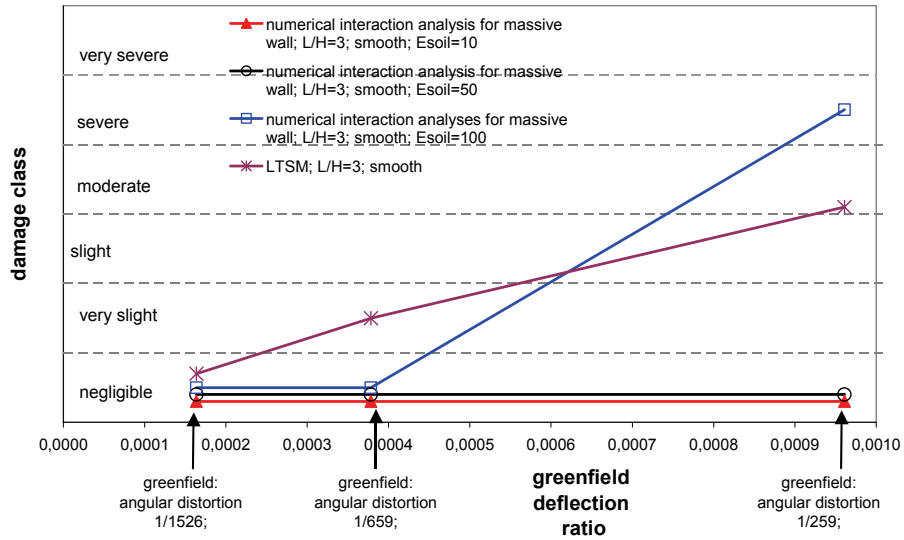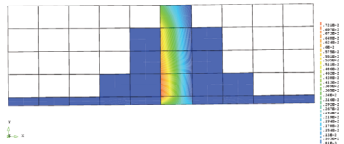
Figure 5.33: Comparison damage results of LTSM and numerical interaction calculations

The LTSM provides a conservative damage prediction for volume loss 1 and volume loss 2 for all smooth cases. The LTSM prediction is however a reasonable conservative approach, as the overestimation of the damage remains very small (between damage class negligible and very slight) for all considered cases. It should also be emphasized, that the LTSM results are independent of the soil stiffness because soil parameters are not included in that approach.

It is remarkable that the LTSM does however underestimate the damage for the upper bound soil stiffness and volume loss 3. This result shows the significance of the nonlinear masonry behaviour. Once a crack occurs the damage can increase rapidly. The LTSM can then obviously not provide a conservative prediction of the damage although it assumes full transfer of differential greenfield ground deformations on the wall and neglects the beneficial interaction effects. The linear elastic strain calculations related to damage classes according to the LTSM are modified significantly if cracking and thus nonlinear behaviour is developing in the masonry wall.

Figure 5.34 shows the comparison for the **rough case** and volume loss 1.

Volume loss 1	E_{soil} =10MPa rough	E_{soil}=100MPa rough
crack pattern	no cracking	
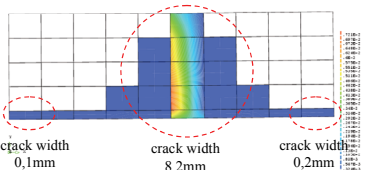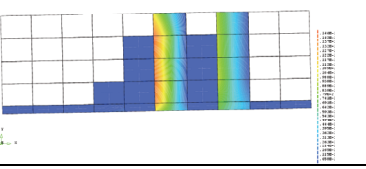
differential horizontal displacements at bottom/top edges [mm]	+0.2mm (tension bottom edge) top edge no horizontal tension/compression	+8.5mm (tension bottom edge) +5mm (tension top edge)
differential vertical displacements at bottom corners [mm]	16.5mm	16.9mm
tilt	1 / 1212	1/1183
deflection	0.05mm (sag)	1.9mm (sag)
tensile strains	average strain bottom edge 0.001%	average strain bottom edge 0.043% average strain top edge 0.025%
cumulative crack width	-	8.5mm
distribution of cracks	-	
damage class	negligible	moderate

Figure 5.34: Comparison for different soil stiffness with rough interface and volume loss 1

Volume loss 1 already reveals significant differences between the damage for E_{soil}=10MPa and E_{soil}=100MPa. The model with the high soil stiffness shows clearly more damage than the model with low soil stiffness (moderate versus negligible). The E_{soil}=100MPa case shows vertical cracking at the centre of the wall which is progressed over the entire height of the wall and consequently separates the wall in two parts. In the E_{soil}=10MPa case, the building only tilts rigidly and the damage is still negligible.

Figure 5.35 shows the comparison for the rough case and volume loss 2.

Volume loss 2	E_{soil} =10MPa rough	E_{soil} =100MPa rough
crack pattern	no cracking	
differential horizontal displacements at bottom/top edges [mm]	+0.6mm (tension bottom edge) -0.2mm (compression at top edge)	+24.4mm (tension bottom edge) +24.6mm (tension top edge)

differential vertical displacements at bottom corners [mm]	38.4mm	39mm
tilt	1 / 520	1/512
deflection	0.3mm (sag)	1.1mm (hog)
tensile strains	average strain bottom edge 0.003%	average strain bottom edge 0.122% average strain top edge 0.123%
cumulative crack width	-	24.6 mm (top edge)
distribution of cracks		
damage class	negligible	severe/very severe

Figure 5.35: Comparison for different soil stiffness with rough interface and volume loss 2

For the E_{soil}=100MPa case the moderate cracking damage from the previous volume loss 1 is further increased in volume loss 3 leading to severe/very severe damage with cumulative crack widths of up to 25mm. It is remarkable that a clear major second vertical crack has developed in the separated, right part of the wall. The consequence is the additional separation of the right half of the wall into two new parts. The E_{soil} =10MPa case remains still uncracked resulting in damage class negligible. The beneficial interaction effects of the lower soil stiffness lead to significant differences in damage between the models with lower and the upper bound soil stiffness.

Figure 5.36 shows the comparison for the rough case and volume loss 3.

Volume loss 3	E_{soil} =10MPa rough	E_{soil} =100MPa Rough
crack pattern		
differential horizontal displacements at bottom/top corners [mm]	+39mm (tension bottom edge) +1mm (negligible tension at top edge)	+65mm (tension bottom edge) +77mm (tension top edge)
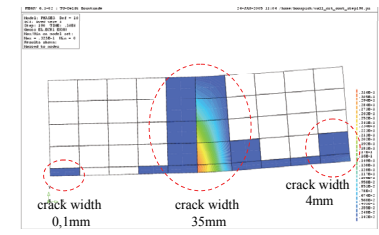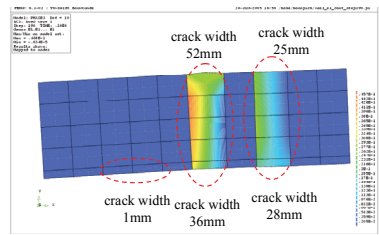
differential vertical displacements at bottom corners [mm]	99.5mm	97.3mm
tilt	1 / 201	1/205
deflection	25mm (sag)	16.5mm (hog)
tensile strains	average strain bottom edge 0,195%	average strain bottom edge 0,33% average strain top edge 0,39%
cumulative crack width	39mm	65mm (bottom) 77mm (top)
distribution of cracks	crack width 0,1mm crack width 35mm crack width 4mm	crack width 52mm crack width 25mm crack width 1mm crack width 36mm crack width 28mm
damage class	very severe	very severe

Figure 5.36: Comparison for different soil stiffness with rough interface and volume loss 3

Volume loss 3 shows an excessive increase of the damage compared to volume loss 2 for the E_{soil}=10MPa case. Vertical cracking is initiated at the bottom edge of the wall progressing rapidly up to the top edge of the wall and consequently leading to very severe damage. The wall is separated in two parts. This significant increase of the damage for the lower bound soil stiffness compared to volume loss 1 and 2 (negligible damage) shows again the significant influence of the nonlinear behaviour of the masonry. Once cracking is initiated, the progress of the cracking can develop rapidly. Despite the fact that the E_{soil}=10MPa calculations were undamaged in volume loss 1 and 2, the same damage class as for E_{soil}=100MPa is reached for volume loss 3. For the E_{soil}=100MPa case the cracking damage from the previous volume loss 2 is further increased in volume loss 3, leading to very severe damage with cumulative crack widths up to 77mm.

The horizontal and vertical interface stresses are presented in Figure 5.37.

Soil-Structure Interaction

E_{soil}=10MPa
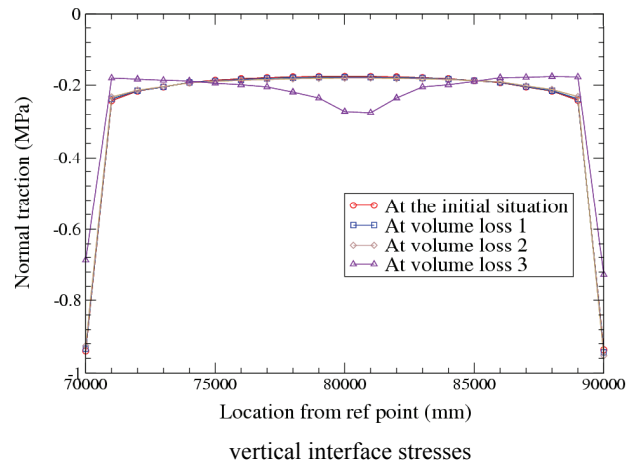
vertical interface stresses
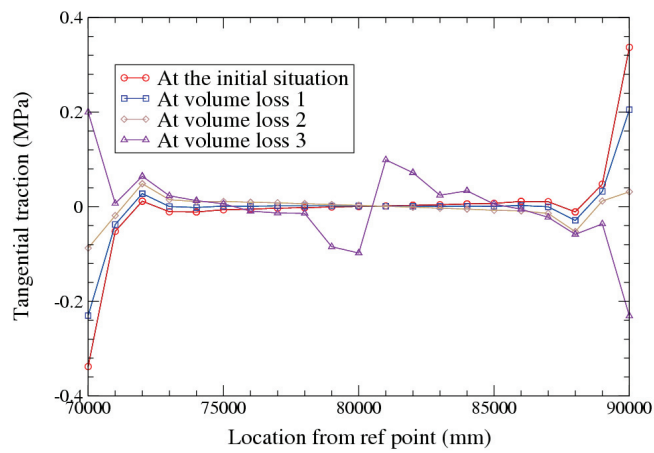
horizontal interface stresses

(a) E_{soil} = 10MPa

E_{soil}=100MPa

vertical interface stresses

horizontal interface stresses
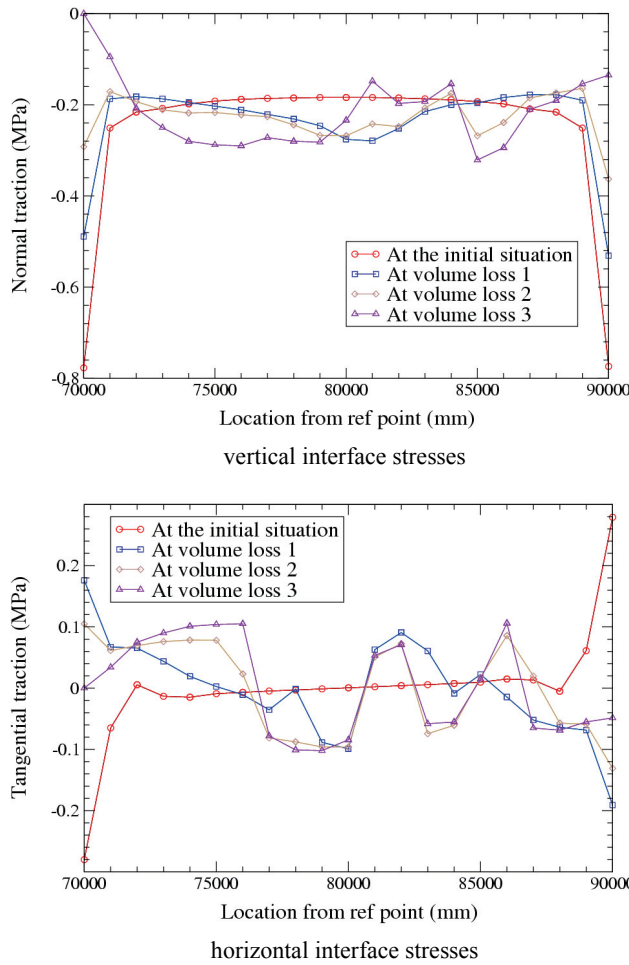
(b) E_{soil} = 100MPa

Figure 5.37: Comparison of interface stresses for different soil stiffness with rough interface

It is noted that a clear redistribution of the vertical and the horizontal interface stresses for the low soil stiffness occurs only at volume loss 3. This redistribution is in line with the rapid development of damage at volume loss 3 for the low soil stiffness. It is remarkable that this redistribution of the vertical and horizontal interface stresses at volume loss 3 for the low stiffness is comparable with the redistribution which occurs for the high soil stiffness of 100MPa already at volume loss 1. This indicates that the beneficial interaction effect reducing the introduced damage in the wall is much stronger for the low soil stiffness than for the high soil stiffness. The strong interaction effects of the lower bound of the soil stiffness prevents the wall from being damaged up to the distortions introduced between volume loss 2 and volume loss 3.

Figure 5.38 presents the damage chart of the calculations with different soil stiffness for L/H=3 and the rough interface. It is noted that the results for E_{soil}=50MPa, which were already presented in the previous section are also included in order to have the direct comparison of all three considered soil stiffness.

Hogging;
L/H=3; rough
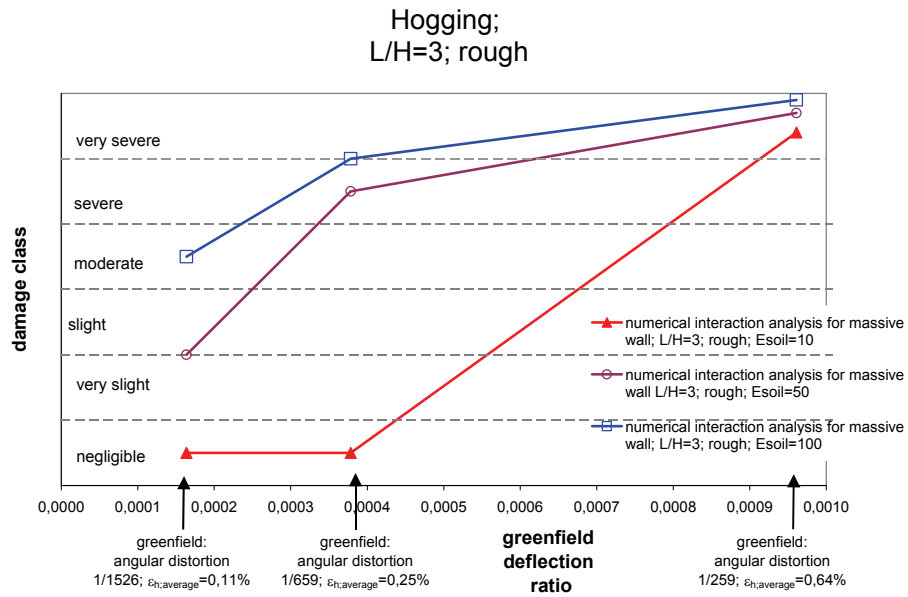
Figure 5.38: Damage results for different soil stiffness and rough interface

The principle general effect that the damage susceptibility is increasing with increasing soil stiffness is clearly shown for the numerical rough case results in Figure 5.37.
In Figure 5.39 the damage prediction result according to the LTSM is added to the chart of Figure 5.38.

Hogging;
L/H=3; rough
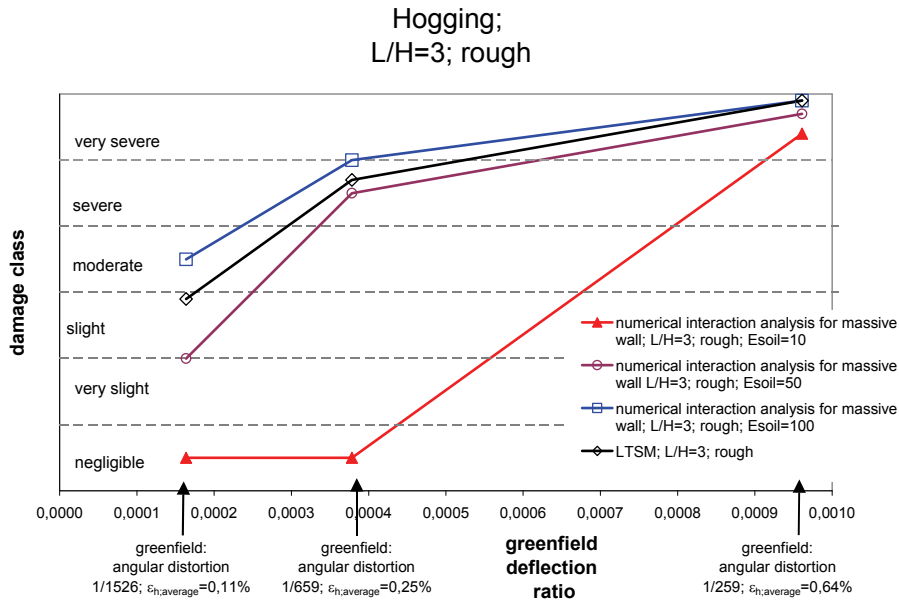
Figure 5.39: Comparison of damage classes between LTSM and numerical calculations

The damage prediction according to the LTSM provides a conservative prediction of the damage for the case with the lower bound of the soil stiffness of 10MPa and volume loss 1 and volume loss 2. For

volume loss 3 however the LTSM provides a very good agreement with the numerical interaction result for E_{soil}=10MPa. The cracking of the wall initiated for volume loss 3 with consequently the highly nonlinear response of the wall and a rapid increase of the damage is responsible for this phenomena. The LTSM as well as the numerical interaction provide very severe damage for volume loss 3 and the lower bound soil stiffness.
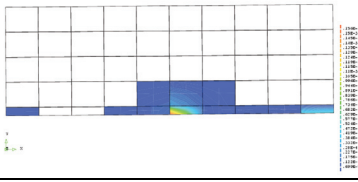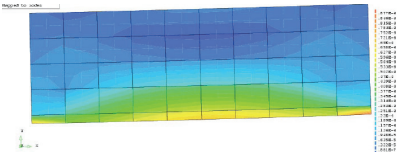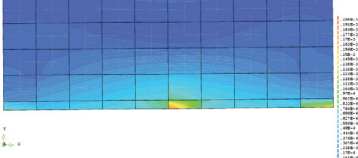
For the soil stiffness of 50MPa the agreement between the predicted damage according to the LTSM and the numerical interaction results are very good. The results for the upper bound value for the soil stiffness of 100MPa show are very slight underestimation of the damage predicted with the LTSM.

5.2.2.3   Influence of linear versus nonlinear masonry model

The influence of the use of the linear and the nonlinear (smeared crack) masonry material model is analyzed in this section for the hogging case with a building *L/H*-ratio of 3, the soil stiffness of E_{soil}=50MPa and the rough interface.

It should be mentioned that the numerical maximum values for the linear strains are used to categorize the linear calculation into damage classes according to the LTSM strain band widths (see Figure 3.5), because the calculation of linear strains in the LTSM considers also the linear maximum strains in the beams.

The results for volume loss 2 are presented in Figure 5.40.

| **Volume loss 1**	**Linear** material model masonry	**Nonlinear** material model masonry
crack pattern	-	
contour plots of the principal tensile strains		
It is emphasized that the scales of the strain contour plots presented above, are not the same for both calculations.		
differential horizontal displacements at bottom/top corners [mm]	+1mm (bottom edge in tension) -0.5mm (top edge in compression)	+1.2mm (bottom edge in tension) -0.3mm (top edge in compression)
differential vertical displacements at bottom corners [mm]	16.4mm	17mm
tilt	1 / 1315	1 / 1190
deflection	0	0.6mm (sag)
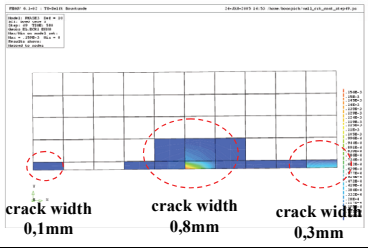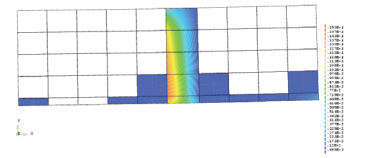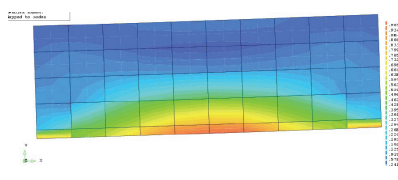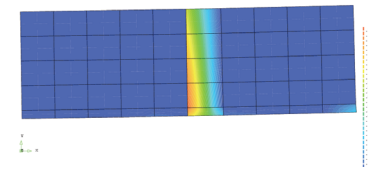
	average strain bottom edge 0.005% max. strains bottom edge 0.0094% bottom mid 0.007%	average strain bottom edge 0.006% max. strain 0.02% bottom mid
tensile strains		
cumulative crack width	-	1.2mm
distribution of cracks	-	crack width 0,1mm crack width 0,8mm crack width 0,3mm
damage class	negligible	very slight/slight

Figure 5.40: Comparison nonlinear versus linear masonry behaviour for volume loss 1

Volume loss 1 shows small differences between the maximum and the average tensile strains at the bottom edge for the two models. This can be explained by the fact that only very slight damage occurs in the nonlinear model for volume loss 1, which causes small differences between the response of the nonlinear and the linear masonry model. The cracking introduced at the bottom centre of the wall in the nonlinear calculation leads to a small sagging mode deflection, which is not developing in the linear calculation. The small sagging mode deflection in the nonlinear calculation is caused by the introduction of the horizontal tensile strains at the bottom of the wall causing an eccentric bending moment of the wall. As a consequence of the vertical cracking at the bottom edge of the wall the bending stiffness of the nonlinear wall is reduced at the section of the cracking and the small sagging deflection is developed (see also explanations in 5.2.2.1).

The results for volume loss 2 are presented in Figure 5.41.

Volume loss 2	**linear** material model masonry	**nonlinear** material model masonry
crack pattern	-	
contour plots of the principal tensile strains		
It is emphasized that the scales of the strain contour plots presented above, are not the same for both calculations.		

differential horizontal displacements at bottom/top corners [mm]	+1.6mm (tension bottom edge) -0.6mm (top edge in compression)	+20mm (tension bottom edge) +10mm (tension top edge)
differential vertical displacements at bottom corners [mm]	38.7mm	39mm
tilt	1 / 536	1 / 514
deflection	1.2mm (sag)	4.1mm (sag)
tensile strains	average strain bottom edge 0,008% max. strain 0,01% bottom mid	average strain bottom edge 0,1% average strain top edge 0,05% max. strain 1,5% bottom mid
cumulative crack width	-	20mm
distribution of cracks		
damage class	negligible	severe

Figure 5.41: Comparison nonlinear versus linear masonry behaviour for volume loss 2

Volume loss 2 shows significant differences between the maximum and the average tensile strains for the two models. The severe vertical cracking of the nonlinear model leads to a significant difference in the damage class. For details of the interpretation of the nonlinear model it is refereed to 5.2.2.1.

The maximum strains of the linear model are still small and result in negligible damage according to the categorization of Figure 3.5. The transfer of horizontal strains in the linear model also leads to a sagging mode deflection due to the introduction of the eccentric bending moment. However the linear behaviour of the wall restricts the strains in the wall. The significance of the nonlinear masonry model for the estimation of damage is obvious.

The results for volume loss 3 are presented in Figure 5.42.

Volume loss 3	**linear** material model masonry	**nonlinear** material model masonry
crack pattern	-	

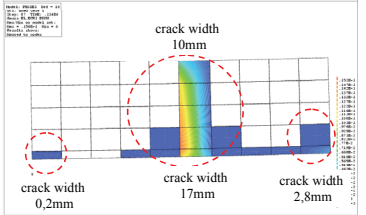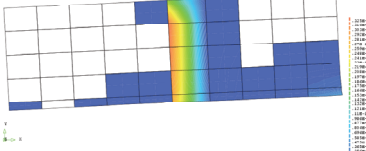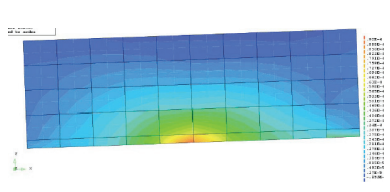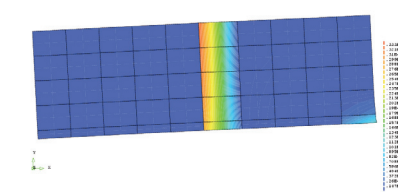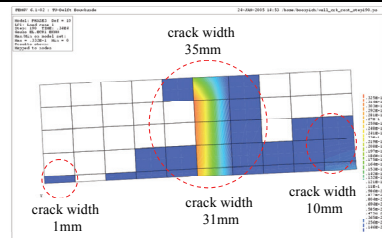| contour plots of the principal tensile strains		
It is emphasized that the scales of the contour plots presented above, are not the same for both calculations.		
differential horizontal displacements at bottom/top corners [mm]	+1mm (bottom edge in tension) no compression at top edge	+42mm (bottom edge in tension) +35mm (top edge in tension)
differential vertical displacements at bottom corners [mm]	98.1mm	99.5mm
tilt	1 / 207	1/201
deflection	0.1mm (sag)	1.8mm (hog)
tensile strains	average strain bottom edge 0.005% max. strain 0.0095 %	average strain bottom edge 0.21% average strain top edge 0.18% max. strain 3.4 %
cumulative crack width	-	42mm
distribution of cracks		
damage class	negligible	very severe

Figure 5.42: Comparison nonlinear versus linear masonry behaviour for volume loss 3

Volume loss 3 shows further increasing significant differences between the maximum and the average tensile strains for the two models. The linear model still remains uncracked and the nonlinear model reveals very severe cracking. For details of the interpretation of the nonlinear model it is referred to 5.2.2.1.

The development of the maximum and average and maximum strains of the linear model from volume loss 2 to volume loss 3 reveal a remarkable change. The tensile strains for volume loss 3 are even reduced compared to volume loss 2, unless the greenfield distortions between the two volume losses are significantly increased ! This phenomena can be explained by the fact that the hogging mode due to the vertical distortions is getting more dominant in volume loss 3. As a consequence the dominant horizontal interaction at the bottom of the wall introducing the horizontal tensile strains at the bottom of the wall for volume loss 1 and 2 is reduced by the vertical hogging mode, which changes the

distribution and orientation of horizontal shear stresses at the bottom of the wall. The resulting tensile strains in the wall are consequently reduced compared to volume loss 2. The interface stresses given in Figure 5.43 and Figure 5.44 also show clearly the modification of the horizontal and vertical load transfer of the wall and the soil. The change in the deflection is also undermining this explanation, because the sagging deflection from volume loss 2 is decreased to almost zero in volume loss 3. As the linear wall cannot develop cracking, this phenomena leads to a reduction of the tensile strains for volume loss 3. The damage in the linear model remains negligible.

Again the results for volume loss 3 show the importance of the nonlinear masonry for the prediction of the damage. The change in deformation mode and stiffness of the wall due to cracking causes major differences in the redistribution of horizontal and vertical loads in the wall, leading to a significant underestimation of the damage with a numerical linear masonry model.

The vertical interface stresses are shown in Figure 5.43.
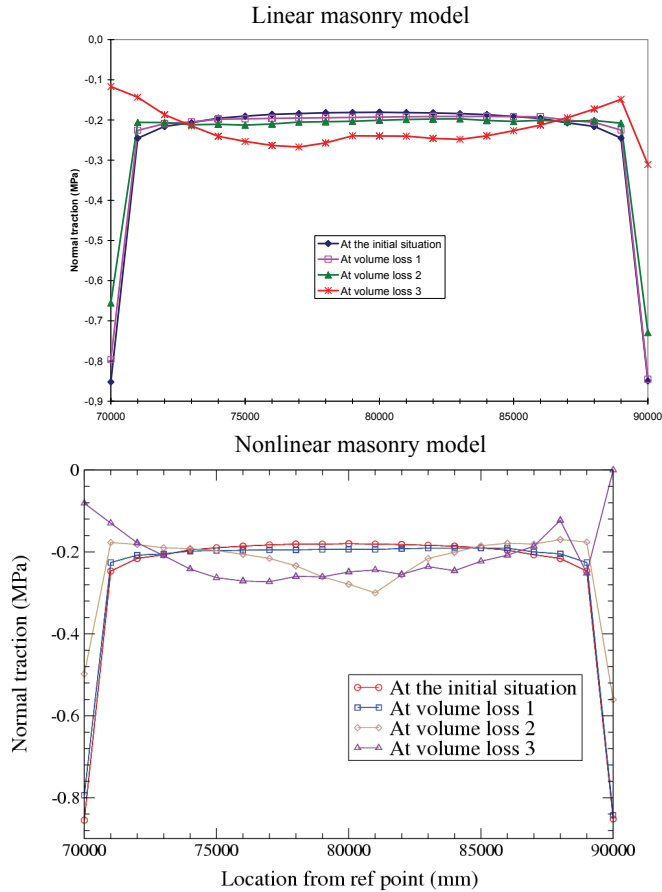
Figure 5.43: Vertical interface stresses

The horizontal interface stresses and the relative horizontal displacements of the interface for the linear model are shown in Figure 5.44.
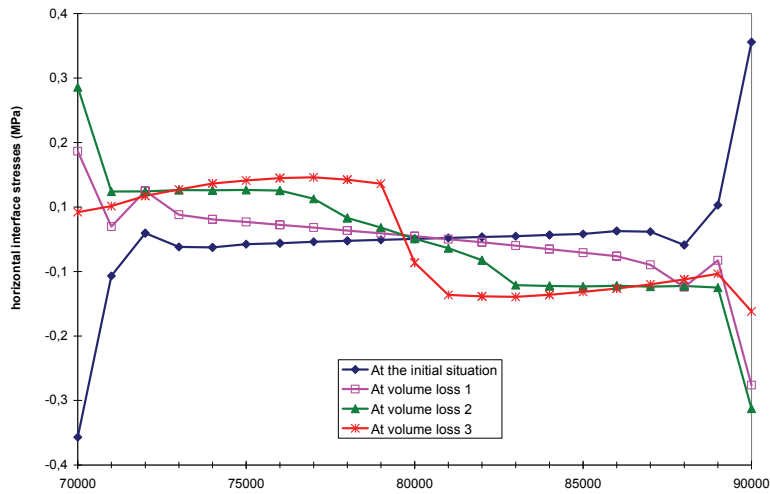
(a) horizontal interface stresses of the linear calculation
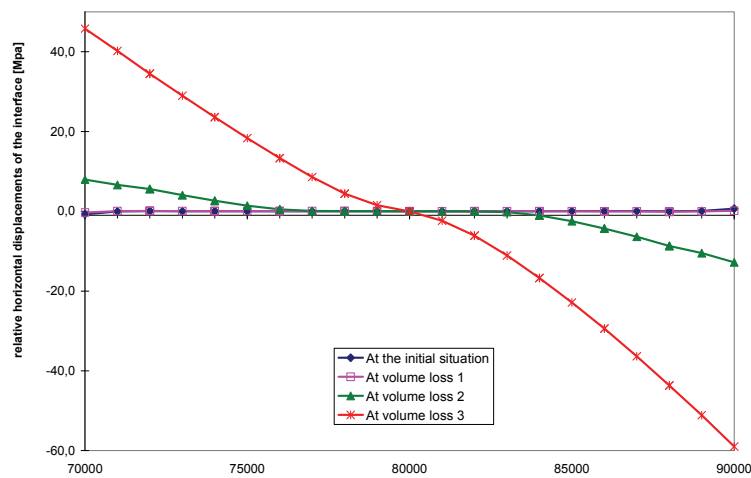
(b) relative horizontal displacements of the interface in the linear calculation

Figure 5.44: Horizontal interface stresses and relative horizontal displacements of the interface for the linear calculation

The calculation for the linear masonry model shows the reduction of the vertical interface stresses at the corners of the wall in volume loss 3 due to the hogging mode deformation caused by the transfer of differential vertical distortions imposed by the soil. This effect is shown in Figure 5.43. The horizontal interface stresses are consequently also reduced at the corners for volume loss 3, as both vertical and horizontal interface stresses are related together via the bi-linear Coulomb friction law, implemented in the interfaces. This reduction at the corners leads to a significant increase of the differential horizontal displacement between wall and soil towards the bottom corners, indicating slipping. The distribution of the relative horizontal displacements of the interface is shown for the linear masonry model in Figure 5.44 (b). Towards the centre of the wall however an increase of the vertical interface stresses is recognized due to the hogging mode deformation in volume loss 3. Consequently the horizontal

interface stresses in the centre of the wall also increases. The interpretation of the development of the horizontal interface stresses is schematically shown in Figure 5.45.
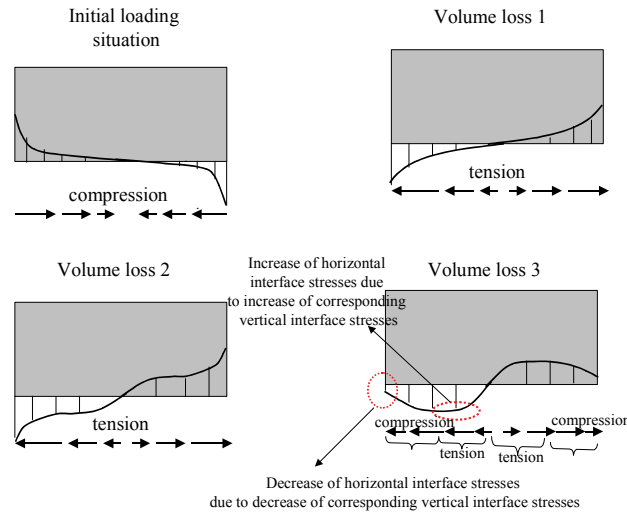
Figure 5.45: Schematic distributions of horizontal interface stresses for the linear calculation

Figure 5.46 shows the direct comparison of the damage class results between the empirical analytical prediction method (LTSM), the linear and nonlinear numerical interaction calculations.
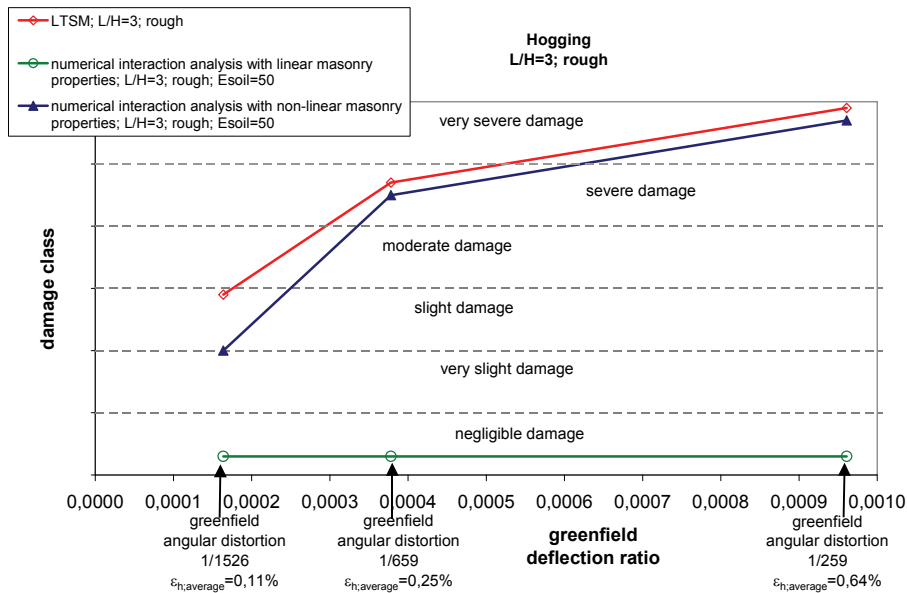
Figure 5.46: Comparison of damage results between nonlinear and linear numerical results and LTSM

It can be concluded that the LTSM provides a conservative approach for the damage prediction for volume loss 1 compared to both numerical calculations. For volume loss 2 and 3 the damage class

according to the LTSM is in very good agreement with the nonlinear calculation (severe to very severe). The linear numerical interaction calculation however strongly underestimates the damage.

The results show the importance of the nonlinear masonry for the prediction of the damage. The change in deformation mode and stiffness of the wall due to cracking causes major differences in the redistribution of horizontal and vertical loads in the wall, leading to a significant underestimation of the damage with a numerical linear masonry model.

The numerical interaction model approach with a linear material model for the masonry can therefore only considered to be appropriate for the determination of strains and damage as long as no cracking is introduced in the wall.

5.2.2.4   Influence of mesh density

In order to judge the sensitivity of the mesh density on the damage results, two calculations with different mesh densities are compared with each other. The calculation of the hogging case with E_{soil}=50MPa, rough interface and L/H=3 is carried out for a fine mesh (element dimensions 0.25m) and the reference mesh with element dimensions of 2m. It is noted that calculation time of the reference mesh is significant lower. It is noted that both calculations are carried out with the nonlinear smeared crack model for masonry.

The results for volume loss 1 are shown in Figure 5.47.
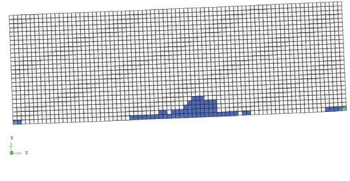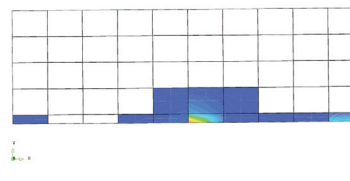
Volume loss 1	Fine mesh	Reference mesh
crack pattern		
differential horizontal displacements at bottom/top corners [mm]	+0.7mm (bottom edge in tension)	+1.2mm (bottom edge in tension)
differential vertical displacements at bottom corners [mm]	17mm	17mm
tilt	1 / 1190	1 / 1190
tensile strains	average strain bottom edge 0,0035% max. 0,02% bottom mid 0,06% bottom edge	average strain bottom edge 0,006% max. strain 0,02% bottom mid
cumulative crack width	0.7mm	1.2mm
damage class	very slight	very slight/slight

Figure 5.47: Comparison numerical results mesh densities for volume loss 1

The results for volume loss 2 are shown in Figure 5.48.
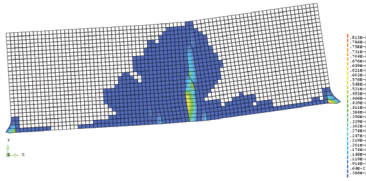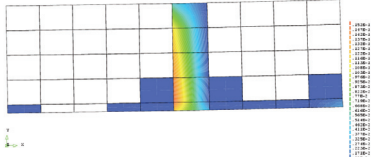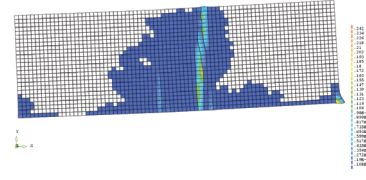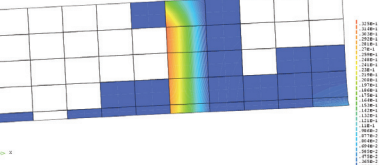
Volume loss	Fine Mesh	Reference
crack pattern		
differential horizontal displacements at bottom/top corners [mm]	+17mm (tension at bottom edge)	+20mm (tension bottom edge)
differential vertical displacements at bottom corners [mm]	39mm	39mm
tilt	1 / 512	1 / 514
tensile strains	average strain bottom edge 0.085% max. strain 6.7% (bottom mid)	average strain bottom edge 0.1% average strain top edge 0.05% max. strain 1.5% bottom mid
cumulative crack width	17mm	20mm
damage class	severe	severe

Figure 5.48: Comparison numerical results mesh densities for volume loss 2

The results for volume loss 3 are shown in Figure 5.49.

Volume loss 3	Fine Mesh	Reference
crack pattern		

differential horizontal displacements at bottom/top corners [mm]	+41mm (tension at bottom edge)	+42mm (bottom edge in tension)
differential vertical displacements at bottom corners [mm]	94mm	99.5mm
tilt	1/213	1/201
tensile strains	average strain bottom edge 0.205% max. strain 20 %	average strain bottom edge 0.21% average strain top edge 0.18% max. strain 3.4 %
cumulative crack width	41mm	42mm
damage class	very severe	very severe

Figure 5.49: Comparison numerical results mesh densities for volume loss 3

The vertical interface stresses for all calculations are presented in Figure 5.50.
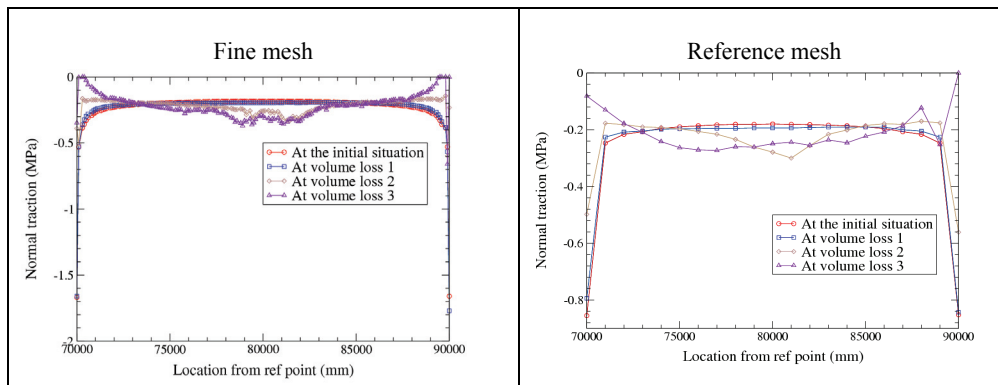
Figure 5.50: Comparison vertical interface stresses for mesh densities

The calculations show minor differences between the refined mesh with element width of 0.25m and the reference model with an element width of 2m. The interface behaviour shows the same pattern.
It is emphasized, that for the refined mesh very local extension and strains occur at four corner elements for volume loss 2 and 3, see Figure 5.51. These numerical singularities are not considered in the determination of the differential horizontal movements and consequently in the determination of the average tensile strains at the bottom edge. The horizontal differential movements just above the lowest row of elements are chosen to be representative.

Representative section for determination of average tensile strain at bottom edge

Numerical singularities at four corner elements
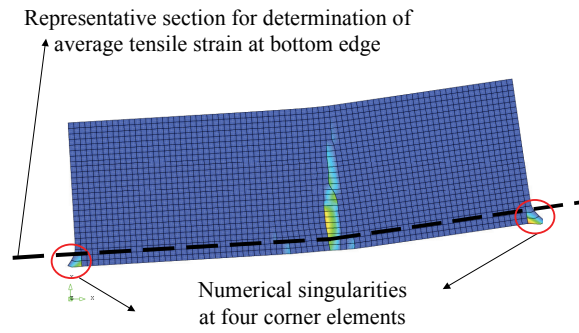
Figure 5.51: Local singularities of the refined mesh for the average tensile strain at the example of volume loss 2

The maximum strain values are increased significantly for the refined mesh and the volume losses 2 and 3, which can be explained by the smaller element widths. This leads to a smaller reference length for an integration point, which leads consequently to locally higher strains at the integration points. However the integration of strains over the element width remains almost the same, yielding reasonably objective results for the cumulative crack width. A comparison of the average strains along the bottom edges gives a better picture, as it does not depend on singular peaks. The average tensile strains at the bottom edge are shown in Figure 5.52.
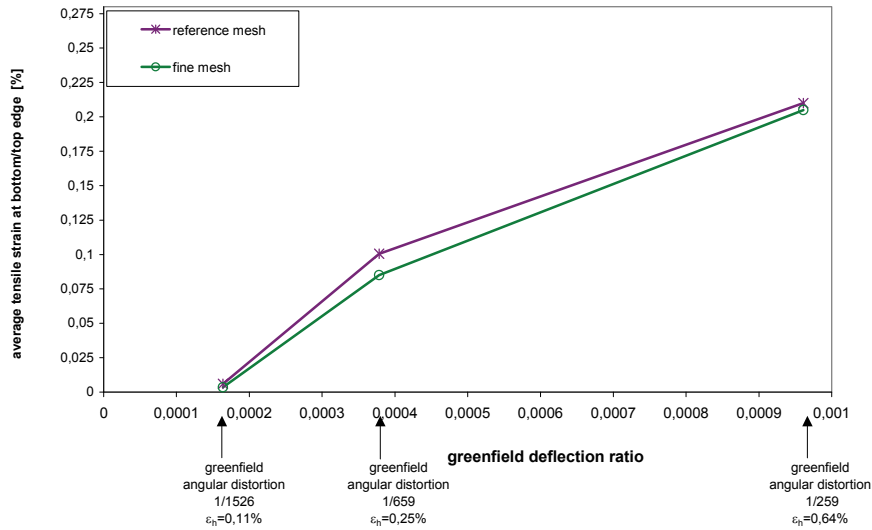
Figure 5.52: Comparison of average tensile strains at the bottom edge for different mesh densities

The differences in the resulting damage can be judged to be negligible as shown in the damage chart of Figure 5.53. The reference mesh can therefore considered to be representative. The results demonstrate the objectivity of crack width predictions with respect to the chosen mesh size. This forms an important issue in softening fracture mechanics using smeared crack models, see Rots (1988).
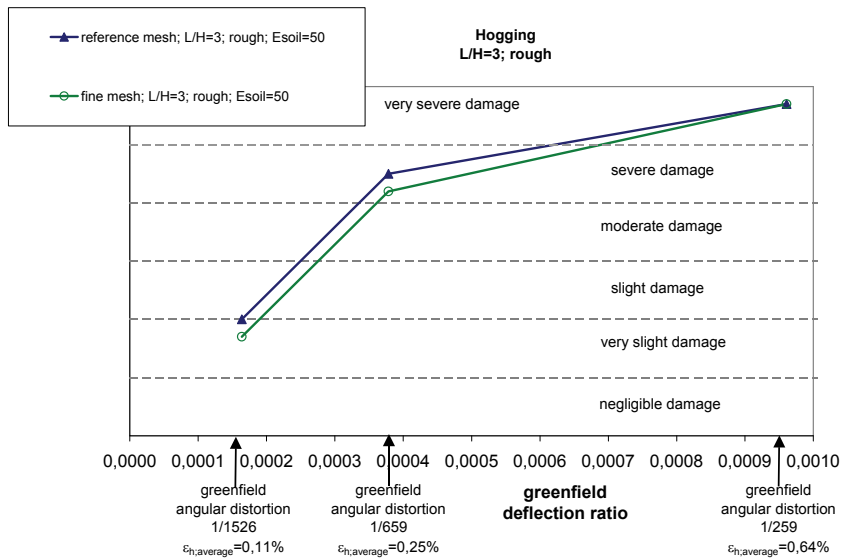
Figure 5.53: Comparison of damage classes for different mesh densities and the LTSM

5.2.2.5   *Influence of L/H-ratio*

In order to analyse the influence of the *L/H*-ratio of the building, the calculations of the building of the same length (20m) and two different heights are investigated for the hogging case with rough and smooth interface and E_{soil} =50MPa. The two considered building heights are 6.5m and 20m, leading to a *L/H*-ratio of 3 and 1 respectively. For a fixed *L*, a decreased *L/H*-ratio of a massive masonry wall means an increase in stiffness of the wall and an increase in the bending capacity as a result of the increase of the second moment of inertia.

The results for the **smooth interface** and the two different L/H-ratio's case are presented hereafter.

It is noted, that the initial load situation for the tall wall with L/H-ratio of 1 and the smooth interface shows already very minor hairline cracking at the bottom corners. This cracking is caused by a local load concentration effect due to the very slightly inclined compression diagonal directed towards the bottom corners of the wall. This effect is visualized in Figure 5.54. No beneficial horizontal restraint is activated at the bottom edge due to the smooth interface. Both cracks at the bottom corners show a width of ca. 0.1mm.

Soil-Structure Interaction
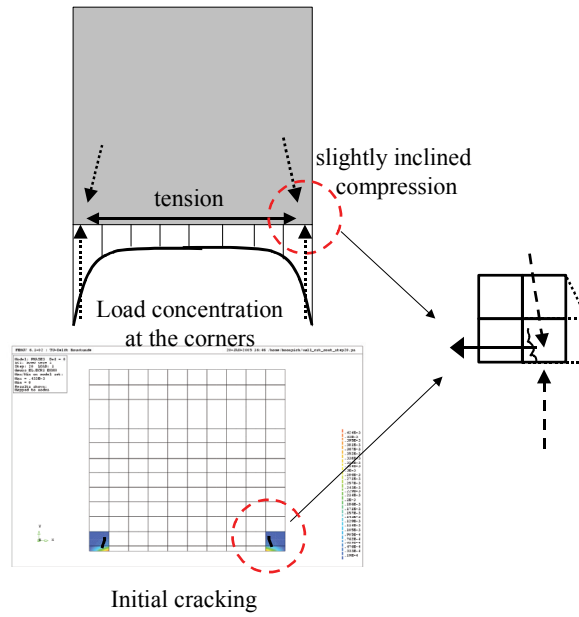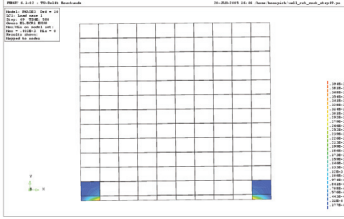
Initial cracking

Figure 5.54: Cracking in the initial situation

The results for volume loss 1 and the smooth interface are shown in Figure 5.55.

Volume loss 1	*L/H*=1 E_{soil} =50MPa smooth interface	*L/H*=3 E_{soil} = 50MPa smooth interface
crack pattern	 reduction of cracking compared to initial situation (see Figure 5.54)	no cracking
differential horizontal displacements at bottom/top corners [mm]	-0.09mm bottom edge slightly compressed top edge no tension or compression	-0.2mm (bottom slightly in compression) +0.2mm (top slightly in tension)
differential vertical displacements at bottom corners [mm]	16.7mm	16.8mm
tilt	1/1196	1/1190
deflection	0,1mm (hog)	0,2mm (hog)
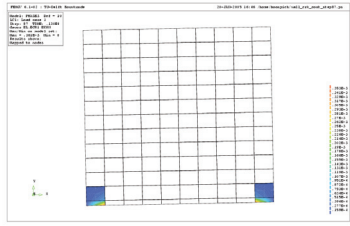
tensile strains	average compressive strain bottom edge -0.00065%	average strain at top edge 0.001%
cumulative crack width	-	-
damage class	negligible	negligible

Figure 5.55: Results for volume loss 1

Volume loss 1 shows a clear difference between the *L/H*-ratio of 3 and the *L/H*-ratio of 1. Although the absolute strains are all negligible, the *L/H*-ratio of 3 shows clear hogging bending behaviour with a linear distribution of strains in the mid section of the wall, causing negligible tensile strains at the top edge of the wall and the same magnitude of compressive strains at the bottom edge, identifying clearly the hogging mode beam behaviour. The hogging deflection of 0.2mm is however very small resulting in negligible damage without any cracking.

The *L/H*-ratio of 1 shows less hogging deflection due to its greater stiffness. It also shows a shell wall behaviour, with a nonlinear distribution of the horizontal strains over the height of the wall. Due to the hogging mode very small horizontal compressive strains are introduced at the bottom edge of the wall. The top edge of the wall is however not influenced by the hogging deformations due to volume loss 1. It is emphasized that the cracking is not initiated by the differential deformations induced by volume loss 1 but was already existing at the initial stage (see Figure 5.54). Anyhow due to the incremental hogging compression at the bottom edge of the wall with *L/H*=1, the initial negligible cracking at the bottom corners is very slightly reduced. The damage is therefore still negligible.

The results for volume loss 2 and the smooth interface are shown in Figure 5.56 .

Volume loss 2	***L/H*=1**	***L/H*=3**
crack pattern	reduction of cracking compared to initial situation (see Figure 5.54)	no cracking
differential horizontal displacements at bottom/top corners [mm]	-0.2mm bottom edge slightly compressed top edge no compression or tension	-0.4mm (bottom edge in compression) +0,4mm (tension top edge)
differential vertical displacements at bottom corners [mm]	38.6mm	38.6mm
tilt	1/518	1 / 518
deflection	0.3mm (hog)	0.5mm (hog)

tensile strains	average compressive strain bottom edge -0.001%	average strain at top edge 0.002%
cumulative crack width	-	-
damage class	negligible	negligible

Figure 5.56: Results for volume loss 2

Volume loss 2 shows the same qualitative pattern as for volume loss 1. The hogging deflection is increased for both cases slightly. Due to the vertical soil-structure interaction both deflections are however reduced significantly and remain still very small. The bottom edges of the wall are further compressed for both cases due to the hogging bending mode. The initial cracking at the bottom corners for the *L/H*-ratio of 1 is further decreased. Both cases still show negligible damage.

The results for volume loss 2 and the smooth interface are shown in Figure 5.57.
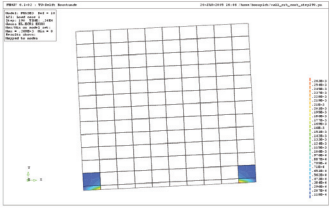
Volume loss 3	L/H=1	L/H=3
crack pattern	reduction of cracking compared to initial situation (see Figure 5.54)	no cracking
differential horizontal displacements at bottom/top corners [mm]	-1mm (bottom edge in compression) top edge no compression or tension	-1mm (bottom edge in compression) +1mm (top edge in tension)
differential vertical displacements at bottom corners [mm]	98.1mm	97.8mm
tilt	1/203	1 / 204
deflection	0.5mm (hog)	1.2mm (hog)
tensile strains	average compressive strain bottom edge -0.005%	average strain at top edge 0.005%
cumulative crack width	-	-
damage class	negligible	negligible

Figure 5.57: Results for volume loss 3

Volume loss 3 still shows negligible damage with slightly increased hogging deflections for both cases.

Soil-Structure Interaction

The results for the distribution of the vertical interface stresses and the relative horizontal interface displacements *L/H*-ratio of 1 are shown in Figure 5.58. The small redistributions of the vertical interface stresses are in line with the negligible damage observations. The distribution of the relative horizontal displacements of the interface show the correct working of the smooth interface with significant relative displacements between the soil side and the wall side of the interface, representing horizontal slipping.

L/H=1

horizontal interface stresses

relative horizontal displacement in the interface
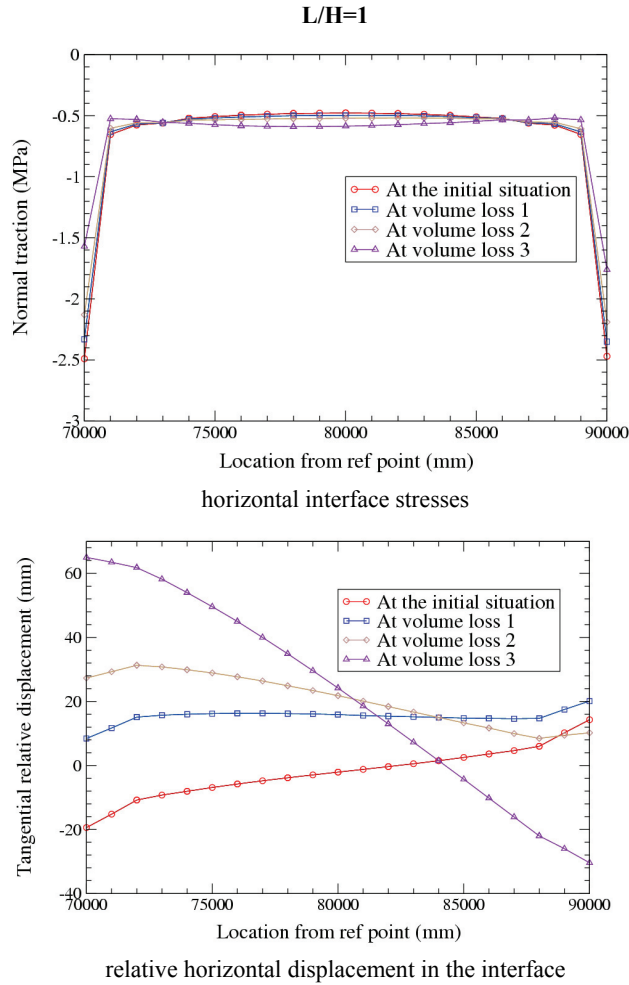
Figure 5.58: Interface behaviour for *L/H*=1 and the smooth cases

The damage chart for the results of the calculations for both L/H-ratio's and the smooth interface are shown in Figure 5.59.
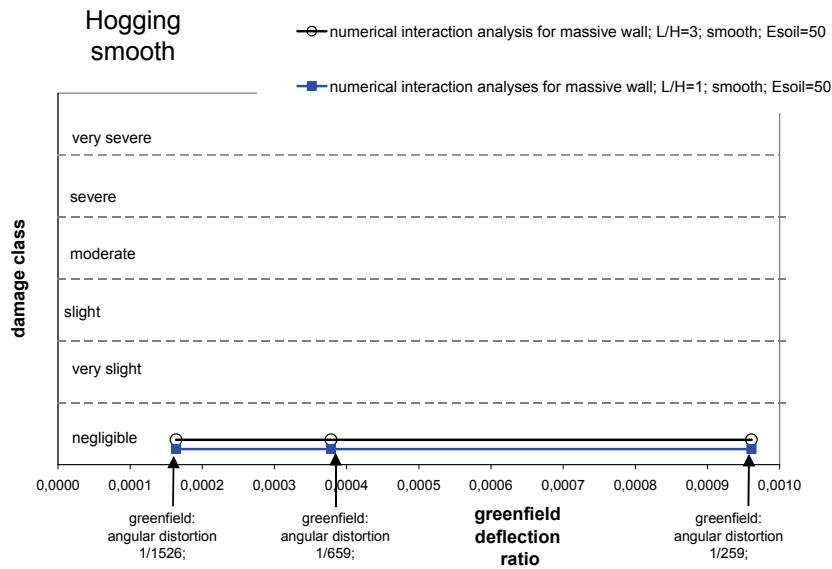
Figure 5.59: Damage chart for both *L/H*-ratio's and the smooth interface

The results of the LTSM are combined with the numerical interaction results in damage chart of Figure 5.60.
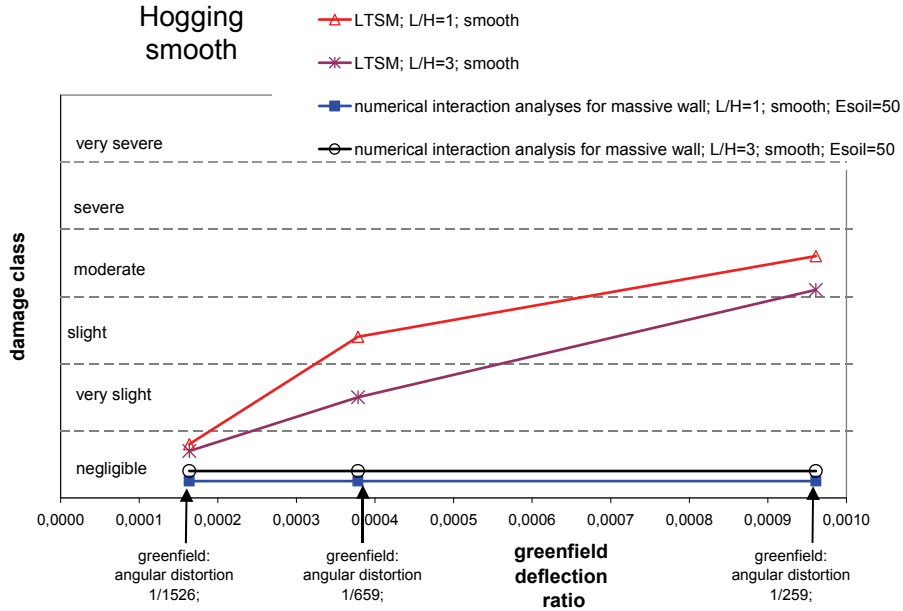
Figure 5.60: Damage chart with LTSM and the numerical calculations for both *L/H*-ratio's and the smooth interface

The LTSM provides good agreement with the numerical damage results for volume loss 1 and both *L/H*-ratio's. It provides a conservative damage prediction for both L/H-ratio's for volume loss 2 and volume loss 3. The difference in the predicted damage is slight for volume loss 2 (damage class negligible versus very slight/slight) and significant for volume loss 3 (damage class negligible versus

slight/moderate). The numerical interaction results show clearly the beneficial effect for the smooth case as both walls remain uncracked. The LTSM prediction provides a slightly more conservative damage for the *L/H*-ratio of 1 than for *L/H*=3.

The comparison for the **rough interface behaviour** and volume loss 1 is shown in Figure 5.61.
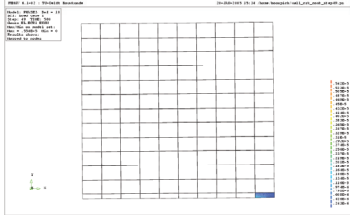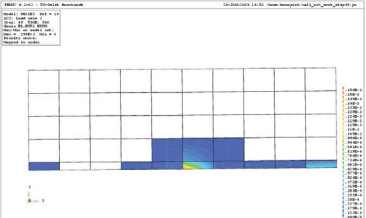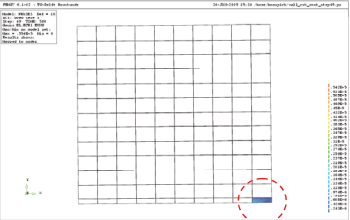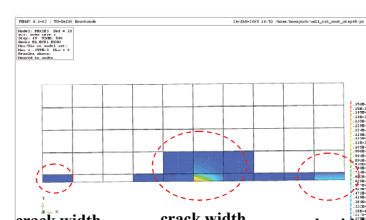
Volume loss 1	*L/H*=1 (L=20m; H=20m) hogging, E_{soil}=50MPa, rough interface	*L/H*=3 (L=20m; H=6,5m) hogging, E_{soil}=50MPa, rough interface
crack pattern		
It is emphasized, that in the plots shown in the following figures, the scale of the wall lengths as well as the division of contours is not the same for both models.		
differential horizontal displacements at bottom/top corners [mm]	+0.9mm (tension bottom edge) no tension or compression at top edge	bottom edge +1.2mm (bottom in tension) top edge -0.3mm (top in compression)
differential vertical displacements at bottom corners [mm]	16.6mm	17mm
tilt	1 / 200	1 / 1190
deflection	0.3mm (sag)	0.6mm (sag)
tensile strains	average tensile strain bottom edge 0.0045%	average tensile strain bottom edge 0.006%
cumulative crack width	0.9mm	1.2mm
distribution of cracks	max. crack width 0.5mm	crack width 0,1mm crack width 0,8mm crack width 0,3mm
damage class	very slight	very slight/slight

Figure 5.61: Comparison different *L/H*-ratio's for volume loss 1

Soil-Structure Interaction

For volume loss 1 the *L/H*-ratio of 1 shows slightly less damage than the wall with *L/H*-ratio of 3. The *L/H*=3 wall is cracked at the bottom mid due to the introduction of horizontal tensile strains. The wall *L/H*=1 however shows no cracking in the bottom mid, but very local and small cracking at the edges due to the singular load bearing concentrations at the outer ends of the building. The *L/H*=1 wall shows the stiffer reaction of the tall wall, resulting in less distortions of the wall than the *L/H*=3 wall.

The comparison for the **rough interface behaviour** and volume loss 2 is shown in Figure 5.62.
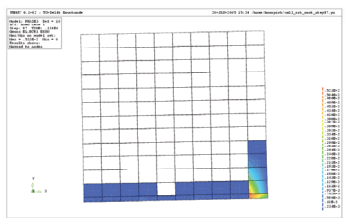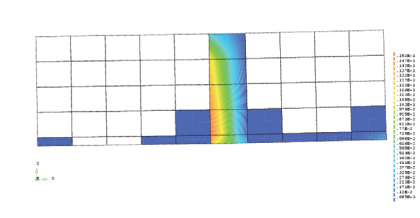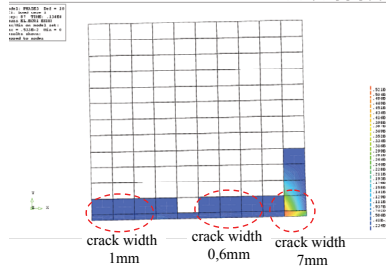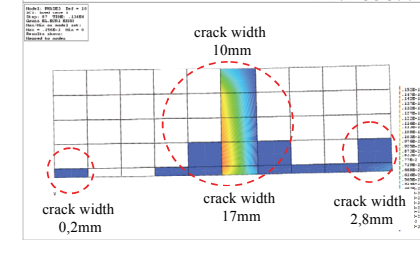
Volume loss 2	*L/H*=1	*L/H*=3
crack pattern		
differential horizontal displacements at bottom/top corners [mm]	+9,2mm (tension at bottom edge) -0.1mm (very small compression at top edge)	+20mm (tension bottom edge) +10mm (tension top edge)
differential vertical displacements at bottom corners [mm]	40.1mm	39mm
tilt	1 / 498	1 / 514
deflection	1.3mm (sag)	4.1mm (sag)
tensile strains	average strain bottom edge 0,046%	average strain bottom edge 0.1% average strain top edge 0.05%
cumulative crack width	9mm	20mm
distribution of cracks		
damage class	moderate	severe

Figure 5.62: Comparison different *L/H*-ratio's for volume loss 2

For volume loss 2 the *L/H*=3 case shows a significant increase of the cracking damage introduced from a vertical crack starting from the bottom mid of the wall increasing over the entire height of the building and splitting the wall into two parts. The cracking is categorized as moderate to severe damage whereas the *L/H*=1 wall only shows moderate damage concentrated in the bottom part of the wall. The dominating vertical cracking for the *L/H*=1 wall occurs at the outer ends and only very slight cracking develops at the bottom mid. Both walls show a sagging mode deflection due to the strong influence of the eccentric horizontal tensile strains introduced at the bottom edge, which are overruling the vertical hogging bending mode. The sagging deflection of the *L/H*=1 wall is however clearly smaller than the sagging deflection of the *L/H*=3 wall. This difference in sagging deflection reveals again more stiffer behaviour of the tall wall resulting in less distortion of the wall and thus less damage.

The comparison for the **rough interface behaviour** and volume loss 3 is shown in Figure 5.63.
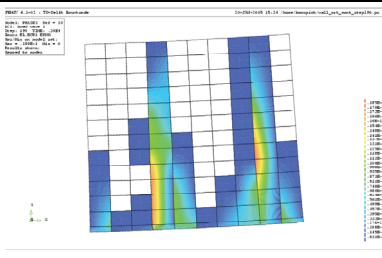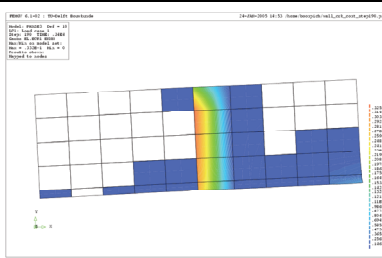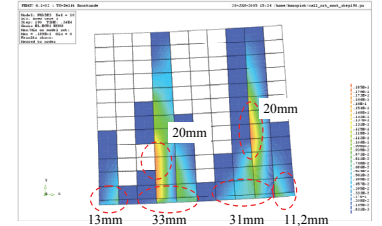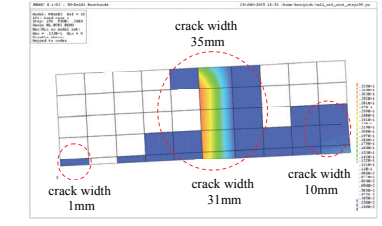
Volume loss 3	*L/H*=1	*L/H*=3
crack pattern		
differential horizontal displacements at bottom/top corners [mm]	+91mm (bottom edge in tension) -1mm (top edge very small compression)	+42mm (bottom edge in tension) +35mm (top edge in tension)
differential vertical displacements at bottom corners [mm]	94.5mm	99.5mm
tilt	1 / 210	1/201
deflection	14mm (sag)	1.8mm (hog)
tensile strains	average strain bottom edge 0.45%	average strain bottom edge 0.21% average strain top edge 0.18%
cumulative crack width	91mm	42mm
distribution of cracks		
damage class	very severe	very severe

Figure 5.63: Comparison different *L/H*-ratio's for volume loss 3

Soil-Structure Interaction

For volume loss 3 the cracking pattern of the *L/H*=1 wall is significantly changed as the wall shows two dominant vertical cracks progressed up to 2/3 of the wall height, splitting the wall into three parts. The vertical cracking is caused mainly by the horizontal tensile strains introduced at the bottom edge. As the three (almost) separated wall parts have clearly smaller *L/H*-ratio's than 1, they almost tilt rigidly away from each other. The overall deflection of the total wall is still sagging mode. The resulting crack damage is categorized as very severe damage as shown by the *L/H*-wall of 3 for volume loss 3.

The vertical and horizontal interface stresses for the *L/H* case of 1 and the rough interface are shown in Figure 5.64. The detailed interpretation of the interface stresses for *L/H*=3 and the rough interface has been already presented in 5.2.2.1. It is emphasized that due to the increasing height of the building of *L/H*=1 and the increasing building loads for the taller building (see also 4.4.4.3) the absolute magnitude of the vertical interface stresses is higher for *L/H*=1 compared to *L/H*=3. The vertical interface stress at the centre of the wall in the initial situation is –0.5MPa for *L/H*=1 case and –0.2MPa for the *L/H*=3 case.

L/H=1

vertical interface stresses

horizontal interface stresses
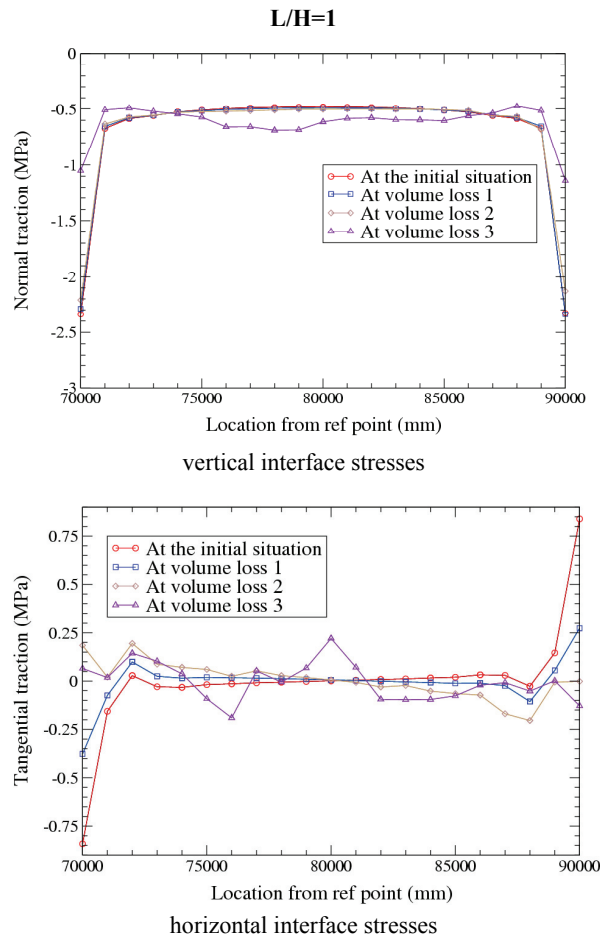
Figure 5.64: Interface stresses for *L/H*=1 and the rough interface

The damage chart for both *L/H*-ratios and the rough interface is shown in Figure 5.65.

Soil-Structure Interaction
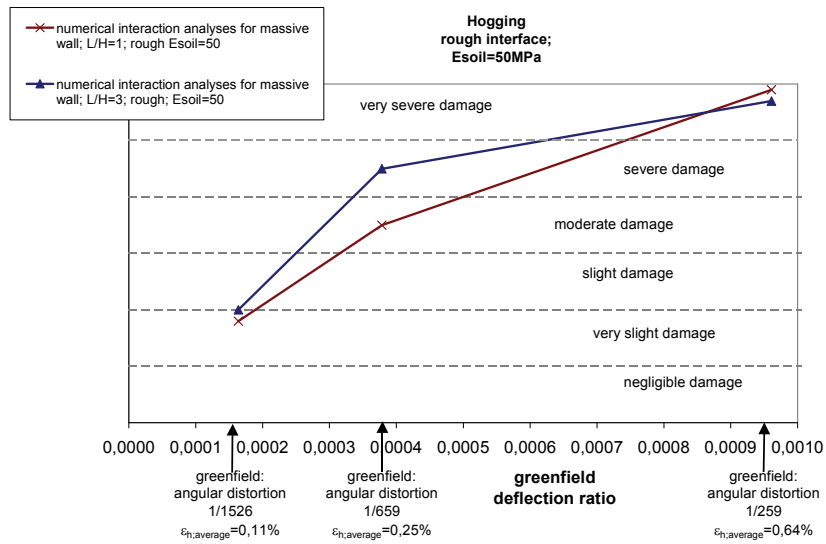
Figure 5.65: Damage chart for both *L/H*-ratio's, *E$_{soil}$*=50MPa and rough interface

The *L/H*=3 wall is only for volume loss 2 more susceptible to damage than the *L/H*=1 wall. For volume loss 1 and 3 both *L/H*-ratio's give the same damage class.
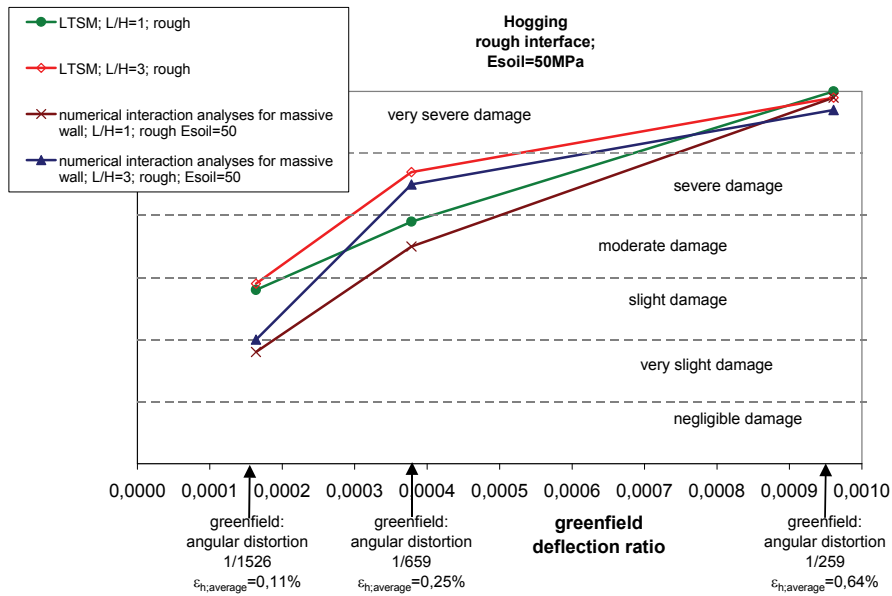
Figure 5.66: Damage chart for the two *L/H*-ratio's compared to the LTSM

The LTSM shows good agreement with the numerical damage for all three volume losses and both *L/H*-ratio's for the hogging zone. Only for volume loss 1 the LTSM overestimates the damage. For both *L/H*-ratio's the LTSM predicts for volume loss 1 slight/moderate damage instead of very slight/slight damage according to the numerical interaction results.

It should be noted that only two different *L/H*-ratio's have been considered, using the same building length (20m) and variation of the height (6.5m and 18m) in order to preserve practical building

dimensions. The possible influence of a *L/H*-ratio where the height is kept constant and the building length is changed can deliver different results and should be investigated in future research.

5.2.3 Sagging

5.2.3.1 Influence of smooth and rough interface

Similar to the approach for the hogging zone the influence of the interface properties is discussed in this section. In the calculations with a rough interface, horizontal shear forces between the soil and the wall can be mobilized. As explained in section 4.4.5 the smooth interface neglects the horizontal transfer of stresses between soil and wall at the bottom edge of the wall. The magnitude of the horizontal forces depends on the vertical loading and is mobilized up to a certain value before horizontal slipping between soil and wall occurs. For the sagging situation the horizontal greenfield movements cause horizontal compression (see also section 4.5.2) at the bottom of the wall and it is therefore expected that for the rough cases horizontal compressive stresses and strains are induced up to a certain degree at the bottom edge of the walls.

The influence of the smooth and the rough interface for the sagging mode is analysed for the example of the case of *L/H*=3 and E_{soil}=50MPa. The numerical model is shown in Figure 5.67.
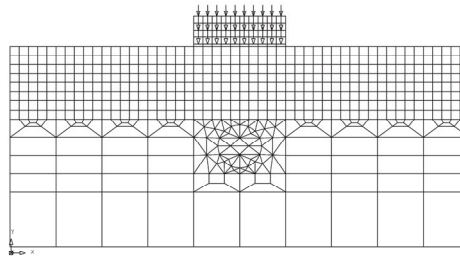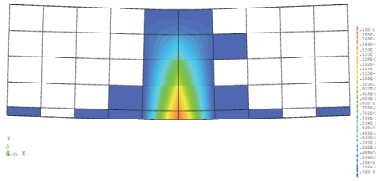
Figure 5.67: Numerical model for L/H=3 and the sagging zone

The numerical results for volume loss 1 are shown in Figure 5.68.

Volume loss 1	E_{soil} = 50MPa smooth; *L/H*=3	E_{soil} = 50MPa rough; *L/H*=3
crack pattern		no cracking
differential horizontal displacements at bottom/top edges [mm]	+32mm outwards (tension at the bottom edge) -0.5mm (relatively very small compression at the top edge)	-0.08mm inwards (compression at bottom edge) -0.2mm (compression at top edge)
vertical displacements at bottom edges [mm]	40mm	50mm
tilt	-	-

deflection	23.6mm (sag)	0.4mm (sag)
tensile strains	max. strain 1.6% average strain bottom edge 0.163%	max. strain 0.0021% average compressive strain bottom edge almost nihil
cumulative crack width	32mm	-
damage class	very severe	negligible

Figure 5.68: Sagging for *L/H*=3 and volume loss 1

The definitions of the presented values of the differential deformations and the deflection from Figure 5.68 for the sagging case are given in Figure 5.69.
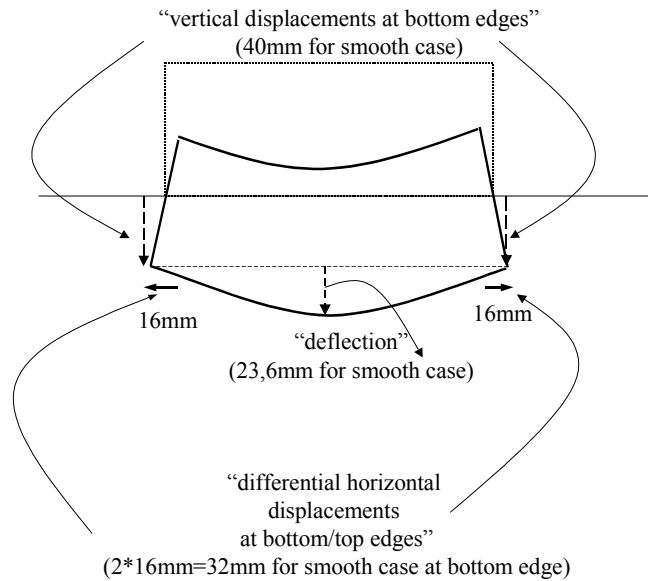
Figure 5.69: Definitions of presented numerical output for the sagging zone

The smooth calculation shows a clear nonlinear reaction for volume loss 1. Vertical cracking is initiated at the bottom centre of the wall and progresses over almost the entire height of the wall. Due to cracking and the lack of beneficial restraint of the soil at the bottom corner for the smooth interface, the damage is classified as very severe. It is emphasized that the numerical deflection at the centre of the wall (23.6mm) is significant greater than the greenfield deflection (13mm, see Figure 4.26). The principle effect of the interaction for the smooth case and volume loss 1 is shown in Figure 5.70. It is noted that the deformation figure of the wall and the greenfield curve is scaled up significantly to show the effects clearly.

Soil-Structure Interaction
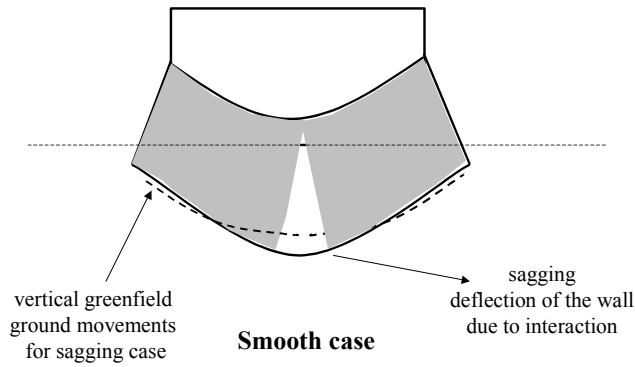
Figure 5.70: Principle of interaction for the smooth sagging case

The rough case shows the very beneficial effect of the transfer of horizontal differential ground movements in the sagging zone, which imposes compressive strains at the bottom edge of the wall. These compressive strains overrule the tensile strains at the bottom edge due to the vertical sagging mode as explained in Figure 5.71. No cracking is initiated, leading to damage class negligible for volume loss 1. The numerical deflection of the wall is consequently significantly reduced compared to the deflection of the smooth case and the greenfield settlements. The horizontal greenfield movement of the soil in the sagging zone is inwards, towards the centre of the wall. This leads to frictional forces at the bottom edge of the wall which are transferred via the interface. Consequently horizontal compression is induced at the bottom edge of the wall, preventing the wall from cracking. The principal effects of soil-structure interaction for the rough case and volume loss 1 are visualized in Figure 5.71.
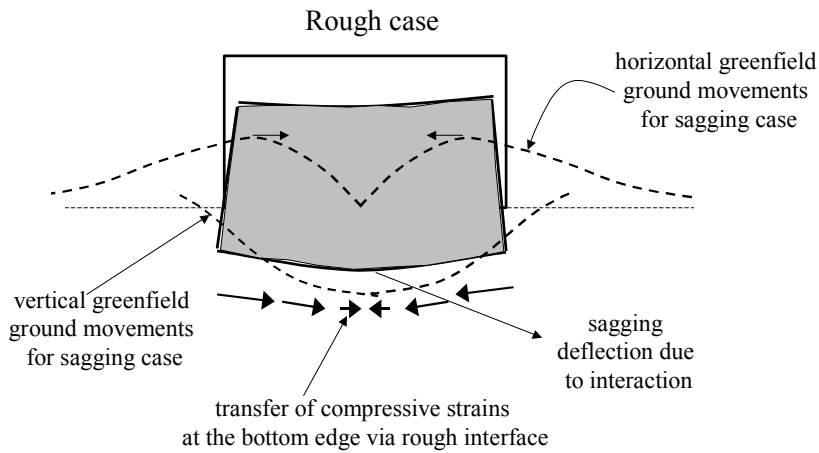
Figure 5.71: Principal effects of the rough case for volume loss 1, sagging zone

The results for the rough and smooth interface for the sagging zone and volume loss 2 are shown in Figure 5.72.
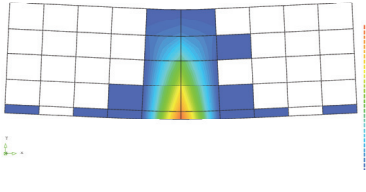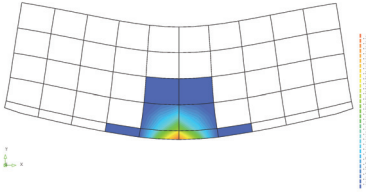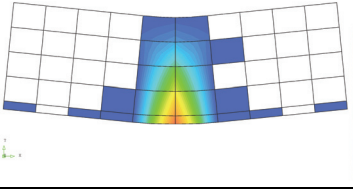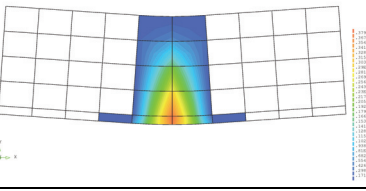
Volume loss 2	E_{soil} = 50MPa smooth; *L/H*=3	E_{soil} = 50MPa rough; *L/H*=3
crack pattern		
It is emphasized that the scale of the deformed mesh plot is not equal for both cases shown above		
differential horizontal displacements at bottom/top edges	+58mm (tension at bottom edge) -1mm (very small compression at top edge)	+0.8mm (tension at bottom edge) -1mm (compression at top edge)
vertical displacements at bottom edges	117mm	116mm
tilt	-	-
deflection	47mm (sag)	2mm (sag)
tensile strains	max. strain 2.9% average strain bottom edge 0.293%	max. strain 0.041% average strain bottom edge 0.004%
cumulative crack width	58mm	0.8mm
damage class	very severe	very slight

Figure 5.72: Sagging for *L/H*=3 and volume loss 2, sagging zone

The results for the smooth case show a further increase of the damage with the same pattern as for volume loss 1. The vertical crack at the centre of the wall is opening further.

The rough case shows initiation of vertical cracking at the bottom edge of the wall leading to very slight damage. Volume loss 2 represents the case where the interaction due to the vertical differential sagging settlements imposed on the wall is just overruling the beneficial effects due to the horizontal interaction in the sagging zone. Thus the beneficial compressive strains transferred at the bottom edge of the wall cannot prevent the wall anymore from cracking for volume loss 2.

The results for the rough and smooth interface for the sagging zone and volume loss 3 are shown in Figure 5.73.

Volume loss 3	E_{soil} = 50MPa smooth; *L/H*=3	E_{soil} = 50MPa rough; *L/H*=3
crack pattern		
It is emphasized that the scale of the deformed mesh plot is not equal for both cases shown above		

differential horizontal displacements at bottom/top edges	+130mm (tension at bottom edge)	+ 84mm (tension at bottom edge)
	-1.6mm (compression at top edge)	-4mm (compression at top edge)
vertical displacements at bottom edges	256mm	269mm
tilt	-	-
deflection	92mm (sag)	62mm (sag)
tensile strains	max. strain 6.4% average strain bottom edge 0.65%	max. strain 3.8% average strain bottom edge 0.42%
cumulative crack width	130mm	84mm
damage class	very severe	very severe

Figure 5.73: Sagging for *L/H*=3 and volume loss 3, sagging zone

The results for the smooth case show a further increase of the damage with the same pattern as for volume loss 1 and 2. The vertical crack widens and progresses further over the height of the wall.
For the rough case a significant increase of the damage compared to volume loss 1 and 2 is recognized. Once the crack is initiated in volume loss 2 the cracking is progressing rapidly in volume loss 3 leading to very severe damage for the rough case at volume loss 3. These results clearly show the importance of the nonlinear masonry behaviour.
The development of the vertical interface stresses for the smooth case for the initial loading situation and all three volume losses is shown in Figure 5.74.
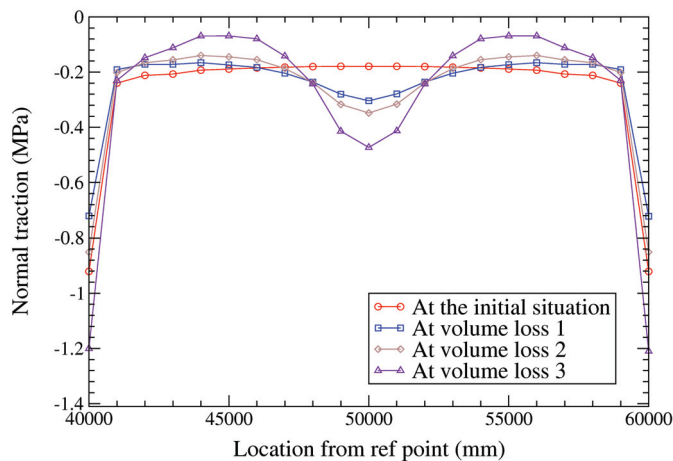
Figure 5.74: Vertical interface stresses for the smooth cases and all volume losses, sagging zone

For the smooth case volume loss 1 already shows a clear redistribution of the vertical interface stresses. Compared to the initial loading situation this redistribution results in an increase of the stresses at the centre of the wall and a decrease of the initial stress peaks at the bottom corners. This is a typical sagging mode effect. The increase of the vertical interface stresses at the centre of the wall can be explained by the fact that the wall is cracked severely in vertical direction at the centre of the wall. The two separated wall parts show load concentrations towards their corners, comparable to the load concentrations which occur in the initial loading situation for the uncracked wall. The load

concentrations at the outer corners are, however, still more developed than at the inner corners at both sides of the crack. This effect develops further with increasing volume loss. For volume loss 3 the further increase of the vertical interface stresses towards the bottom corners is accompanied by a decrease of the vertical interface stresses between the corners of the two separated wall parts. Each centre of the separated wall parts is unloaded up to small stresses over a width of approximately 2 to 3m. The development of the distribution of the vertical interface stresses clearly reflects the soil-structure interaction effects and the corresponding reaction due to the nonlinear cracking behaviour of the wall. Figure 5.75 shows the development of the vertical interface stresses and the horizontal interface stresses between soil and wall for the rough case for the initial loading situation and all three volume losses.

vertical interface stresses

horizontal interface stresses
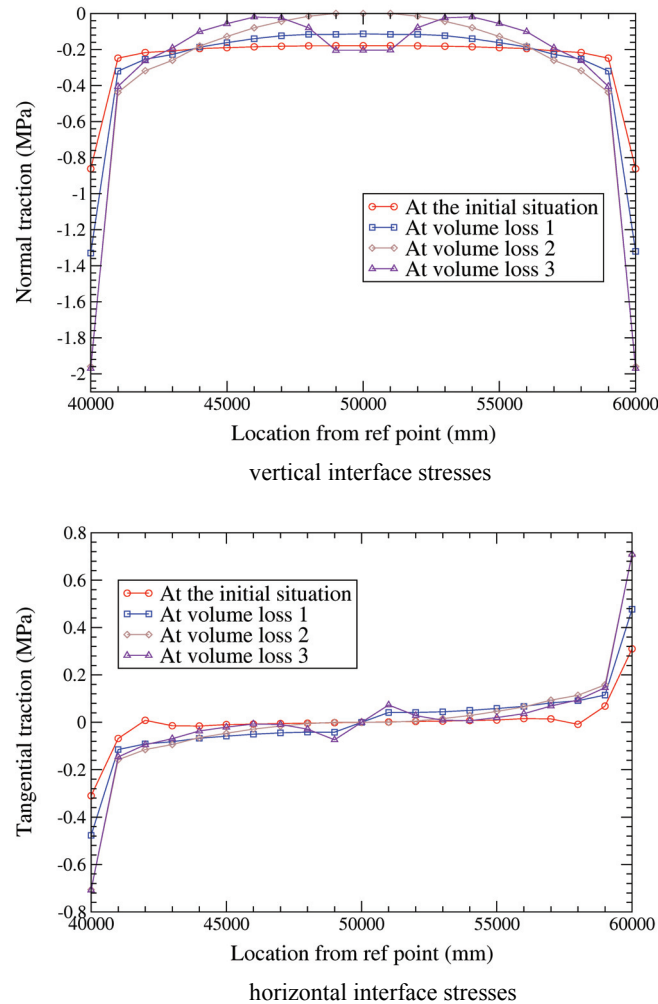
Figure 5.75: Interface stresses for all volume losses and the rough interface, sagging zone

Volume loss 1 for the rough case shows only a small redistribution of the vertical interface stresses with decreasing stresses at the centre of the wall. This unloading effect is characteristic for the sagging mode. As the wall is not cracked for the rough case in volume loss 1, the redistribution effects as described previously for the smooth case are not developing for volume loss 1 and the rough case. Cracking is avoided due to the beneficial effect of the horizontal differential ground movements. This is

clearly shown in the mobilisation of horizontal interface shear stresses acting on the wall and inducing compression in the wall. Figure 5.76 shows the schematic development of horizontal interface stresses for the initial loading situation and volume loss 1.
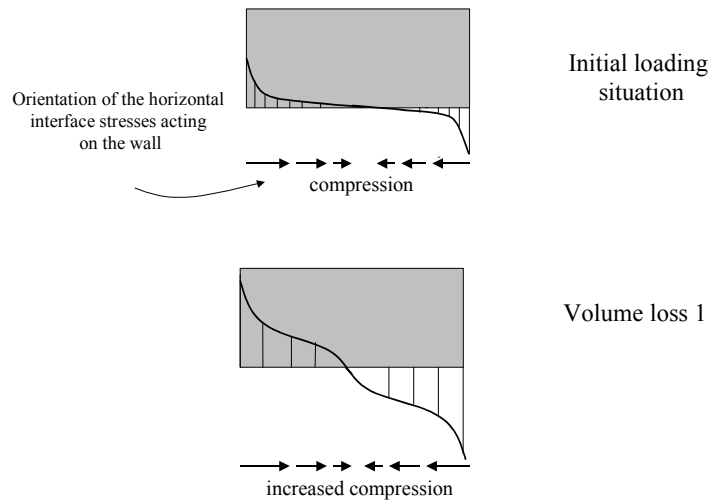
Figure 5.76: Horizontal interface stresses for the rough interface for the initial situation and volume loss 1, sagging zone

For volume loss 2 the development of the vertical and horizontal interface stresses for the rough case is explained schematically in Figure 5.77. Volume loss 2 shows very slight cracking accompanied by a significant decrease of the vertical interface stresses at the centre of the wall. The wall is even completely unloaded over a length of ca. 4m at the centre of the wall. Due to this vertical unloading the horizontal interface stresses are consequently reduced to zero in this part. Figure 5.77 shows the schematic development of vertical and horizontal interfaces stresses for volume loss 2 and the rough interface.
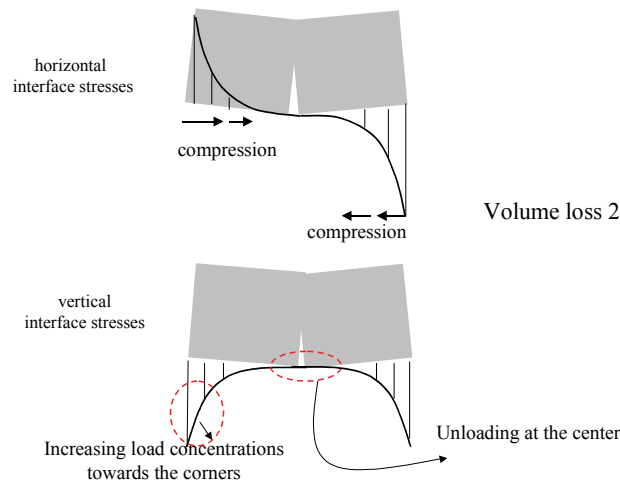
Figure 5.77: Schematic development of interface stresses for the rough case and volume loss 2, sagging zone

For volume loss 3 the development of the vertical and horizontal interface stresses for the rough case is explained schematically in Figure 5.78. Very severe cracking occurs for this case. The redistribution of

the vertical interface stresses shows the same effects as for the very severe cracking of the smooth case described previously. The separation of the wall in two cracked parts leads to a reloading of the vertical interface stresses at the centre of the wall compared to the unloading at volume loss 2. The two separated wall parts show vertical load concentrations at all corners, comparable to the load concentrations which occur in the initial loading situation for the uncracked wall. The load concentrations at the outer corners are however still more developed than at the inner corners at both sides of the crack.
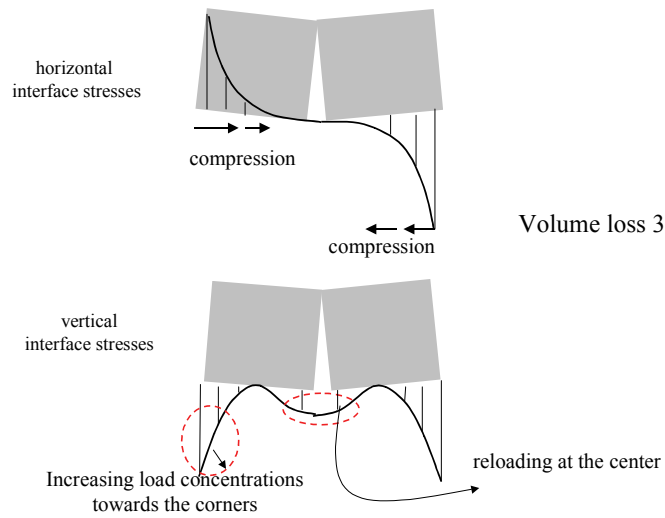
Figure 5.78: Schematic interface stresses for the rough case and volume loss 3, sagging zone

Figure 5.79 summarizes the damage results for all three volume losses and the smooth and the rough interface.
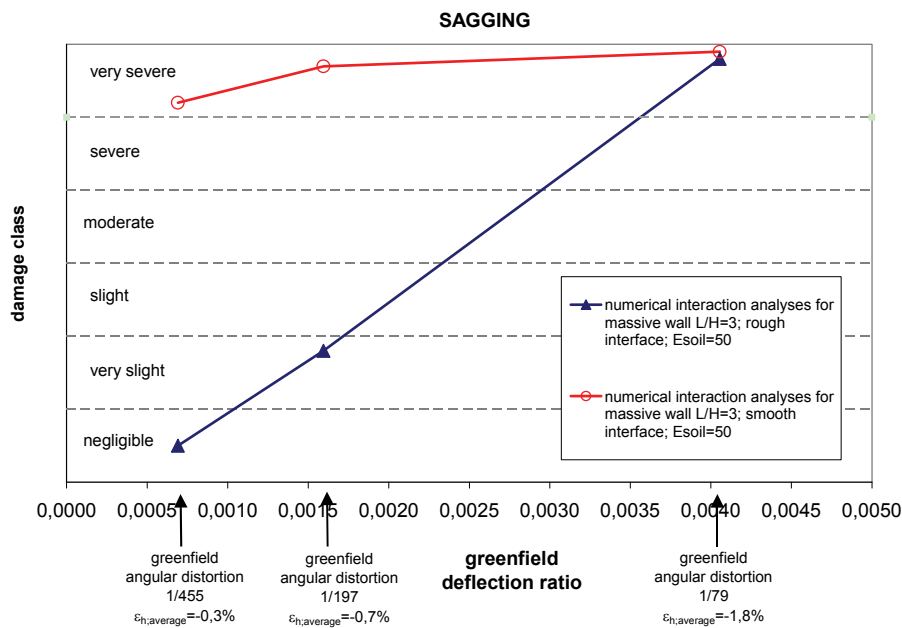
Figure 5.79: Damage classification for the smooth and the rough case for the sagging zone

Soil-Structure Interaction

The figure shows the significant difference in damage sensitivity for the rough and the smooth case. Due to the transfer of the differential horizontal ground movements in the sagging zone via the rough case, the bottom edge of the wall undergoes horizontal shear forces, which cause compressive strains at the bottom edge of the wall. These compressive strains have a beneficial effect on the damage as they reduce the horizontal bending tensile strains introduced by the bending sagging mode. As the transfer of this beneficial effect is neglected for the calculations with the smooth interface, the damage is significantly increased for the smooth calculations. For volume loss 1 and 2 the rough case is far less sensitive to damage than the smooth case. Once cracking is initiated the response is however strongly nonlinear and both cases show comparable damage. Both cases show severe damage for volume loss 3.

Figure 5.80 shows a comparison of the considered sagging cases with results from the LTSM .
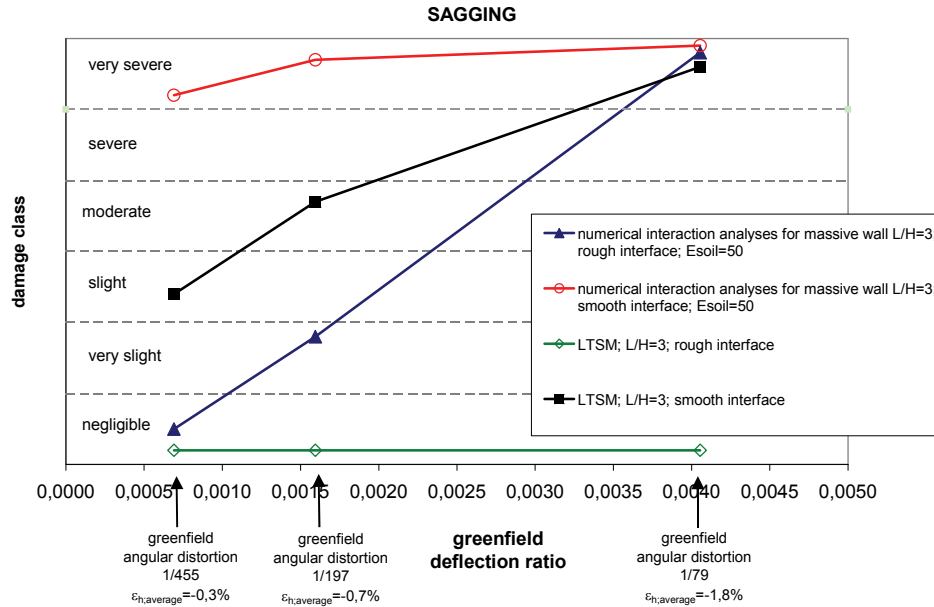
Figure 5.80: Comparison damage for the smooth and the rough case and the LTSM, sagging zone

The LTSM damage predictions for the **rough case** underestimate the damage compared to the numerical interaction analyses. The LTSM does thus not provide a damage result which is at the safe side. The damage for volume loss 3 is significantly underestimated by the LTSM, as the soil-structure interaction calculation reveals more damage due to the appearance of cracking and nonlinear behaviour. A theoretically full transfer of the beneficial horizontal ground movements in the sagging case can considered to be unrealistic and unsafe for the LTSM damage prediction. To obtain a conservative damage prediction with the LTSM it is therefore recommended to neglect the beneficial horizontal, ground movements in the sagging zone. In other words LTSM sagging predictions are recommended to be carried out by neglecting the effect of beneficial horizontal compressive strains in the wall, which can be introduced in a tunnelling sagging zone by the differential horizontal ground displacements.

The LTSM damage prediction for the **smooth case** underestimates the damage compared to the numerical interaction analyses. The result is damage class slight (for the LTSM) versus very severe (for the numerical interaction analyses) for volume loss 1 and moderate versus very severe for volume loss 2. As soon as cracking is introduced in the wall in the numerical interaction analyses, the development of damage can progress more rapidly than according to the predictions with the LTSM.

The smooth LTSM case can thus still provide an unsafe underestimation of the damage compared to the results of the smooth interaction analyses. A clear smooth case is however not a realistic situation for

engineering practice. A certain degree of transfer of horizontal shear stresses via the interface between soil and building will always occur and the nonlinear interface properties in the numerical rough cases are considered to model a realistic degree of transfer of horizontal differential ground movements to the building.

It is therefore recommended to follow the above suggested LTSM approach (neglecting horizontal compression transferred to the building due to differential horizontal ground movements) for tunnelling induced sagging cases. For practical engineering this approach is considered to provide a reasonable damage prediction compared to the numerical interaction results.

5.2.3.2   Influence of soil stiffness

The influence of different soil stiffness is considered separately for the rough cases and the smooth cases. The comparison of the results is presented for the lower and the upper bound value of the soil stiffness, E_{soil}=10MPa and E_{soil}=100MPa. The case for E_{soil}=50MPa has already been presented in the previous section.

The influence of the soil stiffness for the **smooth cases** is presented first in the following figures.

Figure 5.81 shows the results for volume loss 1.

Volume loss 1	E_{soil} =10MPa, smooth	E_{soil} = 100MPa, smooth
crack pattern		
It is emphasized that the scale of the deformed mesh plot is not equal for both cases shown above		
differential horizontal displacements at bottom edges	+0,2mm (tension at boootom edge)	+26mm (tension at bottom edge)
vertical displacements at bottom edges	50.7mm	42.6mm
tilt	-	-
deflection	0,2mm	18,3mm
tensile strain	max. strain 0.0068% average tensile strain bottom edge 0.001%	max. strain 1.3% average tensile strain bottom edge 0.13%
cumulative crack width	0.2mm	26mm
damage class	negligible/very slight	severe/very severe

Figure 5.81: Influence of soil stiffness for smooth case and volume loss 1, sagging zone

The smooth case with the stiff soil is far more sensitive to damage than with the soft soil. Volume loss 1 already shows major differences (negligible/very slight for the soft soil versus severe/very severe for the stiff soil). Cracking is just initiated for the case with E_{soil}=10MPa whereas for the E_{soil}=100MPa case severe vertical cracking is developed over the entire depth of the wall. The larger differences between

the stiffness of the soil and the wall for the soft soil causes more beneficial soil-structure interaction effects introducing less stress and strain concentrations in the building.

Figure 5.82 shows the results for volume loss 2.
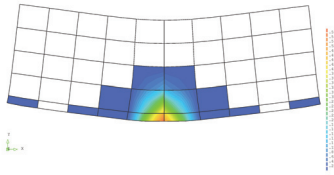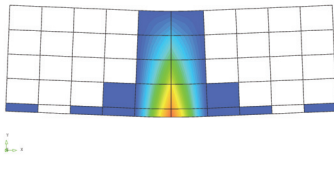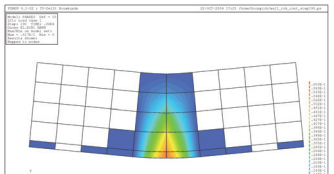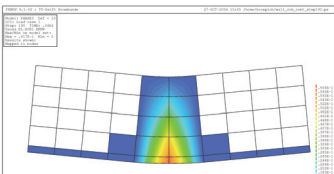
Volume loss 2	E_{soil} =10MPa, smooth	E_{soil} = 100MPa, smooth
crack pattern		
It is emphasized that the scale of the deformed mesh plot is not equal for both cases shown above		
differential horizontal displacements at bottom edges	+1mm (tension at bottom edge)	+54mm (tension at bottom edge)
vertical displacements at bottom edges	117mm	101mm
tilt	-	-
deflection	1mm	36mm
tensile strains	max. strain 0.057% average tensile strain bottom edge 0.0055%	max strain 2.6% average tensile strain bottom edge 0.0055%
cumulative crack width	1mm	54mm
damage class	very slight/slight	very severe

Figure 5.82: Influence of soil stiffness for smooth case and volume loss 2, sagging zone

The damage pattern still shows major differences between the soft soil and the stiff soil. The case for the stiff soil undergoes far more damage than the case for the soft soil.

Figure 5.83 shows the results for volume loss 3.

Volume loss 3	E_{soil} =10MPa, smooth	E_{soil} = 100MPa, smooth
crack pattern		
It is emphasized that the scale of the deformed mesh plot is not equal for both cases shown above		
differential horizontal displacements bottom edges	+186mm	+128mm

vertical displacements at bottom edges	238mm	258mm
tilt	-	-
deflection	132mm	86mm
tensile strain	max. strain 6.7% average tensile strain bottom edge 0.93%	max. strain 6% average tensile strain bottom edge 0.64%
cumulative crack width	186mm	128mm
damage class	very severe	very severe

Figure 5.83: Influence of soil stiffness for smooth case and volume loss 3, sagging zone

The calculations for volume loss 3 show very severe damage for the soft as well as the stiff soil. Both walls are very severe cracked due to the distortions introduced for volume loss 3. No difference in damage class between the soft and the stiff soil is recognized anymore for volume loss 3.

The vertical interface stresses for the initial situation and all three volume losses are shown in Figure 5.84.
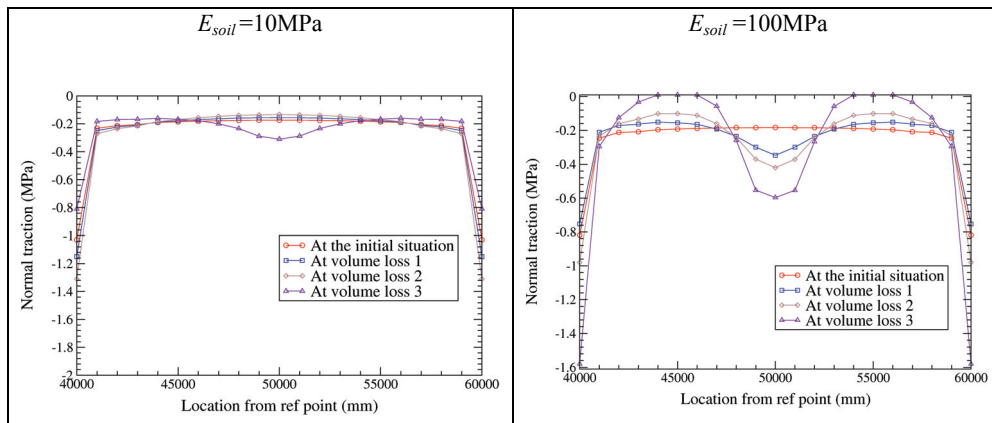
Figure 5.84: Vertical interface stresses for the smooth case and the upper and lower bound of the soil stiffness, sagging zone

The differences in redistribution of the vertical interface stresses shows the differences of the degree of interaction for both cases. Less redistribution of the vertical interface stresses means also less changes of stresses and strains in the building compared to the initial loading situation and thus less damage risks. The E_{soil} =10MPa shows very minor redistributions in the interface stresses for volume loss 1 and 2 corresponding with small damage in the wall. However, the redistribution for the stiff soil E_{soil} =100MPa is significant, which is typical for the sagging mode (see also the interpretation of the interface stresses in the previous section for E_{soil} =50MPa). The stiff case with E_{soil} =100MPa shows for volume loss 3 even a full unloading in the centre part of the two separated wall parts.

Figure 5.85 shows the damage classification for the smooth case and the sagging zone for the different soil stiffness. The case for the medium soil stiffness E_{soil} =50MPa, described in the previous section, is also included in the chart.
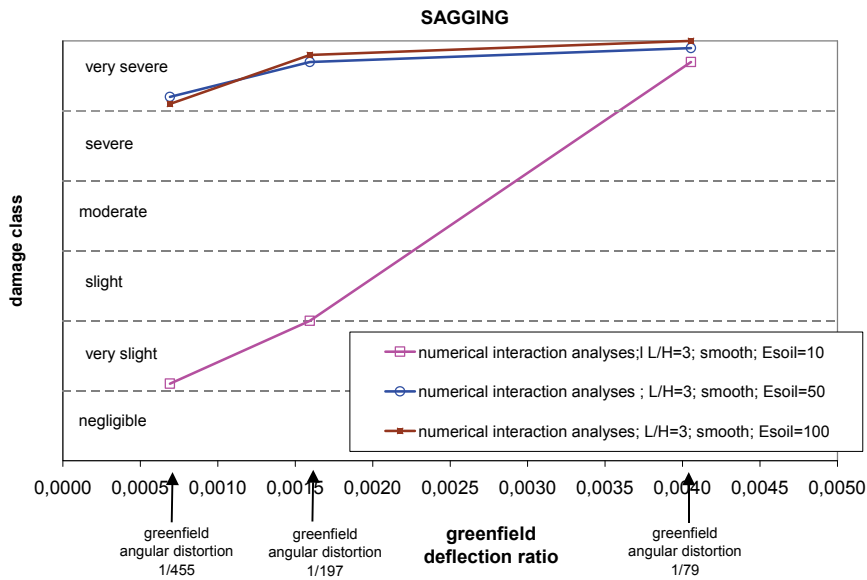
Figure 5.85: Damage classification for the different soil stiffness and the smooth cases, sagging zone

Figure 5.85 shows the significant differences in damage for the lower bound of the soil stiffness and the upper bound. As described previously the lower soil stiffness causes more beneficial soil-structure interaction effects introducing less stress and strain concentrations in the building and consequently reduces the damage significantly compared to the stiffer soil. It is also noted that the damage results for E_{soil}=50MPa and E_{soil}=100MPa are almost the same. Figure 5.86 shows the comparison between the LTSM predictions and the results of the advanced numerical interaction analyses.
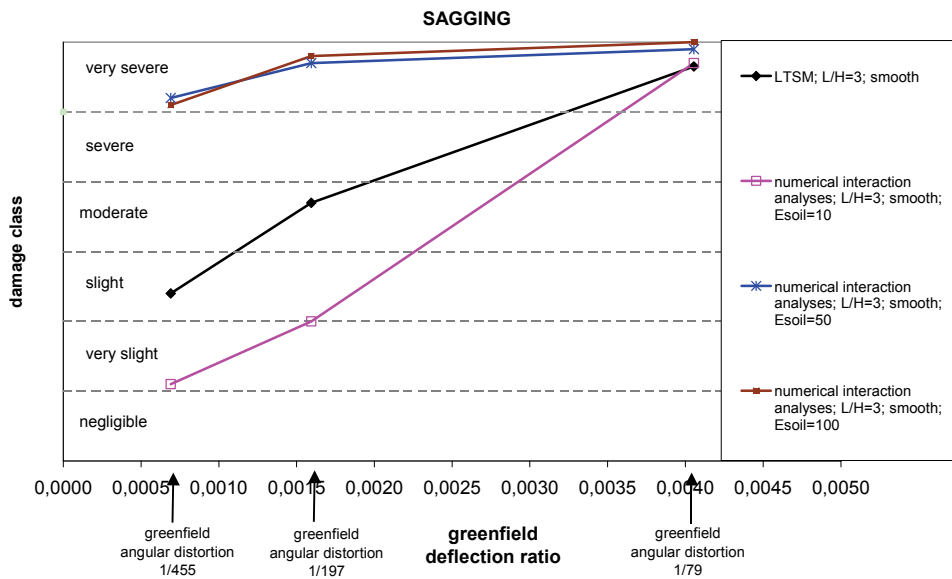
Figure 5.86: Comparison of LTSM and numerical results for the smooth case and different soil stiffness

Soil-Structure Interaction

The LTSM provides a conservative damage prediction only for the numerical case for the lower bound of the soil stiffness with E_{soil}=10MPa. The LTSM approach underestimates the damage compared to the numerical results for E_{soil}=50MPa and E_{soil}=100MPa.

The influence of the soil stiffness for the **rough cases** is presented in the following figures.
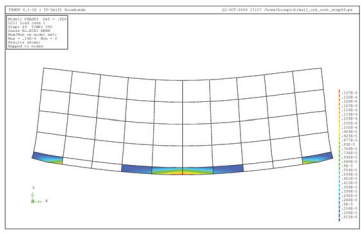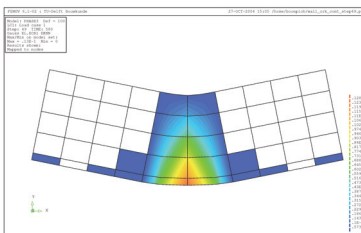Figure 5.87 shows the results for volume loss 1.
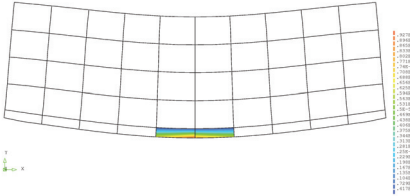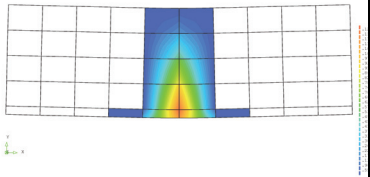
Volume loss 1	E_{soil} =10MPa, rough	E_{soil} = 100MPa, rough
crack pattern	no cracking	
differential horizontal displacements at top/bottom edges	-0.28mm at bottom edge (compression) +0.1mm at top edge (tension)	+0,36mm (tension at bottom edge)
vertical displacements at bottom edges	55mm	50mm
tilt	-	-
deflection	0.05mm (hog)	1.1mm (sag)
tensile strains	max. strain 0.0017% average tensile strain at top edge 0.0005%	max. strain 0.058% average strain bottom edge 0.0018%
cumulative crack width	-	0.36mm
damage class	negligible	very slight

Figure 5.87: Damage results for the sagging zone, the rough case and different soil stiffness for volume loss 1, sagging zone

The results for volume loss 1 and the rough interface show only very small differences in the damage between the lower bound and the upper bound of the soil stiffness. The beneficial effect due to the transfer of differential horizontal ground movements to the wall dominates both cases. However cracking is initiated for E_{soil} =100MPa whereas the wall for the E_{soil} =10 case still remains uncracked for volume loss 1. Thus with increasing soil stiffness the damage is also increased, although the differences in the resulting damage classes are still small for volume loss 1 (negligible versus very slight).
Figure 5.88 shows the results for volume loss 2.

Volume loss 2	E_{soil} =10MPa, rough	E_{soil} = 100MPa, rough
crack pattern	-	
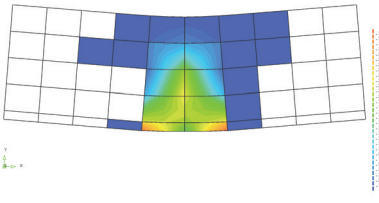
differential horizontal displacements at top/bottom edges	-0.36mm at bottom edge (compression) +0.06mm at top edge (tension)	+28mm at bottom edge (tension) -2.6mm at top edge (slight compression)
vertical displacements at bottom edges	115mm	107mm
tilt	-	-
deflection	0.1mm (hog)	22mm (sag)
tensile strains	max.strain 0.002% average strain at top edge 0.0003%	max. strain 1.25% average strain at bottom edge 0.14%
cumulative crack width	-	28mm
damage class	negligible	very severe

Figure 5.88: Damage results for the sagging zone, the rough case and different soil stiffness for volume loss 2, sagging zone

The results for volume loss 2 show significant differences in the resulting damage. The case for E_{soil}=100MPa shows very severe damage whereas the E_{soil}=10MPa case still remains uncracked. The beneficial interaction effect for the low soil stiffness is obviously confirmed.

Figure 5.89 shows the results for volume loss 3.

Volume loss 3	E_{soil} =10MPa, rough	E_{soil} = 100MPa, rough
crack pattern	-	
differential horizontal displacements at top/bottom edges	+0.014mm at bottom edge (tension)	+98mm tension at bottom edge -6mm at top edge (compression)
vertical displacements at bottom edges	295mm	264mm
tilt	-	-
deflection	0,5mm (sag)	69mm (sag)
tensile strains	max. strain 0.0032% average strain at bottom edge 0.00007%	max strain 3.4% average strain at bottom edge 0.49%

cumulative crack width	-	98mm
damage class	negligible	very severe

Figure 5.89: Damage results for the sagging zone, the rough case and different soil stiffness for volume loss 3, sagging zone

The results for volume loss 3 show further increasing, significant differences in the resulting damage. The case for E_{soil}=10MPa remains still uncracked due to the combination of the beneficial effect of horizontal compressive strains introduced by the differential horizontal ground movements at the bottom edge of the wall and the beneficial effects of vertical interaction.

The results of the vertical and horizontal interface stresses for the rough case and all volume losses are given in Figure 5.90.
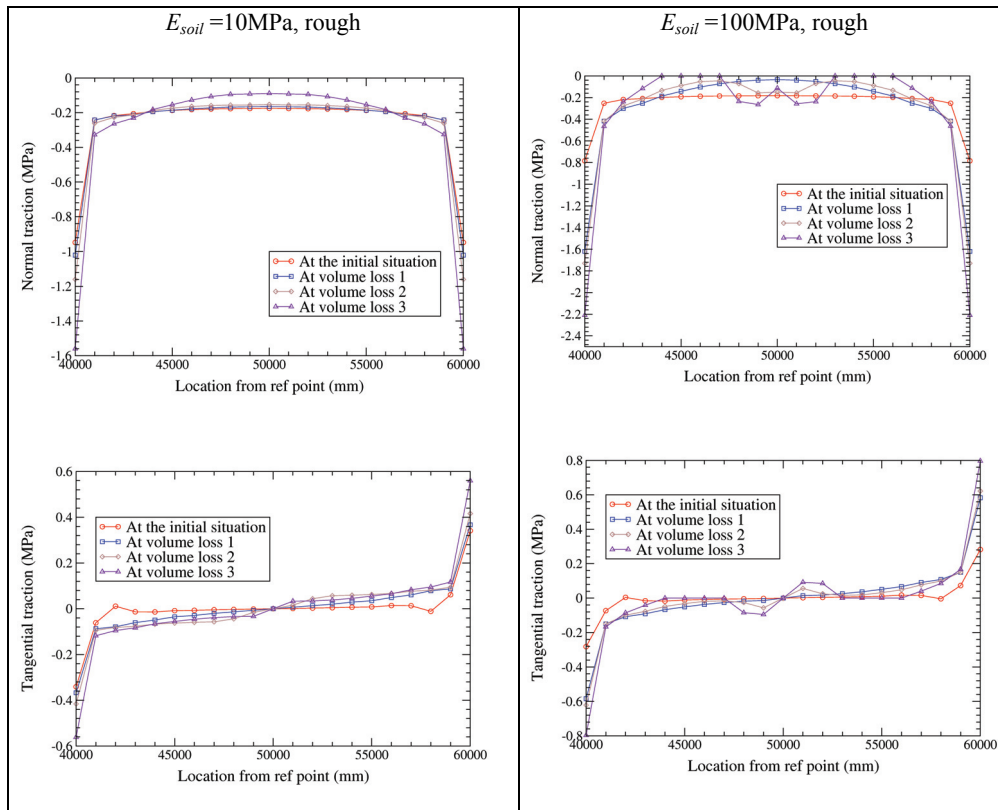
Figure 5.90: Vertical and horizontal interface stresses for the sagging case, the rough interface and different volume losses, sagging zone

The differences in redistribution of the vertical interface stresses show clearly the differences of the degree of interaction for both cases. Less redistribution of the vertical interface stresses means also less changes of stresses and strains in the building compared to the initial loading situation and thus less damage risks. The E_{soil}=10MPa shows very minor redistributions in the interface stresses for volume loss 1 and 2 corresponding with the small damage in the wall for these situations.

The stiff soil E_{soil}=100MPa shows clear redistributions for all volume losses leading to stress and strain redistributions in the wall and consequently to the significant damage patterns. The results for volume loss 3 even show a full unloading in the centre part of the two separated wall parts.

Soil-Structure Interaction

The horizontal *interface* stresses for the lower bound of the soil stiffness cause compression at the bottom edge of the wall. The horizontal interface stresses for this case remain almost the same for all three volume losses after mobilization at volume loss 1. The developments of the horizontal interface stresses for the upper bound of the soil stiffness show clear changes due to the cracking of the wall and the corresponding redistribution of the vertical interface stresses. For volume loss 3 the horizontal interface stresses are reduced to zero for the parts of the wall where the interface is vertically unloaded. This effect corresponds with the relation of horizontal and vertical interface stresses via the friction criteria of the interface.

The damage results for the rough case and all different soil stiffness are summarized in Figure 5.91.

Also the case for E_{soil} =50MPa, which is described in detail in the previous section, is included in the chart.
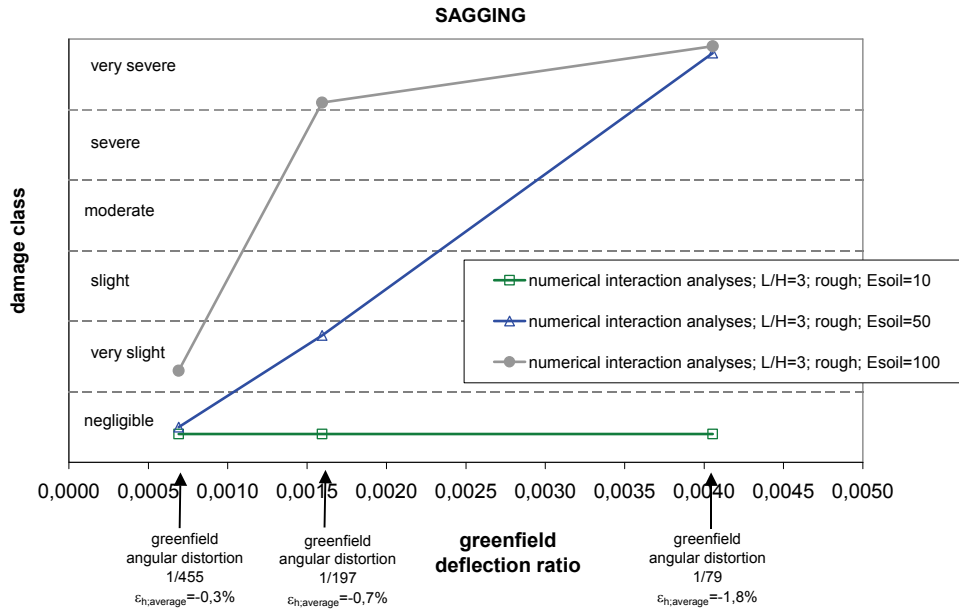
Figure 5.91: Damage classification for the sagging zone, different soil stiffness and the rough cases

Figure 5.91 shows the significant differences in damage sensitivity for the different soil stiffness. The damage increases significantly with increasing soil stiffness. As described previously the lower soil stiffness causes more beneficial soil-structure interaction effects introducing less stress and strain concentrations in the building and consequently reducing the damage significantly compared to the stiffer soil.

The comparison between the LTSM prediction and the numerical interaction results for the rough case and all soil stiffness is shown in the damage chart of Figure 5.92.

SAGGING
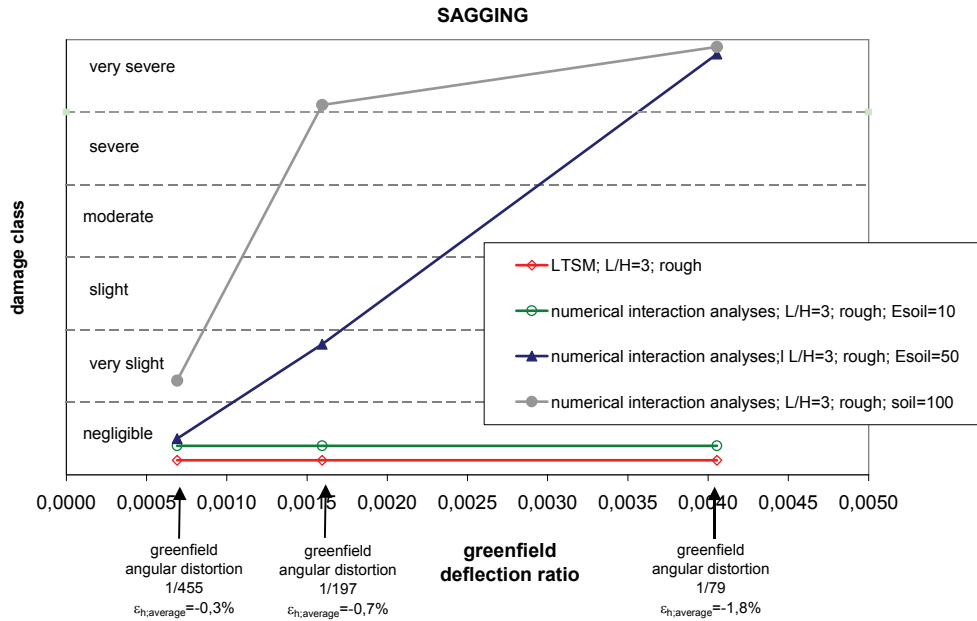
Figure 5.92: Comparison of LTSM with numerical interaction results for sagging zone, rough interface and different soil stiffness

The LTSM for the rough case where the full transfer of differential horizontal ground movements is taken into account underestimates the damage of the numerical rough cases significantly for E_{soil} =50MPa and E_{soil} =100MPa for the volume losses 2 and 3. The numerical cases with the low soil stiffness of E_{soil} =10MPa however provides the same negligible damage for all three volume losses as predicted with the LTSM.

5.2.3.3   *Influence of linear versus nonlinear masonry model*

The influence of the use of the linear and the nonlinear (smeared crack) masonry material model is analyzed for the sagging case with a building *L/H*-ratio of 3, the soil stiffness of E_{soil}=50MPa and the rough interface.

The damage chart in Figure 5.93 shows the summary of the damage results of the LTSM and the numerical calculations with the nonlinear and the linear masonry model for all three volume losses.
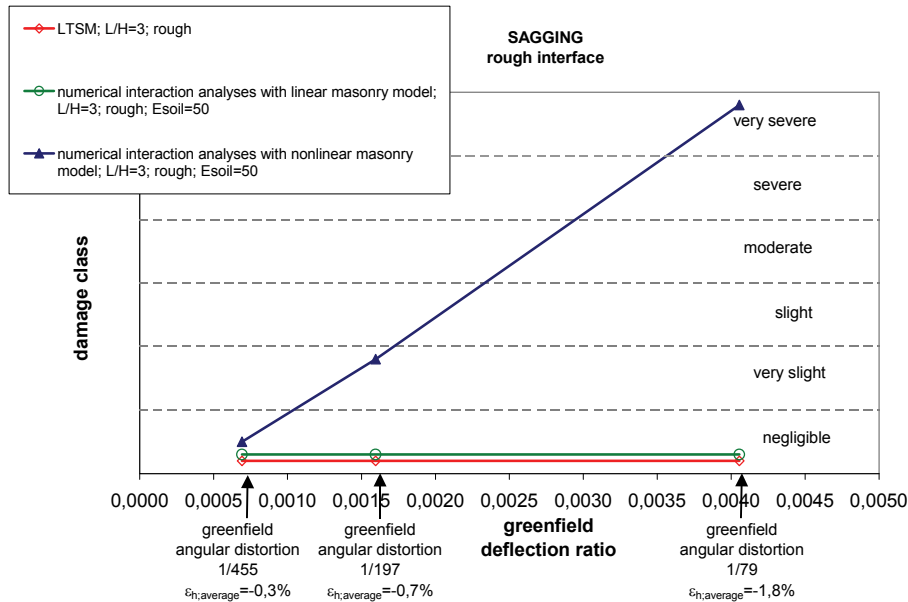
Figure 5.93: Damage classes nonlinear versus linear masonry model and LTSM for all volume losses

The results show that for volume loss 1 the nonlinear and the linear model show very small differences in the resulting damage classes. However, for volume loss 2 and 3 cracking occurs for the nonlinear analyses and the damage is elevated correspondingly. The linear analyses does not include cracking and continues to predict negligible damage. This leads to a significant different behaviour of the wall between both models. The linear model cannot take into account the reduction of bending stiffness of the wall due to cracking and all its nonlinear consequences on the soil-structure interaction.

The LTSM provides the same damage results as the numerical interaction analyses for the linear masonry model, underestimating the advanced numerical interaction calculation with the nonlinear masonry model for the rough case. As concluded previously a full transfer of the differential horizontal ground movements to the building in a tunnelling sagging zone is not a safe and appropriate approach for the LTSM.

5.2.3.4   Influence of L/H- ratio

In order to analyse the influence of the *L/H*-ratio of the building, the calculations of the building of the same length (20m) and two different heights are investigated for the sagging case with rough and smooth interface and E_{soil} =50MPa. The two considered building heights are 6.5m and 20m, leading to a *L/H*-ratio of 3 and 1 respectively.

It is noted that the initial vertical loadings on both walls are also increased with increasing height of the wall. This causes higher vertical bedding stresses and consequently an increased potential for confinement pressures which are transferred via the interface for the rough cases. The interface stresses of the deep and the slender wall are presented later in this section for the interpretation of the results.

First the results for the **smooth interface** and the two different *L/H*-ratio's case are presented.

It is noted, that the initial load situation for the deep wall with *L/H*-ratio of 1 and the smooth interface shows already minor, negligible cracking at the bottom corners. This cracking is caused by a local load concentration effect due to the slightly inclined compression diagonal directed towards the bottom corners of the wall. This effect was already visualized previously in Figure 5.54. Due to the smooth interface, a horizontal restraint cannot be activated at the bottom edge. The two cracks at the bottom

corners show a width of ca. 0.1mm in the initial stage, before the volume losses due to tunnelling are introduced.

The results for volume loss 1 and the smooth interface are shown in Figure 5.55.
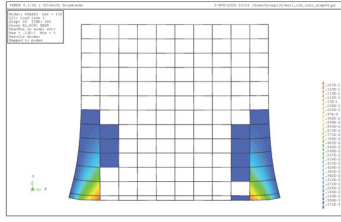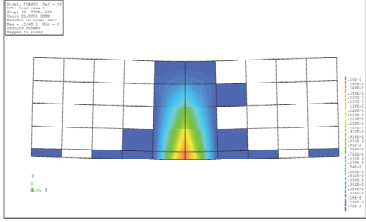
Volume loss 1	*L/H*=1, E_{soil} =50MPa smooth interface	*L/H*=3, E_{soil}=50MPa smooth interface
crack pattern		
differential horizontal displacements at bottom/top edges	+26.8mm (tension at the bottom edge)	+32.6mm (tension at the bottom edge) -0.5mm (very small compression at the top edge)
vertical displacements at bottom edges	48.5mm	40mm
deflection	2.9mm (sag)	23.6mm (sag)
tensile strains	average bottom edge 0.134% max. strains: 1.37% at edges 0.05% at bottom mid	max. strain 1.6% average strain bottom edge 0.163%
cumulative crack width	26mm (two cracks of 12mm and 14mm)	32mm
damage class	moderate/severe	very severe

Figure 5.94: Numerical results for different L/H-ratio's, smooth interface and volume loss 1, sagging zone

The difference between the damage of both cases is moderate/severe versus very severe. The deep wall with the *L/H*-ratio of 1 is less susceptible to damage. It is noted the cracking at the *L/H*=1 wall occurs at the locations of the initial cracks around the bottom corners. The cracking is slightly inclined according to the orientation of the principal strains. No vertical bending cracks are initiated at the bottom centre of the *L/H*=1 wall, which agrees with the expectation, that diagonal shear cracking becomes more dominant over flexural cracking with decreasing *L/H*-ratio. The wall with *L/H*-ratio of 3 shows typical flexural cracking initiated at the centre of the bottom edge of the wall.

The results for volume loss 2 and the smooth interface are shown in Figure 5.95.

.
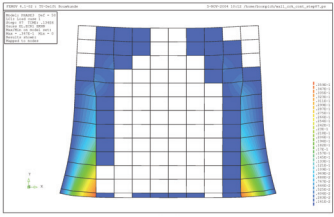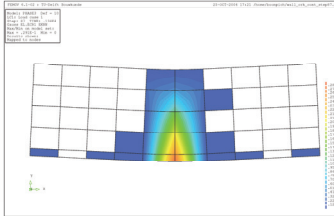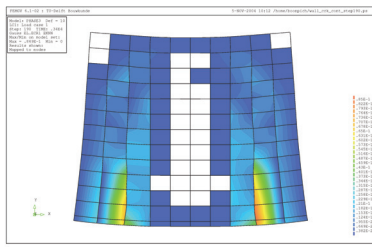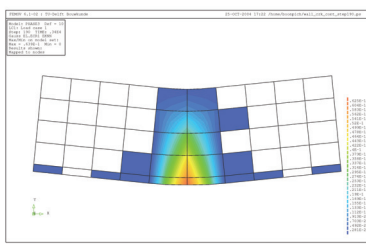
Volume loss 2	L/H=1, E_soil=50MPa smooth interface	L/H=3, E_soil=50MPa smooth interface
crack pattern		
differential horizontal displacements at bottom edges	+80mm (tension at bottom edge)	+58mm (tension at bottom edge) -1mm (very small compression at top edge)
vertical displacements at bottom edges	110mm	117mm
deflection	10mm (sag)	47mm (sag)
tensile strains	max. strain 4% average strain bottom edge 0.4%	max. strain 2.9% average strain bottom edge 0.293%
cumulative crack width	80mm (two cracks of 40mm)	58mm
damage class	very severe	very severe

Figure 5.95: Numerical results for different L/H-ratio's, smooth interface and volume loss 2, sagging zone

Both cases show very severe cracking for volume loss 2. Minor hairline cracking is initiated at the centre of the bottom edge of the L/H =1 wall. The dominant inclined cracking at the bottom edges has progressed further over the wall depth.
The results for volume loss 3 and the smooth interface are shown in Figure 5.96.

Volume loss 3	L/H=1, E_soil=50MPa smooth interface	L/H=3, E_soil=50MPa smooth interface
crack pattern		
differential horizontal displacements at bottom edges	+ 320mm (tension at bottom edge)	+120mm (tension) -1.6mm (compression at top edge)

vertical displacements at bottom edges	262mm	256mm
Deflection	57mm (sag)	92mm (sag)
tensile strains	max. strain 8.8% average strain bottom edge 1.6%	max. strain 6.4% average strain bottom edge 0.65%
cumulative crack width	320mm	120mm
damage class	very severe	very severe

Figure 5.96: Numerical results for different *L/H*-ratio's, smooth interface and volume loss 3, sagging zone

Both cases show very severe damage. The dominant damage pattern is still different for both cases. For the deep structure with *L/H*-ratio of 1 the inclined cracking around the bottom corners is dominant. The wall with *L/H* of 3 is dominated clearly by the flexural bending mode with vertical cracking at the centre of the wall.

Figure 5.97 shows the vertical interface stresses for both cases with smooth interface.
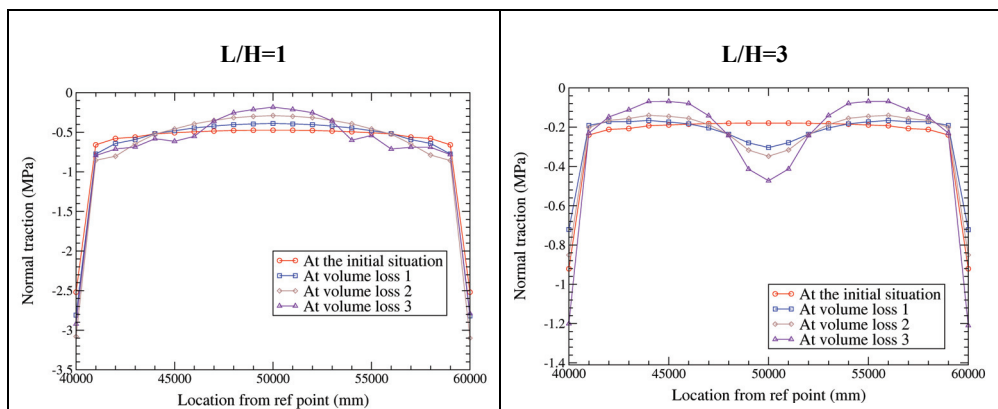
Figure 5.97: Vertical interface stresses for different *L/H*-ratios and smooth interface, sagging zone

The bending sagging mode for *L/H*=3 leads to vertical bending cracking at the centre of the wall, which separates the wall into two parts. For *L/H*=3 the typical pattern of increasing vertical bedding stresses at the outer ends and decreasing bedding stresses at the centre of the separated wall parts can be recognized. This corresponds with the vertical fracture of the wall. In contrast the deep wall of *L/H*=1 does not show this typical sagging redistributions of the interface stresses. Only for volume loss 3 the *L/H*=1 wall shows characteristics towards a decrease of the vertical bedding stresses at the centre of the wall.

The damage results for the walls are summarized in the damage chart of Figure 5.98.
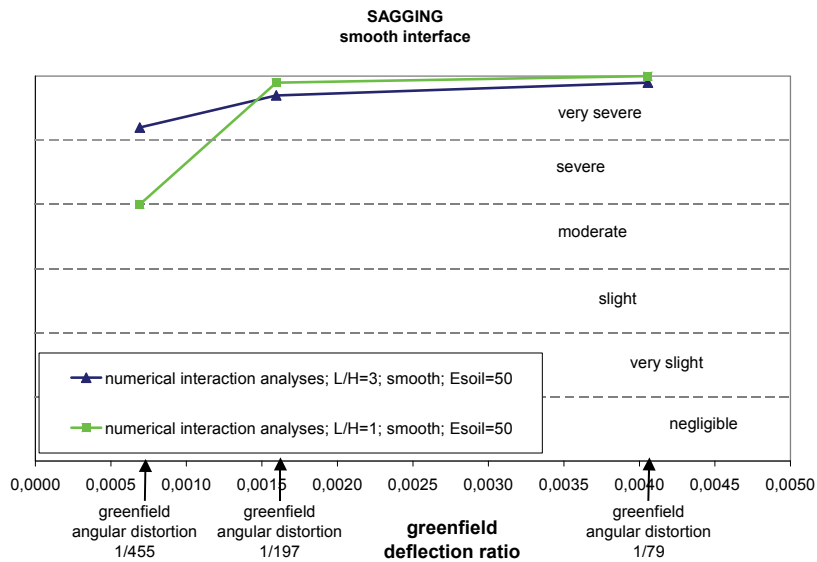
Figure 5.98: Damage chart of numerical results for both *L/H*-ratio's, sagging zone and smooth interface

Volume loss 1 shows a small difference between the damages of both cases. The deep wall with *L/H*=1 is less sensitive to damage than the slender wall with *L/H*=3. However, after cracking is initiated, volume loss 1 and volume loss 2 cause very severe damage for both walls. It is emphasized, that the initial cracking for the tall wall dominates the damage pattern because all further cracking is concentrating at these pre-cracked locations.

The comparison of the numerical results with the LTSM is shown in Figure 5.99.

Figure 5.99: Comparison of LTSM and numerical results for both *L/H*-ratio's, sagging zone and smooth interface

Soil-Structure Interaction

The damage for both cases is underestimated with the LTSM. It should be noted that the numerical damage of the *L/H*=1 wall is however dominated by the initial local hairline cracking at the outer ends of the wall. It is expected that the damage for the deep wall could be less without initial cracking. It is also noted that the LTSM results in the same damage classes for both *L/H*-ratio's for all three volume losses, independent of the fact that the diagonal cracks are the dominant factor for the damage of the *L/H*=1 wall and bending cracking is dominant for *L/H*=3.

The results for volume loss 1 and the **rough** interface are shown in Figure 5.100.

Volume loss 1	*L/H*=1, E_{soil}=50MPa rough interface	*L/H*=3, E_{soil}=50MPa rough interface
crack pattern	no cracking	no cracking
differential horizontal displacements at bottom edges	+0.12mm (tension at top edge) -1.6mm (compression at bottom edge)	-0.16mm (compression at bottom edge) -0.4mm (compression at top edge)
vertical displacements at bottom edges	49mm	50mm
deflection	0.2mm (hog)	0.4mm (sag)
tensile strains	average strain top edge 0.0003% max. strain at bottom edge due to local load concentrations 0.0047%	max. strain 0.0021% average compressive strain bottom edge almost nihil
damage class	negligible	negligible

Figure 5.100: Damage results for sagging zone both *L/H*-ratio's and the rough interface, sagging zone

Both walls show negligible damage due to the beneficial effect of the differential horizontal soil movements in the sagging zone. As they cause horizontal compressive strains at the bottom edge the induced bending and/or diagonal tensile strains due to the differential vertical settlements are overruled. The *L/H*=1 even shows a slight hogging mode, because of the eccentricity effect of the mobilisation of the horizontal compressive stresses at the bottom edge of the wall. It is emphasized that the absolute magnitude of the induced horizontal interface stresses is larger for the deep wall with *L/H*=1 than for the slender wall with *L/H*=3, because the vertical interface stresses are also significantly larger due to the increased loading of the building (dead weight and floor loads).

The results for volume loss 2 and the **rough** interface are shown in Figure 5.101.

Volume loss 2	*L/H*=1, E_{soil}=50MPa rough interface	*L/H*=3, E_{soil}=50MPa rough interface
crack pattern	no cracking	
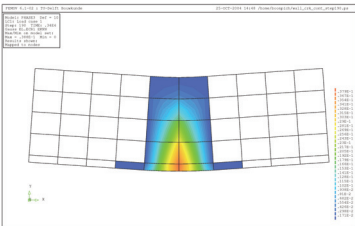
differential horizontal displacements at bottom edges	+0.04mm (tension at top egde) -0.6mm (compression at bottom edge)	+0.8mm (tension at bottom edge) -1mm (compression at top edge)
vertical displacements at bottom edges	116mm	116mm
deflection	0	2mm (sag)
tensile strains	average strain at top edge 0.0002% max. strain at bottom edge due to local load concentration 0.0057%	max. strain 0.041% average strain bottom edge 0.004%
cumulative crack width	-	0.8mm
damage class	negligible	very slight

Figure 5.101: Damage results for sagging zone, both L/H-ratio's and the rough interface, sagging zone

The wall with *L/H*=3 shows a little bit more damage than the wall with *L/H*=1. The *L/H*=1 wall remains uncracked due to the beneficial restraint caused by the effect of horizontal different ground movements in the sagging zone. However very slight bending cracking is just initiated at the bottom edge of the *L/H*=3 wall and the vertical sagging bending mode for the slender wall starts to overrule the beneficial restraint effect for volume loss 2.

The results for volume loss 3 and the **rough** interface are shown in Figure 5.102.

Volume loss 3	*L/H*=1, E_{soil}=50MPa rough interface	*L/H*=3, E_{soil}=50MPa rough interface
crack pattern	no cracking	
differential horizontal displacements at bottom edges	-0.2mm (compression at bottom edge) -0.06mm (compression at top edge)	+ 84mm (tension at bottom edge) -4mm (compression at top edge)
vertical displacements at bottom edges	295mm	269mm
deflection	2mm (sag)	62mm (sag)

tensile strains	the edges are in average both under compression: -0.001% max. strain due to local load concentrations at the bottom edges 0.0088%	max. strain 3.8% average strain bottom edge 0.42%
cumulative crack width		84mm
damage class	negligible	very severe

Figure 5.102: Damage results for sagging zone both *L/H*-ratio's and the rough interface

Volume loss 3 shows significant differences between the damage patterns of both *L/H*-ratio's. The slender wall with *L/H*=3 is very severely cracked and the deep wall still remains uncracked. The initiation of the vertical bending cracking at the mid section of the *L/H*=3 wall leads to a rapid increase of the damage for volume loss 3. For the *L/H*=1 wall the combination of the beneficial effect of vertical interaction, the high bending resistance of the wall and the confinement related horizontal compressive restraint still keep the wall uncracked.

The distribution of the vertical and the horizontal interface stresses for all three volume losses is shown in Figure 5.103.
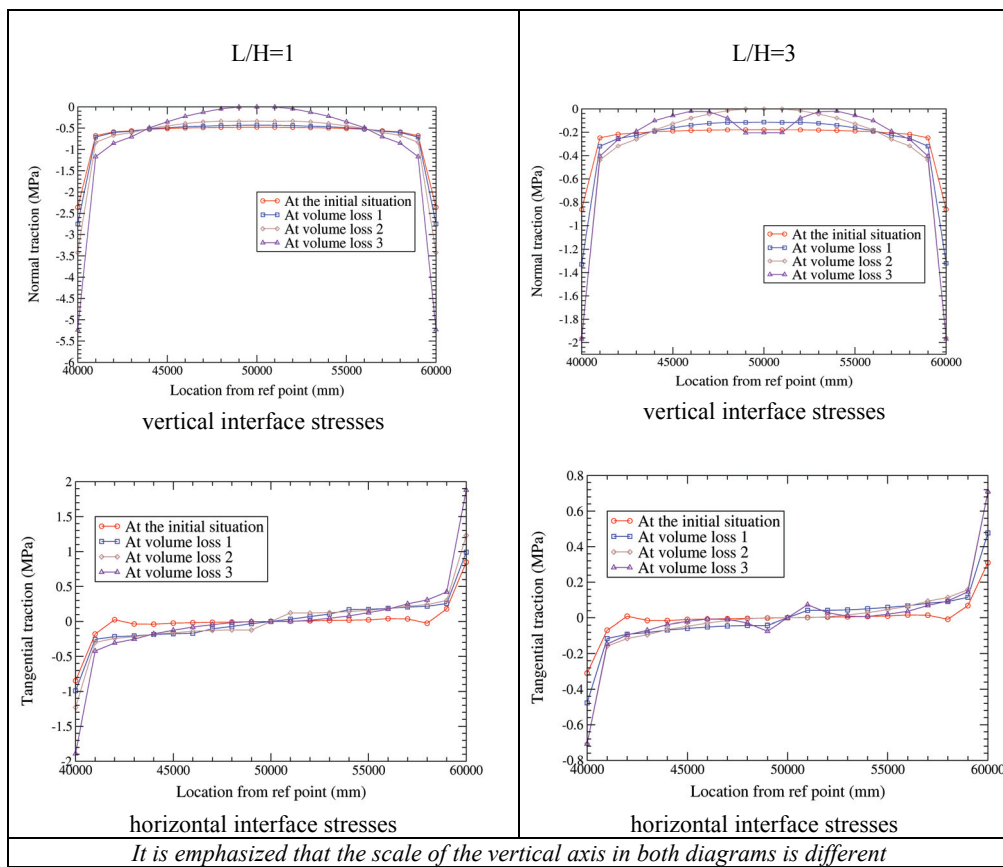
Figure 5.103: Vertical and horizontal interface stresses

The vertical interface stresses show clear differences between the *L/H*=1 wall and the *L/H*=3 wall. Volume loss 1 and 2 show only small redistribution of the vertical interface stresses for *L/H*=1 which is in line with the negligible damage for these situations. As a consequence also the beneficial compressive horizontal interface stresses for this case remain unchanged for volume loss 1 and 2.

The vertical bending cracking of the *L/H*=3 wall starts slightly at volume loss 2 corresponding with the redistributions of the vertical interface stresses, which show the typical sagging behaviour of both cracked wall parts.

Figure 5.103 also shows that the absolute magnitudes of the horizontal interface stresses are significantly higher for the *L/H*=1 wall than for the *L/H*=3 situation. This can be explained by the higher vertical loadings due to increased dead weight and floor loads for the deep wall. As the potential horizontal shear stresses depend on the confinement via Coulomb friction, the deep wall receives more compressive restraint at the bottom of the building. This loading effect would however not be expected if the *L/H*=3 variation would be modelled as a building with the same height as the *L/H*=1 building but a third of the length of the building. More research is therefore suggested for studying different configurations of *L/H*-values.
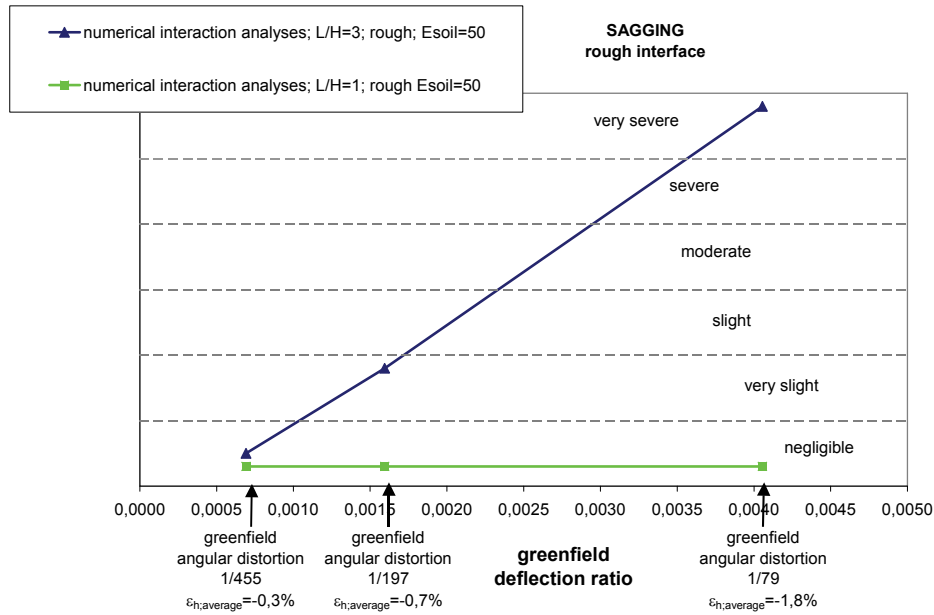
Figure 5.104: Damage chart of numerical results for both *L/H*-ratio's, sagging zone and rough interface

The slender *L/H*=3 wall shows significant more damage for volume loss 2 and 3. The beneficial horizontal compressive strains induced at the bottom edge are overruled by the bending sagging mode due to the vertical differential movements for *L/H*=3 and volume losses 2 and 3. In contrast, the *L/H*=1 building is not dominated by the bending behaviour due to its lower *L/H*-ratio, the increased bending capacity due to the increased wall height and the increased beneficial horizontal compressive strains at the bottom edge. These combination avoids the tall *L/H*=1 wall from cracking for the rough case in the sagging situation.

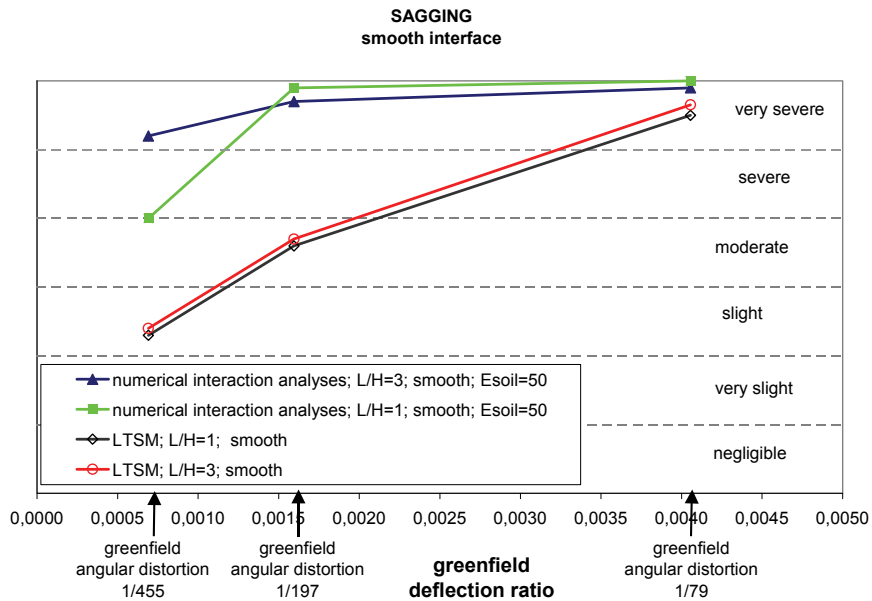Figure 5.105 summarizes the results in terms of a damage chart.
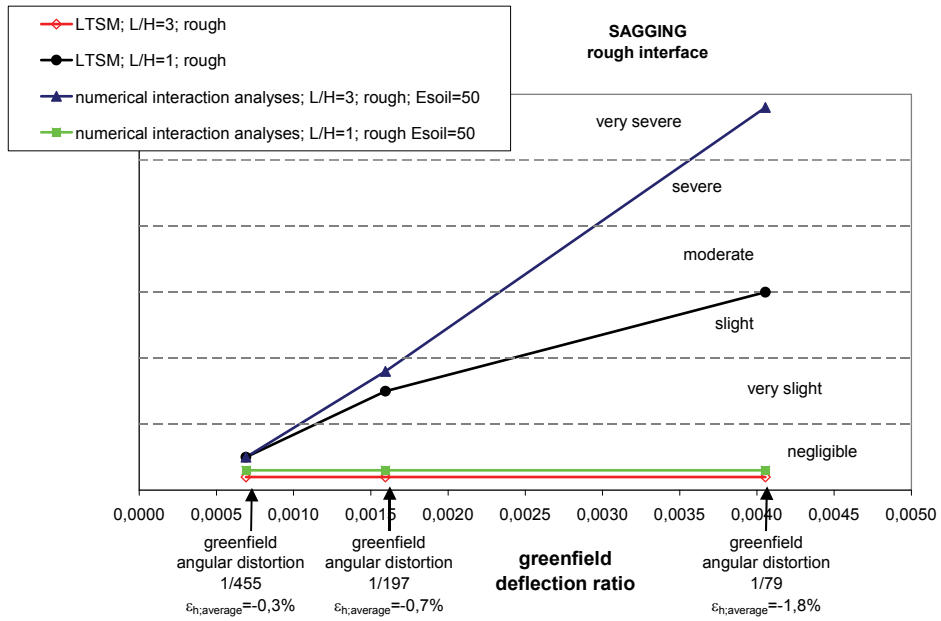
Figure 5.105: Comparison of LTSM and numerical results for both *L/H*-ratio's, sagging zone and smooth interface

The LTSM underestimates the damage of the numerical interaction analyses significantly, because the full transfer of the beneficial horizontal compressive strains is taken into account in the LTSM. As recommended in the previous section, the compression effect of the horizontal differential ground movements in the sagging zone should not be included in the LTSM, in order to circumvent unsafe results.

6 SOIL-STRUCTURE INTERACTION- MASONRY FAÇADE WALL

6.1 Response of the masonry façade wall due to initial loads

The initial principal strains in the façade wall due to the initial loads consisting of the dead weight and the floor line loads are shown in Figure 6.1 for the building geometry L/H=3 and E_{soil}=50MPa with the rough interface.

L/H=3; E_{soil}= 50MPa and rough interface

vectors principal strain ε_1
(max. tensile strain 0.0048%)

vectors principal strain ε_2
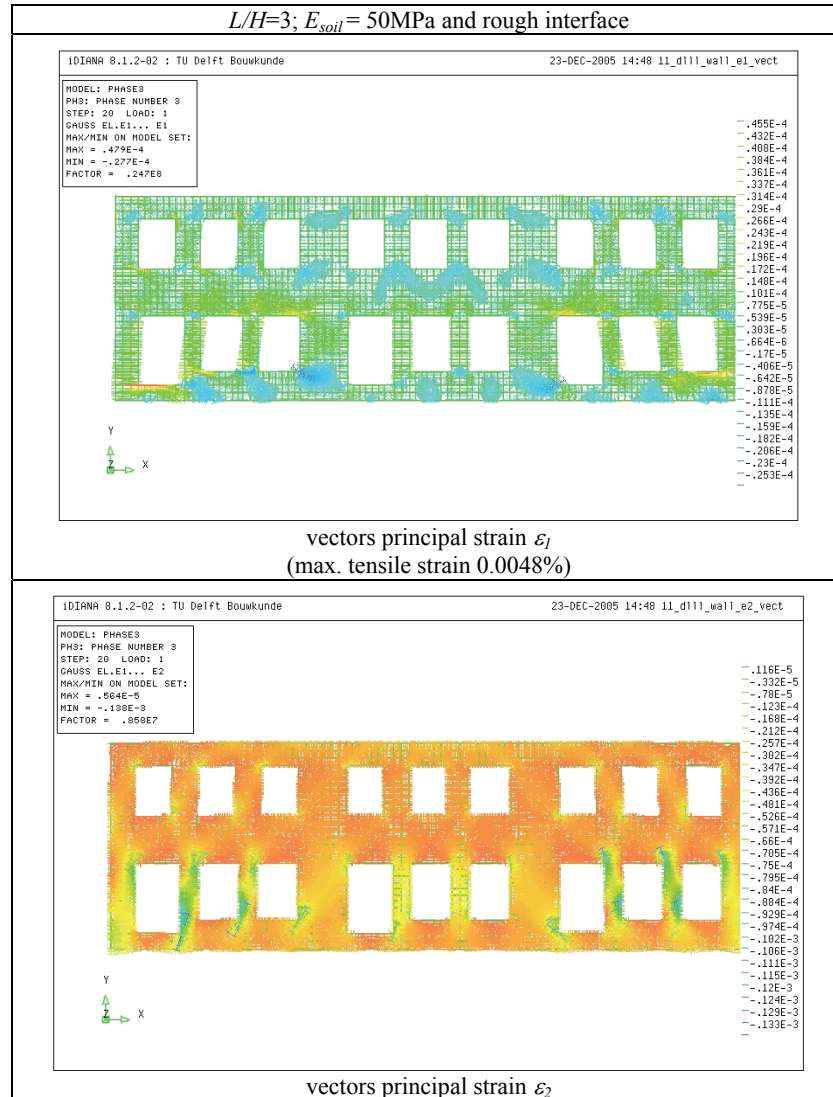
Figure 6.1: Initial principal strains in the façade wall and the rough interface

Soil-Structure Interaction

The façade walls shows strain concentrations around the openings. The maximum initial tensile strain for the rough interface and E_{soil}=50MPa occurs around the openings with 0.0048%. Assuming a smooth interface this value is only slightly higher with 0.0054%. The maximum tensile strains for the lower soil stiffness of E_{soil}=10MPa are 0.0063% and 0.0087% for the rough and the smooth interface respectively. As described already in section 5.1 for the initial situation of the massive walls, the initial loading situation causes increasing strains with decreasing soil stiffness. Initial hairline cracking around the openings occurs. The initiation of cracking starts when the limit of the tensile strength is reached (thus for the masonry properties used in this numerical calculations at approximately f_t/E=0.3/6000= 0.005%, depending on the principal stress situation in different directions). This explains the hairline cracking for the façade walls in the initial situation. The crack strains for E_{soil}=10MPa and the smooth interface are shown in Figure 6.2a. The crack strain contours for E_{soil}=50MPa and the smooth interface are shown in Figure 6.2b.
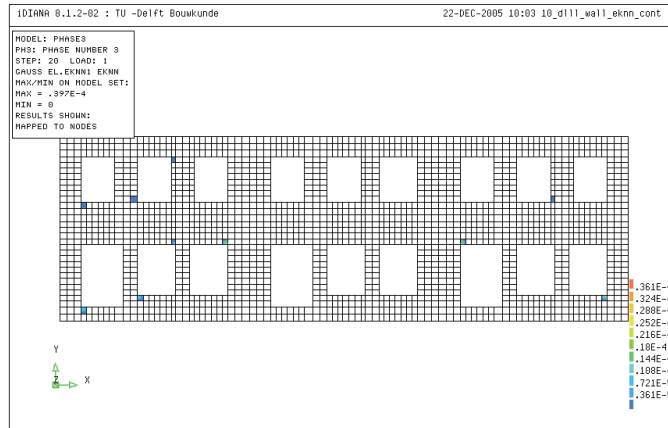
(a) initial crack strains for E_{soil}=10MPa and smooth interface
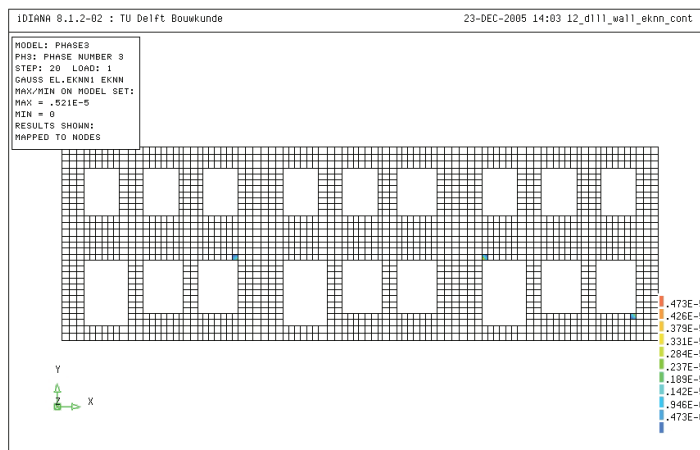
(b) initial crack strains for E_{soil}=50MPa and smooth interface

Figure 6.2: Contour plot initial hairline cracking around openings

The horizontal and vertical interface stresses in the initial load situation for the rough case are shown in Figure 6.3.
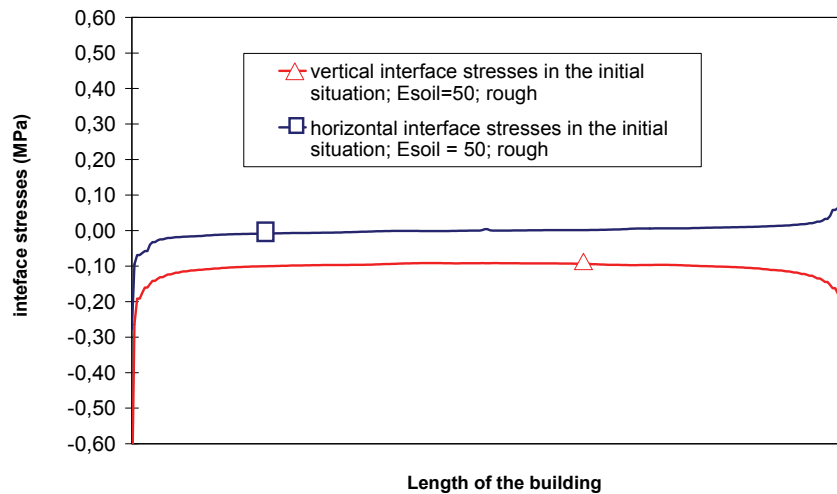
Figure 6.3: Vertical and horizontal interface stresses of the façade wall in the initial loading stage

The vertical interface stresses show the loading concentrations around the outer ends of the wall, which were also recognized for the massive wall (see Figure 5.1). The horizontal interface stresses consequently increase at the outer ends of the wall and cause a beneficial restraint at the bottom edge of the wall. It is however noted that the absolute magnitude of the vertical interface stresses is smaller than for the massive masonry wall due to the smaller floor loads on the wall and the reduced dead weight caused by the openings in the façade wall. Consequently also the mobilized horizontal interface stresses in the initial loading stage are also smaller for the façade wall than for the massive wall.

6.2 Response of the masonry facade wall due to tunnelling induced ground movements

6.2.1 Hogging

6.2.1.1 *Influence of smooth or rough interface*

The influence of the smooth and the rough interface for the hogging mode is analysed for *L/H*=3 and E_{soil}=50MPa. The results for volume loss 1 are shown in Figure 6.4.

Volume loss 1	*L/H*=3, E_{soil}=50MPa **Rough interface**	*L/H*=3, E_{soil}=50MPa **Smooth interface**
crack pattern		 hairline cracking of the initial load stage is not changed
differential horizontal displacements at top/bottom edges	+3.1mm (tension bottom edge) -0.4mm (compression top edge)	+0.23mm (tension top edge) -0.04mm (min. compression bottom edge)
differential vertical displacements at bottom corners	16.6mm	16.7mm
tilt	1 / 1204	1 / 1197
deflection	1.6mm (sag)	0.4mm (hog)
tensile strains	max. strain 2.5% bottom average 0.016%	max. strain 0.0027% top average 0.0012%
cumulative crack width	3.1mm (vertical crack under door opening)	-
damage class	slight	negligible

Figure 6.4: Numerical results for volume loss 1, *L/H*=3, hogging and rough versus smooth interface

The rough case is more sensitive to damage than the smooth case. This result can be explained by the transfer of horizontal strains from the soil to the building in the hogging situation for the rough case. The rough case shows slight vertical cracking under and above the door opening, which is situated near

the bottom-mid of the wall. The smooth case does not transfer any differential horizontal movements from the soil to the building and the beneficial soil-structure interaction effect on the vertical hogging mode deformations in volume loss 1 prevents the façade wall from cracking.

The results for volume loss 2 are shown in Figure 6.5.

Volume loss 2	*L/H*=3, E_{soil}=50MPa **Rough interface**	*L/H*=3, E_{soil}=50MPa **Smooth interface**
crack pattern		 hairline cracking of the initial load stage is not changed
differential horizontal displacements at top/bottom edge	+5.7mm (tension at bottom edge) +0.5mm (min. tension at top edge)	+0.46mm (tension at top edge) -0.2mm (compression at bottom edge)
differential vertical displacements at bottom corners	37.7mm	38.6mm
tilt	1 / 530	1 / 518
deflection	3.1mm (sag)	0.7mm (hog)
tensile strains	max. strain 6.9% bottom average 0.029%	max. strain 0.0037% top average 0.0025%
cumulative crack width	5.7mm	-
damage class	slight/moderate	negligible

Figure 6.5: Numerical results for volume loss 2, *L/H*=3, hogging and rough versus smooth interface

Volume loss 2 shows a further increase of the damage for the rough case. The cracking has developed over the entire depth of the façade wall. Due to the eccentric transfer of the horizontal strains at the bottom, the rough case still shows a sagging mode behaviour, despite the fact that the vertical greenfield ground deformations are hogging.
The smooth case still does not show cracking due to the beneficial interaction effect for only vertical deformations. A small hogging deflection is recognized.

The results for volume loss 3 are shown in Figure 6.6.

Volume loss 3	L/H=3, E_soil=50MPa **Rough interface**	L/H=3, E_soil=50MPa **Smooth interface**
crack pattern		
differential horizontal displacements at top/bottom edge	+11mm (tension bottom edge) +13mm (tension top edge)	+1mm (min. tension bottom edge) +18mm (tension top edge)
differential vertical displacements at bottom corners	96.3mm	98.2mm
tilt	1 / 208	1 / 203
deflection	5,1mm (hog)	13,1mm (hog)
tensile strains	max. strain 12.3% average bottom edge 0.055%	max. strain 13.1% average top edge 0.09%
cumulative crack width	13mm at top edge	18mm at top edge
damage class	moderate	Severe

Figure 6.6: Numerical results for volume loss 3, *L/H*=3, hogging and rough versus smooth interface

The increase of damage compared to volume loss 2 is significant for the smooth case. Severe damage has developed for volume loss 3, whereas volume loss 2 did not show any damage for the smooth case. A clear hogging mode has developed with initiation of cracking at the top edge of the wall. The strong increase of damage confirms the highly nonlinear reaction for volume loss 3. As soon as cracking is initiated for the smooth case a rapid increase of the damage can occur.

The rough case shows an increase of the damage compared to volume loss 2 with one damage class higher (from slight to moderate). It appears that the small sagging deflection of volume loss 2 is changed into a hogging mode deflection. The effect of the vertical displacements is dominating the effect of the horizontal strains for volume loss 3.

The interface stresses for all three volume losses and the rough and the smooth case are shown in Figure 6.7.
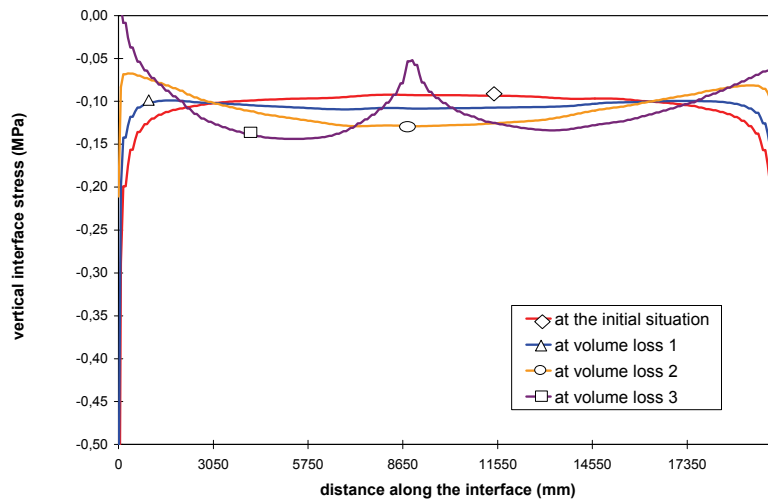
(a) vertical interface stresses for smooth interface
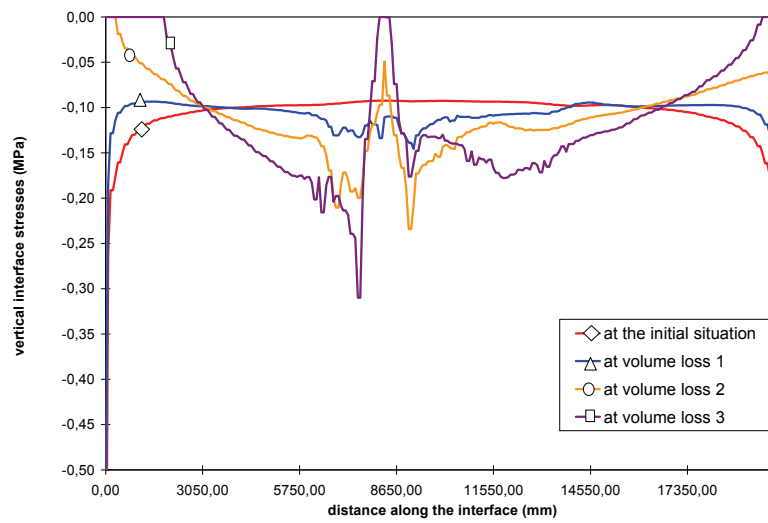
(b) vertical interface stresses for rough interface

(c) horizontal interface stresses for rough interface

Figure 6.7: Interface stresses for all volume losses, rough and smooth interfaces

The vertical interface stresses for the smooth case and volume loss 2 show a typical hogging mode behaviour with increasing interface stresses in the centre of the wall and decreasing stresses towards the edges of the wall. After cracking occurs at volume loss 3 for the smooth case, the vertical interface stresses show the same hogging mode distribution separately for each cracked wall part.

For volume loss 3 the redistribution of the vertical interface stresses in the rough case from the outer ends towards the mid of the building leads even to unloading and gapping between wall over a length of approximately 2m at the outer ends of the wall. Due to the vertical no-tension gap assumption of the interface model the horizontal interface stresses in these parts of the façade wall are also reduced to zero. The vertical interface stresses at the rest of the supporting length of the wall are consequently significantly increased as the sum of all vertical stresses has to be equal for vertical equilibrium.

The damage results of the smooth and the rough calculation are summarized in Figure 6.8.
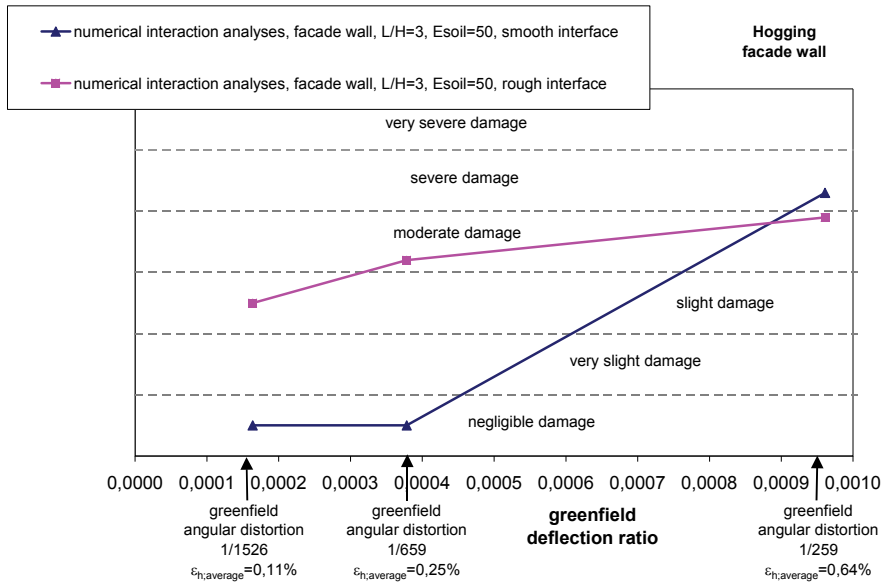
Figure 6.8: Damage results for the façade wall and the hogging case

Figure 6.8 shows the significant differences between the smooth and the rough case for volume loss 1 and 2. The rough case shows significant more damage than the smooth case, which is caused by the additional transfer of horizontal strains at the bottom for the rough case. Volume loss 3 shows moderate to severe cracking for both cases.

The comparison of the numerical results with the results of the LTSM is shown in Figure 6.9.
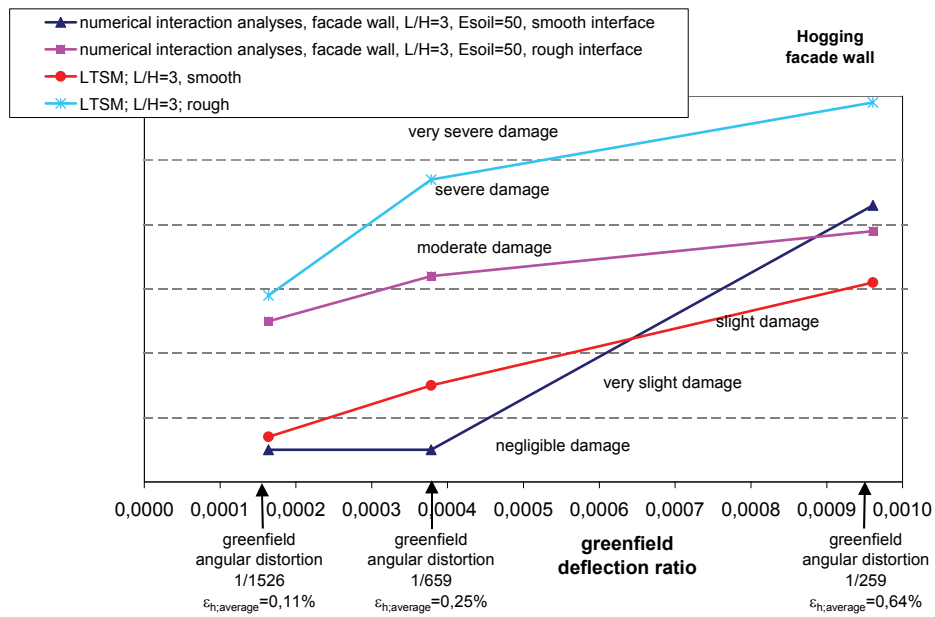
Figure 6.9: Comparisons of numerical results and the LTSM

Soil-Structure Interaction

The LTSM taking into account full transfer of horizontal strains provides a good agreement with the numerical damage prediction for the numerical rough case for volume loss 1 and gives a conservative prediction for volume loss 2 and volume loss 3. For the smooth case, the numerical calculations provide a reasonable agreement with the LTSM for all volume losses.

It can be concluded that for the façade wall in the hogging zone with an *L/H*-ratio of 3 and a soil stiffness of E_{soil}=50MPa, the LTSM prediction, taking into account the full transfer of differential horizontal ground movements, provides a safe upper bound of the damage.

6.2.1.2   Influence of the soil stiffness

This section considers the effect of different soil stiffness for the rough and the smooth cases. The case for E_{soil}=50MPa has been presented in the previous section. The results for the low soil stiffness of E_{soil}=10MPa are presented in this section. It is noted that the E_{soil}=100MPa case, which is also considered for the massive wall in section 5.2, is not included for the façade walls, because the difference between E_{soil}=10MPa and E_{soil}=50MPa appears to give clear insight in the effects of different soil stiffness.

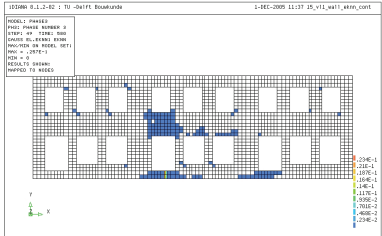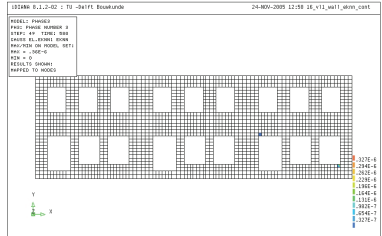The results for volume loss 1 are shown in Figure 6.10.
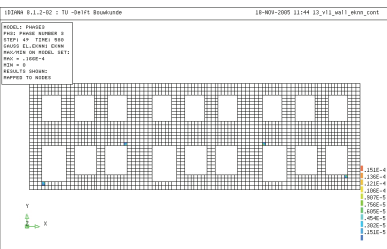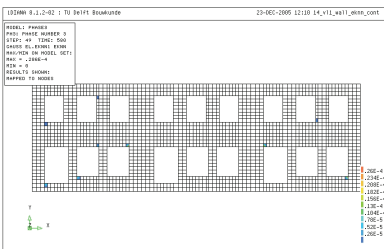
Volume loss 1	*L/H*=3, E_{soil}=10MPa **Rough interface**	*L/H*=3, E_{soil}=10MPa **Smooth interface**
crack pattern	 no changes compared to the initial loading stage	 no changes compared to the initial loading stage
differential horizontal displacements at bottom/top edge	+0.3mm (tension bottom edge) -0.1mm (compression at top edge)	-0.03mm (min. compression bottom edge) +0.06mm (min. tension top edge)
differential vertical displacements at bottom corners	16.7mm	16.7mm
tilt	1/1197	1/1197
deflection	0.05mm (sag)	0.25mm (hog)
tensile strains	max. tensile strain 0.0066% average tensile strain at bottom edge 0.0015%	max. tensile strain 0.0068% average tensile strain at top edge 0.0003%
cumulative crack width	-	-
damage class	negligible	negligible

Figure 6.10: Numerical results for volume loss 1, façade wall, E_{soil}=10MPa

Soil-Structure Interaction

Volume loss 1 shows negligible damage for both situations. The differential vertical displacements of the wall for the smooth case shows a small hogging deflection. The rough case however shows a small sagging deflection, caused by the eccentric effect of the transfer of horizontal shear stresses at the bottom. The beneficial interaction effects for the low soil stiffness prevent both walls from cracking for volume loss 1.

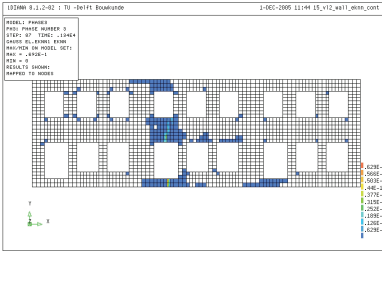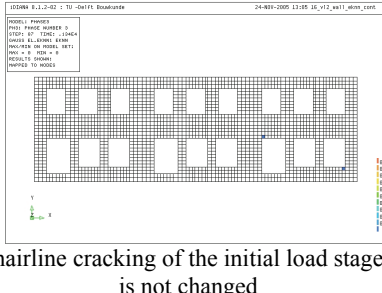The results for volume loss 2 are shown in Figure 6.11.
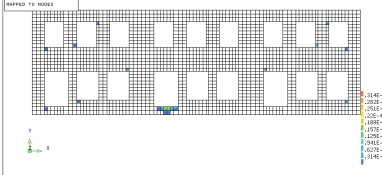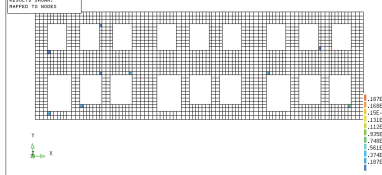
Volume loss 2	L/H=3, E_{soil}=10MPa **Rough interface**	L/H=3, E_{soil}=10MPa **Smooth interface**
crack pattern		 no changes compared to initial stage
differential horizontal displacements at bottom/top edge	+0.6mm (tension at bottom edge) -0.1mm (compression at bottom edge)	-0.1mm (compression bottom edge) +0.13mm (tension top edge)
differential vertical displacements at bottom corners	38.4mm	38.6mm
tilt	1/520	1/518
deflection	0.1mm (sag)	0.5mm (hog)
tensile strains	max. tensile strain 0.0084% average tensile strain bottom edge 0.003%	max. tensile strain 0.0055% average tensile strain top edge 0.00065%
cumulative crack width	vertical crack width bottom edge 0.6mm	-
damage class	very slight	negligible

Figure 6.11: Numerical results for volume loss 2, façade wall, E_{soil}=10MPa

Very slight cracking is initiated for the rough case caused by the increased transfer of horizontal strains at the bottom edge of the wall. The beneficial interaction effect for the soft soil on the vertical differential displacements of the façade wall avoids cracking for the smooth case and volume loss 2. The results for volume loss 3 are shown in Figure 6.12.
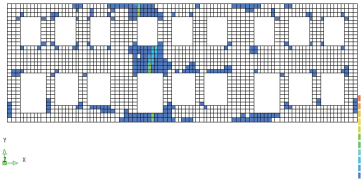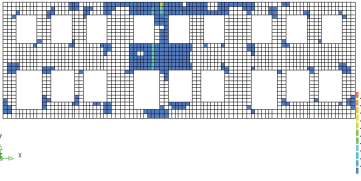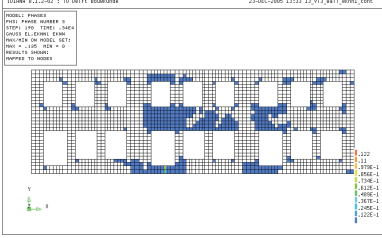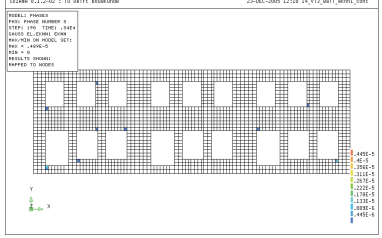
Volume loss 3	L/H=3, E_soil=10MPa **Rough interface**	L/H=3, E_soil=10MPa **Smooth interface**
crack pattern		
differential horizontal displacements at top/bottom edge	+20mm (tension at bottom edge)	-0.2mm (compression bottom edge) +0.3mm (tension top edge)
differential vertical displacements at bottom corners	98.3mm	97.5mm
tilt	1 / 204	1/205
Deflection	11mm (sag)	1.4mm (hog)
tensile strain	max. tensile strain 13.5% average tensile strain bottom edge 0.1%	max. tensile strain 0.0035% average tensile strain top edge 0.0015%
cumulative crack width	20mm	-
damage class	severe	Negligible

Figure 6.12: Numerical results for volume loss 3, façade wall, E_{soil}=10MPa

After the initiation of cracking in volume loss 2 for the rough case, the cracking increases rapidly for volume loss 3 over the entire depth of the building, for the rough case and the low soil stiffness. Severe cracking has developed. It is remarkable, that the rough case still undergoes an increasing sagging deflection. This effect shows, that for the soft soil with E_{soil}=10MPa, the beneficial interaction effect of the vertical movements is that strong, that horizontal transfer of ground movements is still the dominating factor for volume loss 3.

This beneficial interaction effect for the soft soil and the vertical differential displacements is also responsible for the uncracked situation for the smooth case.

The vertical and horizontal interface stresses are shown in Figure 6.8.

Soil-Structure Interaction
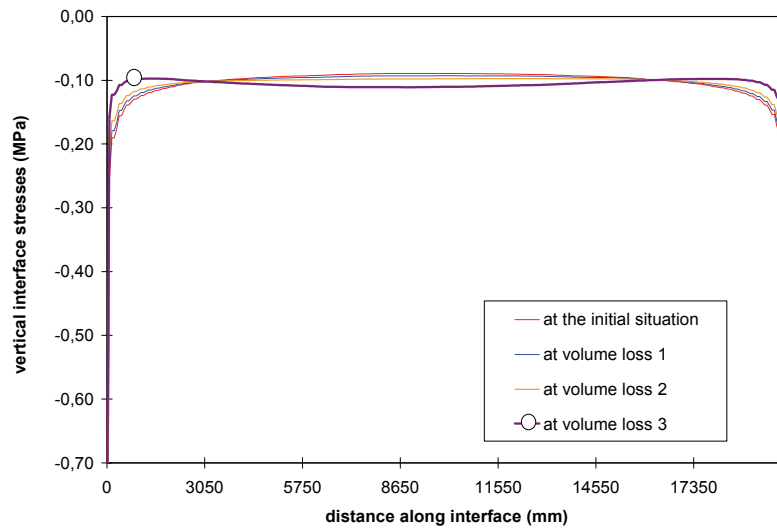
(a) vertical interface stresses for the smooth case
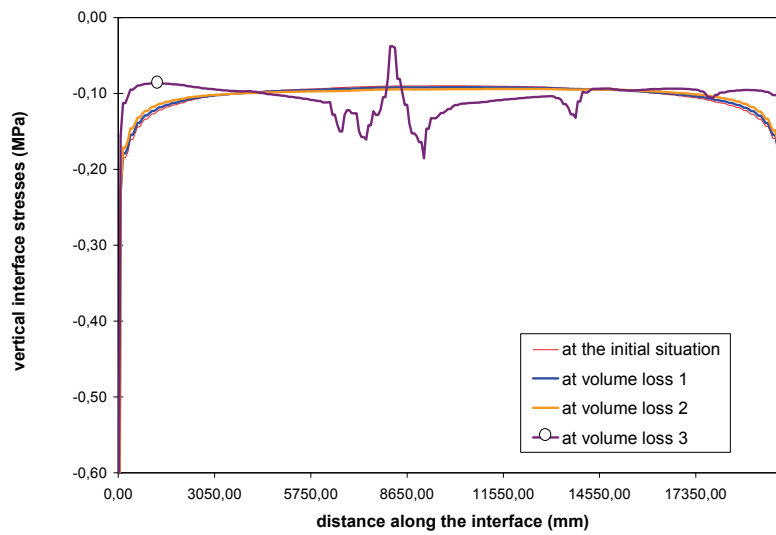
(b) vertical interface stresses for rough interface
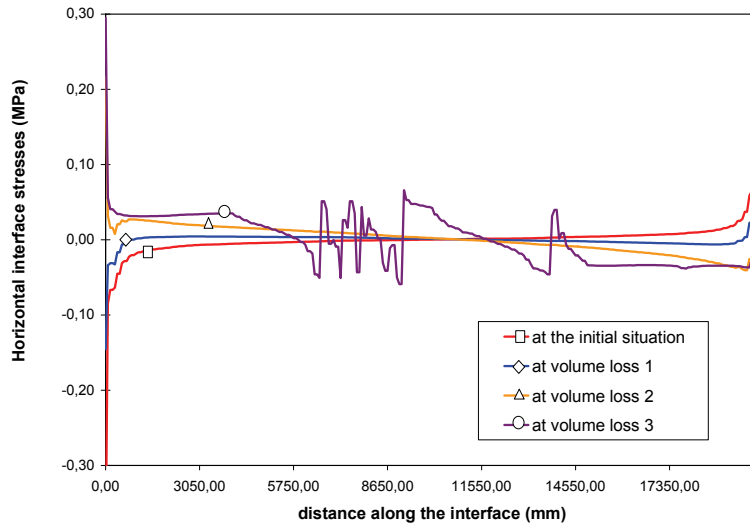
(c) horizontal interface stresses for rough interface
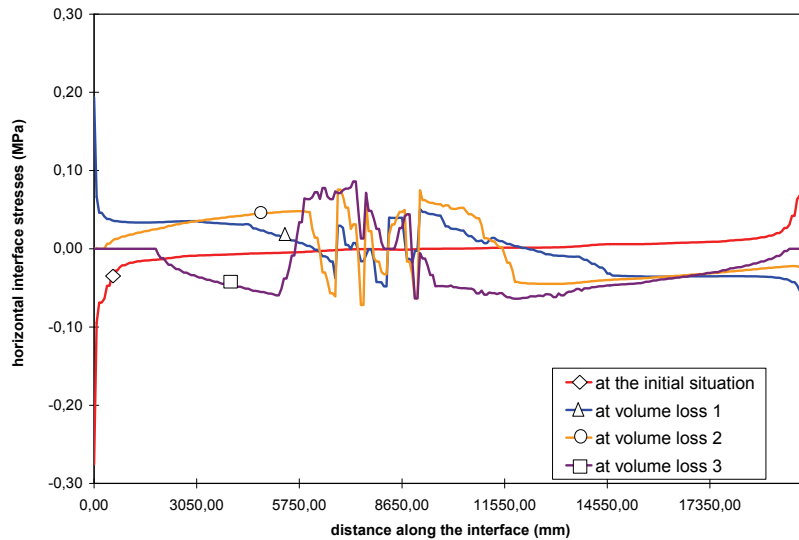
Figure 6.13: Vertical and horizontal interface stresses for all volume losses, façade wall, E_{soil}=10MPa

The vertical interface stresses show a negligible redistribution of the loads for volume loss 1 and 2 which is in agreement with the negligible/very slight cracking for the smooth and the rough case.
Volume loss 3 and the rough case however shows significant redistributions of interface stresses which corresponds with the severe cracking.
The damage results for the two different soil stiffness E_{soil}=50MPa (see previous section) and E_{soil}=10MPa are summarized for direct comparison in Figure 6.14.
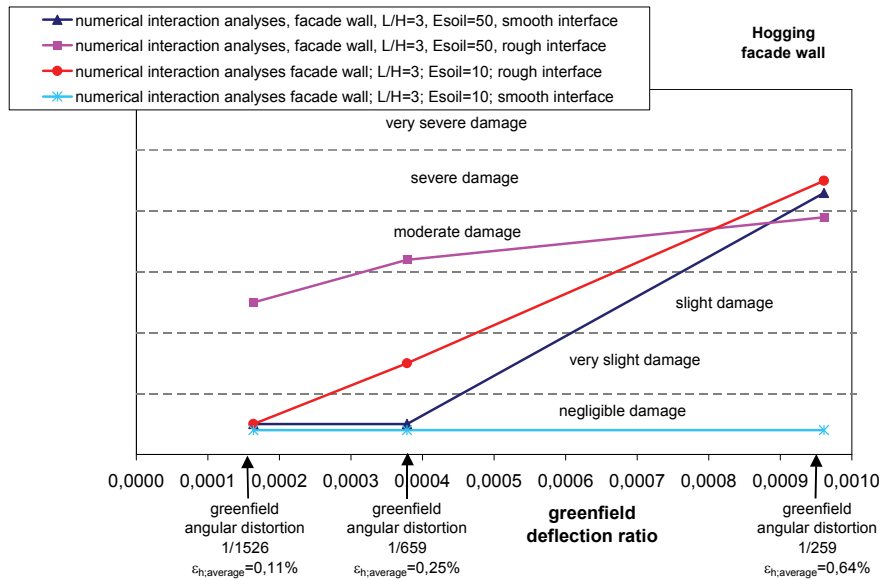
Figure 6.14: Comparison of the numerical results for the façade wall in the hogging zone and two different soil stiffness

For the rough cases and volume losses 1 and 2 the damage increases with increasing soil stiffness. For volume loss 3 however both soil stiffness show equal damage. For the smooth cases and volume losses 1 and 2, the façade remains uncracked for both soil stiffness. For volume loss 3, however, the damage increases significantly with increasing soil stiffness.

The comparison of the numerical results with the LTSM is shown in Figure 6.15.
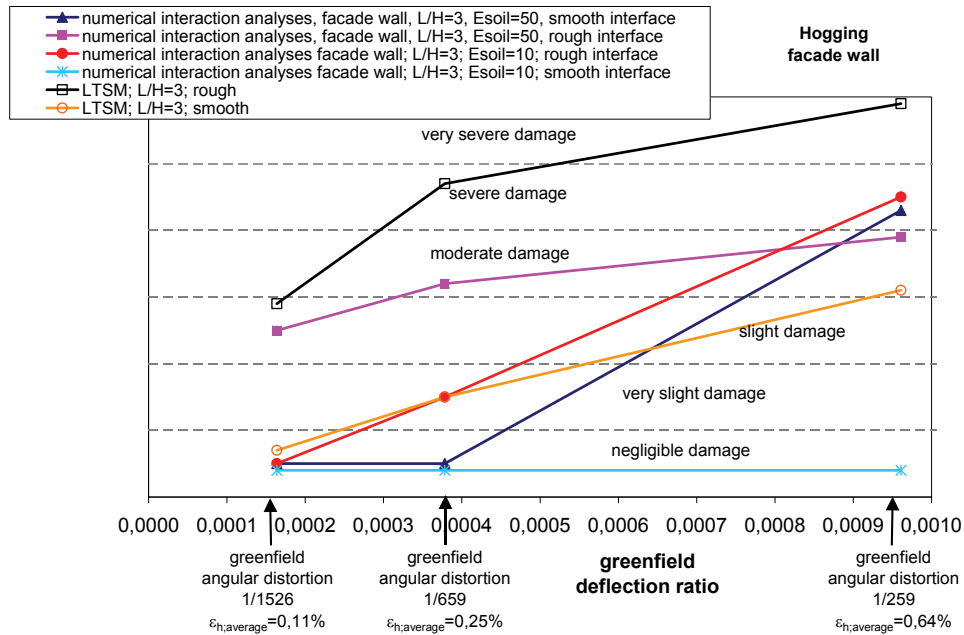
Figure 6.15: Comparison of numerical results and the LTSM for the façade wall in the hogging zone and two different soil stiffness

The LTSM including full transfer of the horizontal greenfield movements to the wall provides for the façade wall in the hogging zone a conservative damage prediction for both soil stiffness and all volume losses.

If the transfer of horizontal movements is neglected in the numerical calculations and the LTSM, the LTSM provides a conservative approach for all volume losses for the low soil stiffness of E_{soil}=10MPa and for volume loss 1 and 2 for the E_{soil}=50MPa case. Volume loss 3 for the smooth cases however shows an underestimation of the damage with the LTSM compared to the numerical calculations with the higher soil stiffness of E_{soil}=50MPa.

6.2.1.3   Influence of the interface friction properties

To study the influence of the degree of transfer of the horizontal differential ground movements to the building, the properties of the interface elements have been varied. The reference calculation with L/H=3, rough interface and E_{soil}=50MPa presented in 6.2.1.1 was carried out for interface properties with a friction angle of 20° corresponding with a friction coefficient tanφ of 0.36. The variation considers a friction angle of 35° corresponding with a higher friction coefficient of 0.7.

The results for volume loss 1 are presented for both interface properties in Figure 6.16.

Volume loss 1	Hogging ; L/H=3; E_{soil}=50MPa, rough **tan φ = 0,36**	Hogging ; L/H=3; E_{soil}=50MPa, rough **tan φ = 0,7**
crack pattern		
differential horizontal displacements at top/bottom edge	+3.1mm (tension bottom edge) -0.4mm (compression top edge)	+6.4mm (tension bottom edge) -0.3mm (compression top edge)
differential vertical displacements at bottom corners	16.6mm	16.8mm
tilt	1 / 1204	1/1190
deflection	1.6mm (sag)	2.6mm (sag)
tensile strains	max. strain 2.5% bottom average 0.016%	max. strain 3.7% bottom average 0.064%
cumulative crack width	3.1mm (vertical crack at bottom edge under door opening)	6.4mm vertical crack bottom edge
damage class	slight	moderate

Figure 6.16: Numerical results for volume loss and different interface properties

The vertical loading and thus the vertical confining stresses at the interface is the same for both cases. Consequently for a higher friction angle, a higher shear stress is transferred from soil to building. In the hogging zone this causes higher tensile strains and therefore more damage than the reference case.
The results for volume loss 2 are shown in Figure 6.17.

Volume loss 2	Hogging ; L/H=3; E_{soil}=50MPa, rough **tan φ = 0,36**	Hogging ; L/H=3; E_{soil}=50MPa, rough **tan φ = 0,7**
crack pattern		
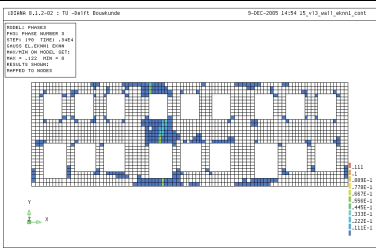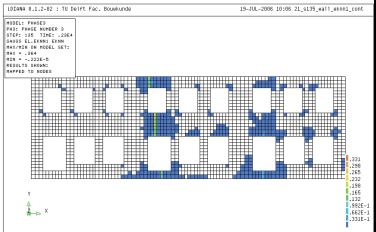
differential horizontal displacements at bottom/top edge	+5.7mm (tension at bottom edge)	+24mm (tension at bottom)
	+0.5mm (min. tension at top edge)	+17mm (tension at top)
differential vertical displacements at bottom corners	37.7mm	40.5mm
tilt	1 / 530	1 / 487
deflection	3.1mm (sag)	0.3mm (sag)
tensile strain	max. strain 6.9% bottom average 0.029%	max. strain 15.8 % bottom average 0.12 %
cumulative crack width	5.7mm	24mm
damage class	slight/moderate	severe

Figure 6.17: Numerical results for volume loss 2 and different interface properties

The results for volume loss 2 show a further increase of the difference in damage for both interface properties. The case with the higher friction coefficient causes significantly more damage than the reference case. The crack pattern for the higher friction coefficient shows cracking over the entire height at two cross sections of the wall.

The results for volume loss 3 are given in Figure 6.18.

Volume loss 3	Hogging ; L/H=3; E_{soil}=50MPa, rough **tan φ = 0,36**	Hogging ; L/H=3; E_{soil}=50MPa, rough **tan φ = 0,7**
crack pattern		*Only numerical feasible up to 68% of volume loss 3*
differential horizontal displacements at top/ bottom edges	+11mm (tension bottom edge)	+45mm (tension bottom edge)
	+13mm (tension top edge)	+41mm (tension top edge)
differential vertical displacements at bottom corners	96.3mm	69.8mm
tilt	1 / 208	1/286

deflection	5.1mm (hog)	4.2mm (hog)
tensile strains	max. strain 12.3% average bottom edge 0.055%	maximum tensile strain 36.5% average strain top edge 0.205% average strain bottom edge 0.225%
cumulative crack width	13mm at top edge	45mm at bottom edge
damage class	moderate	very severe

Figure 6.18: Numerical results for different friction coefficients for volume loss 3

The calculation for volume loss 3 has not been numerically stable for the case with the high friction coefficient. The damage is very severe and the wall is separated in three parts. The volume loss can only be increased up to 68% of the total volume loss 3. The calculation with the low friction coefficient shows only moderate damage for the full magnitude of volume loss 3. The vertical and horizontal interface stresses for the case with the high friction coefficient are shown in Figure 6.18.

vertical interface stresses for tan $\varphi = 0,7$

horizontal interface stresses for tan $\varphi = 0,7$
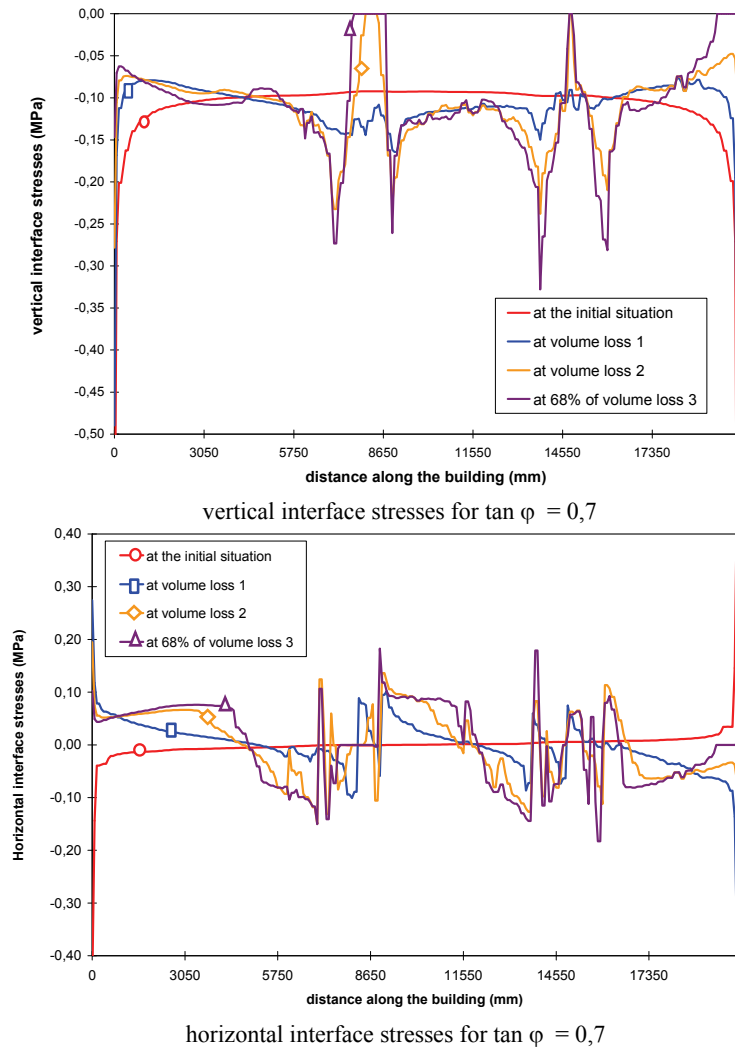
Figure 6.19: Interface stresses for high friction coefficient

Soil-Structure Interaction

Considering the horizontal and vertical interface stresses it is noticed that significant redistributions are introduced for all volume losses resulting in moderate to very severe cracking for all three volume losses. The fluctuations of the stress profiles indicate the positions of major cracks at the bottom. Here the shear tractions change sign at either side of the crack, while the vertical traction in some cases become zero due to local gapping at either side of a crack. The local tortuosity of the profiles is due to secondary cracking and due to possible local convergence problems as a result of bifurcations with softening models, see Rots et al. (1997).

The case with the higher friction coefficient activates higher horizontal interface stresses and thus higher tensile strains introduced at the bottom edge of the wall. An example of the relation of the vertical and the horizontal interface stresses is detailed shown for volume loss 2 in Figure 6.20. For a location of equal vertical interface stress (-0.09MPa), the activated horizontal stresses for both cases are highlighted. The relation between the horizontal and vertical interface stresses corresponds with the different friction coefficients, which confirms the correct behaviour of the interface Coulomb friction model for both cases.
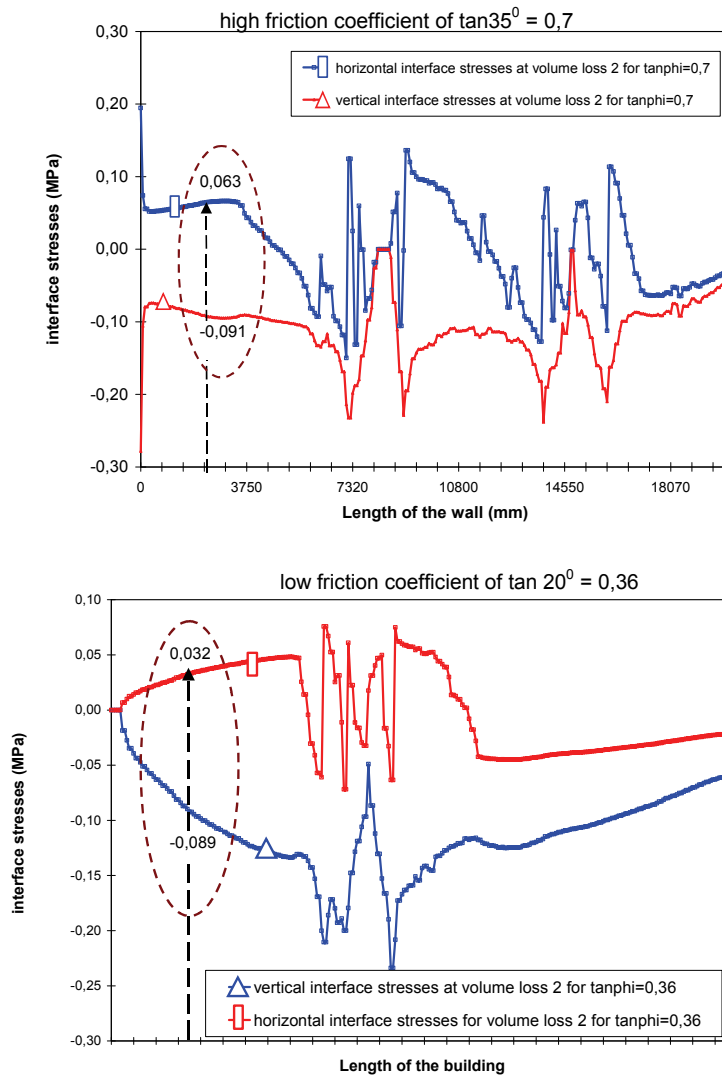
Figure 6.20: Relation of vertical and horizontal interface stresses for both interface properties

The influence of the friction coefficients on the damage and the comparison with the LTSM results is summarized in Figure 6.21.
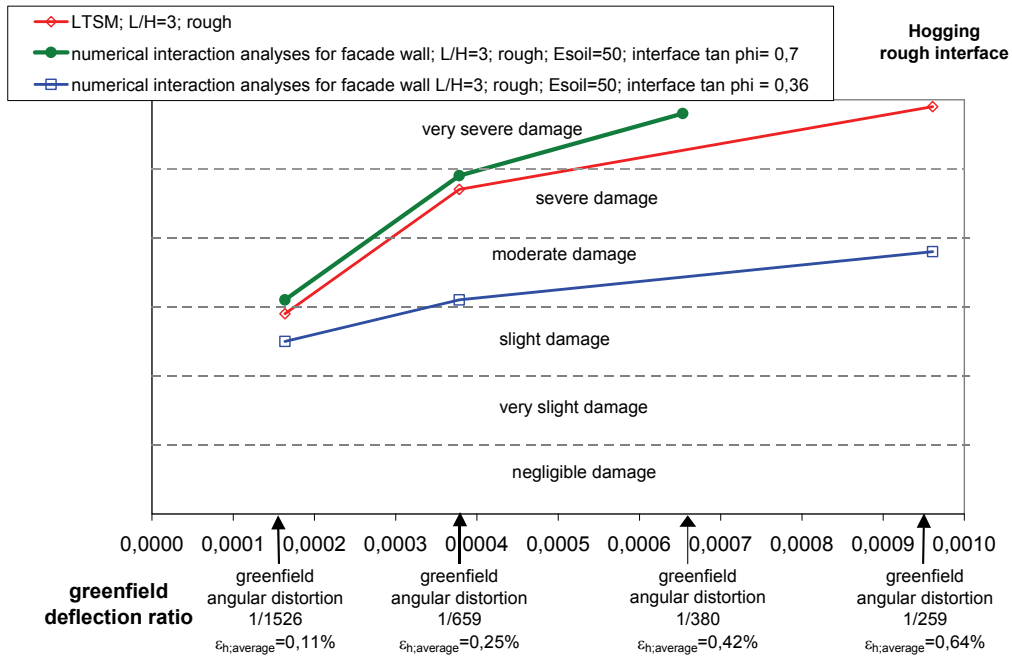
Figure 6.21: Damage class for variation of the friction coefficients of the interface elements

The calculations with the higher friction coefficient show more damage for the hogging case than the low friction coefficient due to the transfer of higher tensile strains at the bottom of the edge. The LTSM provides a very good agreement with the numerical damage predictions for the high friction coefficient and volume loss 1 and 2, whereas it overestimates the damage for the low friction coefficient for all three volume losses. The LTSM provides a conservative damage prediction for the calculations for the low friction coefficient for all three volume losses.

6.2.2   Sagging

6.2.2.1   Influence of smooth and rough interface

The influence of the smooth and the rough interface for the sagging mode is analysed for the façade wall with the example of *L/H*=3 and E_{soil}=50MPa. The results for volume loss 1 are shown in Figure 6.22.

Volume loss 1	*L/H*=3, E_{soil}=50MPa **Rough interface**	*L/H*=3, E_{soil}=50MPa **Smooth interface**
crack pattern		
principal tensile strains		
differential horizontal displacements at top/bottom edge	-0.02mm (min. compression bottom edge) -0.7mm (compression top edge)	+23.6mm (tension bottom edge) -0.9mm (compression at top edge)
tilt	-	-
deflection	1.9mm (sag)	12.5mm (sag)
tensile strains	max. tensile strain 0.25% average strain bottom edge negligible	max. tensile strain 8.1% average strain bottom edge 0,12%
cumulative crack width	0.5mm (diagonal cracking)	24mm
damage class	very slight	severe

Figure 6.22: Numerical results for the façade wall, volume loss 1, the sagging zone and smooth and rough interface

Volume loss 1 shows the dominating effect of the beneficial horizontal compressive strains which are introduced in the sagging case at the bottom of the wall for the rough case. The rough case therefore only shows very slight cracking, whereas the smooth case shows severe cracking due to the lack of the

beneficial transfer of the horizontal compressive strains due to the interface shear tractions at the bottom edge of the wall. The crack pattern for the smooth cases shows a typical sagging mode behavior with vertical cracking initiated at two cross sections of the wall, situated at one third and two third of the wall length.

The results for volume loss 2 are given in Figure 6.23.
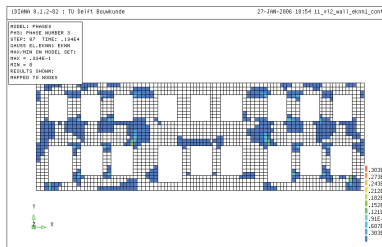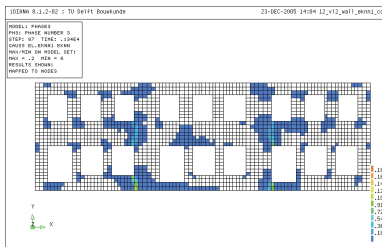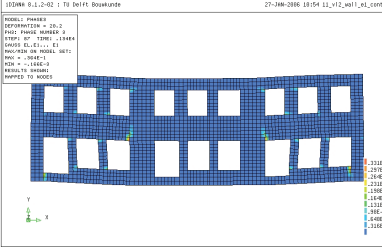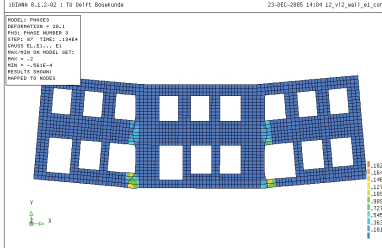
Volume loss 2	L/H=3, E_{soil}=50MPa Rough interface	L/H=3, E_{soil}=50MPa Smooth interface
crack pattern		
principal tensile strains		
differential horizontal displacements at top/bottom edge	+4mm (tension bottom edge) -1.2mm (compression top edge)	+55mm (tension bottom edge) -0.9mm (compression top egde)
tilt	-	-
deflection	12mm	29mm
tensile strains	average tensile strain bottom edge 0.02% max. tensile strain 3.6%	average tensile strain bottom edge 0.23% max. tensile strain 20%
cumulative crack width	15mm	55mm
damage class	moderate/severe	very severe

Figure 6.23: Numerical results for the façade wall, volume loss 2, the sagging zone and smooth and rough interface

The damage results for volume loss 2 show again significant differences between the smooth and the rough case. For the smooth case the damage is further increased to very severe damage.

However, also the rough case shows moderate to severe damage. The beneficial compressive strains at the bottom edge of the wall are obviously overruled by the differential vertical sagging displacements of the wall, resulting in moderate to severe cracking for the rough case. The crack pattern is

characterized by diagonal cracks around the openings at the level of the first floor, occurring at one third and two third of the building length. The diagonal cracks for the rough case indicates a general shear mode of the wall rather than a bending mode. This difference between the smooth and the rough case is very clear from the deformed meshes in Figure 6.23.

The results for volume loss 3 are shown in Figure 6.24.
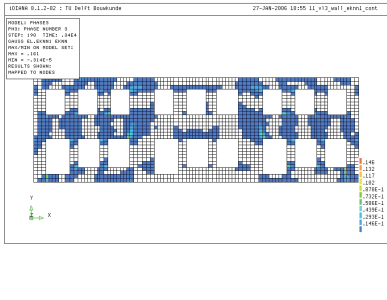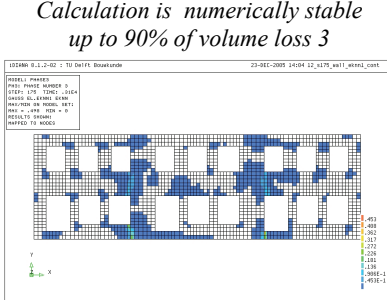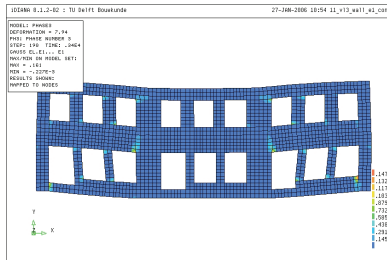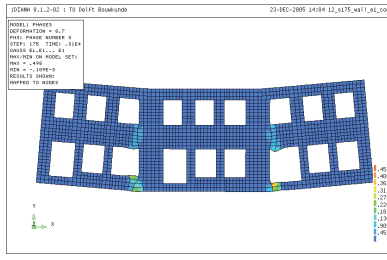
Volume loss 3	L/H=3, E_{soil}=50MPa **Rough interface**	L/H=3, E_{soil}=50MPa **Smooth interface**
crack pattern		*Calculation is numerically stable up to 90% of volume loss 3*
principal tensile strains		
differential horizontal displacements at top/bottom edge	+24.6mm (tension bottom edge) +5.5mm (tension top edge)	+128mm (tension bottom edge) -2mm (compression at bottom edge)
tilt	-	-
deflection	52mm	67mm
tensile strains	average strain bottom edge 0.12% max. tensile strain 16%	Average tensile strain bottom edge 0.64% max. tensile strain 49.8%
cumulative crack width	70mm	180mm
damage class	very severe	very severe

Figure 6.24: Numerical results for the façade wall, volume loss 3, the sagging zone and smooth and rough interface

Soil-Structure Interaction

The smooth case is only numerically feasible up to 90% of volume loss 3. The façade wall is separated into three parts resulting in the damage class very severe. The rough case also shows very severe diagonal cracking around the openings.

The vertical interface stresses for the smooth case are shown in Figure 6.25.

Smooth interface

vertical interface stresses
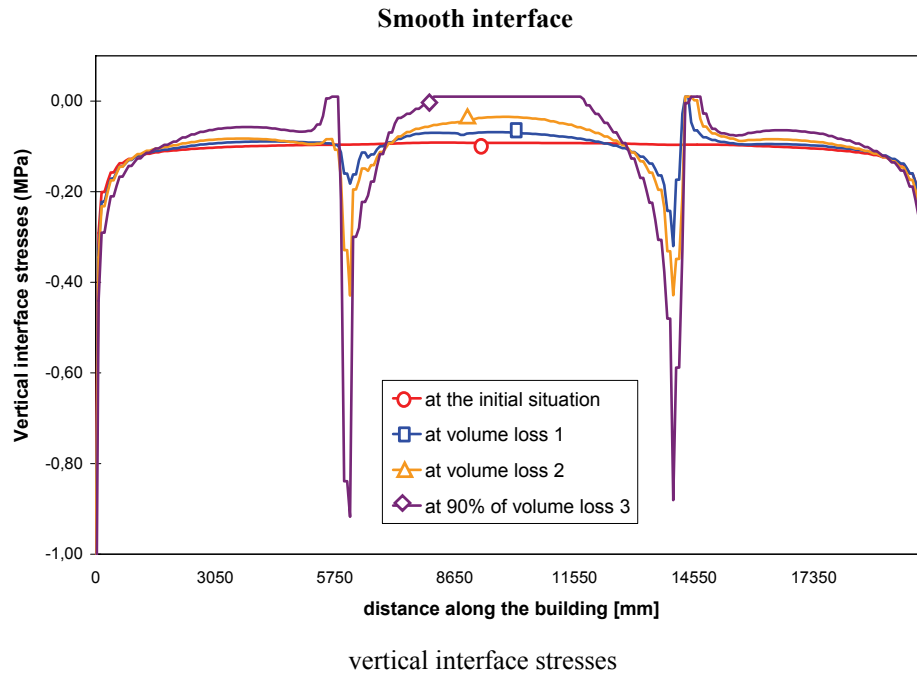
Figure 6.25: Vertical interface stresses for the smooth case

The vertical interface stresses of the smooth case show significant redistributions compared to the initial loading situation for all three volume losses. The vertical load concentrations at one third and two third of the wall length agree with the locations where the dominating vertical cracking is developed. Cracking separates the wall into three parts, which are all undergoing individual sagging modes with increase of the vertical loading towards the corners and decrease of the vertical loading at the centre of the separated parts. For volume loss 3 the vertical interface stresses are even reduced to zero over a significant length (ca. 4m) along the centre part of the building. This unloading leads to a horizontal gap between the soil and the building.

The vertical and horizontal interface stresses for the rough case are shown in Figure 6.26.

vertical interface stresses for the rough case

horizontal interface stresses for the rough case
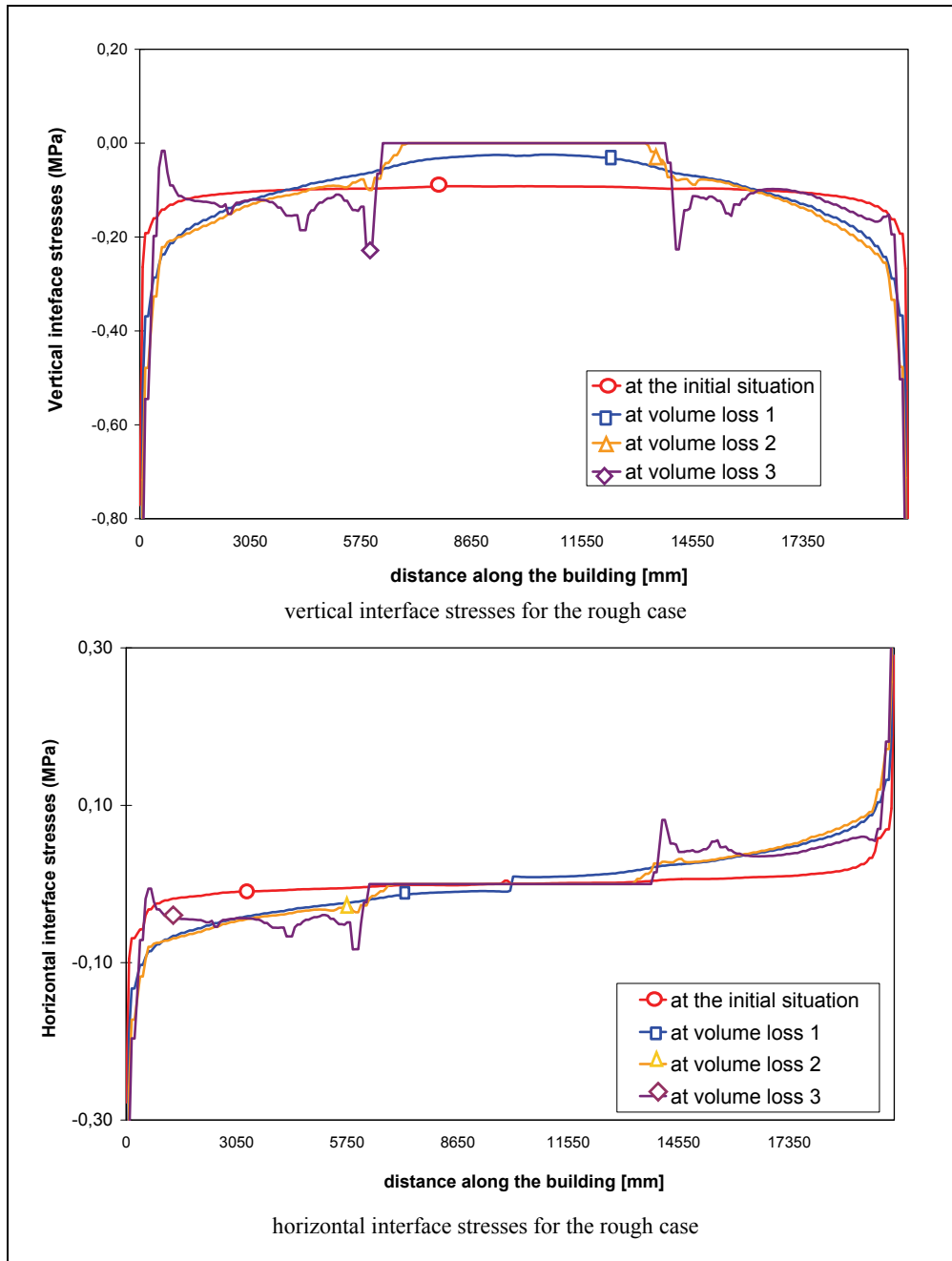
Figure 6.26: Vertical and horizontal interface stresses for the rough case

The vertical interface stresses show load redistributions with increasing loading towards the corners of the wall and decreasing stresses towards the centre of the wall. Volume loss 2 and 3 show unloading of the vertical interface stresses at the centre of the wall, leading to a gap between wall and soil.

The horizontal interface stresses of the rough situation show a clear increase of the horizontal interface stresses compared to the initial situation causing compression at the bottom edge. This compression is

induced by the transfer of the horizontal compressive strains via interface shear tractions from the soil to the building via the interface.

The damage results of the numerical calculations are summarized in Figure 6.27 and compared to the predictions with the LTSM.
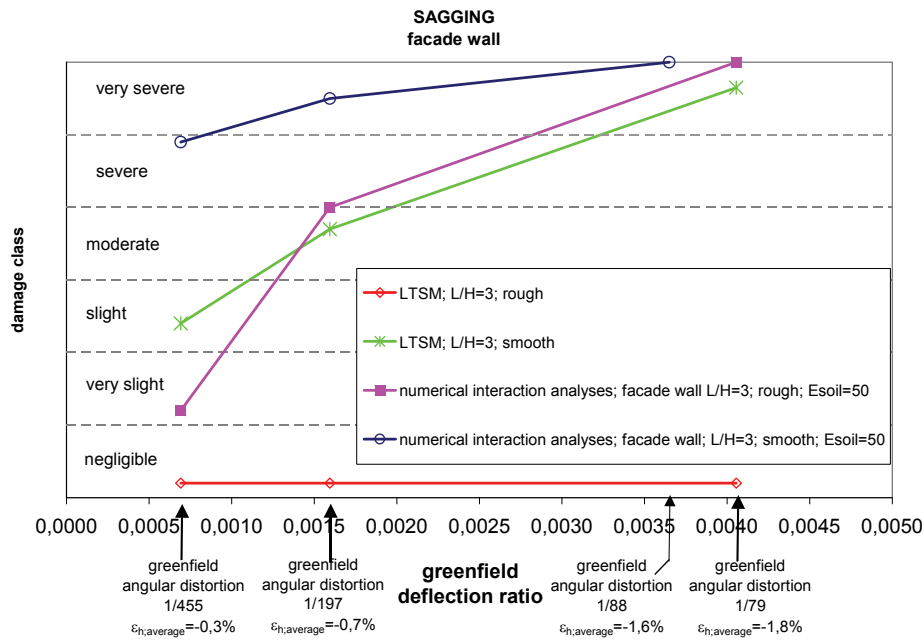
Figure 6.27: Damage results compared with the LTSM

The difference between the rough and the smooth calculation is significant. The rough case introduces compressive strains at the bottom edge of the wall for the sagging zone, making the rough case far less susceptible to damage than the smooth case. The numerical calculations for volume loss 1 show already moderate damage for the smooth interface. The beneficial effect of the horizontal compression induced at the bottom edge in case of the rough interface is clearly visible leading to negligible/very slight damage for the rough interface for volume loss 1.

The LTSM underestimates the damage for the façade wall in the sagging zone. If the beneficial compressive strains are fully included in the damage prediction (rough case) the LTSM underestimates the damage significantly, as it gives negligible damage for all volume losses. However the numerical rough calculations show increasing damage up to very severe damage for volume loss 3. It is therefore recommended to neglect the compressive strains in the LTSM predictions for the sagging zone.

It is emphasized that even when the beneficial horizontal strains are neglected in the LTSM (smooth case), the numerical damage for the smooth case is still underestimated with the LTSM for volume loss 2 and 3. A fully smooth case is however not a realistic situation for engineering practice. A certain degree of transfer of horizontal ground movements will always occur and the nonlinear interface properties in the numerical rough cases are considered to model a realistic degree of transfer of horizontal differential ground movements to the building.

It is therefore recommended to follow the above suggested LTSM approach (neglecting horizontal compression transferred to the building due to differential horizontal strains) for tunnelling induced sagging cases. For engineering practice this approach is considered to provide a reasonable damage prediction compared to the numerical interaction results.

6.2.2.2 Influence of soil stiffness

The analyses on the influence of the numerical models with different soil stiffness are considered for the rough and the smooth cases. The case for E_{soil}=50MPa has been presented in the previous section. The results for the low soil stiffness of E_{soil}=10MPa are presented in this section.
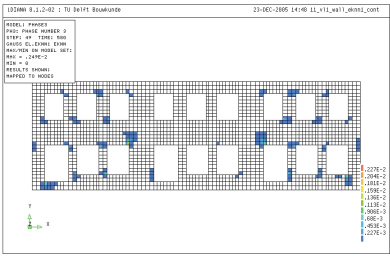
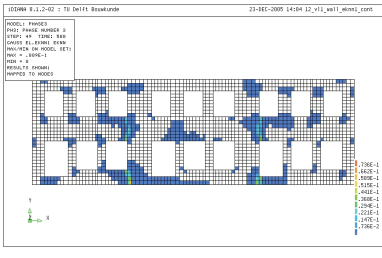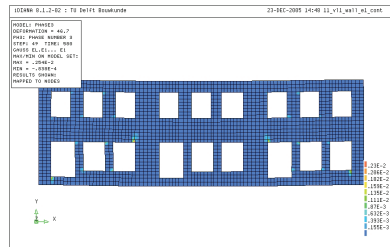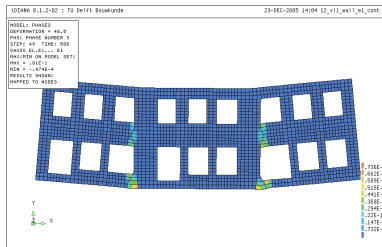The results for volume loss 1 are shown in Figure 6.28.
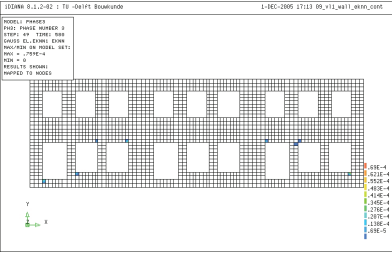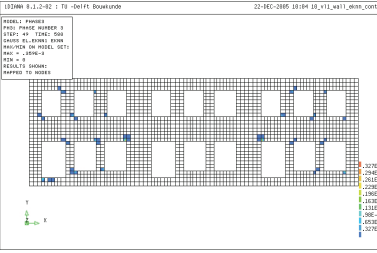
Volume loss 1	L/H=3, E_{soil}=10MPa **Rough interface**	L/H=3, E_{soil}=10MPa **Smooth interface**
crack pattern		
differential horizontal displacements at top/bottom edge	-0.2mm (minimum compression at bottom edge)	+0.1mm (minimum tension at bottom edge)
tilt	-	-
deflection	0.1mm (hog)	0.5mm (sag)
tensile strains	max. tensile strain 0.0128% average compression bottom edge is negligible	max. tensile strain 0.04% average tensile strain bottom edge is negligible
cumulative crack width	diagonal cracking 0.05mm	diagonal cracking 0.1mm
damage class	negligible	negligible

Figure 6.28: Numerical results for volume loss 1

Volume loss 1 results in negligible damage for the low soil stiffness of E_{soil}=10MPa and both interfaces. Compared to the damage results for the stiffer soil with E_{soil}=50MPa (see previous section) the beneficial interaction effects for the low soil stiffness reduce the damage for the smooth case and volume loss 1 significantly. The calculations for the smooth case and the low soil stiffness show negligible damage whereas the stiffer soil results in severe damage for the same volume loss.

The results for volume loss 2 are given in Figure 6.29.
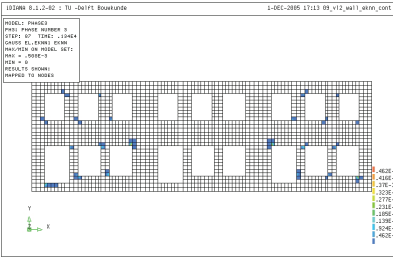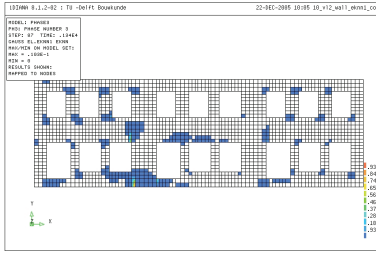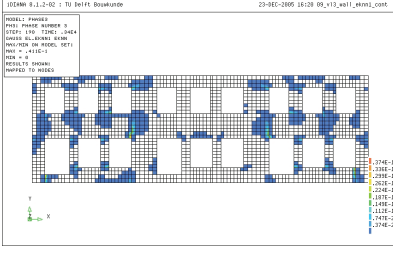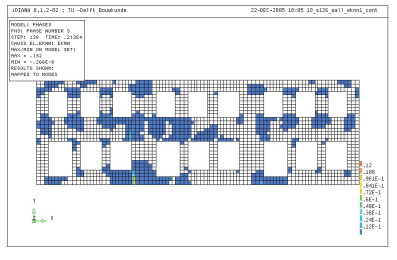
Volume loss 2	*L/H*=3, *E_{soil}*=10MPa **Rough interface**	*L/H*=3, *E_{soil}*=10MPa **Smooth interface**
crack pattern		
differential horizontal displacements at top/bottom edge	-0.22mm (compression at bottom edge)	+0.4mm (tension at bottom edge)
tilt	-	-
deflection	1mm (sag)	3mm (sag)
tensile strain	max. strain 0.051%	max. strain 0.1% average tensile strain bottom edge 0.009%
cumulative crack width	diagonal cracking max. crack width 0.1mm	3mm diagonal cracking max. crack width 1mm
damage class	negligible	slight

Figure 6.29: Numerical results for volume loss 2

The smooth case is more susceptible to damage than the rough case for volume loss 2. Slight cracking is introduced for the smooth case. The rough case however remains uncracked due to the beneficial effect of the soil-structure interaction for the low soil stiffness and the transfer of the beneficial compressive strains at the bottom edge of the wall. Both damage results are significantly lower than for the stiffer soil of *E_{soil}*=50MPa and volume loss 2.

The results for volume loss 3 are shown in Figure 6.30.

Volume loss 3	*L/H*=3, *E_{soil}*=10MPa **Rough interface**	*L/H*=3, *E_{soil}*=10MPa **Smooth interface**
		Calculation only numerically feasible up to 66% of volume loss 3
crack pattern		

differential horizontal displacements at bottom edge	+5.1mm (tension at bottom edge)	+23.8mm (tension at bottom edge)
tilt	-	-
deflection	14mm (sag)	19mm (sag)
tensile strains	max. strain 4.4% average strain bottom edge 0.0255%	max. strain 13.,2% average strain bottom edge 0.12%
cumulative crack width	10mm max. diagonal cracking first floor 4mm	38mm max. diagonal cracking 10mm
damage class	slight	very severe

Figure 6.30: Numerical results for volume loss 3

The smooth case already shows very severe damage when 66% of the volume loss 3 is imposed. The numerical calculation is not numerically stable anymore when the volume loss is further increased, because of the very severe cracking in the façade wall. The rough case shows slight damage for volume loss 3.

The damage results of the low soil stiffness E_{soil}=10MPa and the stiffer soil E_{soil}=50MPa from the previous section are compared with the LTSM predictions in Figure 6.31.
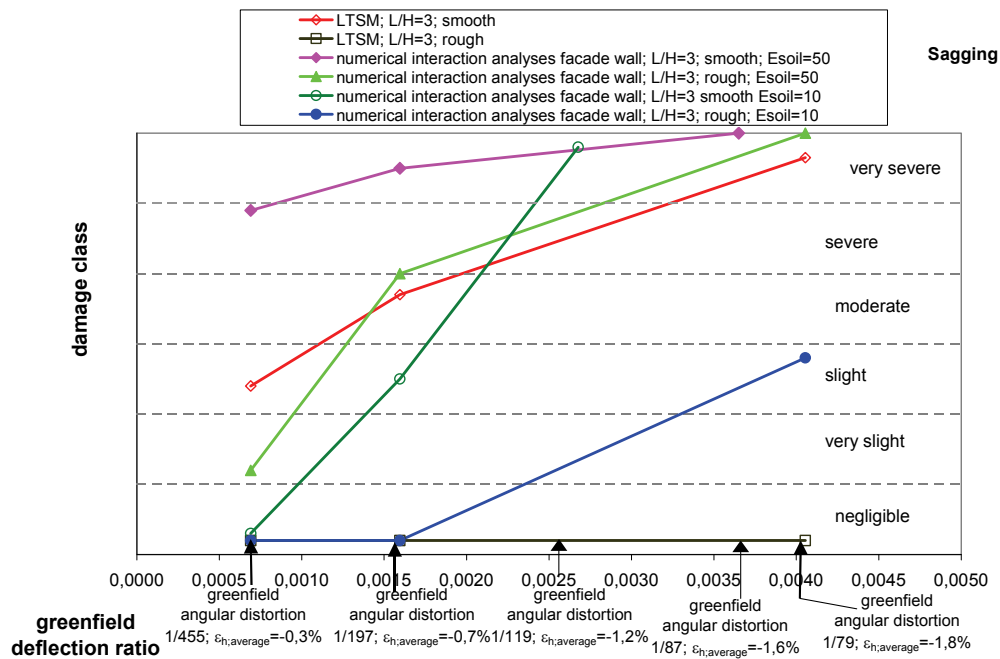
Figure 6.31: Damage results of different soil stiffness compared to LTSM

The LTSM results for the rough case include the full transfer of differential horizontal ground displacements at the bottom edge of the wall. In the sagging zone these differential horizontal movements have a beneficial effect on the damage as they cause compressive strains in the wall, which

Soil-Structure Interaction

reduce the tensile strains induced by the vertical sagging mode deformations. As a consequence the LTSM for the rough case and the assumption of full transfer of the horizontal compressive strains therefore underestimates the damage significantly, compared to the numerical damage for the rough cases. It is therefore recommended to neglect the beneficial differential horizontal ground movements in the damage predictions with the LTSM.

The results for the smooth case for the LTSM show a reasonable conservative damage prediction compared to the numerical results for the smooth case and the low soil stiffness, but the numerical damage for the stiffer soil of E_{soil}=50MPa and the smooth case is underestimated with the smooth LTSM approach. As there will always be a certain degree of beneficial horizontal compressive strain transfer in practice, the underestimations for the smooth cases are considered to be acceptable.

The damage for the softer soil of E_{soil}=10MPa is smaller than the damage for the stiffer soil of E_{soil}=50MPa, if the same differential greenfield ground deformations are imposed on the wall. The damage therefore decreases with decreasing soil stiffness, which is caused by the increase of the beneficial interaction effects for a decrease of the soil stiffness.

.

7 SOIL-STRUCTURE INTERACTION – CONCLUSIONS, LIMITATIONS AND RECOMMENDATIONS

7.1 Conclusions

7.1.1 General

For all considered numerical interaction calculations it is shown that for the same building and the same distribution of imposed greenfield ground deformations, the damage sensitivity increases clearly with increasing soil stiffness. The reason for this effect is shown schematically in Figure 7.1 for the example of vertical interaction in the sagging zone. The mobilized compatibility forces due to interaction between soil and structure increase with increasing soil stiffness. These compatibility forces lead to an increase of the redistribution of the building loads and consequently an increase of tensile strains and damage in the building.

Interaction for imposed ground movements
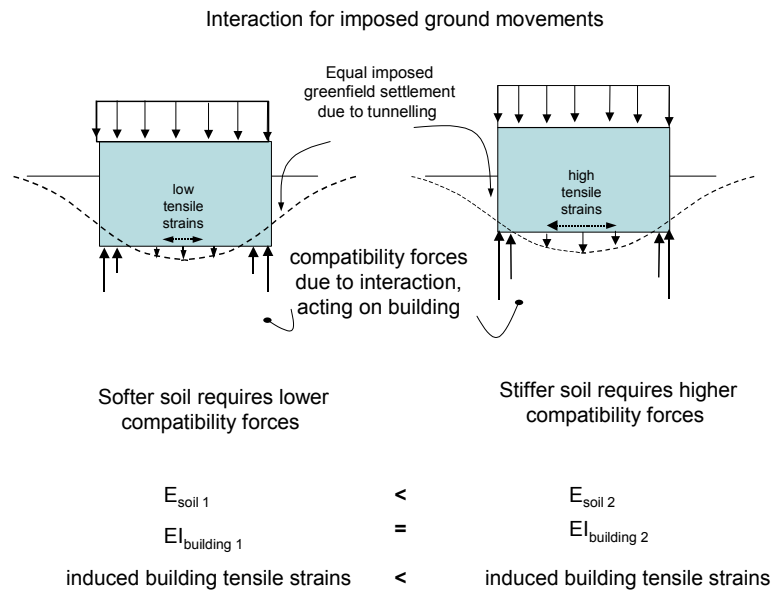
Figure 7.1: Schematic interaction effect depending of the soil stiffness

The nonlinear material behaviour of the wall including the modelling of smeared cracking shows to have significant influence on the damage development once a crack is initiated. A numerical prediction of elastic tensile strains using a linear elastic material model for the wall underestimates the damage significantly. An interaction analyses should take into account nonlinear material behaviour of the wall and the interface in order to obtain appropriate damage results.

The damage and crack width predictions appear to be sufficiently objective with respect to the chosen mesh. This was demonstrated by comparing a coarse and a fine mesh. By relating the crack band width to the finite element dimensions, the energy consumed upon crack propagation is kept constant. This forms an important issue in softening fracture mechanics using smeared crack models. The numerical calculations carried out in this thesis confirm the experience of relevant research on this topic.

Soil-Structure Interaction

For the considered numerical **rough cases**, the horizontal interaction between building and soil mobilizes horizontal shear stresses at the bottom edge of the building, which introduce horizontal strains in the building. These strains are tensile strains for the considered tunnelling hogging zone and compressive strains for the tunnelling sagging zone. For the hogging zone the damage therefore increases and for the sagging zone the damage decreases if the rough case is considered. The magnitude of the horizontal shear stresses which are activated via the interface depend on the properties of the interface, the vertical loads of the building and the differences in the horizontal stiffness between soil and building. The damage in the hogging zone increases with increasing friction coefficient of the interface. This was demonstrated by variation of the interface properties. The friction coefficient depends on details of the connection between wall and soil. It is emphasized that the assumed rough case represents a realistic nonlinear interface behaviour between building and soil.

For the considered **smooth case** any transfer of horizontal movements and shear stresses between the building and the soil is neglected. For a tunnelling hogging zone the damage for the smooth case is in general significant smaller than for the rough case, because no horizontal tensile strains are introduced at the bottom edge of the building due to the differential horizontal ground movements. For the sagging zone, however, the opposite holds, because the differential horizontal ground movements in a tunnelling sagging zone would cause compressive strains at the bottom edge of the wall, if they can be transferred to the building via the interface. However these compressive strains cannot be transferred by friction because a smooth interface is assumed. It is emphasized that the assumed smooth case represents an extreme theoretical assumption, because in reality a certain amount of horizontal transfer of shear stresses will be transferred by friction between building and soil.

7.1.2   Hogging zone

The characteristic results for the relevant hogging cases are summarized in Figure 7.2.
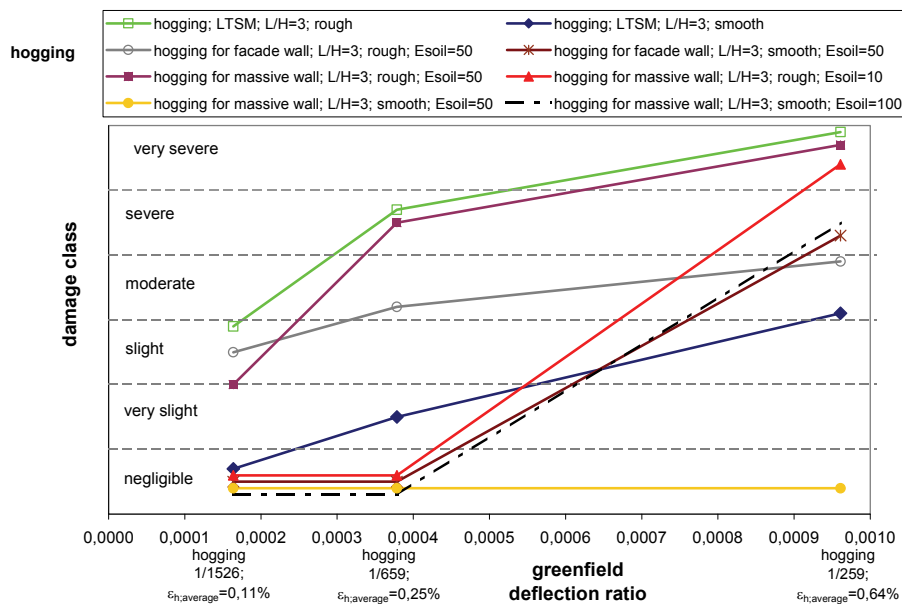
It is noted that the linear connection lines between the three investigated greenfield distortions are only for visual purpose to identify the three results belonging to one case. No linear interpolation can be applied for intermediary greenfield distortions once cracking is initiated.

Figure 7.2: Summary of damage results in the hogging zone

Soil-Structure Interaction

The horizontal axis of the diagram shows the greenfield values for the angular distortion, the deflection ratio and the horizontal ground strain caused by the TBM-tunnelling at the location of the buildings, but in absence of the building. These greenfield values are used as input for the predictions with the modified LTSM, because interaction is neglected in the LTSM. The vertical axis shows the resulting damage class for the LTSM predictions and the numerical interaction damage results, based on the damage classification system derived by the BRE (1981). It is emphasized that the numerical results are obtained with a fully interaction calculation including non-linear respons of the structure (smeared crack model) and non-linear behaviour of the interface between soil and structure.

For the results in the hogging zone the following conclusions can be drawn:

- A characteristic TBM-tunnelling induced hogging zone implies both greenfield vertical and horizontal ground deformations. The differential horizontal components in a hogging zone can cause horizontal strains on a building, depending on the degree of transfer of the horizontal movements from soil to building. The incorporation of the horizontal differential ground movements in the hogging zone has an important influence on the damage profile. The numerical calculations in the hogging zone where rough cases are considered are significantly more vulnerable for damage, than cases where the horizontal interaction is neglected (smooth calculations). This can be explained by the transfer of horizontal strains which are introduced at the bottom of the wall, leading to the initiation of cracking. If no clear defined slipping layers exist between the soil and the building, the horizontal interaction has to be taken into account for a damage prediction in the hogging zone. *A LTSM damage prediction in the hogging zone neglecting differential horizontal greenfield ground movements is incomplete and provides an unsafe damage prediction.* Neglecting of horizontal ground movements and horizontal interaction for a damage prediction is only considered acceptable if detailed information is available which confirms the existence of an effective slipping layer between building and soil, which verifies the assumption of a smooth interface.

- When the *smooth* case can be assumed, i.e. when the transfer of differential horizontal ground movements to the building can be neglected, the LTSM prediction for full transfer of differential vertical movements provides a conservative damage prediction for almost all considered cases. The beneficial interaction effects for vertical movements reduce the numerical damage according to the LTSM prediction for almost all considered numerical cases. Only the numerical cases for the façade wall, soil stiffness E_{soil} =50MPa and for the massive wall and E_{soil} =100MPa volume loss 3 shows slightly more damage due to the highly nonlinear behaviour of the wall for volume loss 3. The difference for these special cases is severe damage for the numerical smooth case calculation and slight/moderate damage for the LTSM.

- When the horizontal and vertical differential ground movements are included in the damage prediction the *comparison between the LTSM and the numerical rough calculations* shows very diverse results:

For the **massive wall** with high soil stiffness of E_{soil} =50MPa and E_{soil} =100MPa the predicted damage shows very good agreement between the LTSM with the assumption of full transfer of horizontal ground movements and the numerical interaction analyses for all three volume losses. However, the damage for the massive wall and the low soil stiffness of E_{soil} =10MPa is overestimated with the LTSM for all volume losses. This shows that the damage is clearly decreasing with decreasing soil stiffness. A result which can be explained by the increase of the beneficial interaction effects for decreasing soil stiffness.

For the **façade wall** the predicted damage for only the E_{soil} =50MPa and the high friction coefficient of the interface shows very good agreement between LTSM and the numerical results for all three volume losses. The other cases show an overestimation of the LTSM damage results compared to the numerical analyses. The overestimation is very conservative for the low soil stiffness of E_{soil}

=10MPa. This is explained by the strong beneficial interaction effect on the vertical ground movements with decreasing soil stiffness.

- In some cases the facade wall appears to be more damage sensitive than the massive wall for the same imposed greenfield distortions. However a general statement cannot be drawn because the reaction can be highly nonlinear for different cases, once cracking is initiated. For the smooth cases the facade wall for the case with the soil stiffness of 50MPa shows for example significantly more damage than the massive wall for volume loss 3. However, for the rough cases and the soil stiffness of 50MPa the facade wall for example shows less damage than the massive wall for volume loss 2 and 3. It is emphasized that if the initial stress and strain situation is different/higher than for the chosen numerical cases it is possible that facade walls can probably provide more damage than for the considered cases. Redistributions of higher initial loads due to differential deformations can enhance local stress and strain concentrations around openings.

7.1.3 Sagging zone

The characteristic results for the relevant sagging cases are summarized in Figure 7.3.
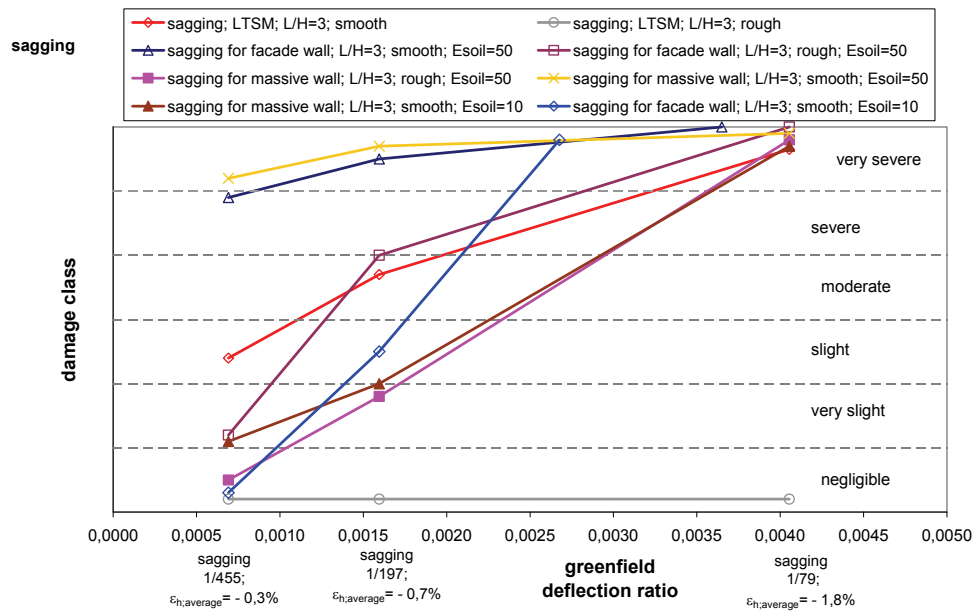
It is noted that the linear connection lines between the three investigated greenfield distortions are only for visual purpose to identify the three results belonging to one case. No linear interpolation can be applied for intermediary greenfield distortions once cracking is initiated.

Figure 7.3: Summary of damage results in the sagging zone

For the results in the sagging zone the following conclusions can be drawn:

- A TBM-tunnelling induced sagging zone implies differential horizontal greenfield ground deformations which can cause horizontal compression at the bottom of the building. The incorporation of the horizontal differential ground movements in the sagging zone has important influence on the damage profile. The numerical calculations where rough cases are considered are significantly less vulnerable to damage in the sagging zone than the smooth cases (neglecting horizontal interaction between soil and building). This is explainable due to the transfer of horizontal compression at the bottom of the wall which reduces the tensile strains induced by the

vertical sagging mode. *A LTSM damage prediction including a full transfer of the beneficial compressive horizontal greenfield movements in the sagging zone results in an unsafe damage prediction. It is therefore recommended to neglect the beneficial horizontal compression transferred to the building due to differential horizontal strains for tunnelling induced sagging cases.*

- The LTSM prediction for the considered sagging cases without encountering the beneficial horizontal ground movements (*smooth case*), does provide a conservative damage prediction compared to the numerical calculations for the low soil stiffness of E_{soil}=10MPa. It does however *not* provide a conservative approach compared to the numerical damage results for the high soil stiffness of E_{soil}=50MPa. For the higher soil stiffness the numerical results for both the facade wall and the massive wall show damage of one or two classes higher than for the LTSM. The smooth case can thus still provide an unsafe underestimation of the damage with the LTSM compared with the results of the numerical interaction analyses and the smooth interface. A clear smooth case is however not a realistic situation in engineering practice. A certain degree of transfer of friction shear forces between building and soil will always occur.
  It is therefore recommended to follow the above suggested LTSM approach (neglecting of horizontal compression transferred to the building due to differential horizontal strains) for tunnelling induced sagging cases. For practical engineering this approach is considered to provide a reasonable damage prediction.

- The numerical calculations for the facade wall show in general slightly more damage than for the massive wall. This is partly to the fact, that the vertical loads on the non-bearing façade wall were assumed lower than for the massive wall, which is a realistic assumption. This reduction of confinement reduces the shear transmission at the interface, which is beneficial for the rough case in the sagging mode and can therefore increase the damage compared to the massive wall for the rough case. It is however emphasized that if the load on the façade wall would be increased, also the initial stress and strain concentrations in a façade wall are higher. This effect can probably provide even more damage for the facade wall than according to the cases considered in this study, although the beneficial confinement for the rough case is higher and thus the damage could also be lower. Small redistributions of loads due to differential deformations can promote damage more quickly for initial higher local stress and strain concentrations around openings. This can overrule the beneficial confinement effect for the rough case in the sagging zone, described above.

7.1.4 Interaction for dead weight versus imposed ground deformations

For the understanding of the damage sensitivity due to differential building settlements, it is crucial to distinguish between settlements of buildings which are caused by the building loads themselves (dead weight) and differential building deformations which are introduced by imposed soil deformations due to nearby excavation works. It should be emphasized that the latter situation is in general far more sensitive for damage. Most important reasons for this are:

- First, dead weight settlements are in general causing only differential vertical deformations, whereas horizontal and vertical differential building deformations are introduced by imposed soil deformations from excavation works. This is a very important difference increasing the damage sensitivity of the latter case, when the transfer of differential horizontal deformations is oriented in such a way, that they can cause tension in the building.
- Another important factor is that the build up/development of the building loads and consequently the settlements due to these building loads increase gradually with the increase in stiffness of the building during the construction work. This means that the settlements occur gradually. Also the stiffness of the building is smaller in the beginning, reducing the damage sensitivity for dead weight settlements. Furthermore the beneficial creep capacity for quasi-brittle materials has its maximum in the early stage of the construction, when also the settlements occur gradually. Both aspects make

the case of dead weight settlements far less sensitive to damage than the short-term excavation induced deformations.

It is also important to understand the different principles of the interaction effects for the two cases correctly. In general the differences in building stiffness and soil stiffness cause interaction between the subsystems, because the compatibility of equal deformations between both systems requires interacting forces between both components. If the magnitude of these compatibility forces increases, the degree of interaction between both subsystems increases. If no interaction occurs no compatibility forces are necessary to guarantee the deformation compatibility.

In order to qualitatively describe the differences of the effects of interaction depending on building stiffness and soil stiffness, the following general definition of an interaction factor is proposed for the further explanations:

$$\text{interaction factor} = \frac{\text{building bending stiffness}}{\text{soil stiffness}}$$

Regarding this factor it is referred to section 4.3, which explains that the widely used system stiffness parameters are judged not to be straightforward. For this reason a more general term of the interaction factor, given above, is used in this section to explain schematically general interaction effects.

For the influence of **dead weight cases** the building and its loads is the actor and the soil is the reactor. For the dead weight case from Figure 7.4, the interaction increases with decreasing soil stiffness for the same building stiffness. The interaction factor k than also increases consequently. With the increasing interaction for dead weight cases, also the internal redistribution of loading in the structure increases and consequently the tensile stresses in the building increase for the considered case. The interaction thus unfavourable affects the internal loading in the building.
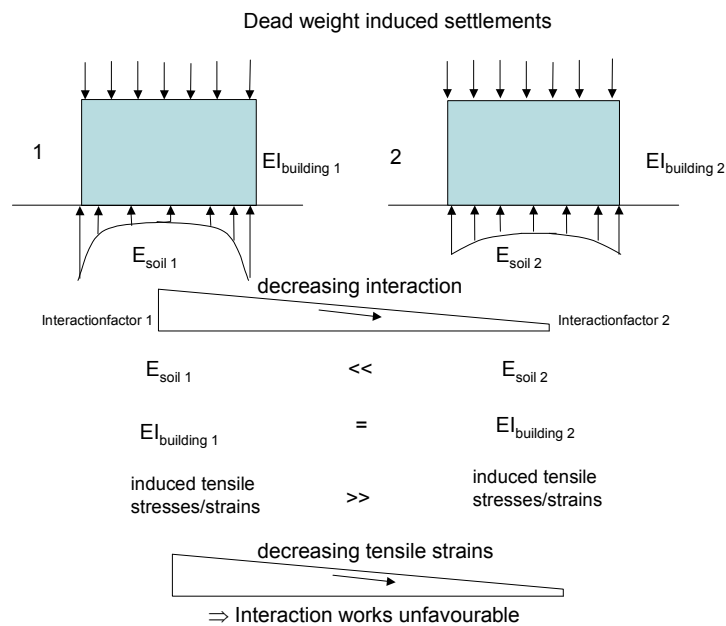
Figure 7.4: Interaction principles for dead weight induced building settlements

Soil-Structure Interaction

The same principle is applicable for the case that the soil stiffness is kept the same and the building stiffness is varied in terms of the Young's modulus. If the building bending stiffness *EI* is for example decreased for a constant soil stiffness parameter, the interaction factor is also decreasing. This results in less interaction and thus less introduction of tensile strains and stresses. For dead weight induced settlements a lower stiffness of the building therefore leads to less damage which is in agreement with empirical and numerical observations, see Netzel D. (1972).

For the effect of **imposed ground deformations** on existing buildings, the interaction effects are different. The ground is the actor and the building is reacting. In this case the damage risk of the building decreases with increasing interaction factor and the interaction thus works favorable, see Figure 7.1. Figure 7.5 shows the considered configurations regarding the interaction factor and the damage. It is emphasized that the starting point is the assumption that the imposed soil deformations are equal for both cases.
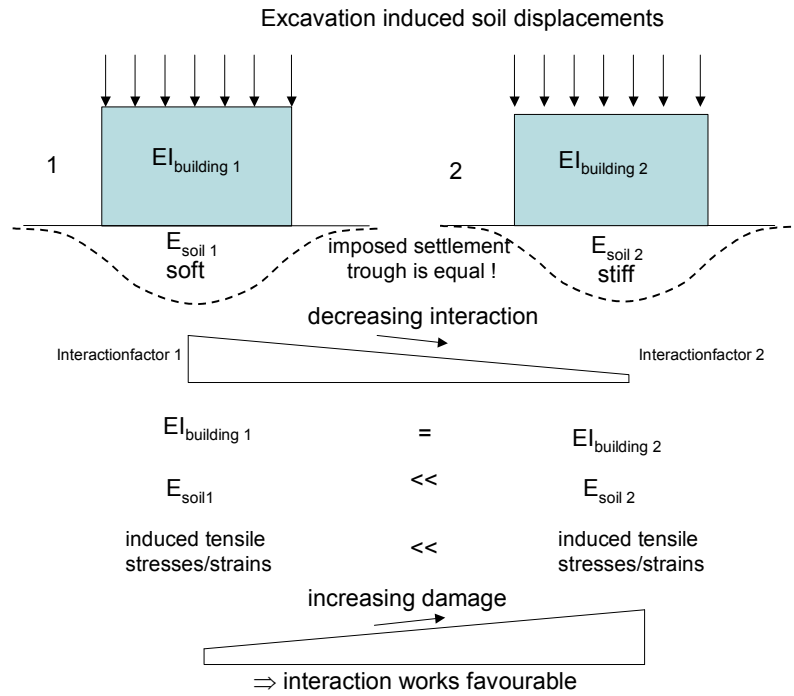
Figure 7.5:   Interaction principles for imposed ground settlements and variation of the soil stiffness

However if the soil stiffness would be kept equal and the building bending stiffness *EI* would be varied, a lower building stiffness would lead to more damage because the interaction factor would decrease. This conclusion is not in agreement with empirical and numerical experience, because the damage will be reduced in the building if the building stiffness is reduced. This considerations undermine the statements given in section 4.3, that the interaction factor or system stiffness parameter is not an appropriate expression to cover all kind of interaction effects for different configurations between soil and building.

7.2   Limitations and recommendations

7.2.1   General

This section addresses some limitations in the numerical interaction models used in this thesis and describes the quantitative influence of these limitations on the building response. Furthermore recommendations are given for future research on the field of numerical interaction analyses of excavation induced building damage.

7.2.2   Effect of nonlinear soil behavior

As described in 4.4.2, the nonlinear behaviour of the soil is not included in the numerical interaction analyses used in this research. The incorporation of nonlinear soil behaviour in combination with brittle masonry fracture leads to complex calculations with a high risk on numerical instabilities. The possible effects of nonlinear soil reactions on the soil-structure interaction are therefore described qualitatively.

- Redistribution of the vertical building loads due to the soil-structure interaction locally increases the vertical soil pressures, which can lead to local plasticity of the soil. Whether these effects cause more or less damage on the wall depends on the overall response of the model. Two different effects are possible:

  - With increasing local absolute settlements due to local plastification, the differential building settlements and thus the building damage could possibly be reduced.

  - The local increase of soil pressures may lead in the worst case to local shear failure of the soil, which can be accompanied by additional large differential settlements of the structure and thus an increase of damage.

  Which of these effects prevails, depends on a combination of factors.

- Vertical cracking in the soil can occur due to horizontal interaction between the relatively soft soil and the stiff structure. Vertical cracking in the soil is than likely to occur next to the buildings for a tunnelling hogging zone situation. Figure 7.6 (a) shows the principal effect for a hogging case. If cracking in the soil occurs next to the building, the differential horizontal ground movements imposed at the structure will be reduced significantly. Consequently horizontal strains in the structure will be reduced, leading to less damage. For the sagging case (Figure 7.6 (b)) vertical cracking in the soil can reduce the benefit of the induced horizontal compressive strains. For rough cases the damage can then be consequently increased.

Hogging

Orientation of horizontal
interaction forces
on the soil and the wall

(a)

Sagging

Orientation of horizontal
interaction forces
on the soil and the wall

(b)
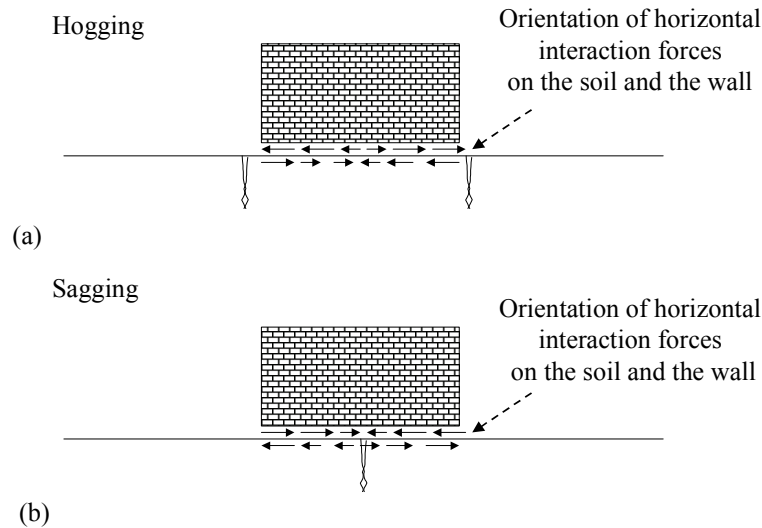
Figure 7.6: Qualitative effects of nonlinear soil behaviour

7.2.3 Effect of 3D behavior of building and soil

The 2D interaction analyses neglect the three dimensional behavior of building and soil.

Due to the differential stiffness of structural parts in different directions of the buildings, the actual load redistribution due to imposed ground deformations can differ from the results of 2D analyses. Especially the connections between construction elements in different directions and of different stiffness can undergo additional loading due to the 3D load redistributions. These 3D redistributions and their effects on the overall damage in a building can only be investigated with advanced 3D numerical models, where the building with its different construction elements and their connections are modeled in detail.

A second 3D effect, ignored in the present 2D study, is the three dimensional load spreading of the foundation loads in the soil perpendicular to the model plane. The stresses in the soil due to the wall loadings in the 2D calculations are therefore overestimated with increasing depth under the foundation. This overestimation of the loads in the soil consequently overestimates the deformations of the soil and thus the stiffness of the soil in the current 2D calculations. As a less stiff soil results in less damage, the damage could be underestimated by neglecting the 3D load spreading in the soil.

7.2.4 Recommendations for future research on the field of numerical damage predictions

Numerical soil-structure interaction analyses are very complex and a lot of different factors can determine the results. For this study it is decided to vary a restricted amount of parameters (see section 4.4.1) in order to be able to investigate and explain significant interaction effects and draw valuable conclusions for engineering practice. However, based on this study, a variation of for example the material parameters of the smeared crack model wall for several models could give more insight in the bandwidth of the results for a bandwidth of structural material parameters. For the case of a single numerical situation this variation of the nonlinear masonry parameters is presented by Boonpichetvong

Soil-Structure Interaction

(2003). The general influence of the most important structural input parameters (Young's modulus, tensile strength and fracture energy) of the walls is qualitatively analysed in this paper. It is recommended to carry out comparable variations in the future.

The numerical studies did not include the incorporation of nonlinear soil behaviour. Future research should aim at combining the nonlinear behaviour of soil and structure, also because computational tools and the developments on the numerical, nonlinear material models for soil and structure become more and more robust and powerful, so that combination of soil nonlinearity and building nonlinearity gradually become feasible.

A numerical study on the influence of initial cracking in a building on the overall damage development due to excavation induced ground deformations forms a challenge for future research. The initial cracking could have been initiated due to other differential ground deformation sources in the past or cracking due to thermal and seasonal influences. The initial cracking could be implemented in the numerical study with for example an initial cracking stage due to a predefined deformation stage or the incorporation of discrete cracks in the building in the initial stage.

3D-effects can influence the damage results as explained in section 7.2.3. For advanced numerical damage predictions detailed structural 3D details of different structural elements and their connections can be implemented in the analyses in order to model a realistic 3D behaviour of the building. The influence of the load spreading in the 3D soil model is already addressed in 7.2.3 and is also included in a 3D calculation.

The numerical interaction analyses should be enhanced/extended in the future with the implementations of framed buildings instead of the masonry walls considered in this thesis. The response of this type of buildings should be investigated further in numerical studies in order to study the modification of bending moments and shear forces in the structural members (beams, columns and foundation plates). As mentioned in section 3.3.6, these considerations form the basis of the damage judgement for framed buildings.

Building on piled foundations form a special case, which requires individual numerical studies. The transfer of greenfield ground movements from the soil to the piles and from the piles to the buildings depends on many factors. The lateral bending of the piles due to the horizontal ground movements can also be a dominant damage criterion for piled foundations.

With a more wide range of variation of input parameters, the statistical analyses of the numerical results with a probability approach is suggested, to be able to determine probabilities of cracking damage for certain damage levels.

8 MONITORING OF THE SURROUNDINGS

8.1 General

Monitoring of the actual influence of the construction work on the surroundings (soil and adjacent structures) is an essential part of settlement risk management, Netzel (1999a, 2001a). The amount, frequency and type of monitoring should be derived from the damage prediction analyses and defined in a monitoring plan, which forms the boundary condition regarding the control of the influence of the construction works on the surroundings. It is emphasized that monitoring is not a (mitigating) measure to avoid or reduce damage but only a tool to signalise deformation trends in time and to take mitigating measures in time. Monitoring can only effectively contribute to risk management if it is used proactively during the construction work. Proactive means that it should be able to anticipate on the development of deformation trends during the construction stage. The damage risks can only be managed if necessary mitigating measures are taken in time on the basis of the processed monitoring data. Experienced engineers have to be involved in the interpretation of the monitoring data during the work on site and the contractor as well as the client have to be aware of the fact that monitoring data determine the boundaries of their work.

For detailed information about different monitoring systems for soil and building deformations and the geodetically aspects of the instrumentation and the readings it is referred to Dunnicliff (1993).

8.2 Natural deformation behaviour of buildings

8.2.1 General

It is important to have information about the natural deformations of adjacent structures and collect data before the start of the construction to have a clear reference of deformations occurring without the additional influence of the construction work. The accuracy of measurements in combination with the natural deformations has to be included in the interpretation of the monitoring results during the construction work. Natural deformations include for example long term autonomous soil settlements and deformation contributions due to seasonal temperature fluctuations.

8.2.2 Temperature effects

Temperature causes an important part of natural fluctuations for settlements and horizontal movements of buildings. On-line deformation monitoring of vertical and horizontal movements of adjacent buildings is carried out two years prior to the construction work for the North-South Metroline in Amsterdam, as presented by Netzel (2001a). The deformations are monitored with a geodetic network of computerized total stations and prism's fixed on the buildings providing monitoring data every two hours. Figure 8.1 to Figure 8.3 show results of vertical and horizontal building movements as a function of the time and temperature.

Z-deformation difference in the period
from 24/07 to 9/11/2001:   ca. 1,5 mm

Temperature difference
in the period from 24/07
to 9/11/2001:   25°
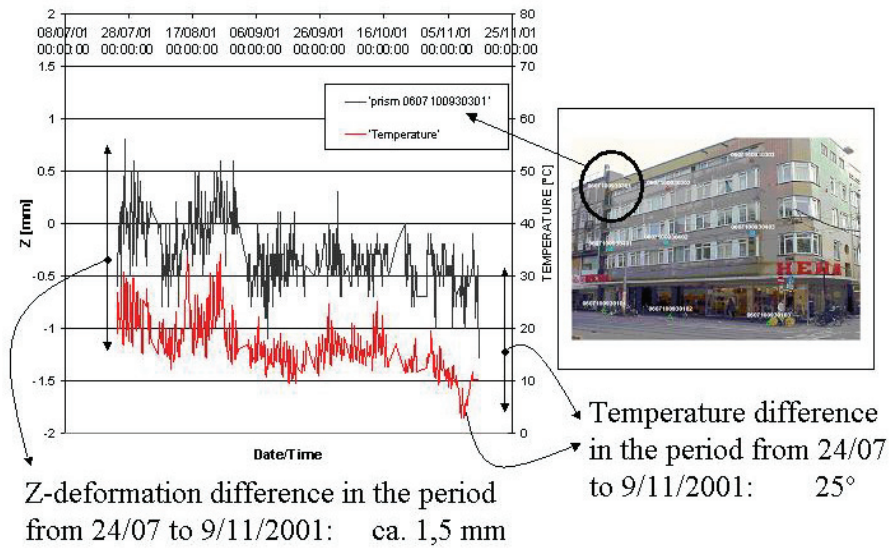
Figure 8.1: Natural vertical settlement in a half year period

Z-deformation difference
on 27/07/2001:   1 mm

Temperature difference
on 27/07/2001:   12°C
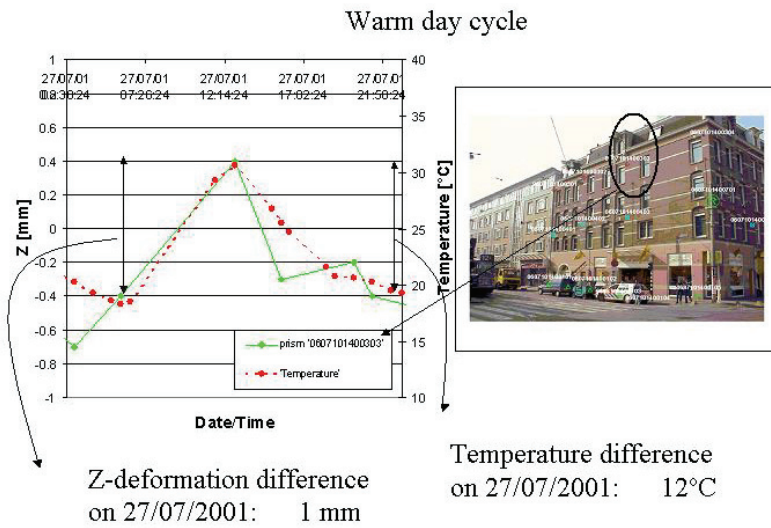
Figure 8.2: Natural vertical settlement on a warm day

Horizontal in plane movements
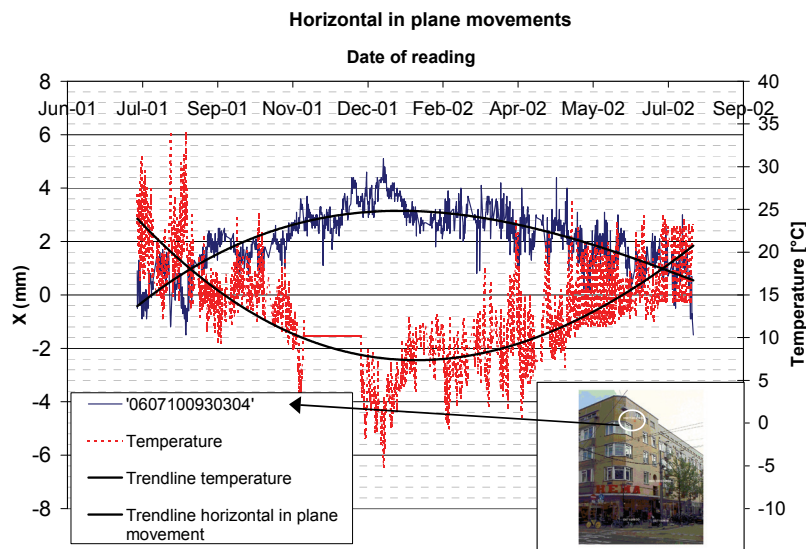
Figure 8.3: Natural horizontal building movement in a year period

Figure 8.1 and Figure 8.2 show natural vertical settlement differences of the considered masonry building. A daily fluctuation of 1mm and an absolute settlement of 1.5mm due to the absolute temperature difference between summer and winter time is recorded.

Figure 8.3 shows differential horizontal movements of ca. 4mm for an air temperature difference of ca. 20°C over the period of one year. The length of the considered façade wall is approximately 35m and the considered sensor is situated at the free end of the building. A rough analytical consideration, assuming a temperature coefficient α of ca. 6*10E-6 (1/K) for masonry, shows, that the horizontal elongation of a 35m wall for a ΔT of 20K is 4.2mm, neglecting the temperature gradient over the thickness of the wall (difference between outer and inner side of the wall) and the possible restraint by transverse walls and floors. It is also observed that the local temperatures on the wall itself are often significantly higher than the air temperature.

The so called "breathing" of the building shows significant fluctuations dependent on the temperature (differences) between winter and summer time, but even during one day between the morning and the afternoon.

8.2.3   Natural ground settlement behaviour

Long term consolidation of cohesive layers (creep) can affect the natural settlement behaviour of buildings. For Amsterdam conditions the masonry buildings on wooden piled foundations (end bearing piles) show natural settlement rates of the structures up to ca. 1.5mm/year, caused by autonomous long term settlement of soil layers on greater depth. The experience in Amsterdam shows that settlement rates of > ca. 2 mm/year can give raise to possible foundation problems.

Settlements due to natural fluctuations of the groundwater table are also a well known natural source of soil and building deformations respectively. The natural fluctuation of the high groundwater table in the Amsterdam situation (the average of the freatic ground water head is ca. 0.5 to 1m below surface level) varies within a bandwidth of ca. +/- 0.2m/year and depends on the weather, rainfall and temperature and can influence the seasonal building deformations.

8.3   Design criteria versus performance criteria

It has to be distinguished between damage criteria (angular distortion, deflection ratio's, absolute settlements or tilts) derived from a continuous line of the predicted deformations curve with a large amount of levelling points in the design stage (design criteria) and damage criteria monitored on site on

a few discrete monitoring points on a structure (performance criteria). The designer should carefully translate the design criteria into the performance criteria. If this translation is not considered major mistakes can occur in the control of the building movements on the construction site.

In the design stage the settlements are predicted from empirical analytical functions, for example the Gaussian curve, or from Finite Element analysis. In the latter case the mesh of the FE calculation (nodes and integration points respectively) defines the amount of points and therefore the continuous character of the predicted deformation line. The possible layout for discrete monitoring points on buildings depends on the practical restrictions of the structure. Although the design approach differs from the real layout of monitoring points, the design criteria are often used as performance criteria.

The following examples will illustrate the significant difference between performance criteria and design criteria and its consequences for the monitoring limits on the site. In the following example it is assumed that the discrete locations of monitoring points on building walls are chosen between ca. 5m and 7m (practically used distances). Three different situations are considered, two for a building in a sagging mode and one for a building in a hogging mode, see Figure 8.4.
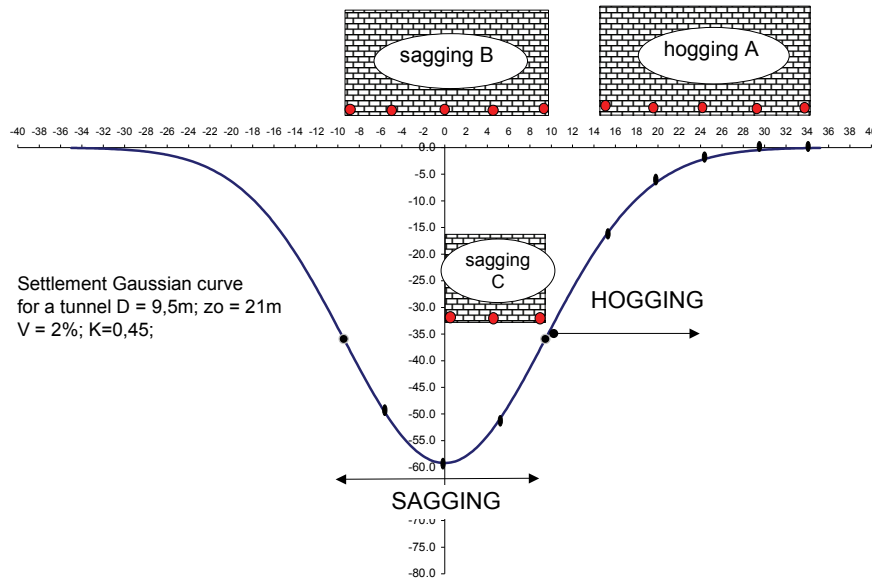
Figure 8.4: Example of difference between design and performance criteria for a Gaussian formed settlement trough
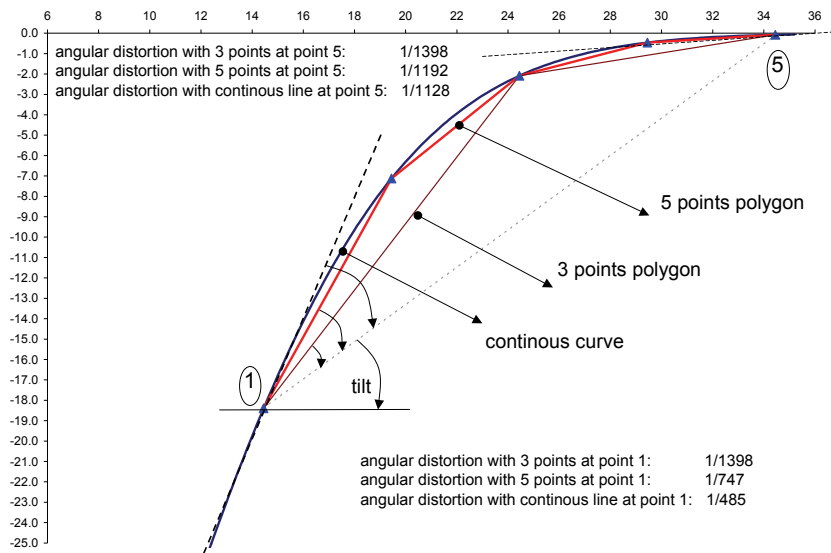
Figure 8.5: Calculation of performance and design criteria in the hogging zone situation A

Figure 8.5 shows the difference for the angular distortion in the hogging zone. The continuous (design) settlement line is compared to the use of three monitoring points and five monitoring points along the structure respectively. It is obvious that a major difference occurs in the value of the maximum angular distortion at point 1, with the value for 3 discrete points being a third of the value for the continuous line. In practice this would mean a highly non-conservative approach. If the limiting angular distortion of the design would be used as the performance criterion without a translation to the discrete points, three times as high values would be tolerated for the monitored angular distortions for the situation of three discrete monitoring points.
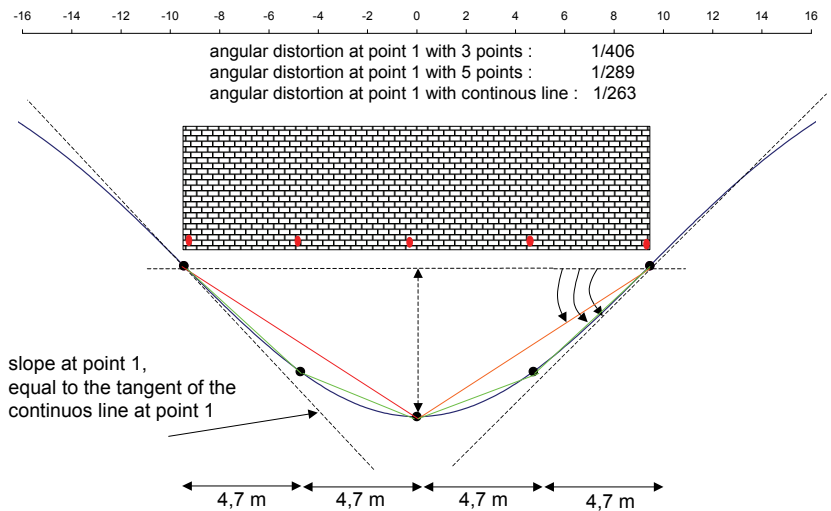
Figure 8.6: Calculation of performance and design criteria in the sagging zone situation B
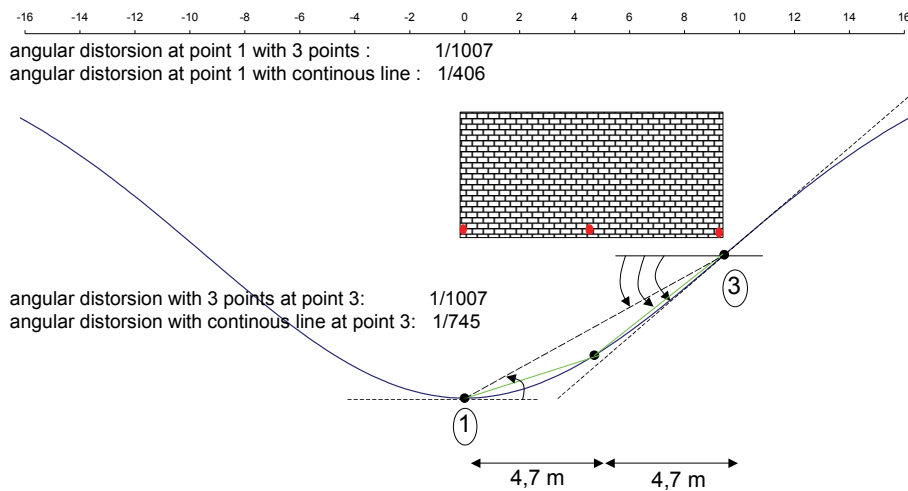
Figure 8.7: Calculation of performance and design criteria in sagging zone situation C

The differences in the sagging zone between the angular distortions for the design criteria and the performance criteria (for three to five discrete points) are up to a factor 2.5. In other words, if the values for the tolerable angular distortion from the design criteria are used for the performance criteria at the discrete monitoring points, the tolerable limits for the angular distortion in practice would be a factor 2.5 higher than the values set in the design ! This would lead to an unsafe monitoring limit of the angular distortion and means that much more damage (than predicted in the design) can occur, before trigger actions for mitigating measures are initiated by the monitoring data.

It should be mentioned that the considerations in the previous examples apply for clarifying the definitions of damage criteria in the design and the performance stage. In reality a difference between the theoretically predicted and the actually measured values occurs due to interaction effects. Nevertheless, the damage criteria have to be determined and checked according to the above stated principles.

In engineering practice absolute maximum surface soil settlements are often used as performance criteria. It should be emphasized, that such a criteria is only reliable if it is derived by a detailed damage prediction of differential settlements on the adjacent buildings in the design stage. The design considerations then have to be translated back to a performance value of the absolute surface soil settlement. If these considerations are omitted such a value is arbitrary and does not reflect the site-specific circumstances of the surroundings and damage risks of each individual project.

It is suggested, that independent of the parameters used as performance criterion in practice (deflection ratio, angular distortion, maximum settlement, tilt or differential settlements between neighbouring monitoring points) a translation has to be carried out from the theoretical design considerations to the monitoring system of the real structure.

9 CASE STUDY ON THE INFLUENCE OF TBM-TUNNELLING ON AN ADJACENT MASONRY BUILDING

9.1 General

A tunnel with a diameter of 9.5m has been constructed close to Rotterdam in Dutch soft soil with the slurry shield mode. The project was referred to as the Sophia Railway tunnel. The COB (Centre Underground Construction) carried out a full scale test on the influence of the TBM-tunnelling on the adjacent soil and building, Netzel (2002a). On line monitoring of deformations was carried out in the soil (on surface and subsurface level in transverse and longitudinal direction of TBM-tunnelling) and on an adjacent masonry building. Monitoring data were collected hourly during the passage of the TBM. The test field and the characteristic cross section regarding the tunnel and the adjacent building are shown in Figure 9.1 and Figure 9.2. The TBM passed the monitoring area in June 2002. The tunnelling progress was 20m/day, however three short TBM stops of several hours were recorded during the passage of the monitoring area. The TBM stops were needed for maintenance of the cutting wheel and the instrumentation in the boring machine. The monitoring results of deformations in the soil and the building as well as the damage observation (defect surveys) at the building are presented in the sections 9.2 and 9.3. A validation of the monitoring data with the analytical and numerical building damage prediction methods is described in section 9.4.
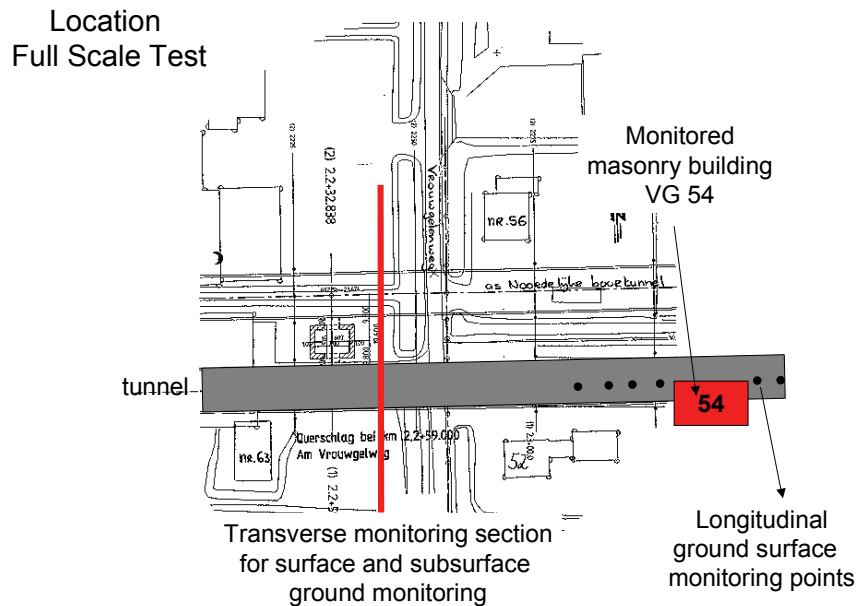
Figure 9.1: Overview COB Full scale test
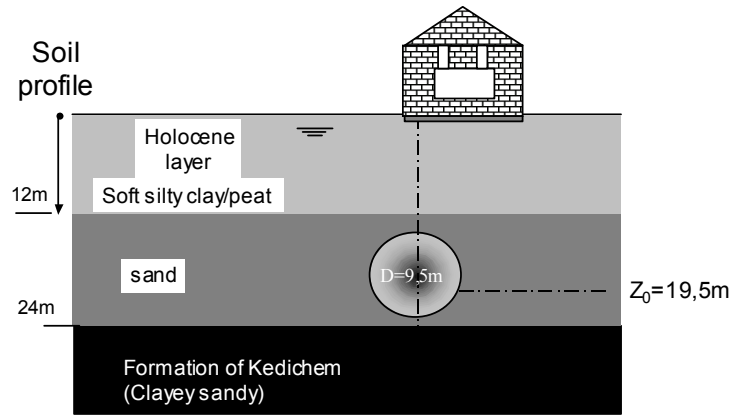
Figure 9.2: Characteristic cross section

Figure 9.3 shows the instrumentation of the ground monitoring cross section. Extensometers monitor the vertical subsurface ground settlements and inclinometers are installed in the subsoil to monitor the horizontal subsurface ground movements. Surface settlement points monitor the surface ground movements.
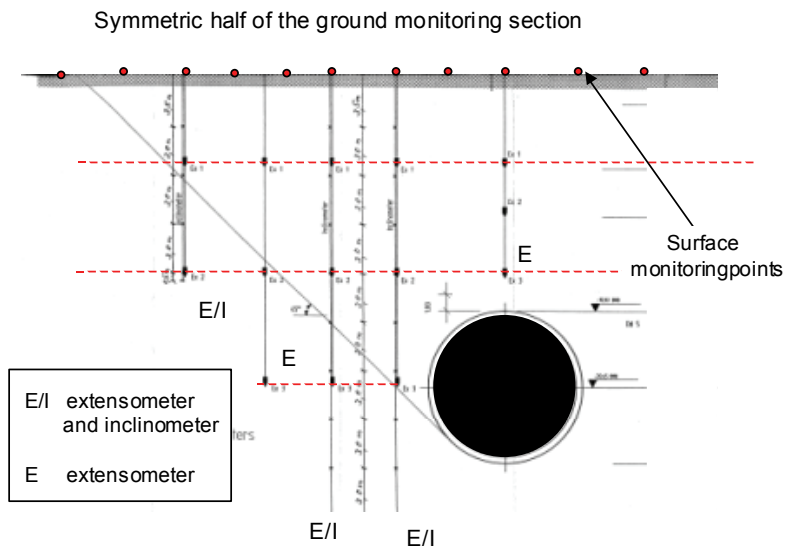
Figure 9.3: Transverse monitoring section for horizontal and vertical ground movements on surface and subsurface levels

Figure 9.4 shows the location of the monitoring points and the initial defect surveys of the façade walls of the adjacent building, before tunnelling. Initial slight cracks are situated around the doors and windows and recorded in a defect survey report.

(a) Transverse facade wall of building Vrouwgelenweg 54 with monitoring points en initial defect survey

(b) Longitudinal facade wall of building Vrouwgelenweg 54 with monitoring points and initial defect survey

Figure 9.4: Monitoring of the building

9.2 Surface ground movements

9.2.1 General

The high frequent monitoring provided an unique monitoring data set showing the detailed development of soil deformations during the passage of the TBM. For detailed information about subsurface vertical and horizontal ground movements and TBM-data (tail void grout pressures and volumes, face pressures etc.) it is referred to Netzel et al. (2004b) and Bezuijen et al. (2004).

9.2.2 Surface settlements of the transverse monitoring section

Figure 9.5 shows the development of the surface settlements in transverse direction during the passage of the TBM. The different settlement lines present different time steps, indicated in the figure in terms of the horizontal distance between the TBM and the monitoring section at a certain time step. The

global trend in the development of the ground settlements on surface level is a small heave effect due to the passage of the TBM front, followed by an incremental settlement due to unforeseen TBM stops and finally an incremental heave associated with the tail void grouting.

Transverse troughs on surface level during TBM passage
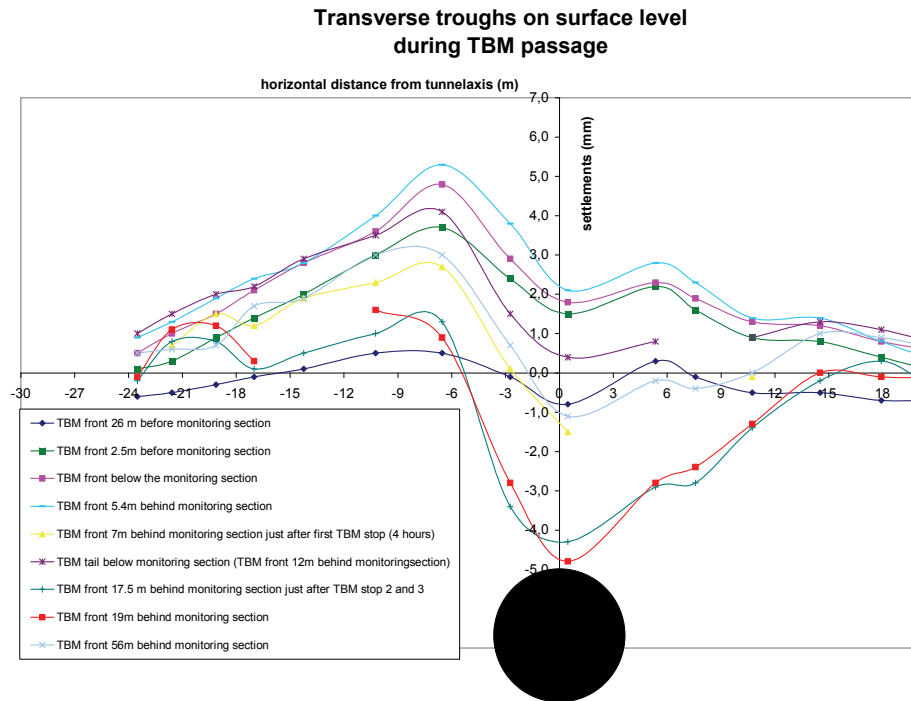
Figure 9.5: Development of surface settlement trough during TBM passage

From this figure the contributions of different phases of the TBM-tunnelling process can be deduced. Three major items are presented in the following figures and the corresponding incremental settlement distributions have been fitted with Gaussian parameters:

- Slight heave due to high face pressures (Figure 9.6).
- Settlement due to TBM stop during passage (Figure 9.7).
- Heave due to tail void grouting with high grout pressures and grout volumes respectively (Figure 9.8).

For the explanation of the characteristic Gaussian parameters V and K see section 2.

Case Study

**Transverse settlements on surface levels
due to passage of the TBM-face**
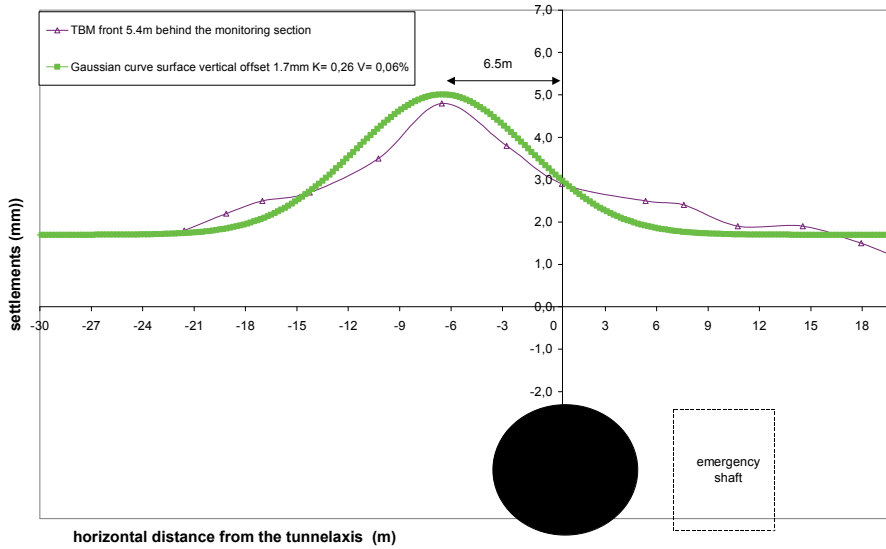
Figure 9.6: Incremental contribution to the surface settlements due to the face pressure

The face pressure causes heave on the surface level. It is recognized that an asymmetric distribution is monitored, which is caused by the existence of an emergency shaft in the soil situated close to the tunnel. As the influence area is wider than found with the fit of the Gaussian distribution, an offset of +2mm is used for the Gaussian curve. The Gaussian distribution describes the differential settlements in the area between the horizontal transverse distances of the tunnel axis of −18m and 18m well. The differential settlements beyond this area are negligible.

**Transverse settlements on surface level
due to passage of the TBM machine with several TBM stops**
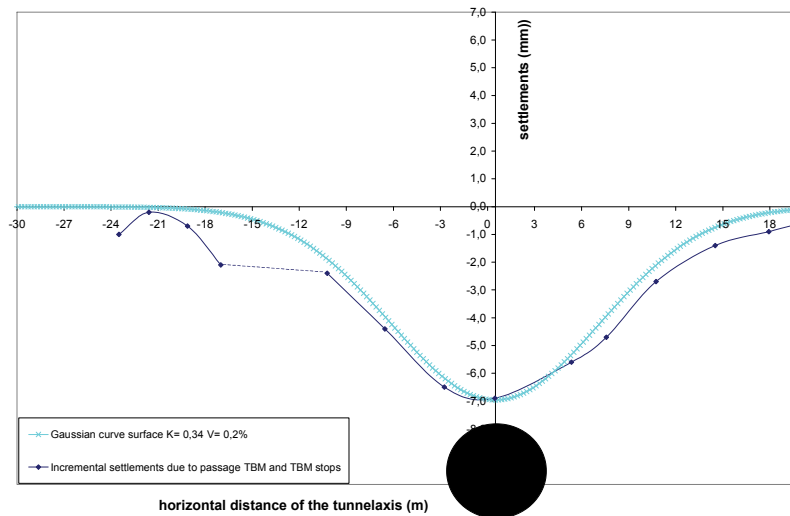
Figure 9.7: Incremental contribution to the surface settlements due to the TBM stop

Figure 9.7 shows incremental settlements due to the TBM stop, caused by the release of the balancing TBM pressures during the stop and the conicity of the machine. The TBM stop took place when the TBM face had passed the monitoring section by 7m.

Transverse settlements on surface due to tail void injection
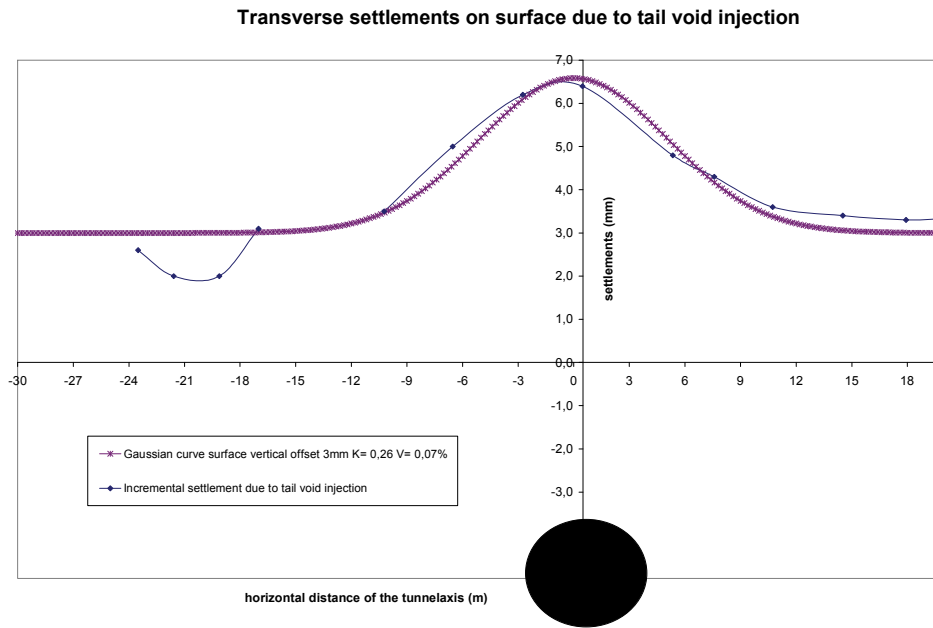
Figure 9.8: Incremental contribution to the surface settlements due to tail void grouting

Figure 9.8 shows clear incremental heave effects due to the high pressures and injection volumes of the tail void grouting. The influence area is wider than found with the fit of the Gaussian distribution, therefore an offset is used for the Gaussian curve. The Gaussian distribution describes the differential settlements in the area between the horizontal distances of the tunnel axis of −18m and 18m well. The differential settlements beyond this area are negligible.

9.2.3   Horizontal ground movements on surface level

Figure 9.9 shows the development of horizontal ground movements on surface level. Positive values of the movements at the left side of the tunnel present horizontal ground movements oriented towards the tunnel. An asymmetric distribution is monitored, which is caused by the existence of an emergency shaft situated close to the tunnel, at ca. 7m distance from the monitoring section in longitudinal direction.
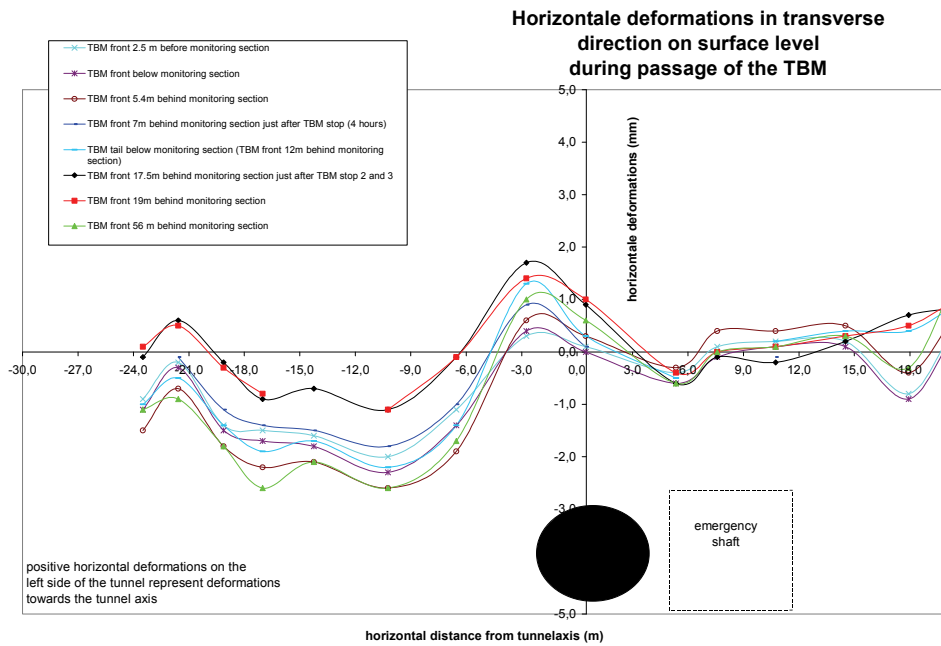
Figure 9.9: Horizontal ground movements in transverse direction

The horizontal deformations vary between +2mm and -3mm. In Figure 9.10 the incremental contributions of the three major parts of the tunnelling process are analysed, corresponding to the contributions considered in 9.2.2 for the vertical ground movements.
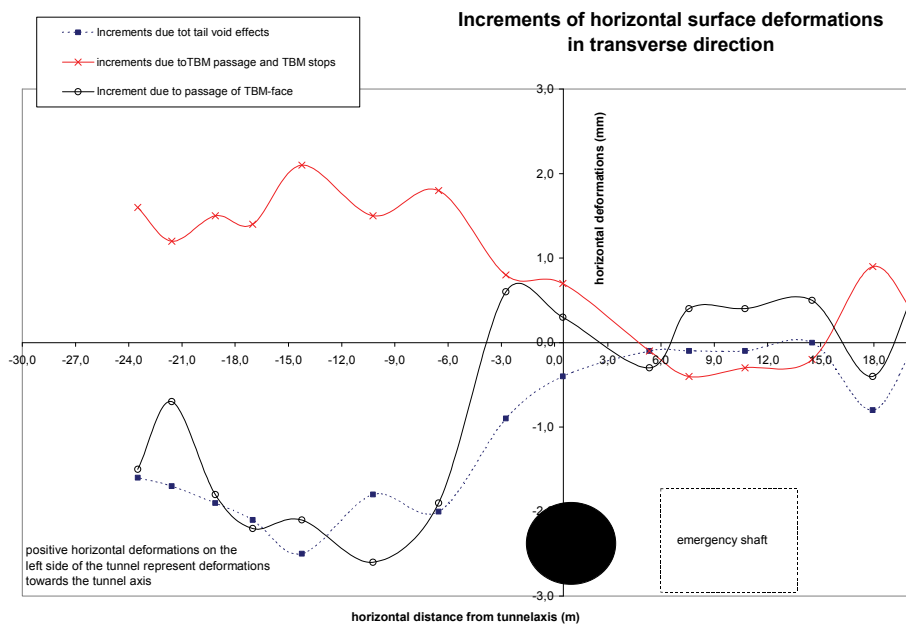
Figure 9.10: Incremental horizontal ground movements in transverse direction

Case Study

Regarding the horizontal movements the following conclusions can be drawn:

- If the vertical ground movements show heave heave, the horizontal deformations are directed away from the tunnel axis. If the vertical ground movements show settlements, the horizontal deformations are directed towards the tunnel axis. This qualitative conclusion is in agreement with the expectations of the relation of horizontal and vertical ground movements according to the empirically derived Gaussian curves.
- The maximum incremental horizontal ground deformation is ca. 35% of the maximum incremental vertical settlement.
- The overall horizontal ground deformations are very small with a maximum of 2.5mm and the lines in Figure 9.10 also show relative large fluctuations between the monitoring points. These fluctuations are explainable by less accuracy of the measurements in horizontal direction compared to the ground movements in vertical direction.

9.2.4 Surface greenfield settlement next to building VG 54

The test field showed fluctuations of the settlements in longitudinal direction of the tunnelling, depending on the applied TBM-process parameters and stops. The detailed evaluation of the distribution of the surface settlements in transverse direction at the location of the monitoring section (see 9.2.2) is used to derive the settlement distribution in transverse direction at the location of the building VG 54. The monitoring data of surface ground sensor nr. 2355 (location see sketch in Figure 9.11) on close distance (2m) of the building VG 54 is used to translate the greenfield Gaussian surface profile derived from the transverse monitoring section to the location of VG 54. Figure 9.11 shows the development of the surface settlements of the surface ground sensor nr. 2355, situated close to the building VG 54.
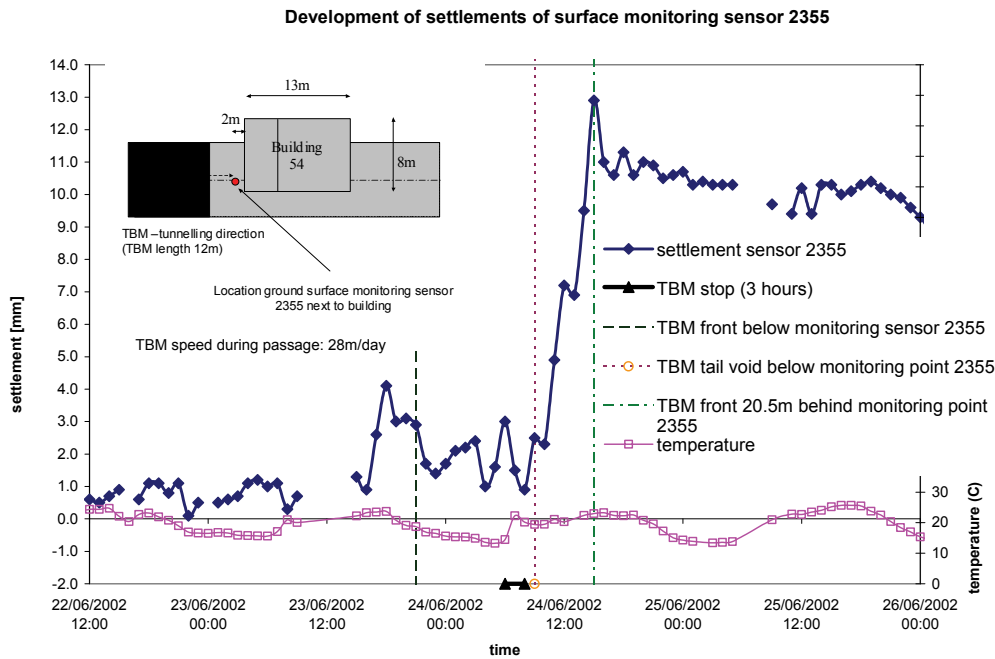
Figure 9.11: Development of surface soil settlements on 2m distance of the building VG 54
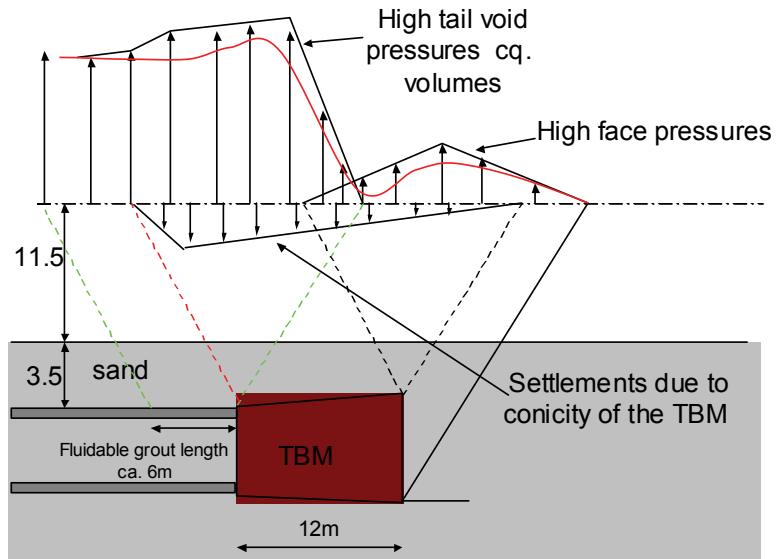
Figure 9.12: Qualitative development of surface settlement due to different TBM processes at sensor 2355

The resulting greenfield settlement profile in transverse direction at close distance of the building VG 54 is shown in Figure 9.13.
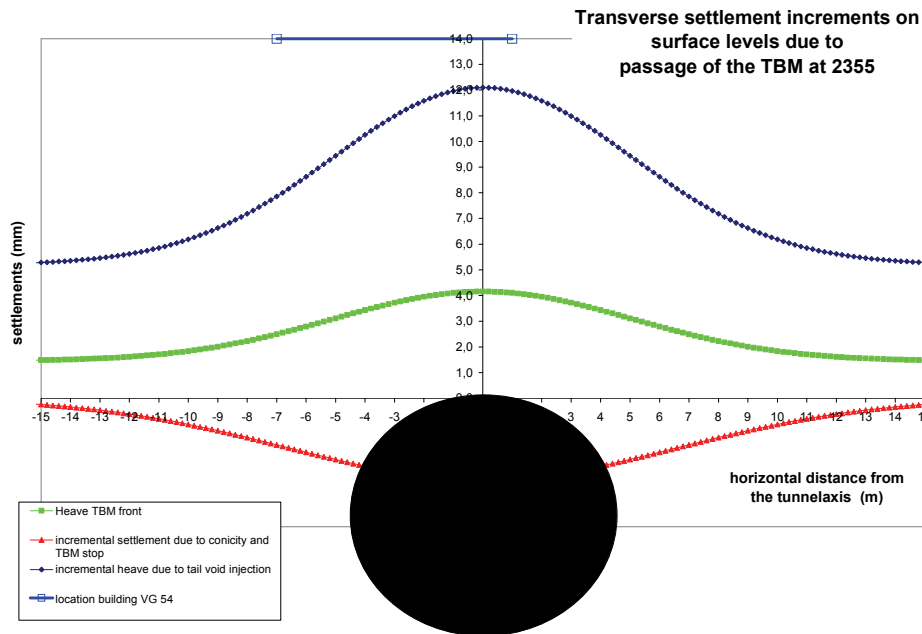
Figure 9.13: Development of greenfield transverse settlements at the building location

9.3   Building response

9.3.1   General

The masonry building VG 54 is founded on concrete strip footings. The initial defect survey before tunnelling shows slight cracking around the openings (maximum crack width 3mm). The location of the monitoring sensors fixed on the building and the results of the initial defect survey are given in Figure 9.4. The development of horizontal and vertical deformations of the transverse façade wall during the passage of the TBM is presented in the following sections.

9.3.2   Settlements of the transverse facade wall

Figure 9.14 shows that the transverse façade wall is heaving and tilting with a maximum value of 1/2000. The deformations are very well in agreement with the greenfield ground heave (see Figure 9.13), although interaction effects due to the stiffness of the building and its foundation (concrete foundation beam) are flattening the curvature of the greenfield line of the soil. This leads to an almost rigid tilt of the building in transverse direction for all the different phases of the TBM passage. The biggest heave increments develop when the TBM face is directly under the centre of the building and the tail void grouting is causing heave of the entire building (see Figure 9.12 for spreading of the influence of tail void grouting to the surface, being the foundation level of the building).
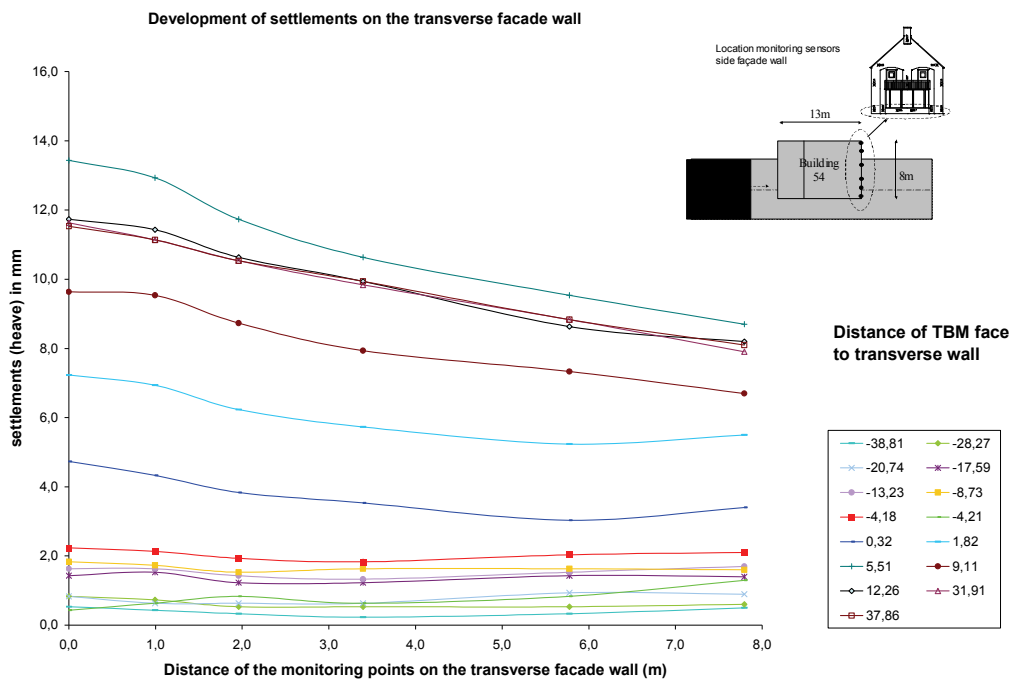
Figure 9.14: Development of vertical deformations of the transverse façade wall during TBM passage

9.3.3   Horizontal deformations of the transverse façade wall

Figure 9.15 shows the development of the horizontal movements of the façade wall.
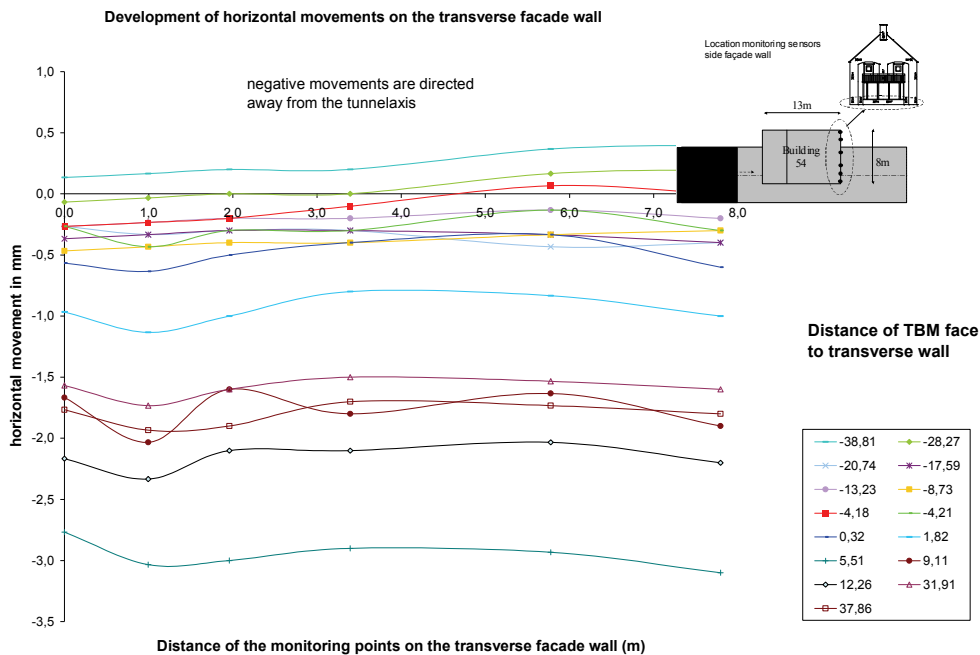
Figure 9.15: Development of horizontal movement s of the transverse façade wall

The largest horizontal translation (3mm) develops when the TBM face is directly under the centre of the building and the tail void grouting is influencing the entire building (spreading of the influence to the surface, see Figure 9.12). The maximum horizontal movement is oriented away from the tunnel axis corresponding with the heave effect of the vertical settlements. The horizontal strain (difference of horizontal movements along the wall) is negligible as the building undergoes an almost rigid horizontal translation for all the different stages of the TBM passage.

9.3.4 Defect survey façade walls before and after TBM passage

A defect survey of the facade wall has been repeated after TBM passage and compared with the initial survey. No additional damage is observed and the existing crack widths did not increase. Despite the monitored deformations of the building as described in 9.3.2 and 9.3.3 no damage is observed due to the passage of the TBM, thus the damage can be classified as negligible.

9.4 Validation of damage predictions with monitoring data

9.4.1 General

This section presents a comparison between the empirical analytical damage prediction, the numerical damage prediction and the observed damage and deformations of the building. The vertical greenfield (differential) deformations (see Figure 9.13) are used as input in the analyses. The very small magnitude of the monitored horizontal ground movements and the low accuracy of the measurements of the horizontal ground movements (see 9.2.3) does not allow to assume a greenfield profile for the differential horizontal ground movements, which could have been used as a valuable input for the damage predictions for the current case. Additionally the monitored horizontal differential movements along the building are shown to be negligible (see Figure 9.15). The vertical greenfield movements are imposed on the building and the damage prediction is carried out with:

- Empirical analytical damage prediction method (modified according to the review results presented in 3.3). This method does not take into account the interaction between soil and building.
- 2D numerical soil-structure interaction model. The stiffness of the soil is modelled as a bedding interface below the building. No horizontal interaction between building and soil is taken into account. The details of the model are given in 9.4.3 and Hart 't et al. (2005) respectively. It is noted, that these simplified interaction models were the first steps in the research program and were performed in 2003 to 2005. The advanced numerical interaction models presented in sections 5, 6 and 7 are developed later in 2005 and 2006.

The results of both prediction methods are compared with the actual measured response of the building in terms of deformations and damage (see 9.3).

9.4.2   Empirical analytical damage prediction with the modified LTSM

The vertical green field movements are projected on the location of the building (see Figure 9.16) and the damage is predicted according to the modified LTSM described in section 3. The transverse façade wall undergoes a hogging deformation.
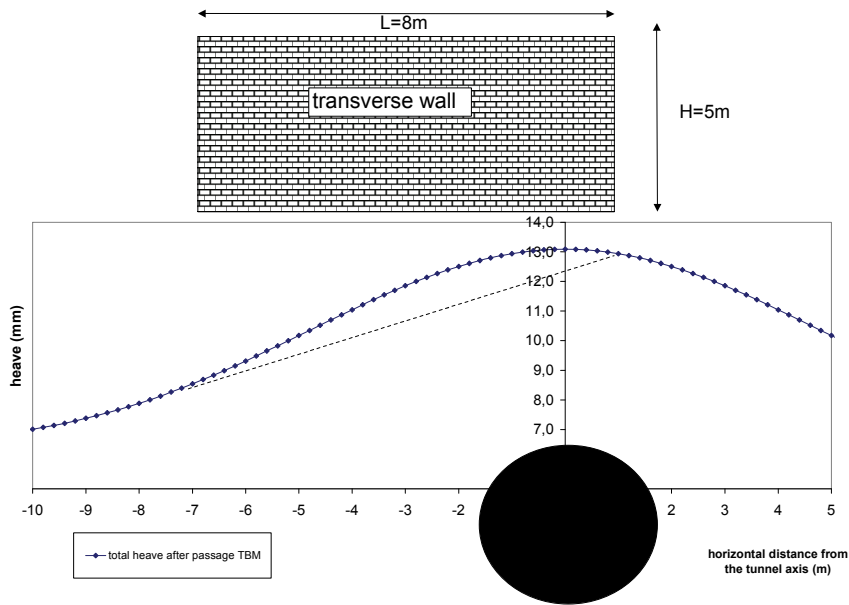
Figure 9.16: Hogging situation vertical settlements of the transverse facade wall

	Length wall	H	L / H	Max. heave	min. heave at the outer end of the building	tilt (rigid body rotation)	max. slope	min. slope	min. angular distorsion	max. angular distorsion	deflection	deflection ratio	Max. total strain	damage class
	m	m	L/H	mm	mm	[1/…]	[1/...]	[1/...]	[1/...]	[1/...]	mm			
neutral axis at the bottom edge	8	5	1,6	13	8,5	1778	1390	3400	6372	1167	1,2	0,00015	0,00041	negligible

Table 9.1: Results damage prediction with modified LTSM

Case Study

The calculated maximum tensile strain is 0.041% resulting in damage class "negligible". The limiting tensile strain for the damage class negligible is 0.05%, see Figure 3.5. These results correspond well with the observations of the defect survey before and after the TBM passage, indicating no damage.

9.4.3   Numerical damage prediction

The numerical model includes:

- Geometry of the transverse facade wall including the openings of doors and windows.
- Nonlinear material behaviour of masonry with a smeared crack model. The concrete foundation beam is modelled with linear elastic material behaviour. A retrospective check on the induced stresses in the concrete beam show that this assumption is reasonable as the tensile strength of concrete is not reached and it can be assumed that the uncracked concrete behaves linearly elastic.
- The initial loading situation with dead weight and 50% of the mobile loads is taken into account. The first calculation phase generates the initial stress situation in the façade wall.
- The normal stiffness of the interface below the building represents the soil stiffness. The interface has nonlinear properties. A "no tension" interface is applied for the vertical connection of the building and the soil. A gap can form between building and soil if the initial compressive foundation stresses are reduced up to zero due to redistribution of the loads, caused by the imposed ground deformations.

For further details of the numerical model it is referred to Hart 't et al (2003, 2005).

The vertical greenfield movements of the three characteristic stages of the TBM-process (see Figure 9.13) are imposed on the building in a phased calculation. The development and changes of the principal tensile strains and cracks in the different stages are shown in Figure 9.17. The maximum tensile strain increases with max. 8% with respect to the initial load situation and appears in the last phase of the calculation (maximum heave due to TBM tail void grouting) in the masonry below the wide window opening. The changes of the maximum strains are thus very small. The absolute maximum principal tensile strain level observed in the model after passage of the TBM is 0.0143%. The maximum initial tensile strain is 0.013%, leading to inital hairline cracking around the windows, because the numerical threshold value for crack initiation is exceeded. This threshold value is defined as the quotient of tensile strength and Young's modulus and amounts in the current model 0.3/6000=0.005%. This initial cracking is not further increased by the very small increase of tensile strains due to the passage of the TBM. The damage response of the numerical analyses is therefore in agreement with the empirical analytical damage predictions and the real observations.
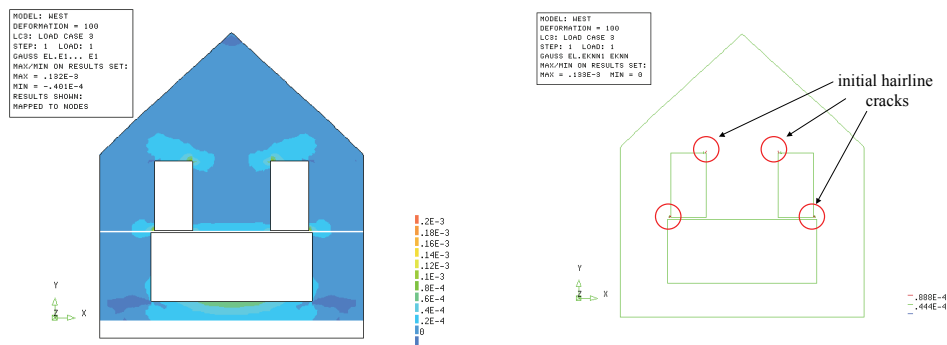
(a) initial loading situation
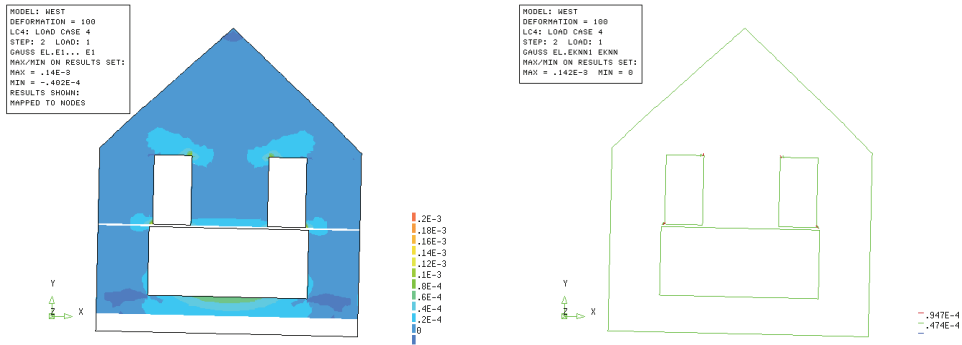
(b) pasaage of TBM front
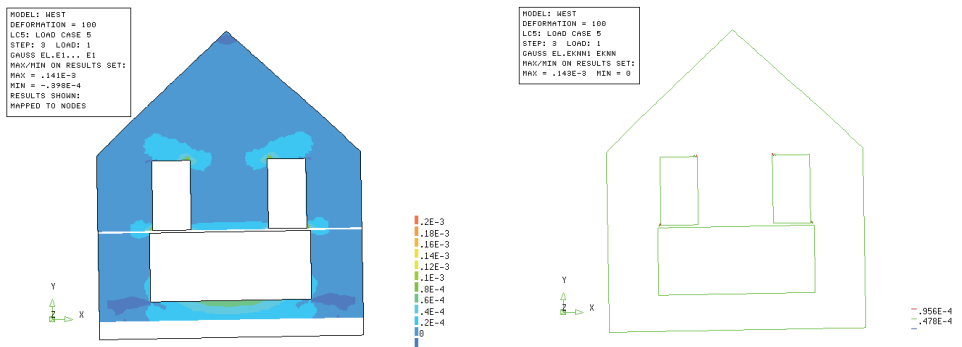
(c) passage TBM
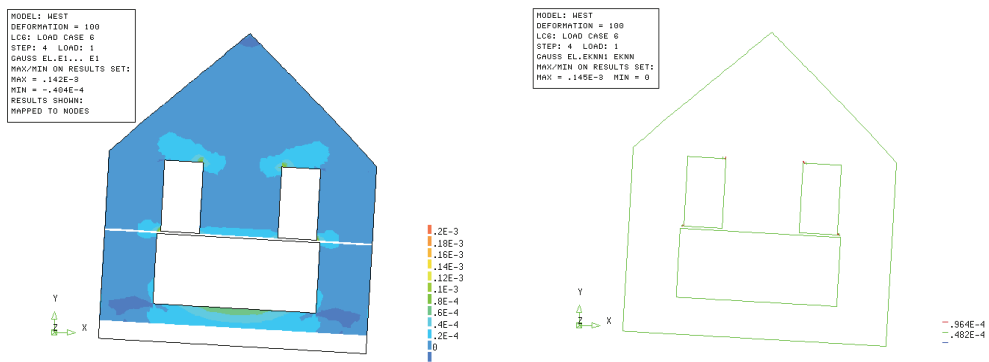
(d) passage TBM tail

Figure 9.17: Development of principal tensile strains and cracks in the transverse façade wall

10 SUMMARY AND CONCLUSIONS

The influence of construction works on the surrounding buildings can have a major impact on the political, economical and technical aspects of a building project in urban surrounding. Prediction of ground movements and the corresponding level of building damage of adjacent structures forms an important part of risk management for excavation works. The aim of this research was to examine and improve existing design approaches and develop more advanced damage prediction methods, which can be used in the design stage of a project to determine the expected damage level of surrounding buildings due to excavation induced ground deformations. Five main research topics can be distinguished:

- Literature study on empirical analytical prediction methods of greenfield ground movements for different sources of excavation works in urban surrounding (TBM-tunnelling, excavation of building pits and groundwater lowering). Moreover the field data of ground movements from three Dutch TBM-tunnelling projects were analysed and compared to the approaches derived for projects outside the Netherlands.
- Review and further development of the existing empirical analytical prediction method (Limiting Tensile Strain Method; LTSM), which is widely used in engineering practice to predict building damage due to imposed greenfield ground deformations.
- A numerical study on the effects of soil-structure interaction on the damage response of masonry buildings founded on shallow foundations for the example of tunnelling induced ground movements.
- Examinations on the translation of the settlement predictions in the design stage into monitoring criteria of buildings, used for the risk control during the construction stage.
- Analyses of the monitoring data of a full scale test, showing the response of a masonry building founded on a shallow foundation due to TBM-tunnelling. The monitored results were compared with the different prediction methods of the building damage.

In this section the results are summarized and the main conclusions of all different parts are addressed separately.

Prediction of greenfield ground movements

From the analyses and evaluation of the monitored settlement field data of three Dutch **TBM-tunnelling** projects, it is shown, that the field data can be properly fitted with a Gaussian settlement distribution of the settlement trough. A bandwidth of K-values is suggested for the prediction of the surface settlement transverse trough for comparable Dutch soil conditions. The K-value determines the point of inflection and thus the steepness of the trough. The measured volume changes of the soil at the surface of all the three Dutch TBM-tunnelling projects varied between 0.15% and 1.5% and showed settlements (volume loss) as well as heave effects (volume increase due to intensive front pressures and tail void grouting applied in the TBM). The fit of the longitudinal settlement wave using the cumulative probability curve according to Attewell et al. (1986) showed slight underestimations of the steepness of the monitored longitudinal troughs, but is proven to be a good approach, also for Dutch tunnelling projects. The longitudinal trough is a temporary trough that occurs during the passage of the TBM, whereas the transverse trough is permanent after the TBM has passed. The important process parameters of the TBM-tunnelling process, determining the ground settlement response, are the applied front pressure and the tail void grouting. On-going research is focused on the numerical implementation of these parameters in order to get advanced settlement predictions as a function of these process parameters.

It is also shown that the wide bandwidths of the empirical approaches from the literature, which are used to predict ground movements due to excavation of **building pits**, reveal the restrictions of these methods and require careful engineering judgement when applying them in a preliminary design stage for a project. The methods should only be used as initial guidance and special attention is required when extrapolating the empirical observations of other projects to the project-specific conditions of a new

Summary and Conclusions

situation. For detailed design purposes it is considered necessary to use powerful numerical modelling to achieve more reliable predictions of ground movements, taking into account the detailed site-specific circumstances like construction sequence, nonlinear soil properties and strutting or anchoring support per project. In engineering practice growing experience is gained in the numerical prediction of ground deformations due to the excavation of a building pit. The choice of the adequate constitutive soil material model and the input of stress-dependant soil stiffness parameters, derived from thorough soil investigation, play an important factor in these predictions.

Review of the Limiting Tensile Strain Method (LTSM)
The limiting tensile strain method is the design approach currently applied for the prediction of building damage due to excavation projects in urban surrounding. The review of the current LTSM is carried out, because several fundamental questions have been raised when using the method in engineering practice. The review leads to the following recommendations for a modified LTSM:

- The equations used for the calculations of the strains according to the current LTSM imply a simplified shear form factor to take into account the contribution of shear deformations. It is however shown that the use of this factor can lead to an underestimation of the damage. New Equations with a modified shear form factor, derived from the more exact theory of elasticity and the method of virtual work respectively, as presented by Timoshenko et al. (1971), are presented in this study. It is recommended to use these equations with the modified shear form factor for the LTSM.

- The currently used assumption of cutting off the beam model of a structure at the 1mm influence line and only considering the part of the structure inside the influence area is not straightforward. Structures extending the influence area of the ground deformations should be considered with their entire length. It is shown that when only a part of the structure inside the influence area is considered, this may result in a significant underestimation of the damage.

- The current approach of the LTSM assumes that a structure extending over the hogging and sagging part can be partitioned for the damage prediction into a separate hogging part and a sagging part. These parts can then be considered separately and independent from each other for the damage prediction. It is shown that this is only valid for structures where the difference between the tilt of the separated parts and tilt of the total structure does not differ more than 15%. If the difference is greater, additional numerical beam calculations for the entire structure are required to quantify the influence. Neglecting this guideline can lead to an underestimation of the damage.

- The two approaches of the current LTSM presented in literature are not consequent in the use of the greenfield damage parameter as input for the damage prediction. Boscardin et al. (1989) use the angular distortion and Burland et al. (1974, 2001) use the deflection ratio as input parameter for the influence of the differential vertical ground movements. It is shown that for Gaussian formed ground deformations the angular distortion has to be used for the calculation of the diagonal strains in the structure and the deflection ratio has to be used for the calculation of the bending strains. Other procedures can cause a significant under- or overestimation of the strains and consequently the damage.

- The increasing damage susceptibility of the hogging deformation mode is an empirical observation born in practice. The current LTSM reflects this observation with the fictitious assumption of the location of the neutral axis of the structure at the bottom edge. It is shown, that if only the influence of vertical ground movements is considered, this assumption does not necessarily provide the aimed effect for all *L/H*-ratio's for structures, For the combination of vertical hogging mode deformations with differential horizontal ground movements introducing tensile strains at the bottom edge of the building, this assumption is however shown to be a reasonable approach.

- The current LTSM suggests a fictitious assumption of an *E/G* value of 12.5 for a frame structure. This is shown not to be straightforward. Additionally the concept of the LTSM for obtaining strains should be limited to wall structures. For frame structures the modification of moments and shear forces in the beams and columns of the structure due to the imposed ground deformations is of

Summary and Conclusions

prime interest to judge the damage sensitivity. A first step for a modified approach for frame structures is therefore presented.

- Additional factors influencing the damage response of a structure are described in section 3.4. Empirical bandwidths for implementation in the LTSM are given for the influence of the initial building condition and the time dependant development of the ground deformations in combination with beneficial creep or relaxation effects in the structure. Additionally, empirically based limiting values for tilt of tall structures with respect to the stability and limiting differential settlement values for the functionality of the connections of services with buildings, as derived from the literature, are given.

Numerical soil-structure interaction

As the analytical empirical LTSM approach neglects the soil-structure interaction, an extensive numerical study has been conducted to study the influence of soil-structure interaction on the building damage due to imposed ground movements. The case of ground deformations induced by TBM-tunnelling and its influence on masonry walls founded on shallow foundations is investigated. The location of the building in the settlement trough of the tunnelling process (hogging or sagging zone), the length to height ratio of the wall (*L/H*), the type of masonry structure (massive wall and façade wall) and the soil stiffness is varied. Different settlement performances of the tunnelling process are considered in order to vary the imposed differential horizontal and vertical ground movements at the location of the building. A nonlinear smeared crack model for the masonry is used and nonlinear properties of the interface between soil and structure are varied to analyse its influence on the building response.

A systematic approach is developed for the interpretation of the numerical damage results in the walls and the comparison of the numerical damage results with the LTSM damage predictions, using the *modified LTSM* method presented in this thesis. The final results are presented in diagrams explaining the differences in the expected damage of the numerical interaction calculations and the LTSM.

The most important conclusions are summarized below.

- For all considered numerical interaction calculations it is shown that for the same distribution of imposed greenfield ground deformations, *the damage sensitivity of a masonry wall increases with increasing soil stiffness*. A decreasing soil stiffness results in beneficial interaction effects, reducing the building damage.
- The nonlinear material behaviour of the wall, including *the modelling of smeared cracking, shows to have significant influence on the damage development* once a crack is initiated. A numerical prediction of elastic tensile strains using a linear elastic material model for the wall underestimates the damage significantly. An interaction analyses should take into account nonlinear material behaviour of the wall and the interface in order to obtain appropriate damage results.
- *The numerical model for the interface between the soil and the structure has important influence on the damage in the wall*, because it determines the degree of transfer of differential horizontal ground movements to the building. In the analyses it is distinguished between a smooth and a rough interface. The smooth interface neglects any transfer of horizontal ground movements resulting in ground slipping along the building. This case represents a fictitious situation, where only differential vertical ground movements are contributing to the introduction of strains and damage in the building. It is emphasized that the assumed smooth case represents an extreme theoretical assumption, because in reality a certain amount of horizontal shear stresses will be transferred by friction between building and soil. The rough interface implies a realistic Coulomb friction relation between the wall and the building. The yield function of horizontal shear stresses across the rough interface is modelled as elasto-plastic behaviour controlled by the magnitude of normal stress and the angle of friction. The assumed rough case is considered to represent a realistic nonlinear interface behaviour between building and soil.

Summary and Conclusions

For the *rough cases*, the horizontal interaction between building and soil mobilizes horizontal shear stresses at the bottom edge of the building, which introduce horizontal strains in the building. These strains are tensile strains for the considered tunnelling hogging zone and compressive strains for the tunnelling sagging zone. For the hogging zone the damage therefore increases and for the sagging zone the damage decreases if the rough case is considered. The magnitude of the horizontal shear stresses which are activated via the interface depend on the properties of the interface, the vertical loads of the building and the differences in the horizontal stiffness between soil and building.

For a tunnelling hogging zone the damage for the *smooth case* is in general significantly smaller than for the rough case, because no horizontal tensile strains are introduced at the bottom edge of the building by the differential horizontal ground movements. For the sagging zone, however, the opposite holds, because the differential horizontal ground movement in a tunnelling sagging zone would cause compressive strains at the bottom edge of the wall, if they could be transferred to the building via the interface. However these compressive strains cannot be transferred by friction because a smooth interface is assumed.

- **Hogging zone:** The results of the damage predictions of relevant numerical cases in the hogging zone, compared to the predictions with the modified LTSM, are summarized in Figure 10.1. The horizontal axis of the diagram shows the greenfield values for the angular distortion, the deflection ratio and the horizontal ground strain caused by the TBM-tunnelling at the location of the buildings, but in absence of the building. These greenfield values are used as input for the predictions with the modified LTSM, because interaction is neglected in the LTSM. The vertical axis shows the resulting damage class for the LTSM and the numerical interaction results, based on the damage classification system derived by the BRE (1981). It is emphasized that the numerical results are obtained with a fully interaction calculation including non-linear respons of the structure (smeared crack model) and non-linear behaviour of the interface between soil and structure.
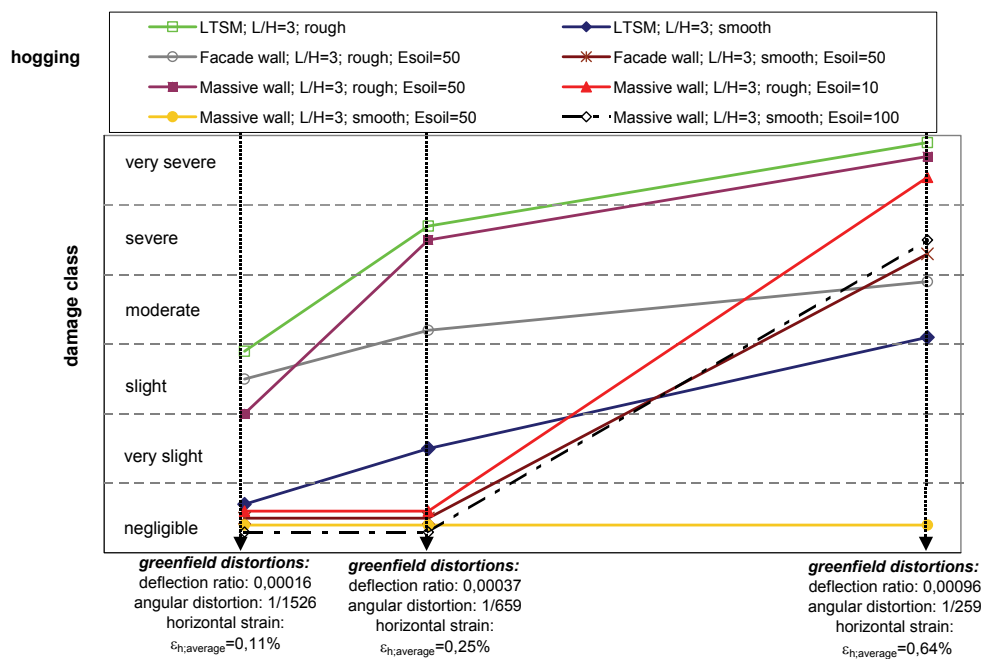
Figure 10.1: Damage results for considered hogging zone cases

Summary and Conclusions

It is noted that the linear connection lines between the three investigated greenfield distortions are only for visual purpose to identify the three results belonging to one case. No linear interpolation can be applied for intermediary greenfield distortions once cracking is initiated.

A characteristic TBM-tunnelling induced hogging zone implies both greenfield vertical and horizontal ground deformations. A LTSM damage prediction in the hogging zone neglects differential horizontal greenfield ground movements and is therefore incomplete, providing an unsafe damage prediction compared to the numerical interaction analyses with rough interfaces. Neglecting of horizontal ground movements and horizontal interaction for a damage prediction is only considered to be acceptable if detailed information is available which confirms the existence of an effective slipping layer between building and soil.

For the *massive wall*, the rough interface and the range of the medium (E_{soil}=50MPa) to high soil stiffness (E_{soil}=100MPa), the predicted damage for the hogging cases shows very good agreement between the LTSM results with the assumption of full transfer of horizontal ground movements and the numerical interaction analyses. However, the LTSM overestimates the damage for the massive wall and the low soil stiffness (E_{soil}=10MPa) and thus provides a conservative damage result compared to the numerical interaction analyses. The beneficial interaction effects, decreasing the damage sensitivity with decreasing soil stiffness lead to this overestimation of the LTSM damage for the low soil stiffness.

For the *façade wall* and the rough interface, the predicted damage for the hogging cases and the medium soil stiffness and the high friction coefficient of the interface show very good agreement between LTSM and the numerical interaction analyses. The other cases show an overestimation of the LTSM damage results compared to the interaction analyses. The overestimation is very conservative for the low soil stiffness. This is explained by the beneficial interaction effect with decreasing soil stiffness.

- **Sagging zone:** The damage results of relevant numerical cases in the sagging zone, compared to the LTSM predictions are summarized in Figure 10.2.
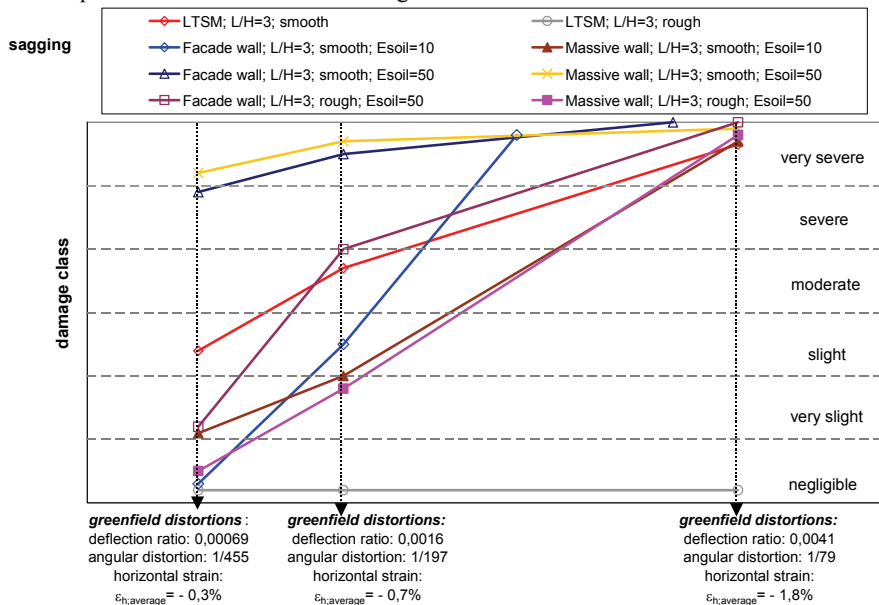
Figure 10.2: Damage results for considered sagging zone cases

Summary and Conclusions

It is noted that the linear connection lines between the three investigated greenfield distortions are only for visual purpose to identify the three results belonging to one case. No linear interpolation can be applied for intermediary greenfield distortions once cracking is initiated.

A TBM-tunnelling induced sagging zone implies differential horizontal greenfield ground deformations which can cause horizontal compression at the bottom of the building. A LTSM damage prediction implies a full transfer of the beneficial compressive horizontal greenfield movements in the sagging zone and therefore results in an unsafe damage prediction compared to the numerical interaction results for a rough interface. It is therefore recommended for the LTSM to neglect the beneficial horizontal compression transferred to the building due to differential horizontal strains for tunnelling induced sagging cases.

For the smooth case, the LTSM can provide an unsafe underestimation of the damage compared with the results of the numerical interaction analyses for the medium of high soil stiffness. A clear smooth case for an interaction calculation is however not a realistic situation in engineering practice. A certain degree of transfer of friction shear stresses between building and soil will always occur. The above suggested LTSM approach for tunnelling induced sagging cases is therefore considered to provide a reliable damage prediction for engineering practice.

Figure 10.3 gives an impression of the typical numerical building response for the sagging zone. Contour plots of cracking strains are shown, along with a schematic interpretation of the deformation modes and interaction effects for the smooth case and the rough case.

Massive masonry wall	
Sagging zone E_{soil} =50MPa, L/H=3 ; smooth interface damage class: very severe	Sagging zone E_{soil} =50MPa, L/H=3 ; rough interface damage class: very slight

It is emphasized that the scale of the deformed mesh plot is not equal for both cases shown above
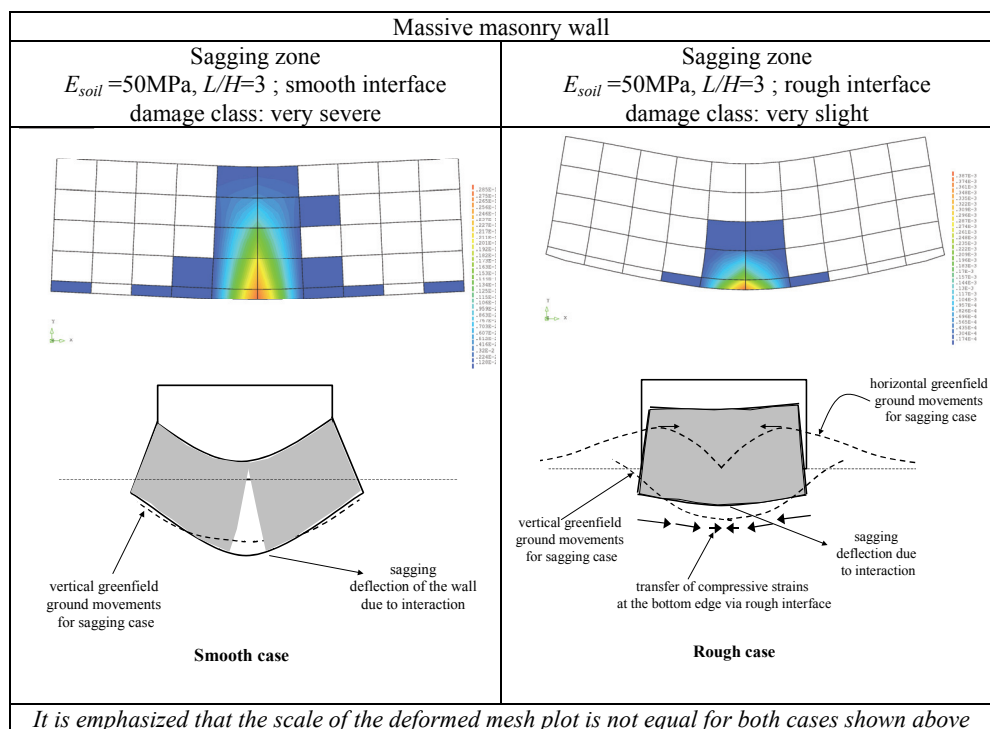
Figure 10.3: Examples of the numerical damage patterns in the sagging zone

The numerical interaction analyses give valuable insight in the complex interaction effects between soil and structure. It is also shown, that for the general understanding of the damage sensitivity due to differential building settlements, it is crucial to distinguish between settlements of buildings which are caused by the building loads themselves (dead weight and or mobile loads) and differential building deformations imposed by soil deformations due to nearby excavation works.

Summary and Conclusions

The latter situation is in general far more sensitive to damage. For the influence of dead weight cases the building and its loads are the actors and the soil is the reactor. For the imposed ground deformations it is the opposite. This has major influence on the different interaction effects for both situations.

Monitoring criteria

The risk control of influences during the construction works on the surroundings requires monitoring of the adjacent structures. The design considerations of the damage predictions have to be translated into a monitoring plan in order to describe deformation limits, which can then be used for the control of the construction process. If these limits are reached an evaluation of the monitored effects has to be carried out and decisions have to be made on considering mitigating measures to manage the building process within the predicted damage profile.

The designer should carefully translate the design criteria into the performance criteria. If this translation is not considered, major mistakes may occur in the control of the building movements on the construction site. The example in Figure 10.4 shows the difference from a continuous line of the predicted deformations curve with a large amount of points in the design stage (design criteria) and damage criteria monitored on site on a 3 discrete monitoring points on a structure (performance criteria).
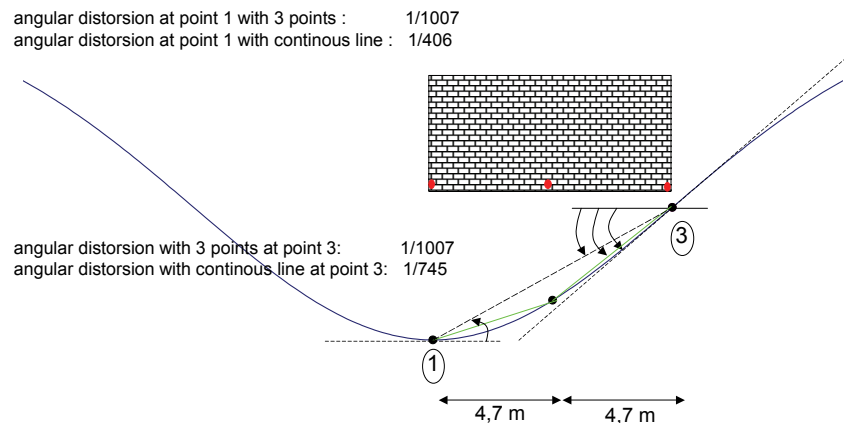
Figure 10.4: Example for difference between design and performance criterion

If the values for the tolerated angular distortion from the design criteria are applied on the performance criteria of the discrete monitoring points, these tolerable limits would in practice be up to a factor 2.5 higher than the values set in the design. This would lead to an unsafe monitoring limit of the angular distortion and means that much more damage than predicted can occur, before trigger actions for mitigating measures are initiated by the monitoring data.

In engineering practice absolute maximum surface soil settlements are often used as performance criteria. It is emphasized here that such criteria are only reliable if they are derived by a detailed damage prediction of differential settlements on the adjacent buildings in the design stage. These design considerations then have to be translated back to a performance value of the absolute surface soil settlement. If these considerations are omitted such values are arbitrary and do not reflect the site-specific circumstances of the surrounding structures and damage risks of each individual project.

It is recommended, that, independent of the parameters used as performance criterion in practice (deflection ratio, angular distortion, maximum settlement, tilt or differential settlements between neighbouring monitoring points) a translation has to be carried out from the theoretical design considerations to the monitoring system of the real structure.

Summary and Conclusions

Case study
COB (Centre Underground Construction) carried out a full scale test on the influence of the TBM-tunnelling on the adjacent soil and nearby buildings for the Sophia railway tunnel.

A tunnel with a diameter of 9.5m and a depth of 19.m has been constructed close to Rotterdam in Dutch soft soil with the slurry shield mode. The tunnel passed an adjacent masonry building founded on a shallow foundation.

On line monitoring of ground and building deformations was conducted as well as defect surveys before and after tunnelling to register the damage development of the building due to tunnelling. A validation of the monitoring data with the analytical and numerical building damage prediction methods is described in this thesis. The results show good agreement between predicted and observed damage level. Unfortunately for the research objectives, the differential ground deformations caused by the tunnelling process at the location of the building were that small, that the damage level on the building was negligible. The negligible damage was observed from the defect surveys as well as predicted with the reviewed empirical analytical LTSM and the numerical damage prediction.

11 RECOMMENDATIONS FOR FUTURE RESEARCH

The following aspects are recommended for future research.

- The influence of differential ground movements on piled foundations requires further research. The interaction between soil, piles and building requires special considerations compared to the behaviour of shallow foundations. Vertical ground deformations on different depths along the piles should be considered to determine the pile settlements. Contributions of negative skin friction and pile point settlements determine the overall settlement of a pile due to excavation induced greenfield ground movements. The interaction between the piles, the soil and the building due to imposed horizontal ground movements, determine the transfer of horizontal strains to the building and the possible lateral pile loading. Both effects have to be considered in the damage assessment of buildings on piled foundations.

- The validation of the numerical and empirical analytical damage predictions with well defined monitoring data of differential ground and building deformations and the clear registration of pre- and post-construction building damage is an ongoing future challenge. The field test of the Sophia railway tunnel close to Rotterdam has been a first step, but further validation is required. The procedure of validation of the modified LTSM method using actual observed damage and monitoring data should be carried out according to the following procedure:

  - Collect monitoring data of green field horizontal and vertical ground movements in a monitoring section close to the structure. This monitoring data should be used to derive a greenfield line for the horizontal and vertical ground movements caused by the excavation process.

  - This greenfield predictions should be projected on the building location and the corresponding greenfield damage parameters angular distortion, deflection ratio and horizontal strain should be determined and used as input for the LTSM prediction. The damage class of the LTSM prediction serves as theoretical damage result.

  - The actual damage should be recorded in detail by defect surveys (in terms of a description of crack locations, crack width and crack length). The registration of pre-and post construction damage forms a crucial item.

  - For the validation it is important to measure the actual differential vertical and horizontal building deformations after interaction between the greenfield movements and the structure.

- Development of a probabilistic approach in order to determine the damage risks due to excavation induced ground movements on adjacent buildings can be a valuable addition to the LTSM, which could make it a more effective tool for risk management. The statistical variation of input parameters for the LTSM prediction can be included in order to be able to determine probability chances for damage risks.

- Numerical soil-structure interaction analyses are very complex and a lot of different factors can determine the results. For this study it was decided to vary a limited amount of parameters which were anticipated to be important for interaction effects and conclusions for engineering practice. However, based on this study, a variation of for example the material parameters of the smeared crack model could give more insight in the bandwidth of the damage results. The reader is referred to Boonpichetvong et al. (2003, 2005) for the influence of the most important structural input parameters (Young's modulus, tensile strength and fracture energy) of the walls. It is recommended to carry out more variation studies in the future.

Recommendations For Future Research

- The numerical studies did not include the incorporation of nonlinear soil behaviour. Future research should aim at combining the nonlinear behaviour of soil and structure. Computational tools and the developments on the numerical nonlinear finite element models for soil and structure become more and more robust and powerful, so that combination of soil nonlinearity and building nonlinearity gradually becomes feasible.

- A numerical study on the influence of initial cracking in a building on the overall damage development due to excavation induced ground deformations forms a challenge for future research. The initial cracking could have been initiated due to other differential ground deformation sources in the past or cracking due to thermal and seasonal influences. The initial cracking could be implemented in the numerical study using for example an initial cracking stage due to previous deformation or the incorporation of predefined discrete cracks in the building in the initial stage.

- 3D-effects can influence the damage results. For advanced numerical damage predictions, detailed structural 3D details of different structural elements and their connections, as well as the 3D behaviour of the soil should be implemented in the analyses in order to model actual configurations more accurately.

- The numerical interaction analyses should be extended in the future towards framed buildings in addition to the masonry walls considered in this thesis. The response of this type of buildings should be investigated further in numerical studies in order to study the modification of bending moments and shear forces in the structural members (beams, columns and foundation plates), as these considerations form the basis of the damage judgement for framed buildings.

LITERATURE REFERENCES

Addenbrooke T.I, (1996), *Numerical analyses of tunnelling in stiff clay*, Phd thesis University of London.

Attewell P.B., Woodman J.P., (1982), *Predicting the dynamics of ground settlement and its derivatives caused by tunnelling in soil, Ground Engineering*, 15, (8), 13-22.

Attewell P.B., Yeates J. and Selby A.R., (1986), *Soil movements induced by tunnelling and their effects on pipelines and structures*, Blackie Glasgow.

Base G.D., Read J.B., Beeby A.W. and Taylor H.P.E, (1966), *An investigation of the crack control characteristics of various types of bar in reinforced concrete beams,* Cement and Concrete Association, Research Report18, Pts. 1 and 2.

Bazant Z.P., Oh B.H. (1983), *Crack band theory for fracture of concrete*. Materials and Structures, RILEM, Vol. 16, No. 94, pp. 155-177.

Beranek W.J., Hannink G., Van der Maarel A.J.G. et al., (1986), Commissie Bodemdaling door Aardgaswinning, *Studieresultaten betreffende ongelijkmatige zakkingen in verband met aardgaswinning in de provincie Groningen.* Grondmechanica Delft, TNO-IBBC en Tauw Infra Consult B.V., in Dutch.

Bezuijen A., Talmon A.M., (2004), *Groutdrukmetingen Sophiaspoortunnel,metingen en analyse beide buizen,* COB rapport F220-O-03-109, onderdeel van commissie F220/230 Praktijkonderzoek Sophiaspoortunnel, in Dutch.

Boone S.J., (1996), *Ground movement related building damage*, J. of Geotch. Engrg. ASCE, 122(11), 886-896.

Boone S.J., (1998), *Ground movement related building damage:* closure, J. of Geotch. Engrg. ASCE, 124(5), 463-465.

Boone S.J., Westland J. and Nusink R., (1999), *Comparative evaluation of building responses due to an adjacent braced excavation*, Canadian Geotech. Journal no. 36, 210-223.

Boone S.J., (2001), *Assessing construction and settlement-induced building damage: a return to fundamental principles,* Proc. Underground construction, Institution of Mining and Metalurgy, London, 559-570.

Boonpichetvong M., Rots J.G., Netzel H., (2003), *On modelling of masonry buildings response in Dutch soft-ground tunnelling***,** Proc. of ITA in Amsterdam.

Boonpichetvong M., Rots J.G., (2005), *Settlement damage of masonry buildings in soft-ground tunneling*, The Structural Engineer, Vol. 83, No.1, pp. 32-37.

Boscardin M.D., Cording E.G., (1989), *Building response to excavation-induced settlement*, J. Geoptech. Engg., ASCE , 115(1), pp 1-21.

Burhouse P., (1969), *Composite action between brick paneel walls and their supporting beams*, Proc. Instn. Civ. Engrs., Vol. 43, 175-194.

Literature References

Building Research Establishment (BRE), (1981; revised 1990), *Assessment of damage in low rise buildings with particular reference to progressive foundation movements*, Digest 251, BRE, Garston.

Burland J.B., Wroth C.P., (1974), *Settlements of buildings and associated damage*, State of the art review, Conf. On settlement of structure, Cambridge, Pentech Press, London, pp 611-654.

Burland J.B., Broms B., De Mello V.F.B., (1977), *Behaviour of foundations and structures* – SOA Report, Session 2, Proc. 9th Conf. SMFE Tokyo, 2; 495 – 546.

Burland J.B., (**1995**), *Assessment of risk of damage to buildings due to tunnelling and excavations.* Invited special lecture to IS-Tokyo '95; 1st Int. Conf. On Earthquake Geotechn. Engrg..

Burland J.B., Standing J.R. and Jardine F. M., (Editors), (**2001**), *Building response to tunnelling*, CIRIA Special Publication 200, Vol. 1 & Vol.2, ISBN 0727730177, Thomas Telford, London.

Clough G.W., Schmidt B., (**1977**), *Design and Performance of excavation and tunnels in soft clay: state of the art report*, presented to international symposium on soft clay, Bangkok.

Clough G.W., O'Rourke T.D., (1990), *Construction induced movements of in situ walls*, Design and performance of earth retaining structures, Geotech. Spec. Publ. No. 25, ASCE, New York, 439-470.

Cording E.J., Hanshmire, W.H. (1975), *Displacements around soft ground tunnels*, - General report 5th Pan. Amer. Conf. on Soil Mech. and Found. Engrg, Buenos Aires, Session IV, pp 571-632.

CUR 162, (1993), *Construeren met grond – grondconstructie op en in weinig draagkrachtige en sterk samendrukbare grond***,** in Dutch, ISBN 90376 0024 7.

Dhanjal H.S., Thurlow P. and Bailey R.P., (2001), *Building settlement on the Copenhagen metro project,* Proc. of Int. Conf. at Imp. Coll. of London Building response due to tunnelling.

DIANA Finite Element Analyses (2002), User's Manual, Release 8.1, TNO Building and Construction Research

Dunnicliff J., (1993), *Geotechnical Instrumentation for monitoring field performance,* John Wily & Sons Inc.; ISBN 0-471-00546-0.

Finno R.J., Harahap I.S. , (1991a), *Finite Element analyses of HDR-4 excavation*, , J. Geotech. Engrg., ASCE 117(10), 1590-1609.

Finno R.J., Harahap I.S., Sabatini P. J., (1991b), *Analyses of braced excavations with coupled finite element formulations*, Comp. and Geotechnics., Vol. 12, 91-114.

Haasnoot J., Netzel H., (2002), *Settlement Risk Assessment; Integrating FEM and GIS***,** Proc. of the NUMOG conference in Rome.

Hart 't C.M.P., (2003), *Numerieke studie belendende panden Sophia spoortunnel*, COB rapport F220-0-03-119. In Dutch.

Hart 't C.M.P., (2005), *Numerieke postdictie belendende panden Sophia spoortunnel*, COB rapport F220-0-04-124. In Dutch.

Hashash Y.M.A, (1992), *Analyses of deep excavations in clay*, PhD thesis, Dept. of Civ. Engrg., massacusettes Inst. Of Technol. (MIT), Cambridge Mass.

Literature References

Hashash Y.M.A. and Whittle A.J., (1996), *Ground Movement prediction for deep excavations in soft clay*, J. Geotech. Engrg., ASCE Vol. 122 no. 6.

Hergarden R., (2000), *Gronddeformaties tijdens het trillend trekken van damwanden*, Master thesis TU Delft Faculty of civil engineering and geotechnics, in Dutch.

Hoekstra J., (1974), *Funderingsonderzoek Dapperbuurt Amsterdam*, Rapportage Grondmechanica Delft.

Kaalberg F.J., Hentschel V., Netzel H., Van Dijk B., (2001), *Big brother for TBM's,* Journal Tunnels & Tunnelling International.

Kolb H., (1988), *Ermittlung der Sohlreibung von Gruendungskoerpern unter horizontalem kinematischen Zwang,* Baugrundinstitut Stuttgart, Mitteilung 28.

Lee J.H., Rowe R.K. and Lo K.Y., (1992), *Subsidence owing to tunnelling I. Estimating the gap parameter,* Canadien Geotechnical Journal, Vol 10, pp 929-940.

Long M.M., (2001), *Database for retaining wall and ground movements due to deep excavations*, J. Geotech. Engrg., ASCE 127(3), 203-224.

Lourenco P.B., Rots J.G., Blaauwendraad J. (1998), *Continuum model for masonry: parameter estimation and validation*. ASCE J. of Structural Engineering, Vol. 124, No. 6, pp. 642-652.

Maidl B., Maidl U. and Ruse N., (2005), *Erfahrungen mit der FEM-Simulation im Rahmen des Prozesscontrollings beim Schildvortrieb*, Bauingenieur, Band 80.

Mair R.J., Taylor R.N. and Bracegirdle A., (1993), *Subsurface settlement profiles above tunnels in clay,* Geotechnique 43, (2), pp 315-320.

Mair R.J., Taylor R.N. and Burland J.B., (1996), *Prediction of ground movements and assessment of risk of building damage due to bored tunnelling,* Proc.of Geotech. Aspects of underground construction in soft ground, Balkema, ISBN 9054108568.

Mair R.J. and Taylor R. N., (1997), *Bored tunnelling in the urban environment*, Proc. 14th Int. Conf. Soil Mech. And Foundation Engineering, Balkema, Amsterdam, Vol 4, pp 2353 – 2385.

Meyerhof, (**1953**)**,** *The settlement analyses of building frames,* The struxctural engineer 25 (1953).

Milligan G.W.E., (1974), *The behaviour of rigid retaining walls in sand*, PhD thesis, Cambridge University, Cambridge UK.

Moh Z. C., Hwangh R.N., (1996), *Ground movements around tunnels in soft ground,* Proc. of Con. On Geotech. asp. of underground construction in soft ground, Balkema Rotterdam ISBN 9054108568.

Netzel D., (1972), *Beitrag zur wirklichkeitsnahen Berechnung und Bemessung einachsig ausgesteifter, schlanker Gruendungsplatten,* Dissertation Universitaet Stuttgart.

Netzel D., (2000), *Wechselwirkung Bauwerk-Baugrund,* Manuskript zur Vorlesung am Institut der Geotechnik TU Stuttgart.

Literature References

Netzel H., F.J. Kaalberg, (**1999a),** *Settlement risk management with GIS for the Amsterdam North/South Metroline*, Proceedings of the ITA World Tunnel Congress 1999 Oslo Norway, Balkema Publ.

Netzel H., Kaalberg F.J., (1999b), *Numerical settlement risk assessment studies for masonry structures due to TBM-tunnelling in Amsterdam*, Proc. Symposium Geotechnical aspects of underground construction in soft ground, Tokyo.

Netzel H., F.J. Kaalberg, (2000a), *Numerical Damage Risk Assessment Studies on adjacent buildings due to TBM-tunnelling in Amsterdam* – Proc. of GEOENG, Melbourne.

Netzel H., Kaalberg F.J., (2000b), *Omgevingsmonitoring van de Noord/Zuidlijn in Amsterdam*, COB Nieuws nr.05 in Dutch.

Netzel H., F.J. Kaalberg, (**2001a),** *Monitoring of the North-South Metroline in Amsterdam*, Proceedings CIRIA conference July 2001, CIRIA Publ.

Netzel H., F.J. Kaalberg, (2001b), *Settlement risk assessment for the North-South Metroline in Amsterdam***,** CIRIA Conference The response of buildings to excavation induced ground movement, London.

Netzel H., Kaalberg F.J., (2001c), *GIS koppelt ontwerp en uitvoering*, Journal Land + Water, nr.7/8, in Dutch.

Netzel H., (2002a), *Full scale test on the building response due to TBM-tunnelling in Dutch soft soil***;** Sec. Int. Conf. on Soil-structure interaction in Urban Civil Engineering, Zuerich.

Netzel H., Kaalberg F.J., (2002b), *On line vervormingsmonitoring van gebouwen in Amsterdam -Het ademen van constructies onder seizoensinvloeden-*, vakblad Cement, in Dutch.

Netzel H., (2002c), *Case studies of building response due to TBM-tunnelling in Dutch soft soil***;** Proceedings of the ITA conference in Sydney.

Netzel H., Kaalberg F.J., (2002d), *Base Monitoring Readings of the North-South Metroline Amsterdam - Natural Breathing of Buildings*, Proceedings of the ITA conference in Sydney.

Netzel H., Rots J.G., (2003a), *Empirische en analytische predicties van grondvervormingen en gebouwrespons,* COB report F220-O-04-122.

Netzel H., Kaalberg F.J., (2003b), *On line monitoring for underground works in Amsterdam,* Proc. of the 15th ICSMGE conference Istanbul Vol.2, Balkema, ISBN 90 2651 8560, p.1503-1507.

Netzel H., (2003c), *Review of the tensile strain method for predicting building damage due to ground movements***,** Proc. of ITA congres in Amsterdam.

Netzel H., Kaalberg F.J., (2003d), *Monitoring the deformation behaviour of buildings in Amsterdam***,** Proc. of ITA congres in Amsterdam.

Netzel H., J.G. Rots, (2004a), *"Geotechnical Innovations/Neue Entwicklungen in der Geotechnik"*,Verlag Glueckauf ISBN 3-7739-5991-5.

Netzel H., Rots J.G., (2004b), *Analyse en evaluatie van grondvervormingen,* COB report F220-O-04-122.

Literature References

Netzel H., Kaalberg F.J., (2004c), *Monitoring of natural deformation behaviour of buildings in Amsterdam – On line Monitoring for the North-South Metroline-*, Proc. of the TC28 conference in Toulouse.

Netzel H., (2004d), *Empirical analytical methods for surface settlement prediction due to TBM-tunnelling in soft soils*, Proc. of 5th Int. conference on case studies in geotechnical engineering, New York.

Netzel H., (2004e), *Review of the limiting tensile strain method for prediction of excavation induced building damage,* Proc.of 13th Int. Brick/Block Masonry conference in Amsterdam, 2004.

Netzel H., (2004f), *Settlement damage criteria- angular distortion or deflection ratio-* Proc.of 5th Int. Phd-Conference in Civil Engineering, Delft.

Netzel H., van Zijl G.P.A.G., (2004g), *Nonlinear numerical simulation of settlement-induced damage to solid masonry walls*, Proc.of 13th Int. Brick/Block Masonry conference in Amsterdam.

Netzel H., Rots J.G., (2004h), *Analyse en evaluatie grond- en gebouwvervormingen*; COB-rapport nr. F220-0-04-122; in Dutch.

Netzel H., (**2004k),** *Review of the limiting tensile strain method for prediction of excavation induced building damage*, Proc. of 5th International PhD-Symposium Delft.

Netzel H. , (2005), *Maaiveldvervormingen door de aanleg van boortunnels*, vakblad Geotechniek; 6e jaargang nummer 1 januari 2005; ISSN1386-2758, in Dutch.

O'Reilly M.P., New B.M. , (1982), *Settlements above tunnels in the United Kingdom - their magnitude and prediction,* Tunnelling 82, M.J. Jones (Hrsg.), S. 173ff., IMM, London.

O'Reilly M.P, (1996), *Discussion: Comments on the risk of damage to structures*, Proc. Of Geotech. Asp. of Undergr. Constr. In Soft Ground, Balkema, Rotterdam, ISBN 9054108568.

O'Rourke T.D., Cording E.D. and Boscardin M., (1976), *The ground movements related to braced excavations and their influence on adjacent structures*, US Department of Transportation, Report nro. DOT-TST-76T-23.

O'Rourke T.D., (1989), *Predicting displacements of lateral support systems*, Design, construction and performance of deep excavations in urban areas, Boston Soc. Of Civ. Engrs. (BSCE), Cambridge, Mass. 35p.

Oversteegen M.J., (**1998),** *Basisrapport: Casco-funderingsonderzoeken. Panden in de 19e eeuwse gordel*, Stedelijke Woningdienst Amsterdam Bureau P/A, in Dutch.

Peck R.B., (1969), *Deep excavations and tunnelling in soft ground*, Proc. 7th Int. Conf. on Soil Mech. and Found. Engrg. 225-290.

Peek R.D. , Willeitner H., (1981), *Behaviour of wooden piles in Long term service,* Proc. Of te 10th Int. Conf. Soil Mechanics and Found. Engrg., Stockholm, Balkema, pp 147-152.

Preene M., (2000), *Assessment of settlements caused by groundwater control*, Proc. Instn. Civ. Engrs. Geotech. Engng., no. 143, 177-190.

Literature References

Rankin (1988), *Ground movements resulting from urban tunnelling; predictions and effects,* Engineering Geology of Underground movement, Geological Society, Engineering Geology Special Publication No. 5,pp 79-92.

Rots J.G., Nauta P., Kusters G.M.A. and Blaauwendraad J. **(1985),** *Smeared crack approach and fracture localization in concrete*. HERON, Vol. 30, No. 1, 48 pp., 1985.

Rots J.G., (1985), *Smeared crack approach and fracture localization in concrete*. HERON 1985, No. 4, The Netherlands.

Rots J.G., **(1988),** *Computational modelling of concrete fracture*. PhD thesis Delft University of Technology, Delft, The Netherlands.

Rots J.G. (Ed.) (1997), *Structural masonry – An experimental/numerical basis for practical design rules,* A.A. Balkema Publishers, Rotterdam, Netherlands, 1997. Based on CUR-report 171, CUR Centre for Civil Engineering Research and Codes, Dutch version, Gouda, The Netherlands, 152 pp., **1994**.

Rowe R.K., Kack G.J., (1986), *A theoretical examination of the settlement induced by tunnelling: four case histories,* Canadien Geotechnical Journal, Vol 20, pp 299-314.

SBR (Stichting Bouwresearch), (1986), *Leidraad voor het onderzoek naar de invloed van een grondwaterstandsdaling op de bebouwing*, Stichting Bouwresearch (SBR), Rotterdam.

SBR (Stichting Bouwresearch), (2003), *Bemaling van bouwputten*, Stichting Bouwresearch (SBR), Rotterdam, Artikelnummer 190.03, ISBN 90-5367-386-5.

Schiphouwer R. A., Van Kessel A., Netzel H., Kaalberg F.J., Teunissen E.A.H., (1999), *IS-database for urban infrastructural projects- Generation of 3D geotechnical soil profiles,* Geotechniek-special in Dutch, ECSMGE-congres.

Schuette J., (1997), *Einfluss der Lagerungsbedingungen auf Zwang in Bodenplatten,* Institut fuer Baustoffe, Massivbau und Brandschutz (IBMB), TU Braunschweig, Heft 132.

Schultze E., (1964), *Zur Definition der Steifigkeit des Bauwerks und des Baugrundes sowie der Systemsteifigkeit bei der Berechnung von Gruendungsbalken und -platten,* Der Bauingenieur 39, Heft 6.

Schultze E., Horn A., (1990), *Setzungsberechnung,,* Kap. 1.8 im Grundbautaschenbuch, Teil 1, 4. Auflage, Berlin 1990.

Stoel A.E.C. van der, (**1998),** *Soil Grouting: Full Scale Injection test North/South metro line Amsterdam*, Tunnels and Metropolises, Proceedings of the World Tunnel Congress 1998 on Tunnels and Metropolises São Paolo Brazil, Balkema Publ.

Stoel A.E.C. van der, (1999), *Injection/grouting near pile foundations: Full Scale Test Amsterdam,* Geotechnical Aspects of Underground Construction in Soft Ground, IS'99 Tokyo Japan, Balkema Publ.

Stoel A.E.C. van der (**2001),** *Grouting for pile foundation improvement*, Phd Thesis Delft University, ISBN 90-407-2223-4, DUP Science.

STUFIB rapport studiecel 154, (2004), *Monitoren van betonconstructies* (J.Walraven, C. van der Veen; H. Netzel, R. Polder, J. Gullikers, J. Leggedoor, F. Kaalberg).

Literature References

Timoshenko S.P., (1957), *Strength of Materials – Part I,* D. Van Nostrand Co. Inc., London, England.

Timoshenko S.P. and Gere J.M., (1971), *Mechanics of materials*, Van Nostrand Reinhold Company.

Vermeer P.A., Bonnier P.G., Moeller S., (2002), *On a smart use of 3D-FEM in tunnelling*, Proc. Of the 8th intern. Symp. on numerical models in geomechanics, NUMOG VIII; Balkema Rotterdam; pp 361-366.

Visschedijk M., (2005), *Rapportage 4D-groutdrukcombinatie*, COB-rapport F220-O-04-120, onderdeel van COB commissie F220/F230 Praktijkonderzoek Sophiaspoortunnel, in Dutch.

Whittle A.J., Hashash Y.M.A. and Whitman R.V., (1993), *Analyses of a deep excavation in Boston*, J. Geotech. Engrg., ASCE 119(1), 69-90.

Wit J.C.W.M. de, Roelands J.C.S., De Kant M., (1999), *Full Scale test on environmental impact of diaphragm wall trench excavation in Amsterdam.*

Appendices

Appendices

Appendix 1
Settlements due to groundwater lowering

Determination of settlements due to increase of effective soil stresses according to CUR 162

$$\frac{\Delta h}{h} = \left(\frac{1}{C_p} + \frac{1}{C_s} \cdot \log \frac{\Delta t}{\Delta t_d} \right) \cdot \ln \frac{p_g}{\sigma'_i} + \left(\frac{1}{C'_p} + \frac{1}{C'_s} \cdot \log \frac{\Delta t}{\Delta t_d} \right) \cdot \ln \frac{\sigma'_i + \Delta\sigma'}{p_g} \qquad (A.1)$$

with
- Δh = total compression of the soil layer
- h = thickness of the soil layer
- C_p = primary compressibility index below limit stress state
- C_s = secondary compressibility index below limit stress state
- C'_p = primary compressibility index above limit stress state
- C'_s = secondary compressibility index above limit stress state
- Δt = time period of the increase of the effective soil stresses, thus the period of the drawdown [days]
- t = 1 day
- p_g = OCR (overconsolidation ratio) * σ'_i [kPa]
- σ'_i = initial effective soil stress in the mid of the soil layer
- $\Delta\sigma'$ = increase of the effective soil stress [kPa]

Appendix 2
Relation between angular distortion and deflection ratio for a simply supported beam with a central point load

Deflection curve v(x)

Neutral axis at the centre of the beam
(sagging zone)
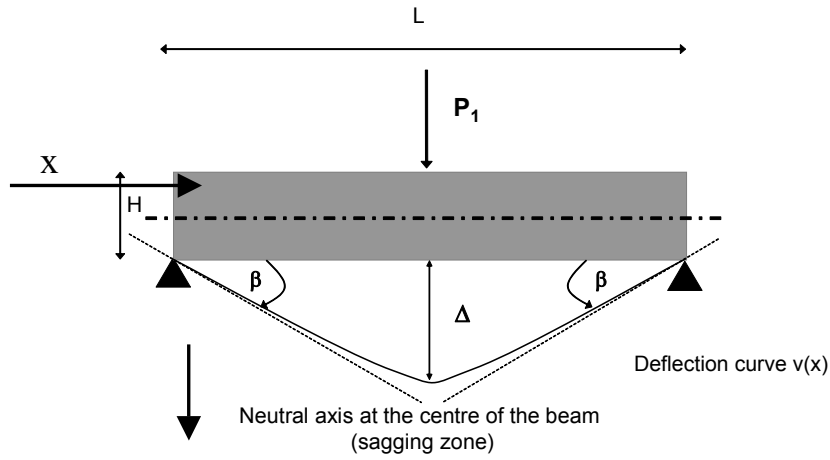
Note: The term α_s used in the following equations is the shear form factor

Deflection curve

$$v(x) = \frac{P \cdot L^3}{48 \cdot EI} \cdot \left(\frac{x}{L}\right) \cdot \left(3 - 4 \cdot \frac{x^2}{L^2}\right) + \frac{\alpha_s \cdot P \cdot x}{2 \cdot GA} \tag{A.2}$$

Slope distribution

$$v'(x) = \frac{P \cdot L^3}{48 \cdot EI} \cdot \left(\frac{3}{L} - 12 \cdot \frac{x^2}{L^3}\right) + \frac{\alpha_s \cdot P}{2 \cdot GA} \tag{A.3}$$

Angular distortion β is equal to the maximum slope at $x = 0$:

$$\beta = v'_{max(x=0)} = \frac{3 \cdot P \cdot L^2}{48 \cdot EI} + \frac{\alpha_s \cdot P}{2 \cdot GA} \tag{A.4}$$

The maximum deflection Δ at $x = L/2$ is:

Appendices

$$\Delta = v_{max\,(x=L/2)} = \frac{P \cdot L^3}{48 \cdot EI}\left(1 + \frac{12 \cdot \alpha_s \cdot EI}{GA \cdot L^2}\right)$$

$$= \frac{P \cdot L^3}{48 \cdot EI} + \frac{P \cdot L \cdot \alpha_s}{4 \cdot GA} \tag{A.5}$$

The deflection ration Δ/L is:

$$\frac{\Delta}{L} = \frac{P \cdot L^2}{48 \cdot EI} + \frac{P \cdot \alpha_s}{4 \cdot GA} \tag{A.6}$$

The relation of angular distortion to deflection ratio is:

$$\frac{\beta}{\left(\frac{\Delta}{L}\right)} = \frac{\left[3 \cdot L^2 \cdot GA + 24 \cdot \alpha_s \cdot EI\right]}{\left[L^2 \cdot GA + 12 \cdot \alpha_s \cdot EI\right]}$$

$$\frac{\beta}{\left(\frac{\Delta}{L}\right)} = \frac{\left[3 \cdot L^2 + 2 \cdot \alpha_s \cdot \left(\frac{E}{G}\right) \cdot H^2\right]}{\left[L^2 + \alpha_s \cdot \left(\frac{E}{G}\right) \cdot H^2\right]}$$

$$\frac{\beta}{\left(\frac{\Delta}{L}\right)} = \frac{\left[3 \cdot \left(\frac{L}{H}\right)^2 + 2 \cdot \alpha_s \cdot \left(\frac{E}{G}\right)\right]}{\left[\left(\frac{L}{H}\right)^2 + \alpha_s \cdot \left(\frac{E}{G}\right)\right]} \tag{A.7}$$

Appendices

Appendix 3
Design charts for the determination of the angular distortions in a Gaussian settlement trough

Definition of β_{left} and β_{right} in the sagging and hogging zone respectively:

Angular distorsion β_{right} in the hogging zone

Angular distorsion $\beta_{average}$ in the hogging zone

Angular distortion β_{left} in the sagging zone

Angular distortion $\beta_{average}$ in the sagging zone

Angular distortion β_{right} in the sagging zone

Legend:
- ssag= 0
- ssag= 0.1i
- ssag= 0.2i
- ssag= 0.3i
- ssag= 0.4i
- ssag= 0.5i
- ssag= 0.6i
- ssag= 0.7i
- ssag= 0.8i
- ssag= 0.9i

X-axis: L/i

Y-axis: $\beta_{right} * (i^2/(V*D^2)) * 1000$
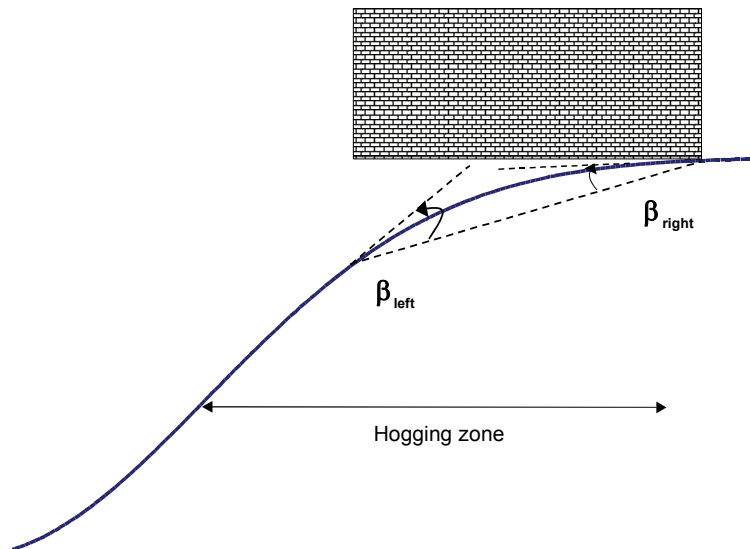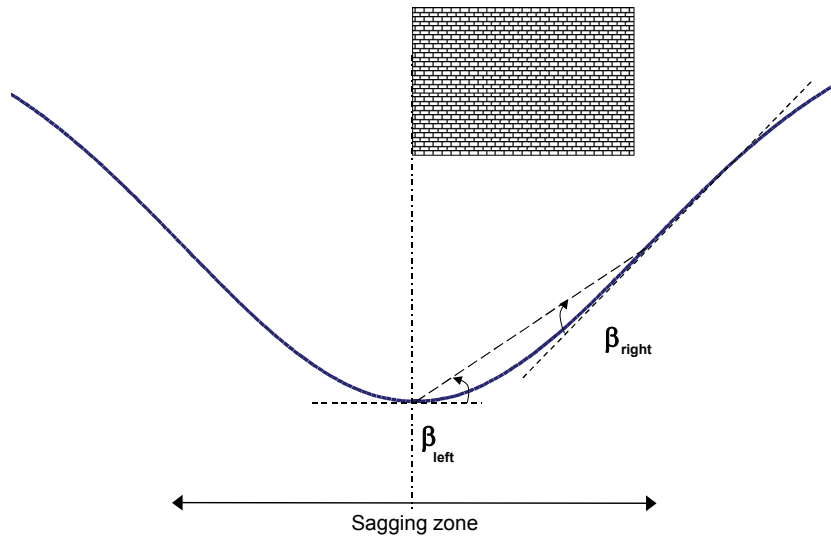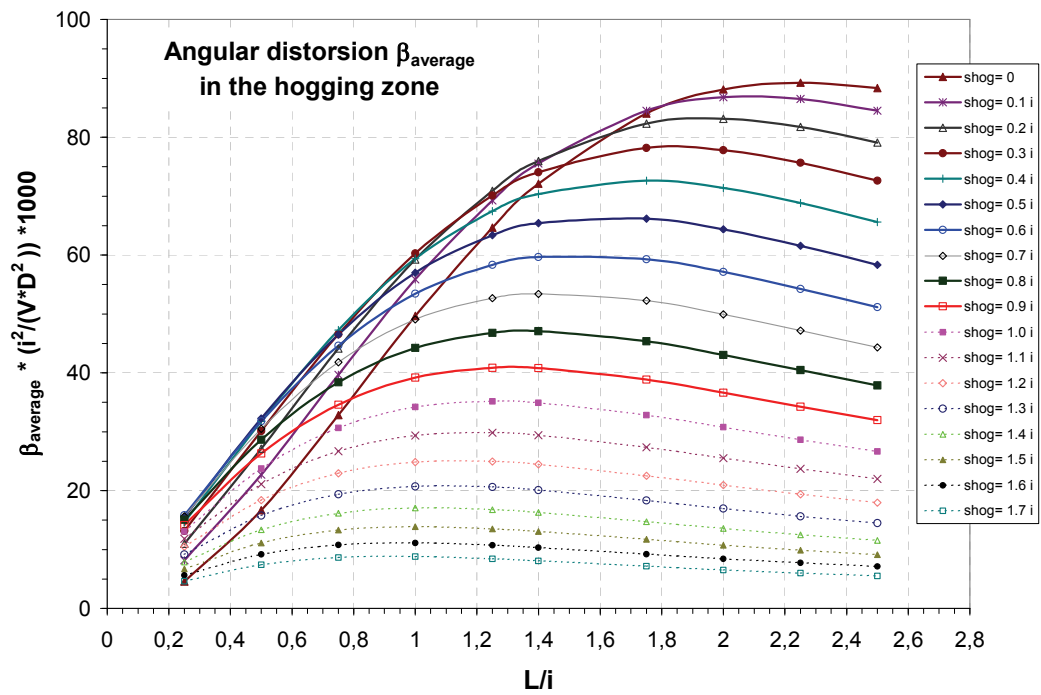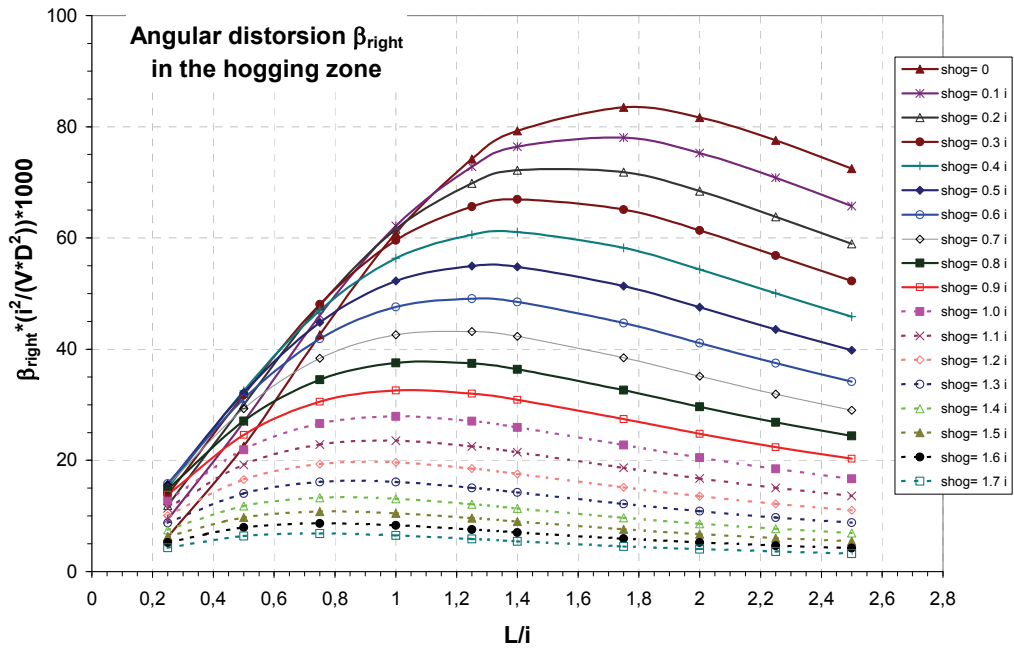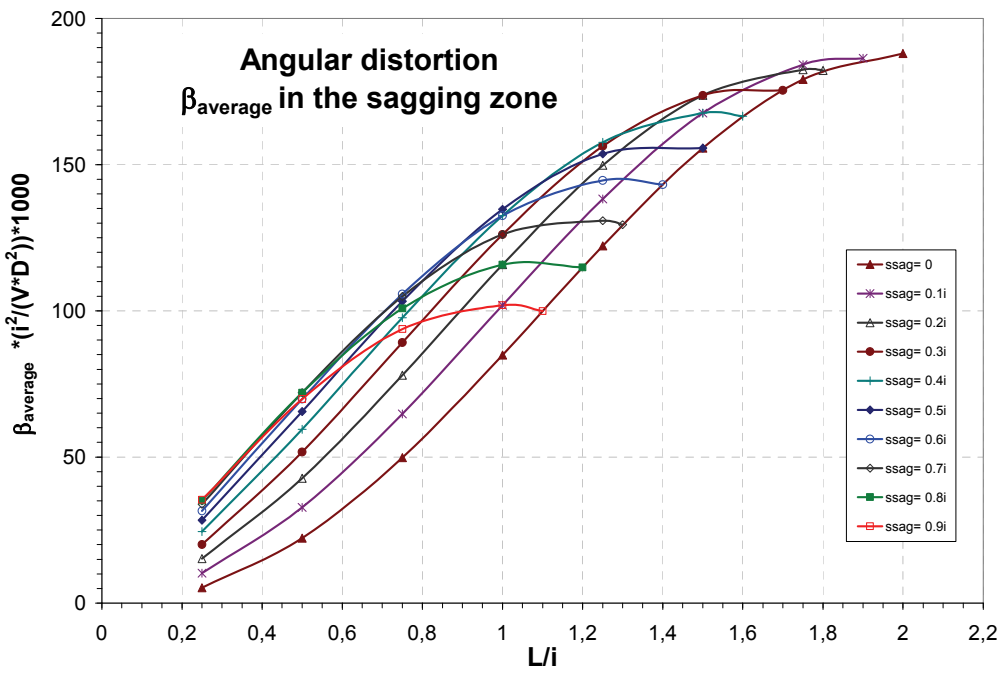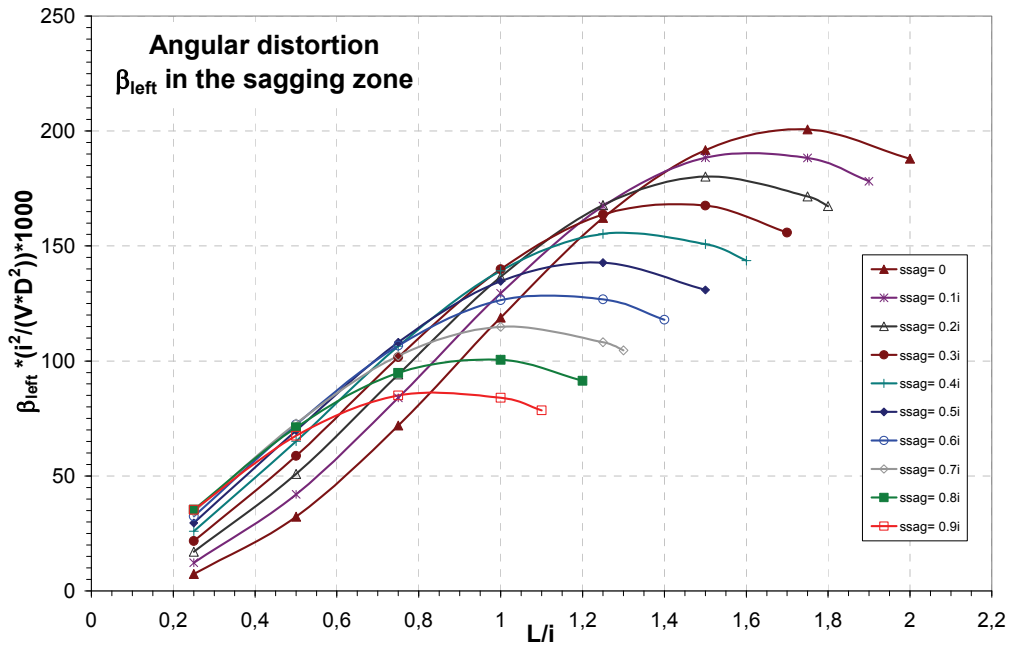
Appendices

Appendix 4
Definition of characteristic soil parameters

The results for the first loading stiffness from *triaxial tests* are in general presented using a value E_{50} which describes the secant stiffness for a mobilisation of 50% of the maximum shear strength (q_f). The normalized value $E_{50,ref}$ is often used in engineering practice and describes the secant stiffness for a mobilisation of 50% of the maximum shear strength q_f and a horizontal reference stress of 100kPa. The figure below shows a characteristic stress-strain curve derived from a triaxial test.
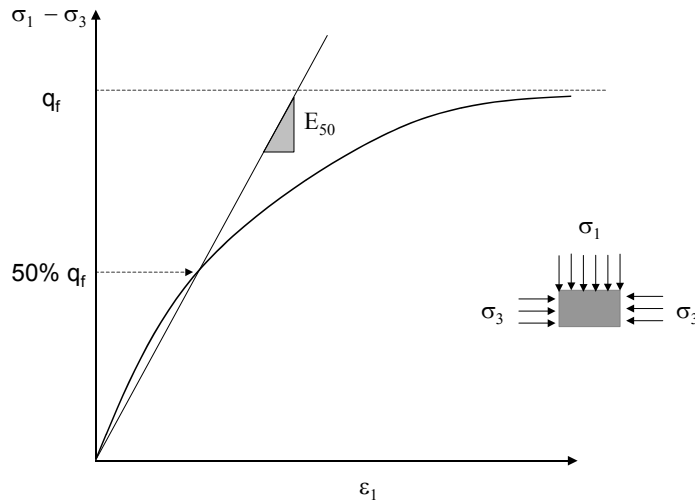
The equation to describe the E_{50} value dependant of the stress level is according to Schanz (1998):

$$E_{50} = E_{50,ref} \cdot \left(\frac{\sigma_3}{\sigma_{ref}} \right)^m \tag{A.8}$$

with σ_3 as the horizontal stress
           σ_{ref} as the horizontal reference stress (100kPa)
           m   as the power, describing the development of the stiffness with depth

The value $E_{soil, linear\ elastic}$ is used as input for the numerical calculations with the linear soil model in the Finite Element code DIANA (2002). The relation between the value $E_{50,ref}$ and the value $E_{soil, linear\ elastic}$ is derived with:

$$E_{soil, linear\ elastic} = 2 \cdot (1 + \nu) \cdot G \tag{A.9}$$

with

$$G = K \cdot \frac{3 - 6\nu}{2\nu + 2} \tag{A.10}$$

Appendices

$$K = K_{ref} \cdot \left(\frac{p'}{p'_{ref}}\right)^{(1-m)} \tag{A.11}$$

with

$p' = \dfrac{\sigma'_1 + \sigma'_2 + \sigma'_3}{3}$ average effective isotropic stress on a certain depth

p'_{ref} effective isotropic reference stress (100kPa)

$K_{ref} = \dfrac{E_{ur,ref}}{3 - 6 \cdot \nu}$

$m = 0.5$

$E_{ur,ref}$ is the tangent modulus at the reference stress σ_{ref} from an unloading/reloading branch in a standard triaxial test. An empirical relation between $E_{ur,ref}$ and $E_{50,ref}$ for sand gives $E_{ur, ref} \approx 4 \cdot E_{50,ref}$. Combining this empirical relation for sand with the equations above gives the following stress (and thus depth) depending relation between $E_{50,ref}$ and the linear elastic soil stiffness $E_{soil, linear elastic}$ used for the input of the numerical calculations:

$$\begin{aligned}
E_{soil, linear\,elastic} &= 2 \cdot (1 + \nu) \cdot G \\
&= 2 \cdot (1 + \nu) \cdot K_{ref} \cdot \left(\frac{p'}{p'_{ref}}\right)^{(1-0.5)} \cdot \frac{(3 - 6\,\nu)}{(2\,\nu + 2)} \\
&= 2 \cdot (1 + \nu) \cdot \frac{4 \cdot E_{50,ref}}{(3 - 6 \cdot \nu)} \cdot \left(\frac{p'}{p'_{ref}}\right)^{(1-0.5)} \cdot \frac{(3 - 6\,\nu)}{(2\,\nu + 2)}
\end{aligned} \tag{A.12}$$

with a Poisson ratio of 0.2:

$$E_{soil, linear\,elastic} = 4 \cdot E_{50,ref} \cdot \left(\frac{p'}{p'_{ref}}\right)^{0.5} \tag{A.13}$$

Appendices

Appendix 5
Eccentricity effect due to transfer of
horizontal differential ground movements

The definition of the imposed greenfield criteria Δ_0, β_0 and h_0 is given in the figures below.

Imposed vertical
greenfield
deformations

Imposed horizontal
greenfield
deformations
$h_0=(h_1 . h_2)/2$
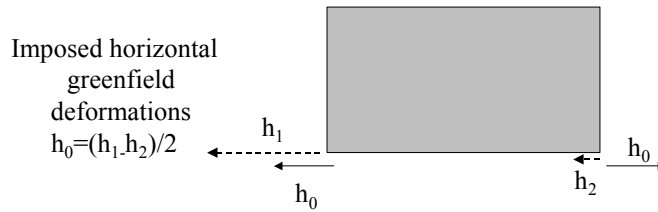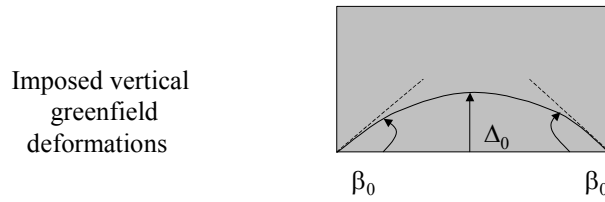
If the neutral axis is situated at the center of the wall, the deformation contributions due to the eccentric transfer of the horizontal deformations at the bottom edge of the wall are given in the figure below.

Neutral axis at center:
Effects of eccentric transfer of
the horizontal deformations
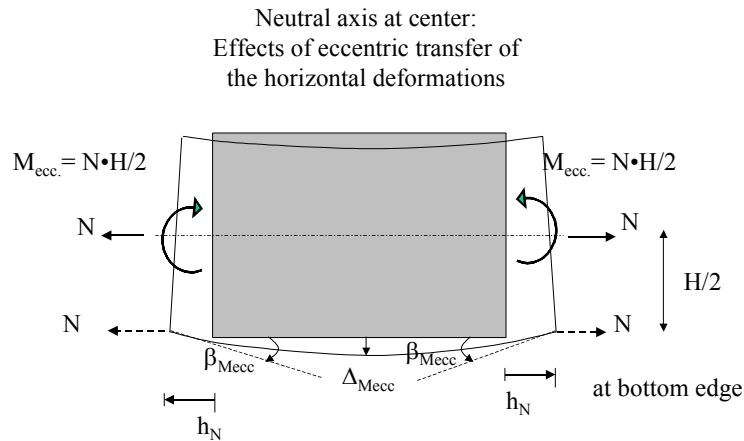
The fictitious central point load P used in the LTSM to impose the beam to predescribed greenfield deformations Δ_0, β_0 and h_0 can be derived from the compatibility of the different vertical and horizontal deformation contributions. The determination of the fictitious point load P_Δ fulfilling the compatibility for the deflection ratio Δ_0, which is used for the calculation of the bending strains, is shown in the figure below.

Appendices

Neutral axis in
the center

Δ_P

P_Δ

$M_{exc.} = N \bullet H/2$

$M_{exc.} = N * H/2$

N

N

$H/2$

Δ_{Mexc}
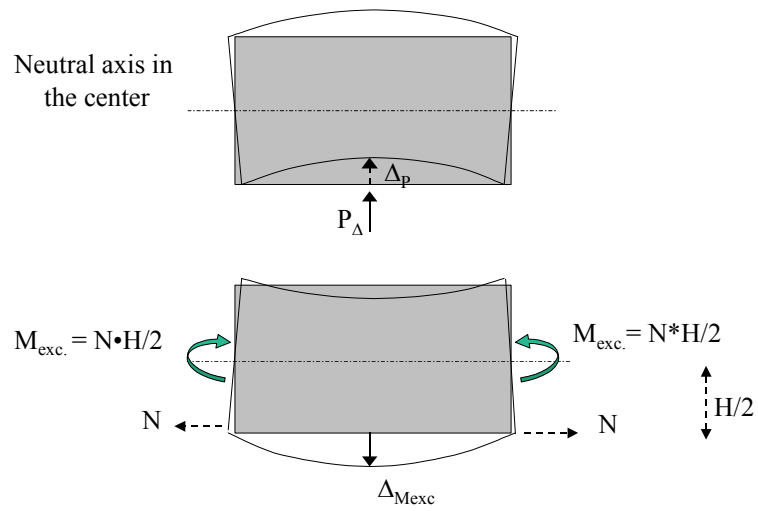
Compatibility deflection: $\Delta_P - \Delta_{Mexc} = \Delta_0$

$$\Delta_P = P_\Delta \cdot \left[\frac{L^3}{48 \cdot EI} + \frac{L \cdot 1,2}{4 \cdot GA} \right]$$

$$\Delta_{Mecc.} = \frac{1}{8} \cdot \frac{Mecc \cdot L^2}{EI} = \frac{N \cdot L^2 \cdot H}{16 \cdot EI}$$

$$\Delta_P - \Delta_{Mecc.} = \Delta_0$$

$$P_\Delta \cdot \left[\frac{L^3}{48 \cdot EI} + \frac{L \cdot 1,2}{4 \cdot GA} \right] - \frac{N \cdot L^2 \cdot H}{16 \cdot EI} = \Delta_0 \qquad (A.14)$$

with

$$h_N = h_0 = \frac{N \cdot L}{2 \cdot EA}$$

$$N = \frac{h_0 \cdot 2 \cdot EA}{L}$$

$$P_\Delta = \frac{\Delta_0 + \left[\dfrac{H \cdot A \cdot h_0 \cdot L}{8 \cdot I}\right]}{\left[\dfrac{L^3}{48 \cdot EI} + \dfrac{L \cdot 1,2}{4 \cdot GA}\right]} \qquad \text{(A.15)}$$

The strain equations given in section 3 can be used to determine the strains with the above calculated fictitious point load.

The determination of the fictitious point load *P* fulfilling the compatibility for the angular distortion deflection β_0, which is used for the calculation of the diagonal strains, is shown in the figure below.

Compatibility angular distortion: $\beta_P - \beta_{Mecc} = \beta_0$

$$\beta_P = P_\beta \cdot \left[\frac{3 \cdot L^2}{48 \cdot EI} + \frac{1,2}{2 \cdot GA} \right]$$

$$\beta_{Mecc.} = \frac{1}{2} \cdot \frac{Mecc. \cdot L}{EI} = \frac{N \cdot L \cdot H}{4 \cdot EI}$$

$$\beta_P - \beta_{Mecc.} = \beta_0$$

$$P_\beta \cdot \left[\frac{3 \cdot L^2}{48 \cdot EI} + \frac{1,2}{2 \cdot GA} \right] - \frac{N \cdot L \cdot H}{4 \cdot EI} = \beta_0 \qquad (A.16)$$

with

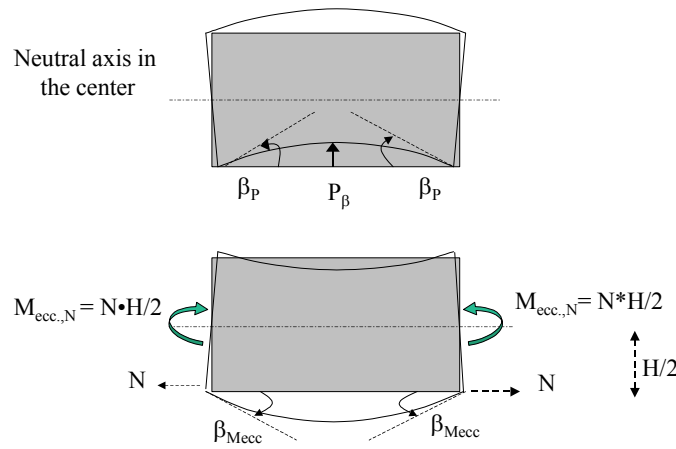$$h_N = h_0 = \frac{N \cdot L}{2 \cdot EA}$$

$$N = \frac{h_0 \cdot 2 \cdot EA}{L}$$

$$P_\beta = \frac{\beta_0 + \left[\dfrac{H \cdot A \cdot h_0}{2 \cdot I} \right]}{\left[\dfrac{3 \cdot L^2}{48 \cdot EI} + \dfrac{1,2}{2 \cdot GA} \right]} \qquad (A.17)$$

The following figure shows the results of the total strains for the current hogging case and the different assumptions for the location of the neutral axis.

Appendices

Hogging zone

Legend:
- combined bending and horizontal strain at top edge with neutral axis at center and eccentricity
- combined bending and horizontal strain at bottom edge with neutral axis at center and eccentricity
- combined bending and horizontal strain at top edge with neutral axis at bottom edge; no eccentricity
- combined diagonal and horizontal strain for neutral axis at center with eccentricty
- combined diagonal and horizontal strain with neutral axis at bottom edge; no eccentricity

y-axis: total strain (0,16%, 0,14%, 0,12%, 0,10%, 0,08%, 0,06%, 0,04%, 0,02%, 0,00%, -0,02%, -0,04%, -0,06%)

x-axis: L/H (0, 1, 2, 3, 4, 5, 6)

SAMENVATTING

Building Response due to Ground Movements

Omgevingsbeïnvloeding vormt vaak een belangrijke randvoorwaarde voor het ontwerp van binnenstedelijke bouwprojecten. Met behulp van een voorspelling van grondvervormingen ten gevolge van de geplande bouwwerkzaamheden en een schadepredictie van de belendende constructies kan hiermee een ontwerp rekenkundig worden beoordeeld met betrekking tot zijn mogelijke gevolgen op de omgeving.

Dit boek behandelt voorspellingsmethodieken voor gebouwschade door grondvervormingen die veroorzaakt worden door een externe bron. Deze rekenmethodieken kunnen enerzijds in het ontwerpstadium worden toegepast, om mogelijk te verwachten zettingsschade aan belendende constructies in beeld te brengen, maar kunnen anderzijds ook worden gebruikt om door middel van een zogenaamde *postdictie* achteraf, rekenkundig verbanden te onderzoeken tussen (geclaimde) schade en bouwwerkzaamheden.

In verband met de grote variatie die in de praktijk kan optreden met betrekking tot de bron voor grondvervormingen van ondergrondse bouwwerkzaamheden en de constructietypes cq. funderingswijzen van de belendende gebouwen, is besloten om in dit onderzoek de focus te leggen op de invloed van grondvervormingen veroorzaakt door de aanleg van een boortunnel op metselwerkgebouwen die op staal zijn gefundeerd. Desalniettemin zijn de principes van de ontwikkelde voorspellingsmethodieken ook toepasbaar voor andere invloedsbronnen (zoals bijvoorbeeld de aanleg van bouwputten en grondwaterstandverlagingen) die verschilvervormingen aan belendende panden kunnen veroorzaken.

Dit onderzoek beschouwt allereerst empirisch-analytische rekenmethodieken ter voorspelling van "*greenfield grondvervormingen*" die veroorzaakt kunnen worden door drie relevante bronnen van grondvervormingen bij binnenstedelijke bouwwerkzaamheden, te weten: de aanleg van een boortunnel, de aanleg van een bouwput en grondwaterstandsverlagingen. In een literatuurstudie zijn de internationale ervaringen met empirisch analytische voorspellingsmethodieken samengevat. Voor de grondvervormingen tengevolge van de aanleg van een boortunnel zijn de internationale ervaringen aangevuld met een analyse van monitoringdata van drie boortunnelprojecten die zijn uitgevoerd in de slappe, Nederlandse bodemgesteldheid. De voorspellingsmethodieken zoals gepresenteerd in dit eerste gedeelte kunnen worden toegepast in een voorontwerpstadium, om een eerste indicatie van de bandbreedte van de te verwachten grondvervormingen te verkrijgen.

Vervolgens worden de resultaten van een review van de methode der grensrekken *(**L**imiting **T**ensile **S**train **M**ethod; hierna: LTSM)* gepresenteerd. Deze empirisch- analytische rekenmethodiek wordt in de huidige ontwerppraktijk vaak toegepast ter voorspelling van gebouwschade door opgelegde grondvervormingen. De methodiek is gebaseerd op de berekening van rekken die door de opgelegde verticale- en horizontale grond(verschil)vervormingen in de constructie worden geïntroduceerd. De berekende rekken worden vervolgens gerelateerd aan te verwachten mate- en ernst van gebouwschade. De review van de bestaande methodiek werd noodzakelijk geacht, omdat bij toepassing van deze methodiek in de praktijk, belangrijke fundamentele vragen zijn ontstaan over de achtergronden en de aannamen die in deze methodiek worden getroffen. Door de review is aangetoond, dat enkele aannamen in de huidige methodiek tot significant onder- of overschatting van de rekken en dus het voorspelde schadebeeld kunnen leiden. Op basis van de analysen is een gemodificeerde LTSM ontwikkeld welke rekenkundig is onderbouwd en waarbij aanbevelingen worden gedaan over verfijnde, aangepaste aannamen en procedures.

Een belangrijk onderdeel van deze dissertatie is een omvangrijke ***numerieke studie naar de effecten van grond-constructie interactie*** op de gebouwschade door opgelegde grondvervormingen. Deze grond-constructie interactie wordt verwaarloosd in de methode der grensrekken, waarbij van een volledige overdracht van de grondvervormingen aan het gebouw wordt uitgegaan. De geavanceerde numerieke interactie berekeningen met de Eindige Elementen methode houden rekening met niet-lineair gedrag van de metselwerkconstructie (*smeared cracking*) en de interface tussen grond en constructie (no tension bedding voor verticale interactie en een elastoplastisch Coulomb wrijvingsmodel voor horizontale interactie). De resultaten van de numerieke berekeningen zijn gepresenteerd in termen van scheurwijdten en scheurpatronen in de constructie, die geclassificeerd worden conform de schadecategorieën die ook in de LTSM worden gebruikt. Op deze manier is een duidelijke vergelijking van de schadevoorspellingen tussen de empirisch-analytische methodiek en de numerieke berekeningen mogelijk en kan de invloed van de grond-constructie interactie worden beoordeeld. In de numerieke berekeningen zijn op staal gefundeerde metselwerkgebouwen onderzocht, die door de grondvervormingen tengevolge van de aanleg van een boortunnel worden beïnvloedt.

Voor alle beschouwde interactie variaties wordt geconcludeerd dat voor hetzelfde verloop van de opgelegde greenfield grondvervormingen, de schade van de metselwerkconstructies toeneemt met toenemende grondstijfheid. Of met andere woorden: bij afnemende grondstijfheid ontstaan gunstige interactie-effecten, die de gebouwschade reduceren. Zodra de eerste scheurvorming wordt geïnitieerd, speelt het niet-lineaire scheurgedrag van metselwerk een zeer belangrijke rol in de ontwikkeling van schade. Een numerieke interactie berekening dient uitgevoerd te worden met een niet-lineair materiaalmodel voor de constructie en de interface. Gedetailleerde conclusies zijn afgeleid uit de vergelijking van de schaderesultaten tussen de gemodificeerde LTSM en de numerieke grond-constructie interactieberekeningen. Voor de interactie-effecten dient zorgvuldig onderscheid te worden gemaakt tussen een *hogging* of een *sagging* situatie, omdat voor grondvervormingen die door de aanleg van een boortunnel worden veroorzaakt, de combinatie van horizontale- en verticale verschilvervormingen in beide situaties zeer uiteenlopende effecten op de gebouwreactie cq. de gebouwschade hebben.

Vervolgens is een hoofdstuk in deze dissertatie gewijd aan belangrijke aandachtspunten voor de vertaling van de schadepredicties in het ontwerpstadium naar monitoringscriteria die voor een actieve risicobeheersing gedurende de uitvoering kunnen worden gebruikt. Ontwerpers zijn zich vaak niet bewust van de noodzaak van deze beschouwingen.

Tenslotte zijn de resultaten van een praktijkproef geanalyseerd en geëvalueerd. In deze proef is langs het tracé van de Sophia Spoortunnel (onderdeel van de Betuwelijn vlakbij Dordrecht), die door middel van een boortunnel is aangelegd, intensive monitoring uitgevoerd van de grondvervormingen en de vervormingen van een belendend metselwerkpand. De monitoringdata van de verplaatsingen in combinatie met de resultaten van schadeopnamen aan het pand, voor- en na de werkzaamheden, zijn vergeleken met de rekenkundige resultaten, die met de in dit onderzoek ontwikkelde empirisch-analytische en numerieke berekeningsmethodieken zijn bepaald. Geconcludeerd wordt dat de resultaten goede overeenkomst vertonen. Het moet worden benadrukt, dat de door de boortunnel veroorzaakte verschilvervormingen in de grond en aan het pand gering waren, waardoor geen schade is veroorzaakt. De rekenkundige beschouwingen resulteerden ook in de schadeklasse "verwaarloosbaar".

Holger Netzel

CURRICULUM VITAE

Holger Dirk Netzel
Geboren 24 januari 1968 te Stuttgart

1990	Abitur Wilhelmsgmnasium Stuttgart *Pre-University Education*
1990-1995	Diplomarbeit Bauingenieurwesen TU Stuttgart (afstudeerrichting "Massivbau") *MSc Civil Engineering*
1995-1996	Adviseur IGB te Stuttgart *Consultant at IGB te Stuttgart*
1996-2002	Adviseur en ontwerpleider bij Witteveen + Bos raadgevende ingenieurs b.v. *Consultant and design leader at Witteveen + Bos consulting engineers; Amsterdam*
2000-2009	Promotieonderzoek aan de TU-Delft (Faculteit Bouwkunde) *PhD TU Delft (Faculty of Architecture, Department Structural Mechanics)*
2002-heden	Oprichter/Directeur CRUX Engineering b.v. te Amsterdam *Founder/Director CRUX Engineering b.v Amsterdam*